



THE PREVENTION OF THERMAL LOSSES FROM  
AUTOMOTIVE LUBRICANTS TO  
IMPROVE COLD START EFFICIENCY

Andrew Peter Roberts. MEng CEng MIMechE

Thesis submitted to the University of Nottingham  
For the degree of Doctor of Philosophy

APRIL 2015

## Abstract

The internal combustion (I.C.) engine remains unrivalled as the primary means of road vehicle propulsion. The frequency of re-fuelling stations, combined with the high energy density of both gasoline and diesel fuel provide users with unrivalled flexibility and vehicle range. However a range of environmental and health concerns exist surrounding I.C. engine emissions; in particular carbon dioxide (CO<sub>2</sub>), nitrous oxides (NO<sub>x</sub>), hydrocarbons (HC) and carbon monoxide (CO). There is therefore increasing pressure on vehicle OEMs to reduce vehicle emissions through tightened emission standards and regulations. A significant challenge in meeting these tightened regulations is the reduced efficiency of the I.C. engine during cold-start which reduces from typical values of 40% when fully warm to values as low as 10% when cold. Increased friction in the engine caused by overly viscous lubricants providing sub-optimal lubrication during cold starts is a primary cause of this reduction in efficiency during cold-start. This is despite the advancements in lubricant technology made that has reduced the sensitivity of lubricant viscosity to temperature variation.

It is therefore desirable to increase the rate of lubricant heating during engine warm-up so that optimal lubrication conditions are reached sooner and frictional losses are reduced. The reduction in frictional losses therefore reduces fuel consumption and hence emissions. In this thesis, the merits of insulating engine oilways are investigated as a means to reduce thermal losses from the lubricant and thus accelerate warm-up rates using a bespoke oil flow rig and simulation model. Through this work, it has been found that, using insulating inserts, it is possible to reduce the thermal losses from the lubricant to the surrounding wall structure by up to 58%. Such reductions have been achieved by installing an insulating insert into the oilway (also commonly referred to as a gallery in I.C. engines) that combines a low thermal conductivity material but also introduces a contact resistance between the insert and the surrounding metal. It has been found that the contact resistance is a highly significant and beneficial feature and, using special inserts designed to enhance the contact resistance, reductions in thermal losses of up to 40% can be achieved using the contact resistance alone without using low thermal conductivity materials.

A computational finite difference model has been developed to simulate heat transfer between flowing engine lubricant and the gallery walls. The model has been correlated with experimental data from the oil flow rig and is capable of simulating the effects of changing the materials properties (density, specific heat capacity and thermal conductivity) of both insulating inserts and the surrounding metal structure. The model is also capable of investigating the effect of changing contact heat

transfer coefficients and changing flow geometry and velocity. Through computational experiments with this model, it has been found that the optimum strategy to achieving reduced thermal losses from the lubricant through the gallery walls is to ensure that the thermal conductivity of the insulating insert and that the thermal mass of the surrounding structure are minimised. Computational experiments have also highlighted the need to consider the flow geometry of different regions of the engine with the variation in bore diameter affecting both the heat transfer surface area and the convective heat transfer coefficient through the Reynolds' effect. It has been found that increasing the lubricant flow velocity for a given bore diameter increases thermal losses to the gallery walls as a result of the Reynolds effect. If the bore diameter is increased, the thermal losses from the lubricant reduce in uninsulated galleries owing to a reduction in the Reynolds number but the reverse happens in insulated galleries owing to the increase in heat transfer area. The change in trend is a result of the interactions between the changing convective heat transfer area, heat transfer coefficient and the temperature differential between the lubricant and gallery wall. In addition, implementation of the insulation into a running engine needs careful consideration to ensure that the insulation does not isolate the lubricant from a potential heat source (such as the cylinder head). The optimum locations will vary between engines but investigations suggest that the return galleries from the head to the sump represent a positive opportunity to reduce thermal losses from the lubricant with a clear reduction in lubricant temperature observed as the lubricant moves down the gallery.

## Acknowledgements

The completion of this work would not have been possible without the support of many people.

I would first like to acknowledge the support and guidance of my two academic supervisors, Dr Richard Brooks and Prof. Phil Shipway.

The financial support of the TSB through grant number 400178 and the EPSRC is also gratefully acknowledged.

Much of the work would not have been possible without the time and technical resources of the project industrial partners. In particular I would like to thank Robert Gilchrist of Jaguar Land Rover and Ian Pegg from the Ford Motor Company for their input and project management. In addition Nigel Fawcett and the Materials Group of the Ford Motor Company deserve a special mention for endlessly tolerating my presence and phone calls during the work.

The technical staff at the University of Nottingham and fellow members of the Polymer Composite Research Group became friends rather than colleagues and I am particularly grateful to Paul Johns for endlessly helping me with experimental changeovers and for keeping me smiling with jokes and mugs of coffee during hundreds of hours of experimental tests.

Without the support of my friends and family this thesis would not have been completed. In particular I would like to thank my parents for their unwavering support throughout and in particular my father, Martin, who painstakingly read each word of this thesis.

John Dominy's friendship and coffee meetings over the past five years have been invaluable both in the capacity of a colleague and a valued friend.

Douglas and Pip MacInnes deserve a special mention for teaching me how to have fun, and going far beyond the call of duty of friendship.

Lastly I unreservedly thank my girlfriend Katie for being a pillar of support and love and for never once complaining about me forever running late or falling asleep.

## Contents

Abstract.....	I
Acknowledgements .....	III
Contents.....	IV
Nomenclature .....	X
Abbreviations and letters used in mathematical formulae .....	X
Greek symbols .....	XIII
1 Introduction .....	1
1.1 The importance of the internal combustion engine in society.....	1
1.2 Legislation and emissions performance .....	2
1.2.1 Alternative measures of engine performance and their comparative nature	3
1.3 The need to improve I.C. engine cold-start performance .....	6
1.4 The thermal balance of the engine during warm-up .....	8
1.5 The significance of engine lubricant and engine coolant temperatures during warm-up .....	11
1.5.1 The sensitivity of engine lubricant to temperature .....	13
1.5.2 Summary.....	25
1.6 Emission control using catalytic convertors during engine cold starts .....	25
1.6.1 NOx emission considerations.....	28
1.7 Conclusions .....	28
2 Literature Review .....	29
2.1 Introduction .....	29
2.2 The fundamentals of heat transfer .....	31
2.2.1 The different mechanisms of heat transfer .....	31
2.2.2 Transient heat transfer.....	33
2.2.3 Heat exchange from fluids and the use of heat exchangers .....	35
2.3 Strategies used to improve I.C. engine efficiency .....	37
2.3.1 Energy re-capture from the exhaust stream .....	42
2.3.2 The use of thermal barrier coatings (TBC) in the combustion chamber	47
2.3.3 External insulation of the engine structure .....	50
2.3.4 Insulation applied to internal structures of the engine .....	53
2.3.5 Active system control methods to improve vehicle cold-start performance.....	55
2.3.6 Use of alternative materials to reduce the thermal mass of the engine	67

2.3.7	Applications of phase change materials to improve engine thermal efficiency .....	72
2.4	The methods of research and their limitations .....	82
2.4.1	Computational Modelling .....	85
2.4.2	Engine test bed experimentation.....	87
2.4.3	Vehicle implementation experimentation .....	88
2.4.4	Levels of confidence in experimental methodologies .....	88
2.4.5	Summary.....	89
2.5	Conclusion.....	90
2.6	Aims of the thesis .....	93
3	Design and construction of the oil flow rig.....	94
3.1	Introduction .....	94
3.2	Rig Design.....	94
3.2.1	Lubricant temperature measurement.....	97
3.2.2	Lubricant pump and flow rate control .....	98
3.2.3	Tank design and heater selection .....	98
3.2.4	Piping geometry and specification .....	101
3.3	Specimen design.....	102
3.3.1	Insulating insert design.....	106
3.3.2	Connection of specimen to the rig.....	108
3.3.3	Storage and usage of test block specimen inserts.....	109
3.4	Variation of lubricant properties with temperature .....	110
3.5	Instrumentation .....	112
3.5.1	Thermocouple instrumentation.....	112
3.6	Experimental methodology .....	119
4	Characterisation of the oil flow rig.....	121
4.1	Introduction .....	121
4.2	Observations of the temperature gradients within the test block specimen 122	
4.2.1	The significance of the temperature differential between the lubricant temperature and specimen temperature .....	124
4.3	The sensitivity of lubricant temperature to specimen structure.....	127
4.3.1	The sensitivity of lubricant temperature to specimen size .....	129
4.4	Overall rig thermal balance.....	131
4.5	The effect of external tank insulation on the rate of rig warm-up.....	134

4.6	The significance of flow rate on the lubricant and specimen warm-up rate	135
4.7	The significance of boundary layer creation on the lubricant temperature measurement .....	140
4.8	The effect of varying the heater power on rig warm-up rate .....	142
4.9	Repeatability of the experimental procedure .....	145
4.10	Conclusion.....	149
5	Experimental results from the characterisation of differing insulating mechanisms .....	151
5.1	Introduction .....	151
5.2	The effect of applying insulating inserts to engine oil galleries on heat transfer to the surrounding metal.....	151
5.2.1	The use of Nylon 12 inserts in engine oil galleries.....	152
5.2.2	Investigation into the significance of the contact interface.....	155
5.3	Attempts to maximise the contact resistance to improve insulating performance .....	158
5.4	Investigation into the effect of the bore surface roughness on heat transfer	161
5.5	The combination of low thermal conductivity material and contact interface	163
5.5.1	Quantification of thermal conductivity .....	164
5.5.2	The benefits of sintered Nylon on the oil flow rig .....	166
5.6	Assessment into the repeatability and confidence of the results .....	167
5.7	Investigation into the variation in fit between polymer inserts and the oil gallery bore.....	169
5.8	The relative performance of external insulation compared to internal insulation methods .....	172
5.8.1	Results.....	174
5.9	Summary .....	178
5.10	Conclusion.....	181
6	Development of the oil flow rig theoretical simulation model .....	184
6.1	Introduction .....	184
6.2	Modelling methodology .....	184
6.2.1	Distance step.....	186
6.2.2	Node $T_x, T_{x+1}, T_{x+2}, T_{outlet}$ .....	187
6.2.3	Node $T_{tank}$ .....	188
6.2.4	Variation of <i>hoil</i> with temperature.....	189
6.2.5	Derivation of outer surface heat transfer coefficient .....	197

6.3	Test block specimen nodes .....	199
6.4	Specimen effective power in .....	200
6.4.1	Variation of effective power with specimen size and structure .....	202
6.4.2	Selection of transferrable rig power function .....	209
6.5	Experimental and theoretical correlation results .....	212
6.5.1	Baseline correlation results .....	213
6.5.2	Correlation of temperature differential between lubricant and specimen as a function of the lubricant temperature .....	222
6.5.3	The sensitivity of the specimen to ambient heat transfer coefficients 227	
6.5.4	Final model optimisation .....	229
6.6	Mesh Sensitivity Study.....	234
6.6.1	Reduced polymer thickness mesh sensitivity study.....	236
6.7	Conclusion.....	237
7	Investigations into the effect of geometry and different material properties on transient warm-up of flowing automotive lubricants .....	239
7.1	Introduction .....	239
7.2	Investigations in to the effect of material properties on energy flow from engine lubricant to the surrounding structure .....	240
7.2.1	Methodology.....	240
7.2.2	Results.....	245
7.3	The significance of flow geometry on heat transfer .....	257
7.3.1	The interaction between flow velocity and varying convective heat transfer area.....	260
7.3.2	Steady state lubricant temperature simulations .....	267
7.4	Investigations into the effect of ambient temperature .....	273
7.5	Conclusions .....	275
7.5.1	Investigations in to the effect of material properties on energy flow	275
7.5.2	The significance of flow geometry on heat transfer .....	277
7.5.3	Investigations into the effect of ambient temperature .....	279
8	Conclusions and scope for further work .....	280
8.1	Conclusions .....	280
8.1.1	Experimental investigations into the effect of applying insulation on oil gallery thermal losses .....	280
8.1.2	Experimental investigations into the effect of contact resistance on oil gallery thermal losses .....	280

8.1.3	Computational investigations into the effect of substrate material properties on oil gallery thermal losses .....	281
8.1.4	Computational investigations into the effect of insulating material properties, insulating thickness and contact conditions on oil gallery thermal losses	281
8.1.5	Computational investigations into oil gallery thermal losses using different engine block materials .....	282
8.1.6	Computational investigations into the effect of flow geometry and conditions on oil gallery thermal losses .....	283
8.1.7	Final conclusions and advances in knowledge.....	284
8.2	Scope for further work .....	284
8.2.1	Refinements to computational modelling.....	285
8.2.2	Development of implementation methodologies .....	286
8.2.3	Alternative methods to address I.C. engine cold-start efficiency.....	289
9	References .....	291
Appendix A	Manufacturer data of Nylon properties .....	298
A.1	Nylon 12 data .....	298
A.1.1	Ensinger data.....	298
A.1.2	PAR data.....	299
A.2	Nylon 6 data .....	301
A.2.1	Ensinger data.....	301
A.2.2	Quadrant data .....	303
A.2.3	PAR data.....	304
A.3	Variation of Nylon properties with temperature.....	305
Appendix B	Oil rig theoretical model nodal equation derivations .....	307
B.1	Internal surface node exchanging heat with the lubricant .....	307
B.2	Internal node exchanging heat by conduction with two neighbouring nodes	308
B.3	External surface node exchanging heat with the ambient air .....	309
B.4	Internal node at the interface of a material change where an insulator has been applied .....	310
Appendix C	Temperature profiles for model predictions .....	311
C.1	100 mm outer diameter uninsulated specimen .....	311
C.2	40 mm outer diameter uninsulated specimen .....	312
C.3	100 mm outer diameter insulated specimen .....	313
C.4	40 mm outer diameter insulated specimen .....	314
C.5	100 mm outer diameter plain aluminium insert .....	315

Appendix D	Flow Chart of Model Structure .....	316
Appendix E	Publications arising from this thesis.....	318

## Nomenclature

### Abbreviations and letters used in mathematical formulae

AH	Auxiliary heater
<i>AFR</i>	Air: fuel ratio
AMEP (bar)	Auxiliary mean effective pressure
Bi	Biot Number
BMEP (bar)	Brake mean effective pressure
BSFC ( $\text{g kW}^{-1} \text{h}^{-1}$ )	Brake specific fuel consumption
<i>c</i> (m)	Bearing clearance
C. I.	Compression ignition
$C_{p\ x}$ ( $\text{J kg}^{-1} \text{K}^{-1}$ )	Specific heat of fluid or material at constant pressure
CO	Carbon monoxide
CO <sub>2</sub>	Carbon dioxide
CoE ( $^{\circ}\text{C}^{-1}$ )	Coefficient of expansion
CFD	Computational fluid dynamics
<i>D</i> (m)	Diameter
DOE	Design of experiments
DSC	Differential scanning calorimetry
<i>dx</i> (m)	Nodal length of oilway
$dx_{short}$ (m)	Discretised length of oilway
EGHR	Exhaust gas heat recovery unit
<i>F</i> (N)	Frictional force within the bearing
<i>F</i>	Radiation heat transfer view factor
<i>f</i>	Friction factor
FMEP (bar)	Friction mean effective pressure

Fo	Fourier Number
FTP	Federal Test Procedure
$g (m s^{-2})$	Acceleration due to gravity (9.81 )
GDTI	Gasoline direct turbo injection
GFRP	Glass fibre reinforced polymer
Gr	Grashoff Number
HC	Hydrocarbon
$h_{contact} (W m^{-2} K^{-1})$	Heat transfer coefficient between the outer surface of the insulating insert and the inner bore of the test block specimen
$h_{oil} (W m^{-2} K^{-1})$	Heat transfer coefficient between the lubricant and the test block specimen
$h_{outer} (W m^{-2} K^{-1})$	Heat transfer coefficient between the outer surface of the test block specimen and ambient
I.C.	Internal combustion
IMEP (bar)	Indicated mean effective pressure
$k_x (W m^{-2} K^{-1})$	Thermal conductivity
LHA	Latent heat accumulator
$L_{ix'} (m)$	Entry length
$m_{ix'} (kg)$	Mass
$\dot{m}_{oil} (kg s^{-1})$	Oil mass flow rate
$m_f (\dot{g} s^{-1})$	Fuel mass flow rate
$N (m s^{-1})$	Relative velocity of the two surfaces
$N (rev s^{-1})$	Revolutions per second
NEDC	New European Drive Cycle
NOx	Nitrous oxides
Nu	Nusselt Number

OEM	Original equipment manufacturer
$P (N m^{-1})$	Applied load per unit width of the bearing
PCM	Phase change material
Pe	Péclet Number
PID	Proportional integral derivative
PM	Particulate matter
PMEP (bar)	Pump mean effective pressure
Pr	Prandtl Number
ppm	Parts per million
$Q_{i,x'} (J)$	Flow of energy between 2 nodes of interest
$\dot{Q}_{i,x'} (W)$	Heat flux between 2 nodes of interest
$R (m^2 K W^{-1})$	Thermal resistance
Re	Reynolds Number
$r_{i,x'} (m)$	Radius of node of interest
$r_s (m^2 K W^{-1})$	Fouling factor
S. I.	Spark ignition
So	Sommerfeld number
$T_y^n (°C)$	Temperature where x denotes the time step and n denotes location
TAN (mg KOH g <sup>-1</sup> )	Total acid number
TBC	Thermal barrier coating
TBN (mg KOH g <sup>-1</sup> )	Total base number
TEG	Thermoelectric generator
$U (m s^{-1})$	Relative bearing speed
$v (m s^{-1})$	Velocity of fluid
VCHP	Variable conductance heat pipe

$V_s$ ( $m^3$ )	Swept volume
$W_b$ ( $W$ )	Brake power
$Z$ ( $^{\circ}C^{-1}$ )	Figure of merit

### Greek symbols

$\alpha$ ( $V K^{-1}$ )	Seebeck coefficient
$\beta$ ( $K^{-1}$ )	Coefficient of volume expansion. Assumed as $T^{-1}$ for gases
$\varepsilon$	Eccentricity ratio
$\varepsilon$	Radiation emissivity value
$\varepsilon$	Overall surface efficiency factor
$\Delta r$ ( $m$ )	Change in radius between 2 nodes of interest
$\Delta T$ ( $^{\circ}C$ )	Temperature differential between 2 nodes of interest
$\delta t$ ( $s$ )	Time step of the model
$\lambda$	$\frac{AFR}{AFR_{stoichmetric}}$
$\mu$ or $Z$ ( $Pa s^{-1}$ )	Dynamic viscosity of fluid. Where subscripts 'b' and 'w' are applied this denotes whether the dynamic viscosity is given at the bulk fluid temperature or the wall temperature
$\nu$ ( $m^2 s^{-1}$ )	Kinematic viscosity of fluid
$\rho_{i,x,i}$ ( $kg m^{-3}$ )	Density
$\rho$ ( $\Omega m^{-1}$ )	Electrical resistivity
$\rho$	Radiation reflectivity value
$\sigma$ ( $W m^{-2} K^{-4}$ )	Stefan-Boltzmann constant

# 1 Introduction

## 1.1 The importance of the internal combustion engine in society

The internal combustion (I.C.) engine remains of paramount importance to both developed and developing economies. Through the burning of fossil fuels (in vehicle applications, this is usually unleaded gasoline or diesel), chemical energy is released from the fuel and converted to kinetic energy. As a by-product of fuel combustion, carbon dioxide ( $\text{CO}_2$ ), water ( $\text{H}_2\text{O}$ ) and nitrous oxides ( $\text{NO}_x$ ) are released to the environment, all of which are greenhouse gases. In addition, during phases of incomplete combustion (typically during warm-up), there is an increased content of additional emissions including carbon monoxide ( $\text{CO}$ ), while diesel engines also produce a high content of particulate matter (PM). PM is highly detrimental to air quality, particularly in densely populated areas, and it is desirable to reduce these emissions as much as possible for the benefit of public health. In light of a range of environmental and health concerns, international and national legislating bodies are keen to minimise the production of  $\text{CO}_2$ ,  $\text{H}_2\text{O}$ ,  $\text{CO}$  and  $\text{NO}_x$ . A significant challenge for vehicle OEMs (original equipment manufacturers) is the reduced efficiency of I.C. engines during the warm-up phase (discussed in Section 1.3) which results in increased fuel consumption and an associated increase in emissions.

The desire by legislating bodies to minimise air pollutants and greenhouse gases is counteracted by the increasing number of vehicles on the roads with private car usage continuing to increase. Between 1994 and 2012, the number of private cars on the United Kingdom's roads rose by 35% from 21.2 million vehicles to 38.7 million vehicles [1]. Vehicle manufacturers have responded to the desire to reduce greenhouse emissions by developing commercially available electric vehicles (e.g. Renault Zoe, Nissan Leaf and Vauxhall Ampera) while there are attempts to develop commercially available hydrogen-fuelled cars [2]; in addition, hybrid vehicles such as the Toyota Prius have gained popularity. However, to date the I.C. engine has remained the primary means of road vehicle propulsion. As an energy source, fossil fuels (in the form of either diesel or unleaded gasoline) provide an unrivalled high density energy source. While the high energy density of fossil fuels is a major benefit in vehicle propulsion, their primary benefit is the flexibility they provide and this is a major obstacle in moving away from fossil fuel usage in vehicles. With the current fuel filling station infrastructure, there are few constraints placed on vehicle range while comparatively, electric vehicles have a limited range that is highly dependent on speed, and vehicle charging locations are limited. Furthermore, the charging process can be prolonged and this places heavy constraints on the use of the vehicle.

While hydrogen fuel cell technology is appealing, there is still the issue of facilitating a safe and convenient method of refuelling.

With alternatives to the I.C. engine still presenting significant drawbacks to the consumer, there is therefore a need to further develop the I.C. engine to both improve fuel efficiency and reduce emissions to minimise the impact on the environment.

## 1.2 Legislation and emissions performance

The New European Drive Cycle (NEDC) is an important performance metric for internal combustion engine efficiency. It is a 1180 second long drive cycle against which all new engines are tested, and aims to simulate a range of driving scenarios from motorway cruising to city centre idling as shown by the speed trace in Figure 1.1 [3]. In the European Union, fuel consumption and emission figures for new cars are quantified from the NEDC and thus any methods to improve cold-start efficiency must be effective in reducing fuel consumption within the timeframe of an NEDC test.

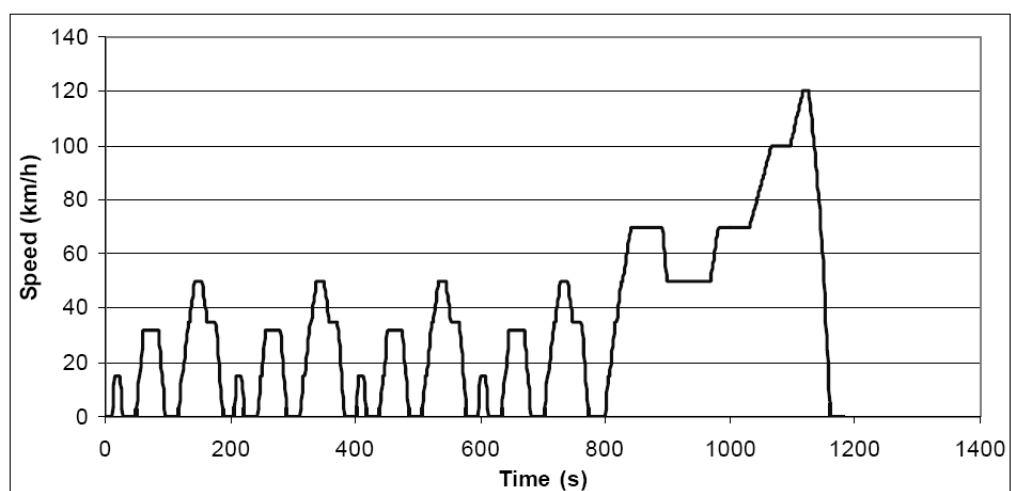


Figure 1.1: Speed-time trace for the NEDC. © TRL (Transport Research Laboratory) [3]

As well as concerns with efficiency, the need to improve cold-start performance is also highly influenced by the need to improve emission quality. As pressure increases to minimise the burden that I.C. engines place on the environment, legislation continues to tighten. Examples include the London Emission Zone that imposes financial penalties on commercial vehicles that fail to meet Transport for London particulate matter legislation.

Furthermore, as of September 2014, all vehicle OEMs will be required to ensure that all class M vehicles (passenger-carrying with less than 8 seats) [4] meet the Euro 6 Emission standards. These emission limits are detailed in Table 1.1 for both diesel compression ignition engines (C.I.) and gasoline spark ignition (S.I.) engines.

**Table 1.1: Upper limits of emission levels allowed under the Euro 6 emission regulations for spark ignition (S.I.) and compression ignition (C.I.) engines [5]**

Carbon monoxide ( $\text{mg km}^{-1}$ )		NOx ( $\text{mg km}^{-1}$ )		Particulate matter ( $\text{mg km}^{-1}$ )	
S.I.	C.I.	S.I.	C.I.	S.I.	C.I.
1000	500	60	80	5.0	5.0

Additional targets have been set in relation to CO<sub>2</sub> emissions. European OEMs are required, under EU law by 1<sup>st</sup> January 2015 to ensure that all models of car manufactured by them produce less than 130 g km<sup>-1</sup> of CO<sub>2</sub> emissions [6]. Shown in Figure 1.2 [1] is a plot showing how the tightened legislation has forced the CO<sub>2</sub> emissions from cars to reduce in the UK. At the end of 2012 the average emissions from all cars was 160 g km<sup>-1</sup> while newly registered vehicles had an average CO<sub>2</sub> emission figure of 133 g km<sup>-1</sup>. Thus it can be seen there is still further work required to meet the mandatory legislation for 2015.

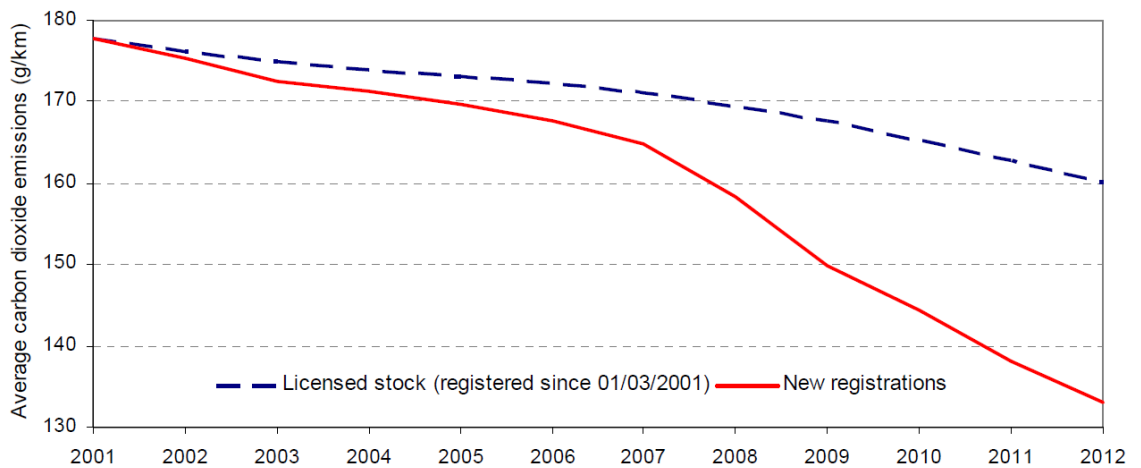


**Figure 1.2: Average CO<sub>2</sub> emissions from both newly registered and existing vehicles for UK registered vehicles against year [1]**

### 1.2.1 Alternative measures of engine performance and their comparative nature

The NEDC is a critical drive cycle for vehicle OEMs, particularly in the European Market, as it is used to quantify whether vehicles have met government targets and is therefore used to classify vehicles for taxation purposes. However, it should be noted that there are other vehicle drive cycles that are commonly used in automotive research and performance quantification and these include:

- The Artemis test profile, commonly used in Europe to represent more realistic driving behaviour relative to the NEDC [3].
- The Federal Test Procedure (FTP) range of tests that are used in the North American market [3].

It must be borne in mind that, while there are differences in these drive cycles, they are each of limited duration and thus any inefficiencies associated with a cold-start

will have a significant effect on the performance metrics. Thus, regardless of the drive cycle used it should be possible for any improvements to be highlighted and quantified within the duration of such tests. However, the applied nature of automotive research does represent a significant challenge in being able to critically appraise and robustly compare different approaches to solving vehicle efficiency. The literature review in Chapter 2 seeks to explore and explain how I.C. engine cold-start inefficiency has been attempted to be improved in the past and the improvements, or lack thereof, seen as a result. The difficulty in assessing such work is assessing the limitations of the repeatability of work and the associated confidence in the results but also attempting to compare different technology strategies using both different engine types and different performance metrics.

Thus far, one has only focused on quantifying the quantity of exhaust pollutants produced by I.C. engines. While this is the focus of government targets the vehicle OEMs have a variety of potential methods of working to meet such targets and hence use different performance metrics to appraise the technologies trialled. It is therefore worth briefly discussing the physical meaning of the performance metrics that will be discussed in Chapter 2.

Of primary interest to the consumer is the overall fuel consumption of the vehicle. This is typically quantified in miles per gallon (mpg) or in litres  $(100 \text{ km})^{-1}$ . While this is arguably the easiest performance metric to understand, its value as a performance barometer of technology is weak, particularly if used as part of a whole vehicle study. Aside from any technology aimed at improving fuel economy, the fuel consumption is also dependent on the nature of the driving carried out (hence the need to use a consistent drive cycle) and also the specific vehicle that it is installed in. Vehicle mass and the aerodynamic performance of the vehicle will therefore be contributory factors in determining the fuel consumption.

In order to isolate the performance of the I.C. engine from that of the vehicle, there are specific powertrain performance metrics that can be used. This includes the use of mean effective pressures to characterise an engine. The definition of a mean effective pressure is the work done per cycle per unit displaced and hence mean effective pressures are measured in Pa or bar. Consequently, mean effective pressures normalise against engines of different displacements (i.e. engine size) and also engine speed and therefore offer a more robust comparison between engines of different architecture. It is important to highlight however that in characterising different engines, there are different types of mean effective pressure and these are listed below:

- Indicated mean effective pressure (IMEP): Gross indicated mean effective pressure from the combustion process

- Brake mean effective pressure (BMEP): Mean effective pressure that is used to transfer work to the output shaft.
- Friction mean effective pressure (FMEP): Mean effective pressure that is used to overcome friction within the engine.
- Auxiliary mean effective pressure (AMEP): Mean effective pressure that is used to drive auxiliary components including the alternator and air conditioning compressor.
- Pump mean effective pressure (PMEP): mean effective pressure used to draw the inlet charge of air into the engine and waste exhaust gases from the engine.

Thus, the BMEP, as a function of engine speed and swept volume is given by:

$$BMEP = \frac{2W_b}{V_s N}$$

Where  $BMEP$  = Brake mean effective pressure (Pa)  
 $W_b$  = Brake power (W)  
 $V_s$  = Swept volume (m<sup>3</sup>)  
 $N$  = Engine speed (revolutions s<sup>-1</sup>)

**Equation 1.1: Definition of BMEP**

The form of Equation 1.1 can be used for any of the respective mean effective pressures providing that the respective work is replaced (e.g. friction work is used to calculate the FMEP). It follows that the IMEP is the sum of all the constituent mean effective pressures, as defined in Equation 1.2. It is desirable for the BMEP to be as high as possible and for the FMEP, AMEP and PMEPP to be as low as possible and it is during a cold-start that the FMEP rises owing to sub optimal lubrication (discussed in Section 1.5.1).

$$IMEP = BMEP + FMEP + AMEP + PMEPP$$

**Equation 1.2: IMEP defined as the sum of all contributory MEPPs**

The final commonly used performance metric is brake specific fuel consumption (BSFC). This is a measure of the fuel used for a given brake power output and is therefore usually quoted in units of g (kW hour)<sup>-1</sup>. This is advantageous over the more commercially popular values of fuel consumption in miles per gallon, as the BSFC gives comparative values relative to the power output and hence prevents the perceived fuel economy increasing but the work output also reducing.

$$BSFC = \frac{3600 \dot{m}_f}{W_b}$$

Where  $BSFC$  = Brake specific fuel consumption ( $\text{g (kW hr)}^{-1}$ )  
 $\dot{m}_f$  = Fuel mass flow rate ( $\text{g s}^{-1}$ )  
 $W_b$  = Brake power (W)

Having established the major performance metrics for I.C. engine efficiency, there is also the need to discuss how such parameters are determined. Typically, when testing full engine builds, the engine is either tested on a laboratory dynamometer, where an electric motor is connected to the output shaft of the engine to provide the resistance load, or the engine is tested while installed in a vehicle. The time and cost of carrying out such tests therefore limits the number of repeat experiments that are carried out and it is common place for the published work in the field to not document the level of repeatability of the results presented, (although discussion of the limited repeatability data available is discussed in Section 2.4.4). When carrying out approval tests for government regulations, there are known issues with the repeatability of engine performance between two assemblies of the same nominal build specification. Consequently there are likely to be variations of up to 2-3 % in performance metrics even if the exact same set of components are disassembled and re-assembled with similar differences between two engines of the same nominal specification.

Thus, in discussing and appraising prior work in the field it is accepted that the absolute values of the performance metric used by the previous authors in the field is not comparable between different studies and this is a major limitation in the current state of the art in the field. It is therefore desirable, in carrying out further work to utilise methodologies that can reduce the uncertainty of the findings relative to prior work in the field.

### **1.3 The need to improve I.C. engine cold-start performance**

The combustion efficiency of an I.C. engine is a measure of how much of the chemical energy contained in a fuel is converted to other forms of energy including thermal and kinetic energy. It is largely accepted that the combustion efficiency of a modern I.C. engine is well optimised, with approximately 98% of the energy contained within the fuel being released on combustion in diesel engines and 95-98% in gasoline engines [7]. However, the useful energy leaving the engine (termed 'brake work') is typically only 40% of the fuel energy [7, 8]. The energy that is used to provide drive to the wheels is less than the brake work, since a fraction of this energy needs to be used to overcome engine friction. This inability to convert all of the chemical energy into useful work output is termed the 'gross indicated thermal efficiency'. The overall efficiency of the engine is termed the 'fuel conversion efficiency' and is defined in Equation 1.3. The fuel conversion efficiency of a modern

I.C. engine is typically 40% (limited by the gross indicated thermal efficiency rather than the combustion efficiency) and this, together with emission quality, has benefitted from the development of common rail fuel injection, improved lubricants, more complex engine control strategies and the use of catalytic converters on most vehicles.

*Fuel conversion efficiency*

$$= \text{Combustion efficiency} \times \text{Gross indicated thermal efficiency}$$

**Equation 1.3: Definition of engine fuel conversion efficiency**

However, while the fuel conversion efficiency and subsequent fuel consumption at steady state operating temperatures have improved, cold-start performance has remained problematic. Andrews et al. [9] demonstrated that engine fuel consumption has a linear dependence on ambient temperature and this is shown in Figure 1.3 [9] for a Euro 1 compliant S.I. engine. Over an urban drive cycle, the fuel consumption was shown to increase by 18% when the ambient temperature decreased from 31 °C to -2 °C. The work of Will and Boretti [8] highlighted a similar trend for three different variants of engine (a 1200 cc 3 cylinder S.I. engine, a 1400 cc 4 cylinder S.I. engine and an 1800 cc S.I. engine) as did Goettler et al. [10] with a 3.3 litre S.I. engine. Such observations are of critical importance to vehicle manufacturers as the NEDC test is required to be conducted from a soak temperature of between 20 °C and 30 °C [11]. Similarly, Kunze et al. [12] presented data showing that the fuel consumption of a gasoline engine reduced by an average of 10% when the start temperature was increased from 25 °C to 90 °C when the engine was run over the NEDC. Will and Boretti [8, 13] estimated that frictional losses in the engine during the early stages of warm-up (when the engine is in the region of 20 °C) can be up to 2.5 times higher than those observed when the lubricant is fully warm. If this temperature is reduced to a cold-start scenario of 0 °C, then Samhaber et al. [14] predicted increases in fuel consumption of up to 13.5 % for an engine starting at 0 °C relative to one that is fully warm.

The effect of reduced operating temperatures on I.C. engine performance has been seen to be an increase in fuel consumption. As a result of burning additional fuel, vehicle emissions consequently rise (2668 g of CO<sub>2</sub> is released per litre of diesel burnt [15]) and hence there is a risk that the vehicle may fail key emission tests. It is therefore critical to make attempts to improve fuel consumption during the warm-up phase particularly as the NEDC is required to be conducted from a soak temperature of between 20 °C and 30 °C.

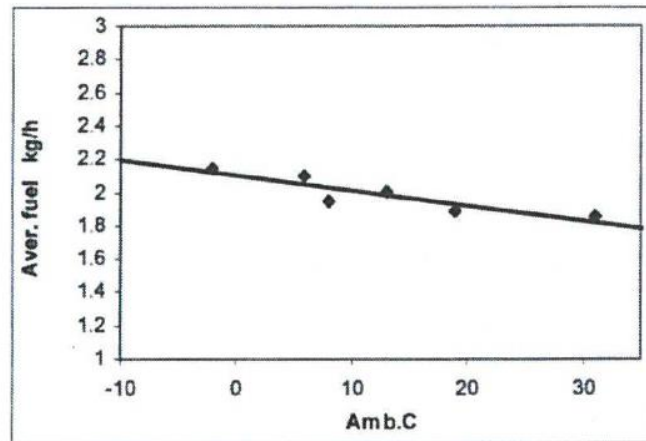


Figure 1.3: Effect of ambient operating temperature on fuel consumption over an urban drive cycle for a Euro 1 compliant S.I. engine. Reprinted with permission from SAE paper 2007-01-2067 © 2007 SAE International and SAE of Japan [9]

While the poor cold-start performance of I.C. engines is problematic during mandated tests such as the NEDC there are also strong consumer trends of making multiple short trips and thus using the engine repeatedly when cold. Such trends further heighten the need to investigate methods of improving the cold-start performance of I.C. engines. Goettler et al. [10] estimated that up to 80% of trips made in the United States of America are less than 15 km in length while Jarrier et al. [16] claimed the mean European car journey is approximately 10 km in duration. Andrews et al. [17] reported the findings of André who found that, from a survey of 35 vehicles, 52 % of the vehicle journeys made were less than 3 km in duration. André [18] later carried out further work investigating the driving habits and trends of vehicles used in real conditions. He found (based on a sample of 55 vehicles and 1840 hours of vehicle running) that approximately one third of the trips made did not enable the engine coolant to exceed 70 °C or the engine lubricant to exceed 60 °C.

#### 1.4 The thermal balance of the engine during warm-up

It has been seen that despite the improvement in emissions and fuel consumption of engines at steady state, the cold-start performance of vehicle engines remains problematic and there is a need to address such an issue to meet legislation.

During the engine warm-up phase, there are effectively three thermal masses interacting with each other, namely the main engine block (including the crankshaft), the lubricant and coolant. Of the three, the coolant is the fastest to respond owing to its temperature being closely coupled to that of the combustion gases [7, 11, 19]. In contrast, the lubricant temperature and block temperature are generally much slower to respond owing to the block having a large thermal inertia and the lubricant being much less closely coupled to the combustion process [12, 20, 21]. Figure 1.4 shows a cross section through a typical I.C. engine cylinder and shows the relative

physical locations of the main engine oil gallery, the coolant jacket and the block structure relative to the cylinder bore. It can be seen how the coolant jacket surrounds the cylinder bores for almost the entire length of the bore and results in the close coupling of the coolant temperatures to the combustion gas temperatures. Conversely, the main engine oil gallery is situated at the bottom of the piston bore and only extends for a fraction of the bore length. The engine oil gallery can also be seen to be in an area of a higher cast thickness and is in close proximity to the rest of the lower block structure which therefore slows down the lubricant heating rate relative to the coolant. It is also worth noting that in the particular example shown, the coolant jacket is abnormally long and it is not unusual for the coolant jacket to only extend for three quarters of the bore length. Such a characteristic would therefore result in a reduction in heat transfer between the coolant jacket and the main engine oil gallery.

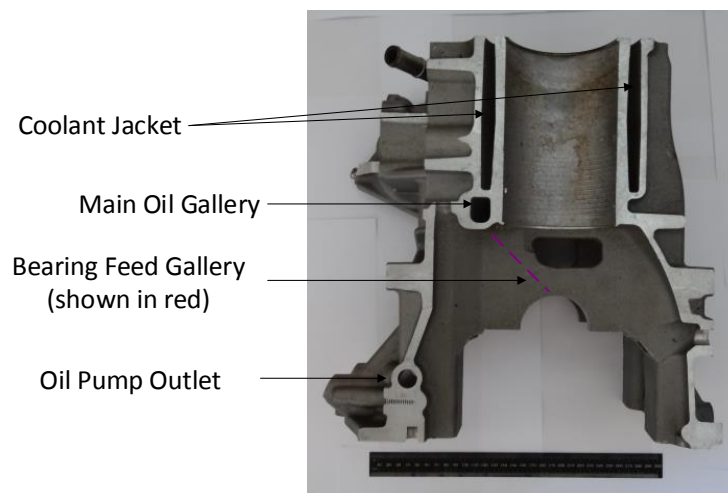


**Figure 1.4: Section through a 2.0 litre S.I. engine showing the relative locations of the main engine oil gallery and coolant jacket to the cylinder bore (the cylinder liner has been removed during the sectioning of the block)**

Figure 1.5 [20] presents data which describe the energy balance of an engine during the warm-up phase. It can be seen that while at steady state typical efficiencies quoted are 40%, during warm-up the fraction of energy available as effective work is only 10%. This is consistent with claims made by Jarrier et al. [16] and Will and Boretti [8]. The left-hand chart of Figure 1.5 provides an energy thermal balance at the combustion chamber and the right-hand chart provides a breakdown of the 53% of energy that is transferred as heat to the cylinder walls; this is a large fraction as a result of the high temperature differential between the combustion gases and cylinder wall generating a high heat flux. Such energy is therefore not available to be used to power the driven wheels. The energy transferred to the cylinder walls causes the coolant, the metallic structure (including the block and crankshaft) and the lubricant to warm up. However, what is indicated is that 52% of this heat energy is not found to warm up any of the ancillary circuits (such as the lubricant or coolant),

but is instead lost directly to the environment (termed 'unused heat'). It should also be noted that only 4% of the heat from combustion will be found to actually warm up the lubricant. Similar trends were observed in the experimental work of Jarrier et al. [16] when using a 1.9 litre diesel engine. Their work, presented in Figure 1.6 [16], shows just over 10 % of the energy being used for brake work with only a small contribution (< 5%) of the energy being input to the lubricant. The work also highlights again how much of the energy is not utilised, with both the ambient air fraction and cabin heating fraction representing heat that is lost from the engine system. Similarly, the theoretical modelling work of Samhaber et al. [14] detailed the energy balance of the heat sink of a diesel engine (offering comparative data to that data presented in the right hand part of Figure 1.5). In this work, it was found that 60% of the energy was used to heat the structural parts, with approximately 20% being absorbed by the coolant and 10% by the lubricant. Thus, the lubricant and coolant once again receive only a small proportion of the energy available. The proportion retained in the metal structure was higher in the work reported by Samhaber et al. [14] and a possible reason may be that Samhaber's simulation work was based on the NEDC with varying load and speed whereas Trapy and Damiral [20] and Jarrier et al. [16] conducted experimental work at a constant speed and load. Also, the work of Trapy and Damiral was conducted on an S.I. engine whereas Samhaber et al. and Jarrier et al. simulated a diesel engine. Thus, the thermal mass of the diesel engine will have undoubtedly been higher to incorporate the higher structural strength required to cope with the higher compression ratios and may account for the smaller fraction of energy held in the metal reported by Trapy and Damiral.

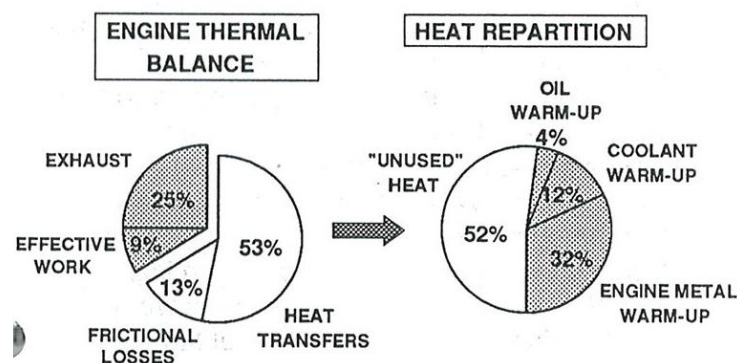
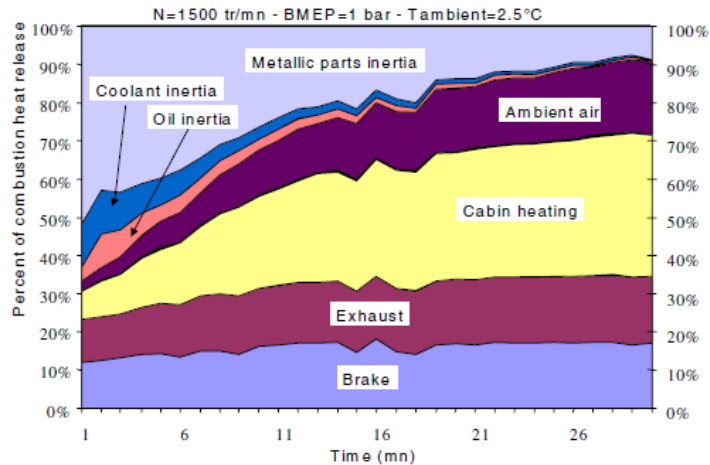


Figure 1.5: Energy thermal balance diagram during warm-up of a 4 cylinder 1.7 litre S.I. engine. Reprinted with permission from SAE paper 902089 ©1990 SAE International [20]



**Figure 1.6: Mean heat balance against time during engine warm-up for a 1.9 litre diesel engine operating at 1500 rpm and 1 bar BMEP (brake mean effective pressure) from a soak temperature of 2.5 °C. Reprinted with permission from SAE paper 2000-01-0299 ©2000 SAE International [16]**

It can therefore be seen that during the warm-up phase of the engine, there is a large proportion of unutilised energy in the engine and that this results in only a small fraction of the energy released during combustion being absorbed by the lubricant and coolant. This is a significant factor in the increased fuel consumption and emission levels during cold-start and the effects are explained in Section 1.5.

## **1.5 The significance of engine lubricant and engine coolant temperatures during warm-up**

Section 1.3 has shown how the internal combustion engine is less efficient when operating at lower temperatures with only a very small fraction (~9%) of the energy contained in the fuel being converted to brake work during warm-up. Meanwhile, Section 1.4 has shown how, of the energy not used as brake work, only a small proportion is used to heat the coolant or lubricant. The slow heating rate of the lubricant and coolant is one factor resulting in poor engine efficiency. However, it is important to understand the role of fluid and component temperatures on thermal efficiency and also the time frames involved for the systems to reach their optimal operating temperature.

Figure 1.7 [20] shows the temperature profile for both the lubricant and coolant for a 1.7 litre S.I. engine when operating at 10 N m load and 2000 rpm. It can be seen that within 7 minutes, the coolant temperature has reached its peak value, which has resulted in the thermostat opening and the system actively dissipating heat to the environment via the radiator. In direct contrast, it can be seen that the lubricant temperature is still not at steady state 15 minutes into the warm-up cycle and it would be desirable to be able to utilise the thermal energy being dissipated to ambient to accelerate the lubricant heating rate. The trend of the lubricant temperature lagging the coolant temperature is verified in the work of Li et al. [21],

Kunze et al. [12], Andrews et al. [9] and Jarrier et al. [16]. The work of Jarrier et al. focused on a diesel engine, indicating that such a problem is not confined to one type of engine. Further work by Andrews et al. [9] compared engine warm-up rates of different designs of engine from the past 20 years and found that over this period of time, the rate of lubricant warm-up had stayed constant with values of  $0.1 \text{ }^\circ\text{C s}^{-1}$  being reported. Comparatively, coolant warm-up rates have typically been in the region of  $0.25 - 0.4 \text{ }^\circ\text{C s}^{-1}$ . This lag in the rate of increase of lubricant temperature is highly significant in the observed inefficiencies during warm-up with Andrews et al. [9] arguing that an increase in lubricant warm-up rate is critical to improving cold-start efficiency.

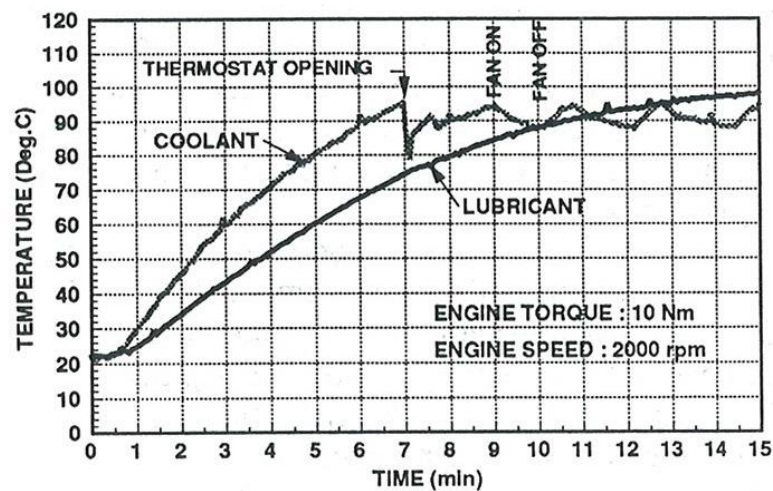


Figure 1.7: Temperature plot against time of coolant and lubricant for a 1.7 litre S.I. engine. Reprinted with permission from SAE paper 902089 ©1990 SAE International [20]

The warm-up process of an I.C. engine is complex with multiple sub-systems and components requiring heating. The coolant system, at steady state, is required to keep components within acceptable temperature limits and consequently the coolant and cylinder liner temperatures are closely coupled [7, 11, 19]. Thus, in a conventionally designed I.C. engine, a high coolant temperature indicates a high cylinder liner temperature. Higher liner temperatures are desirable since they promote the full and effective mixing of the inlet charge and facilitate complete combustion [11, 14, 19, 22]. Consequently, a higher liner temperature facilitates greater energy release from the fuel, improving both fuel consumption [23] and emission quality. Also, the liner temperature has been shown to have a strong effect on the piston- liner friction work, with increased liner temperatures reducing the friction at this interface [19]. Thus, during the warm-up phase, heating of the coolant is desirable as it prevents quenching of the cylinder liners and therefore reduces friction and improves combustion quality. Andrews et al. [9] were able to isolate the effect that low temperature lubricant viscosity has on fuel consumption from the effect of low coolant temperatures and subsequent poor combustion. Such work is discussed in Section 1.5.1.

### 1.5.1 The sensitivity of engine lubricant to temperature

While high cylinder wall temperatures are advantageous to the efficiency of I.C. engines through the promotion of more effective combustion, the more critical observation from Figure 1.7 [20] is that the lower rate of lubricant warm-up when compared to that of the coolant. The primary purpose of the lubricant is to reduce friction in the engine, and if frictional losses rise (due to the lubricant operating at a sub-optimal temperature), an increase in fuel consumption and emissions will result. The systems associated with significant frictional losses in the engine are numerous and include the valve train, crankshaft bearings and piston rings [19, 24-26] with Zammit et al. [27] and Comfort [28] estimating that the main crankshaft bearings account for up to a third of the total frictional losses during warm-up (although the distribution of friction in the engine varies between engines and with operating conditions). A typical breakdown of engine friction was reported by Comfort for a diesel engine and is shown in Figure 1.8 [28].

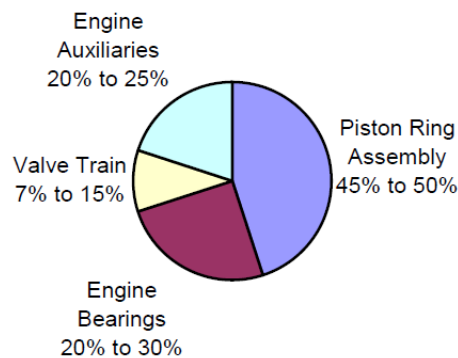


Figure 1.8: Typical breakdown of engine friction for a diesel engine [28]

Frictional losses depend upon a complex relationship between the interacting surfaces together with the lubricant present and is best understood using the Stribeck Curve shown in Figure 1.9 [29]. In this plot, the coefficient of friction,  $\mu$ , is plotted against the dimensionless Sommerfeld Number (defined in Equation 1.4).

$$So = \frac{ZN}{P}$$

Where  $Z$  = Lubricant dynamic viscosity ( $\text{N s m}^{-2}$ )

$N$  = Relative velocity of the two surfaces ( $\text{m s}^{-1}$ )

$P$  = Applied load per unit width of the bearing ( $\text{N m}^{-1}$ )

#### Equation 1.4: Definition of Sommerfeld Number

The vertical lines on the graph separate the three broad lubrication regimes namely, boundary, mixed and hydrodynamic from left to right. The optimal (lowest) frictional

losses are found at the transition from mixed to hydrodynamic lubrication and from this point, either an increase or decrease in the Sommerfeld number results in a higher coefficient of friction and subsequent increases in fuel consumption. In the context of the internal combustion engine, both the load and bearing rotational speed (both of which are variables included in the Sommerfeld number), are largely fixed by drive requirements of the vehicle and therefore minimising friction within the engine is governed by ensuring that an appropriate value of lubricant viscosity is maintained. At low temperatures, there is a need to ensure the viscosity is not so high as to increase the friction when in the hydrodynamic regime while there is a need to ensure that at high temperatures, the lubricant viscosity does not become so low that the lubricant film breaks down and boundary lubrication dominates.

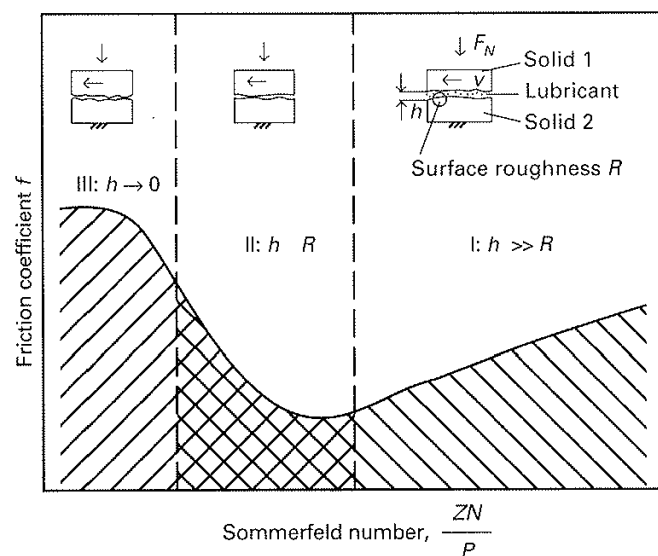


**Figure 1.9: The Stribeck Curve where  $Z$ = lubricant dynamic viscosity,  $N$  is the rotational speed of the bearing and  $P$  is the bearing load [29]**

The challenge of managing engine friction and accounting for the variation of lubricant viscosity is well explained by classical lubrication theory. However, the role of lubricant viscosity in managing engine friction was originally not recognised. Early research focused more on the issue of being unable to start an engine, such was the level of friction within early engines.

Vick [30] highlighted that early researchers argued that a minimum cranking speed existed, below which an engine would not fire, with such behaviour being attributed to there being a minimum cranking speed required to achieve an acceptable air: fuel ratio for combustion. It was the work of Selby in 1964 [31] that linked the effect of high lubricant viscosity to engine starting ability. Selby's theory was based on work by Becker who measured the power required to crank an engine at various engine crankshaft speeds with differing grades of lubricant, with his results shown in Figure 1.10 [30]. Also shown in Figure 1.10 is the output power from a starter motor at different speeds. If the power required to crank the engine at a given speed with a

particular lubricant is below that of the starter motor output, then the engine will fire (conversely, it will not fire if the power requirement is above that of the starter motor output). It should be noted that the work discussed here was carried out with monograde lubricants and therefore, the effect of temperature on the lubricant properties will be more pronounced than that which would be expected for a system operating with a modern multigrade lubricant. However Selby's work [31] (shown in Figure 1.11) was carried out with varying specifications of multi-grade lubricant. The open data points indicate a successful fire-up while the filled data points indicate an unsuccessful fire-up. It can be seen that no successful fire-up was achieved once the lubricant viscosity exceeded 3000 cp. Further tests, reported in the same publication, varied the cranking speed independently of lubricant viscosity and achieved successful fire-ups at cranking speeds as low as 6 rpm but with a lubricant viscosity of 470 cP thus proving beyond doubt that lubricant viscosity was the dominant factor in engine starting ability and not the cranking speed.

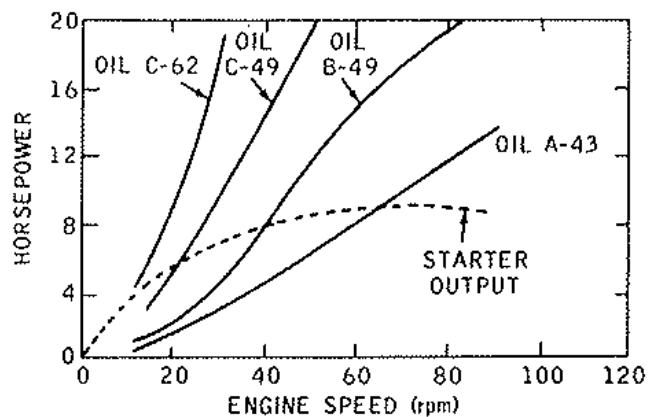


Figure 1.10: Starting power requirements to crank an engine at different speeds when utilising different grades of monograde engine lubricant at 10 °F (-10 °C) compared to the starter motor output. Reprinted with permission from SAE paper 650446 [30]

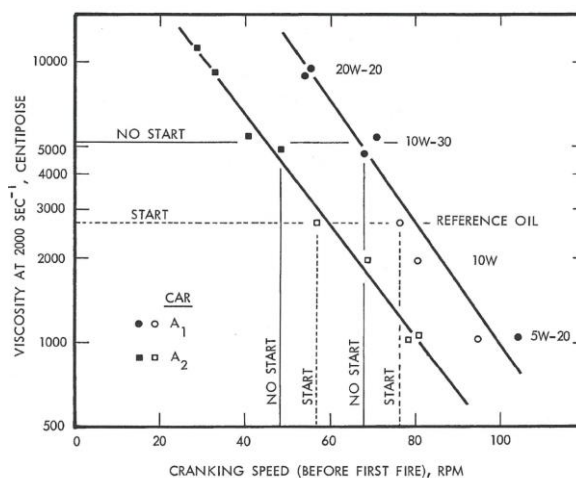


Figure 1.11: Engine lubricant viscosity plotted against engine cranking speed showing the effect of viscosity on achieving a successful engine fire up for two V8 gasoline engines. Reprinted with permission from SAE paper 640427 [31]

The sensitivity of frictional losses to lubricant viscosity is of paramount importance in understanding why a long lubricant warm-up time is undesirable in controlling engine cold-start inefficiencies. There has been much work carried out over the past forty years which has attempted to stabilise the properties of lubricants (particularly viscosity) over the temperature range of operation, with multigrade synthetic oils having become highly complex mixtures with viscosity stabilisers added [26]. The viscosity modifiers are typically polymer molecules and work by the polymer being more soluble in the lubricant at high temperatures than at low temperatures. They therefore interfere with lubricant flow at high temperatures and reduce the temperature thinning effect [32].

However, although desirable, lubricants where the viscosity is independent of temperature have not yet been developed, with typical viscosity-temperature profiles for a range of SAE monograde and multigrade lubricants being shown in Figure 1.12 [33]. The high sensitivity of viscosity to temperature can be observed, as can the benefit of the multigrade lubricants relative to monograde lubricants. It can be seen that the dynamic viscosity of multigrade lubricants is still highly sensitive to temperature, thus highlighting the limitations of using lubricant chemistry to improve cold-start inefficiency. The variation of dynamic viscosity with temperature is typically characterised by a Vogel curve and is described by Equation 1.5 [34, 35]. The values of the constants vary between different lubricants but as an example of typical values, the engine lubricant discussed in Chapter 3 had a value of  $0.0568 \text{ N s m}^{-2}$  for  $k_v$  while  $\theta_1$  and  $\theta_2$  were assigned values of  $1171.2 \text{ }^\circ\text{C}$  and  $135 \text{ }^\circ\text{C}$  respectively.

$$\mu = k_v \exp\left(\frac{\theta_1}{T + \theta_2}\right)$$

Where:

$\mu$  = Lubricant dynamic viscosity ( $\text{N s m}^{-2}$ )

$k_v$  = Constant with the same units as those used for dynamic viscosity

$T$  = Temperature ( $^\circ\text{C}$ )

$\theta_1$  and  $\theta_2$  = Constants with the same units as those used for temperature

**Equation 1.5: Vogel equation to model the variation in lubricant dynamic viscosity with temperature [34, 35]**

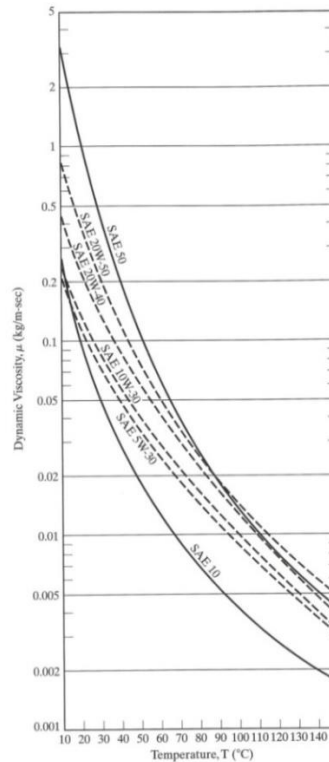


**Figure 1.12: Change in dynamic viscosity with temperature for SAE monograde and multigrade engine lubricants. Multigrade lubricants are shown in dashed lines whereas monograde lubricants are shown with solid lines [33]**

Burke et al. [26] present a similar limitation in the ability of multigrade lubricants to control lubricant viscosity although they base the findings on the kinematic viscosity ( $\nu$ ), rather than the dynamic viscosity ( $\mu$ ). The, kinematic viscosity, defined in Equation 1.6, is simply the dynamic viscosity divided by the density. Consequently, the kinematic viscosity is less sensitive to temperature owing to the density also reducing with temperature and offsetting the reduction in dynamic viscosity.

$$\nu = \frac{\mu}{\rho}$$

**Equation 1.6: Kinematic viscosity as a function of dynamic viscosity**

The effect of lubricant viscosity on engine friction can be observed by numerous performance metrics. The increase in rubbing friction (observed at the bearings and between the pistons and cylinder liners) results in an increase in the friction mean effective pressure (FMEP). In addition, the increased pumping work required to circulate the more viscous lubricant around the engine also results in an increase in auxiliary mean effective pressure (AMEP) as a result of the extra work required to drive the oil pump. The combined effect of increased friction and pumping work results in an increase in fuel consumption as the lubricant temperature is reduced.

Shayler et al. [36] characterised the effect of lubricant viscosity and its variation with temperature by measuring the FMEP of a 2.4 litre direct injection diesel engine filled

with different grades of engine lubricant. Some outcomes of the work, shown in Figure 1.13 [26, 36], indicate a power law increase in FMEP with lubricant viscosity; the dependence of lubricant viscosity with temperature is shown in Figure 1.13b. It can be seen that owing to the effect of lubricant viscosity, the engine FMEP can reach values of up to 8 bar which represents a fourfold increase relative to typical FMEP values for a fully warm engine (typically between 1.5 bar and 2 bar [7]). Such an effect is reflected in Equation 1.7 [37] which enables the FMEP at a given lubricant viscosity to be characterised. The value of  $n$  is typically in the region of 0.19 -0.24 for gasoline engines and 0.25 -0.32 for diesel engines [37]. The power law relationship between lubricant viscosity and engine FMEP enables the effect of sub optimal lubricant viscosity to be appraised in isolation of the benefits in efficiency served by raising the temperature of other thermal masses in the engine (e.g. raising the temperature of the liner walls). The work presented in Figure 1.13 also confirms that the hydrodynamic lubrication regime is dominant in the engine rather than mixed or boundary lubrication. If one refers back to the Stribeck Curve in Figure 1.9, an increase in the coefficient of friction would result in an increase in engine FMEP. When studying Figure 1.9, it is only in the hydrodynamic region where the coefficient of friction rises with increasing Sommerfeld Number (which represents an increase in dynamic viscosity). Comparatively, the coefficient of friction reduces with increasing Sommerfeld Number (and dynamic viscosity) in the mixed and boundary regimes. Thus, the reduction in engine FMEP with decreasing lubricant dynamic viscosity therefore confirms that the hydrodynamic lubrication regime dominates throughout the engine.

$$FMEP = FMEP_{fully\ warm} \left( \frac{\mu}{\mu_{fully\ warm}} \right)^n$$

Equation 1.7: Variation of engine FMEP with lubricant dynamic viscosity [37]

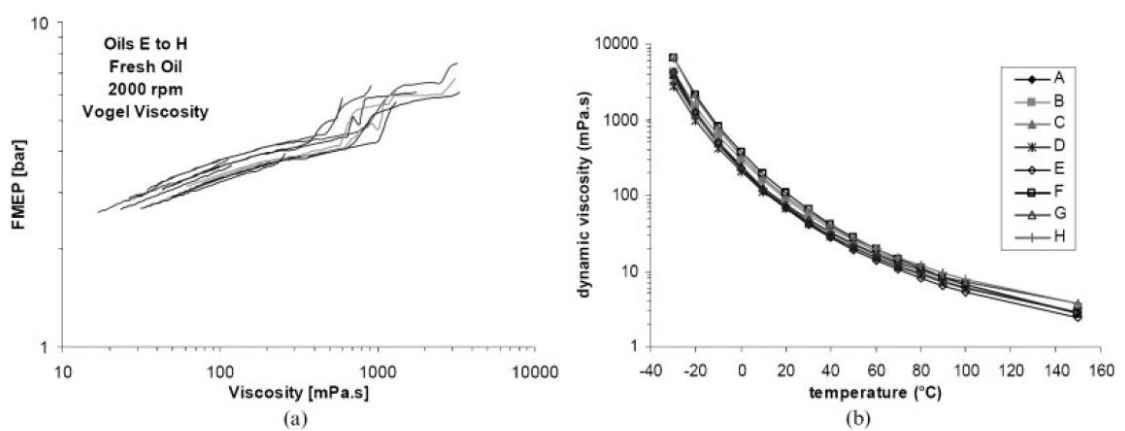


Figure 1.13: Measured engine FMEP against lubricant dynamic viscosity and lubricant dynamic viscosity against temperature for a 2.4 litre direct injection diesel engine running at 2000 rpm. Reprinted with permission from SAE paper 2007-01-1984 ©2007 SAE International and SAE of Japan [26, 36]

Andrews et al. [9] carried out investigative work on both a Ford Valencia and a Ford CVH engine (both S.I.) where the coolant was preheated to 90 °C but the lubricant was allowed to heat up by conventional means, again enabling the effect of high lubricant viscosity to be observed in isolation of the effects of low coolant and cylinder wall temperatures. The results showed that in fixed load tests with 6.6 kW of brake power, fuel consumption was 25% higher as a result of the increased lubricant viscosity at the start of the cycle as compared to when fully warm and an excess in fuel consumption relative to a fully warm situation was observed for over ten minutes in this work.

It is not currently possible to find a lubricant that offers optimal lubrication across the complete lubricant temperature range. It has been shown that the effect of temperature on lubricant viscosity is a key factor in the increase in fuel consumption during cold starts. Shayler et al. [36] have demonstrated how the lubricant viscosity increases by 900% when the temperature is reduced from 90 °C (a typical operating temperature for engine lubricant) to 20 °C. They found that such an increase in viscosity saw the FMEP increase by approximately 60% from 2.5 bar to 4 bar. Such increases in friction have a dramatic effect on fuel consumption; the work of Andrews et al. [9] directly demonstrated that fuel consumption increased by 25% when the lubricant temperature was 20 °C instead of 90 °C. Both the work of Shayler et al. [36] and Andrews et al. [9] attribute the increases in FMEP and fuel consumption solely to the increase in lubricant viscosity. Therefore, with an understanding of the link between lubricant temperature and friction, it is clear to see why the prolonged lubricant warm-up relative to the coolant shown in Figure 1.7 is so undesirable.

#### **1.5.1.1 The mechanism of lubricant heating**

In Section 1.5, it was highlighted how both the lubricant and coolant temperature were critical factors in the efficiency of I.C. engines. It has been seen how the engine lubricant heats up at a slower rate than the coolant but it is desirable for both lubricant and coolant heating rates to be higher. The coolant is heated by heat transfer from the combustion gases through to the coolant jacket and it has already been discussed how the coolant and cylinder liner temperatures are closely coupled [7, 11, 19].

The engine lubricant heating sources are more varied. Section 1.5.1 highlighted how the temperature dependence of lubricant viscosity results in the engine lubricant providing sub-optimal lubrication prior to it reaching its intended operating temperature. A consequence of frictional dissipation in the bearing is heat generation and it will be seen that it is bearing friction that provides the greatest source of heat to the lubricant.

Shayler et al. [25] investigated the effect of main bearing friction during cold-start and demonstrated that frictional work in the bearings (dissipated as heat) is significant during the early stages of warm-up. An unloaded crankshaft was tested from an initial soak temperature of -20 °C to observe the effect of lubricant viscosity on friction at the bearings, and the subsequent heat generation. Figure 1.14 [25] shows the heat flux away from the bearings during the warm-up phase of the engine, with an initially large flux which rapidly decreases with time. The high heat generation in the bearings results from the high frictional losses at cold-start (in this work, there were no other sources of heat). From these data, an empirical equation was developed that relates the friction force in the bearing to a range of parameters, amongst them the lubricant viscosity. This relationship is shown in Equation 1.8. Using this formula, power dissipated as heat in the bearing can simply be related to the product of the frictional force and the surface speed. Thus, the power dissipated at the bearings would be proportional to the product of  $U^{1.6}\mu^{0.8}$ .

$$F = \beta \frac{\pi D L \mu^{0.8} U^{0.6}}{c [(1 - \varepsilon^2)]^{0.5}}$$

- Where:
- $F$ = Frictional force within the bearing (N)
  - $\beta$ =Constant
  - $D$ = Bearing diameter (m)
  - $U$ = Relative bearing speed ( $\text{m s}^{-1}$ )
  - $\mu$ = Dynamic viscosity (Pa s)
  - $c$ = Bearing clearance (m)
  - $\varepsilon$ = Eccentricity ratio (in this work set to 0.6)

**Equation 1.8: Empirical relationship of frictional force within unloaded bearings as a function of lubricant viscosity [25]**

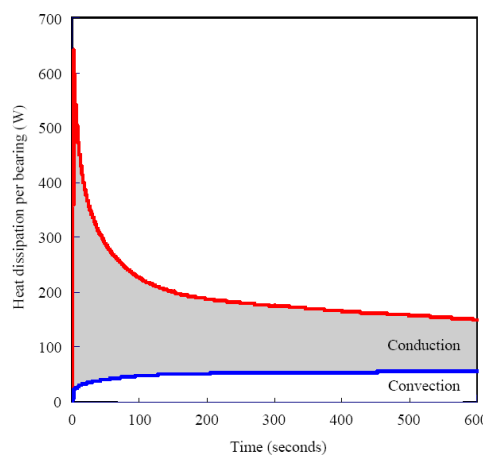


**Figure 1.14: Rate of heat flow from bearing shells during the early stages of engine warm-up [25]**

It should be noted that the equation indicates that the frictional force is not related to the load carried at the bearing with the authors arguing that the friction is essentially independent of engine load during start-up. Instead, the frictional force is dependent on engine speed with the lubricant heating rate having been found to be dependent on engine speed by both Andrews et al. [38] and Shayler and Christian [39], suggesting that the heating rate of the engine lubricant is dependent on frictional heating. If heat transfer from combustion was the dominant source of lubricant heating, it would be expected that the lubricant heating rate would show a positive correlation with engine load owing to the need to burn more fuel to meet the higher load requirements. Instead, the correlation with engine speed (and hence bearing surface speed) indicates that it is the friction in the bearings that dominates as a heat source. Similar heat generation figures to that of Shayler et al. [25] were reported by Zammit et al. [27] (Figure 1.15) using a 2.4 litre diesel engine run at 2000 rpm and 3 bar brake mean effective pressure (BMEP).

In Figure 1.16 [20], Trapy and Damiral demonstrated the overall heating effect of all the bearings (rather than heat flow per bearing) was just over four times the figures presented by Shayler et al. [25] and Zammit et al. [27]. Given that for a 4 cylinder engine, one may expect up to 5 main bearings to be present, this correlates well with the work of Shayler et al. and Zammit et al. It should also be highlighted that Shayler et al. [25] and Zammit et al. [27] investigated C.I. engines whereas Trapy and Damiral [20] investigated S.I. engines. Thus the trend also appears to be consistent across engine types.

Critically, Trapy and Damiral [20] also linked these bearing friction figures to the overall contribution made to lubricant heating, confirming that the main source of lubricant heating during engine warm-up is that of the frictional power dissipated in the bearings themselves (61%). The remaining 39% is provided by what is referred to as 'complementary heat' which encompasses all the other contributions to lubricant heating throughout the engine, including the heat passed to the lubricant from the combustion process, heat transfer from the coolant and other frictional power dissipation. Another key observation is the relative importance of piston cooling jets in lubricant warm-up with Trapy and Damiral [20] reporting the percentage of heat input from 'complementary sources' reducing to as little as 9% when the piston cooling jets were deactivated.

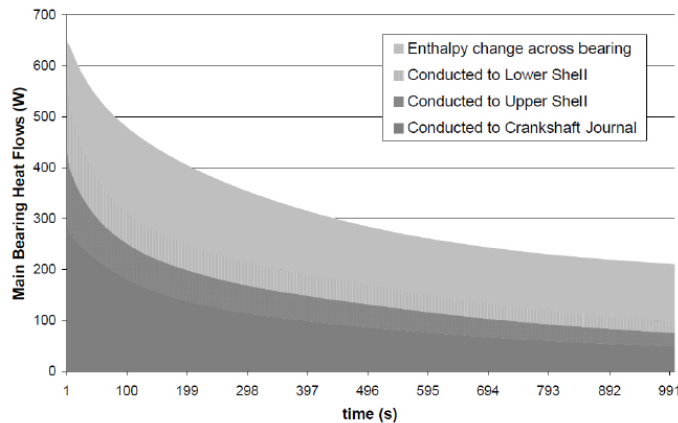


Figure 1.15: Energy flows per bearing from a 2.4 litre diesel engine running at 2000 rpm and 3 bar BMEP during warm-up. Reprinted with permission from SAE paper 2012-01-1216 ©2012 SAE International [27]

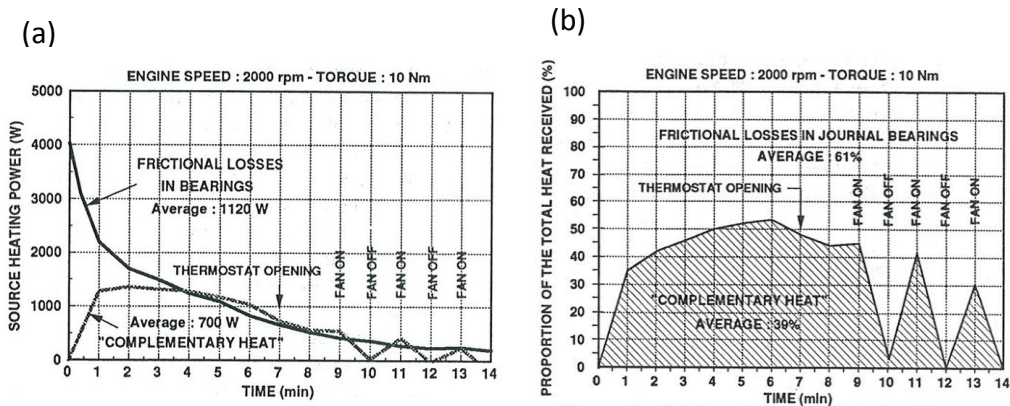


Figure 1.16: Frictional losses within an I.C. engine providing heat input to the lubricant system for a 1.7 litre S.I. engine. Complementary heat to the lubricant is also shown and is a term for all other heat sources to the lubricant including combustion heat and heat from the coolant. Reprinted with permission from SAE paper 902089 ©1990 SAE International [20]

### 1.5.1.2 Variations in lubricant temperature throughout the lubricant circuit

To provide sufficient lubrication to all the components within an I.C. engine requires the lubricant to be pumped around a complex circuit that provides a variety of flow paths. Figure 1.17 shows a schematic of a typical I.C. engine lubricant circuit taken from a 2.0 litre, 4 cylinder direct injection S.I. engine. It can be seen that the lubricant is scavenged by the oil pump and is fed into the rear of the main gallery before being split to serve different parts of the engine including the main bearings, valve train and turbo before the lubricant returns to the sump under gravity feed. Such a set-up is typical of many engines although the presence of individual components (e.g. the turbo) is dependent on the specific engine configuration. The literature referenced thus far characterises the lubricant in the engine based on a single temperature measurement point that is typically taken to be either the bulk lubricant temperature in the sump or at a specific point of interest (e.g. the main gallery temperature or bearing film temperatures). However, there is significant

variation in lubricant temperature between locations in the lubricant circuit. Figure 1.18 [40] shows the lubricant temperature in the engine at various positions at different points in time. It can be seen that at the time steps shown, the lubricant gains approximately 2 °C as it travels through the oil cooler. In this particular engine the oil cooler is coupled to the engine coolant circuit. Consequently, during the early phases of running the coolant actively heats the lubricant and it is only during steady state running that the lubricant is cooled by the coolant. Such an installation is not standard on every vehicle and the effect in this experiment can be seen. The literature review (Chapter 2) highlights the work of Samhaber et al. [14] who modelled the warm-up of a 2.0 litre direct injection diesel engine and found that fuel consumption was either increased or reduced as a result of reduced coolant flow depending on whether a coolant / lubricant heat exchanger was present (Section 2.3.5.2).

When examining the temperature profiles in Figure 1.18 it can be seen that there is negligible difference in the lubricant temperature between the entry point at the rear of the gallery and the exit at the front of the gallery and that the lubricant temperature rises by up to 9 °C (observed at 400 seconds) after flowing through the head. However, a critical observation is the way in which the lubricant loses temperature as it flows down the return channels back to the sump. It can be seen that at 100 seconds the lubricant loses 5 °C in temperature between the head outlet position and lower block return and that this temperature differential remains above 3 °C until 800 seconds. Such a reduction is significant, particularly given that the lubricant viscosity is much more sensitive at these low temperatures. The 5 °C drop in temperature from 30 °C to 25 °C increases the dynamic viscosity of the lubricant by 25% from 69 mPa s<sup>-1</sup> to 85 mPa s<sup>-1</sup>. While the temperature reduction at later points are both lower in magnitude and less significant in terms of viscosity effect, they still contribute to an overall reduction in engine efficiency and contribute to increased fuel consumption and subsequent increases in emissions. A limitation of powertrain research is the lack of repeatability in experimental work. It would be desirable to carry out multiple repeats of a single test to verify the trends discussed are repeatable. However, the cost and time implications of such an approach often prevents research in the field being able to facilitate such data. Such a limitation in the verification of the repeatability of findings is consistent throughout the literature in the field; a point highlighted in the literature review (Chapter 2- Section 2.4.4). Hence, while further repeats would be desirable to verify the trends discussed, such data are not available. However, the temperature measurements were taken using K-type thermocouples that typically read to within +/- 1.5 °C of each other. Thus, a temperature differential of 3 °C can be reliably interpreted as a genuine temperature differential and not a result of experimental noise.

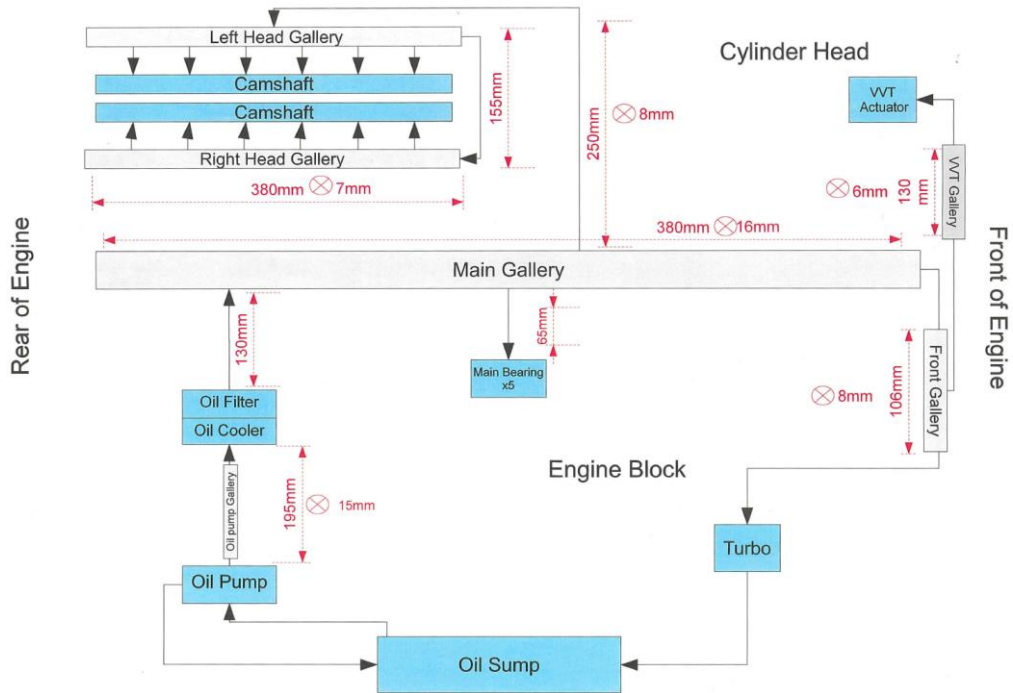


Figure 1.17: Schematic diagram of the experimental test bed engine's lubrication circuit detailing typical lengths and diameters [19]

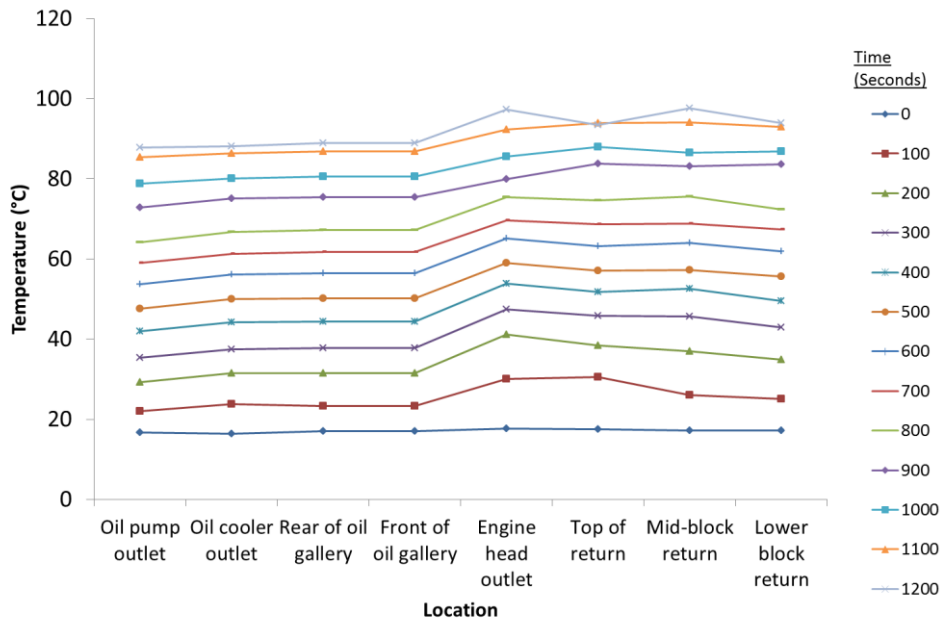


Figure 1.18: Experimental data for engine lubricant during an NEDC test on a 2.0 litre, 4 cylinder direct injection spark ignition engine [40]

### 1.5.2 Summary

The preceding sections have shown how, when operating at a reduced temperature, the I.C. engine is significantly less efficient than at full operating temperature. This is a consequence of cylinder liner temperatures being too low and thus increasing friction between the liner and piston while also failing to promote full and complete combustion. In addition, the viscosity of the engine lubricant has been shown to be highly sensitive to temperature. Consequently fuel consumption is increased owing to the high lubricant viscosities associated with lower temperatures increasing both engine friction and the increased work required more pumping work to circulate it around the engine.

The primary method of coolant heating is via heat transfer from the combustion gases to the coolant jacket while the primary method of lubricant heating is from bearing frictional power dissipation; this is particularly significant at lubricant low temperatures owing to the high viscosity of the lubricants at these temperatures.

In order to improve fuel efficiency and emission quality during the cold-start phase, one must aim to increase the rate of lubricant or coolant warm-up. To achieve this will require a strategy that retains more heat in the lubricant and coolant (i.e. prevents losses) or one that directs more heat to the lubricant or coolant from existing energy sources.

### 1.6 Emission control using catalytic convertors during engine cold starts

Low fuel consumption figures are highly desirable in the NEDC. However, as highlighted in Section 1.2, European legislation is focused on emission figures and not just fuel consumption performance. A critical component in the treatment of exhaust gas emissions on modern vehicles is the catalytic converter which exists to reduce the level of NO<sub>x</sub>, hydrocarbon and carbon monoxide emissions. The catalytic convertors use noble metals to oxidise carbon monoxide and hydrocarbons to carbon dioxide and water while nitrous oxides (NO<sub>x</sub>) are reduced to form water and nitrous oxide (N<sub>2</sub>O), as opposed to NO<sub>x</sub> (NO or NO<sub>2</sub>). Shown in Figure 1.19 [41] is a plot of the conversion efficiency, defined in Equation 1.9, of a typical catalytic converter against temperature. It can be seen that the conversion efficiency of the catalytic converter can approach 100% but that it provides almost no benefit when cold. Thus, the thermal energy in the exhaust gases serves a vital role in ensuring the catalytic converter reaches its light-off temperature (the temperature at which a 50% conversion efficiency is reached [7]) as quickly as possible. Such is the importance of the catalytic converter, engine management strategies will often operate the engine with retarded spark timing (in S.I. engines) relative to a fully

warm condition to increase the exhaust gas temperatures to promote catalytic converter light-off. This is despite the fuel penalty that such a move entails [42].

$$\text{Conversion efficiency} = \frac{\dot{m}_{\text{pollutant in}} - \dot{m}_{\text{pollutant out}}}{\dot{m}_{\text{pollutant in}}}$$

Equation 1.9: Conversion efficiency of a catalytic converter

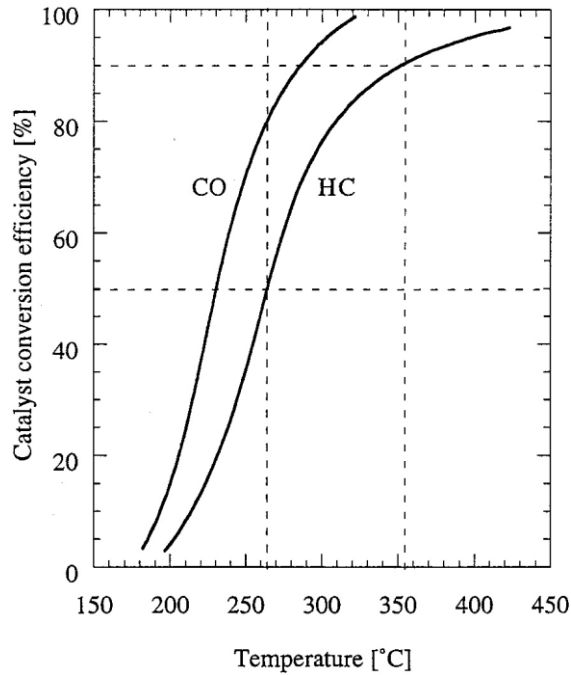
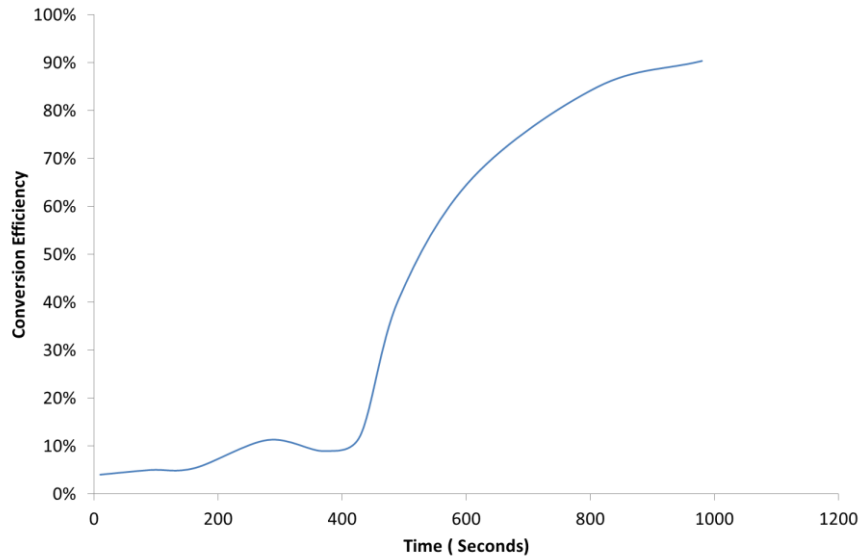


Figure 1.19: Catalytic convertor efficiency against operating temperature for HC and CO emissions [41]

The time frame for the catalytic converter to become active and light-off is variable depending on the engine and load being applied but during real-world driving, Li et al. [21] reported typical light-off times of 150 seconds using a 1.8 litre S.I. engine. Similarly, the work of Zhao and Winterbone [43] reported light-off temperatures being reached in 210 seconds in a wide open throttle scenario but this was extended to 555 seconds in an idling scenario. The work of Gumus [44] investigated methods of improving I.C. engine efficiency and emissions using preheated coolant. The motivation behind doing such work was an attempt to reduce emissions during the phase when the catalytic converter is inactive. The research investigated the merits of phase change materials as an energy store and is therefore discussed in greater detail in Chapter 2. However, as part of the work Gumus [44], monitored exhaust gas composition in the tailpipe both before and after the catalytic converter during warm-up. Thus, using Equation 1.9, it is possible to measure the conversion efficiency of the catalytic converter against time. The results, shown in Figure 1.20, show that the catalytic converter does not begin to improve in performance until after approximately 400 seconds. While the degree of scatter in light-off time is

wide, with time frames of 150 – 555 seconds, even the fastest reacting catalytic converter requires over 10% of the NEDC cycle time to become active. Thus, the challenge of controlling emissions over the NEDC is heightened.



**Figure 1.20:** Plot of HC conversion efficiency against time for a catalytic converter during warm-up at the engine's idle speed for a 4 cylinder 1.6 litre spark ignition engine using data from the work of Gumus et al. [44]

While the light-off temperature of the catalytic converter is paramount in controlling its effectiveness, it is not the only consideration in achieving optimum performance. Another critical parameter is that of the lambda ratio ( $\lambda$ ). The lambda ratio is defined in Equation 1.10 and it follows that a  $\lambda$  value above unity results in a fuel-rich condition whereas a  $\lambda$  value below unity indicates a lean-burning condition. Shayler and Christian [39] highlighted that during the warm-up phase, S.I. engines are usually operated using a rich mixture to help overcome the poor mixing of the inlet charge as a result of the cylinder walls being cold. Such a strategy raises the unburned hydrocarbon emissions as a result of there being too much fuel present to achieve complete combustion [39, 45]. Shayler et al. [45] later highlighted that fuel returning from forming a surface film on the combustion chamber surface is particularly poorly mixed and therefore poorly burnt. However, it is also apparent, based on the work of Li et al. [21], that the conversion efficiency of the three way converter is also impeded due to the rich mixture. Thus, it can be seen that not only does the necessary rich fuel mixture generate higher emissions but also the mechanism of controlling them is limited too.

$$\lambda = \frac{AFR}{AFR_{stoichmetric}}$$

**Equation 1.10:** Definition of the lambda ratio.

### **1.6.1 NOx emission considerations**

The specific control of NOx emissions is beyond the scope of this thesis but is nonetheless worthy of comment in the overall scope of trying to improve emissions during cold starts. Unlike, CO, HC and CO<sub>2</sub> emissions, NOx emissions rise with temperature and such an increase is therefore one of the few negative effects of increased heating rates. Typically, NOx emissions are controlled with exhaust gas recirculation (EGR) which dilutes the air and fuel mixture with exhaust gases from the previous combustion cycle. By using exhaust gas recirculation, NOx emissions are reduced owing to the following effects [26]:

- A reduction in the availability of oxygen for the formation of NOx.
- The increased presence of water and carbon dioxide in the inlet charge raises the thermal capacity of the inlet charge and thus reduces the in-cylinder temperatures.
- A less significant effect is that of the thermal disassociation of carbon dioxide (CO<sub>2</sub>) and (H<sub>2</sub>O). The breaking of chemical bonds in the process of the disassociation is endothermic and consequently the combustion gas temperature is reduced.

Consequently, within the scope of implementing new technology to improve warm-up rates of I.C. engines, there is a potential need to re-tune engine management strategies to control NOx emissions.

## **1.7 Conclusions**

It has been established that when an engine is operating at sub-optimal temperatures there is a significant penalty in terms of increased frictional losses and therefore higher fuel consumption. The higher fuel consumption also results in higher emission levels while the lower cylinder liner temperatures promote incomplete combustion and therefore worsen the emission quality. In addition, the catalytic converter that is used to control NOx, HC and CO emissions is not functional owing to it being at too low a temperature. This thesis therefore aims to investigate methods of improving the warm-up rate of I.C. engines (in particular the coolant and lubricant) to aid OEMs in meeting tighter emissions targets and reducing fuel consumption for vehicle owners.

## 2 Literature Review

### 2.1 Introduction

In Chapter 1, the effect of cold starts on engine emissions and fuel consumption, along with the underlying causes, were discussed. In order to reduce the fuel consumption and emissions from I.C. engines during industry standard drive cycle tests (e.g. the NEDC), it was concluded that there would be a benefit in reducing the time of the engine warm-up phase. The critical role of the catalytic converter was also highlighted, noting that it is imperative to ensure that the catalytic converter reaches its light-off temperature as quickly as possible.

The I.C. engine is a complex thermal system with multiple interrelations between sub-systems. There is therefore a need to ensure that a strategy used to improve the warm-up rate of one system does not impinge negatively on another (e.g. a method of increasing the lubricant warm-up rate having a detrimental effect on the catalytic converter light-off time). Shown in Figure 2.1 is a schematic diagram of the different engine cold-start performance issues and their interrelationships. Various methods have been used to improve cold-start performance across the years and in the sections that follow, these will be discussed in detail.

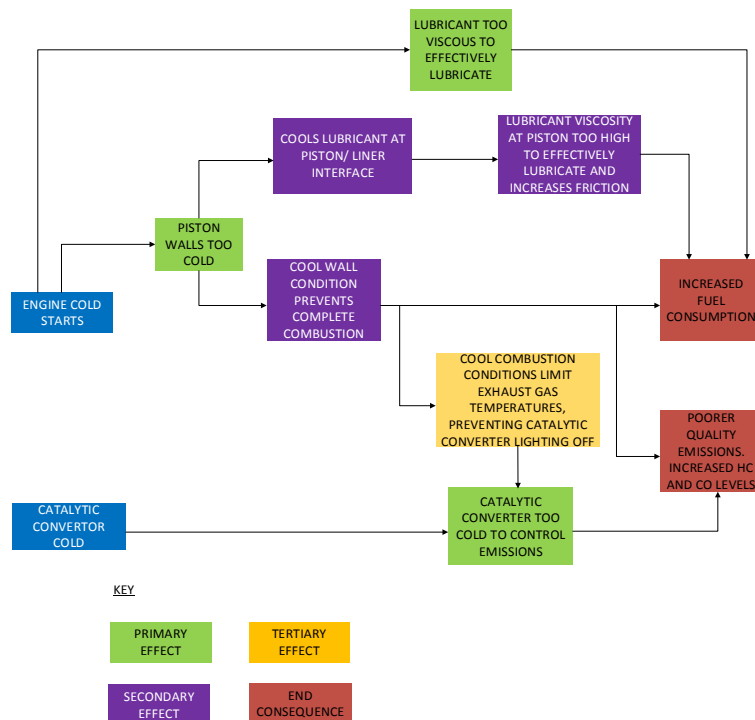


Figure 2.1: Schematic diagram of the causes of cold-start inefficiency and poor emissions

A key differentiator in the merits of different strategies is the nature of the cold-start. In the situation where an engine is being subjected to a full cold-start (i.e. the

whole system is at a temperature close to that of the ambient temperature), there is a need to implement strategies that achieve accelerated warm-up without adding additional thermal inertia to the system. However, there is also, the 'warm start' scenario whereby the engine is below its optimal operating temperature but is at an elevated temperature relative to ambient, having been running a short time before. Such a situation is commonplace, with André [18] finding that an average vehicle made between 5 and 6 trips per day and that the average interval between trips (i.e. from key off to key on) was 3 hours 45 minutes. In addition, over half of the trips were carried out after a stationary period of less than 45 minutes. In such circumstances, energy storage methods may be viable to delay the cool down period, providing the time frame between re-starts is not long enough for the energy storage device to completely discharge. In the event of this happening, there is a subsequent thermal mass to be heated that, depending on how it is installed, could prolong the warm-up phase relative to a conventional full cold-start.

In light of this concern, the solutions discussed attempt to reduce the impact of cold starts by one of two strategies. The first attempts to reduce (or eliminate) the cold-start by trying to keep the engine warmer during periods when the engine is non-operational while the second attempts to re-apportion the energy balance shown in Figure 1.5 [20] in a more effective manner to achieve accelerated warm-up in the regions where it is most beneficial. For example, of the energy transferred to the engine from combustion, only 4% is retained in the lubricant, resulting in its slow warm-up rate; meanwhile, 32% is retained in the engine block, providing little benefit except that this will promote an increase in cylinder liner temperature. However, with 52% of the energy released from combustion being expelled from the system as waste heat, there is clearly scope to improve the efficiency of I.C. engines during warm-up by redistribution of the energy, with (for example) this waste heat being utilised to raise lubricant temperatures more quickly. Commonly, it is believed that between 15%-40% [16, 46-48] of the energy released from combustion is released to ambient via the exhaust gases. Thus, a potential option is to use some of this exhaust heat and energy to accelerate the warm-up of other sub-systems. However, this must be achieved in such a way as to not detrimentally affect the catalytic converter. The figures above are quoted from the work of Trapy and Damiral [20] although the orders of magnitude are in agreement with both Samhaber et al. [14] and Jarrier et al. [16].

The aim of this chapter is to review prior research into improving the energy efficiency of I.C. engines and in particular, the cold-start phase. In doing so, the area for advancement in knowledge from this thesis will be identified. Much of the prior work in the field is related to the re-distribution and transfer of heat and thermal energy. Section 2.2 therefore first introduces the broad concepts of heat transfer before specific attempts to improve I.C. engine efficiency is discussed in Section 2.3.

## 2.2 The fundamentals of heat transfer

The aim of this section is to give a brief overview into the different mechanisms of heat transfer and the associated physical parameters that warrant consideration when attempting to optimise thermal systems. This includes the consideration of the principal mechanisms of heat transfer and also the specific cases of transient warm-up and the use of heat-exchangers.

### 2.2.1 The different mechanisms of heat transfer

Heat transfer can be categorized into three different mechanisms, namely:

- Conduction: The transfer of heat through a solid medium (e.g. through a solid wall).
- Convection: The transfer of heat from a surface to a fluid (e.g. from a surface to air).
- Radiation: The transfer of heat between two bodies via electromagnetic radiation (e.g. between the sun and the earth).

If one first considers heat flow by conduction through a solid, the heat flow (usually measured in  $\text{W m}^{-2}$ ) is a function of both the material thickness, the material thermal conductivity (measured in  $\text{W m}^{-1} \text{K}^{-1}$ ) and also the temperature differential between two points. Comparatively, the heat flux leaving a surface via convection is a function of both the temperature differential between the fluid and the surface and also a range of other physical parameters. These include the velocity of the fluid, viscosity of the fluid and the characteristic length of the object and the surface roughness of the object. The effects of such variables are best represented by empirical correlations and make extensive use of dimensionless parameters but result in a heat transfer coefficient, usually denoted  $h$ , that is expressed in units of  $\text{W m}^{-2} \text{K}^{-1}$ . The heat through a solid as a result of conduction is given by Fourier's law, and is defined in Equation 2.1 while convective heat transfer from a surface is governed by Newton's law of cooling, defined in Equation 2.2.

$$Q_{\text{conduction}} = -\frac{k A \Delta T}{dx}$$

Where  $Q_{\text{conduction}}$  = Heat flow by conduction (W)

$k$  = Material thermal conductivity ( $\text{W m}^{-1} \text{K}^{-1}$ )

$A$  = Area ( $\text{m}^2$ )

$\Delta T$  = Temperature differential between the two points of interest ( $^{\circ}\text{C}$ )

$dx$  = Material thickness (m)

**Equation 2.1: Fourier's law for conduction through a solid**

$$Q_{convection} = -hA(\Delta T)$$

Where  $Q_{convection}$  = Heat flow by convection (W)

$h$  = Convective heat transfer coefficient ( $W m^{-2} K^{-1}$ )

$A$  = Area ( $m^2$ )

$\Delta T$  = Temperature differential between the surface and the fluid ( $^{\circ}C$ )

#### Equation 2.2: Newton's law of cooling

At steady state any heat flow through a solid by conduction will be equal in magnitude to the heat flow at the surface of the solid from convection and it is therefore possible to equate the conductive heat flow in Equation 2.1 with the convective heat flow in Equation 2.2 to form a resistance network of the heat flow by conduction and convection as shown in Equation 2.3.

$$Q_{thermal} = \frac{\Delta T}{R_{conduction} + R_{convection}}$$

$$R_{conduction} = \frac{\Delta x}{k} (m^2 K W^{-1})$$

$$R_{convection} = \frac{1}{h} (m^2 K W^{-1})$$

#### Equation 2.3: Heat flow as a result of convective and conductive heat transfer mechanisms

Radiative heat transfer is of a different nature and therefore obeys the Stefan Boltzmann law. The net radiative heat flow between two surfaces, at temperature  $T_1$  and temperature  $T_2$  is a function of the following variables:

- The temperature of the surfaces (in radiation heat transfer it is imperative that the temperatures are quoted in Kelvin).
- The view factor between the two surfaces,  $F_{12}$  and  $F_{21}$ . This is a measure of the quantity of radiation leaving one surface that would fall on another surface and is a scalar value between 0 and 1.
- The surface emissivity,  $\epsilon$ . This again is a scalar value between 0 and 1 that quantifies the proportion of radiation falling on a surface that is re-emitted relative to the ideal scenario of a black body that would emit all of the possible radiation.
- The surface reflectivity  $\rho$ . This again is a scalar value between 0 and 1 that quantifies the proportion of radiation falling on a surface that is reflected rather than transmitted or absorbed.

Therefore, with an understanding of the parameters associated with radiation heat transfer, the net radiative heat flow between two surfaces as a result of radiation is given by Equation 2.4.

$$Q_{radiation} = \frac{\sigma(T_1^4 - T_2^4)}{\left\{ \frac{\rho_1}{A_1\epsilon_1} + \frac{1}{A_1F_{12}} + \frac{\rho_2}{A_2\epsilon_2} \right\}}$$

- Where
- $Q_{radiation}$  = Heat flow by radiation (W)
  - $\sigma$  = Stefan Boltzmann Constant ( $W\ m^{-2}\ K^{-4}$ )
  - $\epsilon$  = Emissivity of the surface
  - $\rho$  = Reflectivity of the surface
  - $F$  = View factor of one surface relative to another
  - $A$  = Area ( $m^2$ )
  - $T$  = Absolute temperature of the surface (K)

**Equation 2.4: Radiation heat exchange between two surfaces [49]**

The more complex nature of radiative heat transfer presents an interesting debate as to whether or not to account for the effect of radiation in heat transfer calculations and the significance of its impact will vary depending on the individual situation being studied. It follows from Equation 2.4 that radiation is only of significance when the surface has a high emissivity value while Çengel [50] recommends that radiation not be considered significant relative to forced convection scenarios or when the surface considered have low emissivities and low to moderate temperatures.

### 2.2.2 Transient heat transfer

In a steady state situation (i.e. where the temperatures of all the components have equilibrated) the equations presented in Section 2.2.1 can be used to determine the temperature at any point in a thermal resistance network providing that two initial temperatures are known and the relevant thermal properties of the material and the convective heat transfer coefficient is known (or can be calculated). However, in a transient situation there is also a need to consider the rate of accumulation of energy of a component as the temperature profiles approach equilibrium. Thus, an additional term, the energy stored, is introduced and quantifies the amount of energy needed to increase a thermal mass by a given temperature and is given in Equation 2.5. It can be seen from Equation 2.5 that to change the temperature of a body of material or fluid by a given temperature will require more energy if either the mass of the body is increased (either as a result of increased volume or material density) or if the specific heat capacity is higher.

$$Q_{stored} = mC_p\Delta T$$

Where  $m$  = Mass of the body (kg)

$C_p$  = Specific heat capacity of the material or fluid at constant pressure  
(J kg<sup>-1</sup> K<sup>-1</sup>)

$\Delta T$  = Change in temperature (°C)

**Equation 2.5: Change in thermal energy as a result of a change in temperature**

When investigating the transient heat transfer regime it is more complex to model and quantify heat flows than working in the steady state regime. The thermal energy stored results in changing temperature profiles between different thermal bodies but also throughout the thickness of a given body. Depending on the nature of the material or fluid being investigated, it may be possible to model components as lumped capacities. In doing so the assumption is made that there is negligible temperature gradient across the thickness of a component and that the thermal resistance at the convective boundary is far greater than any thermal resistance owing to conduction within the material. In order to quantify the relative magnitude of convective and conductive heat transfer and therefore appraise the validity of using a lumped capacity methodology, the Biot Number,  $Bi$ , defined in Equation 2.6 is conveniently used. For a lumped capacity approach to be valid, the value of  $Bi$  needs to be below 0.1 [39, 50-52]. A more robust methodology, and one that captures all of the changes in temperature distribution throughout the different thermal masses being investigated, is to use a numerical method where the thickness of each thermal mass is discretised into nodes to enable the temperature distribution through the thickness of each thermal mass to be calculated at successive time intervals. However, depending on the time step used and the nodal distribution, this can have a highly detrimental effect on the computational time required.

$$Bi = \frac{h \Delta x}{k}$$

Where:  $h$  = Convective heat transfer coefficient (W m<sup>-2</sup> K<sup>-1</sup>)

$\Delta x$  = Characteristic length (m)

$k$  = Thermal conductivity of the solid material (W m<sup>-1</sup> K<sup>-1</sup>)

**Equation 2.6: Definition of Biot Number [49]**

### **2.2.3 Heat exchange from fluids and the use of heat exchangers**

Section 2.3 discusses a range of strategies that have previously been trialled to improve I.C. engine cold-start efficiency. A recurring theme is the introduction or refinement of heat exchanger technology to improve the thermal balance of the I.C. engine relative to the thermal balance presented in Figure 1.5 and Figure 1.6. Thus this section aims to briefly introduce the concept of heat exchangers and their operating principals.

#### **2.2.3.1 Principal types of heat exchanger**

The aim of a heat exchanger is to transfer heat from one fluid stream to another fluid stream. This is usually achieved by means of the two fluid streams running close to each other and being separated by a thin wall. Heat subsequently flows from the hotter fluid to the colder fluid and results in a convergence of the two fluid stream temperatures. The means by which this can be achieved can be broadly classified in two categories:

- Parallel flow heat exchangers
- Counterflow heat exchangers

In the first scenario, the two fluid streams enter the heat exchanger from the same side and flow parallel to each other before exiting at the opposite side of the heat exchanger. Conversely, the counterflow heat exchangers have the two fluid streams entering the heat exchanger at opposite sides and flowing in the opposite direction to each other. Figure 2.2 [49] shows how the resulting temperature profiles of the two fluid streams change as a result of the different configuration and it is noticeable how the temperature differential between the two fluid streams is more consistent along the heat exchanger length in the counterflow situation. For this reason the counterflow heat exchanger is more efficient and also offers the capability for the cold fluid (i.e. the fluid being used as the heat sink) to exit the heat exchanger at a higher temperature than the exit temperature of the fluid being cooled. However, there are often logistical and cost issues associated with the selection of the counterflow configuration which mandates the use of a parallel flow heat exchanger.

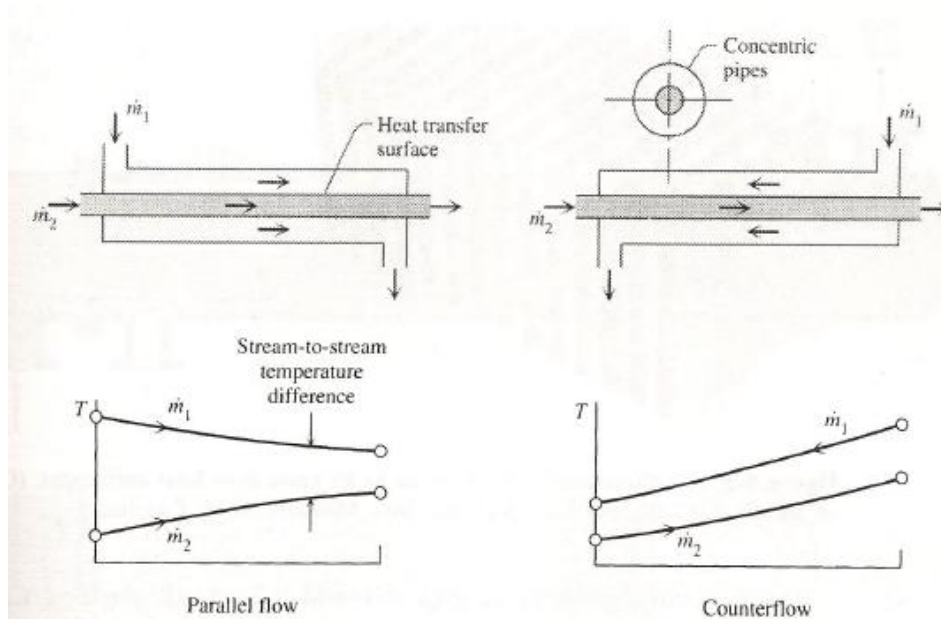


Figure 2.2: Temperature profile of the two fluid streams in parallel and counterflow heat exchangers [49]

### 2.2.3.2 Calculation of the heat flow between fluid streams

The heat flow between the two fluid streams is best quantified using the log-mean temperature difference method and is summarised in Equation 2.7:

$$Q = UA\varepsilon\Delta T_{lm}$$

Where  $U_{overall}$  = Overall heat transfer coefficient ( $W m^{-2} K^{-1}$ )

$A$  = Area ( $m^2$ )

$\varepsilon$  = Overall surface efficiency factor

$\Delta T_{lm}$  = Log mean temperature difference

Equation 2.7: Heat flow in a heat exchanger using the log mean temperature difference [49]

The overall surface efficiency factor,  $\varepsilon$ , accounts for any increase in heat transfer area as a result of the addition of fins. Thus, the value will vary between 0 and 1 depending on the exact ratio of finned to unfinned area. The overall heat transfer coefficient combines the convective heat transfer coefficient for both the hot and the cold fluid but also incorporates the thermal resistance of the wall thickness between the two fluids (hence a thin wall is desirable) but also any thermal resistance owing to the build-up of contaminants and corrosion products (called a fouling factor). The fouling factor typically has values between  $0.0001 m^2 K W^{-1}$  and  $0.0009 m^2 K W^{-1}$  depending on the fluid being used (hard water increases the fouling factor) [49]. Hence, when considering convection from the fluid stream to the separating wall using Newton's law of cooling (Equation 2.2), the overall heat

transfer coefficient is modified to account for any build up in debris reducing the heat transfer effectiveness as shown in Equation 2.8.

$$\frac{1}{U_{overall}} = \left( \frac{r_s}{\varepsilon} + \frac{1}{\varepsilon h} + \frac{\Delta x_{wall}}{k_{wall}} \right)$$

Where  $h_e$ = Overall heat transfer coefficient ( $W m^{-2} K^{-1}$ )

$r_s$ = Fouling factor ( $m^2 K W^{-1}$ )

$h$ = Overall heat transfer coefficient ( $W m^{-2} K^{-1}$ )

$\varepsilon$ =Overall surface efficiency factor

$\Delta x_{wall}$ = Wall thickness (m)

$k_{wall}$ = Wall thermal conductivity ( $W m^{-1} K^{-1}$ )

**Equation 2.8: Heat exchanger effective heat transfer coefficient**

Typical values for the overall heat transfer coefficient can vary between  $30 W m^{-2} K^{-1}$  and  $2500 W m^{-2} K^{-1}$  depending on the combination of hot and cold fluid used.

The log-mean temperature difference, first referred to in Equation 2.7, is defined in Equation 2.9 [49] and it should be noted that in instances where the temperature differential at inlet and outlet are the same then the value of  $\Delta T_{lm}$  assumes the constant temperature differential. This validity and conditions of this simplification is important and is utilised in modelling the experimental work in this thesis and its applicability is highlighted in Section 6.2.2.

$$\Delta T_{lm} = \frac{\Delta T_2 - \Delta T_1}{\ln \frac{\Delta T_2}{\Delta T_1}}$$

Where  $\Delta T_2$ = Temperature differential between the two fluids at the heat exchanger cold fluid outlet.

$\Delta T_1$ = Temperature differential between the two fluids at the heat exchanger cold fluid inlet.

**Equation 2.9: Definition of the log mean temperature differential [49]**

## 2.3 Strategies used to improve I.C. engine efficiency

Having established the fundamental theory behind heat transfer and the issues surrounding the poor performance of I.C. engines during cold-start, the aim of this section is to review prior work in the field relating to improving the energy efficiency of I.C. engines and in particular, the cold-start phase. In doing so, the area for advancement in knowledge from this thesis will be identified.

Prior research into improving the cold-start efficiency of I.C. engines has investigated a wide range of strategies including:

- Energy re-capture from the exhaust stream: By re-capturing thermal energy in the exhaust stream, the warm-up rate of engine components or the lubricant and coolant could be accelerated and therefore either reduce engine friction or improve combustion quality to improve fuel economy or reduce emissions. Alternatively, the thermal energy could be used to generate electricity and therefore reduce the load on the engine's alternator and therefore reduce fuel consumption.
- The use of thermal barrier coatings (TBCs) in the combustion chamber: By using TBCs in the combustion chamber, the combustion process is insulated from the engine block and therefore more of the energy released from combustion will be converted to brake work rather than being transferred as heat to the engine block. This is intended to reduce the fuel consumption, and hence emissions of the engine but also, by virtue of the exhaust gases being at an elevated temperature, enables the catalytic converter to light-off faster and therefore improve the quality of the tail pipe emissions.
- External Insulation of the engine structure: By externally insulating the external structure of the engine, thermal losses from the external surfaces of the engine block are intended to be reduced. This reduces the time required for the engine to reach its intended operating temperature and consequently reduces engine friction; improving the engine's fuel economy and emissions. An associated benefit of such an approach is that the engine takes longer to cool down and therefore subsequent re-starts between short journeys commence at a higher operating temperature than would be the case without insulation.
- Insulation applied to the internal structures of the engine: The heat input to the engine lubricant as a result of friction could be retained in the lubricant better if insulating strategies between the lubricant and the engine block were implemented. Thus, this section investigates the benefits observed as a result of insulating the bearing shells from the engine block and also highlights preliminary investigative work into insulating the engine oil galleries to achieve accelerated lubricant heating rates. Compared to insulating the external structure of the engine, such a benefit offers an immediate benefit to the lubricant heating rate rather than having to heat the entire engine block before any insulating benefit is observed (as would be the case with external insulation).
- Pre-heated coolant: By introducing pre-heated coolant into the engine, such a strategy enables the engine block to be heated and to therefore increase the temperature of the lubricant as a result of reduced losses through the bearing shells or the gallery walls (owing to a reduced temperature differential between the lubricant and the block surface). Such a strategy is

therefore intended to reduce friction work in the engine by means of an increased lubricant heating rate during the cold-start phase.

- Variable coolant flow control: By reducing the coolant flow during engine warm-up, it is intended to reduce the cooling effect on the engine and to therefore achieve optimum operating temperatures sooner. This increased lubricant temperature reduces engine friction but the increased cylinder temperature also facilitates more complete combustion.
- Lubricant flow diversion: By strategically diverting the lubricant flow, it is intended to reduce the thermal losses from the lubricant to increase the warm-up rate of the lubricant and hence reduce engine friction and fuel consumption. The means of achieving this include diverting lubricant away from the sump, separate lubricant circuits for the engine block and the engine head or novel sump designs.
- The use of stop-start technology: Stop-start technology is intended to reduce the fuel consumption of an I.C. engine by turning off the engine when the vehicle is stationary and hence removing the fuel consumed by the engine while idling. Such a strategy, while reducing the net fuel consumed, prolongs the warm-up phase of the engine as a result of heat not being generated during the inactive periods and therefore requires consideration when used in conjunction with other technology strategies.
- Use of alternative materials to reduce the thermal mass of the engine: By using alternative materials the thermal mass of the engine block can be reduced either by using materials of a lower density or materials with a lower specific heat capacity. Such a strategy is intended to increase the warm-up rate of the lubricant and coolant as well as the block owing to the reduced temperature differential between the lubricant, or coolant, and the block surface. Fuel consumption and emissions are intended to be reduced owing to reduced friction (due to the faster heating rate of the lubricant) and also the hotter block surfaces facilitating more complete combustion. However, the need to satisfy the structural requirements of the material also needs to be considered.
- Applications of phase change materials to improve engine thermal efficiency: Phase change materials can be used as high density energy storage as a result of the additional energy stored in the material (termed 'latent heat') as the material undergoes the change in phase. This energy could be used to maintain parts of the engine (either the lubricant directly or structural components of the engine) at a higher temperature during inactive periods and hence reduce fuel consumption and emissions during subsequent re-starts. Material durability and stability must also be considered in such an approach, as must cost.

Having briefly introduced the different concepts previously investigated to improve I.C. engine cold-start efficiency the following sections discuss in more detail, the findings of prior work. While discussing prior work, it will be seen how the positive

impact that an approach has on one sub-system has the potential to be counteracted by a negative effect on a different sub-system and this must be borne in mind when attempting to improve the overall cold-start efficiency of the I.C. engine. An example is the re-capturing of energy from the exhaust gases to improve the rate of lubricant or coolant warm-up. While such an approach may reduce engine friction, and hence reduce the fuel consumed, it may, depending on the approach taken, increase the time taken for the catalytic converter to light-off and therefore cause an undesirable increase in emissions. Such interactions are summarised in Table 2.1 and by reviewing the prior work in the field it is intended to establish the area for advancement in knowledge in this thesis.

Table 2.1: Summary table of potential solutions to engine cold-start issues

	<u>Lubricant warm-up</u>	<u>Combustion warm-up</u>	<u>Catalytic converter functionality</u>	<u>Vehicle integration</u>	<u>Overall effect on fuel economy</u>	<u>Overall effect on emissions quality</u>
Exhaust gas energy recovery (Section 2.3.1)	Green	Green	Red	Red	Green	Yellow
Use of TBCs (Section 2.3.2)	Yellow	Green	Green	Green	Green	Green
External insulation of the engine structure (Section 2.3.3)	Green	Green	Green	Red	Green	Green
Insulation of the bearing shells (Section 2.3.4.1)	Green	Green	Green	Green	Green	Green
Insulation of the engine oil galleries (Section 2.3.4.2)	Green	Yellow	Yellow	Red	Green	Green
Pre heated coolant (Section 2.3.5.1)	Green	Green	Green	Red	Green	Green
Coolant flow control (Section 2.3.5.2)	Red	Green	Green	Green	Green	Green
Lubricant flow diversion (Section 2.3.5.3)	Green	Yellow	Yellow	Green	Green	Green
Stop-start technology (Section 2.3.5.4)	Red	Red	Red	Green	Green	Yellow
Alternative materials (Section 2.3.6)	Green	Green	Green	Red	Green	Green
Phase change material (Section 2.3.7)	Red	Red	Red	Green	Yellow	Yellow

Key

Green	Positive effect
Yellow	Neutral effect
Red	Negative effect

## **2.3.1 Energy re-capture from the exhaust stream**

### **2.3.1.1 Use of exhaust gases in heat exchanger applications**

The exhaust gases leaving an internal combustion engine are at a significantly elevated temperature which can vary between 300 °C and 900 °C depending on engine load [7, 53]. Hot exhaust gases are arguably a wasted form of thermal energy that, if harnessed, could have benefits in achieving accelerated warm-up and reducing fuel consumption. However, caution must be exercised since extraction of heat from the exhaust may increase the catalytic convertor light-off time and thus increase the level of harmful emissions [9] (Figure 2.1). It was highlighted in the introduction how a major consideration during the warm-up of any I.C. engine system is achieving an acceptable catalytic convertor light-off time to manage emissions. A strategy to avoid such an issue would be to capture the exhaust thermal energy downstream of the catalytic converter; however, the broader systems implications must be considered. A typical length from the exhaust manifold to the catalytic convertor could be over 1 metre [43] and experimental data have shown the exhaust gases to reduce in temperature by over 200 °C in the rearward 0.1 m alone. One must also consider that the addition of any energy recovery system for the exhaust gases would add additional weight to the vehicle and may therefore increase fuel consumption.

Investigations into energy re-capture from exhaust gases have a lengthy history in the literature. Goettler et al. [10] investigated the merits of heating the engine coolant via a heat exchanger in the exhaust stream as far back as 1986. The work still provides findings of relevance, although one must consider the advances in technology when comparing with data from more modern vehicles. It is important to note that owing to the age of the vehicle, there was no catalytic converter installed and hence, any negative effect on the catalytic convertor performance did not need to be considered. In the work reported, a coolant to exhaust gas heat exchanger was installed which was aimed at reducing the warm-up times, and hence reduce fuel consumption, of a 3.3 litre S.I. engine. As part of the work, the vehicle was driven on both a high speed dual carriageway (that consequently led to high engine speeds and loads) and a city centre route that mostly comprised low speed and low loads.

The work indicated that the use of a heat exchanger can have a positive effect. For this particular engine, the peak coolant temperature was 85 °C and it was found that the benefit of the heat exchanger was most pronounced in high speed and load applications (i.e. motorway driving). The warm-up time for the coolant was also observed to be highly dependent on ambient conditions but in high speed situations, the warm-up time varied between 5 – 5.5 minutes and this could be reduced by up to 1 minute by use of the heat exchanger. In the low speed situations, the effect was less pronounced and the warm-up time was reduced by approximately 30 seconds

from an initial warm-up time of between 6.5 and 6.75 minutes. The work offered no details on emission levels, but the use of the heat exchanger resulted in a 2.2 % reduction in fuel consumption for both the high and low speed circuits. It must be remembered that the coolant temperature generally leads the lubricant temperature and that using the engine coolant as a means of transferring heat from the exhaust gases to the lubricant is highly inefficient. Will and Boretti [8] estimated that transferring heat from the exhaust gases to the lubricant circuit via the coolant would facilitate approximately 0.8 % of the energy available being transferred to the lubricant. Therefore, the fuel saving is likely to have been as a result of reducing the piston liner friction rather than any dramatic increase in bulk lubricant temperature.

This work is one of the few examples to offer a potential insight into the economic and commercial case for implementation of a technology. The authors focused on the high speed motorway style driving as being the application most likely to offer a successful outcome. The test route was 12.4 km long and was completed in 9 minutes 45 seconds (an average speed of 76 km hour<sup>-1</sup>) and it was found that the engine with the heat exchanger used 40 ml less fuel than the baseline case. The authors assumed that the vehicle would make two cold-starts every day and hence predicted that, the use of the heat exchanger would reduce annual fuel costs by \$23.30 (prices relevant to when the paper was written). If one repeats such a calculation for today's U.K unleaded gasoline prices of £1.27 per litre rather than \$0.40 per litre, the estimated annual fuel saving is £74. The authors felt that the savings represented a marginal case in terms of justifying the expense of such an installation; however, with fuel prices increasing, the merits of such a system become greater.

It has been highlighted that the work of Goettler et al. [10] is unlikely to have had a significant effect on the lubricant heating rate owing to the weak thermal interaction between the exhaust gases and lubricant [8]. The work of Andrews et al. [9] attempted to increase the level of thermal interaction between the lubricant and exhaust gases using additional heat exchangers. A 1.4 litre S.I. engine (operating at 6 kW constant brake power) was configured with a lubricant / coolant heat exchanger to increase the lubricant heating rate but was also configured with a heat exchanger between the coolant and the exhaust gas stream. The baseline condition with neither device active was compared with the following permutations:

- Only the lubricant / coolant heat exchanger active.
- Lubricant / coolant heat exchanger and coolant / exhaust gas heat exchanger active.

It was found that, relative to the baseline tests, the lubricant / coolant heat exchanger alone resulted in a peak reduction in the coolant temperature of 10 °C.

The lubricant temperature had a peak increase in temperature of 6 °C within the first minute of the test, although for the remainder of the test, the lubricant temperature was approximately 4 °C higher than the baseline. Such effects resulted in a 6% improvement in brake specific fuel consumption but it must be highlighted that the reduction in coolant temperature must be carefully managed to ensure that optimum combustion conditions are attained quickly.

When the additional coolant / exhaust gas heat exchanger was used, the increased energy input offset the energy transferred to the lubricant; accordingly, the coolant temperature increased by a maximum of 20 °C and the lubricant temperature increased by a maximum of 12 °C. This resulted in a peak improvement of BSFC of 16%. The work has demonstrated that both technologies have beneficial effects on cold-start fuel consumption and that the combined effects of different technologies can be used to offer an improved benefit and counterbalance the negative effects of different sub-systems.

Research into use of the exhaust gas stream as a source of energy has also been carried out by Will et al. [8, 13] in relation to S.I. engines while Kauranen et al. [15] has examined its use in C.I. engines. The work of Kauranen et al. also included the use of phase change materials as an energy storage medium and is therefore discussed separately in Section 2.3.7.1. In contrast to the outcomes of the work of Goettler et al. [10] which demonstrated the benefit of accelerated coolant heating from the exhaust stream, Will and Boretti [8] focused on improving heat transfer from the exhaust gases to the lubricant. Their analysis suggested that a transfer efficiency of 32% is possible when recovering exhaust heat directly to the lubricant as opposed to an efficiency of 0.8% when using the coolant circuit as an intermediate heat transfer system from the exhaust stream to the lubricant. Their work thus focused on utilising a direct exhaust gas to lubricant heat exchange device. Over the NEDC, the system demonstrated a 7% improvement in fuel efficiency relative to a system without the heat exchanger installed, together with a reduction of 2% in hydrocarbon emissions. This translates into a 27% reduction in CO emissions and a 19% reduction in NO<sub>x</sub>. The reduction in NO<sub>x</sub> emissions is particularly encouraging given that NO<sub>x</sub> usually rises with temperature although Will and Boretti attributed such a trend to be a result of combustion temperatures reducing owing to the reduced friction decreasing the load on the engine. To avoid emissions concerns, the heat exchanger was located to the rear of the catalytic converter. Will and Boretti [8] argued that the increased lubricant temperature has a range of positive effects in addition to the primary objective of reducing friction such as increased piston / liner temperatures that will promote more complete combustion, a fact verified by a range of other sources [11, 14, 19, 22].

Thus, the work in this section has indicated that the use of heat exchangers to directly provide accelerated heating of the engine coolant and lubricant does offer a benefit in terms of reducing fuel consumption. In addition, if the strategy is employed correctly (i.e. energy is recaptured after the catalytic converter), such methods also translate the reduced fuel consumption into improved emission quality. Where possible it has also been shown that the use of exhaust gas energy is most beneficial in terms of improving cold-start fuel efficiency and emissions if it is used to accelerate the lubricant heating rate rather than the coolant heating rate.

### 2.3.1.2 Use of exhaust gases in thermoelectric applications

An alternative method of recovering energy from the exhaust gases is to utilise the thermal energy within the exhaust gases to generate electricity using the Seebeck Effect [46, 48]. The Seebeck Effect is where there exists an electrical voltage across the junction of two dissimilar materials as a result of a temperature difference. Such a strategy could potentially confer a benefit on emissions and fuel consumption by virtue of reducing the load on the engine through the alternator. A typical thermoelectric junction is shown in Figure 2.3 [46].

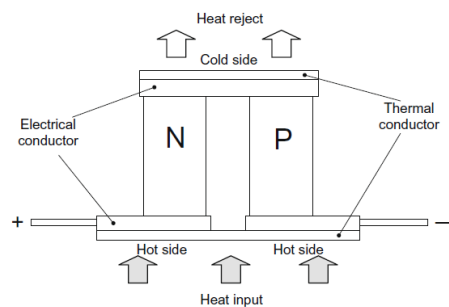


Figure 2.3: Typical thermoelectric junction utilising p-type and n-type doped semi-conductors [46]

The material selection criterion for thermoelectric generator (TEG) applications is governed by the figure of merit, defined as  $Z$  in Equation 2.10 [48, 54]. The values of these parameters are highly temperature dependent but Crane et al. [54] have indicated that the figure of merit will vary between  $2.0 \times 10^{-3} \text{ }^\circ\text{C}^{-1}$  and  $3.7 \times 10^{-3} \text{ }^\circ\text{C}^{-1}$ . Thus, it can be seen that for TEG applications, the material needs to have a high Seebeck Coefficient, low electrical resistivity and low thermal conductivity [48, 54].

$$Z = \frac{\alpha^2}{\rho k}$$

Where  $\alpha =$  Seebeck coefficient ( $\text{VK}^{-1}$ )

$\rho =$  electrical resistivity ( $\Omega \text{ m}^{-1}$ )

$k =$  thermal conductivity ( $\text{Wm}^{-1}\text{K}^{-1}$ )

Equation 2.10: Definition of the figure of merit,  $Z$  [48, 54]

The typical efficiencies of TEG devices are reported as being between 3% and 5% [48, 53, 54], with Matsubara [55] claiming efficiencies as low as 1% and as recently as 2012, BMW only targeting a maximum power output of 1 kW [48]. A possible reason for the poor conversion efficiency is the way in which the energy flux falls dramatically along the length of the TEG unit. Kumar et al. [53] highlighted that the power generated falls by 80% along the 0.4 m length of the TEG unit while Brito et al. [48] also found that achieving power generation along the length of the module was difficult. Furthermore, Yu and Chau [46] demonstrated how maintaining peak power output requires the implementation of complex electronic control strategies. Using such strategies enables the power output of the TEG to be increased by up to 22% relative to its baseline performance. Thus, the literature predicts that with an optimised system, a typical power output could be between 552 W [53] and 600 W [46]. While the conversion efficiency is low, such figures do represent approximately 50% of a vehicle's electrical requirements and would therefore have a benefit on alternator load. The key factor in defining whether such technology is adopted by automotive OEMs would be the cost, with Kumar et al. [53] suggesting the units would need to cost less than 1000 USD to become commercially viable.

A limiting factor in achieving acceptable power outputs is that of the maximum operating temperature, as highlighted by Brito et al. [48]. With the exhaust gases capable of temperatures of 500 °C Brito et al. suggested that the temperature needs to be reduced to between 320 °C and 350 °C. Kumar et al. [53] detailed how heat recovery from the exhaust was carried out with a heat exchanger and that the temperature was controlled by the engine coolant circuit. Figure 2.4 [53] shows an energy balance for a typical TEG device. It can be seen that TEGs have the potential to recover 64 % of the energy within the exhaust gas entering the device. However, 58.7% of the inlet energy is transferred to the coolant owing to operating temperature limitations of TEG devices which hence limits the electrical generation to be only 3% of the total exhaust gas energy.

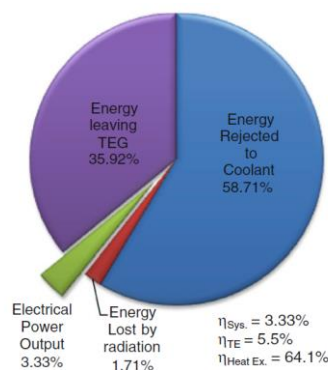


**Figure 2.4: Typical energy balance for a TEG device coupled to the exhaust system [53]**

An alternative approach to managing the operating temperature of TEG devices was proposed by Brito et al. [48] using heat pipes as a heat exchange medium between

the TEG and exhaust gases. The conversion efficiency to electrical power output was still limited to of the order of 1 %, owing to the need to meet operating temperature requirements.

Thus, from this section, it can be seen that TEG devices offer an alternative method to heat exchangers to re-capture energy from the exhaust stream. However, the need to limit their operating temperature is a limitation to realising their maximum potential as is the ability to generate electrical output along the continuous length of the device.

### **2.3.2 The use of thermal barrier coatings (TBC) in the combustion chamber**

The piston liner temperature has a significant impact on the thermal efficiency of the engine with one of the causes of cold-start inefficiency and high emission levels being poor combustion as the cold walls adversely influence flame propagation [17, 39]. Gardiner et al. [19] highlighted the mid-liner temperature as being a critical performance barometer in the efficiency of the engine during cold-start and steady state. A higher piston liner temperature reduces the temperature differential between the liner and the combustion gases and hence results in a lower heat flux to the wall. The energy not transferred to the wall as heat is therefore available to be used as brake work output or in the elevation of the exhaust gas temperature (beneficial in reducing the time to catalyst light-off) [22].

Increasing the cylinder wall temperature can be achieved by the use of a thermally insulating coating material. Thermal barrier coatings are usually of the order of 100  $\mu\text{m}$  thick and have a thermal conductivity of the order of  $1 \text{ W m}^{-1} \text{ K}^{-1}$  [56]. While thermal barrier coating technology has been used to great effect in the gas turbine industry, transfer into the automotive industry has not been significant. It is important to note there are more effective insulators available (i.e. materials with a lower thermal conductivity) but they cannot withstand the high service temperatures or corrosion from the combustion gases (peak combustion gas temperatures are of the order of 2500 K although the surface temperature is much lower with recorded temperatures in the region of 280 °C [7]). Such an issue is illustrated in Figure 2.5 [57] where it can be seen that polymers and foams offer a lower thermal conductivity than technical ceramics but the maximum service temperature is limited to approximately 200 °C and creep concerns would manifest themselves at lower temperatures still (approximately at one third of the melting temperature). Figure 2.5 does indicate that certain foams may be able to both withstand the operating temperature of the bore walls and also offer a lower thermal conductivity but there is also the need to ensure that the material is stable and there is therefore a risk, when using foams, of absorbing by-products of combustion or un-burnt fuel. Hence, the region highlighted is the region of interest

in relation to applying thermal coatings to the bore wall and the piston. Yilmaz et al. [58] also highlighted strain resistance and a high oxidation resistance as material requirements and offered an extensive list of candidate materials. The application of TBCs to engine components appears to have found favour with diesel engines as opposed to S.I. engines with the references discussed here all being based on diesel engines [22, 47, 59, 60].

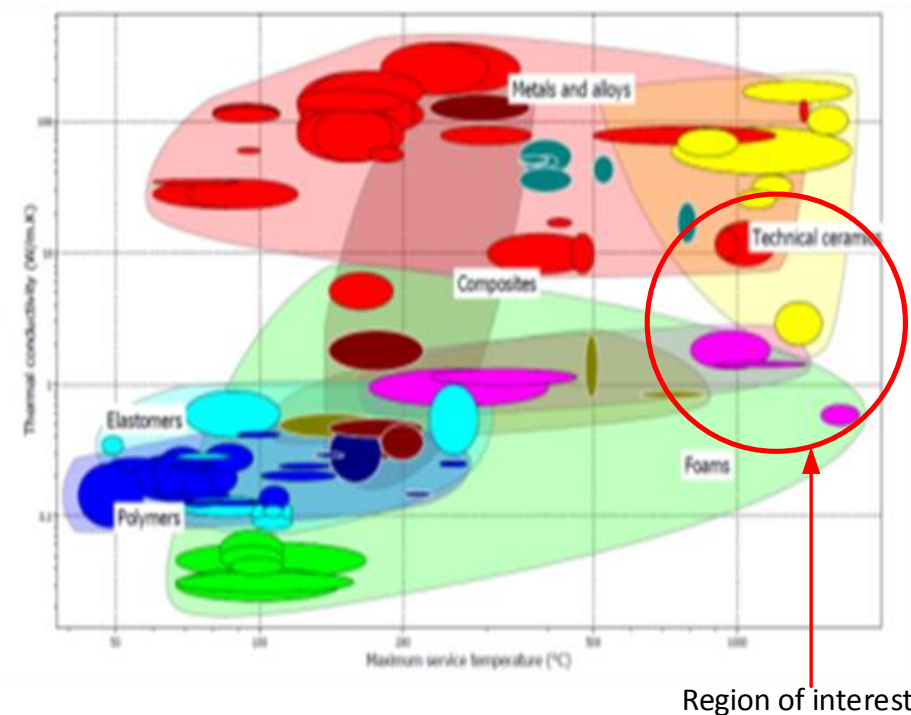


Figure 2.5: Ashby material selection chart plotting thermal conductivity against maximum service temperature [57]

Attempts to utilise thermal barrier coatings in cylinder bores are well documented. Work by Kamo et al. [22] trialled a diesel engine with a cylinder liner coated with a range of TBCs (Table 2.2) and extended the work to a TBC coated piston. For the first case, an improvement in fuel economy of 1% was observed, while the fully insulated case, which also insulated the piston head and cylinder head face (see Figure 2.6) delivered a 2% increase in fuel consumption. Other workers [47, 59] conducted similar trials, with reductions in fuel consumption of between 2% and 4.5% being reported. Such improvements were also translated into reductions in emissions, particularly for CO emissions although Uzun et al. [47] appeared to show a greater gain in emission quality than others with CO emissions reducing by between 35% and 40%, HC emissions reducing by 40% and particulates reducing by 48%. Ciniviz et al. [59] argued that the increased exhaust gas temperatures resulted in the turbo-charger operating more efficiently, thus reducing fuel consumption. It is recognised that the use of TBCs in the bore may change the combustion profile and to therefore

realise the full potential of TBCs, an engine is likely to need ignition timing adjustment to prevent knock phenomena [59].

**Table 2.2: Properties of zirconia and chrome oxide based TBCs [22]**

<u>Coating</u>	<u>Composition</u>	<u>Application method</u>	<u>Density (kg m<sup>-3</sup>)</u>	<u>Specific heat capacity (J kg<sup>-1</sup> K<sup>-1</sup>)</u>	<u>Thermal conductivity (W m<sup>-1</sup> K<sup>-1</sup>)</u>
LT-450	Zirconia & chrome oxide	Slurry TBC	2930	754	1.23
SCA1000	Zirconia & chrome oxide	Plasma sprayed zirconia & post densified chrome oxide	3380	796	2.40

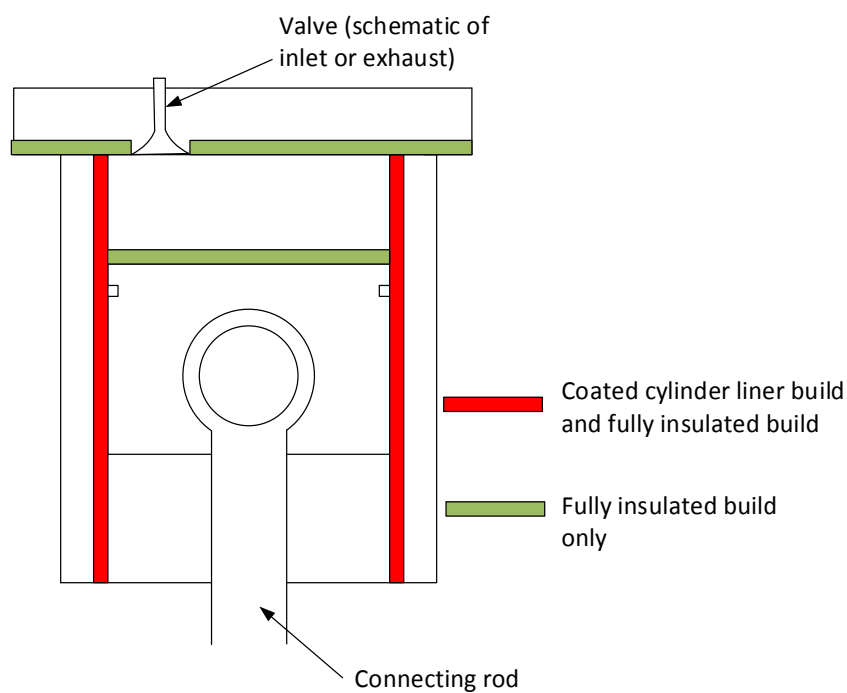


**Figure 2.6: Schematic diagram showing the locations of where TBCs have been applied in I.C. engines in the work of Kamo et al. [22]**

A perceived additional benefit of the use of TBCs is the possibility of removing the cast iron liners owing to both the wear resistance and high operating temperatures of the TBCs. Additionally, the block itself can be made smaller since the need to accommodate the extra thickness of the liners is removed. Dahotre and Nayak [61] argued that the combined weight savings alone could result in significant fuel savings over the life of the vehicle, a fact reiterated by Yilmaz et al. [58].

It must be recognised that the use of TBCs may result in changes to the piston-liner friction; it has been suggested that any increase in friction is detrimental to engine fuel consumption with piston-liner friction typically accounting for 30% of the total engine friction [61, 62]. In addition to the thermal management requirements, the work of Dahotre and Nayak [61] summarised the key properties required from a TBC to be used in an engine. These include compatibility with engine lubricant and the ability to be honed as a post-deposition operation. The honing process is required to ensure an acceptable surface finish is achieved so that low frictional losses result. Further material requirements include good adherence to the substrate, cost effectiveness and the ability to implement the processes on a mass production scale.

Thus, the use of TBCs in the combustion chamber does appear to offer a viable option to improve the cold-start efficiency of the engine. Critically, (as shown in Table 2.1) there are no perceived negative interactions with other sub-systems. However, the literature has highlighted that the use of TBCs in I.C. engine applications must be combined with a possible re-optimisation of injection timing to avoid knock phenomena. In addition, the economic impact of implementing a process usually reserved for high-end aerospace applications into the mass production automotive market must also be borne in mind relative to any potential benefit.

### **2.3.3 External insulation of the engine structure**

Figure 2.1 indicated that all cold-start inefficiencies can be attributed to either the catalytic converter, lubricant or combustion wall being too cold. As such, it is clear that there will be a benefit in bringing the temperature of the whole system up to its normal operational temperature as soon as possible. One method to achieve this is to apply low thermal conductivity materials to the outer surfaces of the engine to insulate the system from the ambient air. This approach may result in more rapid temperature increases, or in slowing down the overall rate at which the temperature falls following a period of engine running. In a cost-constrained and risk-averse industry, such a strategy has the advantage of utilising known technology that can be implemented in a cost effective manner.

Bürgin [63] experimented with applying insulation in what were termed the ‘engine close’ or ‘engine far’ approaches using a diesel engine. The engine close approach places insulation onto the engine block itself while the engine far approach places insulation on the internal panels of the vehicle within the engine bay, as shown schematically in Figure 2.7.

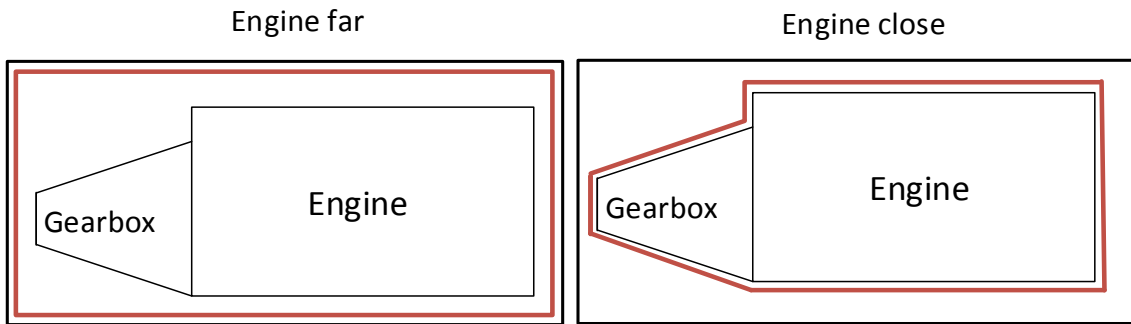


**Figure 2.7: Summary diagram showing the difference between engine far and engine close insulation concepts. The red line denotes where the insulation is applied**

After a cool down period of 12 hours, the engine close solution resulted in engine lubricant and coolant temperature increases of 6 - 7 °C over those observed in baseline tests, whereas the engine far approach resulted in the engine coolant being 7 - 8 °C higher than in baseline conditions but the engine lubricant being only 4 - 7 °C higher.

Critically, percentage coverage is crucial to the successful implementation of any external insulation philosophy with Bürgin [63] suggesting that to achieve noticeable improvements, at least 60% coverage needs to be achieved. If the percentage coverage is less than 50%, the rise in temperature, relative to the uninsulated scenario after 15 hours, is less than 1 °C. Such findings are summarised in Table 2.3; it should also be noted that similar trends were observed by Stouffer et al. [64].

**Table 2.3: Temperature rise relative to an uninsulated baseline test of an engine 15 hours after shutdown when 7 mm thick insulation is applied to the external surfaces of the engine [63]**

<u>% Coverage</u>	<u>Temperature rise relative to uninsulated baseline (°C)</u>
10	0
20	0
30	0.5
40	0.75
50	1
60	1.5
70	2
80	4
90	7
100	16

While the engine close approach was seen as thermally superior, Bürgin argued this approach was likely to incur a higher weight penalty (estimated to be 10%) due to the need to use stiffer structures to cope with increased engine vibrations. Bürgin's

work focused on the retention of heat in an engine after running (i.e. during the cool down period); one concern with such a strategy is that should an excessive mass be added, there is a risk that the additional thermal inertia of the system may cause a delay in the initial warm-up and therefore have a negative effect. No such comparative data were available from Bürgin but the work of Bent et al. [11] does help alleviate such concerns. Bent et al. carried out work on a 1.6 litre 4 cylinder S.I. engine and compared the bulk lubricant temperature in the sump with differing levels of engine encapsulation applied. The insulation material used was a 25 mm thick layer of rockwool, with a thermal conductivity of  $0.04 \text{ W m}^{-1} \text{ K}^{-1}$ ; the reductions in lubricant temperature with time on cool down are shown in Figure 2.8 [11]. It can be seen that during the warm-up, there is negligible difference in lubricant temperature as a result of different levels of insulation but the cool down rate is significantly reduced by the presence of insulation. This would suggest that the additional thermal mass of external insulation is not of significant detriment during warm-up. It does, however, have a significant effect on cool down and it can be seen that with the whole engine insulated, the bulk lubricant temperature is held over  $10 \text{ }^\circ\text{C}$  hotter than the uninsulated case 2.25 hours after the engine finished running. This would suggest that the external energy losses from the outer surface of the engine are suitably de-coupled from the lubricant to make the additional thermal mass of the insulation insignificant during the warm-up phase.

Thus, in attempting to address the increased frictional losses in the I.C. engine during cold-start that result from sub-optimal lubricant viscosity, the use of external insulation is likely to have limited impact; particularly when tested in a NEDC or similar drive cycle test. Thermal losses from the external surface of the I.C. engine occur late in the drive cycle test (when the engine block has reached an elevated temperature) and therefore does not prevent thermal losses from the lubricant circuit to the block during the early phases of the test. Consequently, its impact on reducing the increased friction in the engine due to sub-optimal lubricant viscosity is limited. The data have shown how the external insulation has limited effect on the warm-up rate of the engine but has a more pronounced effect during cool-down and hence is more likely to offer a fuel economy and emissions benefit when the engine is used for multiple short journeys with periods of no use between trips. However, given that mandated drive cycle tests such as the NEDC are required to be conducted from a soak temperature of between  $20 \text{ }^\circ\text{C}$  and  $30 \text{ }^\circ\text{C}$  such benefits will be unable to be observed during such procedures. Consequently, while a benefit may be achieved during real world useage, such a strategy is unlikely to yield a significant benefit during industry standard tests.

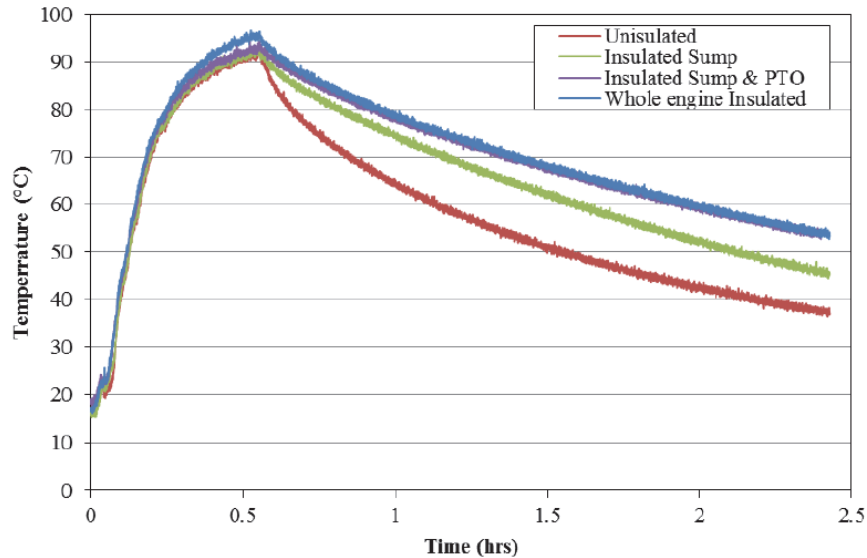


Figure 2.8: Engine oil sump temperatures from a 1.6 litre 4 cylinder S.I. engine during warm-up at 1500 rpm and 2 bar BMEP and subsequent cool down [11]

### 2.3.4 Insulation applied to internal structures of the engine

#### 2.3.4.1 Insulation of the bearing shells from the thermal mass of the engine block

In Figure 1.16a of Chapter 1 data were presented to show the power dissipated as heat in the journal bearings and how this is the primary source of lubricant heating during engine warm-up. The work of Shayler et al. [25] also quantified how much of the heat generated by friction is not transferred to the lubricant but is instead conducted through the bearing shells to the surrounding engine block. The authors therefore investigated reducing heat flow through the bearings as a method of increasing heat retention in the lubricant to accelerate warm-up. The work investigated reducing the contact area between the back of the bearing shells and the engine block by 80% using specially manufactured bearing shells (Figure 2.9 [25]). The aim was to increase the contact resistance between the shell and the engine block to provide an insulating effect and therefore increase the rate of lubricant heating. In computational work, this effect was simulated by reducing the interface heat transfer coefficient by 80%.

The results (shown in Figure 2.10 [25]) indicate that insulating the bearing shells from the engine block has the potential to reduce the frictional force (and have an associated positive benefit on fuel economy) by 22%. Figure 2.10 also shows the maximum potential reduction in frictional force if the bearings could be completely isolated from the mass of the engine block. Thus, it can be seen that there is potential to reduce engine friction, and associated fuel consumption and emissions, by reducing the heat lost from the lubricant through the bearing shells.

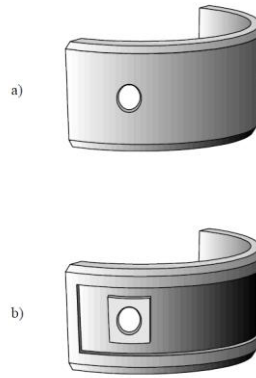


Figure 2.9: Comparison of (a) conventional journal shells and (b) high contact resistance bearing shells used to reduce thermal losses from the lubricant to the engine block [25]

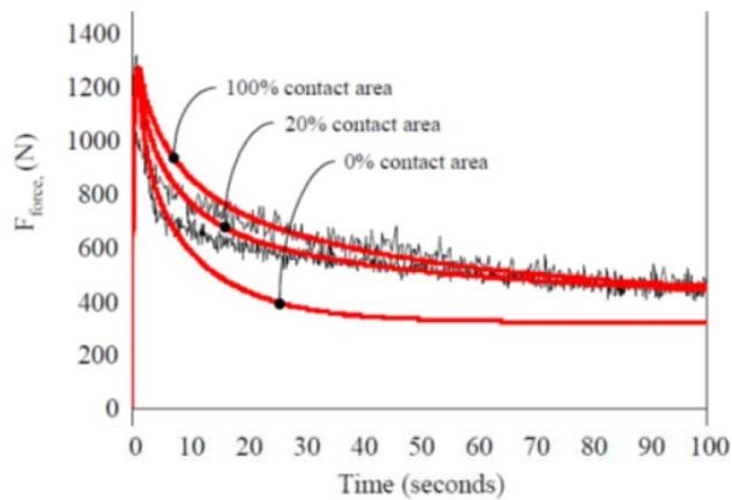


Figure 2.10: The effect of shell contact area on bearing frictional force on the crankshaft assembly of a 1.8 litre diesel engine motored at 1000 rpm [25]

### 2.3.4.2 Insulation applied to the engine oil galleries

In addition to heat being lost from the lubricant through the bearing caps, another potential heat transfer mechanism is through the gallery walls of the lubricant circuit in the engine (shown in Figure 1.17 with a cross section of the engine block showing the main engine oil gallery presented in Figure 1.4). Trapy and Damiral [20] estimated that up to 8% of the heat input into the lubricant (for a 1.7 litre S.I. engine) is lost to the gallery walls while Zammit et al. [65] estimated that this could be as high as 25% (for a 2.4 litre C.I. engine), depending on the location of the main gallery in the engine (a gallery located lower in the engine would promote greater heat losses from the gallery walls). In simulations by Zammit et al. [65], the heat transfer mechanism from the lubricant to the main oil gallery wall (equivalent to the main gallery shown in Figure 1.4) was deactivated to simulate a perfectly insulated main gallery. The simulations predicted that such a strategy could reduce fuel consumption during the NEDC by 0.2%. Moreover, the fuel consumption benefit could be increased further, if the heat transfer from the oil mist to the crankcase

surface was also isolated, to 1.7% (isolation of the oil mist to crankcase surface heat transfer mechanism was predicted to offer a 0.5% fuel consumption benefit). The heat transfer mechanism to the crankcase was highlighted to be of greater significance in the case of insulated lubricant circuits owing to the lubricant being at a higher temperature as a result of reduced heat loss to the gallery walls.

The work discussed above is of significance. The work indicates that insulating the engine oil galleries is likely to give a potential benefit in reducing engine friction as a result of increasing the lubricant heating rate. However, the work is only at a preliminary investigation level and has only been investigated in a computational manner. In the same publication it was discussed how the coupling of the temperature of the lubricant in the gallery to the surrounding structure had a significant effect on the model predictions. If the model was configured to exchange heat with the lower block structure then a heat flow of approximately 200 W was seen to flow from the lubricant to the engine block. However if the model was re-configured so that the engine oil gallery exchanged heat with the outer wall of the coolant jacket (essentially simulating raising the main gallery in the block) then the heat flow was seen to reverse and a heat flow of 200 W was seen to flow from the block to the gallery. Thus, there is a potential benefit to be had by insulating the engine oil galleries on cold-start fuel economy and subsequent emissions. However, research to this date demonstrates significant uncertainty. The complex interactions of an I.C. engine currently makes it difficult to understand the effect that insulation of the engine oil galleries has on heat flow from the lubricant to the engine block. The main engine block is sparsely instrumented with the primary area of interest being the cylinder liners. Consequently there is a lack of understanding of the thermal history of the engine block as it is heated during the warm-up phase and resulting uncertainty as to whether the lubricant is gaining or losing heat at specific points in the engine. Furthermore, the lack of experimental data relating to the engine block temperatures results in a coarse discretisation of the engine in any computational model and hence limits confidence levels in any prediction. In the case of Zammit et al. [65], it has been shown how changing the coupling of the main gallery to a different location in the engine has significant effects on the predicted heat flow to the lubricant and there is clear scope for further investigative work into improving cold-start efficiency by means of insulating the lubricant circuit.

### **2.3.5 Active system control methods to improve vehicle cold-start performance**

The solutions discussed thus far have all been related to a change or addition of material to potentially better suit the cold-start phase of an engine (in situations where the engine is fully-cold or in situations where a short period of non-operation has followed one of engine operation). However, the greater flexibility that modern vehicles offer in terms of control systems allows for the use of fundamentally

different strategies between engines that are fully warm and those that are cold. The benefit of such strategies is the potential to use systems during warm-up to reduce the time to steady state and de-activate such systems during fully warm conditions to avoid overheating.

### **2.3.5.1 Pre-heated coolant**

Using a 2.6 litre diesel engine, Zammit et al. [27] investigated the merits of utilising pre-heated coolant to increase the rate of warm-up of engine lubricant and thus reduce bearing friction. The use of pre-heated coolant could also serve to improve the combustion conditions in the pistons owing to the close coupling of the cylinder liner temperature and the coolant temperature. The engine used during the work had an oil filter cooler assembly (FCA) installed that was used to transfer heat between the coolant and lubricant. The motivation behind installing such devices was to provide lubricant cooling during high load, steady state running and to provide lubricant heating during warm-up (when the lubricant is much cooler than the coolant). Zammit et al. installed a 3 kW electric heater in the coolant tank and preheated the coolant to 90 °C; the hot coolant was streamed into the coolant system when the FCA loop was open (but the main radiator branch was closed) and peak heat transfer rates from the coolant were observed to be over 4 kW. At the point the hot coolant flow was activated, Zammit saw the main gallery lubricant temperature increase from 20 °C to 40 °C (shown in Figure 2.11a) while for the same test, the increase in lubricant temperature in the bearings was only 5 °C (shown in Figure 2.11b). This demonstrates that the local lubricant temperature is highly sensitive to the temperature of the surrounding metal. Nonetheless, a 5 °C increase in lubricant temperature from 35 °C to 40 °C would be expected to reduce the lubricant viscosity of a typical 5W-30 lubricant by 33% if one uses the data of Pulkrabek [33] presented in Figure 1.12 in Chapter 1. The pre-heated coolant was estimated to provide an 8% reduction in main bearing friction work relative to when no heat exchange between the pre-heated coolant and lubricant was utilised. However, the reduction in friction work, as a percentage of the additional energy input to pre-heat the coolant was calculated to be only 26% and therefore highlights the inefficiency of using the coolant as a means to reducing engine friction.

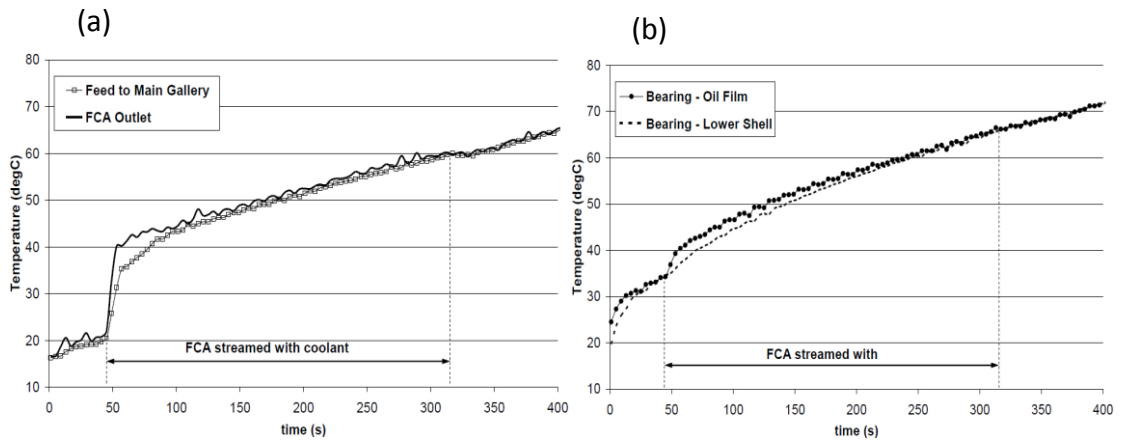


**Figure 2.11: Engine lubricant temperature against time for a 2.4 litre direct injection diesel engine for (a) the main gallery and (b) the main bearing films showing the effect of introducing pre-heated coolant to the FCA device. Reprinted with permission from SAE paper 2012-01-1216 ©2012 SAE International and SAE of Japan [27]**

Bent et al. [11] have also investigated the concept of utilising pre-heated coolant. Relative to the work of Zammit et al. [27] their work was not exclusively focused on reducing bearing friction but was intended to target the whole engine system and was focused on S.I. engines. Consequently, rather than use the coolant as a heat exchange medium for the lubricant, pre-heated coolant was circulated through either the block or the head. Tests were run by circulating the coolant 20 seconds before the engine was fired although a comparative test of coolant circulating only from the moment of firing was also conducted. From the data presented, no benefit was observed in pre-circulating the coolant before firing relative to introducing preheated coolant only once the engine is in use; however the friction levels were reduced relative to the situation with no preheating, with reductions in FMEP of 5% and 9% for block and head pre-heating respectively.

Thus, while the use of pre-heated coolant has been proven to offer a benefit in reducing engine friction and subsequent fuel consumption and emissions, the work presented in this section indicates that it is an inefficient means of doing so. While fuel consumption and emission quality is improved, the work of Zammit et al. [27] has demonstrated that the effective conversion efficiency of the energy input required to heat the coolant relative to the reduction in friction work is 26%. Thus, for the strategy to be economically viable the coolant would need to be pre-heated using waste heat from the engine while running and be subsequently stored. While this is viable and is the set-up used in Bent's work, the approach would only offer a benefit during multiple short trips and would not manifest any benefit during a mandated test situation such as the NEDC owing to the need for the test to be conducted from a soak temperature of between 20 °C and 30 °C.

### 2.3.5.2 Variable coolant flow control

It has been highlighted that one of the contributory factors to poor emissions and fuel consumption during the cold-start phase was the cold cylinder liner temperatures. This wall temperature is very closely coupled to that of the coolant temperature. During the warm-up phase of the engine, the coolant usually circulates through what is referred to as a bypass loop. During this phase, the thermostat is not open and therefore heat is not being rejected by the radiator but coolant flow is maintained to reduce the build-up of hot spots. Such a strategy still circulates coolant through the block and cools the cylinder liners, albeit to a lesser extent than if the radiator was in use. The coolant pump is usually driven from an auxiliary drive belt from the crankshaft and hence the speed of the pump is proportional to the engine speed. A consequence of such a system is that during periods of warm-up or driving conditions that combine low load and high road speed (i.e. motorway cruising) the cooling system is over specified. Brace et al. [66] reported that a conventional mechanically driven coolant pump can only match the required flow rate for  $\approx 5\%$  of the vehicle operation time and that for the rest of the time, the system over cools the engine. An option that has been investigated is to therefore control the coolant flow independently of engine speed. Such technology is already implementable at a commercially effective level with Will [13] reporting such a strategy costs €5 per 1% fuel consumption reduction. However, prior work into this potential strategy has largely concluded that the improvement in fuel consumption as a result of reducing engine friction is negligible. Instead, the fuel consumption reductions observed (between 0.5% and 1%) can be largely attributed to a reduction in the energy consumed by the pump as a result of both its lower speed and power source. Thus the work in this section indicates that variable coolant flow control does not appear to be an effective means of reducing I.C. engine frictional losses.

Gardiner et al. [19] carried out investigations into the effect of coolant circulation rate during the warm-up of a 2.0 litre S.I. engine. Typically, the top of the liner is heated by the combustion process and the bottom of the liner is heated owing to the splashing of warm lubricant; consequently, once up to temperature, the mid-liner temperature is the limiting factor in terms of combustion quality. In addition, the work of Leong et al. [37], has proven that an engine's FMEP is closely correlated to the lubricant's dynamic viscosity when evaluated at the mid liner temperature. This highlights the importance of the mid stroke temperature in minimising friction between the liner and piston also. It is worth noting that while such work was carried out using the hardware from a diesel (C.I.) engine, the actual test was motored (i.e. the engine was turned by an electric motor and hence no combustion was occurring in the cylinders). Thus, the findings are transferrable to both an S.I. and C.I. engine situation.

The effect of varying the coolant pump speed is shown in Figure 2.12 [19] for both warm-up and steady state running for differing positions along the length of the engine liner. It can be seen that the mid-liner position is the coolest of all the locations once the engine has reached steady state and that therefore a potential method of reducing friction to the piston and liner would be to reduce the coolant flow rate. However, despite the coolant flow rate having a noticeable effect on the liner temperatures, the benefit to fuel consumption is limited, with a fuel consumption saving of 0.5 - 1% over the NEDC. This can largely be attributed to the removal of pumping work by the auxiliary drive, with this instead being provided by the electric motor.

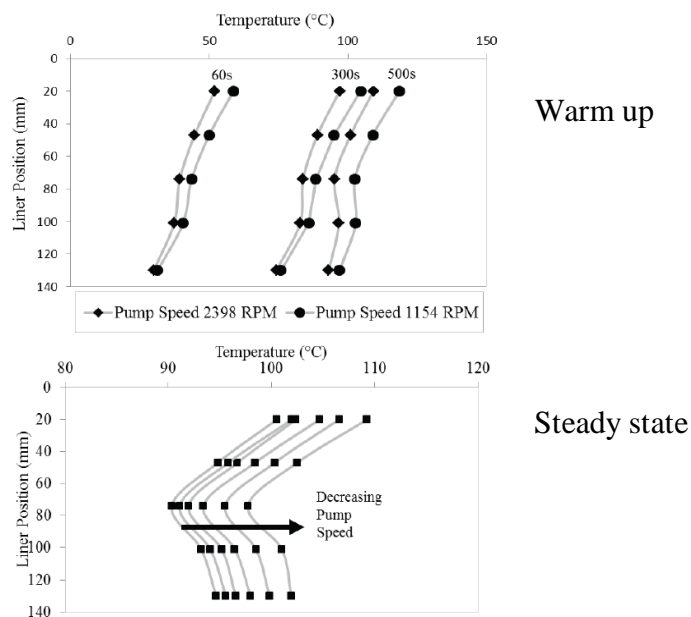


**Figure 2.12: The effect of changing coolant pump speed on cylinder liner temperature at 60 seconds, 300 seconds and 500 seconds after start up and at steady state for a 2.0 litre S.I. engine when running at 1800 rpm and 90 N m load [19]**

Bent et al. [11] also investigated modified coolant flow using a 1.6 litre 4 cylinder S.I. engine. In this case, the coolant flow was turned off until the coolant outlet temperature had reached 60 °C, whereupon the coolant was allowed to flow for 30 seconds and then turned off for 60 seconds (with this cycle being repeated). The authors found that the top liner region was the most affected, with temperatures 10 °C higher than with normal flow; however, the lower liner temperatures were affected to a much lower degree. Similar to the findings of Gardiner et al., the reduction in fuel consumption was estimated to be less than 1% and was primarily attributed to reduced pumping work rather than any thermal benefit. However, the work of Bent et al. [11] did detail some emissions benefits; it was found that in the first 250 seconds, the pulsed coolant flow strategy resulted in an approximately 6% reduction in HC emissions relative to that observed with continuous coolant flow, indicating the significance of liner temperature on combustion conditions and the

piston-liner friction. It was observed that as the liner temperatures associated with the two coolant flow strategies converged, so did the HC emissions (but that a significant reduction was seen in the early phases with a pulsed flow).

An important comparison to the above work is that of Samhaber et al. [14]. Using a lumped capacity model, Samhaber et al. simulated the warm-up of a 2.0 litre direct injection diesel engine that was equipped with a lubricant / coolant heat exchanger. One of the parameters investigated was a reduction in the coolant flow rate. It was found that when the coolant flow rate was reduced by 10%, the coolant temperature was reduced by approximately 5 °C and this was attributed to a reduction in heat pick-up from the head. Such a finding would increase the piston / liner friction owing to increased lubricant viscosity in this area and result in poorer quality combustion. However, owing to the presence of the lubricant / coolant heat exchanger, the bulk lubricant temperature was also reduced by approximately 4 °C. Such a strategy was also highlighted to be negative in the fuel consumption figures; the standard flow rate simulation predicted a fuel consumption of 7.71 l (100 km)<sup>-1</sup>. Even accounting for the reduced pumping work from the lower flow rate, the reduced temperatures caused the simulation to predict that the fuel consumption will rise by 0.6 % to 7.76 l (100 km)<sup>-1</sup>. It is interesting to note the contrasting trends when the lubricant / coolant heat exchanger is removed. If one compares the two baseline simulations (i.e. those without reduced coolant flow), the removal of the cooling effect of the oil cooler resulted in the fuel economy improving from 7.71 l (100 km)<sup>-1</sup> to 7.86 l (100 km)<sup>-1</sup>. In addition, with no oil cooler to transfer heat from the coolant to the lubricant, the effect of reduced coolant flow is to simply raise component temperatures and consequently the lubricant temperature. As a result, with no oil cooler, the reduced coolant flow improves the fuel economy by 1% (including accounting for any reduction in pumping work) from 7.86 l (100 km)<sup>-1</sup> to 7.78 l (100 km)<sup>-1</sup>. Such a finding highlights the need to consider the bespoke combination of thermal management strategies that are in place on an individual engine to ensure that the changes made have a positive impact. In the theoretical simulation work of Samhaber et al. [14], it is worth noting that the pumping work was not entirely removed (unlike the experimental work of Gardiner et al. [19] where the pumping power was provided by an electric motor) but instead was simply reduced owing to the coolant pump speed being reduced but the authors predict that half the fuel economy gain is likely to be a result of reduced pumping work.

The work of Brace et al. [66] focused on using electrically driven coolant pumps to investigate the trade-off of reducing fuel consumption by virtue of increased operating temperatures caused by reduced coolant flow. The work utilised a throttle on the outlet of the coolant pump to simulate the effect of varying pump speed on flow rate using a 2.4 litre diesel engine. In steady state tests where the engine was run at 2000 rpm and at either 2 bar or 8 bar BMEP, it was observed that the lubricant

temperature in the main gallery could be raised by up to 15 °C. At low load, such a change resulted in a 2 % improvement in BSFC but a 10 - 15% increase in NO<sub>x</sub> (although the baseline NO<sub>x</sub> was very low at 2.0 g (kWh)<sup>-1</sup>). Hence, in this situation, it was judged that the fuel consumption benefit justified the increase in NO<sub>x</sub> emissions. At high load, the fuel consumption benefit was only 1.5 % while the NO<sub>x</sub> emissions increased by 45%.

In carrying out transient drive cycle analysis of the effect of variable coolant flow, it was found that the fluid temperatures of the engine were insensitive to changes in flow rate until the latter part of the cycle, although like Gardiner et al. [19], the liner temperatures did show some sensitivity. Burke et al. [26] report that similar findings have been found by Ap et al. and Di Matteo et al. Response models for the drive cycle data suggest that reducing the coolant flow rate from 80 % of the maximum to 4% would only result in a 0.4 % reduction in fuel consumption and increase the NO<sub>x</sub> emissions by 2%.

Thus, from the work presented in this section it has been seen that while there is evidence indicating that reducing the coolant flow rate of the I.C. engine manifests some fuel economy benefit, the sources suggest that any benefit is most likely to be as a result of reduced pumping work rather than any significant reduction in engine friction as a result of elevated temperatures. The work of Bent et al. [11] indicated some potential improvements in emissions as a result of reduced coolant flow, most probably as a result of increased cylinder liner temperatures, while other sources indicate that increased NO<sub>x</sub> emissions are a likely undesirable consequence of reducing the coolant flow velocity. It is therefore felt that such a strategy is ineffective in the primary aim of reducing engine friction and subsequent fuel consumptions and emissions.

### **2.3.5.3 Lubricant flow diversion**

Early work of Will and Boretti [8] highlighted the potential benefit of using the exhaust gases as a means to raising the lubricant temperature during warm-up (discussed in Section 2.3.1.1). Within the same publication, Will and Boretti argued that similar results could be achieved using an alternative method which employed a bypass valve from the cylinder head gallery to return a given fraction of the lubricant directly to the oil pump as opposed to flowing through the sump. In doing so, it was argued that the effective mass of lubricant in the block is reduced which should lead to faster lubricant warm-up rates. The concept of diverting lubricant flow from the sump was encouraged by Andrews et al. [9] who observed large temperature gradients through the lubricant in the oil sump resulting in the lubricant in the top of the sump (having just been returned from the engine) being hotter than the lubricant at the bottom of the sump. However, lubricant viscosity and subsequent friction in the engine was related to the delayed heating profile of the lubricant at

the bottom of the sump owing to this cold lubricant being the lubricant that is scavenged by the engine oil pump. Thus the work in this section discusses methods used to either direct lubricant around the engine in such a way as to minimise thermal losses or methods to temporarily reduce the volume of lubricant in the engine to facilitate an accelerated rate of lubricant heating. The work discussed, while demonstrating that such methods do achieve accelerated rates of lubricant heating and associated reductions in engine friction and fuel consumption, have limited scope to be implemented owing to the complex designs necessary to implement them into an I.C. engine. However, the work is discussed to demonstrate the potential improvements such strategies offer.

Law et al. [67] carried out experimental work on a 2.4 litre direct injection diesel engine with a modified oil sump design. The sump, shown in Figure 2.13, uses an additional thermostat within the sump to reduce the working volume of lubricant during warm-up. Only when the returning lubricant is at a temperature around 70 °C does the thermostat open to allow the working volume of fluid to increase. Such an approach saw the lubricant temperature in the main gallery rise by 5 °C relative to a conventional sump at an ambient temperature of 20 °C and increase by 12 °C when the ambient temperature was reduced to -10 °C. While the reduction in FMEP at an ambient temperature of 20 °C was difficult to quantify, the greater benefit observed at reduced ambient temperatures saw the FMEP during the first two minutes of operation reduce by 10 %.

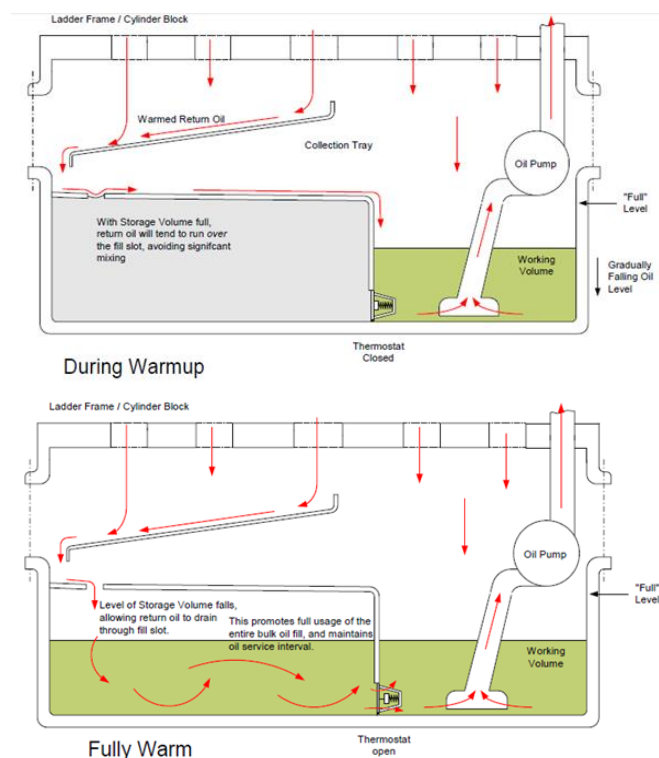


**Figure 2.13: Novel sump design from a 2.4 litre diesel engine to prevent lubricant mixing in the sump and supply hot lubricant to the engine during warm-up [67]**

A lubricant diversion system has been designed in detail and is known as the 'OVER 7' system, short for Oil Viscosity Energy Recovery System [8]. Initial simulations by Will and Boretti [8] predicted that the implementation of such a system would deliver a similar improvement in fuel economy (just over 7%) to the lubricant heat exchange philosophy discussed previously, but with the advantage of much reduced complexity and lower hardware requirements. In a subsequent publication by Will [13], modelling simulations using the bypass return were reported with different bypass ratios. It was found that relative to no bypass flow, the lubricant temperature could be increased by 64 °C and 29 °C with a bypass ratio of 70% and 50% respectively 300 seconds after the start of the NEDC simulation. In using a bypass ratio of 50%, it was found that a peak increase in temperature, relative to the baseline, was 70 °C. This occurred at 700 seconds, after which point the temperature increase reduced as a result of closing the bypass valve in response to the lubricant reaching its peak temperature of 120 °C. Such findings are presented graphically in Figure 2.14 [13].

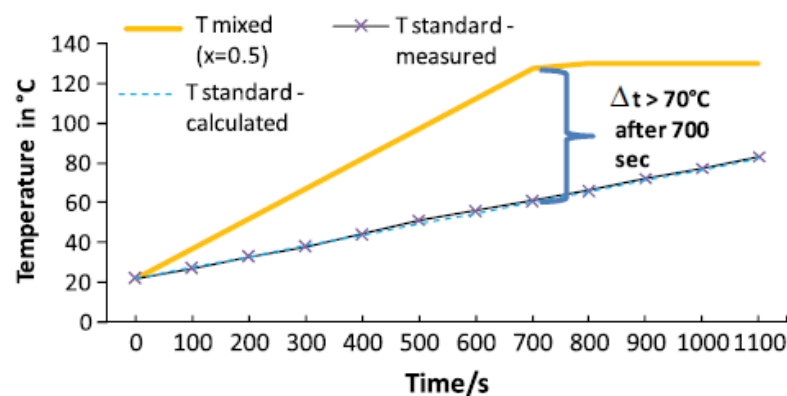


Figure 2.14: Bulk lubricant temperature predictions when implementing lubricant bypass from the cylinder head gallery to the pump inlet based on a 4.0 litre 6 cylinder in line engine [13]

While the practicalities of implementing the above concepts in a production vehicle environment is difficult, the strategies do show synergy with the work discussed in Section 2.3.4 in that by diverting the lubricant flow or temporarily reducing the lubricant volume thermal interaction between the engine lubricant and engine block are reduced. Thus, such work provides further support for developing a practical method of reducing thermal losses from the lubricant to the engine block to facilitate increased lubricant warm-up rates.

#### 2.3.5.4 The use of stop-start technology

Stop-start technology has become more commonplace in the automotive market in recent years, although its role in cold starts is a complex compromise. Stop-start technology is used to eliminate fuel consumption and emissions during idling by turning the engine off.

However, in utilising stop-start strategies, the warm-up period for an engine is prolonged. Consequently, fuel consumption figures will be poorer for longer even if the total quantity of fuel burnt is reduced. In addition, while the engine is turned off, there is no exhaust flow to the tail pipe and hence the catalytic converter will take longer to become active. Bent et al. [11] investigated the use of stop-start technology over the timeframe of the NEDC using a 1.6 litre 4 cylinder S.I. engine. During the NEDC, there are 14 idling periods, totalling 340 seconds in duration; Bent et al. predicted fuel savings of 41.6 g or 7.6% relative to when no stop-start was used. Similar benefits are likely to occur in real world running with André [18] finding that vehicles are stationary for, on average, 18% of the time. However, when examining the work, one can see potential issues, particularly when compared to work already discussed. Results (shown in Figure 2.15 [11]) show that the coolant warm-up rate as a result of using stop-start technology is severely reduced and results in the thermostat opening 177 seconds later. Indeed, at the point that the idling engine thermostat opens (at a coolant temperature of 88 °C), the coolant temperature from the stop-start engine is over 10 °C lower. Such a result is likely to increase fuel consumption owing to the importance of the coolant temperature in reducing piston/ liner friction and achieving complete combustion [14, 19, 22]. Thus, when the engine is running, the net fuel flow is likely to be higher. Similarly, it can be seen that the lubricant at 600 seconds is 10 °C cooler as a result of stop-start technology and that by the end of the NEDC, there is still a 5 °C difference which will result in higher friction in the bearings.

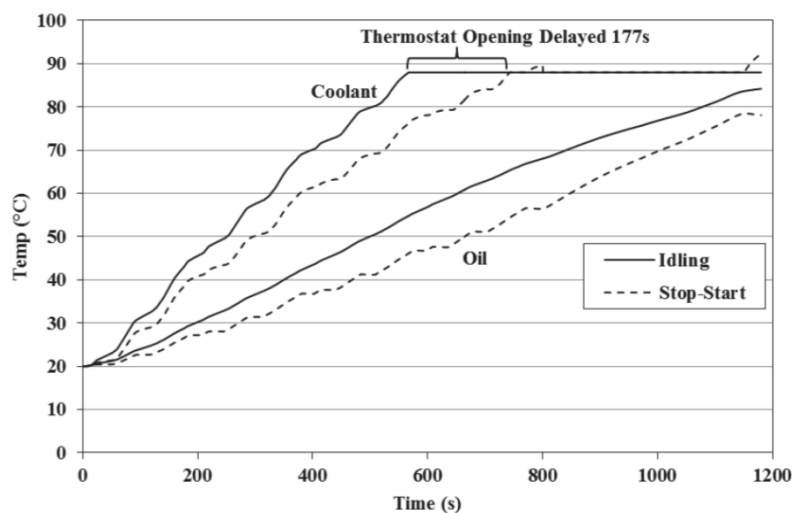


**Figure 2.15: Coolant and lubricant temperatures for a 4 cylinder 1.6 litre S. I. engine during the NEDC both with periods of idling and utilising stop-start technology [11]**

A similar approach is the use of hybrid propulsion vehicles where the wheels can be driven by either an I.C. engine or by an electric motor. Typically, the electric motor is used in lower load scenarios and the batteries are charged when the I.C. engine is operational. Dubouil et al. [68] investigated the effect of hybrid vehicle propulsion on engine warm-up rate and fuel consumption. Simulations were carried out where

a conventional vehicle and one fitted with a hybrid drive unit were both subjected to the NEDC drive cycle from a start temperature of 20 °C and 90 °C. The fuel consumed for the four tests is presented in Figure 2.16 [68] while the temperatures for different parts of the engine are presented in Figure 2.17 [68]. It can be seen how between 450 seconds and 850 seconds, no fuel is consumed on the hybrid vehicle as a result of it operating in electric only mode. It can also be seen how, over the course of the NEDC, the fuel consumed in both the conventional and hybrid vehicle increase as a result of the cold-start and a similar percentage increase is observed between the conventional and hybrid vehicles at the same temperature. Of note however is that the increase in fuel consumed by the hybrid vehicle does not originate from the inactive period of the engine. Instead the extra fuel is consumed in the early phase and is likely to be a result of the extra load of charging the batteries. If one observes the lubricant temperature profile for the two vehicles in Figure 2.17 [68], it can be seen that the temperature of the lubricant at the beginning of the hybrid period for the two vehicles is similar ( $\approx 52$  °C). Thus, the extra fuel consumption for the hybrid vehicle will not have originated from a lubricant viscosity effect but is more likely from the extra load placed on the engine from battery charging. Further examination of Figure 2.17 [68] does show that the period where the hybrid vehicle's I.C. engine is inactive does reduce the lubricant temperature by approximately 20 °C relative to the conventional vehicle; however, this appears to make negligible impact on the fuel consumption. This is most likely to be as a result of the lubricant viscosity being more consistent at higher temperatures.

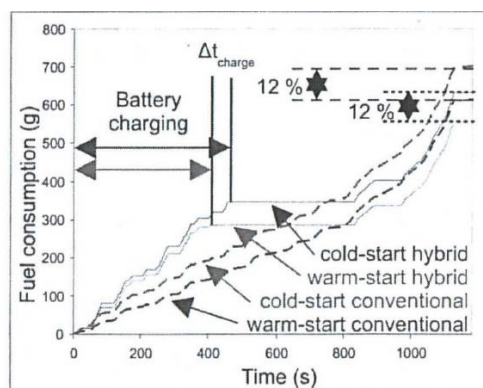


**Figure 2.16:** Cumulative fuel consumed over the NEDC for both a 20 °C start temperature and a 90 °C start temperature for a S.I. engine with and without a hybrid propulsion system. Reprinted with permission from SAE paper 2011-01-1747 ©2011 SAE International and SAE of Japan [68]

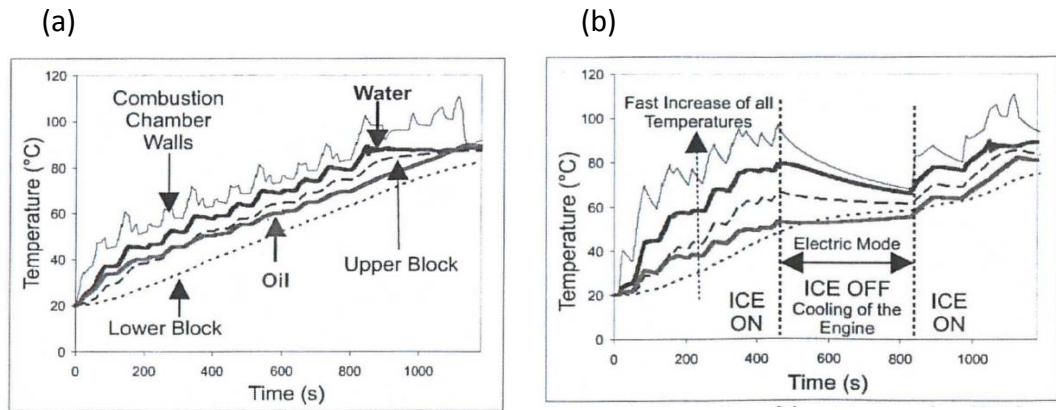


Figure 2.17: Engine temperatures during an NEDC warm-up cycle from 20 °C for (a) conventional S.I. engine and (b) S.I. engine equipped with an electrically powered hybrid propulsion system. Reprinted with permission from SAE paper 2011-01-1747 ©2011 SAE International and SAE of Japan [68]

While stop-start technology is becoming popular with manufacturers, Bent et al. [11] concluded that it does not mitigate the need for improved thermal management in the warm-up phase of an engine. When fully warm, stop-start technology is an attractive option but during cold-start, there still exists a need to achieve optimum lubrication and combustion conditions as soon as possible, making stop-start technology less attractive in this phase of engine operation while the work of Dubouil et al. [68] has highlighted the effect of increased battery load on fuel consumption. To gain further benefit from the use of stop-start technology and the use of hybrid powertrains it would be desirable to increase the thermal energy that is retained in the lubricant. Such a strategy would enable the idling fuel consumption of the I.C. engine to be mitigated while also achieving an accelerated lubricant heating rate relative to the warm-up rate of the current stop-start scenario. To achieve such an objective requires the thermal losses from the lubricant to the block structure to be reduced and, as stop-start technology becomes more commonplace, the need for such a solution will increase.

### 2.3.5.5 The limitations of active control methods

The preceding section demonstrated that from both a fuel consumption and emissions perspective, potential does exist to improve engine cold starts. However, it is worth considering both the limitations of the research investigations and the subsequent issues with implementation of strategies at a mass-production level.

Engine management strategies are both complicated and outside the remit of this thesis but they are nonetheless well developed and based on the known thermal behaviour of the whole engine system. By virtue of introducing new technology and control strategies, the thermal balance of the engine and subsequent interactions between different sub-systems is significantly altered. This can cause conflicts with engine management systems and limit the effectiveness of strategies being trialled.

Such issues were highlighted by Burke et al. [69] where the merits of variable coolant flow and the possibility of EGR cooling with the lubricant rather than with the coolant were discussed. NO<sub>x</sub> emissions for engines generally increase with increasing temperature, and a strategy typically employed to limit NO<sub>x</sub> emissions is to delay injection timing as the engine warms up. Burke et al. [69] highlighted that in instances where experimental data have proven the engine to be hotter, NO<sub>x</sub> emissions decreased unexpectedly. On examination of the combustion behaviour, it was found that the control strategy was too sensitive to the engine temperature and was thus advancing the injection timing too rapidly, resulting in a reduction in NO<sub>x</sub> emissions but also leading to less favourable fuel consumption. Burke et al. also highlighted that the engine temperature was based on a single temperature measurement in the head and that such an approach is not valid in the transient phase of warm-up where dynamic temperature gradients exist.

The work of Burke et al. [69] focused on changing the combustion characteristics of the I.C. engine to achieve greater thermal efficiency. Comparatively, the work of this thesis is focused on achieving greater optimisation and use of the energy released from combustion to improve the warm-up rate of the engine. Consequently, detailed investigations into combustion profiles and engine timing are beyond the scope of this thesis. Nevertheless, it does serve to reinforce the high levels of interactions discussed at the beginning of Section 2.1 and the need to consider the wider implications of any strategy.

### **2.3.6 Use of alternative materials to reduce the thermal mass of the engine**

It has been established that there is a desire to reduce the duration of the warm-up phase of the I.C. engine to improve emissions and fuel consumption. The approaches discussed thus far have all attempted to either adjust the energy balance of the engine in such a way that the thermal energy is directed to the thermal masses that require it most (i.e. the lubricant). An alternative approach however is to reduce the quantity of energy needed to raise the temperature of a thermal mass (be that the coolant, lubricant or engine block). In the context of the lubricant system in isolation, this would require reducing the volume of oil in the lubricant circuit. The work of Jarrier et al. [16], Trapy and Damiral [20] and Law et al. [67] have all investigated the merits of reducing the volume of lubricant in the engine. Jarrier et al. [16] investigated the effect of a reduced lubricant volume in a 1.9 litre diesel engine and found in simulations that reducing the volume of oil in the system from 5 litres to 1 litre increased the lubricant temperature by 7 °C when observed at 3 and 6 minutes into the NEDC. After 20 minutes, the improvement reduced to 3 °C but the large increase in temperature early in the cycle is critical when the lubricant viscosity is more sensitive to temperature. Such changes were reflected in a reduction in FMEP of just over 5% during the first 6 minutes. Similarly Trapy and Damiral [20] predicted

that reducing the lubricant mass from 3.5 kg to 1 kg would reduce the warm-up time from 23 minutes to 19 minutes. The exact lubricant used in the work wasn't specified but if density data for commercially available 5W-30 lubricant at 20 °C (presented in Figure 3.14) are used this equates to a reduction in lubricant volume from 4.1 litres to 1.2 litres and is therefore comparable with the work of Jarrier et al. [16]. Law et al. [67], using their novel sump design discussed in Section 2.3.5.3 effectively facilitated a temporary reduction in the effective oil volume in the system and saw main gallery lubricant temperatures, relative to the standard baseline, rise by up to 12 °C as a result during the first two minutes of the test when trialled at a start temperature of -10 °C. Such changes saw the engine FMEP reduce by 50 kPa over the first two minutes of the test; a reduction of 10% and therefore supporting the work of Jarrier et al. [16]. After this point, the FMEP results from the experimental design converged with the baseline configuration owing to the lubricant viscosity being less sensitive to changes at higher temperatures. The issue with such an approach is the uncertainty as to what effect it could have on reliability. While Law et al. [67] carried out their work experimentally, Trapy and Damiral [20] and Jarrier et al. [16] based their work on computational simulations owing to the risk of oil degradation and pump starvation making it practically unfeasible to operate an engine with such small volumes of lubricant [67].

If reducing the oil volume poses too great a risk to reliability, alternatively, one could attempt to reduce the thermal mass of the engine block. Such an approach could prove beneficial in two ways:

1. Reduce the mass of the engine block and, by association, the vehicle and therefore reduce the fuel consumption by virtue of accelerating a smaller mass (the engine is estimated to account for between 20 % and 25% of the vehicle mass [70]). This is a similar argument to those proposed in the work of Yilmaz et al. [58] and Dahotre and Nayak [61] who argued that being able to remove the cylinder liners would reduce the engine mass and hence reduce fuel consumption.
2. Reduce the thermal mass of the engine and therefore reduce the energy and time required to bring the block up to full operating temperature. This would therefore reduce the heat flux from the lubricant to the block structure and have a positive effect on frictional losses.

If one focuses on point 2 in the above list, the thermal mass is defined as  $mCp$ , where  $m$  is the mass of the object or fluid in question and  $Cp$  is the specific heat capacity. Thus, in order to reduce the thermal mass of the engine block, a material of either a lower specific heat capacity must be used or the mass of the block must be reduced. Attempts to reduce the thermal mass of the engine block have included replacing typically used aluminium casting alloy (an example being A319 [71]) with magnesium alloys [70] or using polymer composite materials [72-74].

Table 2.4 compares the material properties of aluminium A319 casting alloy with magnesium AMC-SC1 and a typical epoxy resin glass reinforced composite. One must remember that the primary aim of the work was to reduce the thermal mass of the engine block and therefore both reduce the mass of the vehicle but also reduce the warm-up time of the block owing to the reduced thermal mass. The practicality of achieving such an objective requires careful consideration of the material requirements of such an application. The I.C. engine subjects components to high temperatures and consequently creep behaviour is of concern [73], as is cyclic loading [70]. Material modulus, particularly at elevated temperatures is therefore critical.

**Table 2.4: Comparative physical properties of magnesium AMC-SC1 alloy and aluminium A319 alloy**

<u>Property</u>	<u>Aluminium A319 alloy</u>	<u>Glass fibre reinforced epoxy resin *</u>	<u>Magnesium AMC-SC1 alloy</u>
Ultimate tensile strength (MPa)	250- 280** [A]	138 – 241 [C]	184 – 206 [D, E]
Thermal conductivity ( $W m^{-1} K^{-1}$ )	130 [B]	0.4 - 0.55 [C]	106 [D]
Young's modulus (GPa)	74 [A]	15 – 28 [C]	44 – 46 [D, E]
Density ( $kg m^{-3}$ )	2720 [B]	1750 – 1970 [C]	1790 [D]
Specific heat capacity ( $J kg^{-1} K^{-1}$ )	1000 [B]	1000 – 1200 [C]	1000 - 1010 [C]
Thermal diffusivity ( $m^2 s^{-1}$ )	$6 \times 10^{-5}$ [B]	$1.86 \times 10^{-7} - 3.14 \times 10^{-7}$ [F]	$5.92 \times 10^{-5} - 6.82 \times 10^{-5}$ [F]

- NB: [A] Values Taken From Materials Handbook, Volume 2 [75]  
 [B] Value From Thermophysical Properties of A201, A319 and A356 Aluminium Casting Alloys, Overfelt, R et al. [71]  
 [C] Value from CES material database [57]  
 [D] Value Taken From AMC-SC1 Data Sheet [76]  
 [E] Value taken from AMC-SC1: A New Magnesium Alloy Suitable for Powertrain Applications [70]  
 [F] Calculated from values presented in table  
 \* All properties will depend on fibre orientation and fibre volume fraction and therefore account for the broad range presented  
 \*\* Value presented is for a T6 heat treated specimen

If one first considers the merits of trying to replace the conventional choice of an aluminium alloy with a glass fibre reinforced polymer (GFRP), it can be seen from Table 2.4 that the density of the GFRP is at least 27% lower than that of aluminium. Thus, while the volumetric heat capacities of both the GFRP and magnesium alloy

are lower than the aluminium alloy, so too is the stiffness of both materials. Consequently, the structural requirements of the intended application must first be satisfied before the thermal masses are compared.

The BRITE Engine Project of 1990 [72] aimed to develop a polymer composite demonstrator engine with the aim being to both reduce the engine's mass and subsequent warm-up time relative to a conventional engine of the time (a four cylinder 1 litre Ford S.I. Lambda engine). However, research at the time indicated that the combination of high loads, particularly at the bearings, and high temperatures would make manufacturing an engine entirely out of polymers unviable [72, 73]. Consequently the design philosophy shown in Figure 2.18 [72] was adopted where the central core of the engine containing the cylinders and coolant jacket were made of conventional aluminium alloy and the outer walls manufactured from glass fibre reinforced polymers. While a successful prototype was manufactured, the approach did limit the potential to reduce the mass with no significant reduction in mass from the baseline 'Lambda Engine' that had a mass of 89 kg [72].

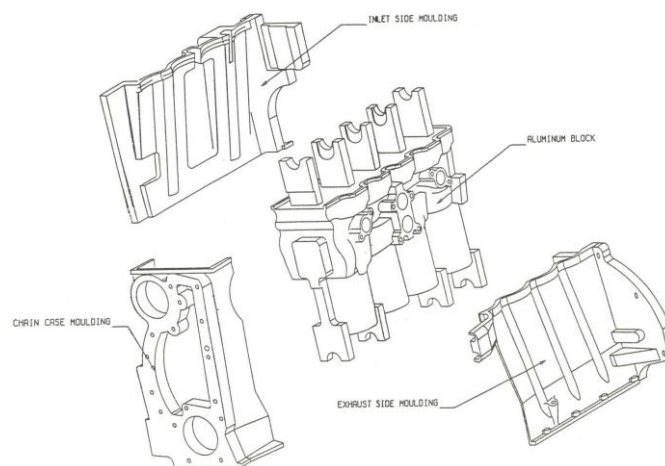


**Figure 2.18: Exploded view of the BRITE Engine's modular components [72]**

Despite a conservative approach to the design, the BRITE engine did indicate a reduction in the warm-up time of the engine relative to the baseline engine, as shown in Figure 2.19 [72]. It can be seen that the BRITE engine achieved a reduction in warm-up time of between 6% and 19% for the coolant which also resulted in hydrocarbon emissions reducing by up to 20% during warm-up. There is no information provided in relation to the lubricant temperature but the increased coolant temperature will have both improved combustion quality and reduced friction between the pistons and liners and this is likely to have accounted for the reduced hydrocarbon emissions.

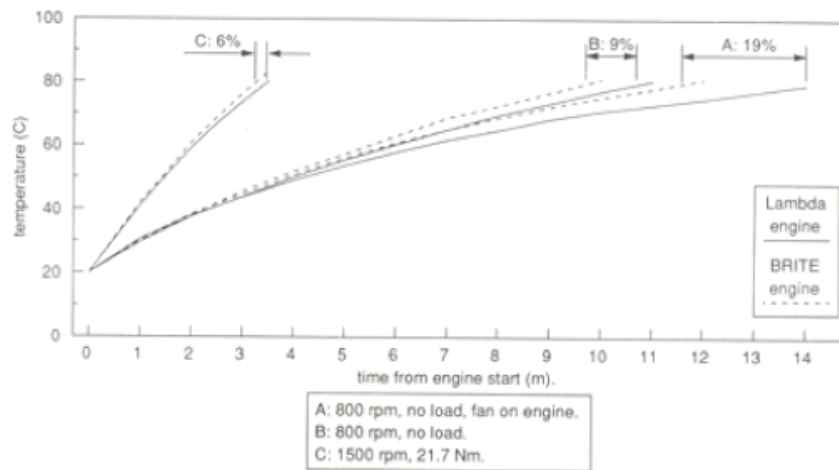


**Figure 2.19: Comparative coolant warm-up times for the BRITE engine compared to an equivalent conventional Lambda engine [72]**

Guimond and Muench [74] developed the concept of the BRITE engine as shown in Figure 2.20 [74]. There is no evidence of this design having been taken any further than the concept stage and so a comparison of mass and thermal performance is not possible. However both Guimond and Muench [74] and Bowman et al. [72] (the BRITE engine) retained a metallic core owing to component operating temperatures and such requirements therefore limits the potential engine mass reduction achievable.

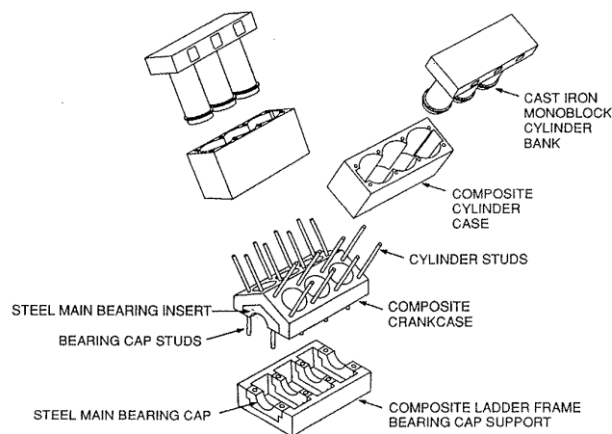


**Figure 2.20: Exploded View of the composite V6 concept. Reprinted with permission from SAE paper 920084 ©1992 SAE International [74]**

From the works listed above, it can be seen that the internal combustion engine is a harsh environment for polymeric materials to operate in. The need for the material to withstand high operating temperatures and high cyclical loads means that there is a limited range of candidate materials while stiffness and strength requirements generally limit any mass reduction possibilities. In addition, there is a need for the materials to be compatible with both engine lubricant and engine coolant [72] with

the work of Krigbaum [77] having demonstrated the deterioration in material properties after exposure to both engine lubricant and engine coolant.

Consequently, an alternative approach is to utilise an alternative metallic alloy. Relative to the use of polymeric materials, the reduced stiffness is generally not as significant. Magnesium alloys are a potential candidate for such an application and a specific alloy for use in engine blocks has been developed. The properties of the AMC-SC1 alloy that was developed by Bettles et al. [70] are listed in Table 2.4. It can be seen that relative to a typical aluminium alloy, the stiffness of the magnesium alloy is 40% less (rather than the 80% reduction with GFRP). This, combined with a density that is 35% lower than aluminium and a similar specific heat capacity, makes thermal mass reduction potentially more viable. However, creep resistance has been a limiting factor in magnesium alloy usage [78]. The work of Bettles et al. [70] was focused on developing a magnesium alloy that presented more favourable high temperature properties. The authors suggested that the new grade alloy compares favourably with aluminium alloys although the full merits of the alloy in an engine application could only be appraised if a prototype block was manufactured and tested.

Thus, the work of Bowman et al. [72] has shown how the use of polymeric materials in the construction of an I.C. engine does have a significant effect on the warm-up rate of the fluids in the engine despite the presence of the aluminium alloy core. However, the availability of lighter metallic alloys, such as those discussed by Bettles et al. [70] that are capable of coping with the structural loads presents an additional method of reducing the thermal inertia of the engine and hence improving warm-up rates. There is therefore scope for further advancement in knowledge in understanding the relative significance of low thermal conductivity materials (i.e. insulating materials) and low thermal inertia materials (i.e. light weight and low specific heat capacity materials) to improve the warm-up rate of the I.C. engine.

### **2.3.7 Applications of phase change materials to improve engine thermal efficiency**

The use of phase change materials (PCMs) in energy conservation and management is a field of research that has grown in interest in recent years. However, before the use of PCMs in increasing automotive cold-start efficiency is discussed, it is necessary to understand their characteristics.

To raise the temperature of a body requires energy; such energy is termed sensible heat and is defined in Equation 2.11.

$$Q_{sensible} = mC_p\Delta T$$

Where  $Q_{sensible}$  = The energy stored in the body as a result of the temperature rise (J)  
 $m$  = The mass of the body (kg)  
 $C_p$  = The specific heat capacity of the material (J kg<sup>-1</sup> K<sup>-1</sup>)  
 $\Delta T$  = The increase in temperature of the body (°C)

**Equation 2.11: Sensible heat contained within a body as a result of a temperature rise**

The use of standard insulation materials results in reduced heat flow away from any source. In comparison, phase change materials offer the potential not only to reduce heat flow, but also to store heat via a change of phase. When a material undergoes a phase change, latent heat is either stored or expelled by the material as a result of a change in phase. A summary diagram of such a process is shown in Figure 2.21; the region of the graph where energy input is causing no change in temperature is the phase change region. The phase change process therefore facilitates a high energy density storage solution that is particularly useful in applications where space and mass need to be conserved [41].

Such a characteristic may be useful in reducing cold-start inefficiency as the additional energy storage in the phase change material can be used to store rejected heat from the engine during running which can then be later liberated (limiting the temperature decrease while the phase change occurs) while the engine is non-operational. Such an approach will be beneficial given consumer trends to make multiple short trips with a relatively short interval between the engine stopping and re-starting (Section 2.1). The use of phase change materials is a strategy that aims to reduce the inefficiencies associated with cold starts by increasing the temperature at engine re-start (rather than increasing the rate of warm-up). While the release of the latent heat as the temperature decreases may be beneficial, the energy absorbed to facilitate the same phase change on heating could prolong the warm-up period and therefore have a negative effect. Thus, in the following section research into the use of PCMs to improve the cold-start performance of I.C. engines is reviewed before the challenges of implementing such solutions into automotive applications are also discussed. As a result of such challenges, attempts to utilise PCMs in improving the cold-start efficiency of I.C. engines were not pursued as an area of investigation. However, it is felt that such technology may be of benefit and there is scope for future work in such areas.

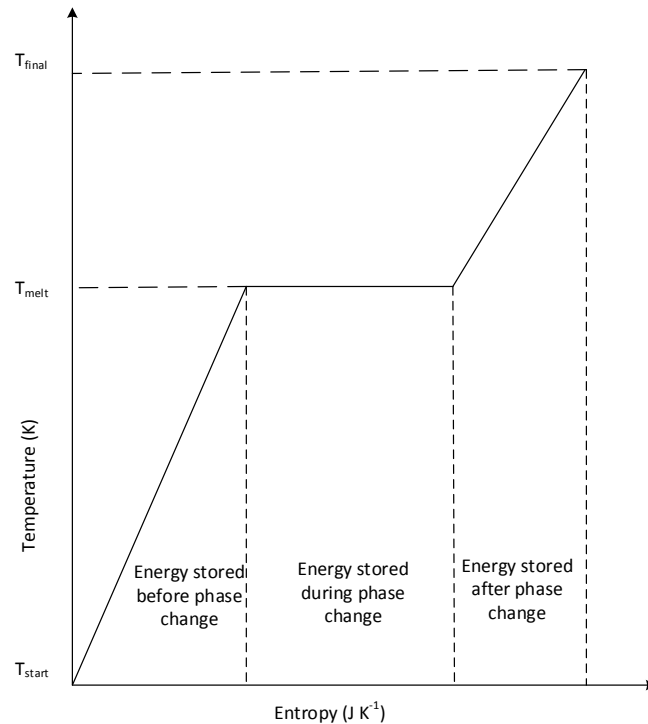


Figure 2.21: Summary diagram of temperatures during a phase change

### 2.3.7.1 Use of phase change materials on the engine and auxiliary systems

The work of Kauranen et al. [15] was briefly referred to in Section 2.2 owing to their work utilising the exhaust stream as an energy source. Kauranen et al. experimented with using a latent heat accumulator (consisting of a phase change material) combined with an exhaust gas heat recovery unit to improve the warm-up times for diesel fuelled mail delivery vehicles. The aim was to find an alternative to the use of an auxiliary fuel burning heater which, while improving warm-up times, ultimately has any benefit to fuel consumption heavily impeded by the burning of additional fuel in the process. In this work, temperatures and emissions were monitored with three configurations;

- A baseline system with an auxiliary fuel burning heater (AH) and no exhaust gas heat recovery unit (EGHR) and no latent heat accumulator (LHA).
- No AH, EGHR active but a discharged LHA.
- No AH, active EGHR and a charged LHA.

Results from this work are shown in Figure 2.22 [15]. A key observation is the comparative performance of the system when the LHA is charged and discharged. Between these two tests (where there is no fuel consumption from the auxiliary fuel burning heater to consider), it can be seen that the emission levels dramatically increase as a result of the LHA being discharged. Such a trend was also reflected in the fuel consumption. The fuel consumption in the instance where the LHA is discharged was  $9.94 \text{ l (100 km)}^{-1}$  whereas this was reduced to  $8.94 \text{ l (100 km)}^{-1}$  when

the unit was charged. Such a trend reinforces the concern that any form of phase change material or latent heat accumulator is best suited to a ‘warm start’ scenario and that if a truly cold-start is being made, the additional thermal inertia could lead to higher emissions or fuel consumption.

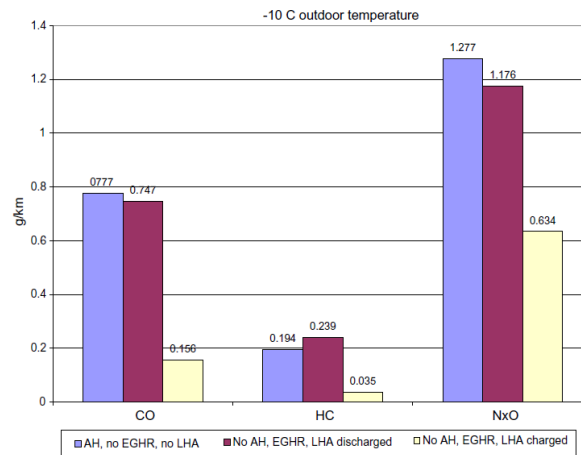


**Figure 2.22: CO, HC and NOx emissions for a 1.9 litre diesel engine running an exhaust gas heat recovery unit and latent heat accumulator in differing conditions [15]**

The work of Gumus [44], referred to in Chapter 1, focused on attempts to improve emission quality while the catalytic converter was below its light-off temperature and therefore inactive. To achieve this, a phase change material ( $\text{Na}_2\text{SO}_4 \cdot 10 \text{H}_2\text{O}$ ) was coupled to the coolant circuit to enable the coolant to charge the device during running and to then act as a heat transfer medium to maintain the engine temperature during its inactive period. Figure 2.23 indicates that preheating the engine via the coolant circuit can reduce carbon monoxide (CO) emissions by as much as 50% and HC emissions by 15% at low temperatures, again highlighting the importance of a well optimised cylinder liner temperature. The results therefore indicate that such a strategy is particularly effective at addressing sub-optimal combustion conditions caused by cylinder liner quenching.

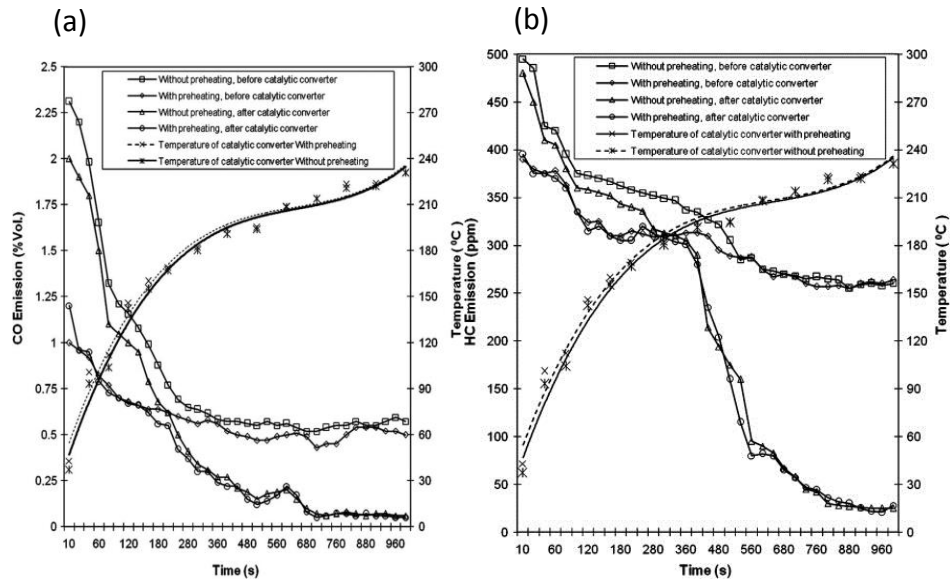


Figure 2.23: Effect of temperature on catalytic converter efficiency of (a) HC emissions and (b) CO emissions [44]

Korin et al. [41] investigated using phase change materials to directly improve the performance of the catalytic converter with the intention being to reduce the rate of temperature decrease during periods of none operation and hence reduce the warm-up time when the engine was restarted. The work looked at ways to best utilise the thermal energy being released by the catalytic converter with emphasis placed on achieving as high a contact area between the PCM and heat source as possible while minimising ambient losses. Thus, the solution shown in Figure 2.23 [41] was chosen. In addition, the outer surface of the combined catalytic converter and PCM was insulated in a wool fibre jacket. The approach showed promise, with the system able to stay above the light-off temperature for approximately four hours after the engine had been switched off.

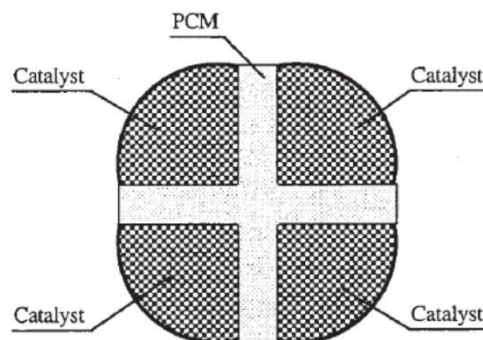


Figure 2.24: Schematic phase change material incorporated into a catalytic converter in order to maximise heat transfer to the PCM and minimise ambient losses [41]

### 2.3.7.2 Use of phase change materials specifically targeting lubricant systems

Stouffer et al. [64] carried out extensive work in improving cold starts for the U.S. Army. Their work examined, in detail, the merits of applying phase change materials to both the oil sump and also the oil filter of an 8.3 litre, 6 cylinder diesel engine. By insulating the oil filter in a phase change material, it was anticipated that the oil filter would heat up faster. Were this to be the case, oil entering the engine would instantly receive some element of heating, helping the lubricant reach its optimum temperature sooner.

Owing to the architecture of the engine, the oil sump is always very low down, thus exposing it to low ambient temperatures, with Samhaber et al. [14] predicting the external surface of the head to be 15 °C higher than that of the outer surface of the lower block. This, combined with a high surface area and high convective heat transfer coefficients at high vehicle road speeds, makes the sump a potential area for high heat losses from the lubricant. Hence, the aim of this work was to limit heat loss from the sump by encasing it in a phase change material. Using a phase change material with the optimum structure and thermal properties for the application intended is key to achieving success. Phase change materials exist in a range of forms, although a solid-to-liquid PCM is commonplace and was used in this research. Alternatives, such as solid- solid phase change materials do exist. At the point of peak operating temperature when the engine system is shut down, it is desirable for the entire volume (thickness) of the PCM to have undergone the phase change and therefore for the minimum of thermal gradients to exist across the thickness of the PCM. If this is not the case and the phase change material furthest from the heat source has not undergone the phase change, the system is being underutilised and the expected benefits will not be realised.

Stouffer et al. combined a theoretical model for optimising the PCM energy storage system design with experimental verification. The model assumed that the ambient temperature was constant at -18 °C and that the lubricant temperature started at 95 °C (these values being based upon experimental data). In their simulation work, Stouffer et al. [64] found that by ensuring the PCM was of a high thermal conductivity, charging times could be reduced and the PCM maximum temperature was increased, enabling it to provide a heating effect to the lubricant for longer. 'Aluminium Flexcore' (a honeycomb structure made of aluminium grade 5052) was added to the PCM assemblies to enhance the thermal conductivity; the temperature of the material nearest the hot lubricant was increased by 30 °C and the temperature differential across the phase change material was reduced from around 100 °C to just over 10 °C compared to running the phase change material without the 'Aluminium Flexcore'. Furthermore, the higher temperatures were achieved in 3

hours, as opposed to the 6 hours required when running the system without the 'Aluminium Flexcore'.

Another measure to ensure a high thermal conductivity in the PCM was the use of a gel-based phase change material over a foam-based phase change material. The work of Sharma et al. [79] and Farid et al. [80] also demonstrated that a high thermal conductivity was necessary for a phase change material to be effectively utilised. However, this does present a compromised situation as the high thermal conductivity phase change material can increase convective losses to ambient if used in a jacketing application. One solution is to effectively insulate the phase change material from the ambient using a conventional insulating material. In the case of the work of Stouffer et al. [64], an 11 mm thick layer of polyisocyanurate insulation with a thermal conductivity of  $0.022 \text{ W m}^{-1} \text{ K}^{-1}$  and a density of  $30 \text{ kg m}^{-3}$  was used to reduce ambient losses. This work shows clear promise, with both oil sump and oil filter insulation with PCMs resulting in a marked increase in lubricant temperature, as shown in Figure 2.25 [64] for the lubricant in the oil filter.

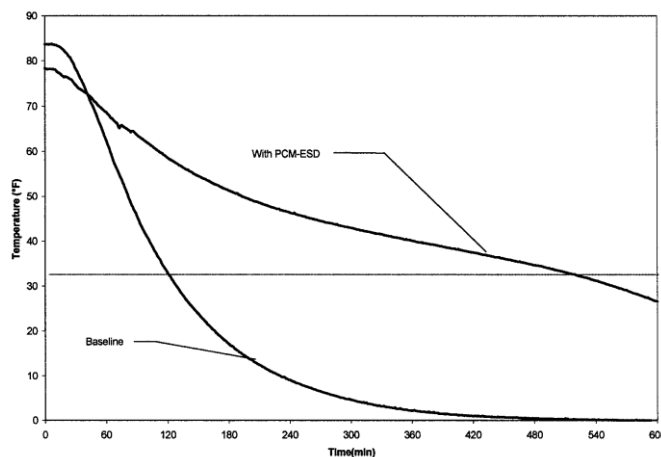


Figure 2.25: Measured oil temperature over time in the oil filter when in a cold chamber at  $0^\circ \text{F}$  ( $-17^\circ \text{C}$ ) both with and without phase change insulation [64]

When looking at the lubricant temperatures in the oil filter, it can be seen that the lubricant temperature, even when exposed to ambient temperatures of  $-17^\circ \text{C}$ , is still above  $0^\circ \text{C}$  some six hours after the baseline, un-insulated engine has reached this temperature. Six hours is approaching a time frame that may span a typical working day and thus, PCMs may offer considerable improvements during a return commute as the initial lubricant fed into the system (during the outgoing commute) is still at an elevated temperature.

The work reviewed suggests that phase change materials present a real opportunity to improve lubricant system warm-up times. However, the addition of phase change materials does add a considerable thermal mass to the system being considered. To investigate this concern, data were taken from the work of Stouffer et al. [64] for two tests to investigate if the additional thermal mass of the PCM had a detrimental

effect on lubricant warm-up. Figure 2.26 [64] shows the warm-up and cool down curve for engine lubricant in two configurations. Figure 2.26a relates to a situation when the engine had an 11 mm thick covering of polyisocyanurate insulation applied to the outer surface of the sump while Figure 2.26b relates to a situation where the PCM was first applied to outer surface of the sump and was then insulated from ambient with polyisocyanurate of 11 mm thickness. Critically, it can be seen that there appears to be negligible difference in lubricant warm-up rate as a result of the presence of the PCM, although there is a clear benefit in a reduced cool down rate. It is worth considering why this may be the case; the transient heating of the oil sump itself is likely to be sufficient to decouple the PCM charging process from the lubricant heating process. The PCM will not start charging until the outer surface temperature of the oil sump is sufficiently hot to facilitate heat transfer to the PCM. Consequently, in the warm-up phase, when the outer wall temperature of the sump is cold, the PCM will not charge and charging only commences once significant heat is being dissipated from the sump. This heat would be dissipated to ambient if the PCM was not present, and so it can therefore be concluded that the PCM does not have a significant effect on limiting lubricant warm-up rates. However, such transient effects do need consideration when deciding where to implement PCMs and are likely to make the use of PCMs internally within the engine a concern.

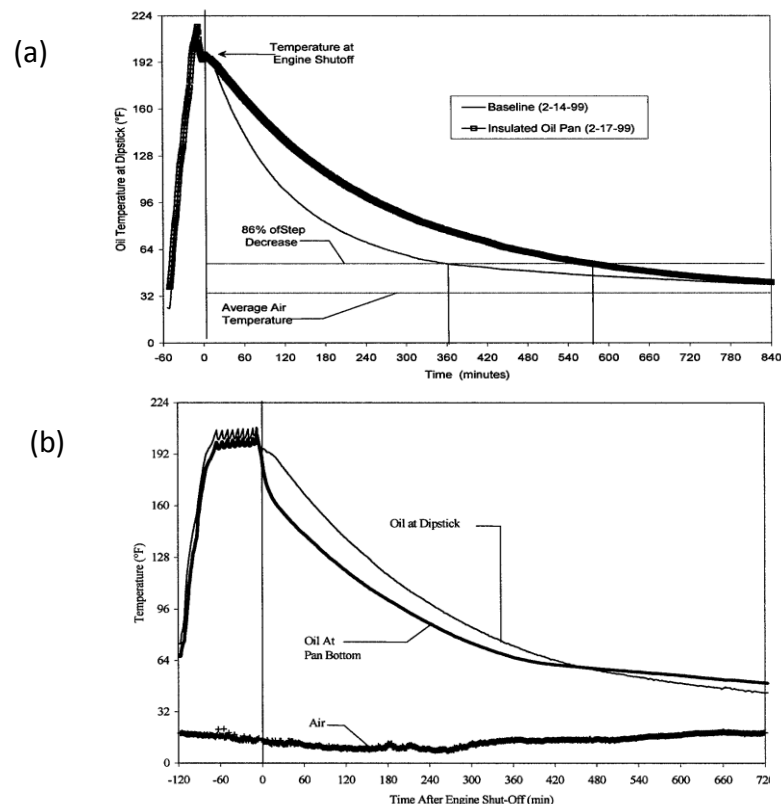


Figure 2.26: Comparative lubricant warm-up and cool down curves for an engine when (a) standard polyisocyanurate insulation is applied to the outside of the oil sump and (b) when a PCM and polyisocyanurate insulation is applied [64]

### 2.3.7.3 The challenges and issues of utilising phase change materials

The use of PCMs in relation to improving engine cold starts has been discussed at length with a range of possible methods shown. However, aside from the thermal considerations that have been presented thus far, there are other factors that warrant consideration.

The range of phase change materials is vast, with many having no specific trade name. Instead they are typically referred to by their composition. The reader is encouraged to consult the work of both Sharma et al. [79] and Agyenim et al. [81] for a comprehensive list of the many PCM variants available.

A critical factor in the selection of a phase change material for a particular application is that of the phase change temperature. In order for the benefits to be realised, it is essential that the phase change temperature is within the operating temperature window. The selection of the phase change materials, with this requirement satisfied, will also be affected by economic considerations, chemical compatibility and ease of installation. A summary of the classes of PCMs is shown in Figure 2.27 [80].

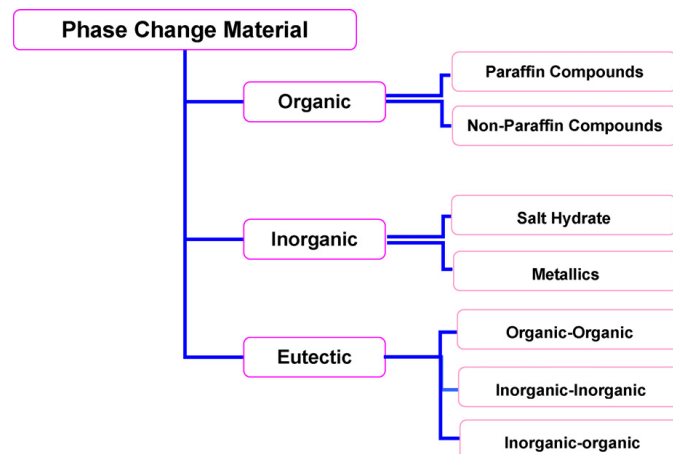


Figure 2.27: Breakdown of phase change materials into different classes [80]

Currently, the most actively used category of PCMs remains the salt hydrates, owing to their higher thermal conductivities and latent heat values with up to  $279 \text{ kJ kg}^{-1}$  being reported [79]. Such a figure is representative of the high energy density storage available, particularly when one considers that the typical specific heat capacity of engine lubricant oil varies from  $1.8 \text{ kJ kg}^{-1} \text{ K}^{-1}$  to  $2.2 \text{ kJ kg}^{-1} \text{ K}^{-1}$  across the working temperature range. They are also economically competitive and are an established technology relative to other developing technologies such as the eutectics.

A major obstacle to be overcome when using salt hydrates in production vehicles would be the degradation over time of their ability to store heat [79, 80, 82]. This is a

concern reported by a range of authors in the literature, although few give any specific information about the rate of degradation. During the phase change, the salt hydrate undergoes a chemical reaction, changing from a hydrated salt (one chemically bonded to water) to either an anhydrous salt and water or to a hydrated salt with fewer moles of water. During the phase change, the issue of incongruent melting can arise, where the water released in the reaction is insufficient to fully dissolve the solid phase. Consequently, the anhydrous or less hydrated salt is unable to be fully dissolved and the high density salt sinks to the bottom of the liquid phase. Such a reaction is chemically irreversible meaning that when the liquid phase reaches its phase change temperature on cool down, the solid salt will not chemically revert back to the original solid PCM and can take no further part in phase change [79]. The lifespan of the salt hydrate is dependent on its application, but across the literature, there appears to be no degree of certainty beyond 1500 cycles. At this point, various sources report a reduction in latent heat storage capacity. Sharma and Sagra [82] reported a reduction of 73% in latent heat storage capacity over 1000 cycles using  $\text{Na}_2\text{SO}_4 \cdot 10\text{H}_2\text{O}$  and also reported a degradation in performance when using  $\text{CaCl}_2 \cdot 6\text{H}_2\text{O}$  after only 2 cycles. In the specific automotive application of Kauranen et al. [15], data were presented for 11 thermal cycles with no indication of degradation. Clearly a life span of 1000 cycles is well within the lifespan of a standard car (particularly in light of André's work [18]) and therefore, before such technology can be widely implemented, these issues of achieving a workable lifespan must be addressed. However, while the literature reports this as a problem primarily associated with salt hydrates, the work of Shukla et al. [83], together with that of Sharma et al. [84, 85] suggests that this is also an issue with paraffin wax based PCMs. Over 500 cycles, Shukla et al. [83] reported degradations in latent heat capacity of paraffin waxes of 18% and 16% from an initial value of  $130 \text{ kJ kg}^{-1}$ . Sharma et al. [85] found the situation to be even more pronounced, with a reduction of latent heat capacity of 31% from an initial value of  $184 \text{ kJ kg}^{-1}$  over 500 cycles. When extended to 1500 cycles, this reduction continued to a 35% reduction over the initial value. Sharma et al. [85] argued that the most likely explanation for this phenomena in paraffin waxes is moisture absorption. Even before the material is subject to thermal cycling, Shukla et al. [83] reported wide variations in material properties in relation to the phase change temperature and latent heat of fusion, particularly with salt hydrates. Such an issue was attributed to the presence of impurities in the materials that are to be expected when using commercial grade materials.

Regardless of long term durability of the phase change material, there exist numerous logistical issues to overcome in consideration of implementation of phase change materials in production vehicles. These include:

- Corrosion issues, with salt hydrates being reported as corrosive to metal containers by Salunkhe and Shembekar [86] and Sharma and Sagra [82], while Sharma et al. [79] reports paraffin waxes as corrosive to polymer containers.
- The need to enhance the thermal conductivity of the phase change material is highlighted across the literature by Farid et al. [80] , Agyenim et al. [81] and Salunkhe and Shembekar [86]. The work of Stouffer et al. [64] using 'Flexcore' aluminium to aid thermal conductivity also supports the argument.
- Another general concern of all phase change materials is the phenomena of sub cooling and super-cooling. Super-cooling in particular has been cited as being undesirable [79]. This is where a material remains in its high-temperature phase even when cooled below the phase transformation temperature (this occurs due to there being no nucleation sites for the phase change to occur). It has been reported that should this occur, then the retrieval of useful energy from the PCM is very difficult. Sub cooling is simply the degree of cooling of a material below its saturation temperature at a given pressure. This is reported as being undesirable [80, 81] presumably because any degree of sub cooling stores thermal energy input as sensible heat (resulting in a temperature rise) as opposed to a latent heat which results in a change of phase.
- Economic considerations must always be considered, with salt hydrates being reported as the most economically viable on a commercial level.

It is a result of the above issues that, while the work reviewed in this section does indicate that PCMs can reduce the cool-down rate of the I.C. engine and the catalytic converter, there is uncertainty surrounding the longevity and reliability of such technology. In addition, with such a vast range of PCM materials available, the success of using PCM materials to aid the cold-start efficiency of the I.C. engine would be highly dependent on choosing a PCM with a phase change temperature within the operating range of the target destination on the vehicle (i.e. the engine or the catalytic converter). This temperature would be variable between different automotive markets depending on geographical location and the specific vehicle in question. It is therefore not felt that such an approach is the optimum way to improve the cold-start performance of the I.C. engine although such an objective may be the subject for future work.

## **2.4 The methods of research and their limitations**

The review of the literature has highlighted a range of possible methods to research improvements to the efficiency of I.C. engines. The approaches taken have been varied and can be broadly placed into three categories, namely:

- Theoretical modelling.
- Engine test bed experimentation.
- Vehicle implemented experimentation.

The nature of the research being conducted will dictate which methodology is most applicable with a summary table of the methods used in the literature shown in Table 2.5. Where experimental and computational methods have been used in the same publication, indicative levels of agreement achieved between simulations and experimental results are highlighted. The correlations between experimental and computational simulations appear to indicate that variations of up to 5 °C are acceptable in the simulation of the I.C. engine during transient warm-up, although some works do report variations that are higher.

There are also instances where experimental engine test bed methodologies have been used in conjunction with vehicle implemented real world driving. However it is not possible to reliably compare data sets from real-world driving and engine test bed conditions. As is discussed in Section 2.4.3 real world driving does incorporate a greater number of variables including the capability of the driver. However, a particular problem associated with the comparison of such data-sets is the increased cooling effect as a result of vehicle speed. One such example is from the work of Goettler et al. [10] who carried out both real world driving and test bed experimentation. He subsequently found that the warm-up times of engines on a test bed were approximately one minute faster than those on a real world driving test. In addition, an engine being subjected to a drive cycle on a test bed procedure will be subjected to a specific speed and acceleration profile that will dictate the heat released from combustion. However the real-world, vehicle implemented testing, will have its speed and acceleration dictated by local traffic conditions and the two are therefore not comparable. However, there are advantages to both methods, as discussed in Section 2.4.2 and Section 2.4.3. Thus, the aims of the following section is to briefly discuss the advantages and limitations of the three broad research methodologies before defining the direction of research in this thesis.

**Table 2.5: Summary of investigative methods used by researchers to assess I.C. engine thermal behaviour and potential methods to improve fuel consumption and emission quality**

<u>Author</u>	<u>Theoretical modelling</u>	<u>Engine test bed</u>	<u>Vehicle implemented</u>	<u>Comment on repeatability between experimental and theoretical process</u>
Andrews et al. [9]				
Andrews et al. [17]				
Andrews et al. [38]				
Bent et al. [11]				

<u>Author</u>	<u>Theoretical modelling</u>	<u>Engine test bed</u>	<u>Vehicle implemented</u>	<u>Comment on repeatability between experimental and theoretical process</u>
Brace et al. [66]				
Burke et al. [69]				
Ciniviz et al. [59]				
Dubouil et al. [68]				
Finlay et al. [23]				
Gardiner et al. [19]				
Goettler et al. [10]				
Gumus [44]				
Jarrier et al. [16]				[A]
Kamo et al. [22]				
Kaplan and Heywood [87]				
Kauranen et al. [15]				
Korin et al. [41]				
Kunze et al. [12]				[B]
Law et al. [67]				
Leong et al. [37]				
Li et al. [21]				
Samhaber et al. [14]				
Shayler and Christian [39]				[C]
Shayler et al. [25]				
Shayler et al. [42]				[D]
Shayler et al. [45]				
Stouffer et al. [64]				[E]
Taymaz et al. [60]				
Trapy and Damiral [20]				
Uzun et al. [47]				
Will and Boretti [8]				[F]
Will [13]				
Zammit et al. [27]				[G]
Zammit et al. [65]				[H]
Zhao and Winterbone [43]				

[A] Correlation between theoretical and experimental results for the lubricant and coolant during warm-up simulations are of the order of between 2 °C and 4° C.

[B] The authors' work clearly stated that the model had not yet been fully refined and correlated to experimental data but peak discrepancies between experimental and theoretical data were approximately 13 °C

and 10 °C for the lubricant and coolant respectively during warm-up although broad trends were in agreement.

- [C] Temperature discrepancy between theoretical and experimental results typically of the order of between 3 °C and 4 °C although peak discrepancies observed reach 5 °C. Only steady state temperatures were presented and were in relation to the cylinder liner temperatures and therefore do not give indicative agreement about the simulation of the rest of the engine structure.
- [D] Typical agreement between experimental values of the bulk lubricant temperature and the bulk coolant temperature are of the order of 2 °C during warm-up simulations.
- [E] Simulation work carried out as initial design proof of concept and therefore does not represent fully the characteristics of the final developmental design. Key variations between the simulation and experimental work include the insulation thickness, variations in the PCM vessel thickness and the percentage coverage.
- [F] Experimental methodology is used to appraise a separate technology to the computational investigation. Discussion of the correlation between the experimental and computational results is therefore not applicable in this instance.
- [G] Temperature discrepancy between theoretical and experimental results typically of the order of 2 °C during warm-up. Where step changes in behaviour occur (e.g. introduction of pre-heated coolant), this increases to approximately 5 °C.
- [H] Temperature discrepancy between theoretical and experimental results typically of the order of 3 °C for steady state results. No correlation was provided for warm-up results.

#### **2.4.1 Computational Modelling**

The appeal of computational modelling, relative to other methods, is the relatively low cost and speed of such work [39, 42]. In addition, computational modelling enables investigation beyond the scope of what is physically possible. In the context of engine warm-up, it is possible to simulate the effect of constant viscosity lubricants or to vary different material properties in isolation of one another (e.g. varying specific heat capacity in isolation of thermal conductivity).

However, while appealing in terms of speed and cost, computational modelling does present limitations. Of note in the literature is the use of the lumped capacity

approach to engine modelling. Rather than use a fully discretised finite element model of the engine, the lumped capacity approach discretises the model into components, with each component being assumed to be uniform in temperature throughout and it has already been discussed in Section 2.2.2 how the Biot Number needs to be below 0.1 for such an assumption to be valid [39, 50-52]. The benefit of using the lumped capacity approach is a drastic reduction in computation time (43 hours for a warm-up simulation using FEA was reduced to 3 seconds using the lumped capacity approach [39]) and reduced processing capability requirements. Of note is the fact that in the review work considered, Jarrier et al. [16], Shayler et al. [39, 42], Samhaber et al. [14] and Kaplan and Heywood [87] have all adopted the lumped capacity approach. However, the lumped capacity approach limits the extent to which one can predict local temperatures. While this does not usually present issues, with Shayler and Christian [39] reporting maximum temperature difference of 4% between a lumped capacity prediction and a full FEA model, localised temperature predictions may be compromised. Thus, while, for example, the mean engine block temperature may be in agreement with experimental data, localised temperatures may not be and could have implications when investigating warm-up strategies in specific engine locations.

As computational power has increased, commercially available packages have been used to model the thermal behaviour of an I.C. engine during warm-up. Seider et al. [88] utilised GT-Suite to incorporate a finite element model within a lumped capacity model. Owing to the cylinder liner having considerable variation in temperature along the length of the bore, key components including the liner, piston and piston rings were modelled using a finite element model that was subsequently linked to a more conventional lumped capacity analysis. Similarly, there is evidence that local variation in fluid temperatures (be that the lubricant, coolant or combustion gases) are of concern in achieving accurate simulations of the thermal behaviour of the I.C. engine during warm-up. Consequently work has been carried out using computational fluid dynamics to increase the accuracy of the exchange of heat between fluids in the engine and the surrounding metal structure. However, a major obstacle to increased use of CFD remains cost and time. The work of Jasak et al. [89] focused on developing algorithms to reduce the time required to simulate the combustion process and associated heat transfer to the block of an I.C. engine. They reported simulation time frames of the order of weeks owing to the number of computational cells required (the work of Tiney et al. [90] reported their CFD model of an I.C. engine required a mesh consisting of 8.6 million cells). While the use of parallel computing by Jasek et al. [89] presented the opportunity to reduce this simulation to the order of days it also required the processing power of over 30 central processing units (CPUs). Thus the cost and computational time of such a methodology is still a significant limitation. In addition, where CFD has been

investigated (the work of Jasak et al. [89] being one such example), the focus of the investigation has usually been in relation to the heat exchange of the combustion gases with the cylinder wall. The work of Rakopoulos et al. [91] reported a comprehensive review into the selection of the optimum function to characterise the heat transfer from the combustion gases to the cylinder wall. There has however, been limited research into the use of CFD to investigate the effect of local fluid temperature variations on the warm-up of I.C. engines. The work of Uppuluri et al. [92] did discuss the need to incorporate the local fluid temperature into any simulation of engine warm-up and found that using CFD, the heat transfer coefficient between the engine block and coolant (although only the coolant heat transfer coefficients were reported) could vary by up to 30% from values calculated using conventional correlations (discussed further in Chapter 6).

A point highlighted in the use of CFD is the difficulty in creating an acceptable mesh to adequately cope with the moving boundary conditions (caused by the reciprocating motion of the piston changing the geometry cyclically) [89, 91]. Thus while there are indications that as computational constraints become less significant, there may be interest in utilising CFD and finite element to develop higher fidelity engine thermal models, the cost and time constraints of such methods are still limiting factors in the use of such technology and is therefore beyond the scope of this thesis. However, there is an accepted need to better incorporate the local fluid and surface temperature variations into investigations into the warm-up of I.C. engines.

#### **2.4.2 Engine test bed experimentation**

Table 2.5 indicates that engine test bed experimentation is the dominant method in the literature. Despite the additional time and cost relative to computational modelling, the use of test bed engines mitigates the risk of inappropriate assumptions being made within the model. The use of engine test beds with dynamometers is more popular relative to vehicle implemented tests owing to the degree of control in test conditions. Moreover, by controlling the engine load and response experimentally, the effect of driver variation (a risk in full vehicle implementation [8]) can be eliminated. Engine test beds also provide the facilities to utilise much more complex instrumentation (such as exhaust gas analysers) while also providing the capability to control ambient temperatures. Hence, engine test beds are particularly well suited to carrying out correlation work with theoretical models. However, the level of instrumentation is critical in defining the quality of the findings. The lubricant and coolant temperature may be measured at multiple points throughout their respective circuits and the cylinder liner temperature may also be measured at multiple points down its length [19]. However, in general, the engine block is sparsely instrumented with the work of Andrews et al. [17, 38], whose work

focused on temperature interactions within the engine, reporting only one thermocouple being installed in the engine head and one in the block. Consequently, there is a lack of data concerning the transient heating profile through the engine block structure, although this is usually of limited concern when correlating lumped capacity theoretical models owing to the coarse discretisation of the model. The engine block temperature is also of limited interest to I.C. engine researchers as it is only the cylinder liner temperatures that affect combustion behaviour.

In addition to the concerns related to a lack of instrumentation of the I.C. engine block, there are also concerns relating to the repeatability of tests between engines of the same nominal build specification, as was highlighted in Section 1.2.1 and discussed in Section 2.4.4. It can therefore be difficult to determine whether changes in performance metric values are a result of experimental noise or a genuine effect. The ability to perform multiple repeat tests on the same engine build is logistically limited owing to the cost and time of running such tests and the need to allow the engine to fully equilibrate and cool down before further subsequent tests are carried out

### **2.4.3 Vehicle implementation experimentation**

The use of vehicle implementation test methods is the most limited of the three methodologies discussed. By carrying out tests in a full vehicle and using real road running, the ability to directly compare data are reduced. The same concerns regarding repeatability exist as those in Section 2.4.2 however there are also additional sources of variation and noise to consider. If one considers driving on populated roads, traffic conditions are highly variable and make carrying out back to back tests difficult. In addition, the ambient conditions are difficult to control. This is particularly important, given the importance of ambient temperature and wind speed in engine warm-up. Another variable is that of driver performance with variation between different drivers and the repeatability of the same driver carrying out comparative tests being identified as a concern [8]. In addition, the instrumentation limitations discussed in Section 2.4.2 remain a concern during vehicle implementation tests.

That said, one advantage of the vehicle implementation method is the opportunity to appraise any developments in the context of the full system and therefore observe any interactions between other vehicle systems such as the cabin heater or rear differential unit (if applicable). Such a benefit is particularly valid at the point of appraising whether or not to implement new technologies into production vehicles.

### **2.4.4 Levels of confidence in experimental methodologies**

Both Section 2.4.2 and Section 2.4.3 have highlighted concerns relating to the repeatability of experimental methods and the absence of repeat data from the

literature although a limited number of references did provide some degree of repeatability assessment. If one first considers the research concerned with engine test bed measurements there are only two sources that make any assessment of the repeatability of such methods. Burke et al. [69] and Leong et al. [37] both report that engine dynamometer test facilities are capable of producing results repeatable to within 5% although neither reference offered comparative data to verify this.

If one considers work that has utilised vehicle implementation methods there is a comparable lack of information regarding repeatability. The work of Goettler et al. [10] did present extensive data points for their work relating to the effect of ambient temperature on warm-up time. However, it did reveal extensive scatter in the results that the authors highlighted was greater in magnitude than the differences observed as a result of different warm-up configurations. However, statistical analysis of the results indicated that there was a 99.9% confidence level that the difference in the regression lines of the two warm-up approaches was a genuine experimental result rather than noise. The work of Will and Boretti reported carrying out 5 repeats of each test configuration to reduce the significance of any variation between tests such as driver influence. Their results were therefore based on the mean of each data set although no indication of scatter was presented and therefore no further comment is possible in relation to the reliability of such findings. The experimental work of Li et al. [21] offered the most comprehensive analysis of test repeatability and reliability. In carrying out experiments into the warm-up time of a test vehicle and engine on a highway circuit, the tests were conducted five times with the vehicle being allowed to cool to a constant soak temperature each time. In assessing the repeatability between the test runs it could be seen that the ambient temperature varied by up to 6 ° C between tests and that the measured lubricant temperature was seen to vary by up to 10 °C. Li et al. [21], in appraising the data between repeats observed standard deviations in the average emissions for the test runs of between 12% and 34% of the mean depending on the emission gas being appraised (CO<sub>2</sub>, NOX or CO). If the most erroneous result was removed this reduced to between 5% and 21% but it does highlight the challenges of achieving repeatability in an applied powertrain test.

It can therefore be seen that there is limited data available to facilitate the accurate appraisal of the repeatability of powertrain research. However, the limited data available does indicate that the complex interactions of the engine, together with the rest of the vehicle if applicable, do limit the confidence and reliability of experimental findings.

#### **2.4.5 Summary**

In assessing the different methods of research utilised in prior work, the following issues have been established:

- The combination of variation in performance between different engine builds and the impracticality of conducting multiple warm-up tests limits the confidence in the experimental findings of the warm-up of I.C. engine and the effect of different strategies.
- Experimental work into understanding the warm-up process of the I.C. engine is limited by a lack of instrumentation in the engine block and thus, high fidelity data of the changing temperature distribution through the engine block during warm-up is not available.
- Computational modelling, while mitigating the effect of experimental noise is based upon the use of lumped capacity models and hence detailed local knowledge of the transient warm-up profile of components is limited. In correlating such models, the absence of high fidelity experimental transient temperature data through the block structure prevents any local variation in component temperatures being incorporated into the model. Significantly, this affects the accuracy of the warm-up profile of the lubricant as the local exchange of heat between the lubricant and engine components is a function of both the lubricant temperature and the component surface temperature.

Therefore, in consideration of the above limitations further work in the area of transient warm-up of I.C. engine structures and fluids should aim to facilitate greater understanding of the local temperature variation through the thickness of components during warm-up. Experimentally this would need to be achieved by increasing the instrumentation through the thickness of components which would therefore facilitate a high fidelity model to be correlated with such data. The computational model would still be of value in such work as it would facilitate the investigation of parameters beyond the physical scope of any experimental set-up. There is also a need to address the repeatability and confidence of the experimental findings in current I.C. engine research. This requires the development of experimental methodologies that offer greater proven repeatability than a fully built I.C. engine.

## 2.5 Conclusion

The warm-up process of the I.C. engine is complex and from the review of the literature it has been seen how increasing the heating rate of both the lubricant and coolant can have a positive effect. However, it is felt that it is the delayed rate of lubricant heating that is currently the greatest limiting factor in the I.C. engine achieving improved efficiency (and associated fuel consumption and emissions) during warm-up. Andrews et al. [9] concluded that the rate of lubricant warm-up had remained at a constant value of the order of  $0.1 \text{ }^\circ\text{C s}^{-1}$  over the past 20 years while coolant warm-up rates have typically been in the region of  $0.25 - 0.4 \text{ }^\circ\text{C s}^{-1}$ . Consequently the lubricant is still not at its operating temperature at the end of mandated test cycles such as the NEDC while the coolant is at its steady state value

(Figure 1.7) and this results in poor fuel consumption and emissions standards. However, from the review of the literature there is no doubt that the lubricant warm-up rate remains problematic. Kunze et al. [12] and Andrews et al. [9], estimated that to heat the 10 litres of lubricant (a typical factory fill) in an S.I. engine would require between 2.0 MJ and 2.5 MJ of energy, depending on ambient conditions. The CO<sub>2</sub> emission penalty for such a process was 12.5 -22 g CO<sub>2</sub> km<sup>-1</sup> which represents 18 % of the 130 g km<sup>-1</sup> target and therefore represents a significant factor in ensuring OEMs meet such constraints. In addition, Will [13] estimated that if engine friction (of which the majority occurs during warm-up) can be reduced then the running cost of the vehicle over a 150000 km lifetime could reduce by €1500 - €2100.

In reviewing the literature it can therefore be concluded that one should aim to develop methodologies that result in an accelerated rate of lubricant warm-up to reduce I.C. engine fuel consumption and emissions, particularly within the constraints of mandated drive cycles such as the NEDC. The strategies therefore need to demonstrate a benefit within a timeframe of 1180 seconds and from a soak temperature of between 20 °C and 30 °C. Consequently, furthering research into the use of TBCs in the combustion chamber is of limited interest as this results in accelerated heating of the cylinder liners but has limited interaction with the lubricant. Similarly, modifying the flow rate of the coolant has implications on the cylinder liner temperatures but is of limited interest in achieving an accelerated lubricant heating rate. The exception to this would be if lubricant to coolant heat exchangers were in place, as was proven in the case of Samhaber et al. [14]. While the use of pre-heated coolant was estimated to reduce friction work by 8% relative to an unheated baseline, the research also demonstrated that the benefit was slight if the additional energy required to pre-heat the coolant was considered.

The use of external insulation on the I.C. engine has been shown to have a positive effect on delaying the rate of lubricant cool-down but has negligible effect on the rate of lubricant warm-up (Figure 2.8) and would therefore be of limited benefit in accelerating the rate of lubricant heating from a constant soak temperature. While the use of PCMs to improve the warm-up rate of either the I.C. engine or emissions treatment equipment has proven to be of some benefit, concerns over the stability of such materials during repeated cycles and the compatibility with surrounding components together with a potential need to use different PCMs depending on the climatic conditions means that it is not felt such technology is viable to implement in a mass production I.C. engine application.

The literature review has shown how a reduction in either friction work or fuel consumption and emissions can be achieved if heat transfer from the lubricant to surrounding structures can be limited by different strategies. This has previously

been achieved by insulating the bearing shells (Section 2.3.4.1) where reductions of 22% in the frictional force were observed. Alternatively, another way of limiting the exchange of thermal energy between the lubricant and engine block structure is to divert the flow away from the engine block by intelligent control strategies (Section 2.3.5.3.) where reductions in FMEP of up to 10% were achieved in the first 2 minutes of engine running. Similarly, Section 2.3.6 demonstrated how reducing the thermal mass of the engine block is another valid way of reducing the warm-up time of engine fluids. The lubricant data for the work of Bowman et al. [72] was not available but the coolant data indicated reductions in warm-up time of between 6% and 19%. Due to the reduced thermal mass, this would be expected to have a positive impact on the lubricant warm-up rate too (unlike when external insulation is used and the coolant and lubricant temperatures show no change in warm-up rate). Since the work of Bowman et al. specific magnesium alloys have been developed for automotive engine applications that would enable the thermal mass of the engine block to be reduced without the associated difficulties of implementing polymeric materials at high temperatures (creep, and softening being two such examples). It is therefore felt that by investigating and optimising the thermal properties of the material surrounding the engine oil galleries that it is possible to reduce thermal losses from the lubricant and therefore increase lubricant heating rates.

Section 2.3.4.2 discussed preliminary investigations into the benefits of insulating engine oil galleries to reduce fuel consumption during warm-up. If the main gallery (first shown in Figure 1.4) was insulated then it was predicted that a fuel economy improvement of 0.2% could be achieved and that this could increase to 1.7% if the oil mist to crank case surface heat transfer was also isolated. Such work has not been validated experimentally and the work also highlighted uncertainty as to how best to model the transfer of heat from the lubricant to the engine block in terms of the local temperature of the metal in the engine. While insulation of the bearings has been investigated, detailed investigation of the merits of insulating the engine oil galleries has not, nor has there been detailed investigation into the sensitivity of lubricant thermal losses to the surrounding material's thermal properties.

The review of the literature and previous work into improving I.C. engine cold-start efficiency has established that the complex system of I.C. engines places limitations on both the repeatability of the work owing to the complex nature of the I.C. engine assembly while the number of repeats carried out in such work is low owing to time and cost constraints. A further limitation of previous work into the warm-up of I.C. engines is the sparse instrumentation of the engine block and other components meaning detailed transient warm-up data is limited in fidelity. Such limitations are subsequently extended into computational modelling with components represented as a single temperature. In furthering research into developing methods of improving the warm-up rate of I.C. engine such limitations needs to be addressed.

## 2.6 Aims of the thesis

Based on the findings of the literature, this thesis aims to investigate methods to reduce thermal losses from the engine lubricant to improve the engine's efficiency during the warm-up phase. The increase in lubricant heating rate need not be of a large magnitude. The sensitivity of lubricant viscosity to temperature has resulted in the lubricant viscosity reducing by 65% when heated from 20 °C to 40 °C and therefore small temperature increases could reduce friction considerably [9]. Indeed, if one uses the experimental results of Shayler et al. [36] presented Chapter 1, the heating of the lubricant from 20 °C to 40 °C saw the FMEP reduce by approximately 20% from 3.3 bar to 2.7 bar.

One method of achieving increased lubricant heating rates is to reduce the thermal losses from the engine lubricant to the engine block structure as it is pumped around the lubricant circuit. This can be achieved by insulating the lubricant circuit of an I.C. engine. While, the concept has been investigated computationally, there is no apparent experimental research into the work. In addition, the thermal losses from the engine lubricant to the engine block could be reduced by greater optimisation of the thermal properties of the engine block. While the operating temperatures of the I.C. make it unviable to construct an entire engine from polymeric materials (remembering that polymers have comparatively low thermal conductivities relative to metallic alloys) it is felt that a detailed investigation of the relative significance of the thermal mass (a function of specific heat capacity and density) is lacking.

It is intended, through this work, to develop a detailed understanding of the transient heat transfer process between flowing engine lubricant and the surrounding metal structure while addressing some of the limitations posed by current computational and experimental methodologies. In particular, it is intended to develop a greater understanding into the relationship between the lubricant and surrounding metal temperature and to account for localised temperature variations within components (as discussed in Section 2.4.1) while improving the repeatability and reliability of the findings relative to conventional powertrain research. In particular the work seeks to:

- Reduce the scatter in results that exists as a result of either variation between engine builds of the same nominal specification or vehicle system interactions by developing an experimental methodology that facilitates comparative testing of greater consistency than that of a full I. C. engine.
- Facilitate investigation of the variation in temperatures through the thickness of components during the transient warm-up phase in experimental work and account for such characteristics in associated computational work.

## **3 Design and construction of the oil flow rig**

### **3.1 Introduction**

In order to investigate the potential benefits of insulating the lubricant circuit of an I.C. engine, an experimental method was required that enabled the heat transfer mechanisms between flowing automotive engine lubricants and the metal structure surrounding the gallery to be investigated. The I.C. engine, both in terms of physical geometry and heat transfer, is highly complex. Thermal interactions exist between multiple components while the coolant and lubricant are both heated and cooled at various points in the system. If one considers only the lubricant circuit, the primary heating source would be from friction heating the bearings but there are also contributions from combustion and the coolant. However, these interactions are dependent on the design of a specific engine and during warm-up are complicated further by complex engine strategies to aid warm-up.

Thus, in order to investigate the benefits of insulating engine oil galleries, a bespoke oil flow rig has been designed and commissioned. The rig enables the heat transfer mechanisms between hot engine lubricant and surrounding metal structures to be studied without the ambiguity introduced by thermal management strategies of I.C. engines during warm-up.

This chapter discusses the design of the oil flow rig and the rationale preceding such decisions; together with the limitations of instrumentation and details of the experimental procedures carried out.

### **3.2 Rig Design**

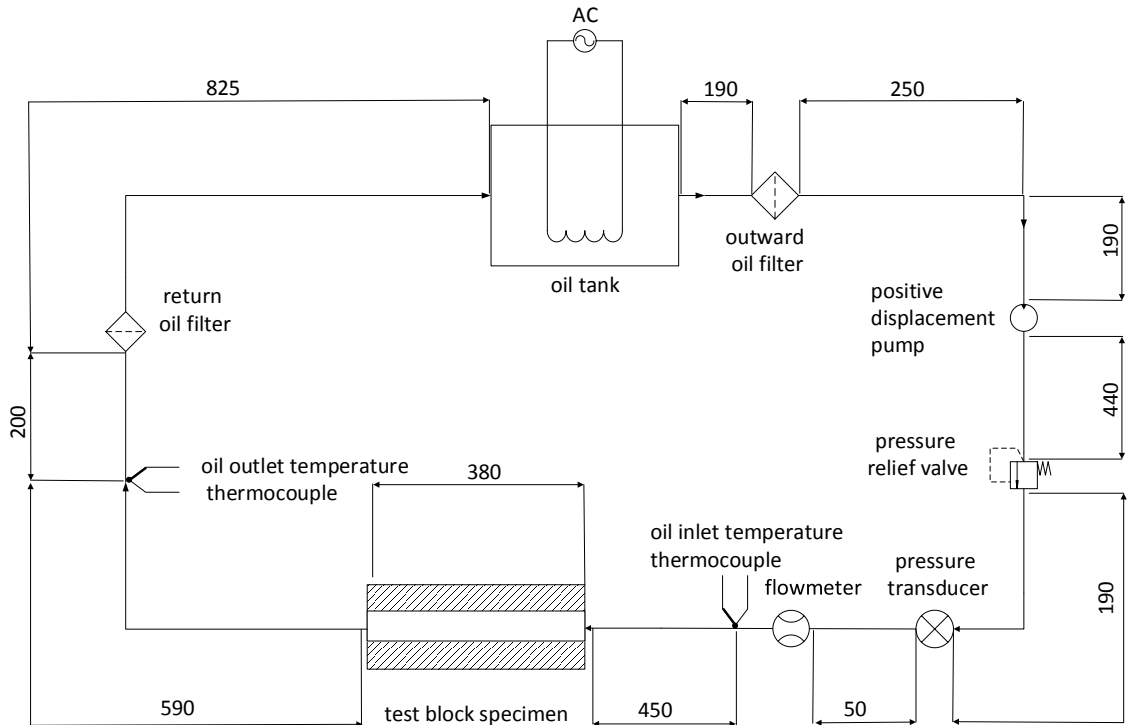
A photograph and schematic of the rig are shown in Figure 3.1 and Figure 3.2. Using this rig it is possible to heat engine lubricant and circulate it through a known thermal mass (in this case the test block specimen) and thus investigate the relationship between the heating rate of engine lubricant and the surrounding metallic architecture.

Aside from offering the capability to install test block specimens of different designs, the rig also offers the capability to vary:

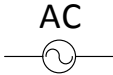
1. The heating rate of the lubricant.
2. The lubricant flow rate.

While the experimental work on the rig focuses on the test block specimen, with the remainder of the rig only being present to heat and deliver lubricant to the specimen, the design and selection of supporting hardware still has a significant role

to play in the thermal behaviour of the rig. In the following sub-sections, the rationale and specification of the various rig components is documented.



**Key**

- |   |                            |   |                 |
|---|----------------------------|---|-----------------|
|  | Oil filter                 |  | AC power supply |
|  | Positive displacement pump |  | Heater element  |
|  | Pressure transducer        |  | Thermocouple    |
|  | Pressure relief valve      |   |                 |
|  | Flowmeter                  |   |                 |

All dimensions in mm

Figure 3.1: Schematic of the oil flow rig

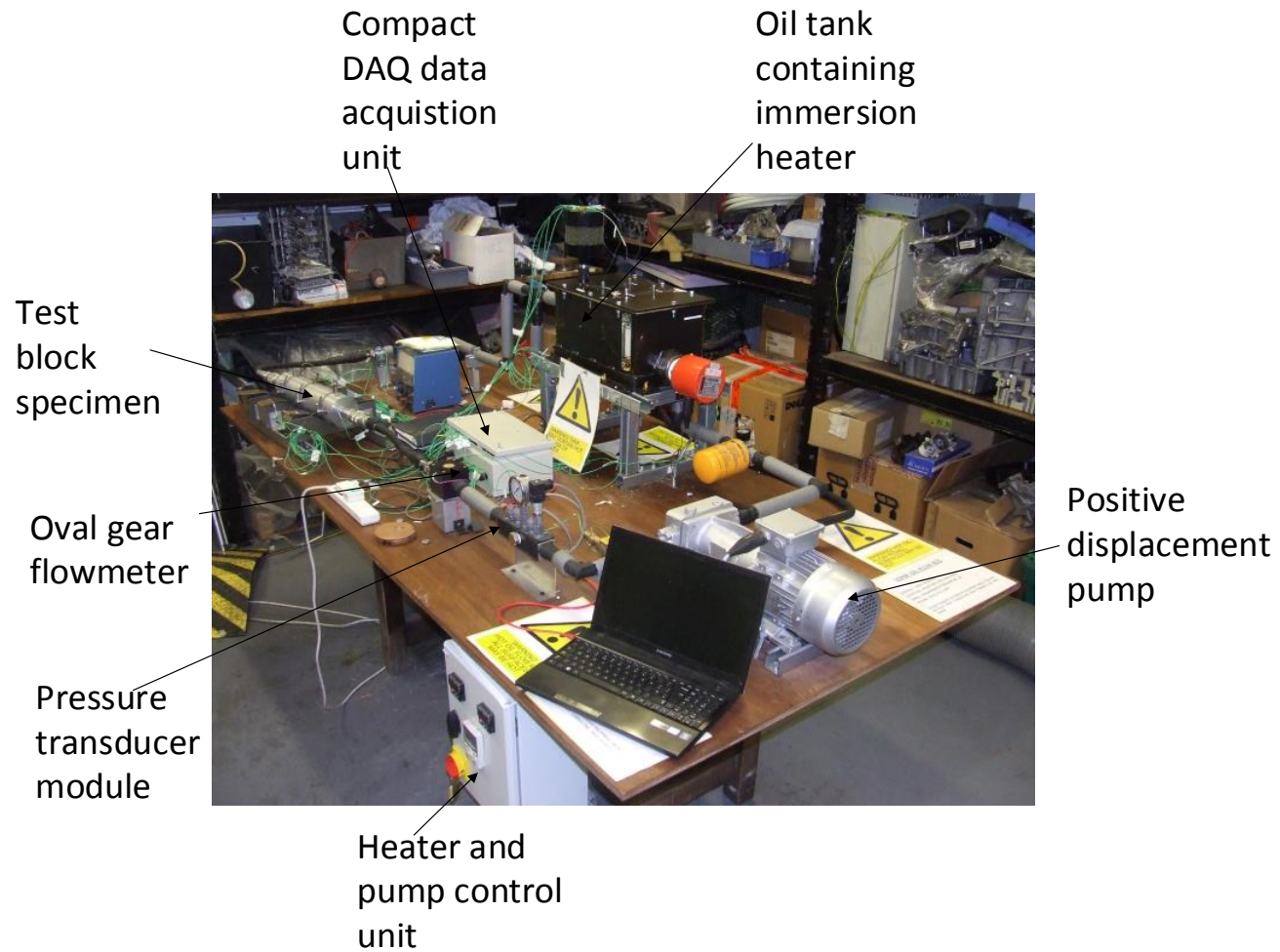


Figure 3.2: Photograph of oil flow rig

### 3.2.1 Lubricant temperature measurement

While the test block specimen is heavily instrumented using K-type thermocouples to record temperatures (detailed further in Section 3.3), there is also a need to measure the lubricant temperature. Figure 3.1 shows that the lubricant temperature is measured at the inlet and outlet to the test block specimen, again using K-type thermocouples. In order to facilitate effective changing of the test block specimens there exists on the rig, two lengths of flexible hosing between the main rig and the test block specimen. These enable clean break couplings to be used to connect the test block specimen into the rig circuit without the need to drain the rig at each changeover. A consequence of the presence of the flexible hoses is the need to install the lubricant temperature thermocouples further away from the absolute inlet and outlet of the test block specimen than would be ideal. In characterising the rig (discussed in Section 3.5.1.2) the reduction in lubricant temperature from the specimen inlet and outlet has been observed to be minimal. It is therefore not felt that the distance between the specimen and the temperature measuring points affects the overall findings of the experimental work. The relative location of the temperature measuring points relative to the test block specimen is shown in Figure 3.3.

The thermocouples installed in the lubricant flow are mounted in such a way that they are level with the bore wall, as shown by the schematic in Figure 3.4. This was motivated by a desire to minimise the disturbance to the flow of lubricant as much as possible. In subsequent experimental work, comparative tests were carried out with the thermocouples mounted in the mid-stream to investigate the significance, if any, of any boundary layer formation. However, negligible difference was observed between the flow thermocouples held at the bore wall and those mounted in the mid-stream. Such findings are discussed in Chapter 4 (Section 4.7).

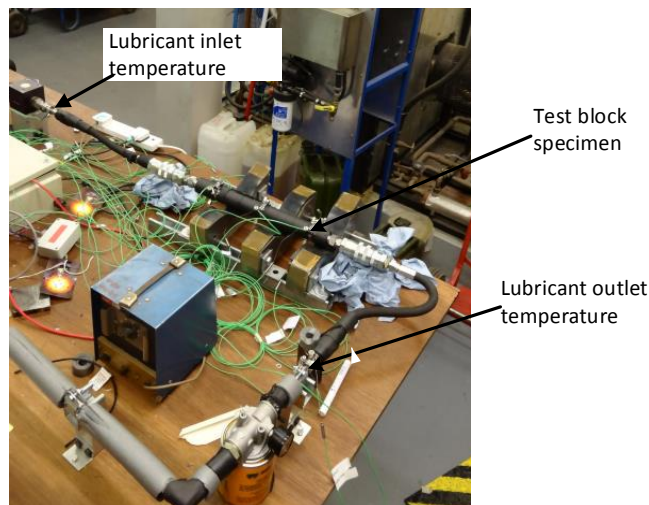


Figure 3.3: Location of inlet and outlet lubricant measuring points relative to the test block specimen

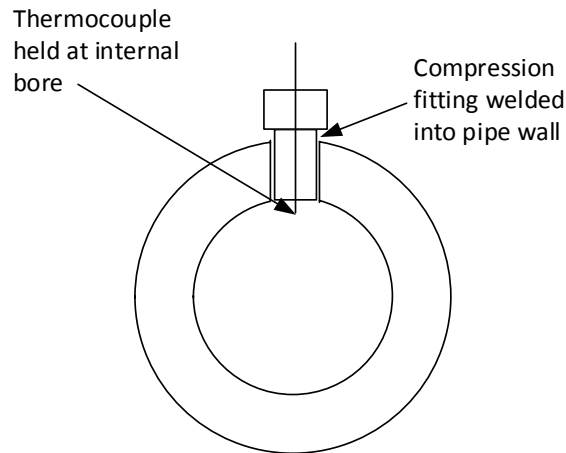


Figure 3.4: Schematic of lubricant temperature measurement (not to scale)

### 3.2.2 Lubricant pump and flow rate control

Lubricant is circulated around the circuit by a positive displacement pump provided by Tuthill Pumps (model number 1012-2S7ICC-00000) that is controlled via a proportional integral derivative (PID) inverter drive, although in this application no derivative control is applied. An oval gear flow meter, supplied by Titan Enterprises (model number OG4-AU1-VHT-B), supplies the control signal to the inverter drive. The motivation behind using flow rate, rather than pressure, to control the pump speed is the fact that the lubricant to specimen heat transfer coefficient is dependent on the velocity, and hence flow rate, of the fluid. A key aspect of the work was to develop a correlated theoretical model of the rig and therefore investigate parameters outside the capability of the physical rig. Thus, in order to correlate the experimental work with the theoretical model, discussed in Chapter 6, it was decided the most appropriate parameter to control was that of flow rate.

### 3.2.3 Tank design and heater selection

The design of the oil tank has two purposes to fulfil:

1. Contain a sufficient volume of lubricant to be representative of heating a car engine's lubricant circuit.
2. House the heater element for the lubricant.

For the experimental work to fulfil its intended purpose it is imperative that the heater element is fully submerged in lubricant for two reasons. Firstly, were this not to be the case, the element could burn the lubricant on the element surface until dry, leading to heavy smoke creation. Secondly without the element being fully submerged, it is not possible to accurately quantify the heat input to the lubricant and some of the heater power would be immediately transferred to the air in the tank.

From the literature, it was seen that average heat to oil figures over the course of engine warm-up is 1120 W [20] for the engine system as a whole and therefore, the heater element needs to provide at least this much power. The heater element, supplied by Watlow, provides a maximum of 2.5 kW of heater power across a combination of 3 elements. A schematic of the heater is shown in Figure 3.5. For the heater selected, the dimension 'B' is 370 mm and therefore necessitated the internal length of the tank to be 400 mm.

The long length of the tank required the heater element to be installed as low as physically possible in order to minimise the volume of lubricant required to completely submerge the element. However, in the bottom of the tank are two bulkhead fittings for the outward feed to the pump and return lubricant to re-enter the tank. Therefore, to provide sufficient clearance around the element for the bulkhead fittings, the internal width of the tank was designed to be 225 mm. A photograph of the interior of the tank showing the heater installation relative to the outlet and return bulkhead fittings is shown in Figure 3.6 where the lubricant has been drained. It can be seen that the outward feed to the pump and the return pipe are positioned diagonally across the tank. This is to promote greater mixing of the lubricant across the heater element and to prevent hotspots forming within the lubricant. To cover the immersion heater, a cold lubricant height of 75 mm is required. Such a constraint, accounting for the volume of lubricant in the pipework and filters of the rig, requires the rig to carry 8.2 litres of lubricant. While this is marginally more than a standard engine fill (the test engine based at Nottingham has a factory fill capacity of 6.4 litres), this is the minimum quantity of lubricant that could be utilised to safely run the rig.

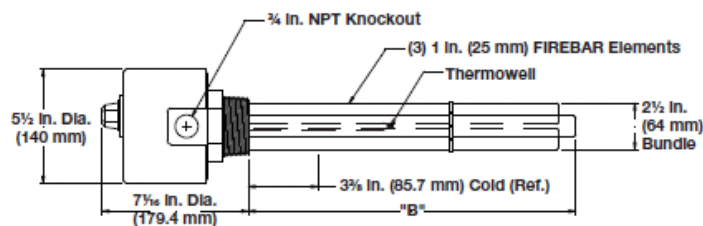
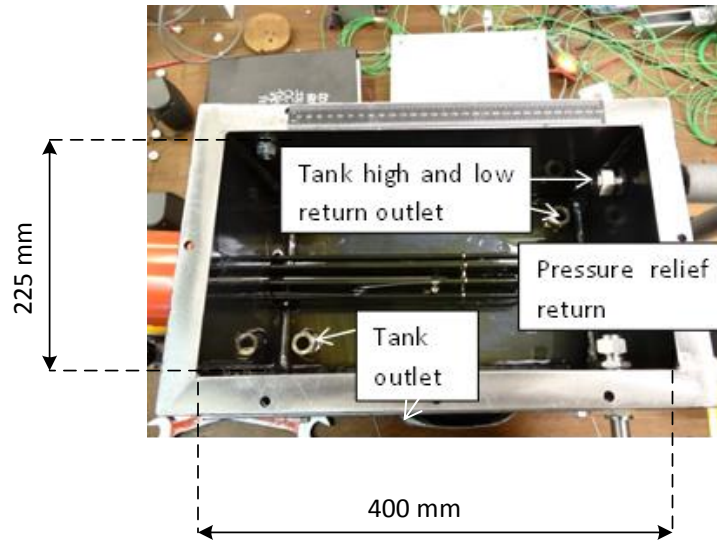


Figure 3.5: Schematic of oil immersion heater



**Figure 3.6: Internal view of oil tank with no lubricant present**

The tank itself is constructed from bright drawn mild steel (BDMS) and is a welded fabrication. The internal surfaces are not coated or painted but remain a bare metal surface. The outside of the tank is painted in black Hammerite Paint to prevent corrosion and a cork gasket is installed between the tank lid and main body. In initial tests it was found that the convective losses from the outer surface of the tank were significant enough to limit the peak temperature of the lubricant in the rig. Consequently, a 40 mm thick blanket of polystyrene foam is applied to all the external surfaces of the tank, as shown in Figure 3.7. The effects of the external insulation on the dynamics of the rig are discussed in Chapter 4 (Section 4.5).

A significant design feature of the tank is that of the wall thickness. The heater element is installed into the wall of the tank on a 2.5 inch national pipe thread (NPT). The original design intent of the tank was to cut the thread within the wall of the tank and therefore, to facilitate effective sealing, the wall thickness was designed to be 10 mm. During manufacture, it became apparent that the internal cutting of such a thread was not viable and consequently, a boss was welded onto the wall of the tank to facilitate the heater installation.



Figure 3.7: Oil rig tank after external insulation applied

### 3.2.4 Piping geometry and specification

All the pipework around the rig is manufactured from stainless steel of grade 316 and is of 13 mm bore diameter and a wall thickness of 1.5 mm. The stainless steel was selected owing to its much reduced thermal conductivity ( $13\text{--}17\text{ W m}^{-1}\text{ K}^{-1}$ ) [57] relative to steel ( $49\text{--}55\text{ W m}^{-1}\text{ K}^{-1}$ ) [57]. Aluminium ( $193\text{ W m}^{-1}\text{ K}^{-1}$  [93]) and copper ( $390\text{ W m}^{-1}\text{ K}^{-1}$  [57]) were rejected for the same reason.

As already highlighted, the primary focus of the rig is the test block specimen and it is therefore desirable to limit the thermal losses around the remainder of the rig as much as possible. While the use of stainless steel pipework aids such an approach, additional steps have also been taken. Firstly, all the pipework is insulated in 13 mm thick polyethylene foam lagging with a stated manufacturer thermal conductivity of  $0.035\text{ W m}^{-1}\text{ K}^{-1}$ . Similarly, around the rig, there are numerous fittings including  $90^\circ$  elbow joints and compression fittings to components such as the pump and oil filters that require insulation. Consequently, where pipe lagging is not a viable option, fittings are insulated in 3 mm thick Armaflex thermal insulating tape with a thermal conductivity of  $0.036\text{ W m}^{-1}\text{ K}^{-1}$ . An example section of the rig showing both the pipe insulation and fitting insulation is shown in Figure 3.8.



Figure 3.8: Example section of oil flow rig piping showing insulation applied to fittings and to the pipe lengths

### 3.3 Specimen design

The critical area of the rig is that of the test block specimen. Through the use of different test block specimens the aim of the experimental rig was to:

1. Identify the potential benefits of applying insulation to engine oil galleries.
2. Quantify the lubricant thermal history in contact with various sized blocks and insulation regimes.

Consistent across all the test specimens utilised in the experimental scheme are:

1. The length is fixed at 380 mm. This dimension was selected to match the overall length of the main engine oil gallery of a 2.0 litre GDTI (gasoline direct turbo injection) test engine.
2. For the same reason, the bore of the test block specimens is fixed at 16 mm. In the instance where insulation is applied the decision was made to compensate for the thickness of the insulation by over boring the test block specimen to allow the insulating insert to be installed and still leave the hydraulic diameter the same and to therefore provide a consistent experimental set-up. Varying the bore diameter causes the velocity, and subsequently the Reynolds Number of the lubricant to change which has an impact on the heat transfer coefficient. In addition, changing the bore diameter also has an effect on the heat transfer area. The relative effect of such variations are investigated and discussed in Chapter 7.

The test block specimen in the rig is intended to be analogous to the thermal mass of the engine block surrounding the gallery in a full engine. Thus, by varying the specimen size, the rig can appraise the relative merits of applying insulation to

regions of the engine block with different cast thicknesses. The test block specimens are manufactured from aluminium 6082 T6 (thermal properties of which are detailed in Table 3.1) in order to closely match the thermal properties of typical cast I.C. engine block.

Worthy of discussion is why a wrought alloy was chosen over a cast alloy such as A319 that was referred to in Table 2.4 of Section 2.3.6 and the associated impact that this may have on results. The test block specimens were manufactured using the in-house manufacturing capability and stock supply of the University of Nottingham. Thus, to reduce material availability and manufacturing lead times grade 6082 T6 was chosen. When comparing the material properties of aluminium alloy A319 (Table 2.4) with aluminium alloy 6082 T6 (Table 3.1) it can be seen that the wrought alloy's thermal conductivity at  $193 \text{ W m}^{-1} \text{ K}^{-1}$  is 48% higher than the cast alloy's thermal conductivity of  $130 \text{ W m}^{-1} \text{ K}^{-1}$ . Such a change can largely be attributed to the silicon content of the two alloys. The silicon content of the casting alloy A319 is 6.1% by weight [71] thus making it a hypoeutectic alloy whereas the silicon content of the wrought alloy is between 0.7% and 1.3% [94]. Increasing the silicon content improves the fluidity of the alloy and reduces shrinkage of the alloy and is therefore desirable for casting applications but has a detrimental effect on the machinability [95]. However the work of Stadler et al. [96] has reported how the silicon content of the alloy causes the thermal conductivity to reduce dramatically. The effect of using the wrought alloy as opposed to a cast alloy is reported in Chapter 7 (Section 7.2.2) and was found to increase the predicted thermal losses from the lubricant by between 2% and 4%. Thus, relative to the changes in energy flow observed when different insulation strategies were investigated, this is negligible.

**Table 3.1: Thermal properties of aluminium 6082 T6 used in the test block specimen**

Property	
Density ( $\text{kg m}^{-3}$ )	2690 [93]
Thermal conductivity ( $\text{W m}^{-1} \text{ K}^{-1}$ )	193 [93]
Specific heat capacity ( $\text{J kg}^{-1} \text{ K}^{-1}$ )	900 [57]
Coefficient of thermal expansion ( $^{\circ}\text{C}^{-1}$ )	$2.3 \times 10^{-5}$ [93]

During the course of this work, two test block specimen sizes have been used with outer diameters of 40 mm and 100 mm to give effective wall thicknesses, in the case of an uninsulated scenario, of 12 mm and 42 mm respectively. Engineering drawings for the uninsulated and insulated 100 mm outer diameter test block specimens are shown in Figure 3.9 and for the 40 mm outer diameter test block specimens in Figure 3.10. The insulated specimens were bored to accommodate an insulating insert (discussed in Section 3.3.1) and the drillings on the outer surface are present to

allow for the installation of thermocouples (discussed in greater detail in Section 3.5.1). The insert, regardless of material, was designed to be a nominal fit and hence no interference between the test block specimen and insert was incorporated.

The temperature of the specimen is monitored at three points along the length and these are shown in Figure 3.9 and Figure 3.10. The first temperature measurement point (L1) is recorded 50 mm from the specimen inlet while position L2 records the temperature at the test specimen midpoint. Location L3 records the specimen temperature 50 mm from the specimen outlet end. At each measurement point, the temperature of the test block specimen is measured at 3 radial increments through the thickness of the metal before a final temperature is measured at the outer surface of the test block specimen. Such locations are denoted as R1 at the deepest point in the test block specimen through to R4 at the outer surface of the test block specimen. The exact locations of the radial thermocouples vary between specimen variants and are shown in Figure 3.9 and Figure 3.10. The temperature measurement configuration was designed to enable any temperature gradient or transient effect in the test block specimen to be observed through both the radial thickness of the test block specimen and along its length. Where an insulating insert is installed, the deepest radial location, R1, is placed on the outer surface of the insulating insert. Owing to the difficulty in installing instrumentation through the interface of the test block specimen and insert, no instrumentation is placed through the thickness of the insert if one was installed.

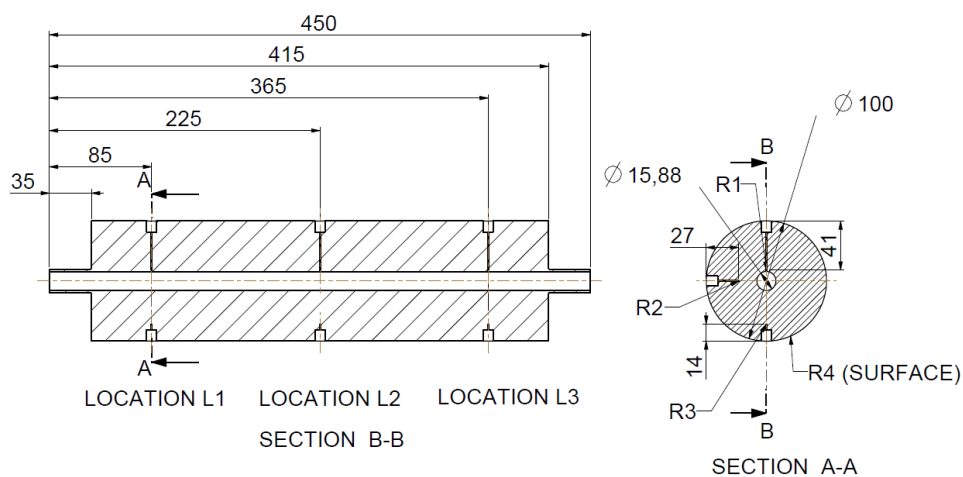


**Figure 3.9a: Cross section through a 100 mm outer diameter uninsulated test block specimen showing the relative longitudinal and radial temperature measuring points**

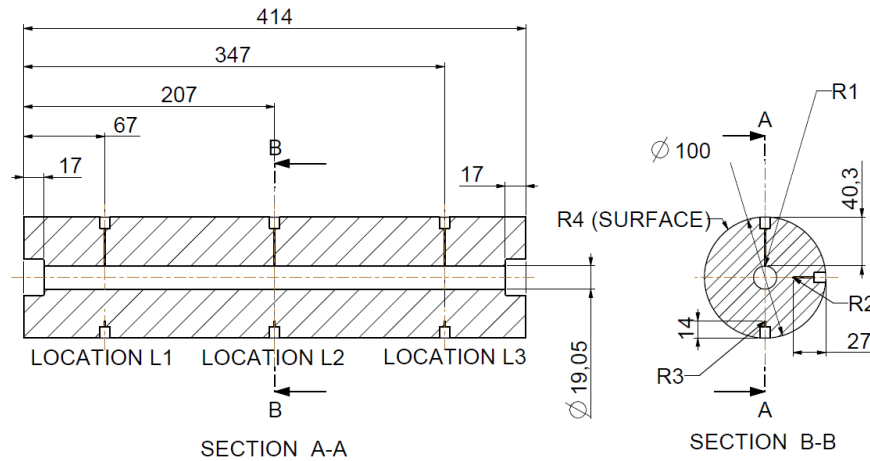


Figure 3.9b: Cross section through a 100 mm outer diameter insulated test block specimen showing the relative longitudinal and radial temperature measuring points (for clarity the insulating insert is not shown)

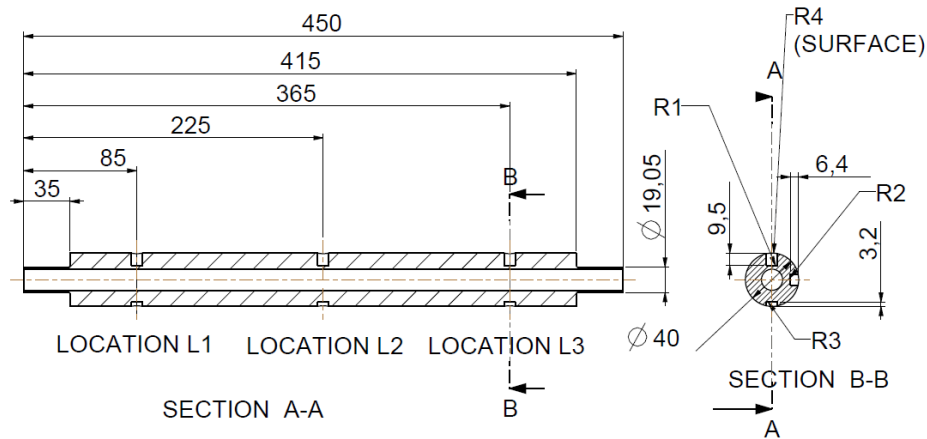


Figure 3.10a: Cross section through a 40 mm outer diameter uninsulated test block specimen showing the relative longitudinal and radial temperature measuring points

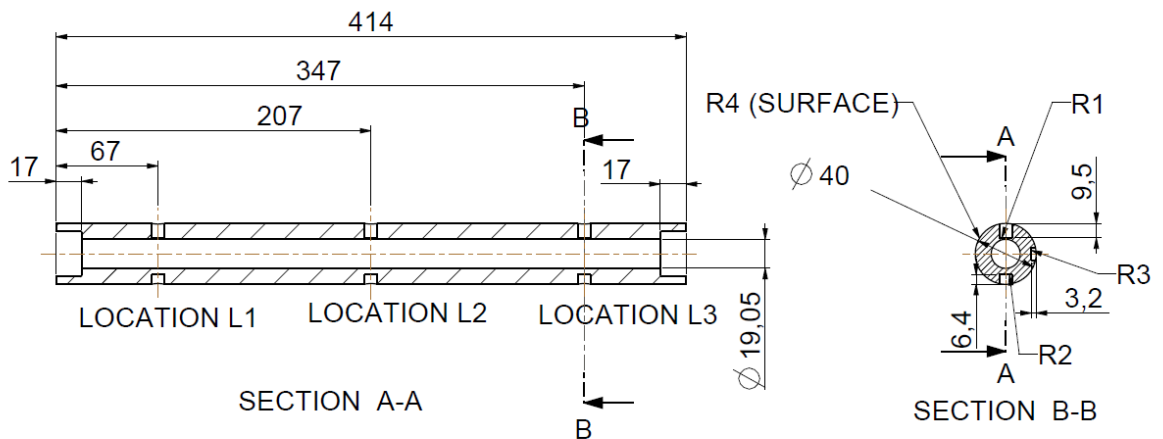


Figure 3.10b: Cross section through a 40 mm outer diameter insulated test block specimen showing the relative longitudinal and radial temperature measuring points (for clarity the insulating insert is not shown)

The specimens, when installed on the rig are supported in three 'V' blocks, identical to the one shown in Figure 3.11. In order to de-couple the thermal mass and thermal inertia of the 'V' blocks from the test block specimen, the top surface, where the test block specimen was seated, is covered in 3 mm thick neoprene rubber sheet (thermal conductivity  $0.1 \text{ W m}^{-1} \text{ K}^{-1}$  [57]).



Figure 3.11: Test block specimen 'V' block support

### 3.3.1 Insulating insert design

All the insulating inserts trialled during the course of the experimental investigation have a nominal internal bore of 16 mm and a wall thickness of 2 mm. Thus, in tests where an insulating insert is installed the effective wall thickness of the test block specimen is reduced to 10 mm and 40 mm respectively in the case of the 40 mm outer diameter specimen and the 100 mm outer diameter specimen.

In total, five variants of insulating inserts were tested to appraise the relative effect of using low thermal conductivity materials (relative to that of aluminium) as an insulator compared to using the combination aluminium and an enhanced contact resistance between the test block specimen as an insulator. It is worth noting that the Nylon 12, while exhibiting a low thermal conductivity relative to aluminium, is relatively conductive compared to engine lubricant that has a typical thermal conductivity of between  $0.144 \text{ W m}^{-1} \text{ K}^{-1}$  and  $0.136 \text{ W m}^{-1} \text{ K}^{-1}$  between  $27 \text{ }^\circ\text{C}$  and  $107 \text{ }^\circ\text{C}$ . The variants tested were:

- A Nylon 12 insert to investigate the benefits of low thermal conductivity materials (the thermal properties are shown in Table 3.2 [57]) although some contact resistance is introduced. Nylon 12 was selected over other polymers of similar thermal conductivity owing to its compatibility with automotive engine lubricants.
- A drawn aluminium (grade 6082 T6) insert to investigate the effect of contact resistance in isolation of low thermal conductivity materials.
- A drawn aluminium insert (grade 6082 T6) with a 0.5 mm step machined into the outer diameter by the faculty workshop to enhance the contact resistance.

- A Nylon 12 insert with a 0.5 mm step (again machined into the outer diameter) to combine high contact resistance with low thermal conductivity.
- Aluminium (grade 6082 T6) insert manufactured by turning and drilling to investigate the effect of surface roughness on the inner bore on heat transfer.

### 3.3.1.1 The variation of Nylon properties

#### 3.3.1.1.1 Variation in Nylon 12 properties between suppliers

The properties listed in Table 3.2 are general properties for Nylon 12 at room temperature. However, the physical properties of polymers vary as a result of small changes in material composition. Such variation may therefore have an impact on the validity and repeatability of the experimental findings and the magnitude of such uncertainty are worth considering. Appendix A.1 presents supplier data for Nylon 12 from two suppliers (Ensinger and PAR) for Nylon 12 at room temperature. It can be seen from supplier data that the thermal conductivity of Nylon 12 is reported to vary from  $0.23 \text{ W m}^{-1} \text{ K}^{-1}$  to  $0.30 \text{ W m}^{-1} \text{ K}^{-1}$  (a variation of 30%)[97, 98] with the values quoted from the literature (Table 3.2) lying within the range of the quoted values. The specific heat capacity quoted in the supplier data are seen to vary by 14% with values of  $1800 \text{ J kg}^{-1} \text{ K}^{-1}$  and  $2100 \text{ J kg}^{-1} \text{ K}^{-1}$  being quoted. Thus the literature quoted value in Table 3.2 lies just outside the minimum value. However, as is discussed in Chapter 7 (Section 7.2.2.2.1), the specific heat capacity of the insulating insert is an insensitive parameter and the thermal losses are instead governed by the thermal conductivity of the insulating insert and hence the variations in thermal conductivity between suppliers are of greater interest.

Table 3.2: Thermal properties of Nylon 12 [57]

Property	
Density ( $\text{kg m}^{-3}$ )	1015
Thermal conductivity ( $\text{W m}^{-1} \text{ K}^{-1}$ )	0.26
Specific heat capacity ( $\text{J kg}^{-1} \text{ K}^{-1}$ )	1760
Coefficient of thermal expansion ( $^{\circ}\text{C}^{-1}$ )	$1.45 \times 10^{-4}$

#### 3.3.1.1.2 The variation in thermal properties between different grades of Nylon

It has been stated that the polymer insulating insert was manufactured from Nylon 12 owing to its compatibility with automotive lubricants and ability to withstand the peak operating temperatures of approximately  $120^{\circ}\text{C}$ . However, there are other grades of Nylon available and a common alternative to Nylon 12 is Nylon 6. A limitation in the use of Nylon for engineering applications is its hydrophilic nature. To counter this problem it is common for Nylon components to be dried prior to any

processing operations being carried out on them [99]; however in applications where dimensional stability and tight tolerances exist, this remains a concern. Owing to the greater number of carbon atoms in the polymer chain of Nylon 12, relative to Nylon 6, it absorbs less moisture and was thus deemed to be more suitable for automotive engine applications [99]. Nonetheless it is worth considering the relative thermal properties of the two grades and these are summarised in Table 3.3. It can be seen how the properties of the two grades are similar with the magnitude of discrepancy between the two different grades of Nylon, no greater than the variation observed between two different suppliers of the same grade. However, while the variations reported are small, they do have an impact on the thermal losses from the lubricant to the surrounding test block specimen and these are investigated and discussed using the theoretical model in Section 7.2.2.2.3

**Table 3.3: Supplier thermal properties of Nylon 12 and Nylon 6**

Property	Nylon 12 [97, 98]	Nylon 6 [100-102]
Density ( $\text{kg m}^{-3}$ )	1020	1130- 1150
Thermal conductivity ( $\text{W m}^{-1} \text{K}^{-1}$ )	0.23– 0.30	0.23– 0.29
Specific heat capacity ( $\text{J kg}^{-1} \text{K}^{-1}$ )	1800- 2100	1700

### 3.3.2 Connection of specimen to the rig

The need to install test block specimens of different sizes necessitated a method of effectively removing the test block specimens from the rig circuit without draining the entire system repeatedly. To facilitate this, clean break fittings, as shown in Figure 3.12, are utilised. These connect to flexible hydraulic hoses to enable the specimens to be manoeuvred into position. The entry side flexible hose is 450 mm in length and the outlet flexible hose is 590 mm in length (Figure 3.1).

While a necessity to have a mechanism of coupling the specimen to the rest of the rig, it is worth considering the possible implications on experimental results as a result of the presence of such features. In the instance of the clean break fitting, there is an unavoidable disruption to lubricant flow as a result of flowing through the fitting. On the inlet side of the specimen, care was taken to ensure that specimen is as far away from a 90 ° bend as possible and also away from any flow rate or pressure measuring equipment to ensure the flow is undisturbed on entry to the test block specimen. This is aided by the 450 mm length of flexible hosing. However the clean break fitting will almost certainly create some entry length effects within the test block specimen, an issue discussed in greater detail in Chapter 6 (Section 6.2.4).

Linked to the issue of entry length and flow disturbances is that of connecting the specimens when an insert is installed. To ensure that no lubricant is able to accumulate in the cavity between the insulating insert and the test block specimen,

the rig is coupled directly to the insert. In the case of the Nylon 12 insert, the compression fittings in use would crush the tube when tightened. Consequently, to enable the fittings to seal and withstand the flow pressure, mild steel top hats, as shown in Figure 3.13, are inserted into the ends of the Nylon 12 inserts. These are inserted into the ends of the Nylon 12 insert and are located by means of the flange resting against the end face of the Nylon 12 insert. When the compression fittings are tightened, the sealing olive is able to compress the Nylon 12 but is able to react against the rigid top hat. Were the top hat not present, the Nylon tube would compress and deform and would therefore be unable to withstand the pressure generated by the flowing lubricant. While not necessary to achieve an acceptable seal in the case of uninsulated and aluminium insert scenarios (the olive deforms to make a seal when compressed against the harder aluminium), the steel top hats are installed in all specimens to provide consistent entry and exit conditions between tests.



Figure 3.12: Clean break fitting connecting test block specimen to oil flow rig circuit

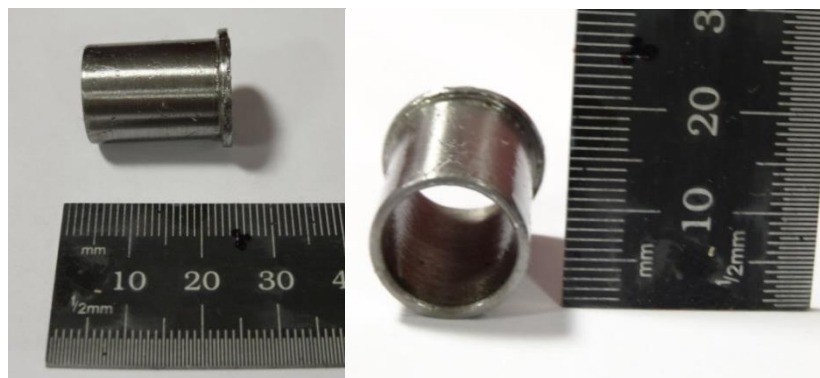


Figure 3.13: Mild steel insert used to enable compression fitting sealing on the end of Nylon 12 insulating inserts

### 3.3.3 Storage and usage of test block specimen inserts

The test block specimen inserts were installed into the rig and a sequence of tests carried out before the inserts were placed in storage whereby they would not be exposed to either extremes of temperature or UV (ultra-violet) sunlight; hence

preventing unwanted degradation. When in use, the test block specimens were usually subjected to the following three tests conditions on both the 40 mm outer diameter test block specimen and the 100 mm outer diameter specimen:

- 1200 W heater power and 10 l min<sup>-1</sup> flow rate.
- 1200 W heater power and 15 l min<sup>-1</sup> flow rate.
- 1800 W heater power and 10 l min<sup>-1</sup> flow rate.

The notable exception to the above usage was the 2 mm thick drawn aluminium insert that was subject to an additional test at 10 l min<sup>-1</sup> flow rate and 1200 W heating power to appraise the sensitivity of the thermocouples between locations (discussed in Section 3.5.1.2).

### **3.4 Variation of lubricant properties with temperature**

The rig is filled with Texaco Energy 5W-30 lubricant in order to match the lubricant installed in the demonstrator engine referred to in Section 3.3. A primary motivator for carrying out this research was to investigate methods of addressing the sensitivity of lubricant viscosity to temperature. However, it is not just lubricant viscosity that is sensitive to temperature but also the specific heat capacity and density. Across the temperature range of the tests (10 °C – 120 °C), the lubricant density reduces by over 10 % and the specific heat capacity increases by 30%, as shown in Figure 3.14 and Figure 3.15. Throughout the experimental work carried out on the rig, the lubricant was not changed between tests and this resulted in the lubricant being heated from ambient temperature (between 17 °C and 20 °C) up to a maximum of 120 °C. While the lubricant underwent multiple heat cycles (82 cycles resulting in approximately 300 hours of service), it was not exposed to by-products of combustion as would be the case in an I.C. engine and it was therefore felt that the lubricant's characteristics would not change or degrade significantly as a result of being circulated through the oil flow rig. In an I.C. engine one would typically expect the lubricant to increase in viscosity relative to a fresh lubricant (at a given temperature) as a result of the lubricant carrying contaminants such as metals and also insoluble compounds within the lubricant that are a by-product of oxidation [103, 104]. It is possible that in the very early phases of lubricant use that an initial thinning could be observed as a result of shear effects on the lubricant [103]. However these effects are slight and lubricant life and usability is governed by the thickening effects of contamination. The typical life span of a modern I.C. engine lubricant can be as high as 18600 miles with S.I gasoline engines and 31 000 miles in the case of C.I. diesel engines [32]. With such lubricant service intervals being deemed acceptable, it was therefore felt that the lubricant in the rig did not require changing throughout the testing phase as it was felt that greater variability would be introduced to the results with repeated lubricant changes rather than maintaining a consistent fill volume.

The notable exception to the above was when the oil flow rig was used for external sub-contractor work (referred to in Section 4.9). During the course of this work, the Texaco 5W-30 lubricant was drained and stored in a sealed container out of direct sunlight to prevent any U.V degradation. The lubricant was subsequently used to re-fill the rig after work for the subcontractor had been completed.

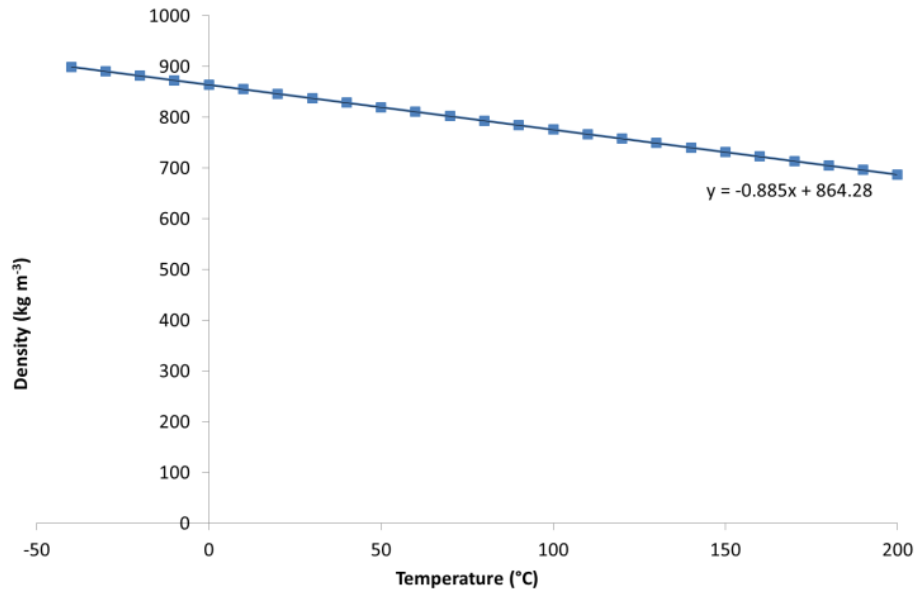


Figure 3.14: Texaco Energy 5W-30 lubricant density as a function of temperature [105]

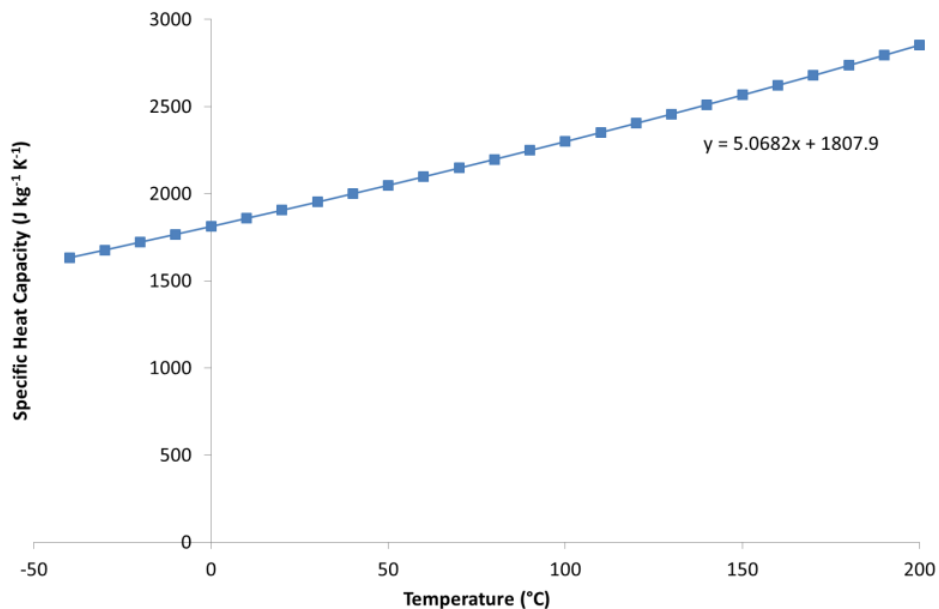


Figure 3.15: Texaco Energy 5W-30 lubricant specific heat capacity as a function of temperature [105]

The variation of the dynamic viscosity with temperature is shown in Figure 3.16. Using data provided by Texaco, the variation of dynamic viscosity with temperature was fitted to the Vogel relationship that was defined in Equation 1.5 [34, 35]. To

model the lubricant dynamic viscosity of this particular lubricant  $k_v$  was assigned a value of  $0.0568 \text{ N s m}^{-2}$ , while  $\theta_1$  and  $\theta_2$  were assigned values of  $1171.2 \text{ }^\circ\text{C}$  and  $135 \text{ }^\circ\text{C}$  respectively.

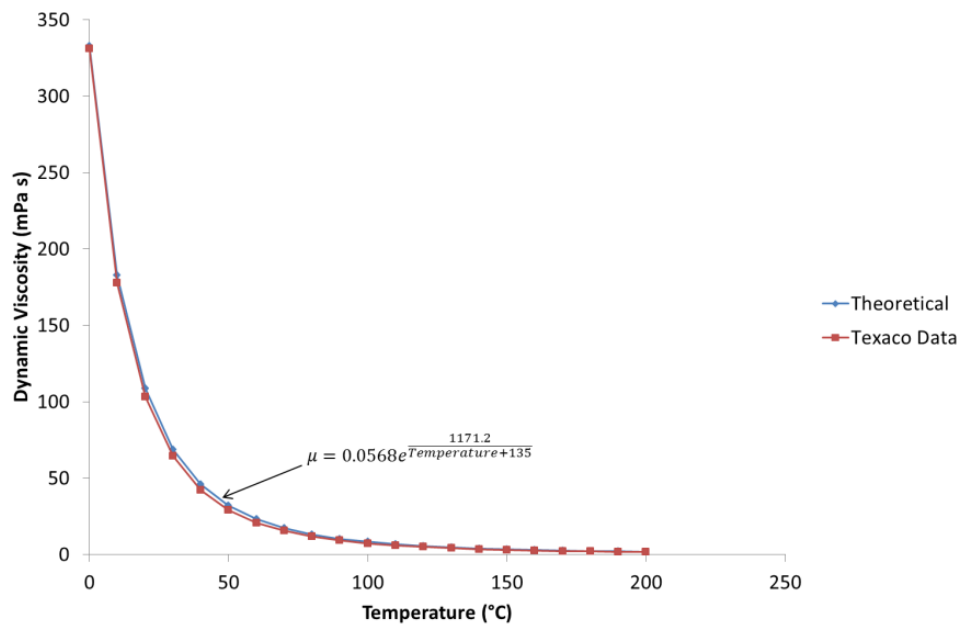


Figure 3.16: Variation of Texaco Energy 5W-30 lubricant dynamic viscosity with temperature [105]

## 3.5 Instrumentation

### 3.5.1 Thermocouple instrumentation

Regardless of whether the test block specimen temperature or the lubricant temperature is being measured, K-type 0.5 mm diameter thermocouples are utilised across the rig. The advantage of a 0.5 mm thermocouple is the faster response time (typically 0.025 seconds [106]) relative to higher sheath diameter equivalents. This is felt to be particularly important, given the transient nature of the investigation.

A notable exception is the thermocouples used to measure the outer surface temperature of the test block specimens. While a K-type thermocouple is still used at these locations, the inability to mount a 0.5 mm diameter thermocouple directly onto the surface requires an alternative solution. Instead 'ring thermocouples' that are mounted in a Jubilee Clip are used, as shown in Figure 3.17. These have a noticeably slower response time (although manufacturer data were not available for such a model) and the data from such thermocouples were consequently infrequently used during the course of the research work. In addition, it was felt the temperature readings from these thermocouples were too sensitive to ambient temperature variations.

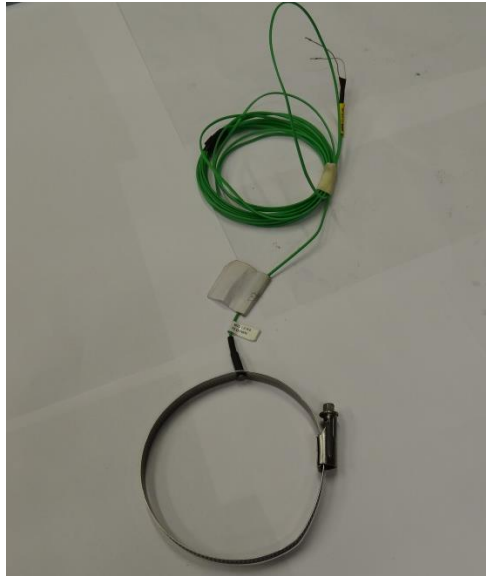


Figure 3.17: Example of ring mounted K-type thermocouple used to measure the outer surface temperature of a 100 mm outer diameter test block specimen

### 3.5.1.1 Thermocouple calibration

The stated manufacturer accuracy of the K-type thermocouples used throughout the experimental work is  $\pm 1.5$  °C. While the absolute temperature of individual components is far higher than such an uncertainty (the lubricant was heated to 120 °C from room temperature), the temperature differential between the lubricant at inlet and outlet or at different positions within the test block specimen is highly likely to be of this order of magnitude.

Consequently, to gain an understanding of the variation in temperature readings between different thermocouples and to reduce the uncertainty between different temperature readings, the thermocouples were calibrated relative to each other using an Isotech dry block Fast-Cal unit. The unit is capable of operating between -35 °C to 140 °C and provides a controlled temperature in a 150 mm deep port, to isolate any ambient effects. By using the block's control temperature as a reference, the system enables the absolute temperature to be controlled and compared to values from the thermocouple, to an accuracy of 0.2 °C. To validate the performance of the inlet flow and outlet flow thermocouples, the Fast-Cal unit was initially set to 15 °C and subsequently increased in 10 °C increments up to a maximum of 125 °C before decreasing the temperature interval back down to 15 °C in 10 °C intervals, as shown in Figure 3.18. At each temperature, the unit was held at a steady temperature for 10 minutes. A series of tests were conducted to enable the 'inlet flow' and 'outlet flow' thermocouples to be compared with the thermocouples from locations L1 R1, L2 R1 and L3 R1 on both the 100 mm and 40 mm outer diameter specimens. The temperature profile for the lubricant thermocouples and the 40 mm outer diameter specimen thermocouples is shown in Figure 3.18, with the same response having

been found for the 100 mm outer diameter specimen thermocouples. In the plot, it is difficult to distinguish between the traces for each of the different thermocouples owing to the close performance of each thermocouple channel and thus, closer examination is paid to specific thermocouples across a smaller temperature range in Figure 3.19.

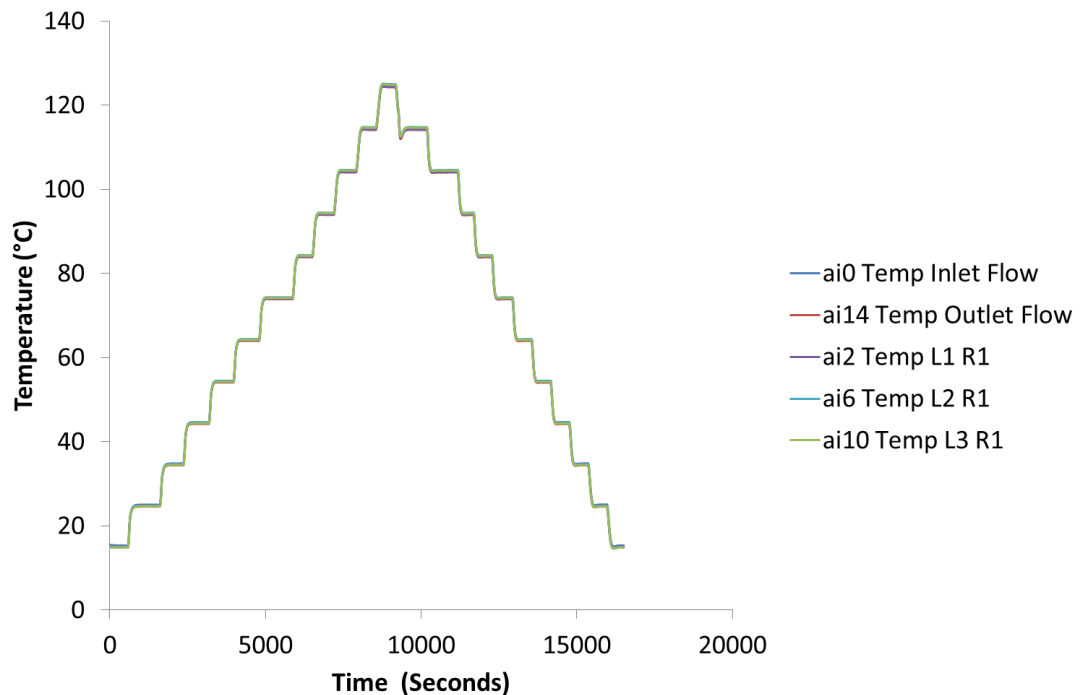


**Figure 3.18: Temperature against time for the 40 mm outer diameter test block specimens and oil flow thermocouples in the Fast Cal unit.**

An important parameter to understand is the differential temperature between the thermocouples at the inlet flow and outlet flow positions. The small time frame that the lubricant spends in the test block specimen ( $0.47 \text{ seconds at } 10 \text{ l min}^{-1}$  flow rate) means that the reduction in lubricant temperature as it passes through could be less than  $1 \text{ }^\circ\text{C}$ .

Shown in Figure 3.19 is a close up plot of the inlet and outlet flow temperature thermocouple readings. It can be seen that regardless of the temperature range in question, the inlet thermocouple reads consistently  $0.5 \text{ }^\circ\text{C}$  higher than the outlet temperature, suggesting that any temperature differential in the lubricant would need to be greater than  $0.5 \text{ }^\circ\text{C}$  to be reliably identified. While not as significant, the temperature differential between the flow thermocouples and those mounted at radius R1 in the test block specimen were observed to be within  $0.5 \text{ }^\circ\text{C}$  of the flow thermocouples also. The possible small temperature differences between the inlet and outlet lubricant temperature, meant that it was necessary to ensure that there was no physical temperature differential within the calibration block test port. Consequently, the thermocouples were swapped in location relative to the test in

Figure 3.19. It was found that the inlet thermocouple still recorded a temperature 0.4 °C higher than the outlet thermocouple, suggesting no temperature gradient exists within the calibration unit itself.

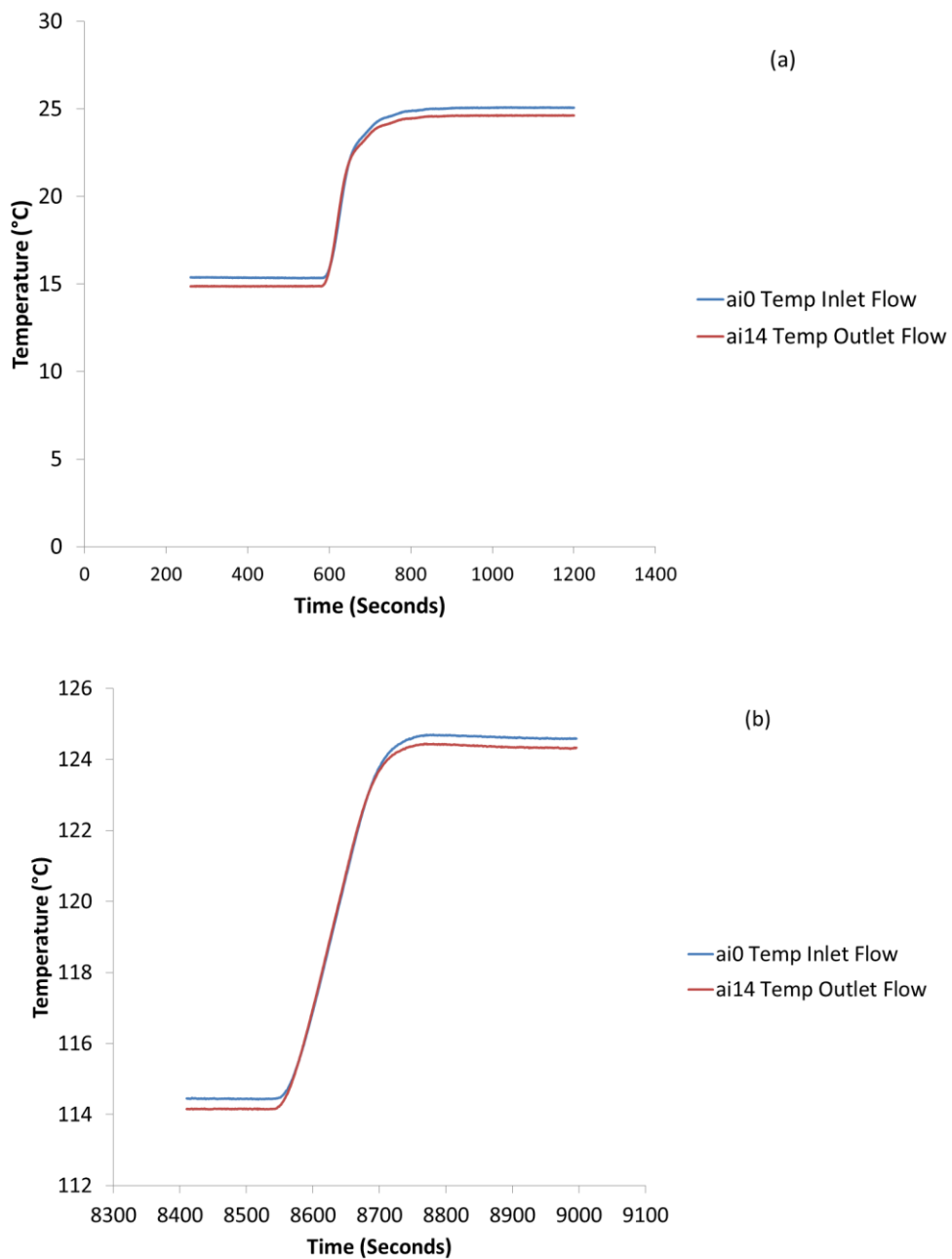


**Figure 3.19: Temperature profile between (a) 15- 25 °C and (b) 115-125 °C for the inlet flow and outlet flow thermocouples in the Fast Cal unit**

Critically, as will be seen in the experimental results in Chapter 4 and Chapter 5, the uncertainty of the temperature differential between the lubricant and specimen at location R1 has been proven to be a maximum of 1 °C. If one considers an un-insulated 40 mm outer diameter specimen, the peak temperature differential between the lubricant and specimen was 7 °C, indicating a percentage uncertainty of 14 %. However, when using the 100 mm outer diameter specimen, the temperature

differentials were far higher, with a peak uninsulated temperature differential of 22 °C in the uninsulated scenario and up to 56 °C when insulation was applied, reducing the uncertainty to 4.5% and 1.8% respectively.

### 3.5.1.2 Verification of lubricant temperature differential along the specimen using the oil flow rig

To investigate if the temperature differential between the lubricant temperature at the inlet and outlet was identifiable using the instrumentation, two identical tests were carried out with the following parameters.

- 40 mm outer diameter specimen with a 2 mm thick drawn aluminium insert.
- 1200 W heater power.
- 10 l min<sup>-1</sup> flow rate.

In one test, the thermocouples of the inlet lubricant position and outlet lubricant position were the same as used in all the other tests while in the second, the thermocouples were swapped relative to each other. The specimen thermocouples during this test were unchanged. An overview of the temperature profiles from the two lubricant temperature thermocouples during the two tests is shown in Figure 3.20. It can be seen that owing to variations in the ambient temperatures in the laboratory, the test with the switched thermocouples was approximately 3 °C cooler than the original test, but is nonetheless a representative comparison of thermocouple performance.

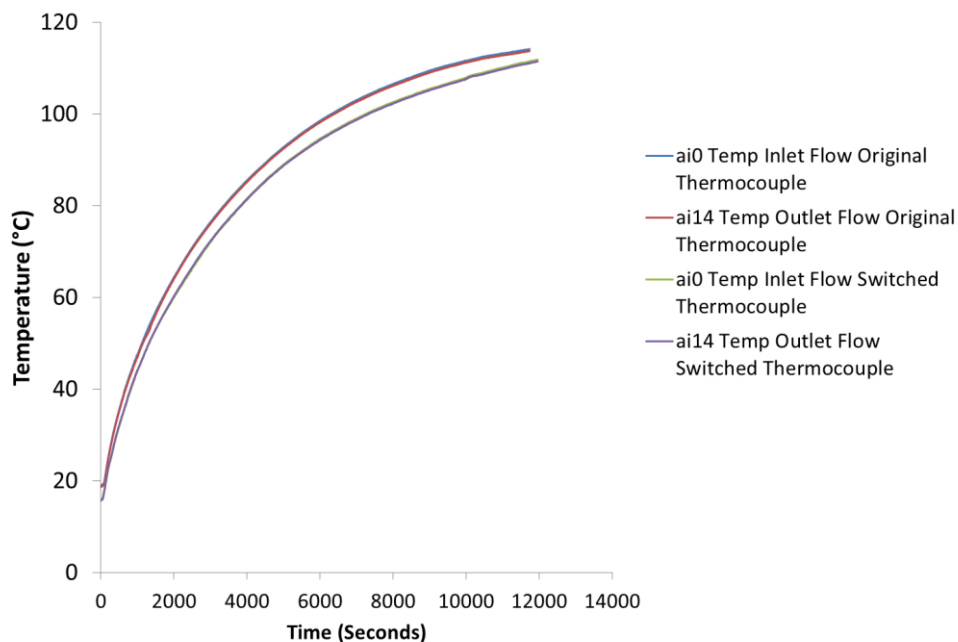
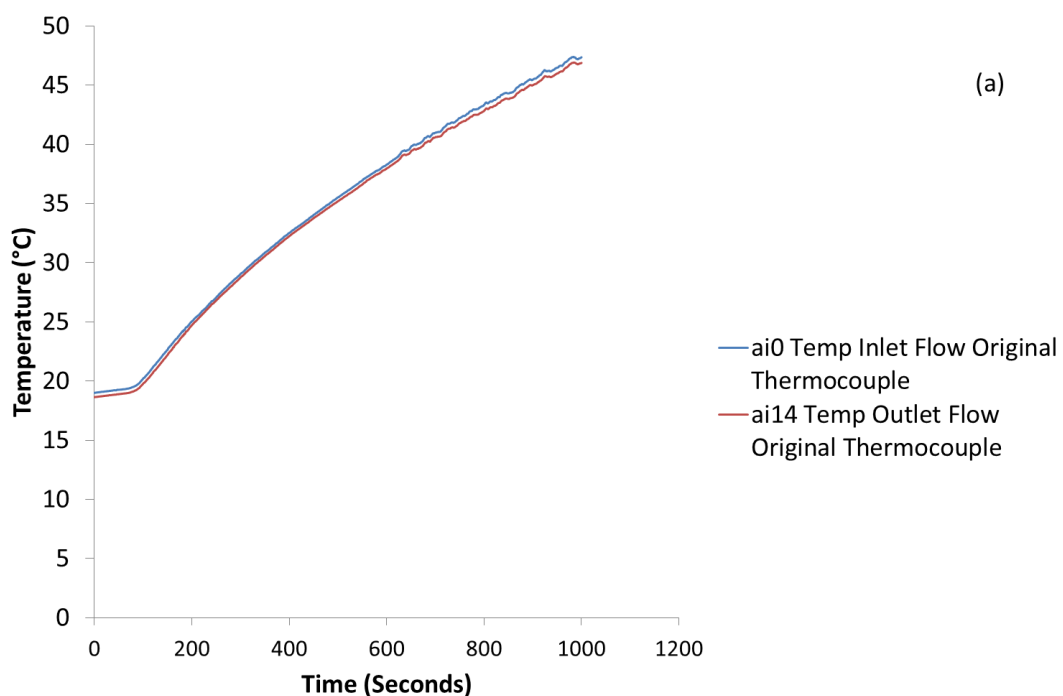


Figure 3.20: Lubricant temperature profiles at the specimen inlet and outlet when the flow thermocouples are in their original position and when they have been swapped. The heater power was set to 1200 W and the lubricant flow rate controlled at 10 l min<sup>-1</sup> while the specimen was 40 mm outer diameter with a 2 mm thick aluminium insert installed

Figure 3.21 and Figure 3.22 plot the temperature profile of the inlet and outlet thermocouples between 0–1000 seconds and 9000–10000 seconds when the thermocouples are in their original and swapped locations respectively. Comparing the two, it can be seen that in the original location, the inlet temperature reading is approximately 0.5 °C higher than the outlet temperature reading. Comparatively, when the thermocouple locations are swapped, the inlet temperature reading, in the latter stages of the test, is approximately 0.2 °C higher, though in the early stages of the test the outlet temperature can read higher than the inlet.

Such observations, combined with the calibration unit, indicate that the temperature differential of the lubricant between the inlet and outlet of the specimen cannot be reliably determined from the experimental data. Instead, the two temperature readings are better used as an average lubricant temperature. Such small temperature differentials between the inlet and the outlet also prove that the lengths of connecting hoses, discussed in Section 3.2.1, do not detrimentally affect the validity of the measured lubricant temperature in the specimen.



**Figure 3.21a: Lubricant temperature at specimen inlet and outlet when the thermocouples are in the original position when the heater power was set to 1200 W with a lubricant flow rate of 10 l min<sup>-1</sup> and the specimen is 40 mm outer diameter with a 2 mm thick aluminium insert installed between 0- 1000 seconds**

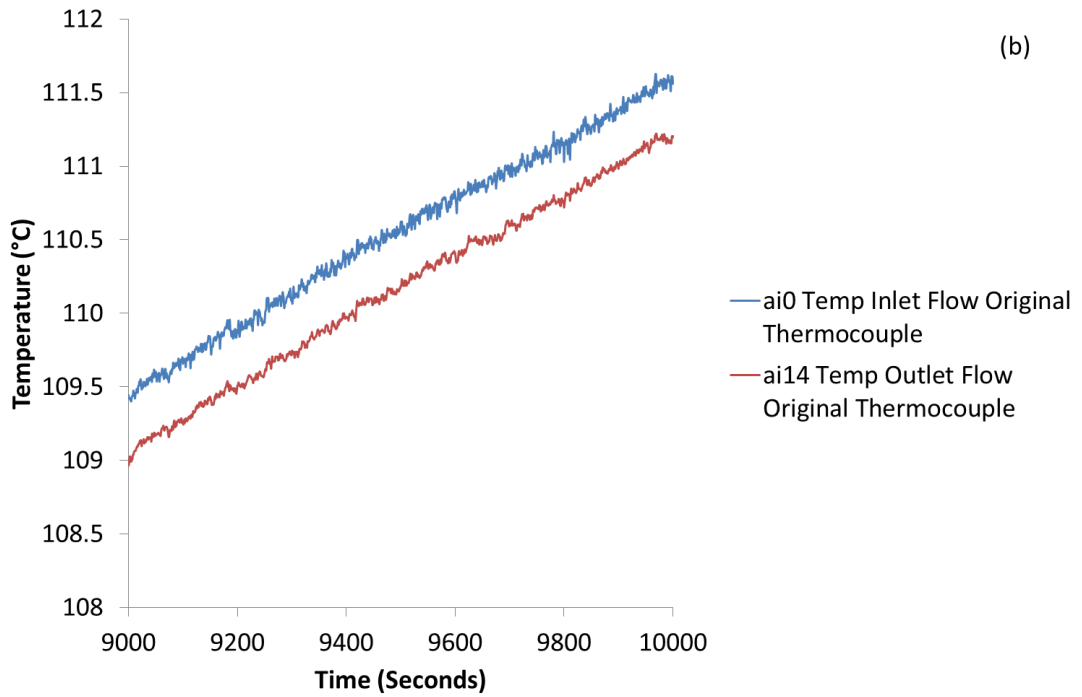


Figure 3.21b: Lubricant temperature at specimen inlet and outlet when the thermocouples are in the original position when the heater power was set to 1200 W with a lubricant flow rate of 10 l min<sup>-1</sup> and the specimen is 40 mm outer diameter with a 2 mm thick aluminium insert installed between 9000 – 10000 seconds

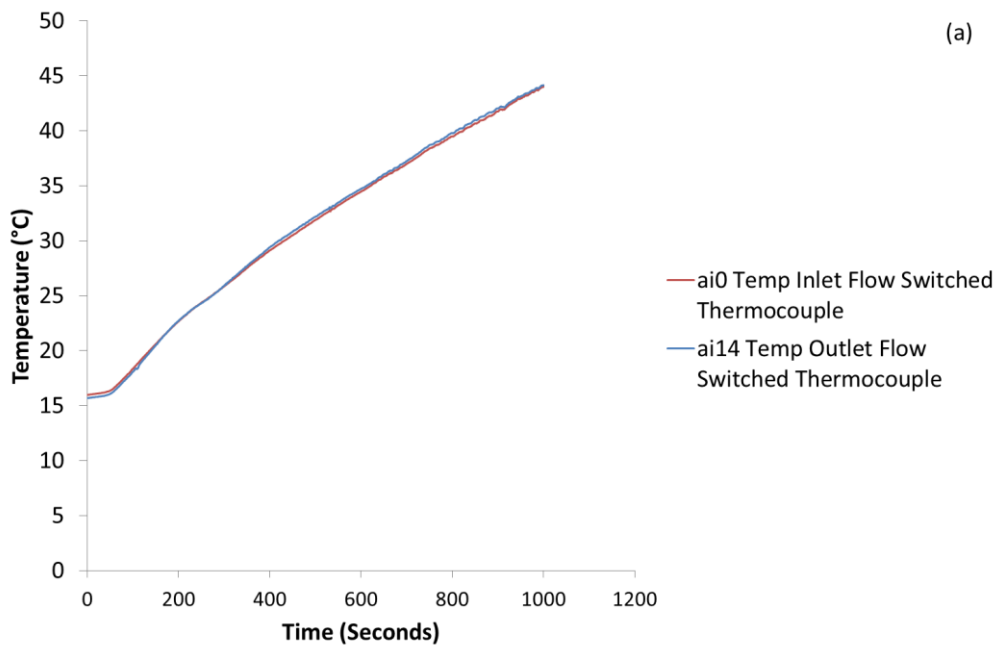


Figure 3.22a: Lubricant temperature at specimen inlet and outlet when the thermocouples are swapped in position relative to Figure 3.21 when the heater power was set to 1200 W with a lubricant flow rate of 10 l min<sup>-1</sup> and the specimen is 40 mm outer diameter with a 2 mm thick aluminium insert installed between 0- 1000 seconds

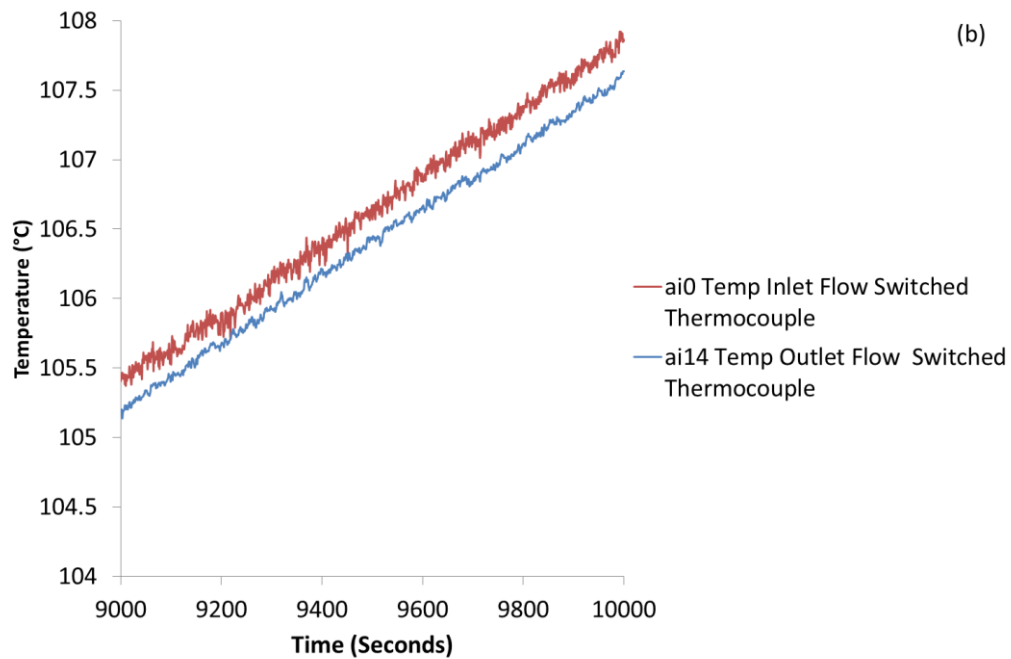


Figure 3.22b: Lubricant temperature at specimen inlet and outlet when the thermocouples are swapped in position relative to Figure 3.21 when the heater power was set to 1200 W with a lubricant flow rate of  $10 \text{ l min}^{-1}$  and the specimen is 40 mm outer diameter with a 2 mm thick aluminium insert installed between 9000 – 10000 seconds

### 3.6 Experimental methodology

Within the rig, the following parameters are variable:

- Heater power.
- Lubricant flow rate.
- Specimen outer diameter.
- Presence or absence of an insulator.
- Insulator material.

Within the scope of the experimental work, across a given test, the heater input power was kept constant via the heater controller. The baseline heater power was set to 1200 W to replicate common heat to oil figures reported across the literature [20, 25, 65] though subsequent work did investigate the significance of increasing the heater power to 1800 W and reducing the heater power to 600 W (Chapter 4, Section 4.8).

The lubricant flow rate was set to a baseline flow rate of  $10 \text{ l min}^{-1}$ , to ensure cavitation did not occur at the pump inlet when the lubricant was at its most viscous during the early phase of a test. The flow rate was subsequently increased to  $15 \text{ l min}^{-1}$  to investigate the sensitivity to flow rate, as reported in the results of Chapter 4 (Section 4.6).

The rig facilitates the installation of test block specimens of varying sizes and compositions and the rationale behind the design of specimen variants has already been documented. During a test procedure, the lubricant flow rate was selected on the control panel of the pump and the pump speed ramped to a steady state value. During this time, the heater was not activated to allow the pump speed to stabilise. Once the pump speed had stabilised, the heater was activated. Such an approach ensured that the heat transfer coefficient between the lubricant and specimen was changing only as a result of temperature-dependent fluid properties and not due to the flow rate. As will be discussed in Chapter 6, a known flow rate was vital in developing the correlated simulation model which was developed in conjunction with the experimental results from the rigs.

Once activated, the rig was left to heat up naturally, until the lubricant reached a temperature of 120 °C or the lubricant was approaching steady state temperature.

While each test conducted on the rig was carried out using the same procedure, it is important to highlight the greatest variable across the spectrum of tests carried out was the ambient temperature of the laboratory which could range from 23 °C to 13 °C over the course of a year's testing. The implications of such a variation are discussed in Chapter 4 (Section 4.6 and Section 4.9), Chapter 5 (Section 5.8) and Chapter 7 (Section 7.4).

## 4 Characterisation of the oil flow rig

### 4.1 Introduction

The purpose of this chapter is to develop an understanding of the dynamics and sensitivities of the rig to parameters before the key experimental findings are discussed in Chapter 5. The primary aim of the oil flow rig is to develop an understanding of the potential benefits of internally insulating engine oil galleries during warm-up. However, to best understand the data it is necessary to develop an understanding of the performance metrics used in conjunction with rig.

This chapter investigates the transient response of the test block specimens to heating from the lubricant and pays particular attention to the presence or absence of temperature gradients both throughout the radial thickness and along the horizontal length of the test block specimen. Similarly, the sensitivity of the lubricant temperature profile to changes in test parameters is also examined. Closely linked to the experimental results from the oil flow rig has been the development of a theoretical simulation model for the rig to investigate parameters outside the physical capability of the rig. The development of the model and the underlying physical assumptions are discussed in greater detail in Chapter 6. Both within the oil flow rig results in Chapter 5 and the model development in Chapter 6, the average lubricant temperature,  $T_{Average}$ , is referred to frequently. This is the mean temperature of the inlet and outlet lubricant thermocouple readings and the validity, relative to the accuracy of the instrumentation, has already been investigated at length in Chapter 3. Similarly, the specimen temperature,  $T_{specimen}$ , refers to the average temperature of the thermocouples at locations R1, R2 and R3 i.e. the three longitudinal locations. A key deliverable of the initial rig characterisation is the validity of using an average temperature for the specimen rather than discretising along the length of the specimen and through its thickness.

The temperature differential between the lubricant and the test block specimen is fundamental to understanding and quantifying heat flow. With an understanding of the sensitivity of the lubricant and test block specimen temperatures in isolation, this chapter seeks to explain how the temperature differential profile can be used to understand the relative effects of different insulating strategies.

The focus of the experimental work and the results is the test block specimen. However, to best interpret the results an understanding of the effect of other rig variables is necessary. Thus this chapter investigates the effect of tank insulation and the relative effect of varying the heater power (analogous to heat to oil) on both lubricant and specimen heating rates. Consequently, the concept of the effective power is introduced which quantifies the energy flow to both the lubricant and specimen in isolation of the effects of other rig hardware.

Key limitations into the experimental methodology are also investigated and appraised. This involves quantifying the repeatability of the experimental procedure and also quantifying any limitations in temperature readings as a result of fluid boundary layers.

## 4.2 Observations of the temperature gradients within the test block specimen

In Chapter 3, it was shown that the temperature differential between the lubricant at the specimen inlet and outlet was too small to be distinguished from the sensitivity in temperature readings of the individual inlet and outlet thermocouples

In a steady state situation, one would expect the temperature gradient across the radial thickness and the longitudinal length of the specimen to be too small to be measured. Indeed, owing to the high thermal conductivity of the aluminium (193 W m<sup>-1</sup> K<sup>-1</sup> [93]) one would expect to be able to treat the test block specimen as a lumped capacity. However, during the transient warm-up phase it is critical to gain an understanding of the rate of heat propagation through the test block specimen during warm-up. In any thermal resistance network, the thermal resistance between two locations is given by Equation 4.1:

$$R_{thermal} = \frac{\Delta x}{k}$$

Where:  $R_{thermal}$  = The thermal resistance in m<sup>-2</sup> K W<sup>-1</sup>.

$\Delta x$  = The characteristic length (in this case the radius) in m.

$k$  = The thermal conductivity of the material in W m<sup>-1</sup> K<sup>-1</sup>.

### Equation 4.1: Thermal resistance through a solid object

Of the two specimen sizes used in the experimental work, the 100 mm outer diameter specimen would present the highest radial temperature gradient owing to the higher thermal resistance. This specimen is therefore used to investigate the variation in temperature through the specimen. Owing to the different dynamics of heat transfer with the presence of an insulator, both an insulated and uninsulated specimen were investigated. Figure 4.1 and Figure 4.2 show plots of temperature against time for a 100 mm outer diameter specimen when the lubricant flow rate and heater power are set to the baseline parameters of 10 l min<sup>-1</sup> and 1200 W respectively. In Figure 4.1, the temperature gradient through the radial thickness is compared against time. The specimen was heated until the lubricant reached an apparent steady state temperature (in this instance the lubricant reached a temperature of 112 °C and had shown less than 0.2 °C change in temperature in 6 minutes). It can be seen that regardless of the point in time of the test, there is no

identifiable temperature differential between the R1, R2 and R3 locations in either the insulated or uninsulated specimens. Similarly, if one looks at Figure 4.2, one can see that, in the case of the insulated specimen, there is no observable temperature gradient along the length of the specimen. Meanwhile, along the length of the uninsulated test block specimen, the temperature at L1 shows an apparent trend to be 2 °C higher than the thermocouples at L2 and L3. This may be due to variations in the seating of the thermocouple in the specimen, although this is unlikely given the rest of the material showing homogenous performance. However, the difference observed is of the order of 2 °C at 100 °C and therefore represents a small percentage variation. Thus it was felt that the assumption of a single average specimen temperature remained valid for the purposes of this work. Having also proven that the lubricant temperature is constant along the length of the test block specimen, relative to the uncertainty of the thermocouples, in Section 3.5.1.2, it is also worth highlighting that the log mean temperature difference, discussed in Section 2.2.3.2, is the value of the inlet or outlet temperature differential.

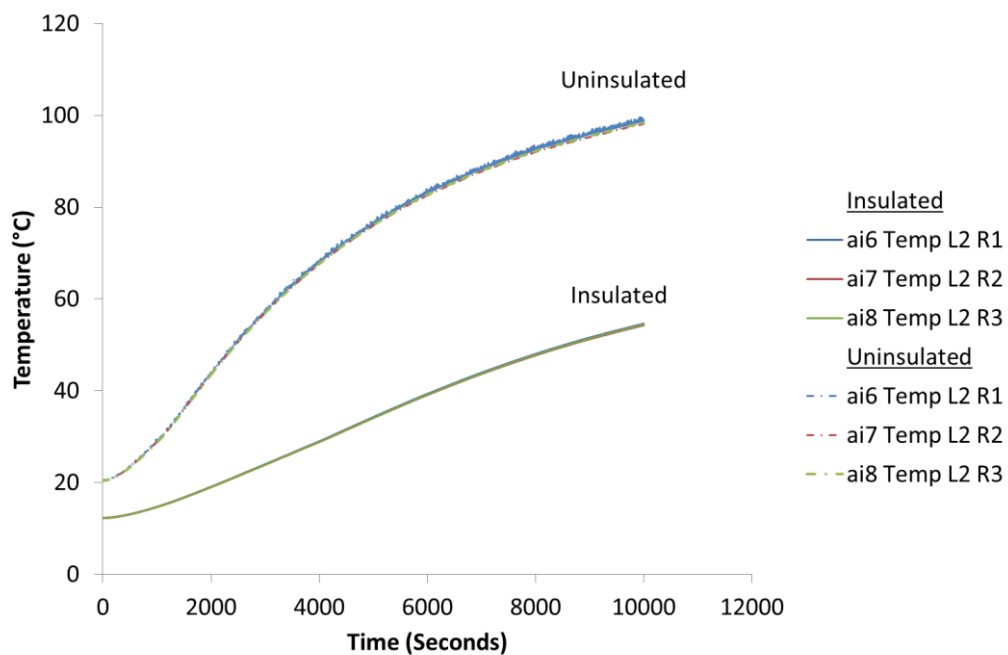


**Figure 4.1: Comparison of specimen metal temperatures through the radial thickness of a 100 mm outer diameter specimen when the heat input is 1200 W and the lubricant flow rate is 10 l min<sup>-1</sup> with an externally insulated tank in the case of an uninsulated specimen and a specimen with a 2 mm thick Nylon 12 insert installed**

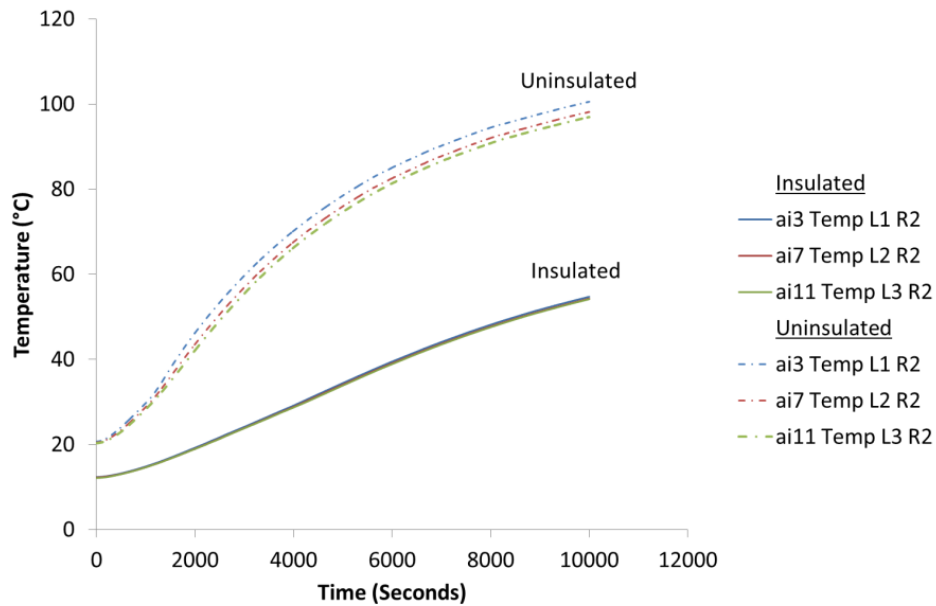


Figure 4.2: Comparison of specimen metal temperatures along the longitudinal length of a 100 mm outer diameter specimen when the heat input is 1200 W and the lubricant flow rate is  $10 \text{ l min}^{-1}$  with an externally insulated tank in the case of an uninsulated specimen and a specimen with a 2 mm thick Nylon 12 insert installed

#### 4.2.1 The significance of the temperature differential between the lubricant temperature and specimen temperature

The results presented thus far show that the test block specimen and lubricant temperature noticeably take of the order of 10000 seconds to reach either a steady state temperature or reach the peak lubricant temperature limit of  $120 \text{ }^\circ\text{C}$ . However, the nature of this research is concerned with lubricant warm-up performance in the 1180 seconds timeframe of the NEDC. The longer time frame for these experiments is a consequence of the supporting rig hardware also undergoing transient warm-up. The lubricant and test block specimen form only a small part of the thermal balance of the rig. This is discussed in greater detail in Section 4.4. However, in order to generate performance measures that are relevant to the time frame of engine lubricant in a vehicle engine, one can use the plot of the temperature differential between the lubricant and specimen plotted against the lubricant temperature (rather than time). In doing so, the results are effectively normalised against time and one can see the relative performance of an insulating mechanism at a given lubricant temperature.

It is worth considering the desired output from applying insulation. To raise the temperature of any thermal mass, be it liquid or solid, requires an input of energy. The only source of thermal energy to the test block specimen is from the hot lubricant circulating through the bore. Therefore, a positive result would be one whereby the test block specimen is kept at a lower temperature as it indicates less

energy has been transferred from the lubricant. Thus a higher temperature differential between the specimen and the lubricant is perceived as beneficial.

The temperature differential plot is also a valuable tool in being able to understand the transient dynamics of the heat transfer mechanism from the lubricant to the test block specimen and the effects that both insulation and changes in thermal mass have on the relationship between the lubricant and specimen heating rate. Figure 4.3 shows a plot of the temperature differential between the lubricant and test block specimen metal for the two different test block specimen sizes (100 mm and 40 mm outer diameter), both with and without 2 mm thick Nylon insulation inserts applied. Within the temperature frame of each test, one can see up to 3 distinct transient regimes, labelled A-C. This section aims to develop an understanding of the underlying mechanisms behind such changes in thermal behaviour and how the different regimes change between specimens of different size and configuration.

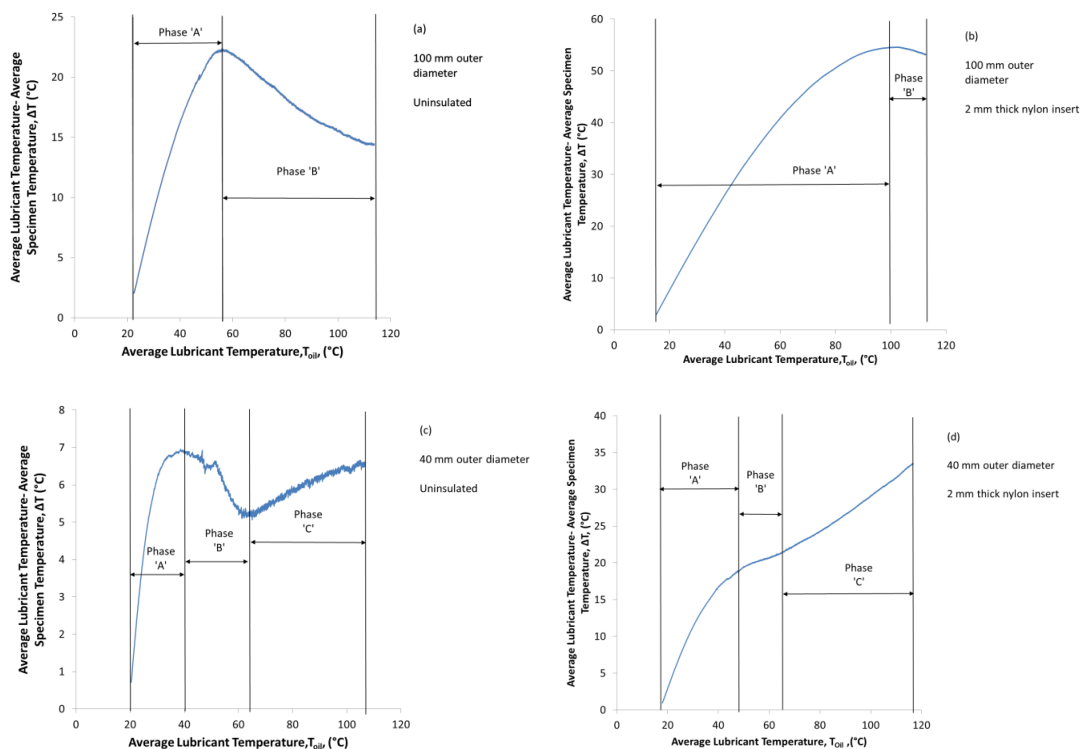


**Figure 4.3: Temperature differential between the lubricant and test block specimen metal plotted against lubricant temperature when the heater power is set to 1200 W and the lubricant flow rate is  $10 \text{ l min}^{-1}$  for (a) a 100 mm outer diameter uninsulated specimen, (b) a 100 mm outer diameter specimen with a 2 mm thick Nylon insert, (c) a 40 mm outer diameter uninsulated specimen and (d) a 40 mm outer diameter specimen with a 2 mm thick Nylon insert**

In phase A of all the test block specimens, one can see the lubricant temperature increasing owing to the heater but the energy transferred from the lubricant to the specimen is insufficient to cause the temperature of the specimen to rise, hence the temperature differential rises without exception.

In phase B, it can be seen that the temperature differential between the lubricant and test block specimen starts to fall in three of the cases (Figure 4.3a- Figure 4.3c). In Figure 4.3a and Figure 4.3c this results from there having been sufficient energy transferred to the test block specimen, relative to its thermal mass, to cause the temperature of the test block specimen to start to rise and the temperature differential subsequently falling. It is important to note that the onset of Phase B occurs at a lubricant temperature of approximately 55 °C in the case of the 100 mm outer diameter uninsulated specimen but that the smaller thermal mass of the 40 mm outer diameter specimen results in the onset of Phase B occurring earlier, at 40 °C. The late onset of Phase B in the case of the 100 mm outer diameter insulated specimen (Figure 4.3b) is a result, of the specimen temperature profile being both delayed by the presence of insulation but also having a slow rate of increase owing to its large thermal mass (the thermal mass of the 100 mm outer diameter specimen is 8 times greater than the 40 mm outer diameter specimen). One must remember that the lubricant temperature heating profile is similar between all four test block specimen variants as the heating rate is dominated by thermal losses to the rest of the rig system. Consequently, at the point that the lubricant temperature rate of increase is slowing down in the case of the 100 mm outer diameter insulated specimen (a consequence of the thermal losses from the supporting hardware of the rig), the rate of increase of the specimen temperature is higher than that of the lubricant as the external surface of the specimen is not yet sufficiently hot enough to create a heat flux to ambient that limits the specimen temperature rise.

Relative to the other specimens, Figure 4.3d (40 mm outer diameter insulated specimen) presents a unique case where one sees the rate of increase of the temperature differential (i.e. the gradient of the curve) reduce but never become negative. To understand why, warrants focusing on comparing the insulated and uninsulated temperature differential profiles from a 40 mm outer diameter specimen as shown in Figure 4.3c and Figure 4.3d. One can see, relative to the 100 mm outer diameter specimens, an additional phase, denoted phase C, that shows the temperature differential between the lubricant and specimen metal increasing again. This is a result of the outer surface temperature reaching a high enough temperature to generate a high heat flux to the ambient that ultimately limits the rate of temperature increase of the specimen. Such a phenomenon is not observed in the case of the 100 mm outer diameter specimens owing to the high thermal mass of the specimens requiring far more energy before the temperature differential between the ambient and outer surface is high enough to become a limiting factor.

With this in mind it is now possible to understand why the 'Phase B' shown Figure 4.3d is not a negative gradient. The two insulated specimens both exhibit a delay in the onset of specimen heating relative to the uninsulated equivalent specimens. This is illustrated in Figure 4.4 where one can see the lubricant temperature profiles for

an insulated and uninsulated 40 mm outer diameter specimen are almost identical. However, the specimen temperature profiles are dramatically different. In addition to the delayed onset of specimen heating, the insulated specimen temperature profile is also characterised by a slower rate of temperature rise relative to the uninsulated profile. The negative gradient of Phase B in Figure 4.3c (40 mm uninsulated) is a result of the rate of temperature increase in the specimen being higher than that of the lubricant whereas Figure 4.3d (40 mm insulated) shows the reverse to be true as the heating rate of the specimen is reduced although the gradient decreasing does represent the rate of specimen temperature increase rising. Thus, the reason for the presence of a positive gradient in Phase B of Figure 4.3d is twofold. Relative to the equivalent sized uninsulated specimen, the insulating insert has delayed both the onset and reduced the heating rate of the test block specimen. However, the small thermal mass of the test block specimen still sees the specimen temperature rising and hence the rate of increase of the temperature differential is reduced in this phase, although the gradient does not become negative. The small thermal mass of the test block specimen results in the external heat transfer mechanism becoming active and hence one sees the temperature differential rising at an increased rate again at the end of the test.

Thus, through this section it has been possible to develop an understanding into the significance of the temperature differential profiles for both the different sized test block specimens and also those of different material composition. However, in appraising these temperature differential profiles it is important not to ignore the thermal energy that is retained in the polymer insert. While an increased temperature differential between the lubricant and test block specimen does indicate reduced heat flow, the heating of the polymer insert still requires energy and is a critical variable in reducing the temperature differential, and subsequent heat flow, between the lubricant and the bore wall. Thus there is an apparent need to consider the specific heat capacity of any insulating material when trying to reduce the thermal losses from the lubricant. Such investigations are discussed in Chapter 7.

### **4.3 The sensitivity of lubricant temperature to specimen structure**

The aim of this research was to investigate possible ways of improving lubricant warm-up by reducing the thermal energy transferred to the metallic structure of the engine block from the gallery walls. Thus before discussing the full suite of experimental results it is necessary to understand the sensitivity of the lubricant temperature to changes in the test block specimen design.

It has been shown in Section 4.2.1 that the presence of the insulator has a significant effect on the heat transfer to the test block specimen. A comparison of Figure 4.3a -

Figure 4.3d shows that the peak temperature differential between the lubricant and test block specimen increases from 22 °C to 54 °C as a result of installing a 2 mm thick Nylon 12 insert into a 100 mm outer diameter specimen and from 6 °C to 34 °C in the case of a 40 mm outer diameter specimen. However, if one looks at Figure 4.4, it can be seen that the primary effect is to lower the temperature of the specimen and not increase the temperature of the lubricant. Figure 4.4 shows the peak specimen temperature is reduced from 100 °C when uninsulated to 76 °C when the Nylon 12 insert is installed into the 40 mm outer diameter specimen. Such trends are not reflected in the lubricant temperature warm-up which appears almost identical. Such a trend is highly unintuitive and the two trends observed should be mutually exclusive based on the conservation of energy. However, if one looks more closely at the lubricant temperatures in Figure 4.4 it can be seen that the lubricant temperature in the insulated scenario commences the test 2 °C lower than the temperature in the uninsulated scenario. If such an offset were removed, the insulated lubricant temperature would appear marginally higher than the uninsulated scenario but still does not reflect the large differential in specimen temperature. Such an occurrence is a consequence of the varying laboratory conditions from test to test.

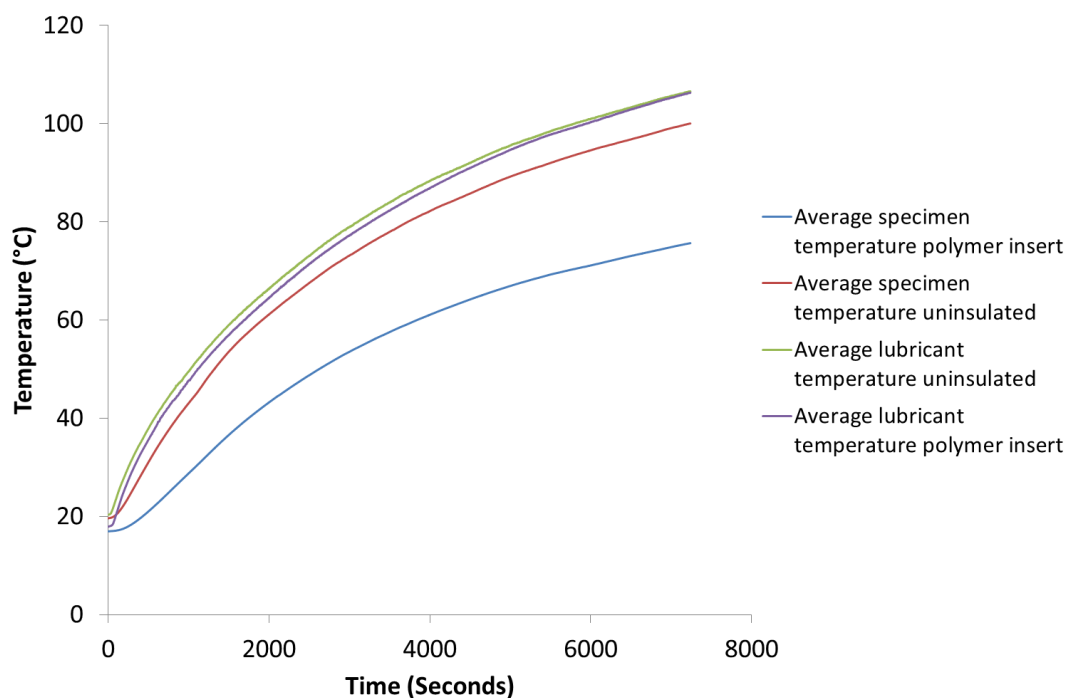


**Figure 4.4: Comparison of specimen metal temperatures and lubricant temperatures for both a 40 mm uninsulated specimen and one with a 2 mm thick Nylon 12 insert installed when the heat input is 1200 W and the lubricant flow rate is 10 l min<sup>-1</sup> with an externally insulated tank**

To understand why the above observation occurs requires an appreciation of the size of the specimen relative to the rest of the rig architecture. The size and length of the test block specimens were designed to replicate the length and bore of the main

engine oil gallery of a typical engine while enabling the thickness of the surrounding casting to be investigated. However, as a result of the size of the specimen, it represents only a small fraction of the total thermal inertia of the rig. The heating rate of the lubricant is therefore dominated by other components including the tank and the cast pump head while the two oil filters provide an effective heat transfer mechanism to ambient.

While the rig has the ability to demonstrate the effectiveness of insulation by reducing the specimen temperature, the benefit to the lubricant temperature is masked by other rig hardware dominating the transient timeframe of the rig. Consequently, the results analysed from the rig focus on the temperature differential between the lubricant and the specimen and the cumulative energy lost to the specimen as a measure of relative performance.

#### **4.3.1 The sensitivity of lubricant temperature to specimen size**

To understand if the specimen size affects the lubricant temperature, two comparative tests were carried out with an uninsulated specimen. One was conducted with an uninsulated 100 mm outer diameter specimen and the second was conducted with an uninsulated 40 mm outer diameter specimen with the heater power being controlled at 1200 W and the flow rate maintained at 10 l min<sup>-1</sup> in both cases. Shown in Figure 4.5 is a plot of the temperature differential between the lubricant and specimen in both cases. One can clearly see that the specimen size does generate a significantly different transient regime with the peak temperature differential in the case of the 100 mm outer diameter specimen reaching 22 °C and the 40 mm outer diameter specimen only reaching a value of 6 °C.

The physical dynamics of the differing transient regimes has already been discussed in Section 4 but despite such differences, Figure 4.6 indicates the effect of specimen size on lubricant temperature is negligible. The variation in temperature differential is instead almost entirely a result of variations in the specimen temperature and the lubricant temperature profiles remain within 1 °C of each other. Thus, in the same way that specimen composition effects are reflected by the specimen temperature but not the lubricant temperature, the same has been proven to be true of specimen size.

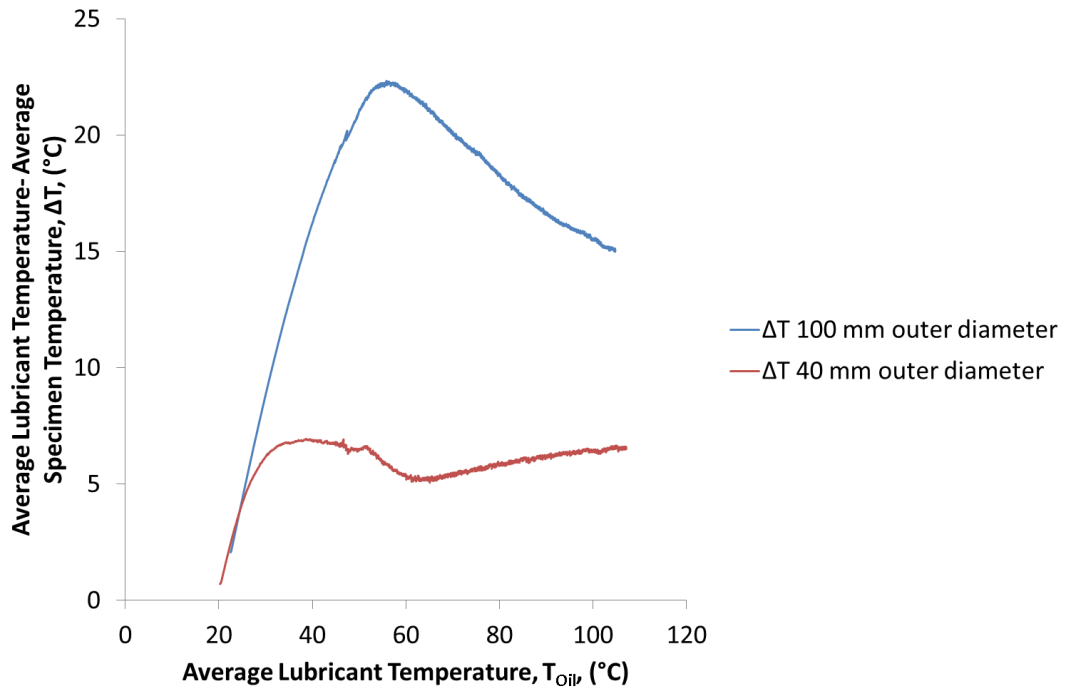


Figure 4.5: Temperature differential between the lubricant and test block specimen a when using a 100 mm outer diameter and 40 mm outer diameter uninsulated specimen with 1200 W heater input power and  $10 \text{ l min}^{-1}$  flow rate

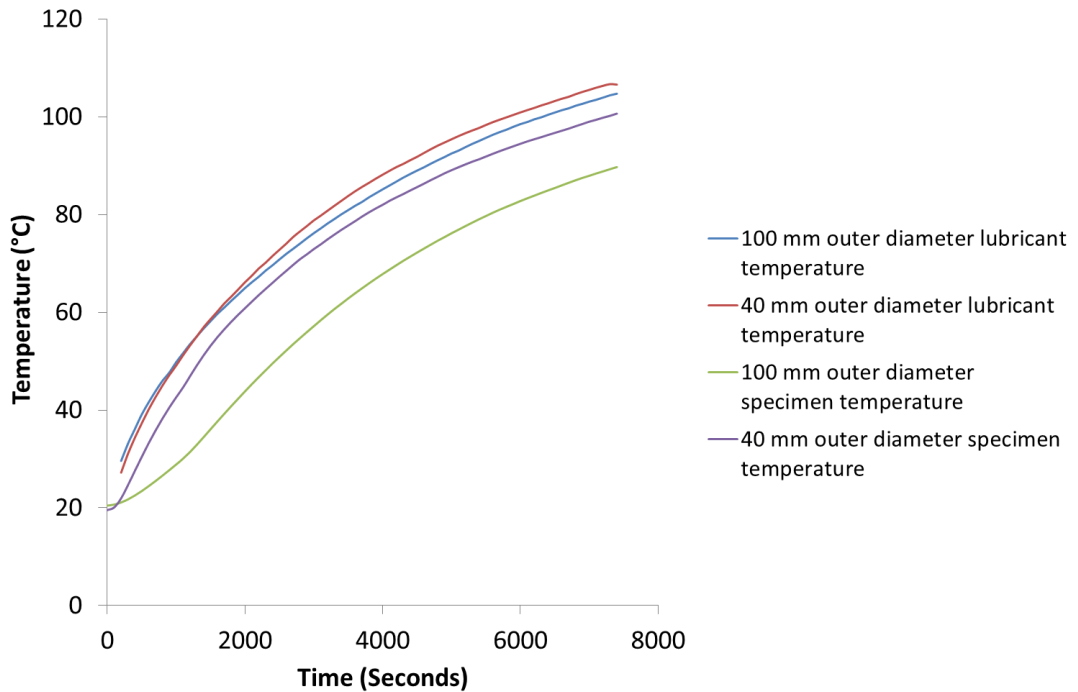


Figure 4.6: Average lubricant and specimen temperatures for the oil flow rig when using a 100 mm outer diameter and 40 mm outer diameter uninsulated specimen when the heater power was set to 1200 W and the flow rate set to  $10 \text{ l min}^{-1}$

## 4.4 Overall rig thermal balance

To understand why the lubricant temperature is seemingly inert to the specimen size and composition, an energy audit of the rig has been undertaken. The only source of energy input to the rig is that of heat from the electrical heater. The energy then has four possible destinations as detailed in Figure 4.7. The right hand branch of the flow network is very difficult to quantify as different items of hardware operate at different temperatures and the external surface area for heat transfer to ambient is highly variable across the rig. However, the left hand branch, associated with the lubricant and test block specimen, is much more readily analysed.

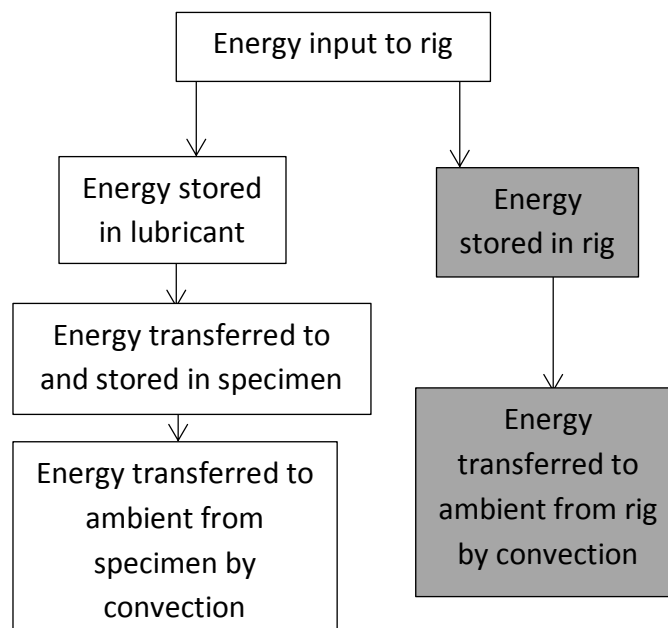


Figure 4.7: Energy flow chart for oil flow rig

The cumulative energy stored in the lubricant, as a result of the energy input by the heater is defined in Equation 4.2. It should be noted from Chapter 3 that the specific heat capacity and density of the lubricant are highly sensitive to temperature and therefore, an incremental approach is needed to calculate the energy stored in the lubricant.

$$Q_{\text{stored lubricant}} = \int_{T_{\text{start}}}^{T_{\text{finish}}} m_{\text{lubricant}} C_{p_{\text{lubricant}}} dT$$

Equation 4.2: Cumulative energy stored in lubricant

The cumulative energy stored in the test block specimen is defined in Equation 4.3 and is identical in form to that of the lubricant however, the mass and specific heat capacity are assumed constant in the case of the aluminium. In order to fully understand the energy flow from the lubricant and the specimen, it is necessary to account for the energy transferred from the outer surface of the test block specimen

to ambient by convection using Equation 4.4. However, the outer heat transfer coefficient,  $h_{outer}$ , varies with the surface temperature of the test block specimen. A Nusselt correlation, defined in Equation 4.5, was used to determine the external heat transfer coefficient in conjunction with Equation 4.6. It should be noted that all the fluid properties were analysed at the film temperature, that being the average of the ambient air and surface temperature. By the summation of Equation 4.3 and Equation 4.4 it is possible to calculate the total energy transferred from the lubricant to the test block specimen over time, and see how the thermal balance of the rig changes with different designs of specimen. The total effective energy supplied to the rig (i.e. energy accounted for in the left hand branch only of Figure 4.7), including heating the lubricant, is given by the summation of Equation 4.2, Equation 4.3 and Equation 4.4.

$$Q_{stored\ specimen} = \int_{T_{start}}^{T_{finish}} m_{specimen} C_{p_{specimen}} dT$$

**Equation 4.3: Cumulative energy stored in test block specimen**

$$Q_{ambient} = \int_{T_{start}}^{T_{finish}} \pi D_{outer} L_{specimen} h_{outer} (T_{R3} - T_{ambient}) \delta t dT$$

**Equation 4.4: Cumulative energy transferred to ambient from the outer surface**

$$Nu = \left\{ 0.6 + \frac{0.387 Ra^{1/6}}{\left[ 1 + \left( \frac{0.469}{Pr} \right)^{9/16} \right]^{4/9}} \right\}^2$$

**Equation 4.5: Nusselt heat transfer correlation for a horizontal cylinder due to natural convection**

$$h_{outer} = \frac{Nu k_{air}}{D_{outer}}$$

**Equation 4.6: Heat transfer coefficient as a function of Nusselt Number.**

To demonstrate the change in the overall thermal balance of the rig, the two variants of the specimen were compared to show the effect of specimen size. The two specimens compared were:

1. 100 mm outer diameter uninsulated specimen.
2. 40 mm outer diameter uninsulated specimen.

Figure 4.8 compares the cumulative effective energy input between the two specimen variants. It can be seen that by reducing the specimen size from 100 mm outer diameter to 40 mm outer diameter, the cumulative energy supplied to the

lubricant and specimen reduces from 2.0 MJ to 1.5 MJ in the case of the uninsulated specimens over 6900 seconds. Table 4.1 compares the average effective power supplied to the rig for the two variants of specimen and one can see a reduction from 290 W to 212 W as a result of specimen size. In all these tests, the heater power was maintained at 1200 W and thus the figures in Table 4.1 indicate that between 75% and 82% of the heater power is either used to heat auxiliary hardware on the rig or is dissipated to ambient via the rig hardware. This is despite all pipework, fittings and the tank being insulated. The dependence of the effective power on specimen size has important implications when deciding upon the most beneficial locations to apply insulation and these findings are discussed further in Chapter 5 (Section 5.2.1.1).

Based on these observations one can now see that relative to the rest of the rig, the test block specimen, is only a very small fraction of the rig and thus, most of the thermal losses from the lubricant are in fact to auxiliary components on the rig. It is such a characteristic that makes the temperature of the lubricant insensitive to the design of the test block specimen. Consequently, the temperature differential between the lubricant and specimen and the cumulative energy transferred to the specimen from the lubricant, are deemed to be the most appropriate performance measures for the rig.

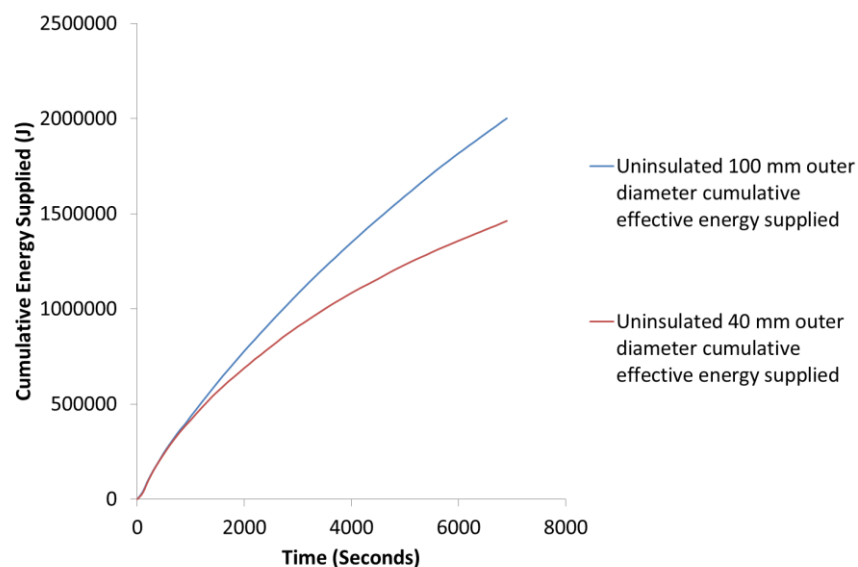


Figure 4.8: Cumulative effective energy supplied to the oil flow rig with different design test block specimens when the heater power was set to 1200 W and the lubricant flow rate maintained at 10 l min<sup>-1</sup>

Table 4.1: Average effective power supplied to the oil flow rig for different specimens when the heater power was set to 1200 W and the flow rate maintained at 10 l min<sup>-1</sup>

Specimen variant	Average effective rig power (W)
100 mm uninsulated	290
40 mm uninsulated	212

## 4.5 The effect of external tank insulation on the rate of rig warm-up

At any given instant in time, the majority of the lubricant in the rig is in the tank. Consequently, the architecture of the tank was likely to be significant in the overall warm-up rate of the rig. To minimise heat losses it was decided to insulate the external surfaces of the oil tank in 40 mm thick polystyrene insulation (See Chapter 3). In order to determine the effect of this insulation, two comparative tests were carried out using an uninsulated 100 mm outer diameter test block specimen. In these tests the flow rate was maintained at the baseline value of  $10 \text{ l min}^{-1}$  and the heater input power maintained at a constant  $1200 \text{ W}$ .

Figure 4.9 shows a plot of both the average lubricant temperature and average specimen temperature against time to compare the effect of the external tank insulation. It can be seen that in the early phases of the test there is no noticeable difference between the two test profiles but as the test progresses, the lubricant temperature, with the tank lagging applied, deviates from the uninsulated tank profile resulting in a temperature that is  $10 \text{ }^\circ\text{C}$  higher at the end of the test. Given that the hot lubricant is the only heat source to the test block specimen, it is therefore not surprising to see the specimen temperature, when the tank is lagged, to be also higher at the end of the test than the uninsulated variant. i.e.  $6 \text{ }^\circ\text{C}$  higher.

Based on these findings, it was decided that all tests would be conducted with the outer surface of the tank insulated in order to increase the significance of the test block specimen relative to the overall size of the rig.

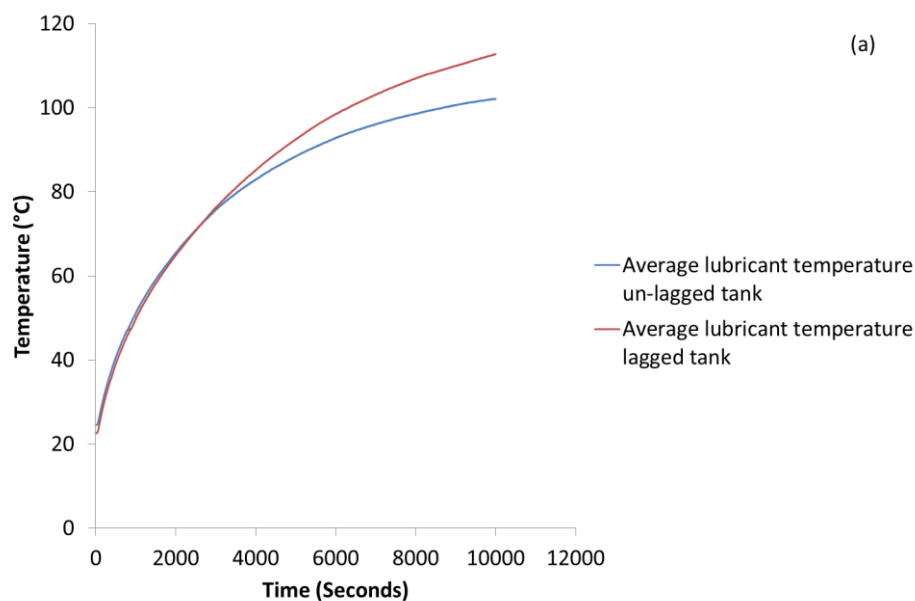


Figure 4.9a: Comparative temperatures from the oil flow rig for an uninsulated 100 mm outer diameter specimen with a  $10 \text{ l min}^{-1}$  flow rate and  $1200 \text{ W}$  heater power comparing lubricant temperatures when external tank insulation is and is not applied

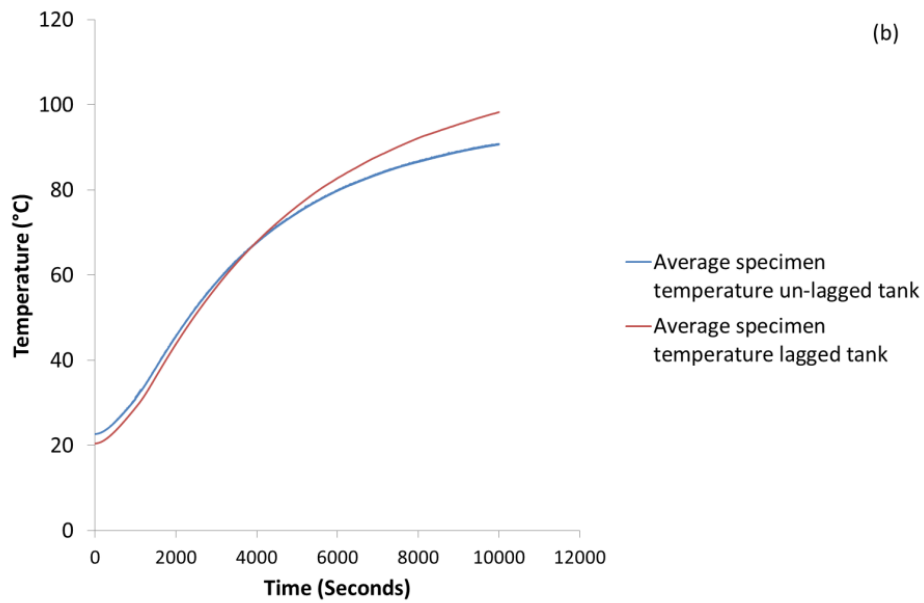


Figure 4.9b: Comparative temperatures from the oil flow rig for an uninsulated 100 mm outer diameter specimen with a  $10 \text{ l min}^{-1}$  flow rate and 1200 W heater power comparing specimen temperatures when external tank insulation is and is not applied

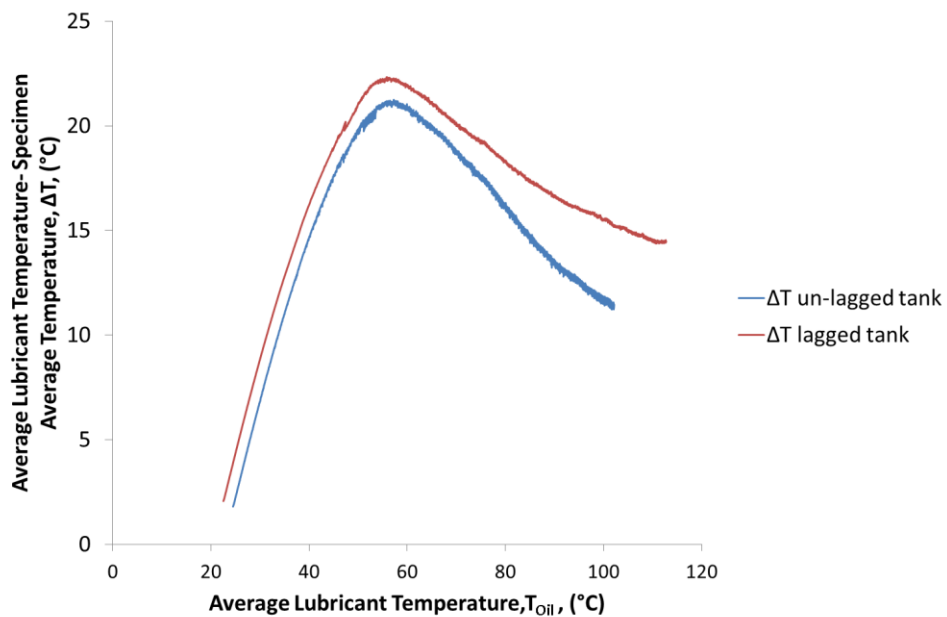


Figure 4.10: Comparison of the temperature differential between the lubricant and test block specimen metal from the oil flow rig for a 100 mm outer diameter specimen of 380 mm length with a  $10 \text{ l min}^{-1}$  flow rate and 1200 W heater when external tank insulation is and is not applied

#### 4.6 The significance of flow rate on the lubricant and specimen warm-up rate

Throughout the course of this work, tests have been carried out at both  $10 \text{ l min}^{-1}$  and  $15 \text{ l min}^{-1}$  to investigate the significance of changing flow rate. The effect of flow

rate on heat transfer is significant, with the lubricant to specimen heat transfer coefficient,  $h_{oil}$ , being a function of the Reynolds Number, that increases linearly with flow rate. Consequently, one would expect for the Reynolds Number effect to increase the value of  $h_{oil}$ , with flow rate and therefore increase the energy transferred from the lubricant to the test block specimen. Such an effect has been used in the past to promote greater heat transfer in regions of the engine that require intense cooling by Clough [107] and Finlay et al. [108] (See Chapter 7 Section 7.3) while the magnitude of the Reynolds effect in terms of the oil flow rig is discussed in greater depth in Chapter 6. It is also worth highlighting that although a lower flow rate prolongs the time period that a given volume of lubricant is in contact with the specimen (and therefore for a constant heat flux would transfer more energy to the test block specimen), such an effect is counteracted by the delivery rate of newly heated lubricant (the only heat source to the specimen) being reduced. The same effect is also true when considering the manner in which the lubricant picks up heat from the heater element at a lower flow rate.

One will see in Chapter 6, the value of the Reynolds Number does not change by a considerable margin between these two flow rates and therefore, the value of  $h_{oil}$  has stayed consistent too. Therefore, it would not be expected to see any drastic differences in temperature profiles between flow rates. Nonetheless such an analysis has been carried out to verify such a trend. Figure 4.11 shows a comparison between the specimen and lubricant temperatures at the two flow rates while Figure 4.12 compares the temperature differential between the specimen and lubricant for the scenario of a 100 mm outer diameter specimen that is uninsulated when the heater power is set to 1200 W. As one can see from Figure 4.11a, the lubricant temperature profiles are very closely matched for the two flow rates, with a maximum discrepancy of 2 °C between the two tests. When one looks at the temperature distribution for the specimen, one can see the temperature profile for the higher flow rate scenario is slightly higher than the baseline 10 l min<sup>-1</sup> test. By the end of the test, the test block specimen is 5 °C higher when flowing at a 15 l min<sup>-1</sup> than when flowing at 10 l min<sup>-1</sup>; a result of the enhanced heat transfer caused by a higher Reynolds Number.

To further compare the experimental effect of the two trends, Figure 4.12 compares the temperature differential between the lubricant and test block specimen as a function of the lubricant temperature. Again the differences are subtle with the early regime being almost identical. The peak temperature differential in the lower flow rate scenario is 1 °C higher than in the higher flow rate scenario and this offset is maintained throughout the latter stages of the test. The lower peak temperature differential is consistent with a reduced flow rate reducing the convective heat transfer coefficient and effectively providing an insulating effect relative to the higher flow rate scenario. Hence, the higher flow rate demonstrates a lower peak

temperature differential owing to the specimen temperature beginning to rise earlier as a result of increased energy flow. The slight offset in the two test profiles in the early phase of Figure 4.12 is consistent with the 15 l min<sup>-1</sup> ambient temperature being approximately 2 °C lower than the 10 l min<sup>-1</sup> test and therefore increasing the initial temperature differential between the specimen and the lubricant.

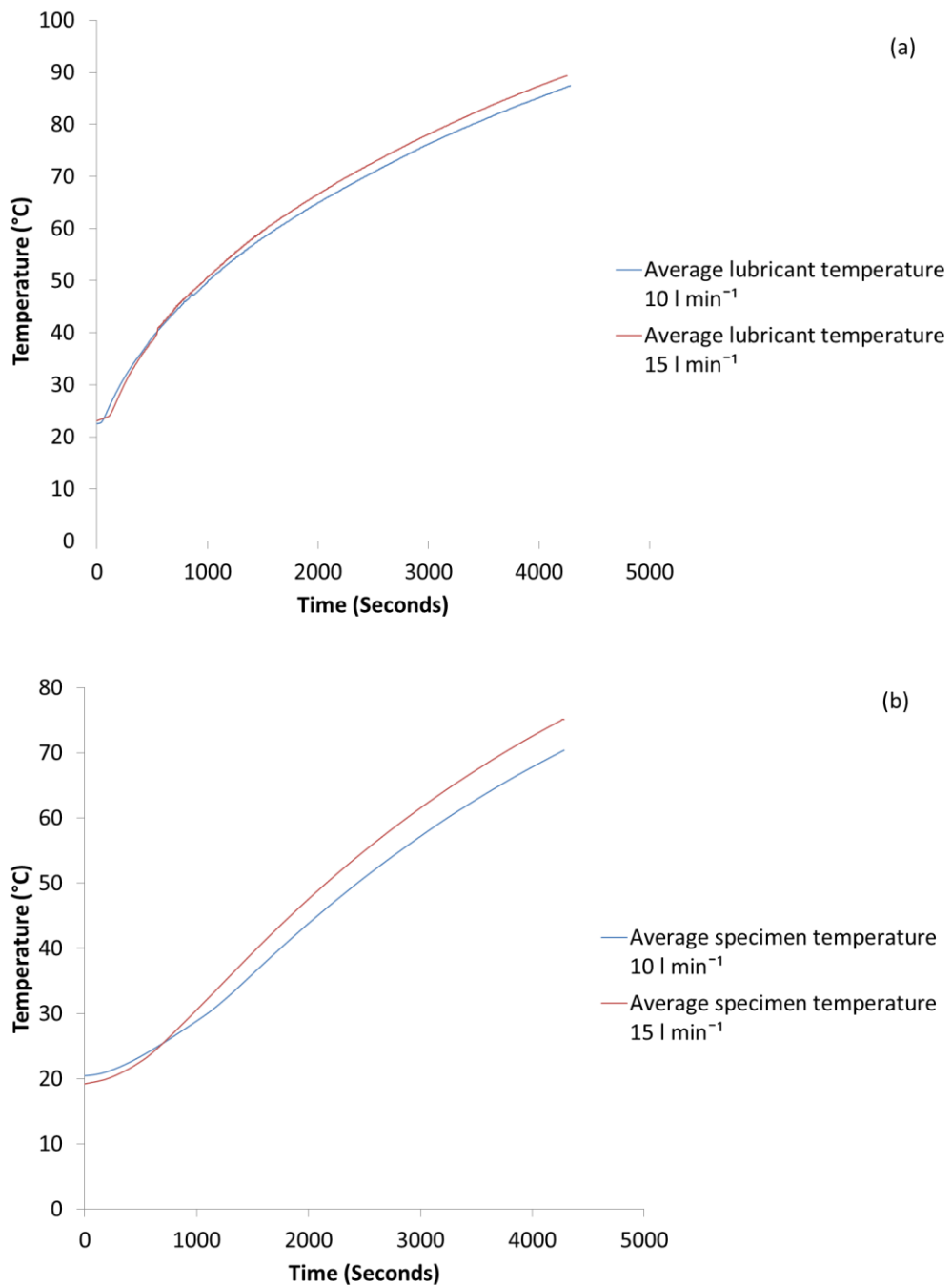


**Figure 4.11: Temperature profiles over time from the oil flow rig using a 100 mm outer diameter uninsulated specimen with 1200 W heater power and a flow rate of 10 l min<sup>-1</sup> 15 l min<sup>-1</sup> comparing (a) lubricant temperatures and (b) specimen temperatures**

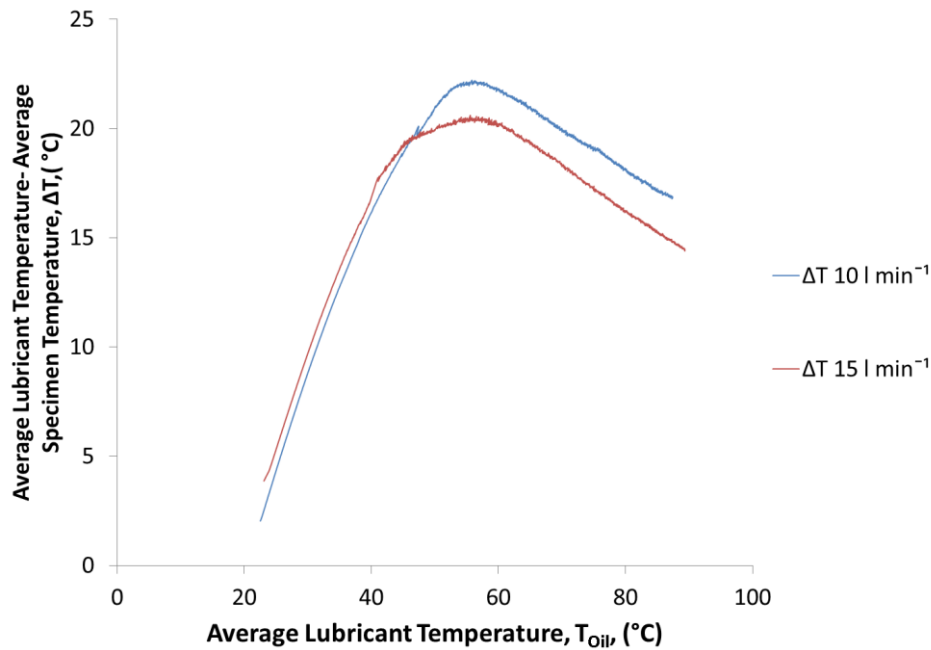


**Figure 4.12: Temperature differential between the lubricant and test block specimen plotted against lubricant temperature from the oil flow rig using a 100 mm outer diameter uninsulated specimen with 1200 W heater power applied flowing at  $10 \text{ l min}^{-1}$  and  $15 \text{ l min}^{-1}$**

To further validate the effect of flow rate on experimental findings, two flow rates were also compared utilising a 40 mm outer diameter specimen insulated in 2 mm thick Nylon 12. As was seen in Section 4.2.1, the transient heat transfer behaviour is very different to that of a 100 mm outer diameter insulated specimen and was thus chosen as an extreme contrast to see if the flow rate was more of a factor in insulated scenarios. As one can see in Figure 4.13, there is no noticeable difference in either the lubricant or specimen temperatures with a peak temperature differential between the two flow rates of 4 °C when comparing both the specimen and lubricant temperatures. Such a difference is difficult to apportion to any physical change of test parameters when one can see an offset in temperature at the beginning of the test resulting from a change in ambient conditions in the laboratory.

If one compares the temperature differential between the lubricant and test block specimen metal when plotted against the lubricant temperature, one observes a peak discrepancy between tests of less than 2 °C, thus further confirming that the flow rate of the rig within the boundaries of this study is not a significant parameter.

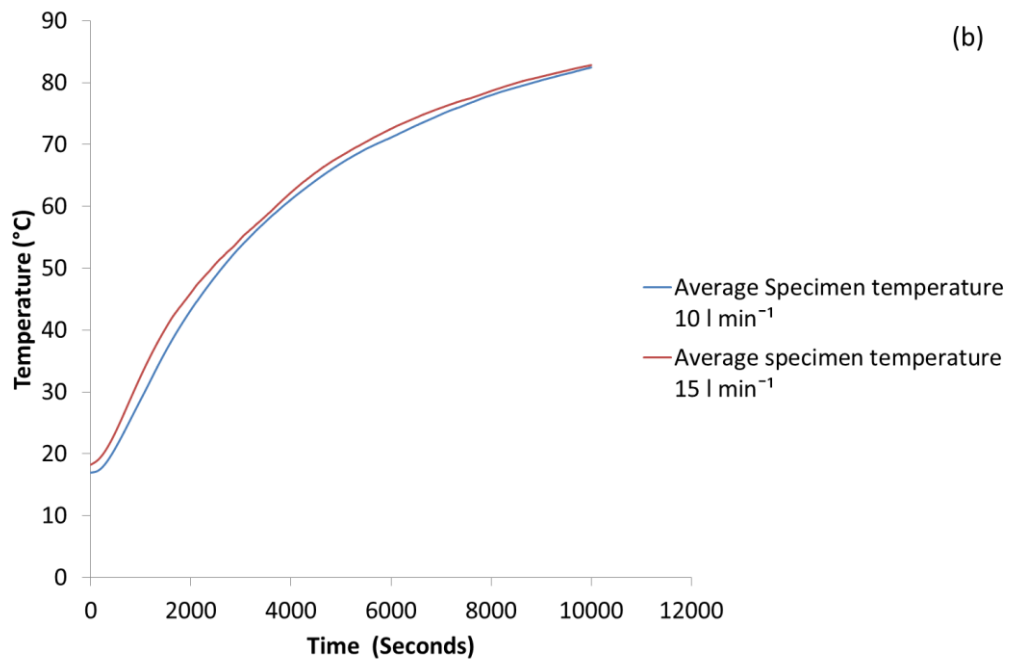
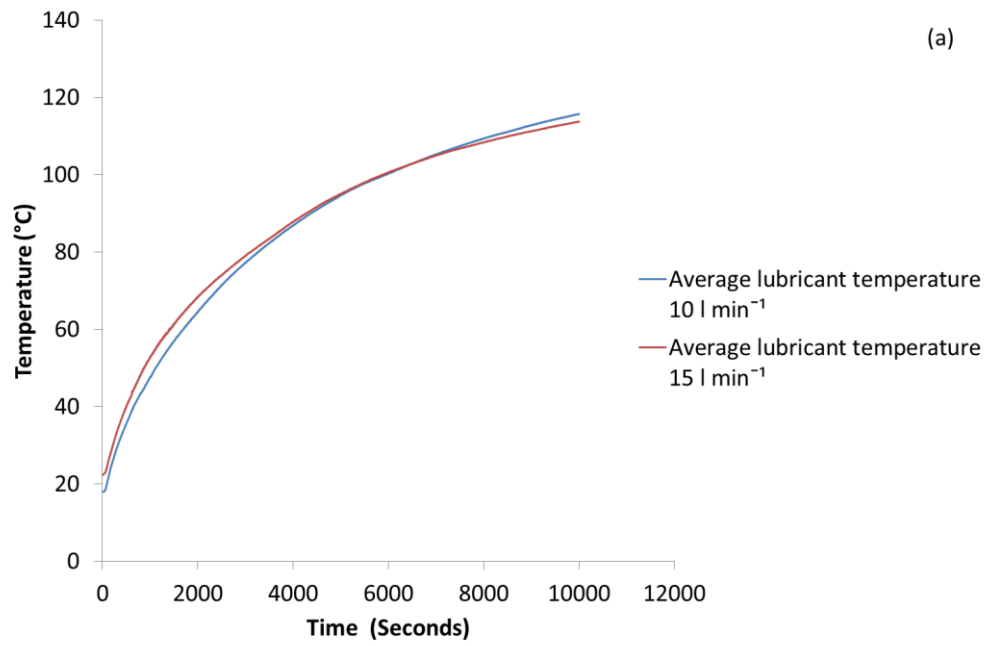


Figure 4.13: Temperature profiles over time from the oil flow rig using a 40 mm outer diameter specimen with 1200 W heater power applied and insulated with a 2 mm thick Nylon insert flowing at 10 l min<sup>-1</sup> and 15 l min<sup>-1</sup> for (a) the lubricant temperature and (b) the specimen temperature

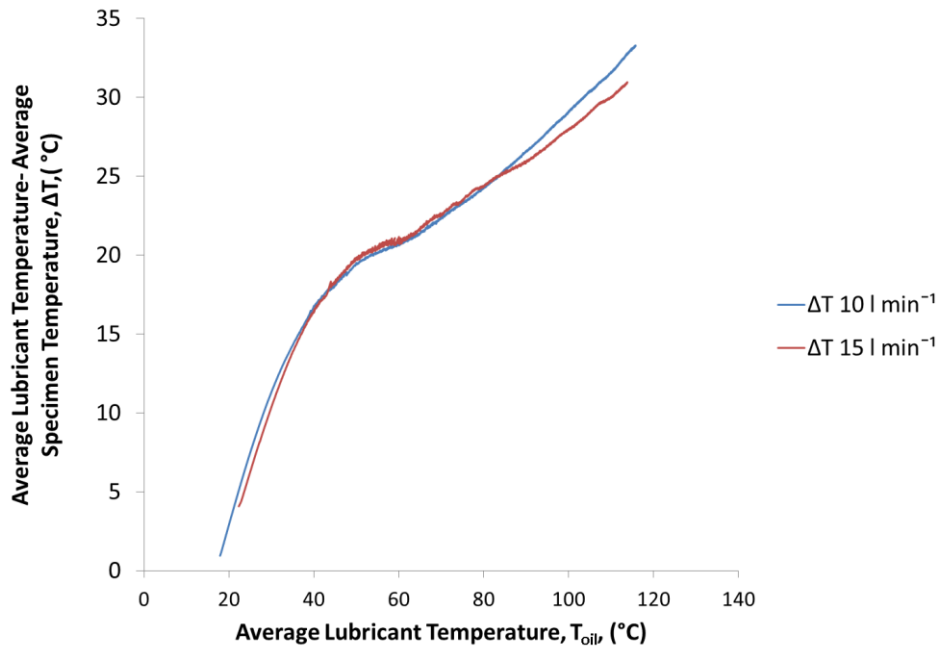


Figure 4.14: Temperature differential between the lubricant and test block specimen plotted against lubricant temperature from the oil flow rig using a 40 mm outer diameter specimen with 1200 W heater power applied and insulated with a 2 mm thick Nylon insert flowing at 10 l min<sup>-1</sup> and 15 l min<sup>-1</sup>

#### 4.7 The significance of boundary layer creation on the lubricant temperature measurement

As discussed in Chapter 3, the thermocouples installed on the rig to measure the temperature of the lubricant at the specimen inlet and outlet were positioned to be flush with the bore wall of the pipe. Such a design decision was based on a desire to minimise flow disturbance. A subsequent concern however was the effect of boundary layers. Across a boundary layer there exists a temperature gradient within the fluid that varies from the bulk fluid temperature in the centre of the bore to the fluid in contact with the wall having the temperature of the wall, as shown schematically in Figure 4.15.

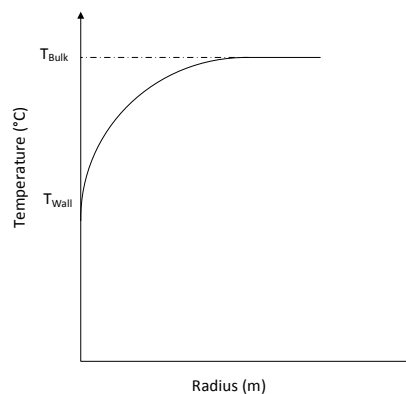
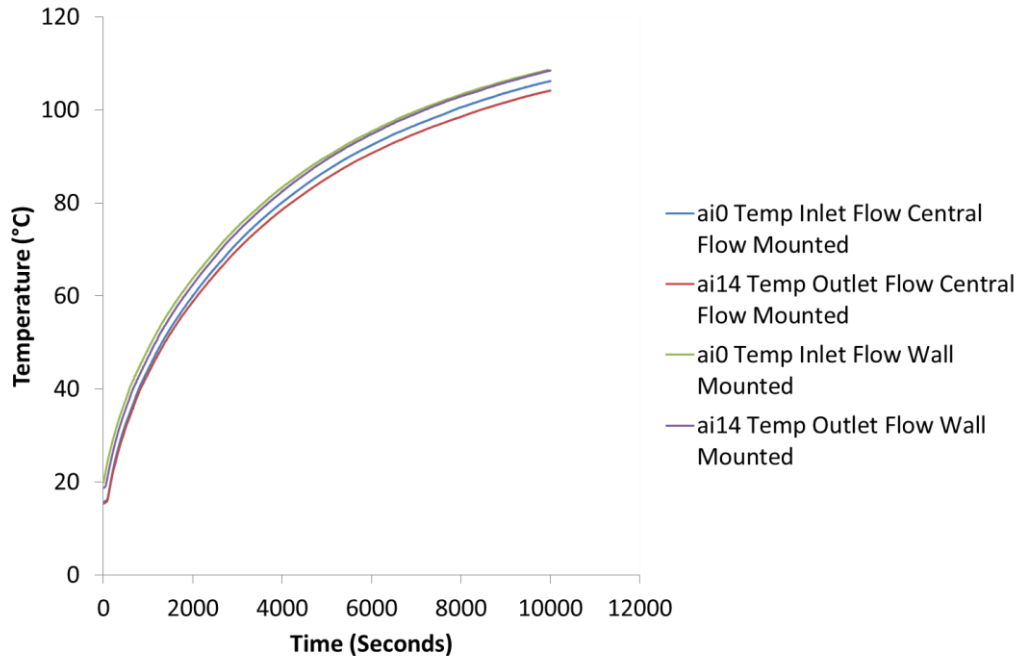


Figure 4.15: Schematic diagram showing the variation of fluid temperature with distance from the bore wall

To investigate if such variations in temperature were significant relative to the temperature variation of the rig during warm-up, two tests were conducted. In the first, the thermocouples were located flush with the bore wall, while in the second test, the thermocouples were moved to be in the mid-stream of the lubricant. The tests were conducted with the heater power set to 1200 W and the lubricant flow rate set to  $10 \text{ l min}^{-1}$  while the test block specimen installed was of 100 mm outer diameter and had a 2 mm aluminium insulating insert installed. Figure 4.16 shows a comparison of the lubricant temperature at the specimen inlet and outlet when measuring the lubricant temperature at the bore wall and in the centre of the flow. One would expect, should boundary layer effects be significant, for the lubricant temperature in the centre of the flow to measure higher than those at the wall. However, it can be seen that there is no noticeable difference between the temperature measurements at the two locations. Figure 4.17 shows the temperature differential between the lubricant and test block specimen using the two thermocouple locations. Whereas the absolute temperature plotted against time highlights any difference in start temperature, the temperature differential against lubricant temperature normalises this. As one can see, the trends from the two experiments are consistent to within  $1 \text{ }^\circ\text{C}$ . Thus, it was felt that there was no risk of boundary layer effects within the specimen affecting the overall trend of the experimental data from the rig.



**Figure 4.16:** Lubricant temperature plotted against time from the oil flow rig using a 100 mm outer diameter specimen with a 2 mm thick aluminium insert. The heater power was set to 1200 W and the flow rate set to  $10 \text{ l min}^{-1}$ . The lubricant thermocouples were installed both level with the bore wall and in the centre of the flow in comparative tests

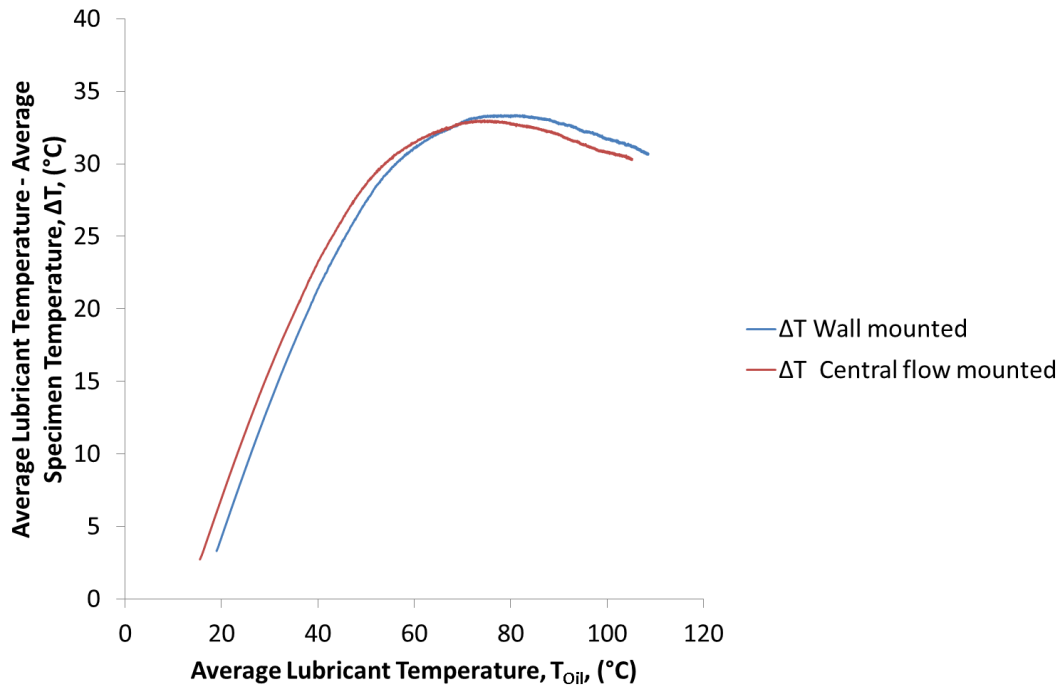


Figure 4.17: Temperature differential between the lubricant and test block specimen plotted against lubricant temperature from the oil flow rig using a 100 mm outer diameter specimen with a 2 mm thick aluminium insert. The heater power was set to 1200 W and the flow rate set to  $10 \text{ l min}^{-1}$ . The lubricant thermocouples were installed both level with the bore wall and in the centre of the flow in comparative tests

#### 4.8 The effect of varying the heater power on rig warm-up rate

The heater power in the experimental work was typically set to a value of 1200 W. This was to simulate average values of frictional heat to oil reported in the literature [25, 27] during engine warm-up. The immersion heater in the tank was capable of delivering up to 2500 W of power. Therefore, to investigate the sensitivity of the lubricant temperature to the heater power, two additional tests were conducted. The first increased the heater power to 1800 W while the second reduced the heater power to 600 W. Figure 4.18 compares the lubricant and specimen temperatures for the three heater powers. It can be seen that in the case of both the lubricant and specimen temperatures, the reduced heating power of 600 W reduces the rate of warm-up and reduces the final steady state temperature value. When 1200 W or 1800 W heating power is applied at the heater, the test is terminated before the rig reaches a natural state of equilibrium, though the 1800 W test condition sees the rate of temperature rise increase dramatically.

The heater power clearly affects the transient behaviour of the rig and this is most clearly shown in Figure 4.19 where the temperature differential between the lubricant and specimen is plotted against the lubricant temperature. One can see the peak temperature differential increases with the heater power. With a higher heater

power the lubricant temperature can increase at a faster rate owing to more energy being supplied to the same thermal mass in the same time frame. However, the transient heating of the test block specimen is less closely coupled to the heater element and is instead more a function of the specimen's thermal properties (including thermal conductivity, specific heat capacity and external heat transfer area). Thus while an increased heater power has a direct result on accelerating the lubricant heating rate, the response of the specimen to such a change is less pronounced. The result is a higher peak temperature differential between the specimen and lubricant that occurs at a higher temperature.

If one looks at the late regime of the test, the final temperature differential is determined by Newton's law of cooling, the general form of which was defined in Equation 2.2 and is explicitly defined for this particular example in Equation 4.7. In the context of Figure 4.19, when comparing points at a given lubricant temperature for different heater powers, the lubricant temperature is constant, as is the area over which heat transfer is occurring. In the late regime of the test, the rig is approaching steady state. Thus, if one ignores the rest of the rig and focuses solely on the interaction between the lubricant and test block specimen, the net heat input applied to the fluid by the heater element (after losses to the rig have been accounted for), must equal that transferred to the test block specimen as the rig approaches steady state. Given that the value of  $h$  is dominated by the lubricant temperature and the area of the bore is the same, if the heater power is increased, then, in a steady state scenario, the temperature differential between the lubricant specimen must increase also to conserve energy. Thus, in the late regime of the test the temperature differential is observed to increase with heater power in the manner shown in Figure 4.19.

$$\dot{Q} = h A (T_{oil} - T_{specimen})$$

Where  $\dot{Q}$  = Rate of heat transfer (W)

$h$  = Convective heat transfer coefficient ( $\text{W m}^{-2} \text{K}^{-1}$ )

$A$  = Area ( $\text{m}^2$ )

$T_{oil}$  = Temperature of lubricant in the test block specimen ( $^{\circ}\text{C}$ )

$T_{specimen}$  = Temperature of the test block specimen ( $^{\circ}\text{C}$ )

**Equation 4.7: Newton's law of cooling**

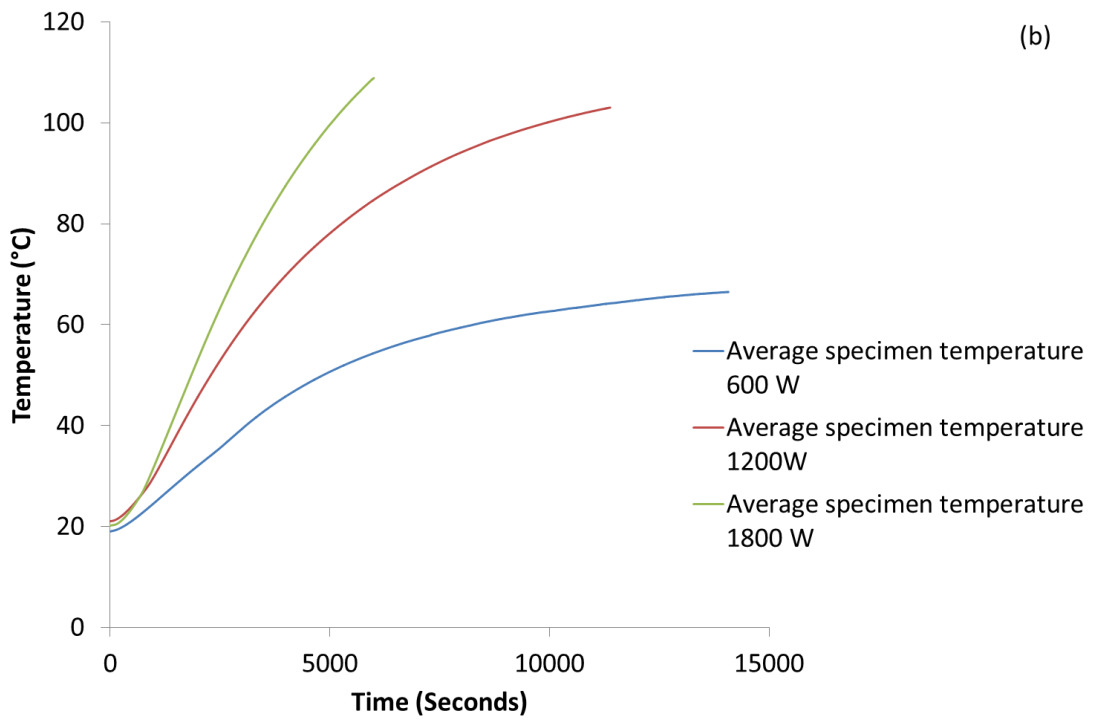
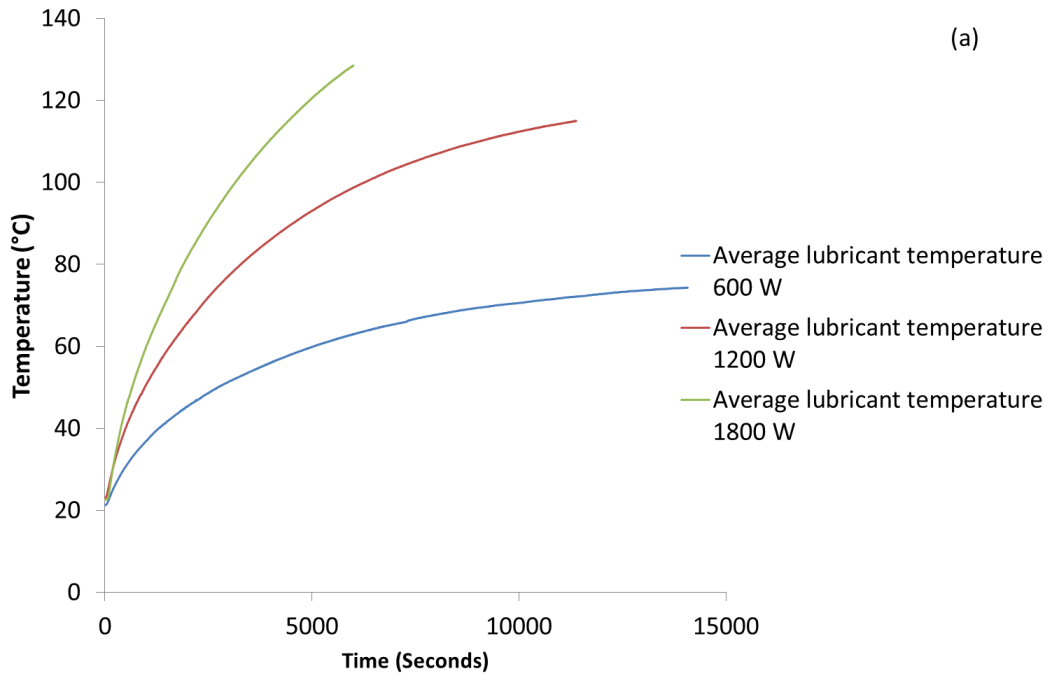
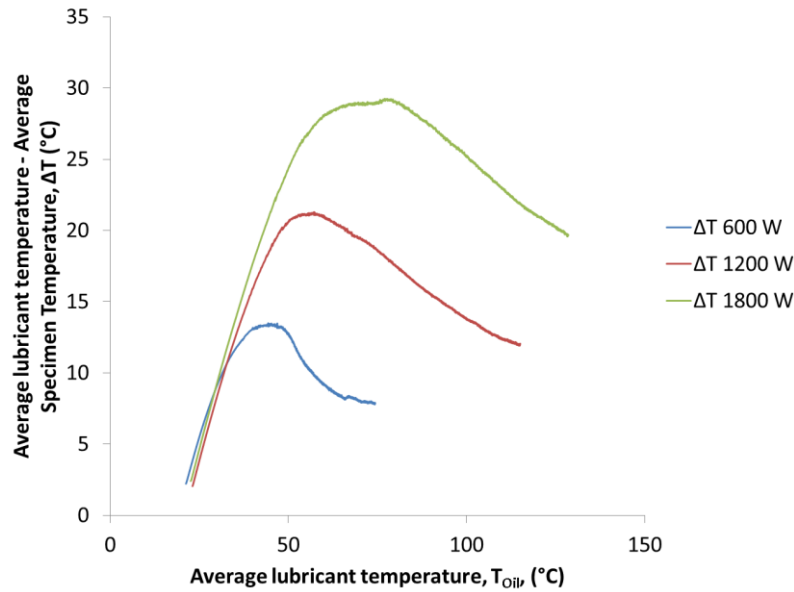


Figure 4.18: Comparative temperatures from the oil flow rig for a 100 mm outer diameter uninsulated specimen with  $10 \text{ l min}^{-1}$  flow rate and varying heater power comparing both (a) lubricant temperatures and (b) specimen temperatures



**Figure 4.19: Comparison of the temperature differential between the lubricant and test block specimen from the oil flow rig for a 100 mm outer diameter uninsulated specimen with  $10 \text{ l min}^{-1}$  flow rate and varying heater power**

Thus, from this work it can be seen how the relationship between the lubricant temperature and the specimen temperature does change as a result of variable heater power. The transient regimes identified and discussed in Section 4.2.1 are still present; however the magnitude and duration of these phases vary with changing heater power. For the data from the oil flow rig to be comparable between tests, it is therefore important to maintain a constant heating rate from the lubricant heater and in all further work the heater power is maintained at 1200 W.

#### 4.9 Repeatability of the experimental procedure

The use of the oil flow rig spanned the period from May 2012 to November 2013. Much of the data from the rig are relative and it is therefore imperative to have confidence in the repeatability of the rig. In order to validate the rig's repeatability, three sets of repeat tests were carried out.

The first set of repeatability tests utilised a 100 mm outer diameter uninsulated specimen together with the Texaco Energy 5W-30 lubricant first discussed in Section 3.4 to conduct two repeat tests using 1200 W heater power and  $10 \text{ l min}^{-1}$  flow rate. The first test was carried out on 20<sup>th</sup> June 2012 and the second was conducted on 4<sup>th</sup> June 2013 and was used to establish if any systematic degradation of the rig had occurred over the time frame that the majority of the rig was used over. Figure 4.20 shows the temperature differential between the lubricant and test block specimen plotted against the lubricant temperature for the two respective tests. As one can see, in the regime of the test up to the peak temperature differential, the two tests are in almost exact agreement with each other and the peak temperature

differential deviates by only 1 °C. This would suggest no systematic degradation of the rig has occurred during the twelve months between tests.

It must be noted that the two tests diverge in the high lubricant temperature regime and the discrepancy between tests increases to 2.5 °C. The fact this occurs in the late regime of the test, when heat transfer to ambient from the outer surface of the specimen is significant, means variations in ambient conditions are a likely cause of the discrepancy, particularly given the facility's absence of climatic control that has already been discussed. The recorded soak temperature (the temperature that the test commenced at) is 2.5 °C higher in the June 2013 test and will therefore have contributed to the specimen not being as heavily cooled by ambient, reducing the temperature differential to the lubricant. The heat flux from the external surface of the test block specimen to ambient is only a significant mechanism in the late regime of the test where the specimen temperature has increased sufficiently for there to be a temperature differential between the test block specimen and ambient that is high enough to produce a sizeable heat flux. Thus, for a given lubricant temperature it would be expected that the temperature differential between the lubricant and the test block specimen would be consistent until such point that heat transfer to ambient from the external surface of the test block specimen became a limiting factor. At such a point the test with the warmer ambient conditions (June 2013) would be expected to be able to achieve a higher peak specimen temperature (resulting in a reduced temperature differential between the test block specimen and the lubricant) and maintain this differential owing to the reduced heat flow between the test block specimen and the warmer ambient air. Such a trend is demonstrated in Figure 4.20 and the impact of variations in ambient temperature on the heat flow between the lubricant and test block specimen, and the associated uncertainty introduced to data, is discussed further in Section 7.4.

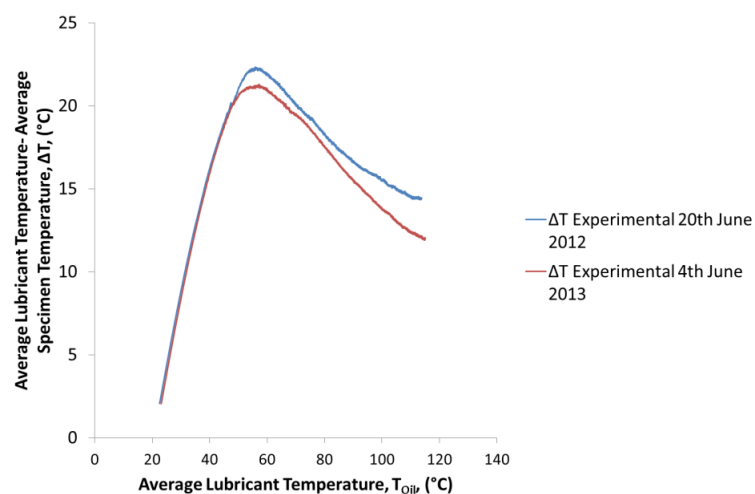


**Figure 4.20: Temperature differential between the lubricant and test block specimen when using a 100 mm outer diameter uninsulated specimen with 1200 W heater input power and 10 l min<sup>-1</sup> flow rate on two respective dates**

To further appraise the repeatability of the experimental rig, two further sets of repeatability tests were carried out. During August 2012, the experimental rig was utilised to carry out lubricant compatibility work for BP. In order to ensure that none of the additives from different lubricants remained in the rig, the oil flow rig was flushed out using a specific flushing lubricant supplied by BP. Thus the lubricant, while similar to the Texaco Energy 5W-30 lubricant, was not identical and no data relating to the specific heat capacity and density were provided for confidentiality reasons. However, the tests do provide sufficient data to appraise the repeatability of the temperature differential between the lubricant and test block specimen when plotted against the lubricant temperature.

In these tests the lubricant was heated to 120 °C by setting the heater power to 1800 W and the lubricant flow rate was set to 10 l min<sup>-1</sup>. Figure 4.21a shows the temperature differential between the lubricant and test block specimen using the flushing lubricant supplied by BP with a 100 mm outer diameter test block specimen installed. It can be seen that good agreement is achieved between the two tests carried out on the 28<sup>th</sup> August 2012 and 30<sup>th</sup> October 2012 with the typical discrepancy in temperature differential no more than 2 °C in the early phase of the test and this reducing to less than 1 °C in the latter phase of the test. It is worth noting that between these two tests, a cross over is observed at a lubricant temperature of approximately 95 °C. Such a characteristic is not believed to be of physical significance and is most likely to be experimental noise, rather than evidence of a significant trend.

Of concern is the offset performance of the test carried out on 14<sup>th</sup> August 2012 which demonstrates a similar profile of the temperature differential against the lubricant temperature relative to the other two tests but with a noticeable offset along the lubricant temperature axis. This results in a discrepancy in temperature differential for a given lubricant temperature of up to 5 °C. However, the discrepancy is constant throughout the test and is a result of the test carried out on 14<sup>th</sup> August 2012 commencing with a lower initial temperature differential relative to the other two tests. In appraising the data, it can be seen that the soak temperature of the specimen is of the order of 4 °C higher than the other two tests and hence, the temperature differential is reduced throughout the test as a result. If this initial offset is removed, by subtracting 4 °C from the lubricant temperature then it can be seen in Figure 4.21b that much closer agreement is obtained.

Figure 4.22 plots the temperature differential between the lubricant and the test block specimen using the BP flushing lubricant when used in conjunction with an uninsulated 40 mm outer diameter specimen. It can once again be seen that across the three tests, good repeatability was seen between successive tests with a

maximum discrepancy of 3 °C seen in temperature differential for a given lubricant temperature and a maximum variation in peak temperature differential of 1 °C.

Across both the repeatability tests carried out using the 100 mm outer diameter specimen (Figure 4.21) and the 40 mm outer diameter specimen (Figure 4.22) no evidence of any systematic degradation in the rig has been observed and the maximum variation in peak temperature differential that has been observed is approximately 1 °C. This places confidence in the validity of comparing the trends between different tests. However, the ambient soak temperature has been discussed as a cause for any constant offset in test profile. However, while the variation in ambient temperature may affect the temperature differential profile, such a variation is accounted for when calculating any change in energy flow from the lubricant to the specimen (and subsequently to ambient). Thus by using the energy flow between the lubricant and test block specimen as a measure of performance (see Section 5.9, Figure 5.17) the variation in ambient temperature and soak conditions is normalised and enables comparisons between specimens of different designs and compositions to be compared with confidence, thus addressing the limitations in previous work discussed in Section 2.4.4.

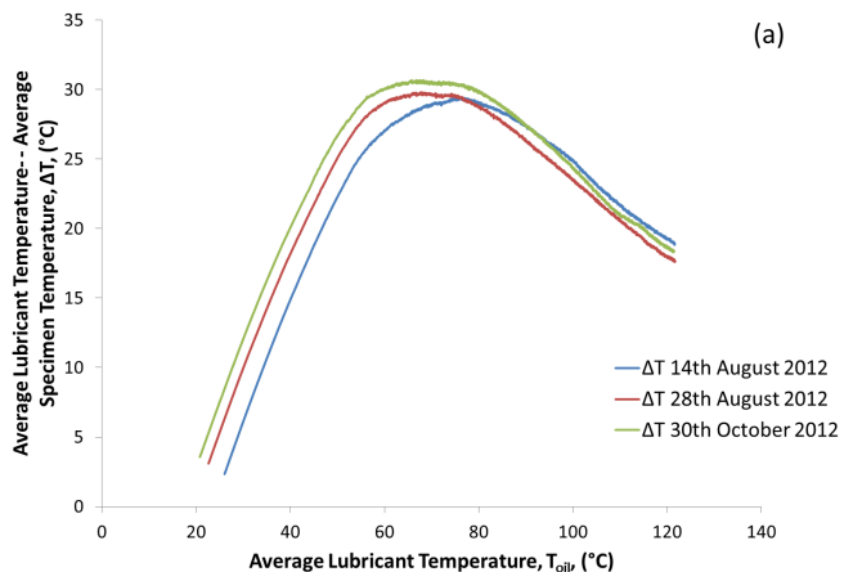


Figure 4.21a: Temperature differential between the lubricant and test block specimen when using a 100 mm outer diameter uninsulated specimen with 1800 W heater input power and 10 l min<sup>-1</sup> flow rate on three respective dates using an undisclosed flushing lubricant supplied by BP

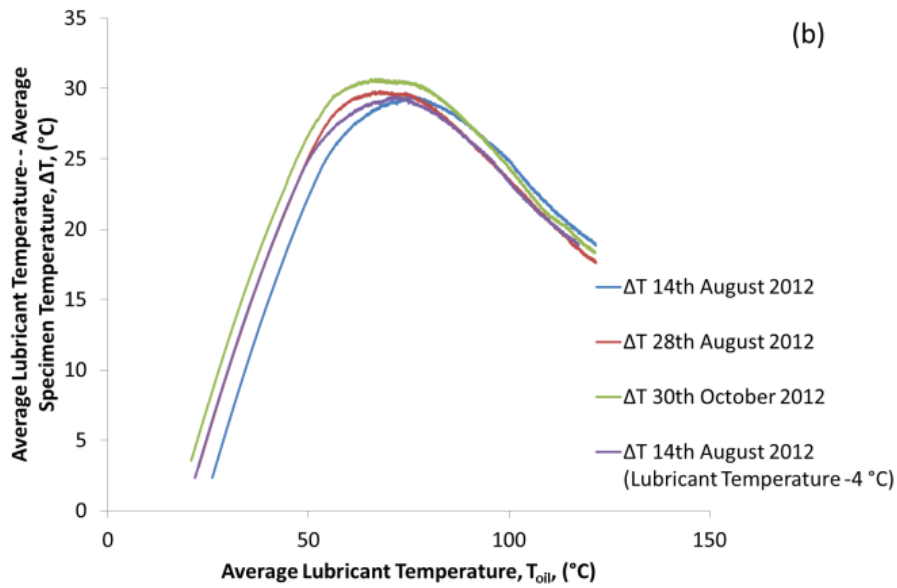


Figure 4.21b: Temperature differential between the lubricant and test block specimen when using a 100 mm outer diameter uninsulated specimen with 1800 W heater input power and  $10 \text{ l min}^{-1}$  flow rate on three respective dates using an undisclosed flushing lubricant supplied by BP using an offset lubricant temperature

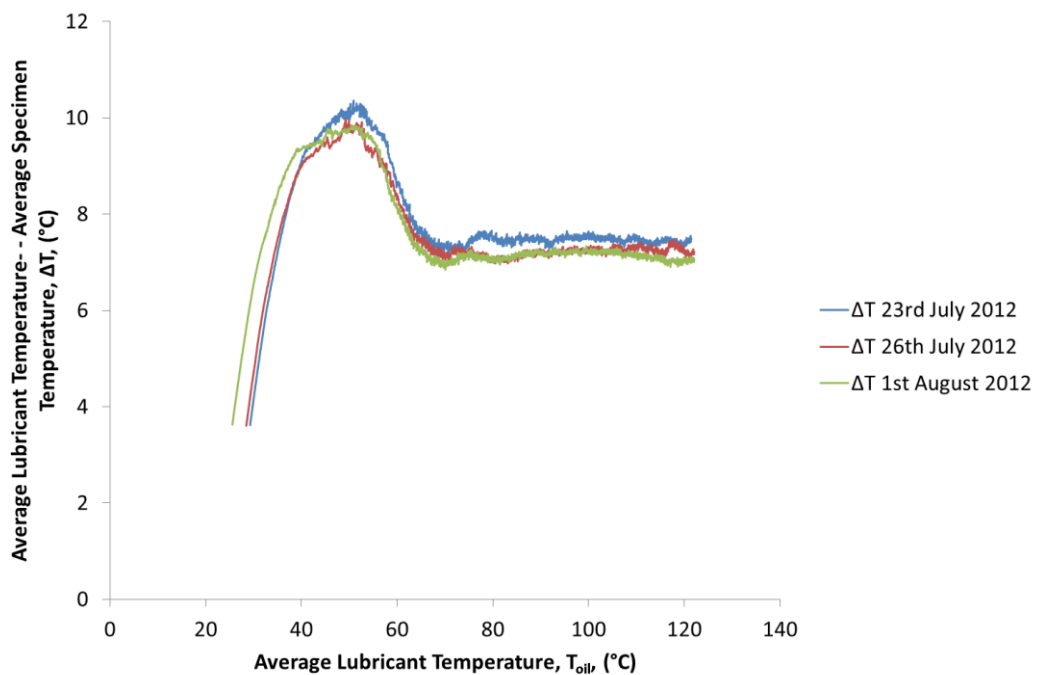


Figure 4.22: Temperature differential between the lubricant and test block specimen when using a 40 mm outer diameter uninsulated specimen with 1800 W heater input power and  $10 \text{ l min}^{-1}$  flow rate on three respective dates using an undisclosed flushing lubricant supplied by BP

## 4.10 Conclusion

Through these preliminary tests, the fundamental performance characteristics of the rig have been established. It has been shown that the rig is suitably sensitive to

insulation mechanisms in the test block specimen to yield measurable differences in heat transfer from the lubricant to the test block specimen.

However, it has also been shown that the majority of the thermal losses from the lubricant are transferred to other rig architecture components and not the test block specimen. This is despite all pipework and fittings being insulated as far as is reasonably practicable. A consequence of such a characteristic is the way in which the lubricant temperature is insensitive to any change in the size or construction of the test block specimen. Thus, the most appropriate performance measure of any insulating mechanism is the cumulative energy transferred to the test block specimen from the lubricant over the timeframe of the test.

The measured lubricant temperature has also been proven to be representative of the bulk flow temperature and through comparative tests it has been shown that the temperature gradient across the boundary layer is beyond the resolution of the thermocouples used.

Over the period of experimentation from May 2012- November 2013, the rig showed no sign of any systematic degradation and repeatability was good. Therefore the test data to be discussed in Chapters 5 does provide valid, comparative data.

## **5 Experimental results from the characterisation of differing insulating mechanisms**

### **5.1 Introduction**

Having established the broad performance characteristics of the rig in Chapter 3 and Chapter 4, the aim of this chapter is to discuss the findings from investigating various methods of insulating oil galleries.

Through the characterisation work discussed in Chapter 4, it was seen how a specimen of a larger thermal mass represents a greater percentage of the thermal mass of the rig. Consequently, the concept of an 'effective power' was introduced. The effective power represents the rate of thermal energy input to the rig that results in one or several of the following:

- An increase in the lubricant temperature.
- An increase in the specimen temperature.
- A transfer of energy to ambient from the outer surface of the specimen.

Through the experimental data presented in Chapter 4, it was observed that the effective power to the rig increases with specimens of a larger size. A logical development of such a performance characteristic is to investigate whether the benefit of applying insulation increases with specimen size.

Thus, the investigations discussed in this chapter include:

- The effects on heat transfer mechanisms of insulating inserts of both different design and material composition.
- The relative merits of insulating thermal masses of differing sizes.
- The significance of bore surface finish on heat transfer.
- Relative performance of externally insulating the test block specimen as opposed to internal insulation.

### **5.2 The effect of applying insulating inserts to engine oil galleries on heat transfer to the surrounding metal**

By installing a polymer insert into the bore of an engine oil gallery, the intention was that the low thermal conductivity of the insert relative to the surrounding material would provide an insulating effect. The significance of the temperature differential between the lubricant and test block specimen has already been highlighted and a successful outcome would be that the temperature differential would increase as a result of installing the insert. The resulting colder specimen would mean that less energy has been transferred to the specimen and therefore allow scope for a faster rate of lubricant temperature increase.

One has also seen how the lubricant temperature in the rig is insensitive to the specimen design and construction, and the associated reasons why this is the case have already been discussed. Thus this section focuses on the temperature differential between the lubricant and the specimen and the cumulative energy transferred from the lubricant to the specimen.

### **5.2.1 The use of Nylon 12 inserts in engine oil galleries**

In the first instance, a Nylon 12 insert (as detailed in Section 3.3.1 of Chapter 3) was installed into the test block specimen. As was highlighted in Chapter 3, the inner bore of the insert was maintained at 16 mm and the outer diameter was 20 mm, to give a 2 mm wall thickness. Thus in comparative work, the hydraulic diameter and convective heat transfer area between the specimen and the lubricant was constant for a given combination of lubricant and bore wall temperature.

One can see in Figure 5.1 that the addition of a 2 mm thick Nylon 12 insert when using a 100 mm outer diameter specimen increases the peak temperature differential from 22 °C to 54 °C, an increase of 150%. On the other hand, if one compares the performance of the Nylon 12 insert when used in the smaller specimen of 40 mm outer diameter, the peak temperature differential is increased by 470% from 6 °C to 34 °C. Such differences between both specimens of different size and those with and without insulation are indicative that the potential benefits of applying insulation to engine lubricant circuits does depend on the size of the thermal mass being insulated. While the percentage change in temperature differential as a result of insulation is higher in the case of the smaller 40 mm outer diameter specimen, to fully appraise the relative merits requires a full audit of the energy flow through the different specimens.

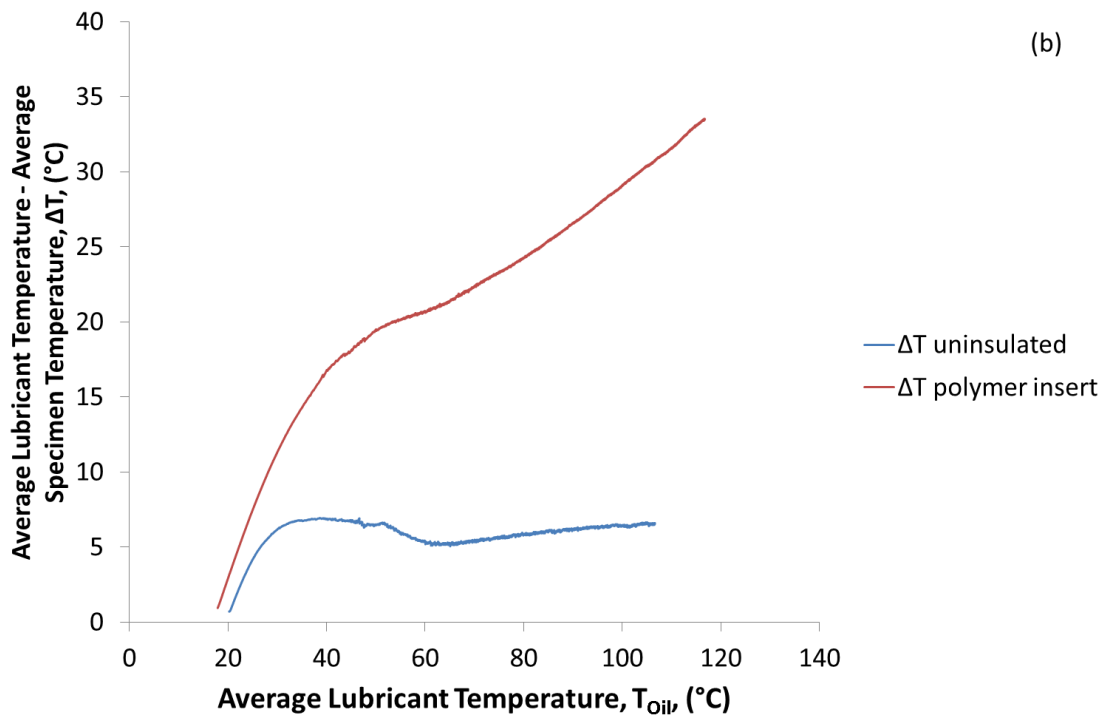
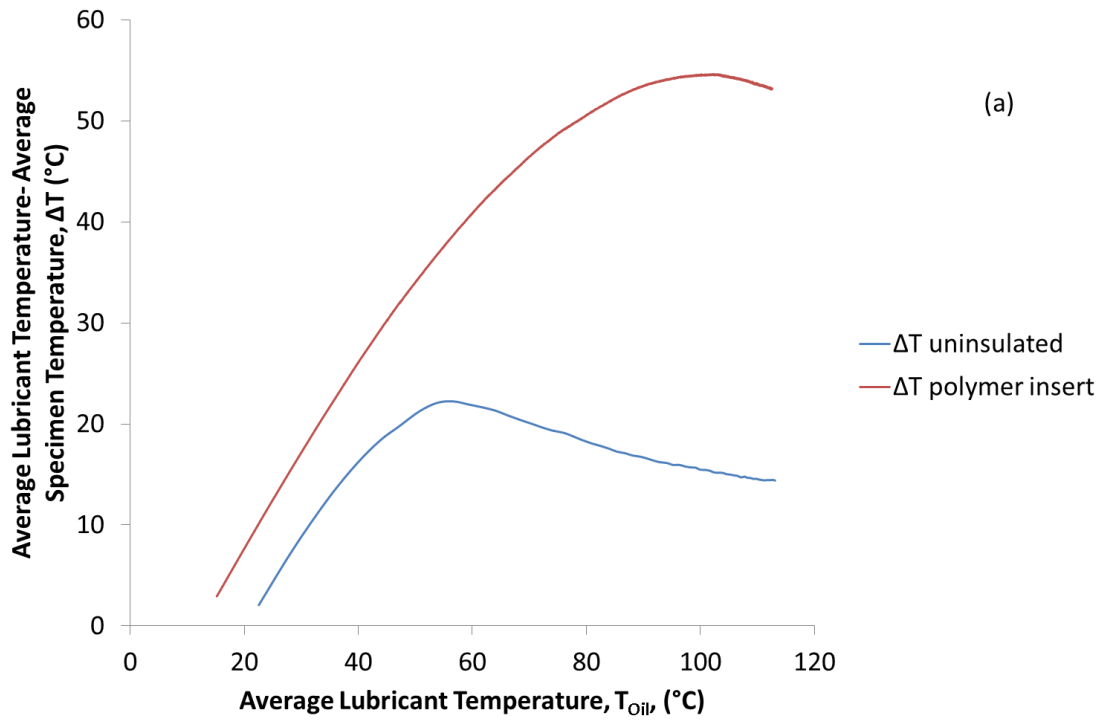


Figure 5.1: Temperature differential between the lubricant and test block specimen when the specimen is both uninsulated and when a 2 mm thick Nylon 12 insert is installed with 1200 W heater input power and  $10 \text{ l min}^{-1}$  flow rate for (a) a 100 mm outer diameter specimen and (b) a 40 mm outer diameter specimen

### 5.2.1.1 Implications of insulation on energy flow

The results presented in Figure 5.1 clearly indicate that the installation of polymer inserts in to the test block specimens has a significant effect on heat transfer. To determine the effect of the insulation in terms of energy lost from the lubricant, the energy audit approach, developed in Chapter 4 (Section 4.4), was again utilised, and the results summarised in Table 5.1. The results are taken from a set of comparative tests of 6900 seconds in duration to enable average heat fluxes to be calculated. It can be seen that the effect of specimen size is apparent when comparing the two uninsulated test results. The heat flux to the specimen is reduced from 124 W to 39 W simply as a result of the specimen size and mass being reduced. However of greater interest are the relative merits of insulation between the two specimen sizes.

If one first looks at the case of a 40 mm outer diameter specimen, the average heat flux to the specimen, including accounting for losses to ambient from the outer surface of the specimen, is 39 W. This can be reduced by 25% to 29 W when the Nylon 12 insert is installed. While a significant saving, the benefits are even more pronounced when insulating the larger specimen with the average heat flux being reduced by 56% from 124 W to 54 W. If the assumption is made that the reduction in energy transferred to the specimen is all retained in the lubricant (e.g. the 0.07 MJ not transferred to the specimen in the 40 mm outer diameter as a result of insulation instead increases the energy transferred to the lubricant to 1.28 MJ), it is possible to predict a best case scenario of the increase in lubricant heating rate as a result of insulation. These are presented in Table 5.1 and show that insulating the smaller 40 mm outer diameter specimen can increase the lubricant heating rate from 176 W to 186 W and insulating the larger 100 mm outer diameter specimen could theoretically increase the lubricant heating rate from 161 W to 231 W.

**Table 5.1: Energy balance of the lubricant and specimen showing the effect of insulation with different specimen sizes over test duration of 6900 seconds**

	<u>40 mm</u> <u>insulated</u>	<u>40 mm</u> <u>uninsulated</u>	<u>100 mm</u> <u>insulated</u>	<u>100 mm</u> <u>uninsulated</u>
Cumulative energy transferred from lubricant to specimen (MJ)	0.20	0.27	0.37	0.85
Average heat flux from lubricant to specimen (W)	29	39	54	124
Cumulative energy transferred to lubricant (MJ)	1.21	1.19	1.11	1.12
Average heat flux to lubricant (W)	176	172	161	163
% of heat input to rig transferred to specimen	2%	3%	4%	10%
Assumed potential power to lubricant (W)	186		231	

Therefore, it can be concluded that, regardless of the size of the specimen, the installation of an insulating insert presents the opportunity to reduce the heat flux from the lubricant to the specimen by between 25% and 56% with the benefits increasing when insulating a larger thermal mass.

Having established such a performance characteristic all further analysis work is conducted utilising the 100 mm outer diameter specimen.

### **5.2.2 Investigation into the significance of the contact interface**

The effect of applying a Nylon 12 insulating insert to the bore of the test block specimen showed a dramatic ability to reduce heat transfer from the lubricant to the surrounding metal. While the low thermal conductivity of the Nylon 12 would be expected to reduce the heat transfer, the interface between the Nylon insert and test block specimen is also likely to have been a contributory factor in the insulating mechanism. This is particularly relevant given that the specimen was designed to be a nominal fit and thus had no interference with the inner bore of the test block specimen.

In the theoretical modelling of the rig that is discussed in Chapters 6 and 7, a heat transfer coefficient, denoted  $h_{contact}$ , is included to account for this interface and allow for a temperature differential between the outer surface of the insert and the inner surface of the specimen bore to exist. To validate if such an approach is representative of the physical contact resistance effect and not a further change in the dynamics of the rig, the Nylon 12 tube was replaced with a drawn aluminium tube of equal wall thickness. Given that the thermal mass of the specimen and the outer convective heat transfer areas are the same in the case of the uninsulated specimen and that with the aluminium insert installed, one would expect the temperature distribution of the lubricant and test block specimen to be the same in both situations were the contact resistance not significant. Instead, as can be observed in Figure 5.2, a marked difference is observed as result of the aluminium insert being installed.

Using a 100 mm outer diameter specimen it can be seen that the use of an aluminium insert, as opposed to a homogenous test block specimen, sees the peak temperature differential between the lubricant and test block specimen increase from 22 °C to 34 °C. Such a plot also verifies that the high thermal resistance of the polymer does have an effect as the temperature differential with the Nylon 12 insert increases to a peak value of 54 °C. However, the variation is also likely to be contributed to by a difference in fit between the two respective inserts and the test block specimen. Therefore, an investigation into the limits and fits of the insert

installation is carried out in Section 5.7. Contact heat transfer coefficients are difficult to quantify and the correlations that exist do not offer completely acceptable results [50, 52, 109] and will be sensitive to contact pressure and surface roughness [50, 109]. Correlations reported in the literature are often valid only for specific combinations of material and specific geometries and are hence not transferrable to other situations. The review work of Fletcher [110] discusses a wide range of contact resistance applications however, the specific case of concentric tubes is sparsely dealt with. Madhusdana [111] is one of the few authors to have investigated the case of two concentric tubes of dissimilar materials, claiming that no satisfactory correlation exists for such a case. Work by Madhusdana [111] highlighted that the value of contact heat transfer coefficient is dependent on a range of parameters including:

- The contact pressure between the two mating surfaces.
- Surface roughness.
- The temperature gradients through the two concentric tubes.
- The softer material's microhardness.
- The initial fit between the two tubes. The fit also affects the rate of change of contact heat transfer coefficient with a closer fit seeing the contact coefficient increase at a faster rate with temperature than a fit with greater clearance.

The work of Madhusudana and Litvak [112] did investigate the case of composite cylinders and quote values of contact heat transfer coefficient of between  $2286 \text{ W m}^{-2} \text{ K}^{-1}$  and  $3300 \text{ W m}^{-2} \text{ K}^{-1}$  for stainless steel interfaces. Fuller and Marotta [113], while they did not investigate cylindrical joints, did investigate the contact coefficient of aluminium and polymer flat plate joints using polycarbonate and PVC. Their work suggested that contact heat transfer coefficients, depending on interface pressure, could be between  $30 \text{ W m}^{-2} \text{ K}^{-1}$  and  $240 \text{ W m}^{-2} \text{ K}^{-1}$ . In the context of the experimental rig, there is insufficient instrumentation available to attempt to derive the contact heat transfer coefficient from experimental data. However, the contact heat transfer coefficient will almost certainly vary between the two cases of an aluminium tube inserted into the test block specimen and a polymer tube being inserted into the test block specimen. Across, the temperature range, the variation between the two scenarios is also unlikely to be constant owing to the expansion and softening of the Nylon 12 tube at high temperatures changing both the contact pressure and area. At high temperatures, the insert was seen to sag at the extreme ends where the hydraulic couplings were positioned and would have resulted in a tangential contact in the centre of the specimen between the test block specimen and insert. The Nylon 12 and aluminium also possess differing coefficients of thermal expansion that will cause the contact heat transfer coefficients to vary over the temperature range of the test owing to changes in contact pressure [109]. Thus, the

incorporation of the variable  $h_{contact}$  into the model does appear to represent well the physical mechanisms of heat transfer. However, the use of a constant value across the temperature range is likely to be a limitation in the model depending on the material combination in use and such limitations are discussed in Section 6.5.4.

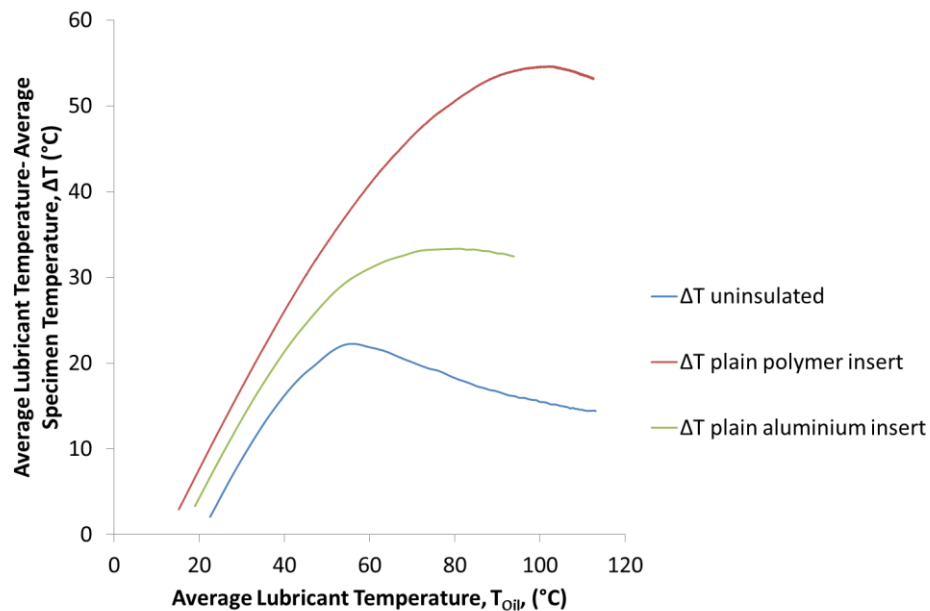


Figure 5.2: Temperature differential between the lubricant and test block specimen when a 100 mm outer diameter specimen is uninsulated, insulated with a 2 mm thick Nylon 12 insert and insulated with a 2 mm thick aluminium insert. The heater power was 1200 W and the flow rate set 10 l min<sup>-1</sup>

### 5.2.2.1 Increase in contact heat transfer coefficient using contact paste

As a final verification that the interface between the insert and test block specimen has an important effect in reducing the energy lost to the test block specimen, thermal contact paste was used to reduce the thermal resistance at the interface of the insert and specimen. The contact paste used was Wakefield Type 120 silicone based thermal compound with a manufacturer stated thermal conductivity of 0.735 W m<sup>-1</sup> K<sup>-1</sup>. To conduct this comparison, the 100 mm outer diameter specimen was again tested with the same aluminium insert as used in Section 5.2.2 to avoid the effects of any differing thermal expansion properties between the specimen and insert affecting the results.

Figure 5.3 shows the comparative performance of the differing configurations of insulating inserts. It can be seen that, relative to when the aluminium insert is used without contact paste, the insulating benefit is much reduced. Prior to the contact paste being applied, the aluminium insert achieved a peak temperature differential between the specimen and lubricant of 34 °C. While this is a reduction of 20 °C from

the peak temperature differential of 54 °C achieved with the Nylon 12 insert, it is nonetheless still significant. With the contact paste applied, it can be seen that the peak temperature differential reduces to 24 °C and produces a trend highly similar to that of the homogenous uninsulated specimen. Such a performance trait confirms that the contact resistance at the interface of the insert and specimen is very important in achieving the insulating benefits observed thus far.

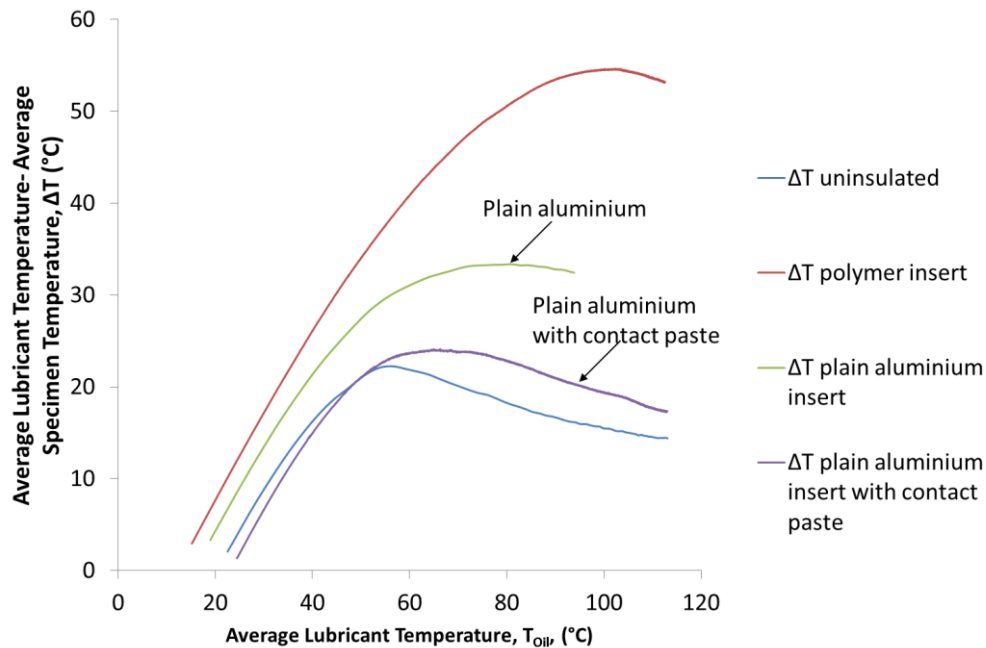


Figure 5.3: Temperature differential between the lubricant and test block specimen when a 100 mm outer diameter specimen is uninsulated, insulated with a 2 mm thick Nylon 12 insert and insulated with a 2 mm thick aluminium insert (both with and without contact paste). The heater power was 1200 W and the flow rate set 10 l min<sup>-1</sup>

### 5.3 Attempts to maximise the contact resistance to improve insulating performance

The results presented in Section 5.2 established that the contact resistance between an insert and the test block specimen is critical to achieving the reduced heat flow from the lubricant to the surrounding metal structure. Thus, the merits of purposefully increasing the contact resistance to reduce energy losses from the lubricant were investigated.

To increase the contact resistance, a standard aluminium insert of 16 mm bore and 2 mm wall thickness was modified to incorporate a 0.5 mm step in the outer surface, as shown in Figure 5.4. Figure 5.5 shows the comparative performance of the stepped aluminium insert relative to a plain aluminium and plain polymer insert. As one can see, the stepped aluminium insert is able to significantly increase the peak temperature differential relative to the plain aluminium insert from 34 °C to 46 °C. With no differing thermal properties between the insert and specimen to account

for, the only physical mechanism that can be responsible for such a performance trait is that of the reduced contact area between the insert and the specimen.

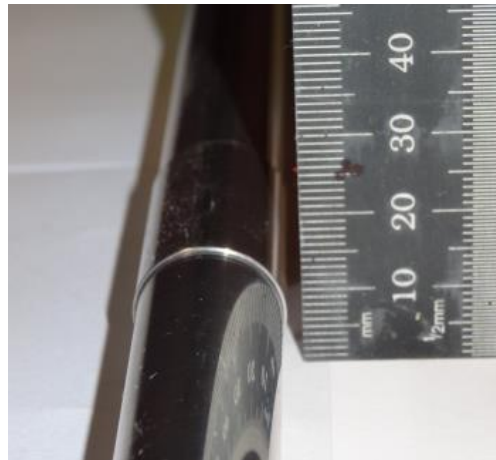


Figure 5.4: Stepped aluminium insert showing reduction in diameter

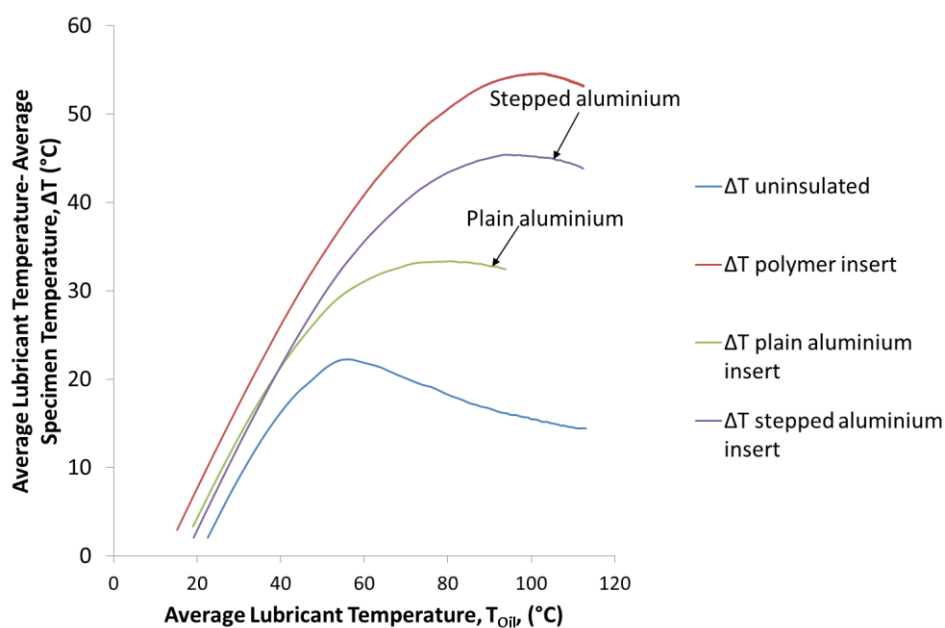
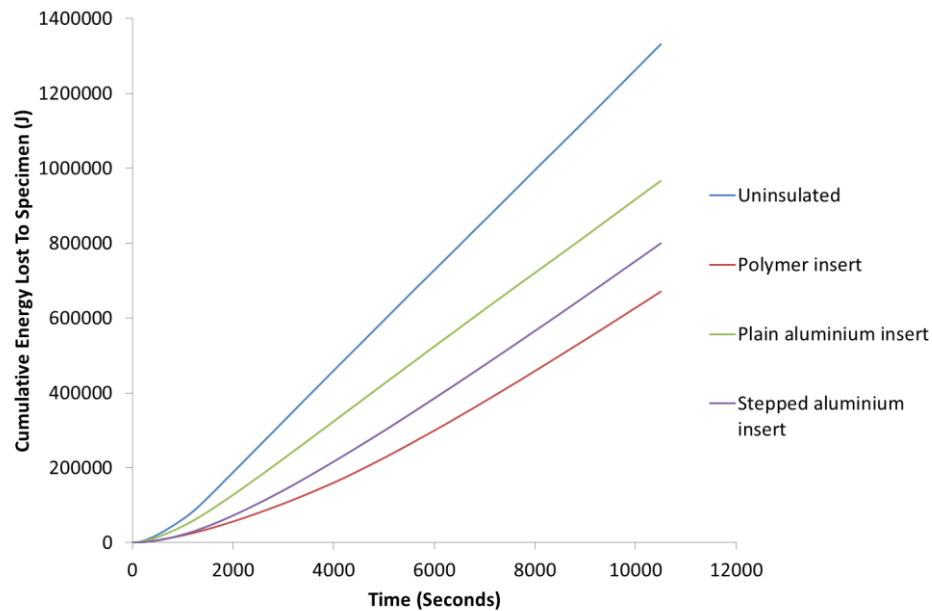


Figure 5.5: Temperature differential between the lubricant and test block specimen when a 100 mm outer diameter specimen is uninsulated and insulated with different insulating insert designs. The heater power was 1200 W and the flow rate set 10 l min<sup>-1</sup>

Using the energy audit method discussed in Chapter 4, it is again possible to see how the reduced temperature of the specimen, as a result of differing insulation methods, translates into a reduction in the energy transferred from the lubricant to the test block specimen. A plot of cumulative energy transferred to the specimen against time is shown in Figure 5.6 and shows how the benefit accumulates over the timeframe required for the lubricant to reach the target temperature. It can be seen that, while the stepped aluminium insert does not reduce the energy losses to the

levels of the polymer insert, it does nonetheless reduce the cumulative energy lost to the specimen from 1.3 MJ in the uninsulated scenario to 0.8 MJ when using the stepped aluminium insert across the 10408 second test duration. This represents a reduction of 40% whereas the plain aluminium insert transfers 1 MJ of energy to the test block specimen, representing only a 23% reduction relative to the uninsulated baseline.



**Figure 5.6: Cumulative energy lost from the lubricant to a 100 mm outer diameter test block specimen including energy lost to ambient by convection when different insulating inserts are used. The lubricant flow rate was  $10 \text{ l min}^{-1}$  and the heat input controlled at a constant  $1200 \text{ W}$**

Having seen such a dramatic increase in performance when increasing the contact resistance between the aluminium insert and the test block, the same design strategy was transferred to the Nylon 12 insert. Hence, a Nylon 12 insert was modified to incorporate the same 0.5 mm air gap (shown in Figure 5.4 on the aluminium insert) on the outer surface to increase the contact resistance.

One can see in Figure 5.7, that compared to the aluminium stepped insert, the Nylon 12 stepped insert only shows a marginal improvement of  $2 \text{ }^\circ\text{C}$ , from  $54 \text{ }^\circ\text{C}$  to  $56 \text{ }^\circ\text{C}$  in insulation effect relative to a plain outer diameter Nylon 12 insert. However, the effect of such a change on the energy transferred to the test block specimen is still significant. Over the 10408 seconds of the test, 0.55 MJ of energy was transferred to the test block specimen, representing a 58% reduction in energy transferred to the specimen over the uninsulated baseline as opposed to the 50% reduction when using the standard Nylon 12 insert (0.66 MJ). Thus the effect of the increased contact resistance is far less pronounced than it was when using the aluminium insert. However, the explanation is likely to be linked to the relative fit of the original, plain diameter, specimens in the gallery bore with the original aluminium bore having a

tighter clearance than the original Nylon 12 insert. Findings from such investigations are presented in Section 5.7.

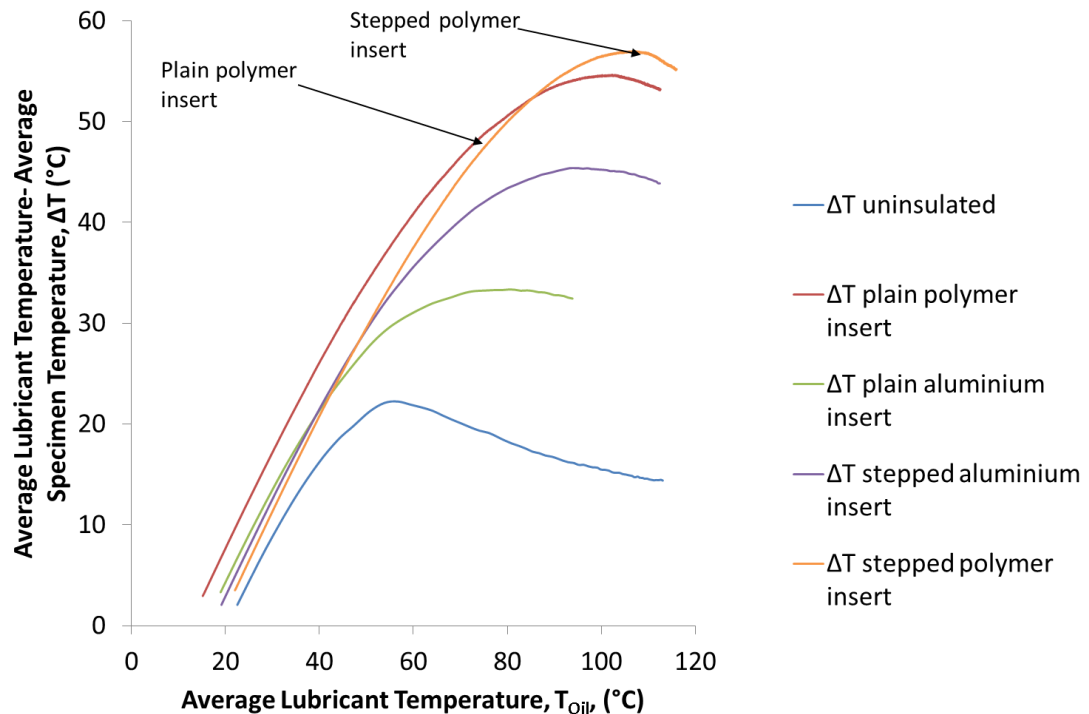


Figure 5.7: Temperature differential between the lubricant and test block specimen when a 100 mm outer diameter specimen is uninsulated and insulated with different insulating insert designs. The stepped inserts had a 0.5 mm step machined into the outer diameter of the insulating insert while the heater power was 1200 W and the flow rate set 10 l min<sup>-1</sup>

#### 5.4 Investigation into the effect of the bore surface roughness on heat transfer

The work presented in Section 5.3 clearly showed how the insertion of a plain aluminium insert into the test block specimen delivered reductions in energy flow to the test block specimens that were significantly higher than had been expected. Such an observation was attributed to the introduction of a contact resistance between the test block specimen and the insert. The stepped aluminium and Nylon 12 inserts, whose reduced external contact areas increase the contact resistance, provided further evidence that the contact resistance was the dominant factor in reducing heat flow from the lubricant. However, regardless of whether a deliberate step was included in the insert and whether the aluminium or Nylon variant was used, an unavoidable consequence of installing the insert was a change in the bore surface roughness.

In the homogenous specimen, the oilway was created by a continuous drilling process in order to replicate the process used in a full engine. Thus, the surface finish

was left as drilled. Comparatively, the drawn aluminium tube had a significantly smoother surface finish, as did the Nylon 12 tube. Such a change may have affected the boundary layer formation and flow characteristics in the lubricant and hence impacted on heat transfer to the specimen through the effect on the heat transfer coefficient at the fluid bore boundary.

In an attempt to isolate such a variable, a comparable insert to that of the drawn aluminium tube was manufactured. The insert was manufactured from solid aluminium 6082 T6 stock and the outer diameter turned to match that of the drawn insert. The inner bore was manufactured by drilling the insert in the same manner as the uninsulated specimen. Thus, the contact interface was present but with a consistent bore surface finish.

The comparative temperature differential of the drilled insert, relative to the Nylon 12 insert is shown in Figure 5.8. It can be seen that relative to the standard aluminium insert, the peak temperature differential increases by 8 °C. Were the surface finish of the bore to prove significant, one would have expected the temperature differential between the lubricant and specimen, relative to the drawn aluminium insert, to decrease. Such a hypothesis centres on a rougher surface promoting more turbulent flow and hence increasing the heat transfer coefficient between the lubricant and specimen. The increased temperature differential between the specimen and the lubricant suggests that less energy has been lost to the specimen using the drilled insert. As highlighted previously, the work of Madhusdana [111] showed that the contact resistance between two concentric tubes is dependent on a range of parameters including the degree of initial interference and surface finish. Hence, the observations seen in this section are likely to be more as a result of slight differences in the fit between the insert and test block specimen. A quantitative study of the interference between the specimens is presented in Section 5.7.

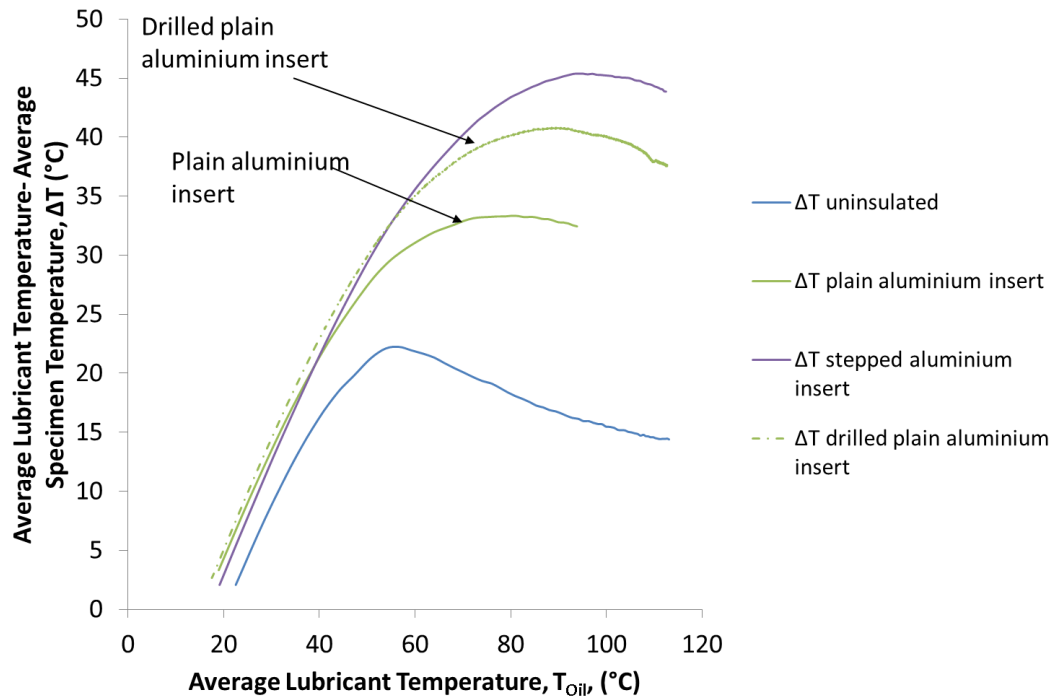
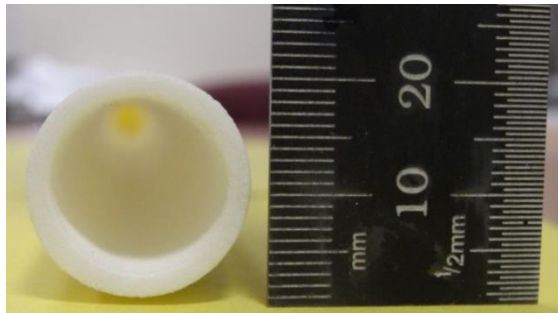


Figure 5.8: Temperature differential between the lubricant and test block specimen when a 100 mm outer diameter specimen is uninsulated and insulated with inserts of different surface roughness. The inserts were all manufactured from aluminium but were either a conventionally drawn tube or manufactured from stock billet and the bore drilled out. The heater power was 1200 W and the flow rate set 10 l min<sup>-1</sup>

## 5.5 The combination of low thermal conductivity material and contact interface

The work presented thus far has focused on increasing the contact resistance between an insert and the surrounding thermal mass. An alternative approach is to use an insert of a lower thermal conductivity. As part of the development of a novel test engine, the Ford Motor Company made extensive use of rapid prototyping facilities and sintered Nylon 12. The company chose to seal the sintered Nylon 12 to improve durability in coolant and lubricant environments and after extensive durability tests on the material, Ford could find no indication of material degradation or lubricant absorption as result of exposure to hot engine lubricant. Owing to the sintering process, the Nylon material would be expected to have a lower thermal conductivity than conventionally extruded Nylon tube as a result of the presence of voids and thus the thermal conductivity of sintered Nylon is a function of packing density. Work by Yuan [114] investigated the thermal conductivity of sintered nylon and found that the thermal conductivity at room temperature varied from 0.093 W m<sup>-1</sup> K<sup>-1</sup> at a density of 456 kg m<sup>-3</sup> to 0.11 W m<sup>-1</sup> K<sup>-1</sup> at a density of 560 kg m<sup>-3</sup>. However, the work also reported how bulk sintered Nylon 12 with a density of 990 kg m<sup>-3</sup>, and thus similar to stock Nylon 12, had a thermal conductivity value of 0.26 W m<sup>-1</sup> K<sup>-1</sup> and thus within the bounds of the expected value of stock Nylon 12

presented in Table 3.3 and highlighting the significance of the packing density and void content. Thus, were the two interfaces between the insert and specimen the same, it would be expected that the temperature differential between the lubricant and test block specimen, in the case of a sintered Nylon insert, would be higher than with the conventional extruded Nylon tube. In order to investigate the relative merits of attempting to reduce the thermal conductivity of any insert, an insert was manufactured from sintered Nylon to be installed into the oil flow rig test block specimen, as shown in Figure 5.9.



**Figure 5.9: Sintered Nylon insert provided by the Ford Motor Company for use in the oil flow rig showing wall thickness**

### **5.5.1 Quantification of thermal conductivity**

Before any testing of the sintered Nylon was carried out, the thermal conductivity of the material was compared to that of standard stock Nylon 6. To achieve this, a calibrated C-Therm thermal conductivity analyser was utilised. The equipment utilises a small heater that applies a heat flux across the interface of the specimen and heater. The resulting input of heat causes a rise in the temperature at the interface of the heater and specimen and causes a reduction in the voltage across the heat flow sensor. The rate of change of the voltage is critical in determining the thermophysical properties of the sample as it is proportional to the thermal conductivity of the specimen being measured. Hence, with a correctly calibrated unit, the C-Therm thermal conductivity analyser can provide rapid measurement of a material's thermal conductivity.

Within the scheme of work, six materials were tested. These were:

- Sintered Nylon post sealing.
- Unsealed sintered Nylon.
- Stock sheet Nylon 6.
- Pyroceram.
- Pyrex.
- LAF6720.

The latter three materials in the above list were provided by C-Therm as calibration materials and were therefore tested to ensure the rig was performing within acceptable limits. Figure 5.10 shows the results for the six tested materials. For each material, the average thermal conductivity from ten tests is presented with error bars showing one standard deviation. Repeatability is very good for a specific material with standard deviations all below 2%. If one first examines the calibration materials, it can be seen that the unit shows excellent agreement with the expected values. In the instance of the Pyrex, the unit overestimates by 0.6% while the pyroceram material overestimates by 1.6%. The worst performing calibration material is LAF6720 that overestimates the thermal conductivity by 34%. However, the expected value was  $0.082 \text{ W m}^{-1} \text{ K}^{-1}$  and the overshoot is therefore only  $0.028 \text{ W m}^{-1} \text{ K}^{-1}$ . It should also be noted that the thermal conductivity of the polymers of interest vary between  $0.21 \text{ W m}^{-1} \text{ K}^{-1}$  and  $0.3 \text{ W m}^{-1} \text{ K}^{-1}$  depending on the supplier and the operating temperature (such variations are discussed further in Section 7.2.1.2.2) and hence the thermal conductivity of this reference material is 10 times lower than the materials of interest.

Having established confidence in the test equipment's performance, the relative thermal conductivities of the application materials were analysed. It can be seen that the sintered Nylon, regardless of whether sealant was applied, does as expected, possess a lower thermal conductivity than the sheet Nylon 6, albeit by a small margin of  $0.1 \text{ W m}^{-1} \text{ K}^{-1}$ . A key observation is the measured data for the Ensinger Nylon 6 are recorded at  $0.42 \text{ W m}^{-1} \text{ K}^{-1}$  whereas the manufacturer data state the thermal conductivity as being  $0.23 \text{ W m}^{-1} \text{ K}^{-1}$ . While this does introduce uncertainty into the absolute values of the material's thermal conductivity, the relative values of the sintered and stock Nylon would still be valid and gives an indication as to the effect of using sintered materials as opposed to solid stock. In addition, the excellent performance of the calibration material tests, suggest that one can have a high level of confidence in these results and that the sintered Nylon insert does represent a material with a lower thermal conductivity than the stock Nylon 6.

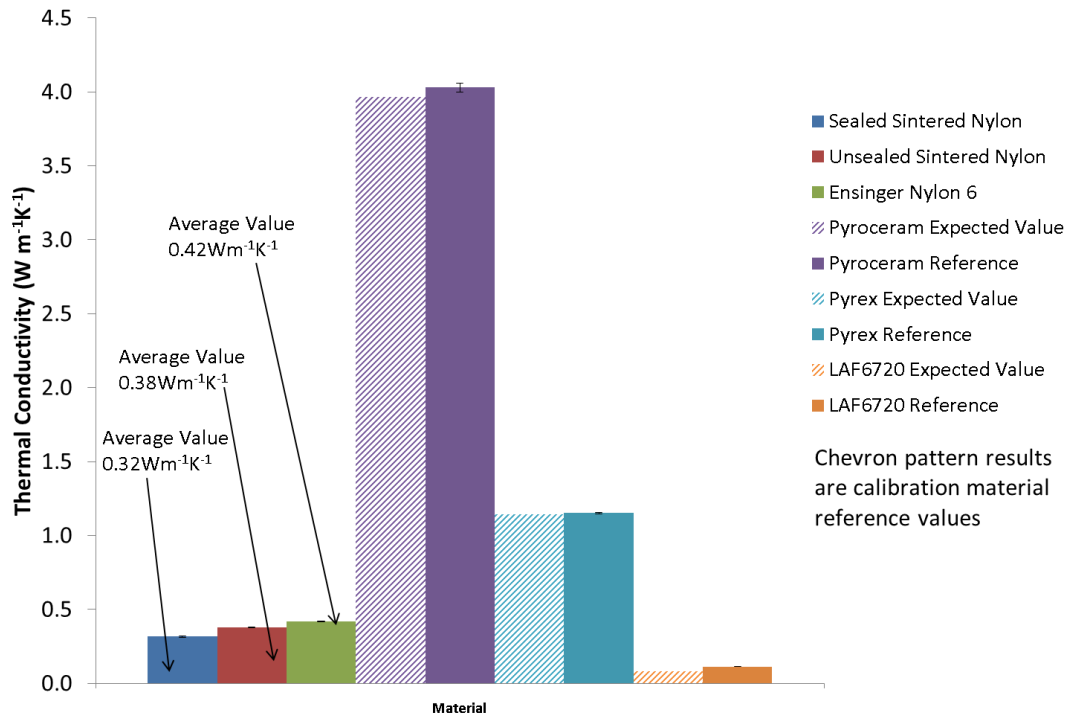


Figure 5.10: Measurement of thermal conductivity of different materials from the C-Therm thermal conductivity analyser where the average value is taken from 10 tests and each error bar represents 1 standard deviation

### 5.5.2 The benefits of sintered Nylon on the oil flow rig

While the work presented in Section 5.5.1 indicated that the thermal conductivity of the sintered Nylon was a maximum of  $0.1 \text{ W m}^{-1} \text{ K}^{-1}$  lower than stock Nylon 6, this still represented a 25% reduction in thermal conductivity. Therefore, to develop an understanding of the relative sensitivity of the thermal conductivity of the insert material relative to the contact resistance, the sintered Nylon insert shown in Figure 5.9 was installed in the oil flow rig.

Figure 5.11 presents the temperature differential between the lubricant and specimen for the sintered Nylon insert relative to the results already discussed. The peak temperature differential, and subsequent insulating performance, of the sintered Nylon insert is  $6 \text{ }^\circ\text{C}$  higher than the stepped aluminium insert. However, both the standard Nylon 12 insert and stepped Nylon 12 insert do provide a greater insulating effect than the sintered Nylon insert by up to  $6 \text{ }^\circ\text{C}$  in the case of the stepped polymer insert. While one can see a physical reason for the stepped polymer insert offering a greater insulating benefit than the sintered Nylon insert, it would have been expected that the polymer insert (shown in red in Figure 5.11) would provide less of an insulating benefit than the sintered Nylon were the contact coefficients the same. However, as is shown in Section 5.7, the clearance between the test block specimen and the insert is reduced in the case of the sintered Nylon

insert relative to the standard Nylon insert and consequently the insert provides a reduced insulating effect; a similar result to that found in Section 5.4.

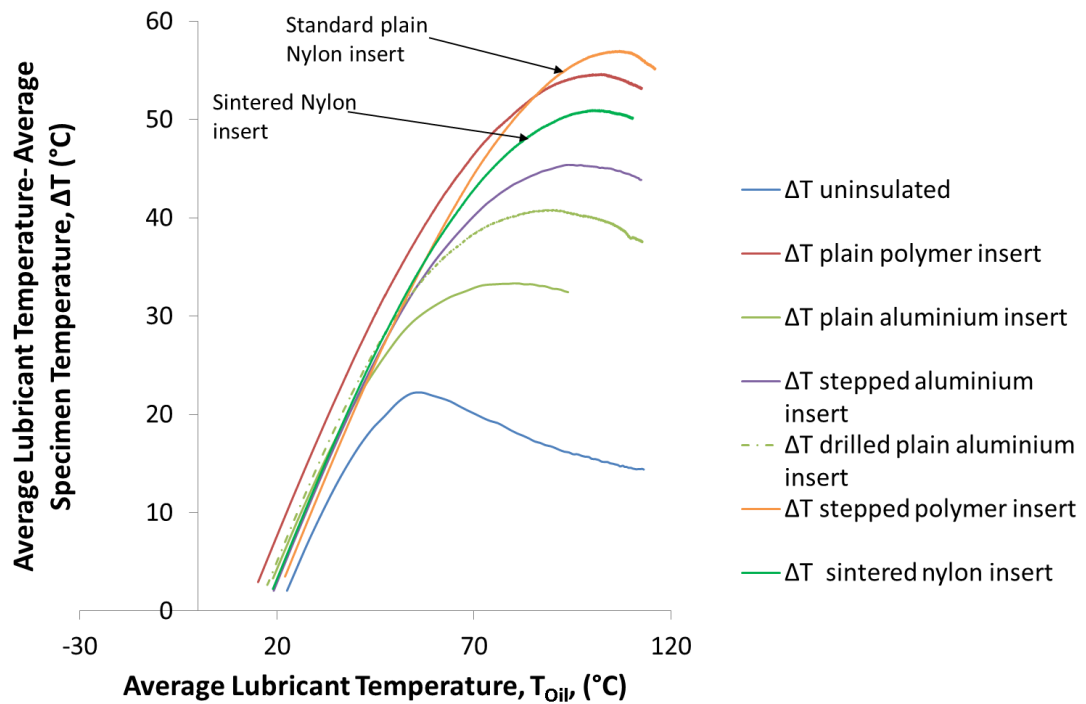


**Figure 5.11: Temperature differential between the lubricant and test block specimen plotted against average lubricant temperature when a 100 mm outer diameter specimen is uninsulated and insulated with different designs of insert. The lubricant flow rate was  $10 \text{ l min}^{-1}$  while the heater power was 1200 W. The figure compares the respective performance of sintered Nylon inserts with that of high contact resistance inserts**

## 5.6 Assessment into the repeatability and confidence of the results

An advantage of the work and methodology presented in this thesis relative to equivalent research work carried out on a fully built engine is greater control over the operating parameters of the rig. It was discussed in Section 1.2.1 and Section 2.4 how the majority of the work presented in the powertrain research field is based on single tests and a limitation in the work is being able to distinguish between genuine changes in performance as a result of parameter optimisation and the variation that may be expected between two engines of the same nominal build specification. The reasons for the absence of repeat tests has been apportioned to the cost and time required to carry out such repeat work with long soak periods required between tests to ensure comparable start conditions between tests and the same constraining factors are valid when using the oil flow rig for repeat work. However, the removal of the need to assemble an entire engine to the exact same specification, does enable greater confidence in the oil flow rig to be ascertained relative to full engine tests and the work presented in Section 4.9 has shown how the

oil flow rig can produce a peak temperature differential that is repeatable to within 1 °C for two tests that are nominally the same.

When such repeatability is placed in the context of the oil flow rig it can be seen how even the plain aluminium insert increases the temperature differential between the lubricant and test block specimen by 12 °C (from 22 °C to 34 °C) indicating that the changes in temperature distribution far exceed any associated experimental noise. That said, there are specific instances that warrant particular investigation. When one considers the change in performance between the plain aluminium insert to a stepped aluminium insert a 12 °C increase in temperature differential was observed (from 34 °C to 46 °C) and there is therefore clear confidence to be had that such a change was a result of the change in insulating strategy and not an inconsistency in the performance of the rig. It is also worth highlighting that the increase in temperature differential from the plain aluminium insert to that of a Nylon 12 insulating insert is 20 °C and hence far exceeds the uncertainty of 1 °C shown in Section 4.9 and reinforces that the low thermal conductivity of the Nylon 12, relative to the aluminium 6082 does produce an insulating benefit beyond that caused by the contact interface.

While the repeatability and associated confidence of the oil flow rig results has been shown to be good there are nonetheless weaknesses that warrant discussion. In considering the two Nylon 12 inserts (one being of a plain outer diameter and the other containing a 0.5 mm step) the increase in temperature differential as a result of the higher contact resistance produced by the 0.5 mm step was only shown to be 2 °C. It is shown in Section 5.7 how the inclusion of a 0.5 mm step onto the outer diameter of the insulating insert causes a much greater increase in clearance on the aluminium insert than it does on the Nylon 12 insert and this will have been a contributory factor in the increase in the contact resistance on the Nylon 12 insert having a lesser impact. However, it must also be accepted that a change in temperature differential of 2 °C between the two Nylon 12 inserts does present a higher degree of uncertainty than the other comparative results and hence further repeat experimentation would be desirable.

Section 5.4 presented data that attempted to investigate if the bore surface roughness was a significant factor in ensuring that heat transfer between the lubricant and gallery wall was minimised. A drawn tube would typically have a surface roughness of between 3.2 and 0.8 µm whereas a drilled tube would be expected to have a surface roughness of between 6.3 and 1.6 µm [115]. One would therefore expect that a drilled tube, with a rougher internal surface, would be expected to transfer more heat from the lubricant to the test block specimen owing to the effect of the surface friction factor on the Reynolds Number. By manufacturing an aluminium insert of the same nominal dimensions as the drawn

aluminium insert tube, but instead manufacturing the tube by turning the outer diameter and drilling the bore, it was expected to see an increase in energy transferred to the test block specimen (and a subsequent reduction in the temperature differential between the lubricant and the test block specimen) relative to the drawn tube. Instead, the drilled insert saw a peak differential of 42 °C as opposed to 34 °C in the case of the drawn aluminium insert. Such a difference is of a magnitude that is eight times higher than the uncertainty in the experimental results and there is therefore confidence that the trend observed is not a result of experimental noise. Instead, the result indicates that the degree of initial fit between the surrounding metal and the insulating insert is of far greater significance than any variation in bore surface roughness caused as a result of variation in manufacturing processes. The work presented in Section 5.7 supports such a conclusion as the clearance between the drawn aluminium insert and the test block specimen is 0.27 mm whereas this increases by 33% with the drilled insert and hence results in a higher insulating effect. From the experimental results it is therefore not possible to appraise the independent effects of the bore wall roughness. Where this has been attempted, it has been observed that the contact resistance effects dominate over any change in surface roughness. The investigations using the correlated computational model of the oil flow rig in Chapter 7 (Section 7.2.2.2.1) similarly indicate that the contact resistance effect is the dominant insulating mechanism. By halving or doubling the value of the contact heat transfer coefficient,  $h_{contact}$ , one observes a reduction in heat flow of 18% or an increase in heat flow of 13% respectively (Table 7.11). Comparatively, assuming the same value of  $h_{contact}$  but decreasing the insulating thickness by 0.5 mm only saw the thermal losses from the lubricant increase by 5% (Table 7.10).

## **5.7 Investigation into the variation in fit between polymer inserts and the oil gallery bore**

The results discussed thus far have highlighted that the presence of a contact resistance of any sort is likely to be the most effective insulating mechanism. This has been most graphically illustrated by the increase in temperature differential when a 0.5 mm step was machined into an aluminium insert. However, when looking at Figure 5.11 it can be seen that, contact interference alone does not account for some of the observed trends. These include:

1. The sintered Nylon insert creating a peak temperature differential 4 °C higher than the stepped aluminium insert.
2. The sintered Nylon insert creating a peak temperature differential 4 °C lower than that of the standard Nylon tube.

3. Why the 0.5 mm step when applied to the polymer insert only results in a 2 °C increase in peak temperature differential while the same strategy on an aluminium insert increases the peak temperature differential by 12 °C.

To further understand the significance of material thermal conductivity relative to the contact resistance, the clearance between the specimen bore and outer diameter of the specimen was measured for each of the cases studied. In doing so the mean external diameter of the insert was calculated from five measurements for each specimen and the mean diameter of the bore was calculated from the mean of four measurements of the inner bore diameter. The results are shown in Figure 5.12.

The first key observation is in the comparison between the stepped aluminium insert and the sintered Nylon. The sintered Nylon has the smallest clearance of all the inserts and therefore, the peak temperature differential achieved of 50 °C, particularly relative to the stepped aluminium insert that has a clearance eight times greater, is demonstrative that there is a benefit to be found in utilising low thermal conductivity materials in addition to increasing the contact resistance. Similarly, the clearance measurements offer an explanation into the anomalous result that showed the lower thermal conductivity sintered Nylon producing a lower temperature differential than the standard Nylon tube. The standard Nylon tube had a measured clearance of 0.4 mm relative to the 0.17 mm clearance for the sintered Nylon tube. The increase in clearance of 35% is highly likely to account for the 4 °C higher temperature differential achieved by the standard Nylon insert relative to the sintered Nylon insert.

Through the results presented in Figure 5.12 it can also be seen how the initial clearance between the test block specimen and the insulating insert differs between the drawn plain aluminium insert and the aluminium insert that was manufactured by turning and drilling and that the associated increase in contact heat transfer coefficient dominates over any effect that the surface roughness of the bore has on heat transfer from the lubricant. It can be seen that the drawn aluminium insert has an initial clearance between itself and the test block specimen of 0.27 mm. Comparatively, the drilled aluminium insert has a clearance of 0.36 mm; an increase of 33% and this has resulted in the peak temperature differential rising from 34 °C in the case of drawn aluminium insert to 42 °C in the case of the drilled aluminium insert.

Another key insight achieved by this investigation is why the increase in contact resistance achieved by machining a 0.5 mm step yielded so much greater a benefit when applied to the aluminium relative to the Nylon 12. The addition of the step to the insert in the case of the aluminium increased the peak temperature differential from 34 °C to 46 °C, an increase of 35%. Comparatively, the inclusion of a step on the Nylon 12 insert only increased the peak temperature differential by 4%, from 54 °C

to 56 °C. However, when one studies Figure 5.12 it can be seen that the increase in clearance is less significant in the case of the Nylon insert than it is with the aluminium insert. The addition of the step causes the clearance with the Nylon insert to increase from 0.4 mm to 1.5 mm, an increase of 275 %. Comparatively, the addition of the step in the aluminium insert increases the clearance from 0.28 mm to 1.4 mm, an increase of 400%. Such comparative dimensions are likely to be a significant factor in the relative gains seen as a result of increasing the contact resistance. Although difficult to quantify, another factor in the varying heat transfer dynamics between specimens is that of varying coefficients of thermal expansion between the Nylon inserts and the aluminium test block specimen. Whereas, the aluminium inserts would expand at the same rate during a test, the coefficients of thermal expansion for Nylon 12 (CoE between  $10 \times 10^{-5}$  and  $16 \times 10^{-5} \text{ }^\circ\text{C}^{-1}$ ) [97, 98] is over four times that of aluminium (CoE  $2.3 \times 10^{-5} \text{ }^\circ\text{C}^{-1}$ ) [93]. Hence, the level of clearance between the specimen and the Nylon inserts would reduce at higher temperatures owing to the Nylon expanding more than the aluminium. In doing so, the contact pressure (highlighted as being a key factor in determining the contact resistance at interfaces [50, 109-112]) would increase and cause a subsequent reduction in contact resistance at high temperatures. Such an effect would therefore limit the peak temperature differential achieved as the contact resistance reduced.

The significance of the contact resistance between the test block specimen and the insulating insert (and the associated value of  $h_{contact}$ ) reducing thermal losses from the lubricant presents a challenge for implementation. To ensure reliability vehicle OEMs require tight tolerances and this usually relates to minimising clearances (an example is the clearance between the piston and the bore wall). However, in this instance there is a need to ensure that the clearance is as high as possible when an insulating insert is installed but also to ensure that this is achieved in a repeatable manner in order to be able to guarantee that the insulating effect is achieved. It has been seen through the results presented in this chapter that even small variations in fit can potentially have a significant effect on the thermal losses from the lubricant and there is therefore a need to develop a method of implementation that facilitates achieving the maximum possible clearance with a very tight tolerance.

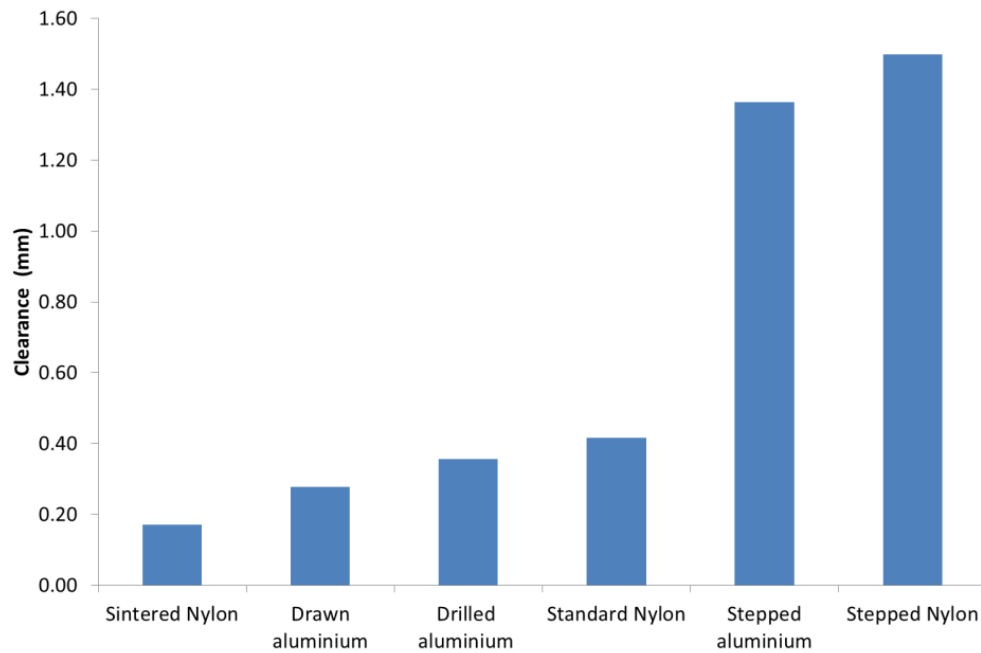


**Figure 5.12: Average clearance between the test block specimen bore and outer diameter of insulating inserts based on an average of five measurements along the length of the specimen and four measurements of the bore diameter**

## 5.8 The relative performance of external insulation compared to internal insulation methods

The internal geometry of an internal combustion engine is complex and to therefore achieve acceptable internal insulation is logistically challenging. It is worth remembering, from the aims of the thesis why internally insulating the engine oil galleries is hypothesised to be of greater benefit than externally insulating the engine.

If it is anticipated that if one was to externally insulate the engine, no benefit would be served to the lubricant circuit until such point that the outer surface of the engine was sufficiently hot to generate a significant temperature differential between the metal surface and ambient. The time frame for this to occur is variable both between engines and also specific points on a given engine (the metal temperatures in the engine head are typically 5 °C higher than those in the block [17]). During the warm-up phase of the metal, the lubricant, assuming it to be hotter than the metal, would still lose energy to the surrounding metal at the same rate until such a point that the external metal temperature was sufficiently hot for any external insulation mechanism to be able to reduce losses to ambient. Hence, because any external insulation does not thermally isolate the lubricant from the thermal mass of the engine, an external insulation strategy would not be anticipated to offer as large a benefit to lubricant warm-up as internally insulating galleries. Such a hypothesis assumes that the primary source of heat to the lubricant is from bearing friction and

that the lubricant is hotter than the surrounding metal. The primary source of lubricant heating is agreed to be from bearing friction by a range of literature sources including Andrews et al. [38], Trapy and Damiral [20], Zammit et al. [27] and Shayler et al. [25]. However the lack of detailed temperature measurements for the engine block at different locations during warm-up means that, depending on the specific engine, there may be regions in the engine where gallery insulation would isolate a secondary heat source to the lubricant rather than preventing cool down. There are likely to be regions where the current level of technology will not facilitate effective internal insulation of the I.C. engine owing to access restrictions and therefore, where internal insulation is not applied, the lubricant heating rate may benefit from insulation applied to the external block (similar to the work of Bürgin [63] and Bent et al. [11]).

To investigate the relative merits of external insulation compared to the benefits observed when using internal insulation methods, both a 100 mm outer diameter specimen and 40 mm outer diameter specimen were externally insulated in 3 mm thick Armaflex lagging tape. This tape was the same as that used to insulate fittings around the rig circuit and has a manufacturer specified thermal conductivity of between  $0.034 \text{ W m}^{-1} \text{ K}^{-1}$  and  $0.038 \text{ W m}^{-1} \text{ K}^{-1}$  between  $20 \text{ }^\circ\text{C}$  and  $40 \text{ }^\circ\text{C}$ . A photograph of the 100 mm outer diameter specimen externally insulated is shown in Figure 5.13. It can be seen that the R4 jubilee clip thermocouples have purposefully been installed on the external surface of the insulation. It was highlighted earlier in the thesis that the response times of the jubilee clip mounted thermocouples were significantly slower than the standard 0.5 mm diameter thermocouples and hence were of negligible benefit. However, in this work, they do enable the effect of the insulating layer to be seen.

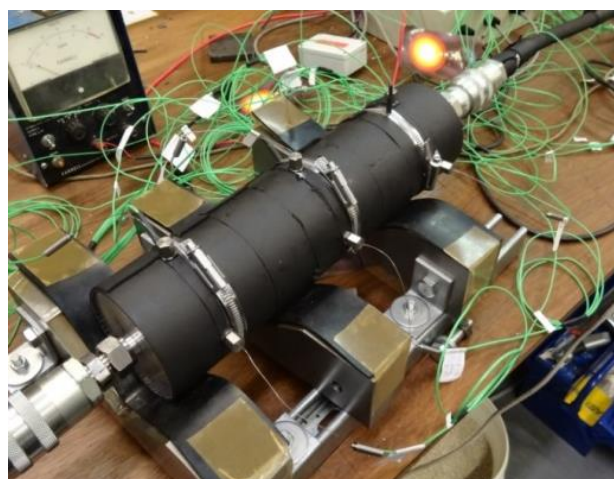


**Figure 5.13: 100 mm outer diameter specimen externally insulated in 3 mm thick Armaflex insulation tape**

### 5.8.1 Results

Figure 5.14 shows the average lubricant temperature profile for two tests conducted using the 100 mm outer diameter specimen with no internal insulation. In one, the test has been externally insulated and in the other, the original aluminium surface is exposed to ambient. It can be seen that during warm-up, there is no identifiable difference in trend for the two scenarios. If anything, the externally lagged specimen shows a prolonged warm-up phase relative to the uninsulated equivalent. Such a trend was also observed when testing the 40 mm outer diameter specimen. It was highlighted in Chapter 4 that the test block specimen, regardless of design, makes only a small overall contribution to the overall thermal inertia of the rig. This was highlighted when the 100 mm outer diameter specimen was installed. In this instance, accounting for energy that was subsequently transferred to ambient from the test block specimen's outer surface, the cumulative energy used to heat the lubricant and test block specimen, was only 25% of the total energy input to the rig. Hence, it is understandable why the lubricant temperature profile remains insensitive to the presence or absence of external insulation.

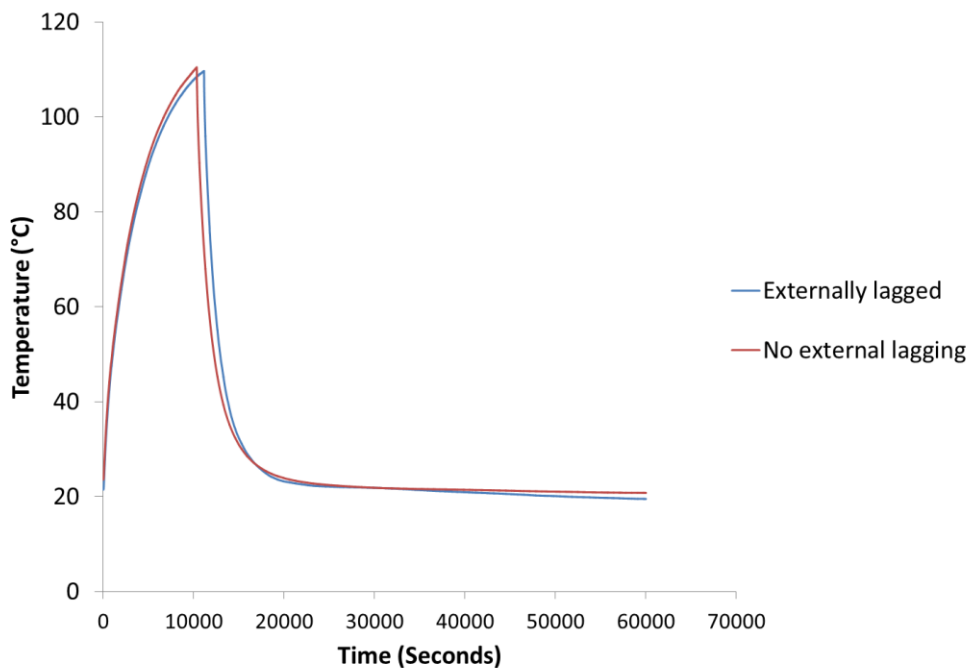


**Figure 5.14: Average lubricant temperature in the oil flow rig for a specimen of 100 mm outer diameter with no internal insulation applied when the heat power is controlled at a constant 1200 W and the lubricant flow rate during warm-up is 10 l min<sup>-1</sup>**

To understand if the external insulation has any meaningful effect on the metal transient warm-up rate requires closer inspection of the temperatures through the thickness of the test block specimen. In doing so, there are possible indications that external insulation does provide some benefit, though the magnitude of the effect is governed by the thermal inertia of the test block specimen. Figure 5.15 shows the

average specimen temperature of both a 100 mm outer diameter specimen (Figure 5.15a) and a 40 mm outer diameter specimen (Figure 5.15b) during both a heating and cooling cycle when the lubricant was heated to 120 °C.

If one first examines the relative performance of the two 100 mm specimens (Figure 5.15a), it can be seen that the specimen with external lagging reaches the peak temperature of 98 °C in 11100 seconds compared to 10300 seconds when no external lagging is applied. This would initially indicate that the presence of external insulation has a negative effect on performance. However, it must also be observed that the starting temperature, owing to ambient variations, is 4 °C lower in the insulated case than in the uninsulated test. Hence, not only is the externally insulated specimen required to increase by a further 4 °C but the heat lost to ambient throughout the entire warm-up cycle will be higher owing to the higher temperature differential between the specimen and ambient. Such a variation also explains why the final temperature of the externally lagged specimen is lower than the lagged equivalent.

Comparatively, the 40 mm outer diameter specimen indicates a more positive result for the use of external insulation. Figure 5.15b shows that while there is still an offset in start temperature, the two tests are more closely aligned with the externally lagged specimen starting at 21.5 °C and the uninsulated specimen starting at 23.5 °C. The externally lagged temperature reaches a peak temperature of 105 °C, compared with 104 °C when no lagging was applied. However, of greater significance is the relative performance of the lagged and un-lagged specimens during cool down. It can be seen that although the two specimens reached peak temperatures to within 1 °C of each other, during cool down, the lagged specimen is, at certain instances in time up to 8 °C higher than the un-lagged equivalent, giving firm indications that the lagging does provide a benefit in the correct scenario.

It is worth considering why the 100 mm outer diameter specimen appears to show no sensitivity to the external lagging yet the 40 mm outer diameter specimen does. The heat flux from the specimen to ambient is a function of the surface area and would thus be proportional to the specimen diameter. One would therefore expect, in a steady state situation, for the larger specimen to show a greater benefit than the smaller counterpart owing to the insulation being over a larger area. However, the transient regime is more complex. The 100 mm outer diameter specimen has a thermal mass 8 times greater than the 40 mm outer diameter specimen. Owing to the high thermal conductivity of aluminium ( $193 \text{ W m}^{-1} \text{ K}^{-1}$  [93]), the specimen reacts as a lumped capacitance body, with negligible temperature gradient across the radial thickness of the metal. Consequently, a specimen with a smaller thermal mass will generate a higher heat flux to ambient sooner than one with a larger thermal mass owing to less energy being required to heat the mass, and the corresponding outer

surface, to an elevated temperature. In the context of the tests conducted with external insulation, the lubricant was heated to 115 °C with both the 100 mm and 40 mm outer diameter specimens. It has already been established that the lubricant temperature profile is insensitive to the specimen design in the rig. Consequently, for a given lubricant temperature, the smaller specimen will be at a higher temperature. This can be seen when comparing Figure 5.15a and Figure 5.15b as the peak specimen temperature is 8 °C higher in the case of the 40 mm outer diameter specimen and the positive gradient noticeably steeper. Thus, when the external insulation is added, there is a greater potential heat flux to insulate owing to the higher temperature between the specimen surface and ambient.

While the transient dynamics of the specimens undoubtedly account for some of the performance characteristics linked to the presence or absence of external lagging, it is also possible that the insulation was simply very ineffective, despite having a thermal conductivity of between  $0.034 \text{ W m}^{-1} \text{ K}^{-1}$  and  $0.038 \text{ W m}^{-1} \text{ K}^{-1}$  and a thickness of 3 mm. This results in a thermal resistance (defined in Equation 4.1) of between  $0.088 \text{ m}^2 \text{ K W}^{-1}$  and  $0.079 \text{ m}^2 \text{ K W}^{-1}$ . Comparatively, the external heat transfer coefficient is seen to vary from between  $14 \text{ W m}^{-2} \text{ K}^{-1}$  and  $4 \text{ W m}^{-2} \text{ K}^{-1}$  (Figure 6.7 in Section 6.2.5) depending on the temperature and size of the test block specimen. The thermal resistance as a result of this boundary condition (the inverse of the heat transfer coefficient) varies between  $0.25 \text{ m}^2 \text{ K W}^{-1}$  and  $0.07 \text{ m}^2 \text{ K W}^{-1}$ . Thus, it may be the case that the external insulation made negligible impact on the temperature profiles owing to the insignificant contribution it makes to the thermal resistance of the system relative to the convective boundary condition. If one compares the external surface of the test block specimen with the internal bore surface, the polymer insert (ignoring the introduction of any contact resistance) has a thermal resistance of  $7.60 \times 10^{-3} \text{ m}^2 \text{ K W}^{-1}$  based on the thermal conductivity of the Nylon 12 being  $0.26 \text{ W m}^{-1} \text{ K}^{-1}$  and the thickness being 2 mm. Comparatively, the internal heat transfer coefficient is between  $225 \text{ W m}^{-2} \text{ K}^{-1}$  and  $500 \text{ W m}^{-2} \text{ K}^{-1}$  (Figure 6.5 in Section 6.2.4.2) and hence represents a thermal resistance of between  $2 \times 10^{-3} \text{ m}^2 \text{ K W}^{-1}$  and  $4.41 \times 10^{-3} \text{ m}^2 \text{ K W}^{-1}$ . Thus the thermal resistance of the Nylon 12 insert is up to 3 times greater than the convective boundary condition whereas on the external surface of the test block specimen the insulation contributed a thermal resistance that was up to 3 times smaller than that provided by the convective boundary condition.

Were the insulation effective, one would expect the radial thermocouples at location R4 to read lower in the insulated case than the uninsulated case as the thermocouples are mounted externally on the insulating tape. If one examines Figure 5.16, this can indeed be seen. When examining the 100 mm and 40 mm outer diameter specimens respectively, it can be seen that the peak outer surface temperature is 10 °C and 7 °C lower respectively when the insulation is applied. This

does indicate that the insulation is effective and that a significant temperature gradient does exist across the external insulation. An interesting trend is the way in which during cool down, the outer surface temperature for the insulated scenario rapidly converges on the uninsulated cool down phase, further reinforcing the theory that the external insulation is only of benefit in the late phase of heating.

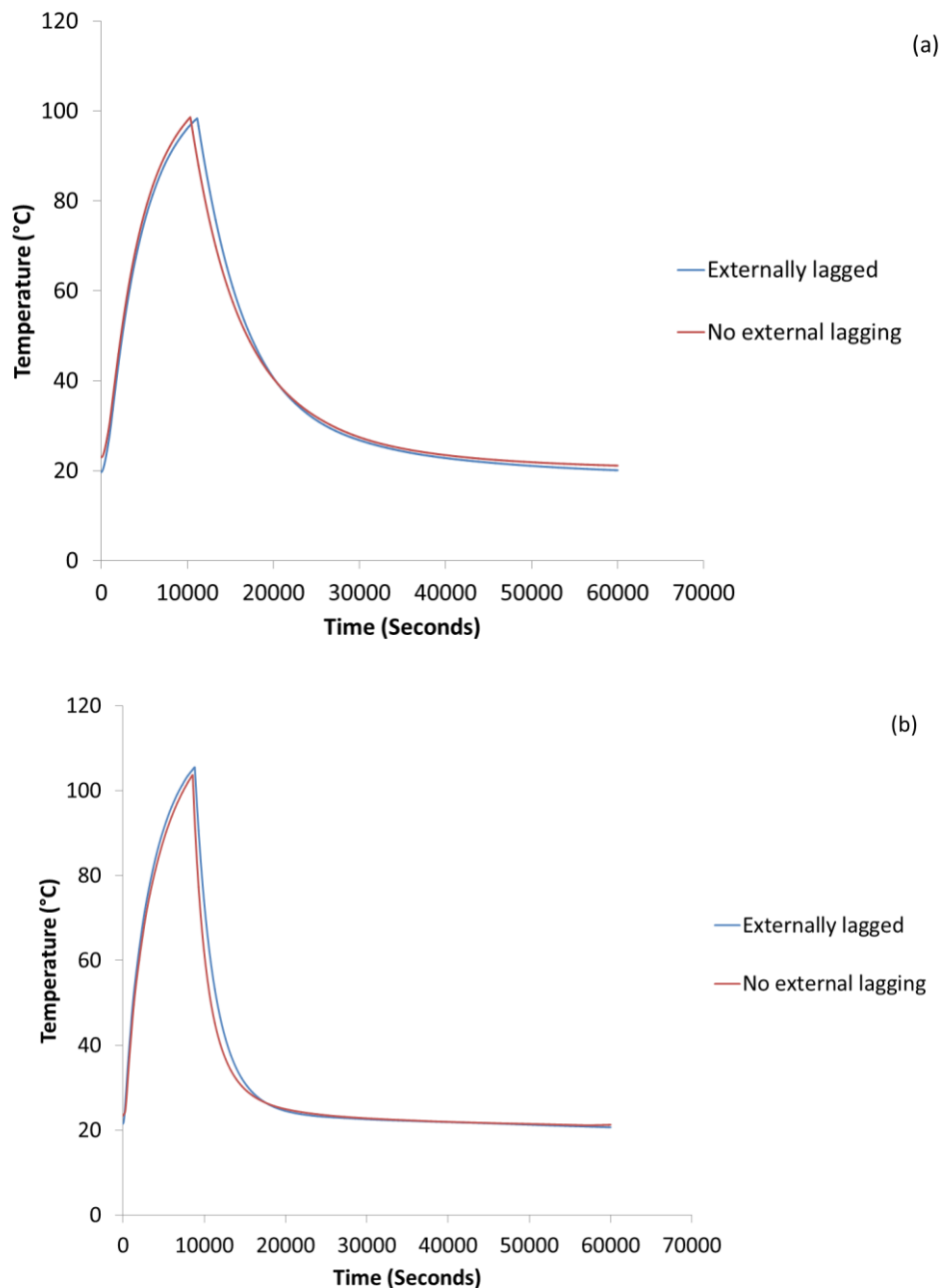


**Figure 5.15: Average specimen temperature in the oil flow rig for specimens without internal insulation when the heat power is controlled at a constant 1200 W and the lubricant flow rate during warm-up is 10 l min<sup>-1</sup>. The specimen outer diameter is (a) 100 mm and (b) 40 mm and were trialled both with and without external insulation**

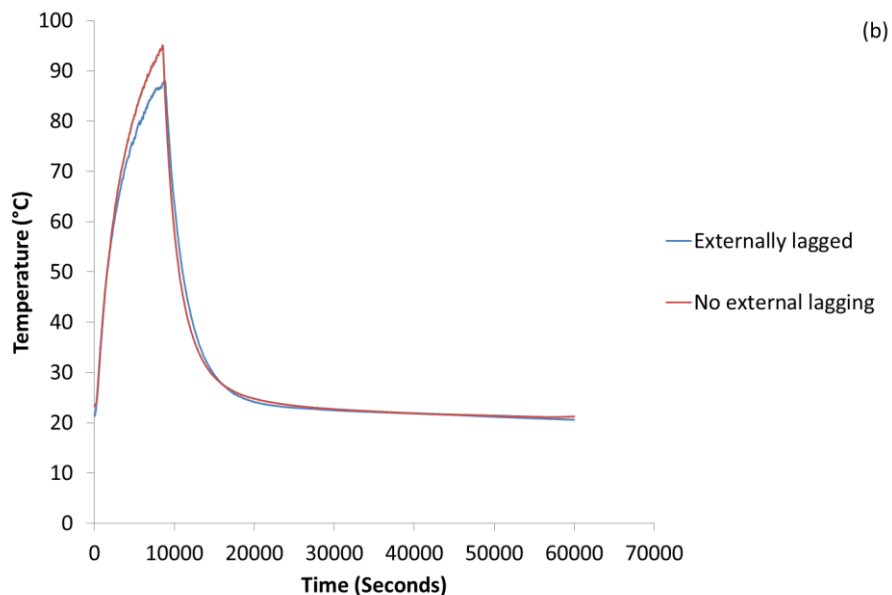
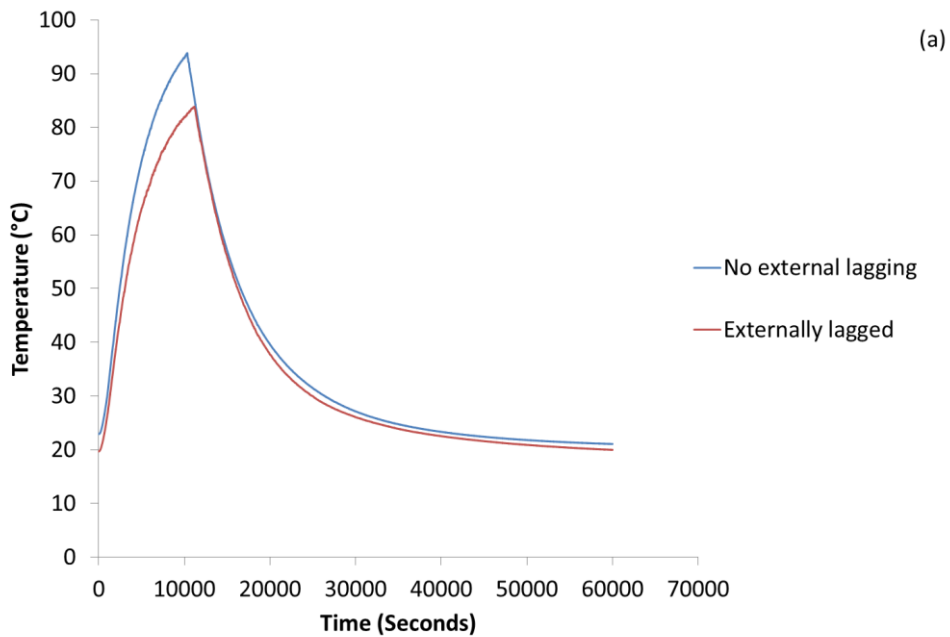


Figure 5.16: Average R4 temperature in the oil flow rig for specimens without internal insulation when the heat power is controlled at a constant 1200 W and the lubricant flow rate during warm-up is 10 l min<sup>-1</sup>. The specimen outer diameter is (a) 100 mm and (b) 40 mm and were trialled both with and without external insulation

## 5.9 Summary

The work presented in this chapter has discussed the changes in observed heat flow from the lubricant to the test block specimen as a result of different insulation strategies. By comparing the experimental results with initial repeatability tests presented in Section 4.9 it has been discussed how the changes in heat flow observed as a result of insulation are of a magnitude that enables them to be

confidently distinguished from variation that has been seen as a result of experimental noise.

Through the experimental results presented, it has been possible to confidently show that the installation of a low thermal conductivity insert has the potential to reduce the heat flow from the lubricant to the surrounding metal structure. Moreover, the insulating effect can be further enhanced by increasing the contact resistance between the insulating insert and the surrounding metal structure. It has been seen that even slight variations in the fit between the insert and the test specimen can have a significant effect on the contact resistance and dominate the thermal conductivity benefits (e.g. the tighter clearance of the sintered Nylon insert relative to the standard Nylon 12 insert). This presents a significant challenge when attempting to implement such technology into a full I.C. engine as there is a need to maintain tight tolerances to ensure reliability in the engine. However, in order to achieve the greatest benefit in reducing thermal losses from the lubricant, there is a need to ensure that as large a clearance as possible is facilitated between the insulating insert and surrounding metal. Critically, such a clearance must also be repeatable to ensure that the intended improvement is achieved.

In order to best summarise the findings, Figure 5.17 presents the average heat flux to the test block specimen for the different designs of insulating inserts. To ensure such a comparison is valid, the cumulative energy transferred to the test block from the lubricant was compared at 10408 seconds into each test and divided by the test duration to provide an average heat flux.

It can be seen that in the uninsulated scenario tested in this work, the average heat flux from the lubricant to the specimen is 127 W and that the most effective insulator (the stepped Nylon 12 insert) can reduce this to 53 W. It can also be seen that the addition of a 0.5 mm air gap to both the Nylon 12 and aluminium inserts has a further positive effect on the heat flux to the specimen. In the case of the Nylon insert, the average heat flux is reduced by 16% from 64 W to 53 W while the aluminium insert is reduced by 17 % from 92 W to 76 W. This, combined with the ability to reduce the benefit of installing an insert into the gallery by applying a thermal contact paste has established that the interface alone, between the surrounding metal and insert, is a highly effective insulating mechanism.

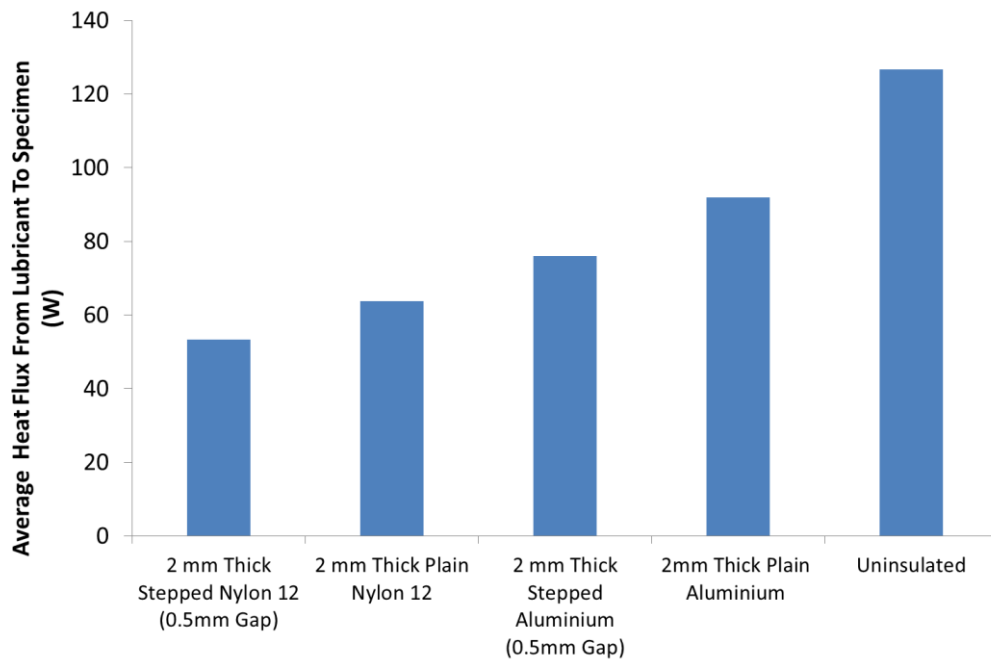


Figure 5.17: Average heat flux from the lubricant to the test block specimen over the duration of 10408 seconds on the oil flow rig for a 100 mm outer diameter specimen with different insulating inserts when the heater power was controlled at 1200 W and the lubricant flow rate set to 10 l min<sup>-1</sup>

In discussing the architecture and characteristics of the rig, it has been highlighted at length that the lubricant temperature is largely insensitive to the size and composition of the test block specimen structure. In highlighting the effect of insulating against thermal masses of different size, Section 5.2.1.1 presented a methodology that enabled a hypothetical accelerated lubricant heating rate to be calculated based on the reduced energy flow to the test block specimen. The methodology assumes that, for a given insulation method, the difference in energy transferred to the specimen, relative to the uninsulated baseline scenario, is all retained in the lubricant and therefore results in a higher lubricant heating rate.

The results, presented in Table 5.2, indicate that the percentage of heat input that can be retained as a result of lubricant gallery insulation can be increased from 124 W, i.e. 10 % of the total heater power to 197 W (16% of the total heater power). This is achieved by combining a high contact resistance and low thermal conductivity material. In carrying out this work, the desires of OEMs must be considered. The use of a metallic insert that does not present any concerns with regard to creep and relaxation over time is potentially a more appealing option for implementing at a production level. If one attempts to maximise the contact resistance, the results show that the theoretical maximum lubricant heating rate could be increased by 13% from 157 W to 177 W.

**Table 5.2: Potential improvements to lubricant heating rate as a result of insulation when a 100 mm outer diameter specimen is installed and the heater power and lubricant flow rate are controlled at 1200 W and 10 l min<sup>-1</sup> respectively**

<u>Specimen</u>	<u>Average heating rate of lubricant (W)</u>	<u>Average heat flux from the lubricant to the specimen (W)</u>	<u>Assumed potential lubricant heating rate (W)</u>
2 mm thick stepped Nylon 12 (0.5 mm Gap)	124	53	197
2 mm thick plain Nylon 12	123	64	186
2 mm thick stepped aluminium (0.5 mm Gap)	126	76	177
2 mm thick drilled aluminium	124	80	170
2 mm thick plain aluminium	122	92	157
Uninsulated	124	127	124

## 5.10 Conclusion

The work presented in this chapter has, through a broad range of experimental tests, characterised the transient process of engine lubricant heating and the effect of the surrounding metal structure on this heating.

It has been quantifiably observed that the use of insulating inserts in engine oil galleries has the capability to reduce the heat flux from the lubricant to the surrounding metal by as much as 60% depending on the system being utilised.

The insulating mechanism has been found to be a combination of two physical phenomena. In the first instance, the insertion of low thermal conductivity materials into the engine gallery bore wall does undoubtedly reduce the heat flow from the lubricant to the surrounding metal structure. However, a critical observation has been the importance of contact resistances to the heat transfer from the lubricant to the specimen. Results presented in this chapter saw the insertion of a 2 mm thick drawn aluminium tube into the 100 mm outer diameter test block specimen reduce the average heat flow to the lubricant by 27% relative to the uninsulated baseline from 127 W to 92 W. Such a change can only have been as a result of the introduction of the contact resistance given that the thermal masses of the two cases are virtually identical owing to the insert being manufactured from the same material as the test block specimen. If the contact resistance was purposefully increased by machining a 0.5 mm air gap into the outer diameter of the specimen,

the reduction in heat flow increased to 40%, resulting in an average heat flux from the lubricant to the specimen of 76 W. Moreover, it has been shown that the effect of the contact resistance is dominant over any change in heat flow that may be as a result of changes in the bore surface roughness. When utilising a plain aluminium insert of the same dimensions as the drawn tube but with a drilled bore, the heat flow from the lubricant to the test block specimen decreased from 92 W with the drawn aluminium to 80 W with the drilled aluminium insert (a decrease of 13%). Were surface roughness effects dominant one would have expected the rougher drilled bore to increase the heat flow from the lubricant to the test block specimen. The most effective combination utilised both a high contact resistance and a low thermal conductivity material by using a 2 mm thick Nylon 12 tube with a 0.5 mm air gap machined into the outer surface. This achieved a 58% reduction in the heat flow, resulting in an average heat flux of 53 W, compared to 127 W in the uninsulated scenario.

Through the experimental results, it has also been observed that during the transient regime the application of insulation to engine oil galleries has a greater benefit when insulating against larger thermal masses. When comparing an uninsulated specimen of 40 mm outer diameter and 100 mm outer diameter specimen, one saw that over a test of equal length, the average heat flux from the lubricant to the specimen was 124 W in the case of the 100 mm outer diameter specimen and 39 W in the case of the 40 mm outer diameter specimen. When a 2 mm thick plain Nylon 12 insert was installed in both specimens, the average heat flux from the lubricant to the specimen reduced from 124 W to 54 W (a reduction of 76 %) while the 40 mm outer diameter specimen reduced from 39 W to 29 W (a reduction 34 %).

By comparison, when external insulation was applied to the test block specimens, one could see negligible change between the bulk specimen temperatures during warm-up or cool down as a result of the external insulation. The outer surface temperature was seen to peak at a lower value than the uninsulated counterparts but during cool down, quickly converged on the uninsulated results.

The results therefore indicate that the most effective insulating strategy is to insulate regions of high thermal mass (i.e. thick wall castings) and that wherever possible, to use a combination of the lowest thermal conductivity and highest contact resistance that the operating conditions will allow. However, for such an approach to yield meaningful benefits in the efficiency of an I.C. engine there is a need to apply insulation to the lubricant circuit in a way that is applied to the most appropriate regions of the engine lubricant circuit. As was detailed in Section 1.5.1.2 (Figure 1.18) there are regions of the engine where the lubricant increases in temperature as a result of heat exchange with other engine components and one must therefore only insulate regions where thermal losses are observed. An

associated challenge of implementing insulation in regions of the engine that are the most desirable is developing an installation or application method that is feasible to use in regions of the engine that are difficult to access. The concept of installing an insulating insert in the same manner that has been used on the oil flow rig is applicable to regions of the engine such as the main oil gallery as the drilling is straight and there is good access from both ends of the engine block. However in the case of bearing feed galleries or the galleries to the valve train and return galleries (see Figure 1.17), the cast geometry is far more complex and such an approach would not be viable. There is therefore clear scope for further work to develop a method of installing thermal insulation to the lubricant circuit of an I.C. engine in regions of limited access.

## 6 Development of the oil flow rig theoretical simulation model

### 6.1 Introduction

Through the experimental work conducted on the oil flow rig, it has been seen that the incorporation of insulation has a significant impact on the thermal behaviour of the test block specimen. The scope of the experimental work has been broad and allowed significant physical parameters, such as the presence of a contact resistance, to be identified. However, a well correlated theoretical model of the heat transfer between the lubricant and the test block specimen allows for further investigative work to be carried out beyond the physical limitations of the rig.

The lubricant temperature within the test block specimen and the specimen temperatures are fundamental to any theoretical or experimental work. It was established in Chapter 3 that the remaining rig architecture is of limited interest in the investigation of oilway insulation. However, the supporting hardware on the rig such as the tank, filters and pump are significant in affecting the thermal behaviour of the lubricant and specimen owing to the large thermal inertia associated with the components. Hence, this chapter details the underlying physical principals of the model, how the specific dynamics of the rig are incorporated into any assumptions and the subsequent validation with experimental data. This model focuses on the heat transfer between the lubricant and the test block specimen and does not explicitly model heat transfer to the remaining rig structure. Through the use of the model, it is intended to be able to carry out parametric studies into the effects of different physical parameters on heat transfer between the specimen and the lubricant. Whereas a change in material on the experimental rig would result in multiple properties changing, the model enables properties to be varied independently of each other (e.g. specific heat capacity and thermal conductivity) while also simulating the combined effects of using different materials, both as insulators and test block materials. The model will also facilitate the effect of variations in flow parameters to be investigated.

### 6.2 Modelling methodology

To simulate the rig discussed in in Chapter 3 – Chapter 5, a mathematical finite difference model was constructed (the flow chart of the model structure is available in Appendix D). Figure 6.1 shows a schematic section through the longitudinal length of the specimen and how the lubricant temperatures along the length of the specimen are discretised and linked to the bulk lubricant temperature in the tank,  $T_{Tank}$ . Figure 6.2 shows the nodal setup through the radial thickness of the specimen. One can see in Figure 6.1 and Figure 6.2 that the model has only explicitly modelled temperatures for the following variables:

- The lubricant along the length of the test block specimen.
- The temperature of the specimen through the radial thickness.
- An additional node,  $T_{tank}$ , to simulate the bulk lubricant temperature in the tank

Such an approach was taken to aid the subsequent tuning process of the model to experimental data. Relative to the physical rig, the model does not explicitly model significant thermal masses including the pump, tank and oil filters. The approach developed has minimised unknowns and has utilised experimental temperature data to select appropriate heat transfer coefficient correlations from the literature. The experimental temperature data, combined with heat transfer coefficients has enabled the model to incorporate an empirical function to model the ‘effective power’ supplied to the system. The effective power represents energy that is either:

- Stored as sensible heat in the lubricant and causes the lubricant temperature to rise.
- Stored as sensible heat in the specimen and causes the specimen temperature to rise.
- Is transferred by convection from the outer surface of the specimen to ambient.

Consequently, by incorporating the effective power of the rig into the simulation, the thermal inertia and unknowns of the supporting rig hardware are mitigated. This section details the heat transfer equations between nodes through the radial thickness of the test block specimen in addition to the modelling of the loss of temperature from the lubricant as it traverses the longitudinal length of the specimen. The combination of these two mechanisms and incorporation of the effective power to account for the thermal inertia of the supporting rig hardware enables the model to simulate the heating of engine lubricant in a rig test environment.

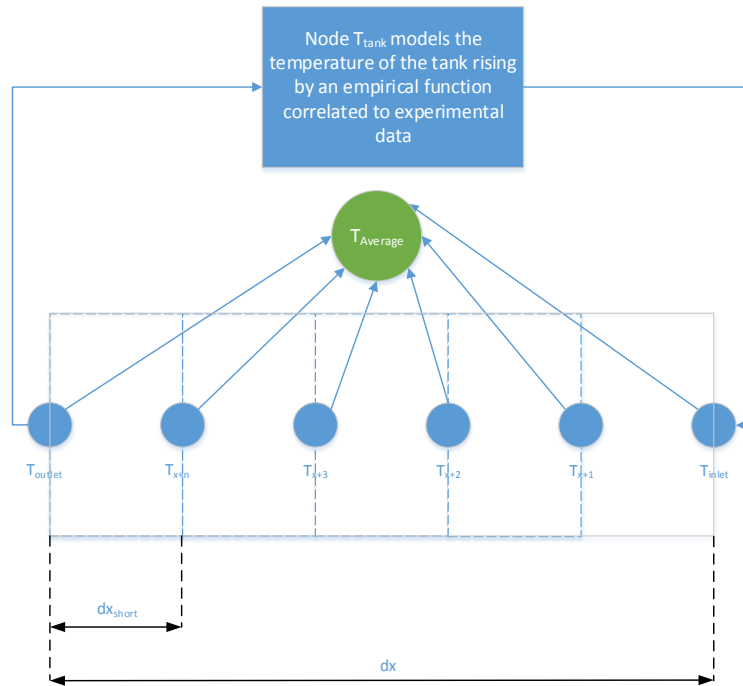


Figure 6.1: Schematic lubricant nodal structure along the longitudinal length of the test block specimen in the theoretical model

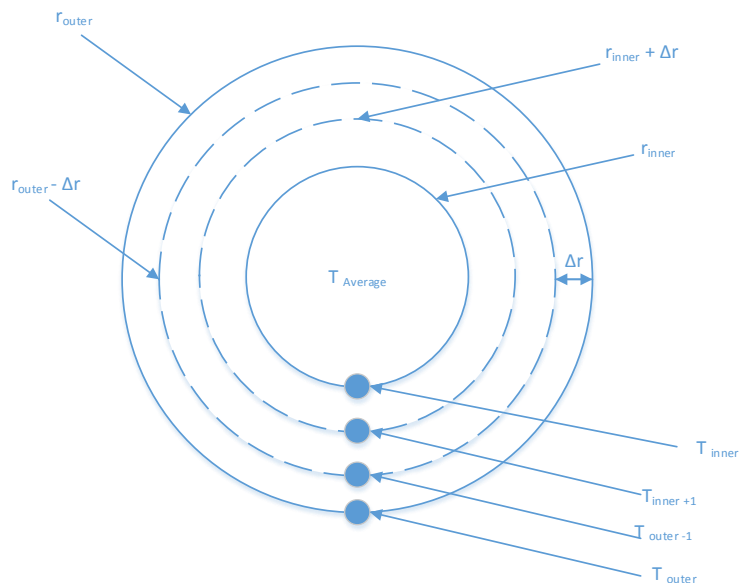


Figure 6.2: Radial nodal arrangement from the oil pipe centre

### 6.2.1 Distance step

The model incorporates a lubricant tank with a fixed volume of lubricant and a lubricant volumetric flow rate. The lubricant is modelled to enter the test block specimen at an input temperature of  $T_{inlet}$ . Assuming the block to be cooler than the lubricant, the lubricant loses heat to the block as it traverses the length of the specimen and, by conservation of energy results in the block temperature rising. For the model to work effectively, the nodal distance,  $dx_{short}$ , needs calculating and is a

function of the time step, internal bore cross sectional area and lubricant density. The time step is governed by the need to match a stability criterion provided by the nodal equations discussed in Section 6.3 and is subsequently used to calculate the nodal distance as shown in Equation 6.1.

$$dx_{short} = \frac{\dot{m}_{oil} \delta t}{\pi r_a^2 \rho_{oil}}$$

**Equation 6.1: Oilway nodal length dependency on oil mass flow rate, cross sectional area, density and time step**

A key assumption within the model structure is that within any time step, the control volume of lubricant along the length  $dx_{short}$  is entirely replaced. Consequently, depending on the time step required to meet stability demands, the lubricant within the test block specimen is discretised into cells. The number of cells required is defined in Equation 6.2.

$$Longitudinal\ steps = \frac{dx}{dx_{short}}$$

**Equation 6.2: Longitudinal steps required as a function of distance step**

With the parameter  $dx_{short}$  determined each individual longitudinal cell can be subject to its own energy balance.

### 6.2.2 Node $T_x, T_{x+1}, T_{x+2}, T_{outlet}$

The number of longitudinal steps is a function of the specimen length and model time step. As such, the number of nodes depicted in Figure 6.1 is illustrative only; however the approach taken is the same along the length of the specimen.

As the lubricant flows through the test block specimen, the only means of the lubricant losing thermal energy, and thus reducing temperature, is by convection to the bore wall of  $r_{inner}$ . Taking  $T_{inlet}$  as an example, the energy lost from the lubricant across a length  $dx_{short}$ , is defined as

$$Q_{block} = h_{oil} dx_{short} 2\pi r_{inner} \delta t (T_{inlet}^n - T_{inner}^{n-1})$$

**Equation 6.3: Heat flow to the block from the oil**

The associated temperature change in the lubricant at the node of interest as a result of the energy lost to the block,  $Q_{Block}$ , is defined as:

$$T_x^n = T_{inlet}^n - \frac{Q_{block}}{\dot{m}_{oil} C_{p\ oil} \delta t}$$

**Equation 6.4: Derivation of oil flow node temperature as a function of the preceding flow node temperature**

Equation 6.4 is subsequently repeated along the length of the specimen, taking the temperature of the upstream lubricant node,  $T_{x-1}^n$ , and calculating the new temperature as a function of the heat flux to the bore wall temperature at the previous time step,  $T_{inner}^{n-1}$ . Given that in this work, the specimen is being heated by the lubricant, the lubricant leaves the test block specimen at a temperature  $T_{outlet}$  that is lower than  $T_{inlet}$ .

The average temperature of the lubricant in the node,  $T_{average}$  is used to determine the temperature differential between the lubricant in the specimen and the test block specimen. Having established in Section 4.2 that the temperature differential between the test block specimen and lubricant is constant along the length of the test block specimen, this therefore is a valid log mean temperature differential ( $\Delta T_{lm}$ ).  $T_{average}$  is taken as the average of lubricant temperatures along the length of the test block specimen at a given time step, as shown in Figure 6.1.

The heat input rate over the length of the test block specimen is therefore given by:

$$\dot{Q}_{block} = h_{oil} dx 2\pi r_{inner} (T_{average}^n - T_{inner}^n)$$

**Equation 6.5: Heat flow to the block from the lubricant**

It should be noted here that Equation 6.5 has a sign convention whereby a positive heat flow is one that flows from the lubricant to the test block specimen.

### 6.2.3 Node $T_{tank}$

The tank in this model has been modelled as being a perfectly insulated block and therefore has no convective heat transfer mechanism built into it. Instead, the effective power that was referred to in Section 6.2 accounts for such losses. The quantification and validation of the effective power is discussed in greater detail in Section 6.4. The change in energy of the lubricant in the tank is a function of the tank lubricant temperature at two separate time steps:

$$\Delta Q_{tank} = m_{oil\ tank} C_{p\ oil} (T_{tank}^n - T_{tank}^{n-1})$$

The energy input into the rig and lubricant is provided by the immersion heater and for a given time step is given by

$$Heat\ Input = Q_{in}\delta t$$

The bulk lubricant temperature in the tank is effectively reduced by cooled lubricant returning to the tank. The effective heat lost by the lubricant in the tank as a result of this is given by:

$$\dot{m}_{oil} \delta t C_{p\ oil} (T_{outlet}^n - T_{tank}^{n-1})$$

Equating the change in overall energy of the tank lubricant with the summation of the energy inputs gives:

$$m_{oil\ tank} C_{p\ oil} (T_{tank}^n - T_{tank}^{n-1}) = \dot{m}_{oil} C_{p_{oil}} \delta t (T_{outlet}^n - T_{tank}^{n-1}) + Q_{in} \delta t$$

A final re-arrangement gives:

$$T_{Tank}^n = T_{Tank}^{n-1} \left( 1 - \frac{\dot{m}_{oil} \delta t}{m_{oil\ tank}} \right) + T_2^N \left( \frac{\dot{m}_{oil} \delta t}{m_{oil\ tank}} \right) + \frac{Q_{in} \delta t}{m_{oil\ tank} C_{p_{oil}}}$$

Equation 6.6: Nodal equation for node  $T_{Tank}$

Using such an approach, the inlet temperature to the test block specimen,  $T_{inlet}$ , is assumed to be the same as the tank lubricant temperature,  $T_{tank}$ , owing to the effective power being used to reduce the lubricant warm-up rate.

## 6.2.4 Variation of $h_{oil}$ with temperature

### 6.2.4.1 Reynolds Number effects

A key variable within the model is the selection of an appropriate value of the parameter  $h_{oil}$ . While the emphasis of this work is not a detailed study of the fluid mechanics of engine lubricant, it must be acknowledged that the convective heat transfer mechanism from the lubricant to the test block specimen is dependent on a range of fluid mechanics factors. The value of heat transfer coefficient is known to be dependent on:

- Hydraulic diameter and length.
- Fluid properties, most noticeably viscosity and density.
- Flow velocity.

The use of engine lubricants makes this issue ever more significant owing to the lubricant's temperature sensitivity in relation to viscosity, as was shown in Chapter 3 (Section 3.4). A fundamental parameter to be considered in the selection of an appropriate  $h_{oil}$  is that of the Reynolds Number. The Reynolds Number, defined in Equation 6.7, is the ratio of inertial forces to viscous forces and therefore quantifies whether the flow regime is laminar, transitional or fully turbulent. Typically, it is accepted that should the Reynolds Number fall below 2000 then the flow is laminar and for the flow to be considered fully turbulent, the Reynolds Number needs to be above 10000. However, such boundaries are not absolute and a degree of tolerance is allowed in the transition between such regimes. For a given flow rate, the velocity of the fluid can be calculated using the internal bore cross sectional area. By combining lubricant temperature data from the oil flow rig with the lubricant dynamic viscosity data presented in Figure 3.16 of Chapter 3 and the lubricant density data presented in Figure 3.14 of Chapter 3 the Reynolds Number can be

calculated. Figure 6.3 shows how the Reynolds number changes over time for a 100 mm outer diameter specimen when 1200 W heat input is applied at the element and the flow rate is maintained at 10 l min<sup>-1</sup> and 15 l min<sup>-1</sup>. When looking at Figure 6.3 one can see the Reynolds Number increases from 140 at the beginning of the test to 1400 when testing at 10 l min<sup>-1</sup> and varies between 180 and 1500 at 15 l min<sup>-1</sup>. In both tests, the period where the pump speed was increasing was omitted. Hence there is no variation in the Reynolds Number as a result of a change in flow rate. Thus the variation seen is purely an effect of lubricant viscosity and density changing with temperature. The Reynolds number remaining below 2000, indicates that the flow remains laminar throughout both test cycles, a condition observed in the actual engine oil galleries according to the work of Zammit et al. [116]. However, it is possible some transition effects will have begun to manifest themselves at the higher Reynolds Number.

$$Re = \frac{\rho_{lubricant} v D_{hydraulic}}{\mu_{lubricant}} = \frac{v D_{hydraulic}}{\nu_{lubricant}}$$

Equation 6.7: Definition of Reynolds Number

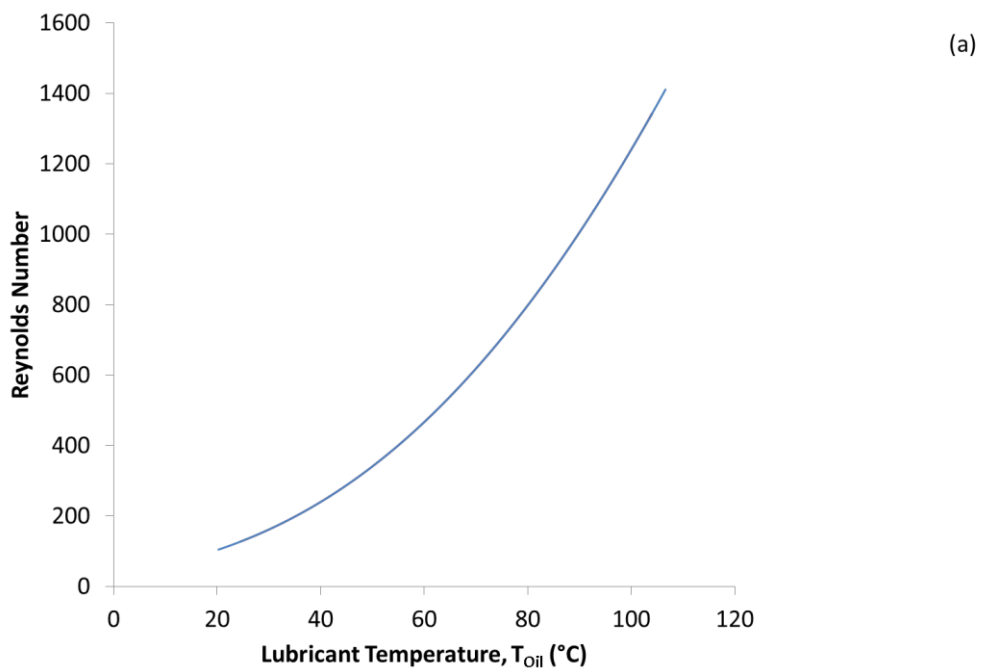
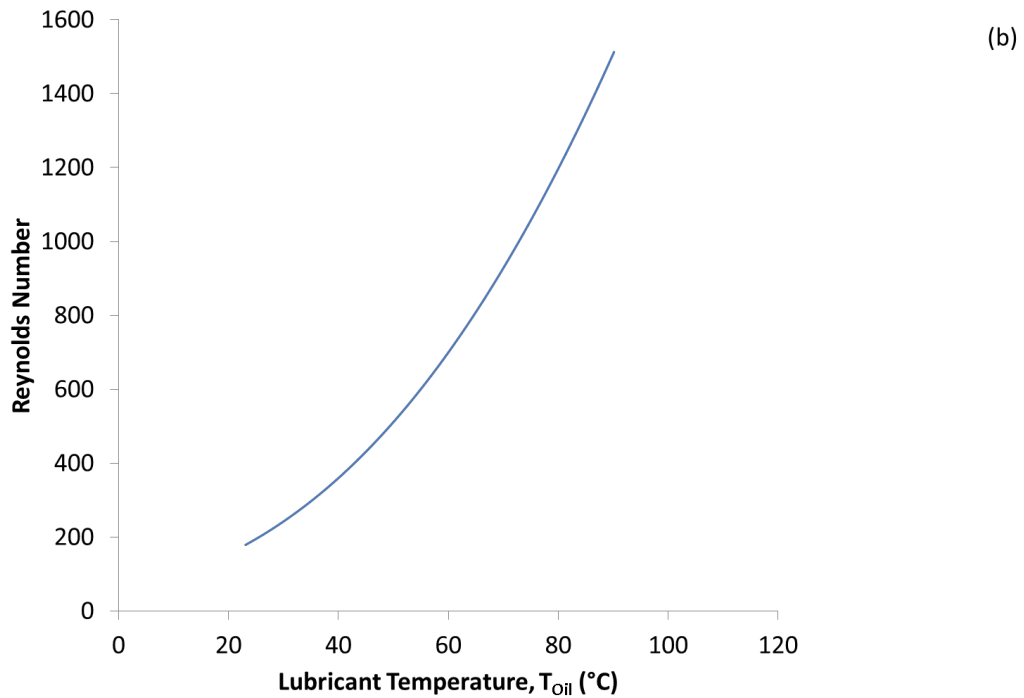


Figure 6.3a: Reynolds Number against lubricant temperature for the oil flow rig when flowing at 10 l min<sup>-1</sup> through an uninsulated specimen of 100 mm outer diameter with a 16 mm bore and 1200 W constant heat input



**Figure 6.3b: Reynolds Number against lubricant temperature for the oil flow rig when flowing at  $15 \text{ l min}^{-1}$  through an uninsulated specimen of 100 mm outer diameter with a 16 mm bore and 1200 W constant heat input**

The quantification of the Reynolds Number in Figure 6.3 suggests that the flow regime in the gallery is laminar and is supported by the work of Shayler et al. [39]. Hence, any correlation used should focus on correlations based on laminar flow. Such an approach would be valid in the instance of fully developed flow; however, one has to consider the entry length effects of the test block specimen. At the entry and exit of the test block specimen are two clean break fittings (first shown in Figure 3.12 of Chapter 3) to allow the specimen to be removed from the rig. An unavoidable consequence of their presence is the high likelihood to cause some flow disturbance and consequently introduce entry length effects into the test block specimen.

The typical entry length for laminar flow is defined in Equation 6.8 [50] and represented graphically in Figure 6.4 and it is interesting to observe the increase in entry length as the test progresses. This is a result of the Reynolds Number of the lubricant increasing and therefore becoming more turbulent. However, the critical observation is that the specimen (of 380 mm length) is well within the entry length of the flow regime being studied and as such a heat transfer coefficient for fully developed laminar flow is not likely to be relevant in this instance.

$$L_{hydraulic\ entry} = 0.05 Re D$$

$$L_{thermal\ entry} = 0.05 Re Pr D$$

**Equation 6.8: Definition of entry lengths for laminar flow [50]**

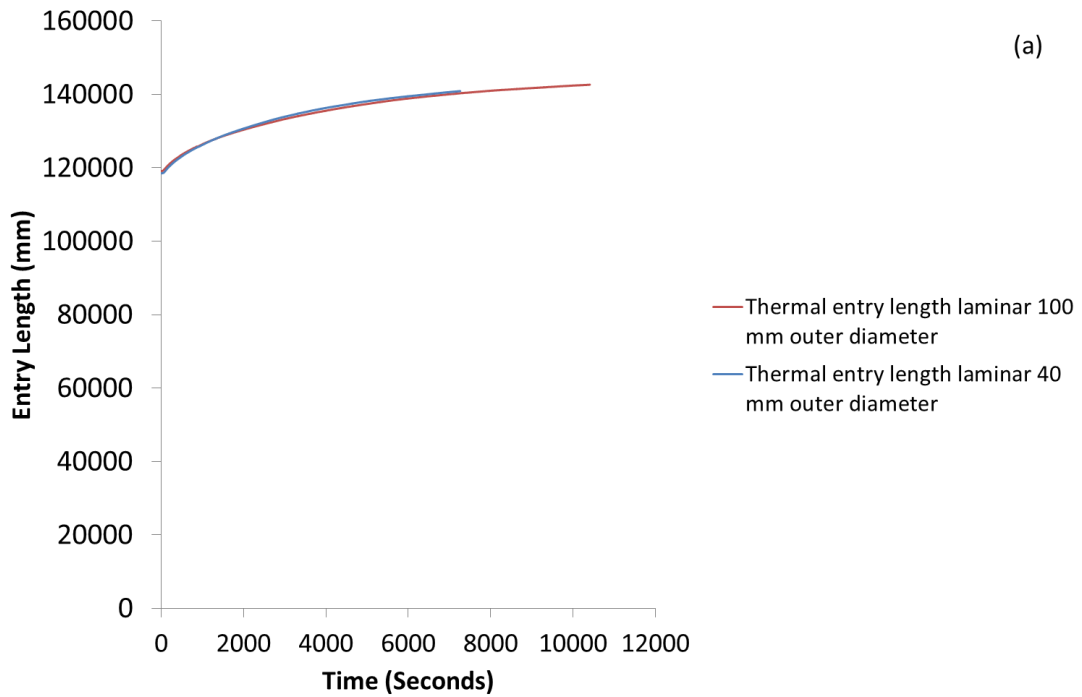


Figure 6.4a: Thermal entry length for developing laminar flow using both a 40 mm outer diameter and 100 mm outer diameter specimen with 1200 W heater power and  $10 \text{ l min}^{-1}$  flow rate through a 16 mm diameter bore

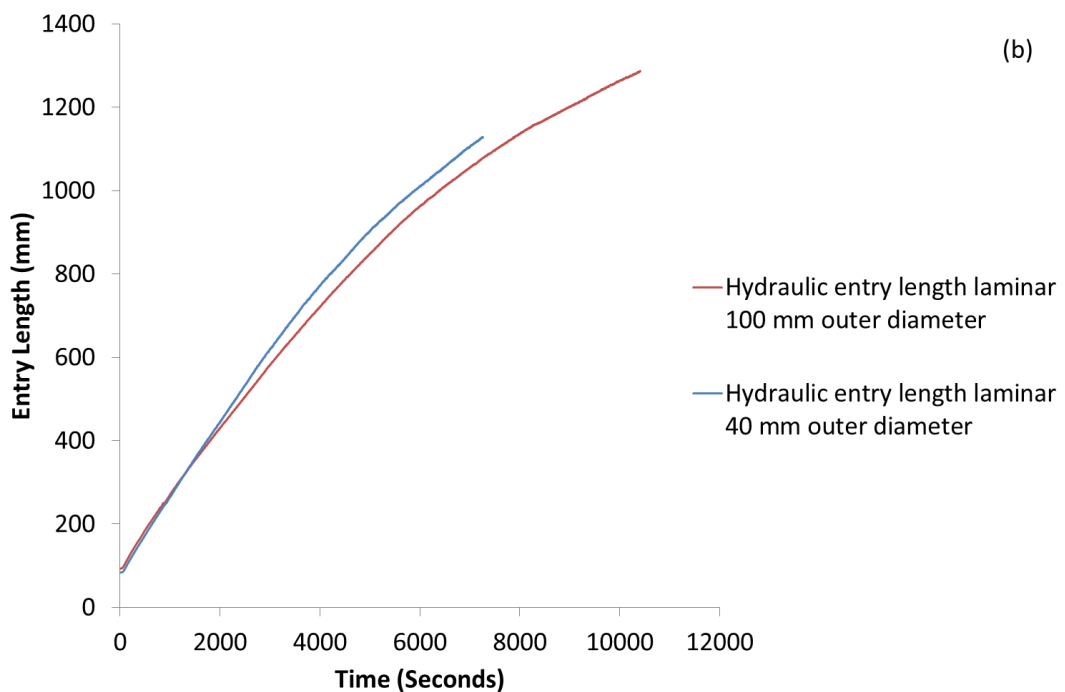


Figure 6.4b: Hydraulic entry length for developing laminar flow using both a 40 mm outer diameter and 100 mm outer diameter specimen with 1200 W heater power and  $10 \text{ l min}^{-1}$  flow rate through a 16 mm diameter bore

From the work presented it can be concluded that the lubricant viscosity reducing as the lubricant temperature increases has a significant impact on the Reynolds Number at both of the flow rates tested. The Reynolds Number is seen to approach a maximum value of 1600 meaning that it is possible the flow is not fully laminar. This, together with flow disturbances caused by entry effects at the inlet of the specimen would indicate that the flow regime will span both the laminar and transition flow regimes.

#### 6.2.4.2 Selection of $h_{oil}$ correlation

It is possible to gain an indication of magnitude and trend of the value of  $h_{oil}$  from the experimental data. The energy transferred from the lubricant to the specimen is either retained in the specimen and causes an increase in the temperature of the metal or is transferred to ambient by convection at the outer surface of the specimen, as summarised in Equation 6.9.

$$\dot{Q}_{specimen} = \frac{m_{specimen} C p_{specimen} \Delta T_{specimen}}{\delta t} + h_{outer} 2\pi r_{outer} dx (T_{outer} - T_{ambient})$$

$$\dot{Q}_{specimen} = h_{oil} 2\pi r_{inner} dx (T_{oil} - T_{inner})$$

$$h_{oil} = \frac{\dot{Q}_{specimen}}{2\pi r_{inner} dx (T_{oil} - T_{inner})}$$

Equation 6.9:  $h_{oil}$  as a function of experimental data

It should be noted that such a methodology is only valid when considering uninsulated specimens as the temperature differential across any insulator would give a false indication of the heat transfer coefficient. Across the literature there exists a wide range of heat transfer coefficient correlations for use in a range of applications. These are summarised, together with their recommended limitations in Table 6.1.

Table 6.1: Range of empirical heat transfer coefficients for internal forced convection

Name	Correlation	Remarks	Reference
Sieder and Tate laminar flow	$Nu = 1.86 \left( Pe \frac{D}{L} \right)^{1/3} \left( \frac{\mu_b}{\mu_w} \right)^{0.14}$		[51]
Sieder and Tate turbulent flow	$Nu = 0.027 Pr^{1/3} Re^{0.8} \left( \frac{\mu_b}{\mu_w} \right)^{0.14}$		[49, 50, 52]
Dittus and Boelter	$Nu = 0.023 Re^{0.8} Pr^n$	n = 0.4 for heating n = 0.3 for cooling	[49, 50]

Name	Correlation	Remarks	Reference
Nusselt Turbulent developing flow	$Nu = 0.036Pr^{1/3}Re^{0.8}\left(\frac{d}{L}\right)^{0.055}$		[13, 52]
Ghajar and Tam laminar flow	$Nu = 1.24\left[\left(\frac{RePrD}{L}\right) + 0.025(GrPr)^{0.75}\right]^{1/3}\left(\frac{\mu_b}{\mu_w}\right)^{0.14}$		[50]
Ghajar and Tam turbulent flow	$Nu = 0.023Re^{0.8}Pr^{0.385}\left(\frac{x}{D}\right)^{-0.0054}\left(\frac{\mu_b}{\mu_w}\right)^{0.14}$		[50]
Edwards laminar flow	$Nu = 3.66 + \frac{0.065\left(\frac{D}{L}\right)RePr}{1 + 0.04\left[\left(\frac{D}{L}\right)RePr\right]^{2/3}}$	Laminar thermal entry region	[50]

In determining the most appropriate heat transfer coefficient, the empirical correlations highlighted in Table 6.1 have been calculated using experimental data from both a 40 mm and 100 mm outer diameter test specimen without insulation. Figure 6.5 shows a comparison of the experimental value of  $h_{oil}$  (calculated using Equation 6.9) against a range of empirical correlations at  $10 \text{ l min}^{-1}$  flow rate. In all instances both the experimental and empirical correlations show a value of  $h_{oil}$  that is increasing with temperature; a consequence of the lubricant kinematic viscosity reducing and therefore causing the Reynolds Number to increase (see Figure 6.3). One can see in both instances the laminar Sieder and Tate, laminar Ghajar and Tam and the transition Ghajar and Tam correlations are wholly unrepresentative of the experimental trend observed. Given that the Reynolds Number clearly indicates that the flow should remain laminar at both  $10 \text{ l min}^{-1}$  and  $15 \text{ l min}^{-1}$  over the duration of the test this is surprising. However, it has already been established that the flow is unlikely to be fully developed upon entry to the test block specimen and as a result, the flow is likely to be much more mixed than in a fully developed situation. The Edwards correlation is intended to be used for developing flow situations and one can again see that the correlation with experimental data is poor. The most likely cause of such disagreement is the sensitivity of the lubricant viscosity to temperature making the viscosity based Reynolds Number term a dominant factor in determining the heat transfer coefficient. Similarly, an analysis of the various correlations was carried out at the higher  $15 \text{ l min}^{-1}$  flow rate using a 100 mm uninsulated specimen. Based on the Reynolds Number plot shown in Figure 6.3b, the flow should, even at this higher flow rate, remain laminar; albeit with the entry

length considerations already considered. When looking at Figure 6.6 one can see that the Dittus and Boelter turbulent correlation shows particularly good agreement with the experimental data and this was also the correlation that gave the closest agreement at  $10 \text{ l min}^{-1}$  flow rate. The literature [49, 50] highlights the Sieder and Tate turbulent correlation to be particularly relevant when applied to fluids with temperature dependent viscosity, hence the inclusion of a viscosity term that analyses the viscosity at both the bulk fluid and wall temperature. However, this particular correlation does not offer an improved performance in any of the instances discussed and was hence discounted. In addition, the Sieder & Tate correlation for turbulent flow is recommended for use only when the Reynolds Number is above 10000 [49-51]. This is clearly beyond the scope of the experimental work considered.

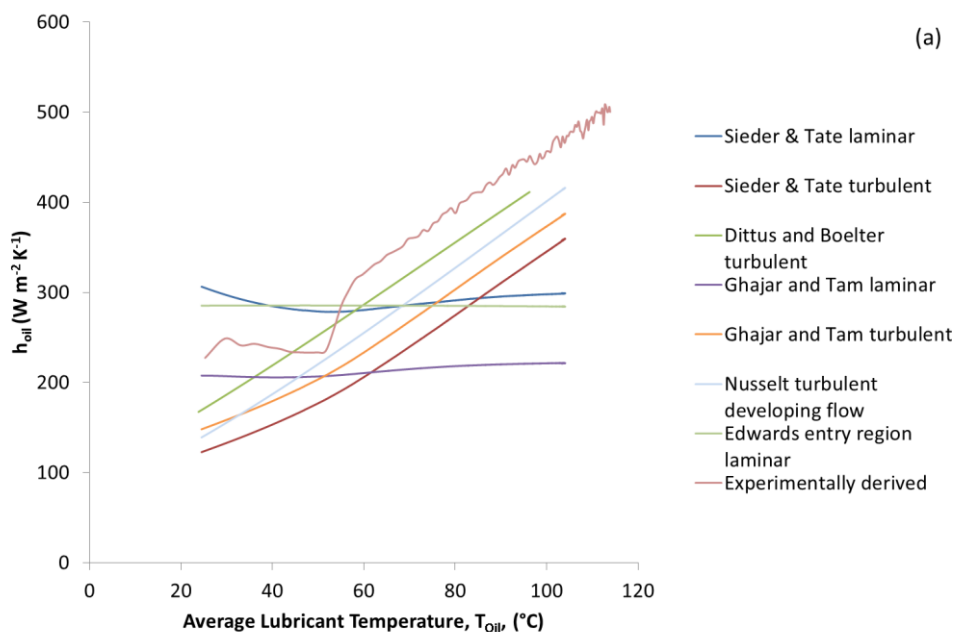


**Figure 6.5a: Comparison  $h_{oil}$  values using different correlations and derivations from experimental results using a 100 mm outer diameter specimen with a 16 mm bore and  $10 \text{ l min}^{-1}$  flow rate with 1200 W element heater power**

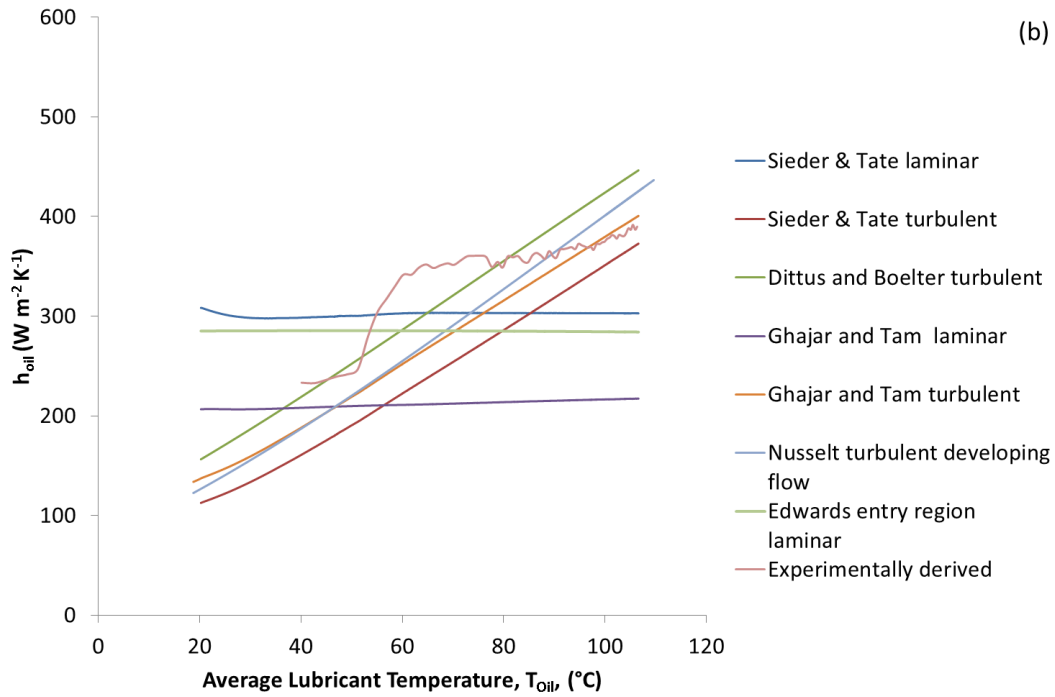


Figure 6.5b: Comparison  $h_{oil}$  values using different correlations and derivations from experimental results using a 40 mm outer diameter specimen with a 16 mm bore and  $10 \text{ l min}^{-1}$  flow rate with 1200 W element heater power

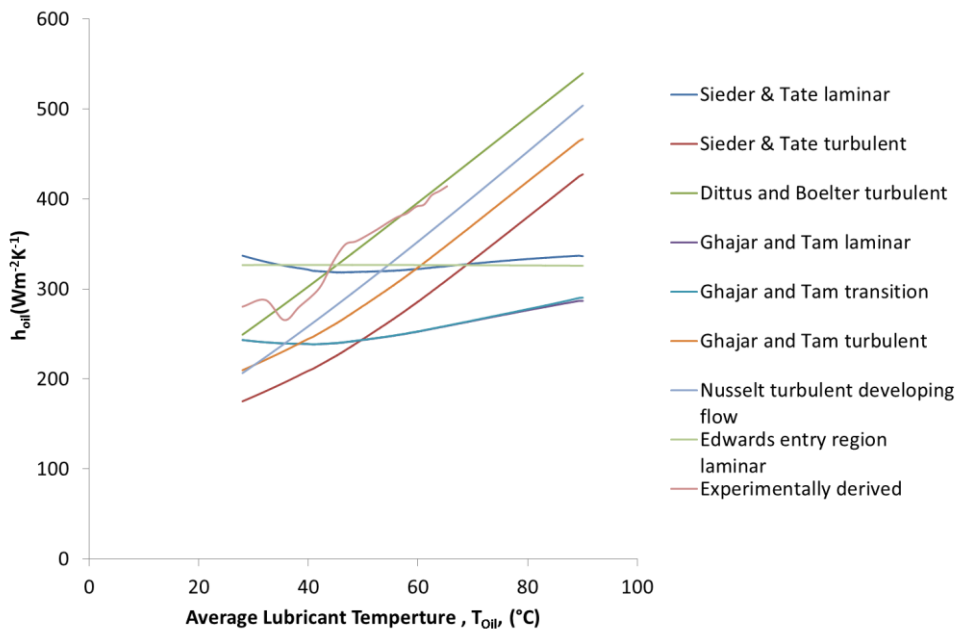


Figure 6.6: Comparison of  $h_{oil}$  values using different correlations and derivations from experimental results using a 100 mm outer diameter specimen with a 16 mm bore and  $15 \text{ l min}^{-1}$  flow rate with 1200 W element heater power

It should be noted that the literature accepts that the correlations offer an accuracy of between 25% [50] and 40% [49]. With the accepted percentage error of correlations so high, the remaining correlations that have not been discounted are all within the stated limits of percentage error. Based on this analysis, it was felt that

the most appropriate correlation to utilise in the simulation was the Dittus and Boelter turbulent correlation, as it was, without exception, the correlation that provided values closest to the experimental data. It is accepted that the Dittus Boelter correlation is recommended for Prandtl Numbers from 0.7 [49-51] with a maximum of 160 [50] whereas the experimental results present values of 1000 - 125. That said, owing to the Prandtl Number being a function of the dynamic viscosity, the Prandtl number falls very quickly, resulting in it being in the range of interest for over 50% of the experimental test duration.

### 6.2.5 Derivation of outer surface heat transfer coefficient

The convective heat transfer coefficient of the outer surface of the test block specimen is calculated in the model using a Nusselt correlation of the form:

$$Nu = \frac{hD}{k}$$

Where  $h$  = Convective heat transfer coefficient ( $W m^{-2} K^{-1}$ )

$D$  = Characteristic length (in this case the outer diameter) (m)

$k$  = The thermal conductivity of the fluid ( $W m^{-1} K^{-1}$ )

**Equation 6.10: Nusselt correlation for convective heat transfer coefficients [50-52].**

For a horizontal cylinder with only natural convection, the Nusselt number is defined as:

$$Nu = \left( 0.6 + \frac{0.387Ra^{1/6}}{\left[ 1 + \left( \frac{0.559}{Pr} \right)^{9/16} \right]^{8/27}} \right)^2$$

Where:  $Ra = Rayleigh Number = \frac{g\beta(T_{surface}-T_{ambient})D^3Pr}{\nu^2}$

$Pr = Prandtl Number = \frac{c_p\mu}{k}$

**Equation 6.11: Nusselt Number correlation for a horizontal cylinder [50]**

To verify the validity of such a correlation, experimental data were utilised to calculate the outer surface convective heat transfer coefficient. The R3 radial location temperatures were used as the surface temperatures as it was felt the surface temperature readings off the ring mounted thermocouples were too sensitive to ambient temperature fluctuations. Figure 6.7 shows plots against time of the experimental outer surface heat transfer coefficient showing values between 4.5

$W m^{-2} K^{-1}$  and  $14 W m^{-2} K^{-1}$ . This is within the expected range of heat transfer coefficient for a natural convection scenario. The subsequent optimisation of the external surface Nusselt Number is discussed further in Section 6.5.3.

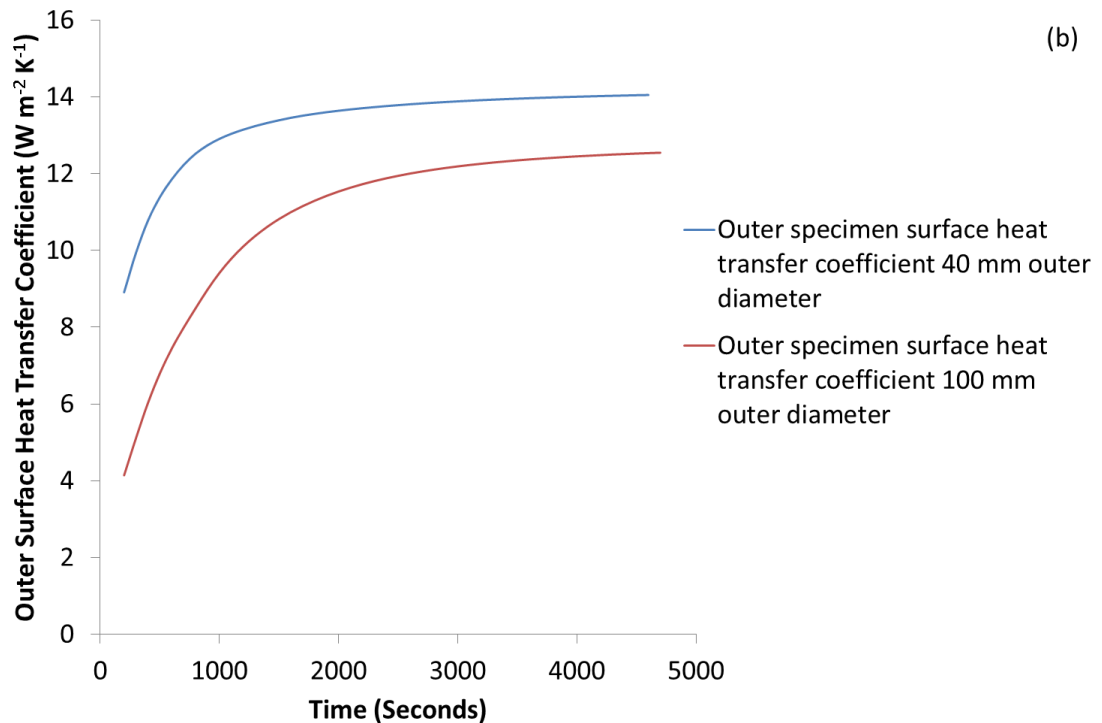
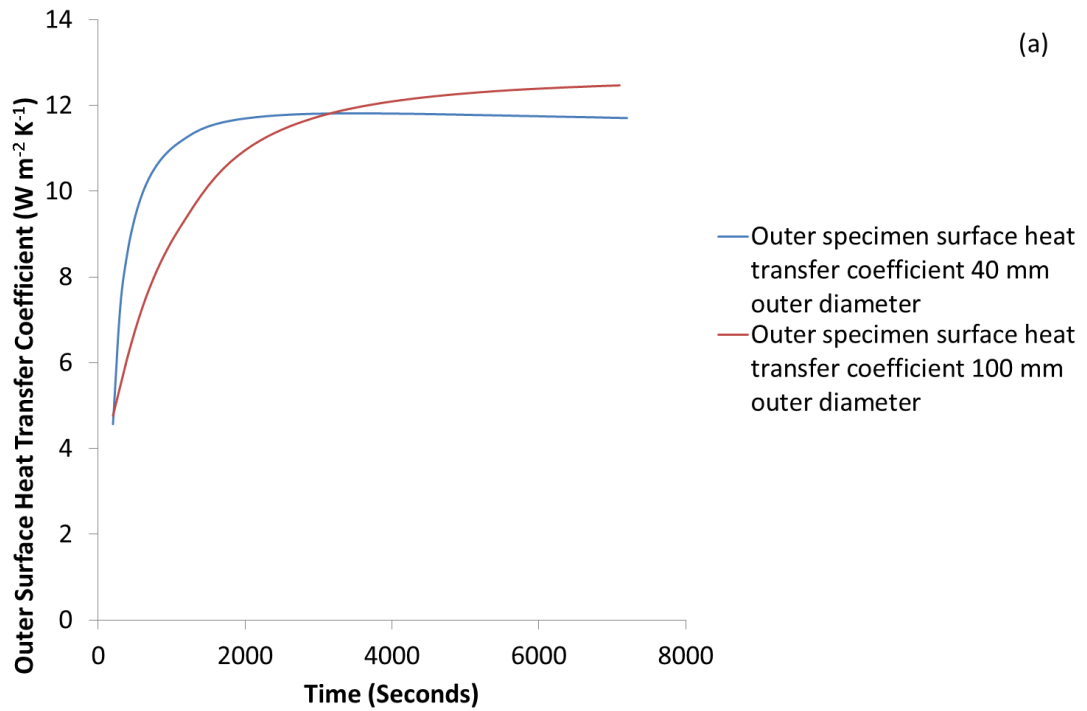


Figure 6.7: Variation of test block specimen outer surface heat transfer coefficient for different uninsulated specimens at different heat input rates and flowing at  $10 l min^{-1}$  and a heater power of (a) 1200 W and (b) 1800 W

### 6.3 Test block specimen nodes

In this work, it has been assumed that from a steady state soak temperature, the only source of additional thermal energy to heat the test block specimen is the hot lubricant. It was observed through the experimental data that there was no identifiable temperature gradient along the length of the specimen and consequently, a one dimensional radial model has been developed to model heat transfer through the radial thickness of the specimen.

For the one dimensional model to be effectively implemented, the lubricant temperature used to provide the temperature differential to the test block specimen is calculated as the average of the longitudinal flow nodes at each time step, and is defined as  $T_{average}$ .

Within the test block specimen, there exists four possible configurations of nodes:

- Internal surface node exchanging heat with the lubricant.
- Internal node exchanging heat by conduction with two neighbouring nodes.
- External surface node exchanging heat with the ambient air.
- Internal node at the interface of a material change where an insulator has been applied.

The full derivation of the nodal equation for each node type is provided in Appendix B however Table 6.2 summarises the four equations used for the different node types when modelling the heat transfer through the radial thickness of the test block specimen.

**Table 6.2: Summary table detailing the nodal temperature equations of the four node types used in the oil flow rig theoretical model through the radial thickness of the specimen**

Node type	Nodal temperature equation
Internal surface node exchanging heat with the lubricant	$T_{surface}^n = T_{surface}^{n-1} \left( 1 - Fo_{metal} \left( \left( 2 + \frac{\Delta r}{r_{inner}} \right) + \frac{\Delta r h_{oil}}{k_{metal}} \right) \right) + Fo_{metal} \left( 2 + \frac{\Delta r}{r_{inner}} \right) T_{inner+1}^n + \frac{2Fo_{metal} \Delta r h_{oil}}{k_{Metal}} T_{oil}^{n-1}$
Internal node exchanging heat by conduction with two neighbouring nodes	$T_{inner+1}^n = T_{inner+1}^{n-1} (1 - 2Fo_{metal}) + T_{inner}^{n-1} \left( Fo_{metal} \left( 1 - \frac{\Delta r}{2r_{inner+1}} \right) \right) + T_{inner+2}^{n-1} \left( Fo_{metal} \left( 1 + \frac{\Delta r}{2r_{inner+1}} \right) \right)$
External surface node exchanging heat with the ambient air	$T_{outer}^n = T_{outer}^{n-1} \left( 1 - Fo_{metal} \left( \left( 2 - \frac{\Delta r}{r_{outer}} \right) + \frac{\Delta r h_{outer}}{k_{metal}} \right) \right) + Fo_{metal} \left( 2 - \frac{\Delta r}{r_{outer}} \right) T_{outer-1}^n + \frac{2Fo_{metal} \Delta r h_{outer}}{k_{metal}} T_{ambient}^{n-1}$

Node type	Nodal temperature equation
Internal node at the interface of a material change where an insulator has been applied	$T_{inner\ metal}^n = T_{inner\ metal}^{n-1} \left( 1 - F_{O_{metal}} \left( \left( 2 + \frac{\Delta r}{r_{inner\ metal}} \right) + \frac{\Delta r h_{contact}}{k_{metal}} \right) \right)$ $+ F_{O_{metal}} \left( 2 + \frac{\Delta r}{r_{inner\ metal}} \right) T_{inner\ metal+1}^n$ $+ \frac{2F_{O_{metal}} \Delta r h_{contact}}{k_{metal}} T_{outer\ polymer}^{n-1}$

In testing and correlating the model, the baseline material properties of the nodes in the test block specimen were assumed to be the same as those discussed in Chapter 3 and are provided again below in Table 6.3 for reference. However further investigative work into the effect of the change in aluminium thermal properties between different grades of alloy and the effect of changes in Nylon thermal properties as a result of supplier variation, different grades of Nylon and temperature effects are discussed further in Chapter 7 (Section 7.2.2).

**Table 6.3: Material properties used through the modelling work**

Property	Aluminium 6082 T6	Nylon 12 [57]
Density (kg m <sup>-3</sup> )	2690 [93]	1015
Thermal conductivity (W m <sup>-1</sup> K <sup>-1</sup> )	193 [93]	0.26
Specific heat capacity (J kg <sup>-1</sup> K <sup>-1</sup> )	900 [57]	1760

## 6.4 Specimen effective power in

The power supplied to the oil flow rig is controlled at the heating element. Depending on the test being conducted, this was typically set to a constant 1200 W or 1800 W using the heater control system. Such values were used to reflect typical ‘heat to lubricant figures’ from the literature [20, 25]. The rig is effectively an open system with electrical energy input via the immersion heater, as shown in Figure 6.8. However, in simulating the rig, it must be remembered that only a small percentage of the total energy input to the rig will be retained in the lubricant or conducted to the specimen. Indeed the energy input to the rig has a range of possible destinations:

- Be retained as sensible heat in the rig architecture (observed through an increase in the temperature of rig hardware).
- Be transferred to the ambient air via the outer surface of the rig hardware.
- Be retained as sensible heat in the lubricant (observed through an increase in the temperature of the lubricant).
- Transferred to and retained as sensible heat in the test block specimen.
- Transferred to ambient air via the outer surface of the test block specimen.

The heating of the supporting rig was of limited experimental interest and the focus of the experimental work was on the heating process of the lubricant and test block

specimen. Consequently, detailed experimental temperature data are only available for the test block specimen and the lubricant and hence only the latter three destinations listed above are measurable. It is energy that is transferred to these destinations that is collectively termed the ‘effective power’. Thus, the cumulative effective energy input to the rig (the integral of the ‘effective power’ over time) is given by Equation 6.12 and can be calculated using experimental data.

$$\int_0^t m_{lubricant} C_{p_{lubricant}} \Delta T_{lubricant} dt + \int_0^t m_{specimen} C_{p_{metal}} \Delta T_{specimen} dt + \int_0^t h_{outer} \pi d_{outer} dx (T_{outer\ surface} - T_{ambient}) dt$$

Equation 6.12: Total effective energy input to the rig

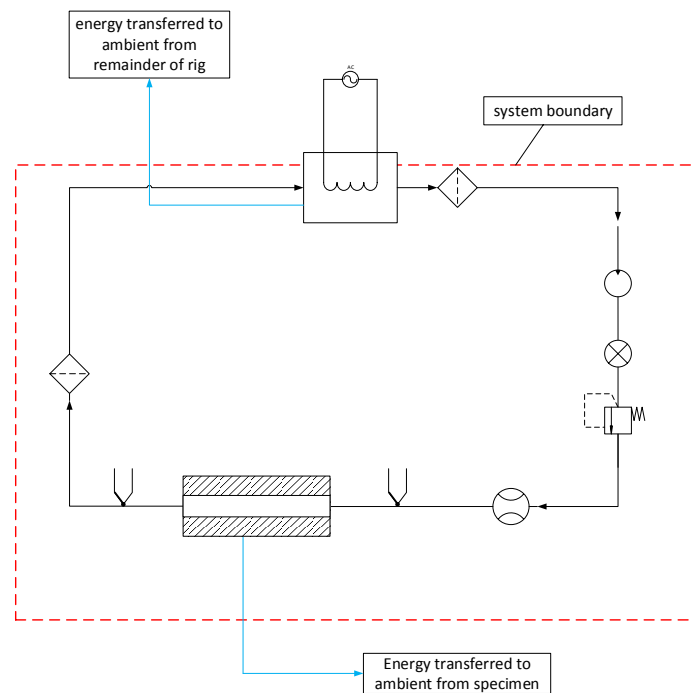


Figure 6.8: Schematic rig diagram showing system boundaries and possible energy throughput routes

It was discussed earlier in the thesis how the lubricant temperature profile, for a given heater power, is insensitive to changes in the specimen size and composition but that the specimen temperature does vary significantly (Figure 4.4 and Figure 4.6 of Chapter 4). The variation in specimen size alone, without any insulation effect was seen to increase the peak temperature of the specimen from 89 °C in the case of the 100 mm outer diameter specimen to 100 °C in the case of the 40 mm outer diameter specimen (for a heater power of 1200 W).

If one refers back to Equation 6.12, it can be seen that, owing to the lubricant temperature profiles being almost identical, the total energy input to the lubricant is very similar between tests. However the energy transferred to the specimen, and from the specimen to ambient, will vary owing to differences in the thermal mass and external convective heat transfer area of the specimens. By processing the data from a range of tests of differing heater element and specimens the effective power can be calculated across the time frame of the test. Thus, if one refers back to Equation 6.12, by taking the temperature differentials at set intervals of time from experimental data, the variation in effective power for each of the terms in Equation 6.12 can be calculated. The fill volume of the lubricant is known, as is the temperature of the lubricant (from experimental data) and therefore the mass of the lubricant at any instant in time can be calculated using the temperature dependent density data in Figure 3.14. If one takes the lubricant temperature from two nominal points in time, then it is possible to calculate the increase in energy stored in the lubricant (using the specific heat capacity data presented in Figure 3.15) and to therefore calculate the average heating rate of the lubricant over the time interval. In addition, the cross sectional area of the gallery bore is known and, with the lubricant flow rate controlled, the lubricant velocity, and as a result  $h_{oil}$ , can be determined. Similarly, the temperature and mass of the test block specimen is known and one can therefore, taking the difference in temperature of the specimen at two points in time ( $\Delta T_{specimen}$ ) and the specific heat capacity data for aluminium (Table 6.3 [93]), calculate the average heating rate of the specimen. The final term in Equation 6.12 is calculated by means of the external surface temperature of the specimen being known and this therefore enables Equation 6.10 and Equation 6.11 to be used to calculate an average heat transfer coefficient and hence calculate the average heat flux to ambient over a given time interval. The time interval chosen when using this methodology was 100 second intervals and therefore gave sufficiently high increments in temperature between sampling points to remove any noise in the signals from the thermocouples. The overall trend observed is one of the effective power supplied to the rig decreasing as the specimen and lubricant temperature increase and the contribution of each of the individual components that make up the effective power is assessed further in Section 6.4.1.1. However, using this approach has demonstrated dramatic changes in the effective power to the rig over a test as a result of varying the specimen geometry and composition.

#### **6.4.1 Variation of effective power with specimen size and structure**

As was first detailed at the beginning of Section 6.4, the effective power is the combined rate of transfer of energy that raises the test block specimen temperature and the lubricant temperature together with instantaneous heat flux from the outer surface of the test block specimen to the ambient. Figure 6.9 shows the observed

effective power into the rig against lubricant temperature for both a 100 mm and 40 mm outer diameter uninsulated specimen with 1200 W and 1800 W heater element powers. Comparatively, Figure 6.10 plots the effective power for a 100 mm and a 40 mm outer diameter specimen insulated with a 2 mm thick Nylon 12 insert. The plots present data from a point 200 seconds after the heater element was activated and hence removes uncertainty about whether the heater element had equilibrated and ensures that the flow rate was at a steady state value. In the case of Figure 6.10 it should be highlighted that the effective power presented, neglects the energy required to heat the Nylon 12 insert owing to there being no temperature readings through the thickness of the insert.

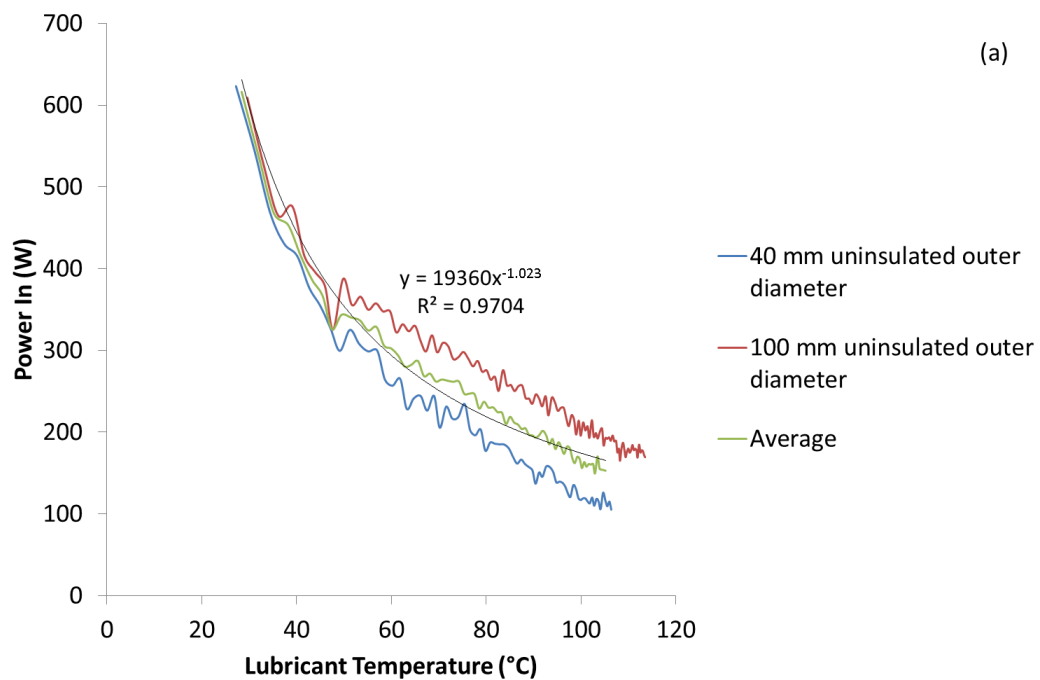


Figure 6.9a: Effective rig power supplied to the lubricant and specimen for both 40 mm and 100 mm outer diameter uninsulated test block specimens with the first 200 seconds of data omitted and plotted against average lubricant temperature when the flow rate is controlled at  $10 \text{ l min}^{-1}$  and the heater input is set to 1200 W

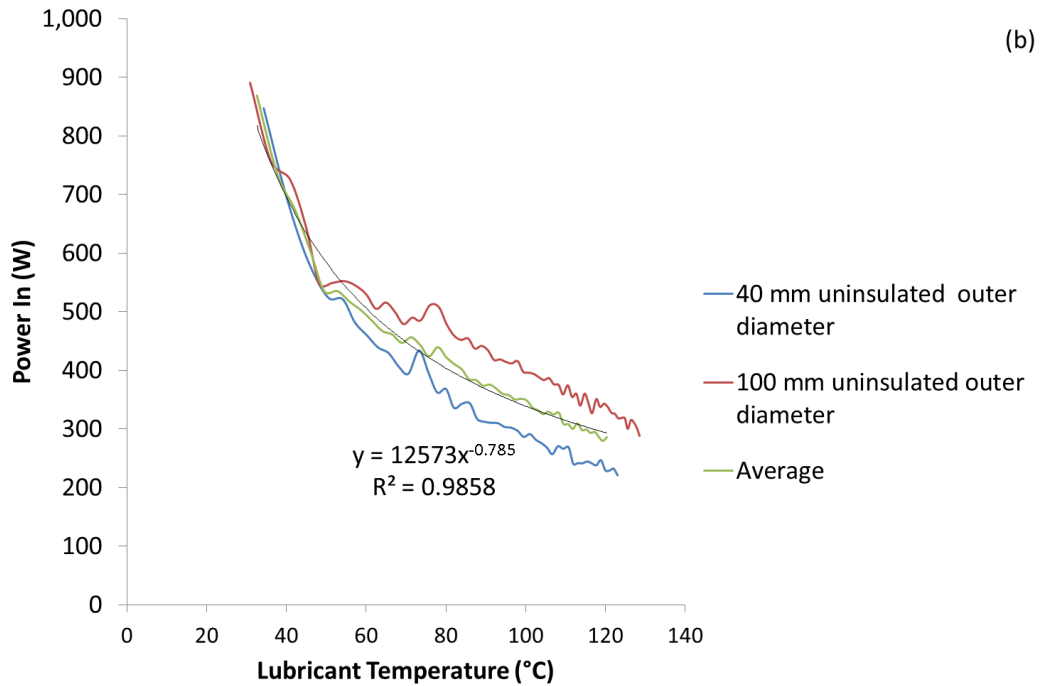


Figure 6.9b: Effective rig power supplied to the lubricant and specimen for both 40 mm and 100 mm outer diameter uninsulated test block specimens with the first 200 seconds of data omitted and plotted against average lubricant temperature when the flow rate is controlled at  $10 \text{ l min}^{-1}$  and the heater input is set to 1800 W

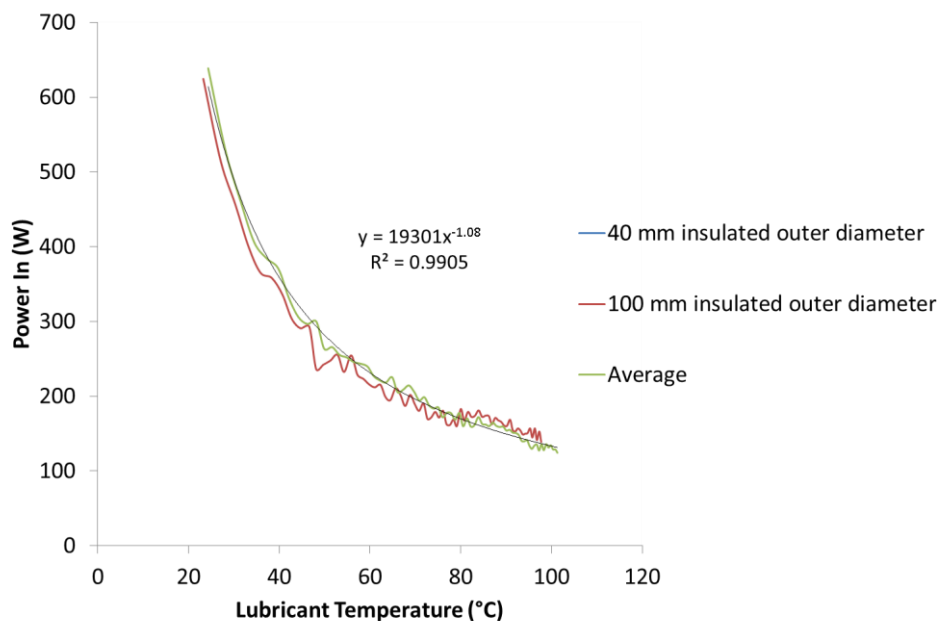


Figure 6.10: Effective rig power supplied to the lubricant and specimen for both 40 mm and 100 mm outer diameter test block specimens insulated with 2 mm thick Nylon 12 plotted against average lubricant temperature when the flow rate is controlled at  $10 \text{ l min}^{-1}$  and the heater input is set to 1200 W

When considering the uninsulated specimens both Figure 6.9a and Figure 6.9b highlight the same trends. Most noticeably, the peak effective power in both instances is much lower than that of the element power. In the case of the scenario

where 1200 W heater power is supplied to a 40 mm outer diameter specimen, the peak effective power is only 50% of the heater power, at 600 W. Similarly when applying 1800 W, both specimens demonstrated effective powers of between 820 W and 860 W which is only 46% and 47% of the element heater power. A key observation in both Figure 6.9a and Figure 6.9b is the way in which the two specimen sizes diverge at higher lubricant temperatures with the larger 100 mm outer diameter specimen remaining higher. Such an occurrence is a result of the 100 mm outer diameter specimen having a surface area that is 2.5 times greater than the 40 mm outer diameter specimen. However, the larger thermal mass of the 100 mm outer diameter specimen also increases the effective power, but has implications on the temperature differential, and subsequent heat flux, between the test block specimen and ambient. Such factors are discussed in greater detail in Section 6.4.1.1. While it has been highlighted at length that the energy flows to the test block specimen are only a small fraction of the total energy input to the rig (between 2% and 4 % based on the results shown in Table 5.1), the effective power eliminates the effect of the supporting hardware of the rig and enables closer examination of the differing transient dynamics of test block specimens of differing sizes.

When studying Figure 6.9a Figure 6.9b one can see that there are small oscillations in the trend lines that can be attributed to noise in the experimental data. However in Figure 6.9a one can see a significant decrease in effective power at approximately 40 °C before the calculated effective power rises again while a noticeable increase in effective power is observed at approximately 65 °C in Figure 6.9b. While these features are greater in magnitude than the surrounding experimental noise, it is not felt that the magnitude or direction of such features warrant further investigation. While it is noted that Figure 6.9a features an increase in effective power and Figure 6.9b features a decrease in effective power it is felt that the features are most likely experimental artefacts and are a result of the external surface heat flux increasing in significance rather than a physical phenomenon worthy of investigation.

The insulated results in Figure 6.10 show that the peak effective power is, relative to that of the heater element power, reduced in both instances with 680 W peak power being input for the 40 mm outer diameter specimen and 620 W for the 100 mm outer diameter specimen. A key observation to be made is the much closer trend of the two between specimen sizes, relative to the uninsulated profiles being plotted against lubricant temperature (Figure 6.9). Owing to the presence of the insulation, the specimen has become less closely coupled to the rest of the oil flow rig. Consequently, the composition of the rig between the two experiments is now effectively very similar (i.e. the test block specimen is essentially a 2 mm thick Nylon tube in both instances, particularly in the early regime of any tests). The heating of the aluminium test block specimen in response to lubricant heating is therefore delayed. Were the lubricant temperatures to be elevated further, it would be

expected that the two profiles would diverge at higher temperatures once the thermal inertia and surface area effects of the two specimens could manifest themselves.

In both the uninsulated and insulated scenarios, a key contributor to the low effective power to the element electrical power will be the large cooling effect of the tank wall on the lubricant temperature. The tank wall is 10 mm thick owing to the need to install the heating element and as such is a large thermal mass that will draw energy from the lubricant at the source of heat. However, without further instrumentation of the tank, it is not possible to individually quantify the exact magnitude of the thermal losses that occur at the tank and at other significant hardware components (e.g. the pump head and pipe work).

#### **6.4.1.1 The effect of different heat transfer mechanisms on the effective power**

While the insulation reduces the impact of the different specimen sizes on the effective power it was seen that the effective power for the uninsulated specimens diverged from each other. When looking at the 1200 W scenario, the heat input at the end of the test is 180 W for the 100 mm diameter specimen and 120 W for the 40 mm diameter specimen. Similarly when the 1800 W heater power is applied, the effective power at the end of the test is 300 W for the 100 mm outer diameter specimen and 220 W for the 40 mm outer diameter specimen. This section seeks to explain the interaction of different heat transfer mechanisms during the heating process that result in diverging trends.

The lubricant heating rates, having proven to be so similar between different test specimens, is not the source of the divergence. Instead, the divergence is a result of the temperature rise of the different specimen designs and the different heat fluxes to ambient from the outer surface of the test block specimen (discussed in Chapter 4, see Figure 4.6). Figure 6.11 shows a breakdown of the instantaneous power received and subsequently stored by the specimen as heat (i.e. energy that results in the specimen temperature rising) and the instantaneous heat flux to ambient from the specimen for the tests shown in Figure 6.9.

In both instances (40 mm and 100 mm outer diameter) the power absorbed by the specimen (not transferred to ambient) initially increases; shown by blue lines in Figure 6.11. This occurs owing to the lubricant temperature rising and hence increasing the temperature differential (and associated heat flux) between the lubricant and specimen. In the initial phases of the test, the specimen temperature has not risen relative to ambient and there is therefore no significant heat flow from the outer surface (shown in red). Once sufficient energy has been transferred to the specimen to raise the specimen temperature, the temperature differential between

the lubricant and the specimen starts to reduce (resulting in a reduction in heat flow from the lubricant) and also the heat flux to ambient starts to increase. These two mechanisms therefore cause the rate of energy stored in the specimen to reduce; in a steady state situation this rate of energy storage would be 0 W. Comparatively the external surface heat flux continues to increase with specimen temperature as both  $h_{outer}$  and the temperature differential between the specimen and ambient increase.

The sum of the instantaneous rate of energy storage in the specimen and the instantaneous heat flux to ambient is equal to the effective heat flux leaving the lubricant via the specimen and summed with the power required to heat the lubricant equates to the effective power of the system. The divergence of the effective powers is a result of the differing thermal masses of the two specimen sizes (the mass of the 100 mm outer diameter specimen and the 40 mm outer diameter specimen are 8.0 kg and 0.96 kg respectively assuming the density of aluminium 6082 T6 alloy to be  $2690 \text{ kg m}^{-3}$ ). The high thermal conductivity of the specimens results in the specimens responding in a lumped capacitance manner meaning that the outer surface temperature of the specimen is, to within 0.5 °C, the same temperature as the innermost R1 radial location. Consequently, the time frame between the start of the test and the onset of the external surface heat transfer to ambient is dictated by the thermal mass of the specimen controlling both the rate of heat retention in the specimen and the temperature differential to ambient ( $T_{R3} - T_{ambient}$ ) and results in the effective power diverging for the two specimens.

In addition, the outer surface area of the 100 mm outer diameter specimen being 2.5 times greater than the 40 mm outer diameter specimen also has an effect on the heat flow through the specimen. The combined effects of these different mechanisms results in the 100 mm outer diameter specimen power (not including the lubricant heating power) being 70% higher than the 40 mm outer diameter specimen. Table 6.4 details the relative percentage of the total energy input to the rig received by each possible destination. The larger thermal mass of the 100 mm outer diameter specimen retains a further 5% more energy than the 40 mm outer diameter specimen. Interestingly, if one looks simply at the energy received by the specimen, rather than the energy received by the rig, it can be seen that the 40 mm outer diameter, even accounting for a reduced convection heat transfer area transfers 25% more of this energy to ambient than the 100 mm outer diameter. This is owing to the higher temperature differential to ambient discussed earlier in the case of the 40 mm outer diameter specimen and the reduced thermal mass of the specimen offering a much lower energy storage capability than the larger specimen.

**Table 6.4: Comparative rig energy balance for the oil flow rig comparing a 100 mm outer diameter uninsulated specimen with a 40 mm outer diameter uninsulated specimen when 1200 W heater power is input and the flow rate set to 10 l min<sup>-1</sup>**

Specimen	<u>% of rig input to specimen</u>	<u>% of rig input stored in specimen</u>	<u>% of rig input transferred to ambient via specimen</u>	<u>% of rig input stored in lubricant</u>	<u>% of energy transferred to specimen lost to ambient</u>
100 mm uninsulated	11%	6%	5%	13%	45%
40 mm uninsulated	3%	1%	2%	14%	75%

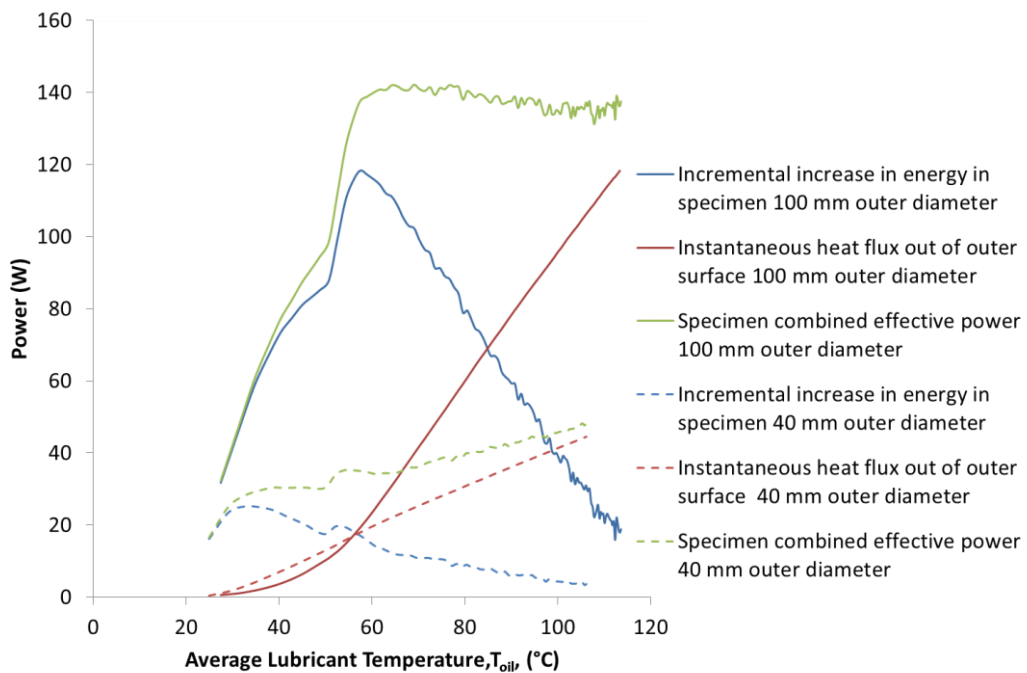


**Figure 6.11: Instantaneous heat fluxes through the test block specimen plotted against lubricant temperature when the heater input power is set to 1200 W and the flow rate controlled at 10 l min<sup>-1</sup> for both a 100 mm outer diameter specimen and 40 mm outer diameter specimen**

Through this analysis, it has been comprehensively proven that, while initially counter intuitive, particularly with such similar lubricant temperature profiles, the effective power supplied to the rig is indeed specimen size dependent. Consequently, in using a single function, that is consistent between specimens of different size and material composition, to model the effective power supplied to the rig it is accepted that an exact correlation between experimental and theoretical data will not be possible. It would be expected that the use of single effective power

function would result in an overestimate of specimen temperatures in the case of the 40 mm outer diameter uninsulated specimen simulations or an underestimate of temperatures in the case of the 100 mm outer diameter uninsulated specimens. Having proven that the lubricant temperature is an unsatisfactory method of characterising this effective power, Section 6.4.2 details the method chosen to model the rig's effective power.

#### **6.4.2 Selection of transferrable rig power function**

The work presented in Section 6.4.1 has demonstrated how the effective power supplied to the test block specimen and lubricant is dependent on specimen size and material composition. For the model to serve as an effective tool, the effective power supplied to the rig is required to be modelled as a function of a single variable that is consistent between specimens of different size and composition.

The results presented in Figure 6.9 and Figure 6.10 demonstrated that while the effective power as a function of lubricant temperature was acceptable in the case of the insulated specimens, the profiles deviated too much between uninsulated specimens of different sizes. Comparatively, if one used the average specimen temperature to characterise the power, improved agreement was found between uninsulated specimens of different size. However, the dramatic reduction in specimen temperature owing to the insulation resulted in the specimen temperature range between insulated and uninsulated specimens being too broad to characterise the effective power using a single function for both insulated and uninsulated specimens of different sizes.

The lubricant temperature correlation offered greater stability in the transition from uninsulated to insulated specimens while the specimen metal temperature offered greater stability when transferring between uninsulated specimens of different sizes. Thus, it was felt that the specimen bore temperature was a valid compromise between insulated and uninsulated specimens to characterise the heat input. In the instance of the uninsulated specimens, this would make negligible difference to using the average specimen temperature owing to the aluminium's high thermal conductivity. However in the case of the insulated scenario, the temperature of the inner wall of the polymer tube will be noticeably higher than the aluminium temperature. This is a result of both the temperature gradient across the thickness of the polymer and also the temperature gradient across the interface of the polymer tube and aluminium test block specimen. The difficulty with such an approach is the inability to accurately measure the polymer tube temperature on the rig due to the installation issues discussed previously.

Presented in Figure 6.12 is a plot of the observed effective power supplied to the rig as a function of the specimen bore temperature. No plot is presented for the

insulated scenarios as a result of the instrumentation limitations discussed. However, when comparing Figure 6.9 with Figure 6.12 one can see a marked improvement in correlation with a reduction in the divergence of the two specimen sizes as a result of using the bore wall rather than the lubricant temperature (shown in Figure 6.9). This is particularly the case at higher temperatures where the greatest concern lay with the lubricant temperature correlation. However, it is worth highlighting the apparent divergence of the effective power for the two specimen temperatures at low bore wall temperatures (up to 20 °C). Unlike in Figure 6.9 the effective power for the 100 mm outer diameter specimen appears to begin by being lower than the 40 mm outer diameter specimen before the two trends cross over and the 100 mm outer diameter specimen ends the test with the higher effective power. There is no physical explanation for such a phenomenon and it is again felt that such a feature, and the associated higher magnitude fluctuations on the 100 mm outer diameter specimen profile, is an experimental artefact.

The motivation for using the specimen bore wall temperature to model the effective power lay in having observed that the specimen metal temperature was too isolated from the lubricant to characterise the effective power in insulated scenarios. It was therefore concluded that it was desirable to use a variable that did lag the lubricant temperature to control the effective power supplied. Thus, having discussed the reduced divergence at higher temperatures and discussed the presence of a likely experimental artefact present at lower temperatures it is felt that the specimen bore wall temperature has shown improved consistency between specimens of different size relative to the lubricant temperature correlation. However, it is worth considering why the divergence between the two specimens sizes at higher temperatures is not eliminated using such an approach. It must be remembered that the effective power only accounts for energy that is used to heat either the lubricant, the test block specimen or is transferred to ambient from the specimen. Thus, for a given bore wall temperature (this being very similar to the external surface temperature in the case of the uninsulated specimens) the external heat flux to ambient will differ between the two specimen sizes owing to the different external heat transfer areas (the 100 mm outer diameter specimen has a heat transfer area 2.5 times greater than the 40 mm outer diameter specimen). However, the surface temperature of the larger specimen is only 8 °C cooler than the 40 mm outer diameter specimen and hence any increase in heat transfer coefficient in the case of the 40 mm outer diameter owing to the increased surface temperature, is insufficient to counteract the increase in area. Consequently, the heat flux to ambient through the specimen will be much higher from the 100 mm outer diameter specimen than the 40 mm outer diameter equivalent. It is worth highlighting however that, for the same bore wall temperature, the lubricant will be hotter in the case of the 100 mm outer diameter specimen than the 40 mm outer diameter

specimen and hence the heating power for the lubricant will be reduced in the case of the 100 mm outer diameter specimen; a consequence of the lubricant being closer to steady state and dissipating more heat to ambient via the rest of the supporting rig hardware. However, as is shown in Figure 6.12 the outer surface area effects dominate over any difference in lubricant heating rate and hence a divergence in trends, albeit reduced relative to the lubricant temperature correlation, is still observed. Hence, one would still expect there to be an overestimate of specimen temperatures in the case of the 40 mm outer diameter uninsulated specimen simulations or an underestimate of temperatures in the case of the 100 mm outer diameter uninsulated specimens, as discussed in Section 6.4.1.1. However, such overshoots would be less than if the lubricant temperature was used to characterise the effective power input.

Consequently, by using the average of the effective powers for both the 100 mm and 40 mm outer diameter uninsulated specimens, the effective power as a function of specimen bore wall temperature, when 1200 W heater power is applied is shown in Equation 6.13.

$$Q_{effective} = 8709.6T_{specimen\ bore}^{-0.871}$$

Equation 6.13: Effective power as a function of bore wall temperature when heater element power is 1200 W

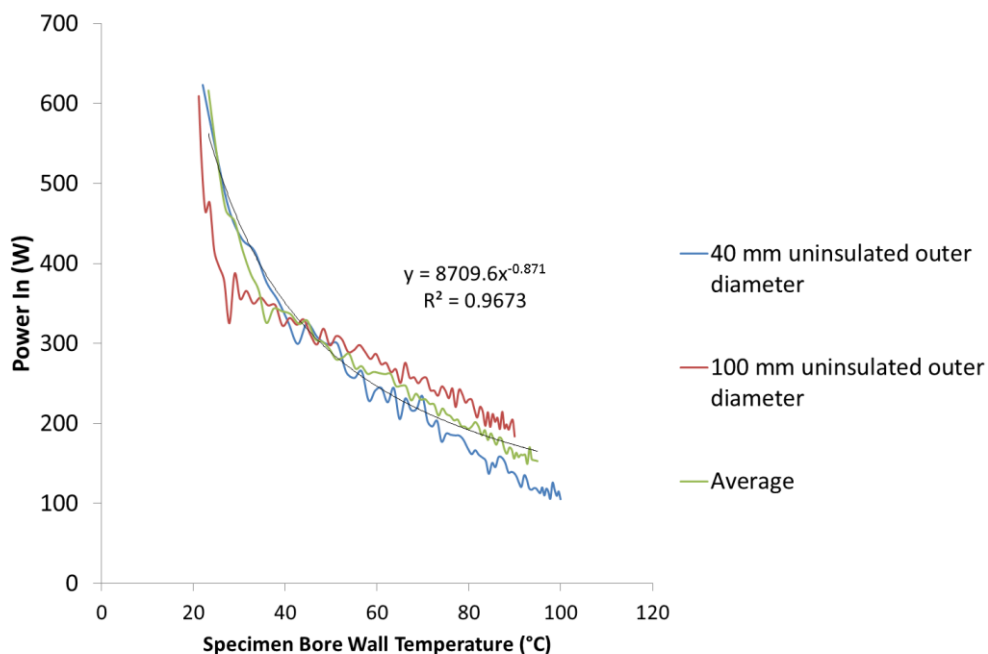
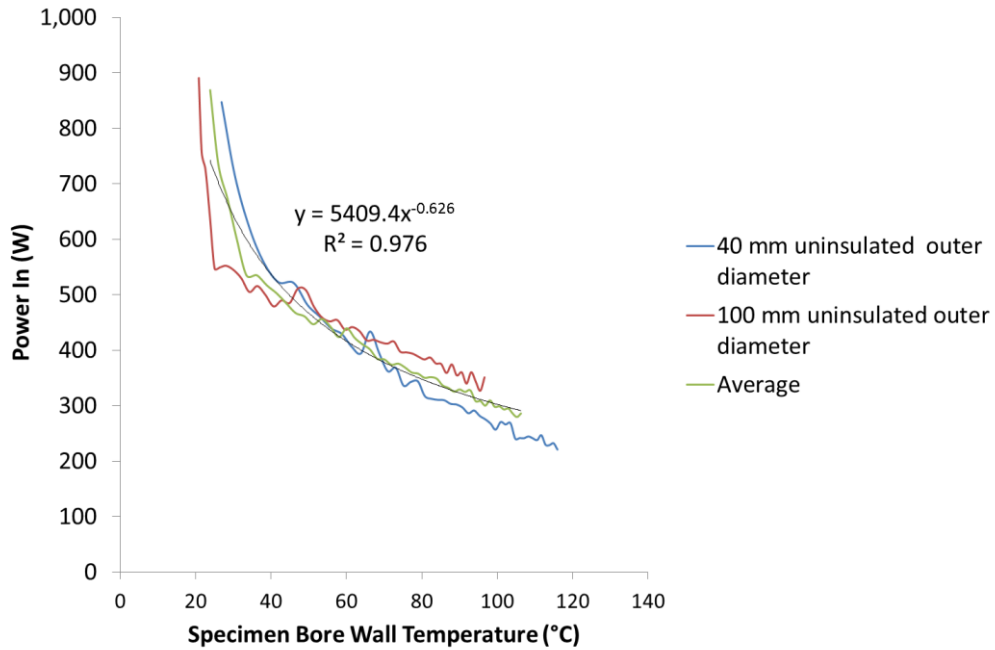


Figure 6.12: Effective power plotted against specimen bore wall for different sized uninsulated specimens for a lubricant flow rate of  $10\text{ l min}^{-1}$  and a heater input of 1200 W

Similarly, when carrying out the same analysis when 1800 W heater power is applied, the trend demonstrated in Figure 6.13 was observed.



**Figure 6.13: Effective power plotted against specimen bore wall for different sized uninsulated specimens for a lubricant flow rate of  $10 \text{ l min}^{-1}$  and a heater input of 1800 W against bore temperature**

Thus the effective power, as a function of the bore wall temperature when the heater power is set to 1800 W is shown in Equation 6.14.

$$Q_{effective} = 5409.4T_{specimen\ bore}^{-0.626}$$

**Equation 6.14: Effective power applied to the oil flow rig when 1800 W heater power is applied**

## 6.5 Experimental and theoretical correlation results

Having established the inter-dependence of specimen geometry to the effective power supplied to the rig, it is unrealistic to expect a perfect correlation for a constant effective power in. However, one would still expect the time frame of the rig and simulation to be similar in terms of the rate of change of any temperatures. In Section 6.4.1 it was highlighted how the effective power from experimental data was appraised from 200 seconds after the heater had been activated to allow the power to equilibrate. This raises an issue in comparing the experimental and theoretical data. While the element power is still increasing to provide the desired power output, it is still heating the lubricant resulting in an offset between the lubricant and specimen temperatures at the point that the effective power reaches its peak value. Consequently, when comparing the data between the simulation and the experimental data, the start point of the simulation is taken to be 200 seconds after the heater was activated. Thus one will observe that the lubricant and

specimen temperatures commence at different start temperatures. This accounts for the increase in lubricant temperatures as a result of churning from the pump and any heat applied from the element.

## **6.5.1 Baseline correlation results**

### **6.5.1.1 Uninsulated results**

Figure 6.14 and Figure 6.15 show a comparison between experimental and theoretical data for both a 100 mm and 40 mm outer diameter test block specimen. It can be seen that the approach taken has reflected in a reasonable agreement, albeit one that demonstrates the limitations of using a consistent effective power method between specimens of different size. When looking at the lubricant data, a maximum discrepancy between the theoretical and experimental data of 2 °C was observed in the case of the 100 mm outer diameter specimen. Similarly, the specimen temperature for the 100 mm outer diameter specimen maintains good agreement with the experimental data with a maximum deviation of 4 °C. These peak discrepancies both occur in the mid-phase of the test and it is important to note that the overall trend of the temperatures is reflected well between the experimental and theoretical results in this instance. Figure 6.14 shows that at the end of the test both the lubricant and specimen temperature show a discrepancy between the experimental and theoretical data of less than 1 °C and that, as predicted the theoretical model underestimates these temperatures relative to the experimental data. Thus, the results suggest that the physical mechanisms of heat transfer have been well represented by the model, albeit that the accuracy of the model is limited by the use of a constant function for the effective power. It can be seen, if one refers back to Figure 6.12, that the region where the peak temperature overestimate occurs in Figure 6.14 (between 35 °C and 60 °C) coincides with where the discrepancy between the average effective power and the effective power for the 100 mm outer diameter specimen is at its maximum. The convergence between these two effective powers at higher temperatures also coincides with how the theoretical and experimental temperatures also converge at higher temperatures

By comparison, the 40 mm outer diameter specimen demonstrates a maximum deviation from the experimental data of 6 °C. This occurs at the end of the test and of concern is that this discrepancy is diverging. However, for the majority of the test one can see that the 40 mm outer diameter lubricant temperature is within 1 °C of the experimental data while the specimen temperature for the 40 mm outer diameter specimen maintains good agreement to within 1 °C for the majority of the test but deviates in the latter stages. The poorer performance of the 40 mm outer diameter specimen at the end of the test is not surprising when one refers back to the difference in effective power trends for the two sizes of specimen and the limitations of using a single effective power function for different sized specimens.

Indeed, it was discussed in both Section 6.4.1.1 and Section 6.4.2 how one would expect that the use of a single effective power (Equation 6.13) for both specimen sizes would result in either an over-estimate of the temperatures in the case of the 40 mm outer diameter specimen temperatures or an underestimate of the 100 mm outer diameter specimens.

Figure 6.12 showed that the greatest discrepancy in effective power between specimen sizes was late in the test and the reasons for this were discussed in Section 6.4.2. However, whereas the discrepancy between the average effective power and the 100 mm outer diameter effective power was greatest in the early phase of the test and then subsequently converged (this also being reflected in the correlation in theoretical and experimental temperatures), the discrepancy between the average effective power and the 40 mm outer diameter effective power is generally better in the early phase of the tests but is more apparent at high temperatures. The diverging trend between the experimental and theoretical results for the 40 mm outer diameter specimen therefore coincides with the greatest discrepancy in effective power between the two specimens.

These initial correlation results have therefore confirmed the hypothesis that the single effective power would over-estimate temperatures for the 40 mm outer diameter specimen and under-estimate temperatures for the 100 mm outer diameter specimen. However, the model does reproduce the trends of the temperature profiles of the rig. In particular, the sensitivity of the rig to the size of the test block specimen is clearly evident in the theoretical results and this is highlighted by the correlation of the temperature differential (average lubricant temperature – average specimen temperature) when plotted against the average lubricant temperature in Section 6.5.2. It is nonetheless worth considering whether the average effective power is the most appropriate means of modelling the rig. The limitations of such an approach and the limitations of achieving a satisfactory correlation (and why such issues occur) have been discussed. However, the aim of the rig and computational model were to develop an understanding as to the significant factors in reducing thermal losses from automotive lubricant as it flows through engine oil galleries. The experimental results have already shown how reducing the size of the test block specimen outer diameter from 100 mm to 40 mm reduces the average heat flow from the lubricant by 69 % and that the benefit of applying insulation is more than halved as a result of such a change (Section 5.2.1.1). Thus, the model seeks to advance knowledge beyond the scope of the physical rig by being able to adjust material or geometric parameters independently of one another. This includes the thickness or presence of insulation and to observe the respective trends of thermal losses relative to changing different parameters it is necessary to maintain a constant effective power. Thus, while the concept of a single effective power is an oversimplification of the physical problem, it is felt to be the

optimum method of modelling the localised thermal losses from the lubricant to the test block specimen. Alternative methods of modelling the rig would require much greater knowledge of the thermal history of the supporting rig hardware and would be at the expense of the high fidelity data of the test block specimen; a novelty of the work presented in this thesis.

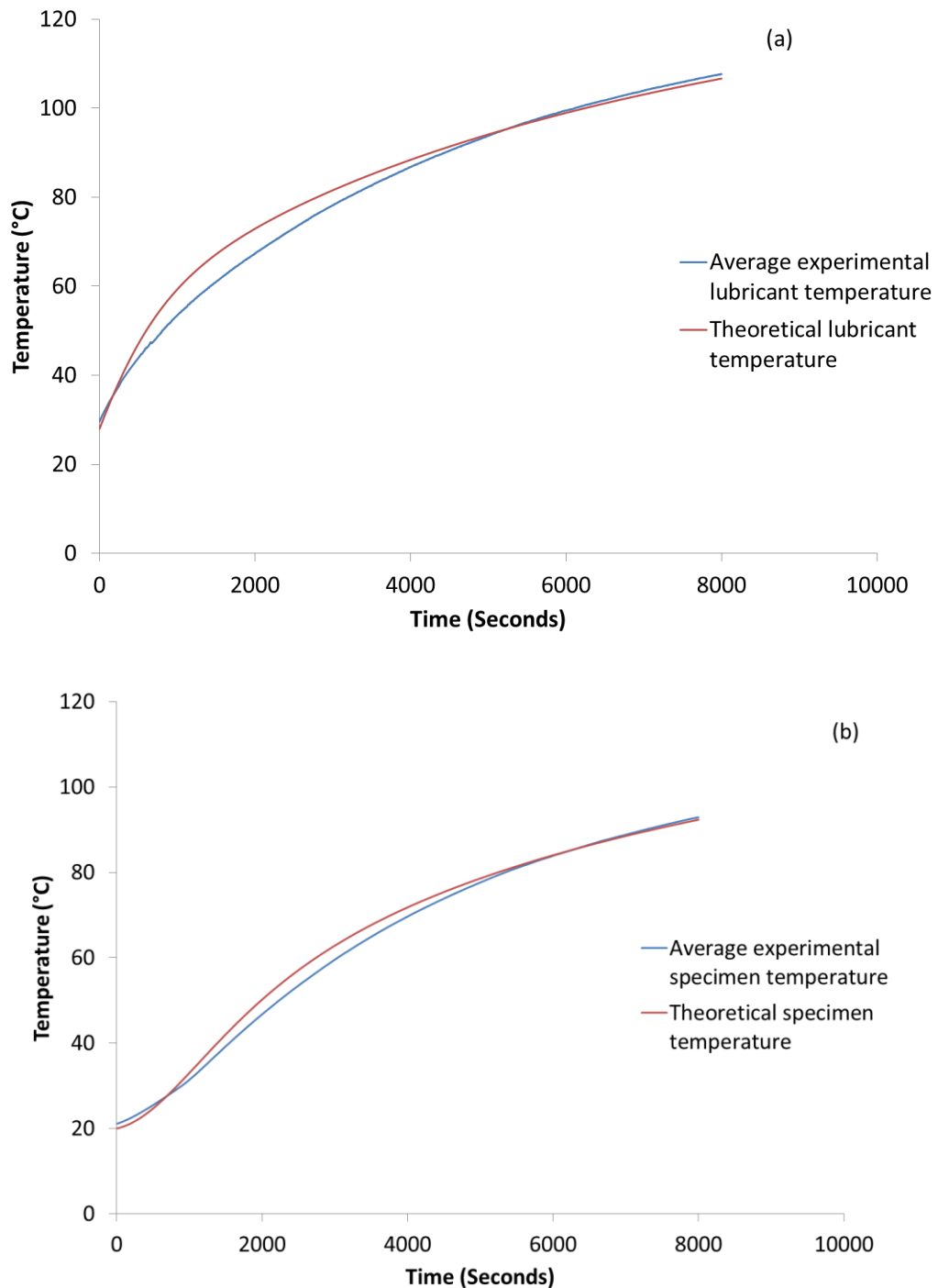


**Figure 6.14: Comparison between theoretical and experimental data for the oil flow rig when 1200 W heater power is input using a 100 mm outer diameter uninsulated specimen and a lubricant flow rate of  $10 \text{ l min}^{-1}$  for (a) the lubricant temperature and (b) the specimen temperature**

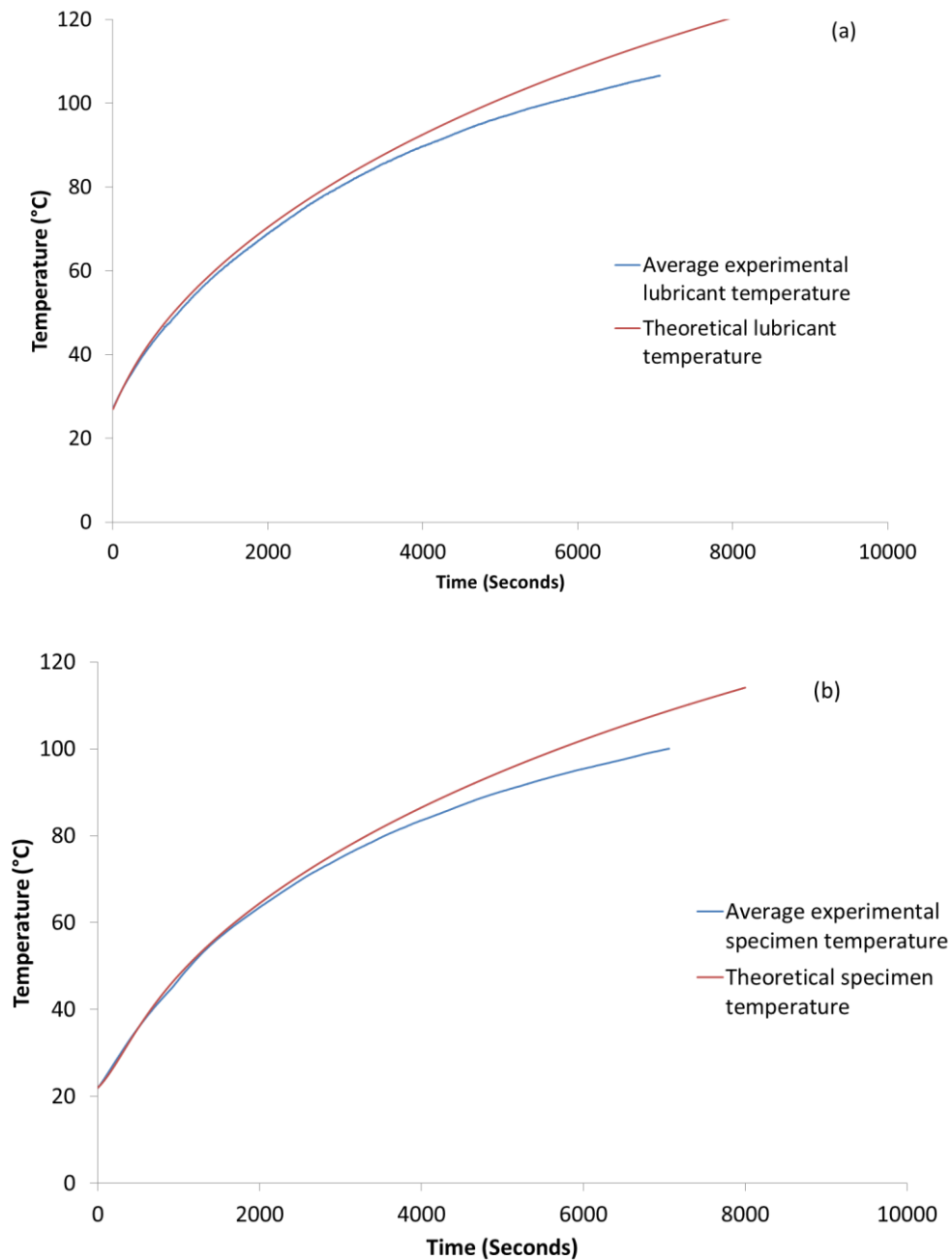


Figure 6.15: Comparison between theoretical and experimental data for the oil flow rig when 1200 W heater power is input using a 40 mm outer diameter uninsulated specimen and a lubricant flow rate of  $10 \text{ l min}^{-1}$  for (a) the lubricant temperature and (b) the specimen temperature

### 6.5.1.2 Insulated results and the effect of contact resistance on heat transfer

When modelling the radial heat transfer through the test block specimen with polymer insulation, the code effectively contains a separate thermal resistance network for both the metal and polymer with a variable boundary condition coupling the two. This variable boundary condition takes the form of a variable defined as

$h_{contact}$  with units  $W m^{-2} K^{-1}$ . The presence of such a variable allows there to exist a contact resistance and subsequent temperature differential between the outer surface of the insert and inner surface of the drilled out bore in the test block specimen. The quantification of contact resistances is notoriously difficult and the value is likely to differ even between specimens manufactured in the same way owing to its dependence on surface roughness and initial clearance (both of which have an allowed manufacturing tolerance) [52]. The implications of other material properties and processing factors on contact resistance have been discussed in Chapter 5 (Section 5.2.2). To optimise the value of the modelled contact resistance, experimental and theoretical data were compared and the value of  $h_{contact}$  adjusted to provide the best agreement possible. As discussed previously (Section 6.4.1), the trend of the effective power curve plotted for the insulated scenarios neglects the thermal energy stored in the Nylon 12 tube owing to the logistical difficulty in installing instrumentation across the interface of the polymer tube and metal. Consequently, the decision was made to leave the effective power curve, the same as the uninsulated scenario.

In the first instance, the model was configured to have a perfect interface between the polymer insert and the test block specimen by having an extremely high value for  $h_{contact}$  ( $10000 W m^{-2} K^{-1}$ ). The performance of the model in such a configuration was seen to drastically over predict the specimen metal temperature and by a process of trial and improvement, an optimum value of  $h_{contact}$  was found to be  $65 W m^{-2} K^{-1}$ . The theoretical and experimental correlation for such a value is shown in Figure 6.16 and Figure 6.17.

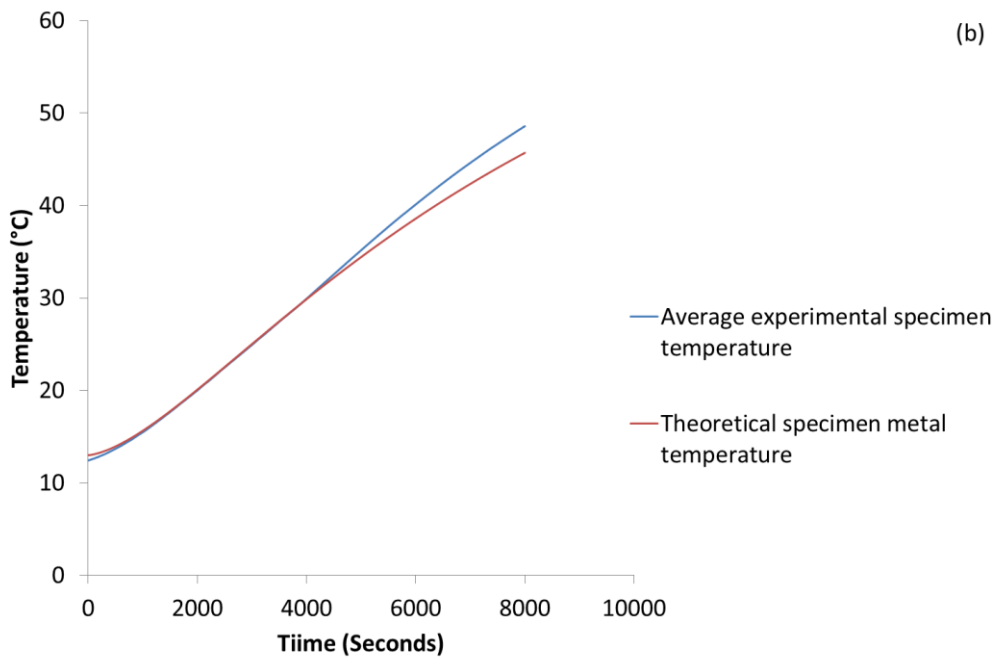
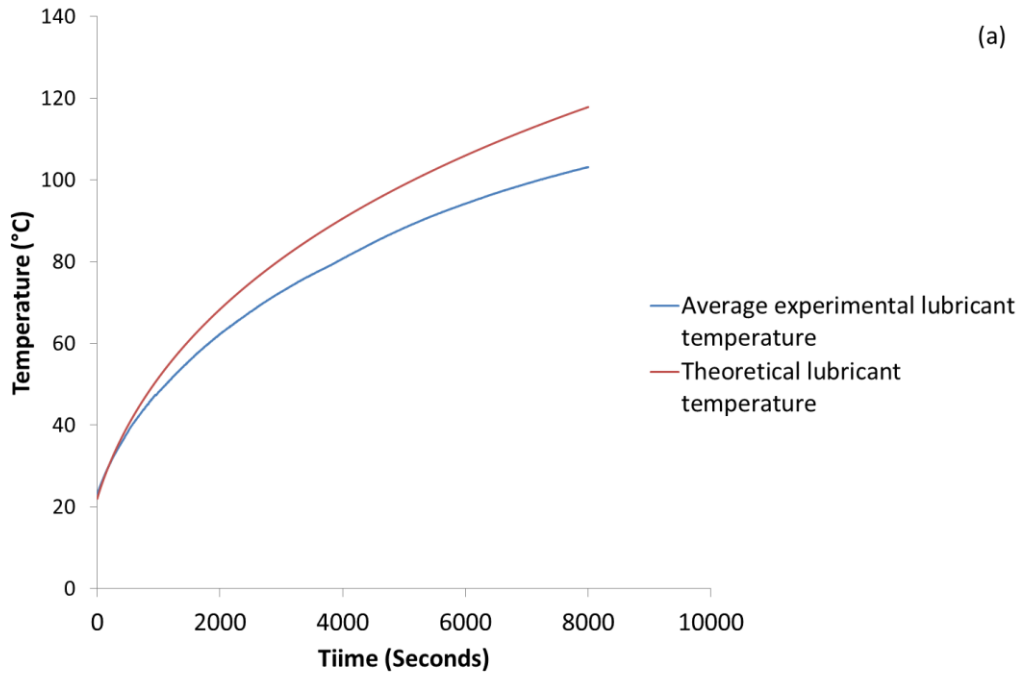


Figure 6.16: Correlation between experimental and theoretical results for the oil flow rig using a 100 mm outer diameter specimen insulated in 2 mm thick Nylon 12 with 1200 W heater power and  $10 \text{ l min}^{-1}$  flow rate and a contact heat transfer coefficient of  $65 \text{ W m}^{-2} \text{ K}^{-1}$  comparing (a) lubricant and (b) specimen temperatures

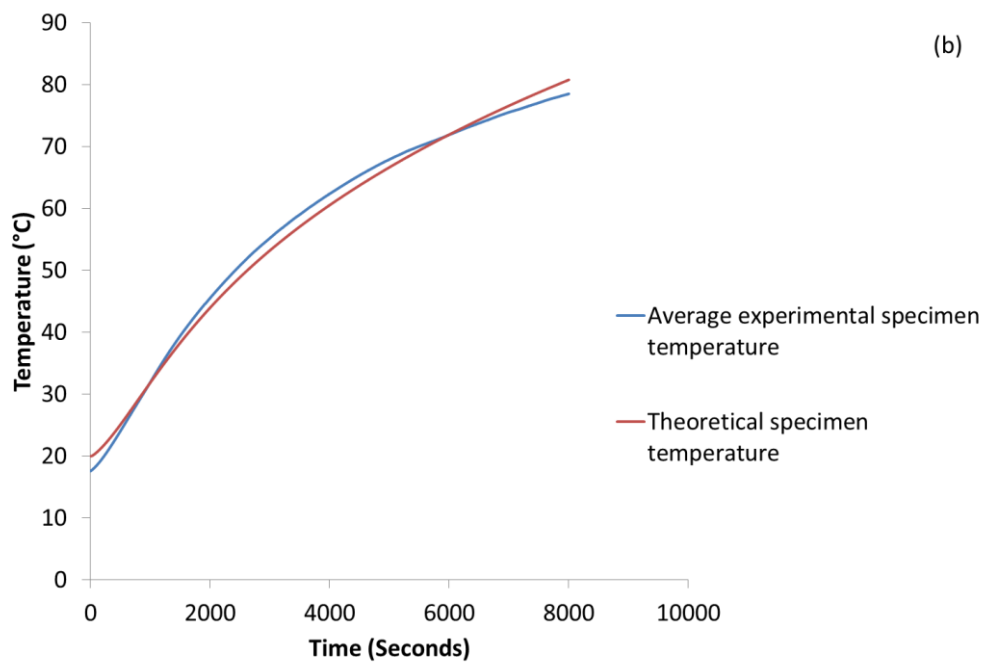
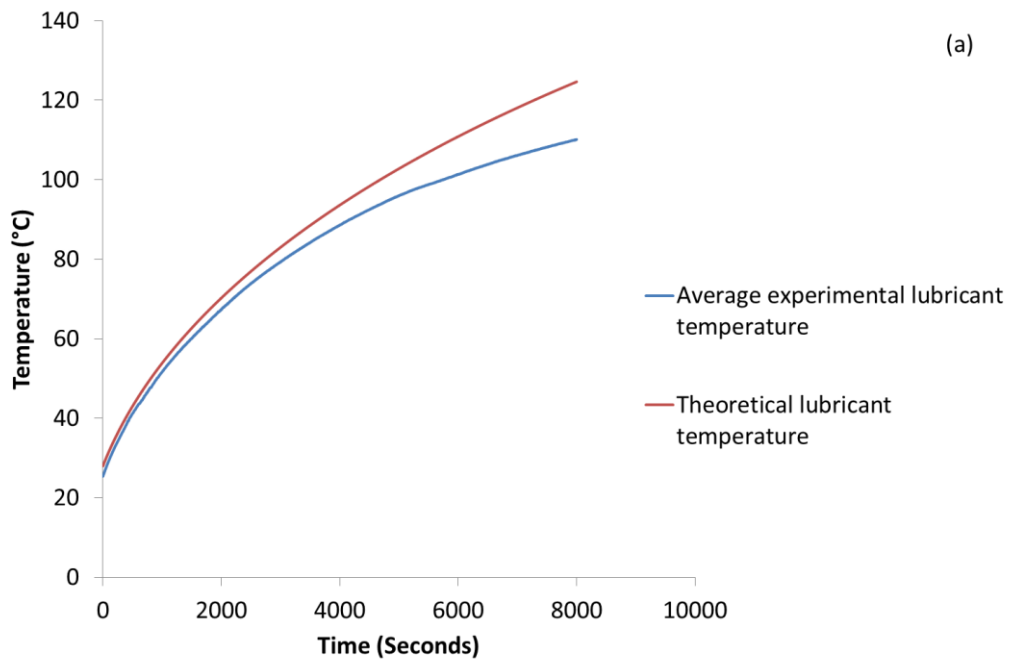


Figure 6.17: Correlation between experimental and theoretical results for the oil flow rig using a 40 mm outer diameter specimen insulated in 2 mm thick Nylon 12 with 1200 W heater power and 10 l min<sup>-1</sup> flow rate using a contact heat transfer coefficient of 65 W m<sup>-2</sup> K<sup>-1</sup> comparing (a) lubricant and (b) specimen temperatures

#### 6.5.1.2.1 Verification of the behaviour of $h_{contact}$

The structure of the theoretical model utilises two forms of the code depending on the specimen design being investigated. The homogenous specimen consists of only one radial heat transfer network while if an insulator is being investigated, the model contains two radial heat transfer models, coupled by a convective boundary

condition using the contact heat transfer coefficient,  $h_{contact}$ . To validate the behaviour of such a boundary condition, the material properties of the insulator were set to the same aluminium properties of the test block specimen and the value of  $h_{contact}$  increased to  $1000000 \text{ W m}^{-2} \text{ K}^{-1}$ . In doing so the model should closely match the prediction of the uninsulated model owing to there being no insulating materials and the effect of any contact resistance being very small with such a high contact heat transfer coefficient.

Figure 6.18 shows a comparison of the lubricant and specimen temperature profiles using the two model structures. It can be seen that the two approaches give almost identical results, with a maximum variation of 0.2% in lubricant temperature and 0.6% in specimen temperature. Figure 6.19 also illustrates how such consistency is also carried forward into the energy predictions with a maximum variation of 1% in the cumulative energy transferred to the specimen. Such results do verify that the implementation of the contact coefficient boundary condition is a valid method of modelling the physical mechanism of heat transfer at the interface of the specimen and insulating insert.

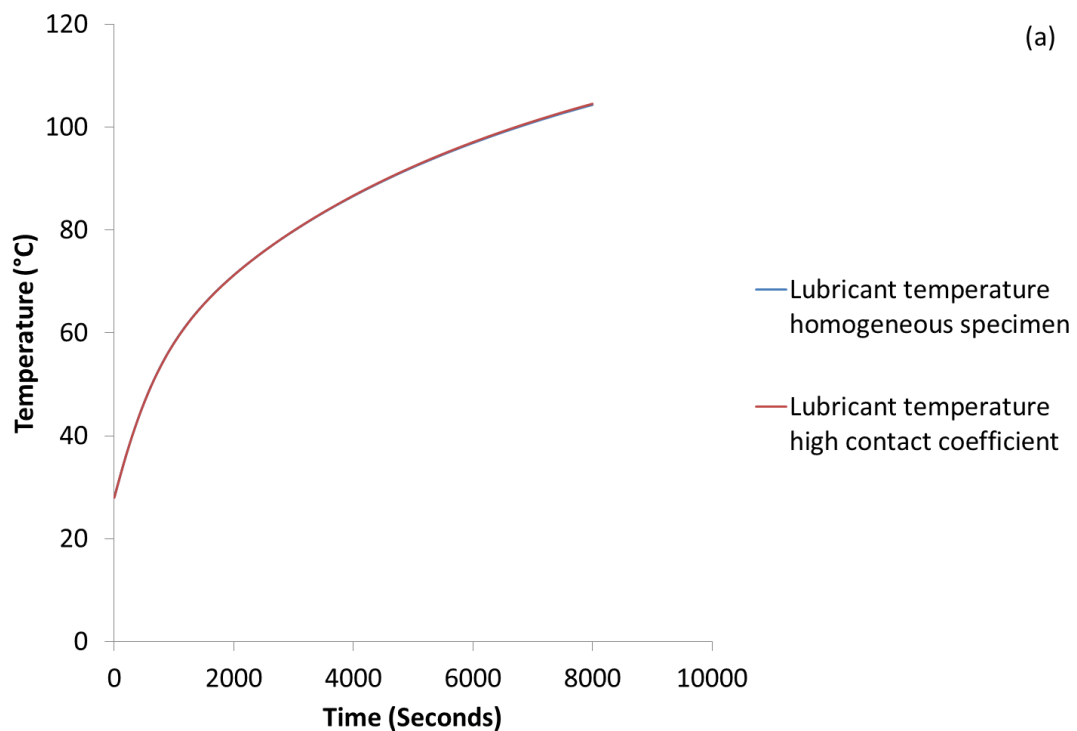


**Figure 6.18a: Comparative temperatures from the oil flow rig simulation model for a 100 mm outer diameter uninsulated specimen with a  $10 \text{ l min}^{-1}$  flow rate and 1200 W heater power using both the uninsulated and insulated model structures comparing lubricant temperatures**

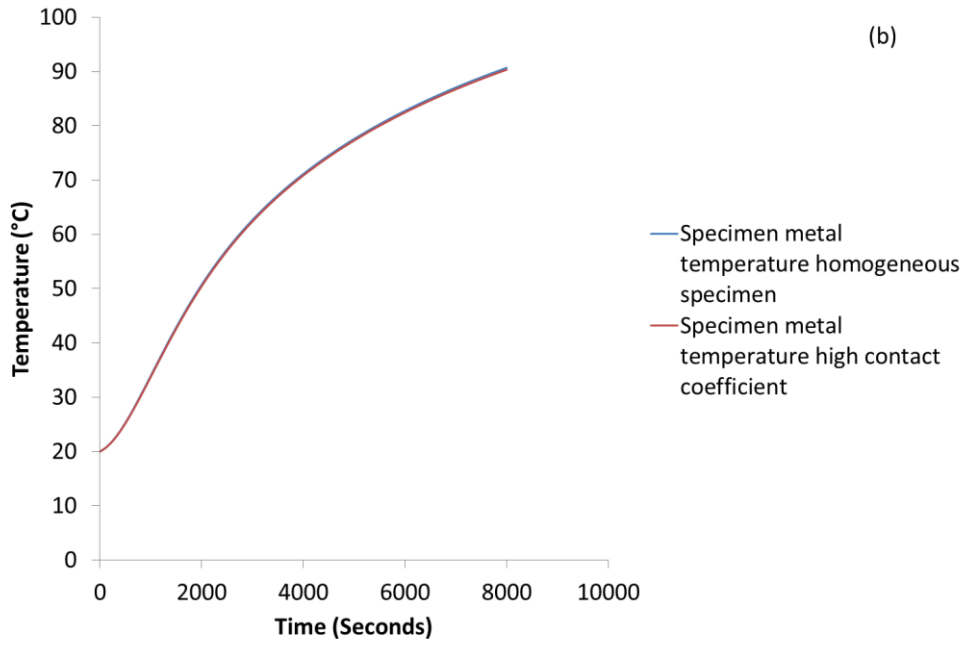


Figure 6.18b: Comparative temperatures from the oil flow rig simulation model for a 100 mm outer diameter uninsulated specimen with a  $10 \text{ l min}^{-1}$  flow rate and 1200 W heater power using both the uninsulated and insulated model structures comparing specimen temperatures

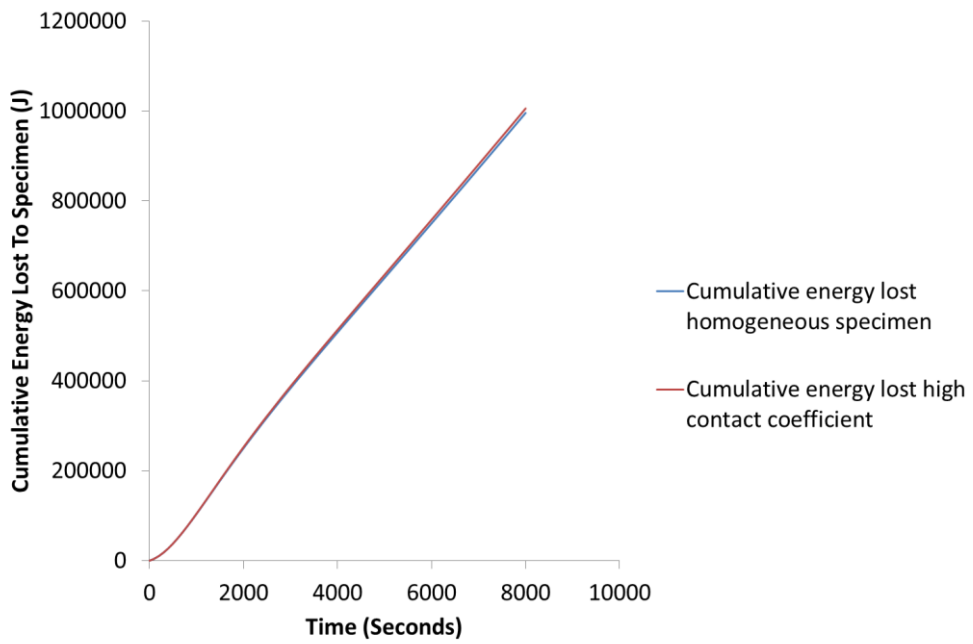


Figure 6.19: Comparison of the cumulative energy lost from the lubricant to the test block specimen in the oil flow rig simulation model for a 100 mm outer diameter specimen with a  $10 \text{ l min}^{-1}$  flow rate and 1200 W heater power using both the uninsulated and insulated model structures

### **6.5.2 Correlation of temperature differential between lubricant and specimen as a function of the lubricant temperature**

A satisfactory correlation between the experimental rig and theoretical simulations is characterised by more than the isolated temperatures of the lubricant and test block specimen. In Chapter 4 and Chapter 5, the variation of the temperature differential between the lubricant and test block specimen was highlighted as being highly significant in characterising the transient thermal behaviour of the rig. Consequently, it is important to validate that the trends in temperature differential relative to lubricant temperature are well reflected in the model. Figure 6.20 and Figure 6.21 compare the theoretical and experimental temperature differentials between the lubricant and specimen as a function of lubricant temperature.

If one first examines the performance of the model in the uninsulated scenario (Figure 6.20), it can be seen that in the instance of the 100 mm outer diameter specimen an encouraging performance is seen with a maximum deviation from the experimental data of 4 °C. The 40 mm outer diameter specimen performs exceptionally well in the early phase and the model appears to replicate the trends of differential profile. However, in the latter stages of the test one can see the peak discrepancy between theoretical and experimental data is 4 °C with an apparent diverging trend.

Of greater concern is the performance of the model when applying the 2 mm thick insulating insert, as shown in Figure 6.21. It can be seen that in the instance of the 100 mm outer diameter specimen, excellent agreement is achieved up to a lubricant temperature of 60 °C. However the model, at this point, does not appear to replicate the physical rig in an acceptable manner. The theoretical model, at a lubricant temperature of 112 °C predicts a temperature differential between the specimen and lubricant of 70 °C and is increasing whereas the experimental data shows a temperature differential of 53 °C and is decreasing. The insulated 40 mm outer diameter specimen exhibits similar issues in the simulation with diverging trends between experimental and theoretical predictions at high temperatures. In this instance the peak discrepancy at a lubricant temperature of 116 °C is 8 °C.

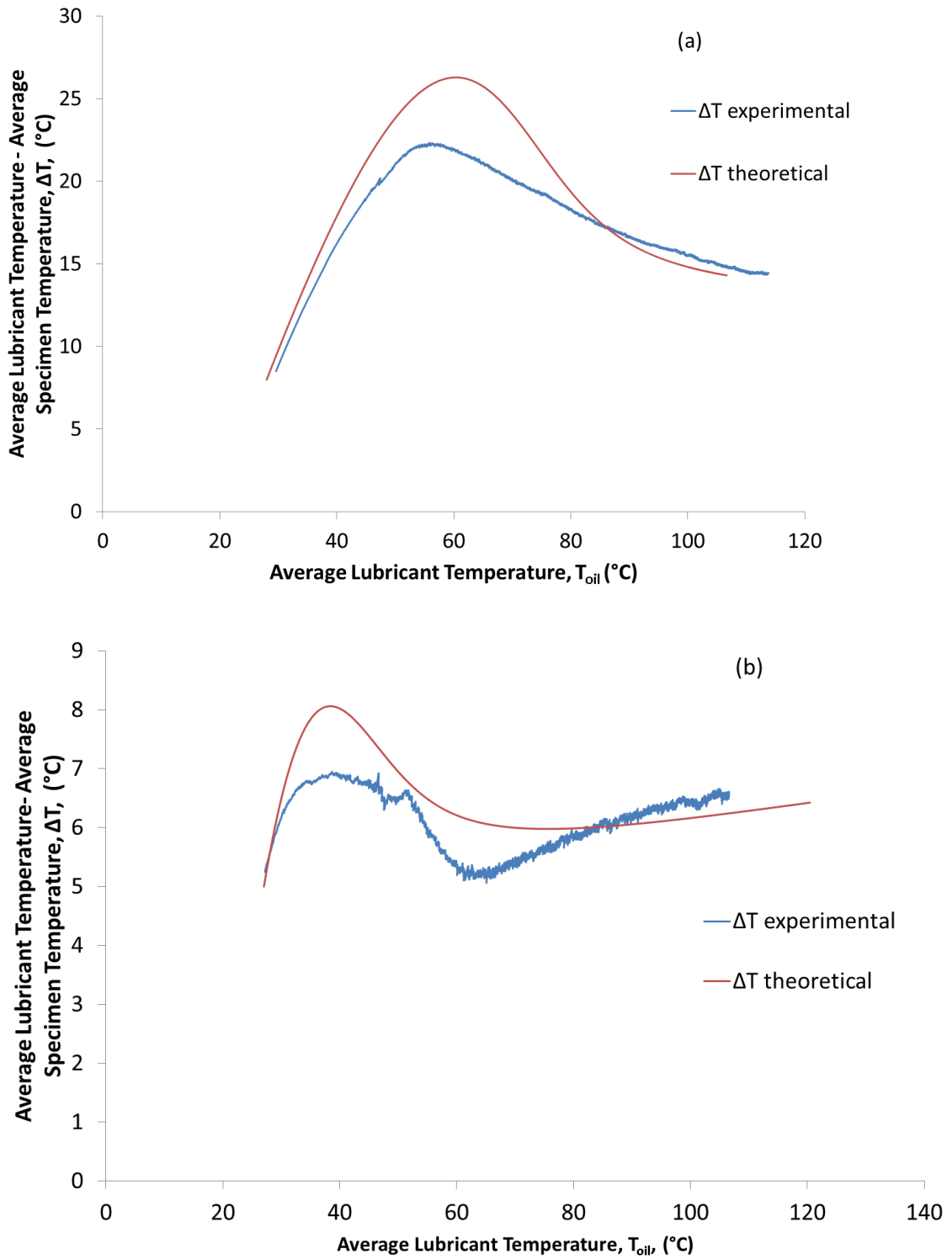


Figure 6.20: Comparison between theoretical and experimental data for the oil flow rig when 1200 W heater power is input using (a) 100 mm outer diameter and (b) 40 mm outer diameter uninsulated specimens and a lubricant flow rate of  $10 \text{ l min}^{-1}$

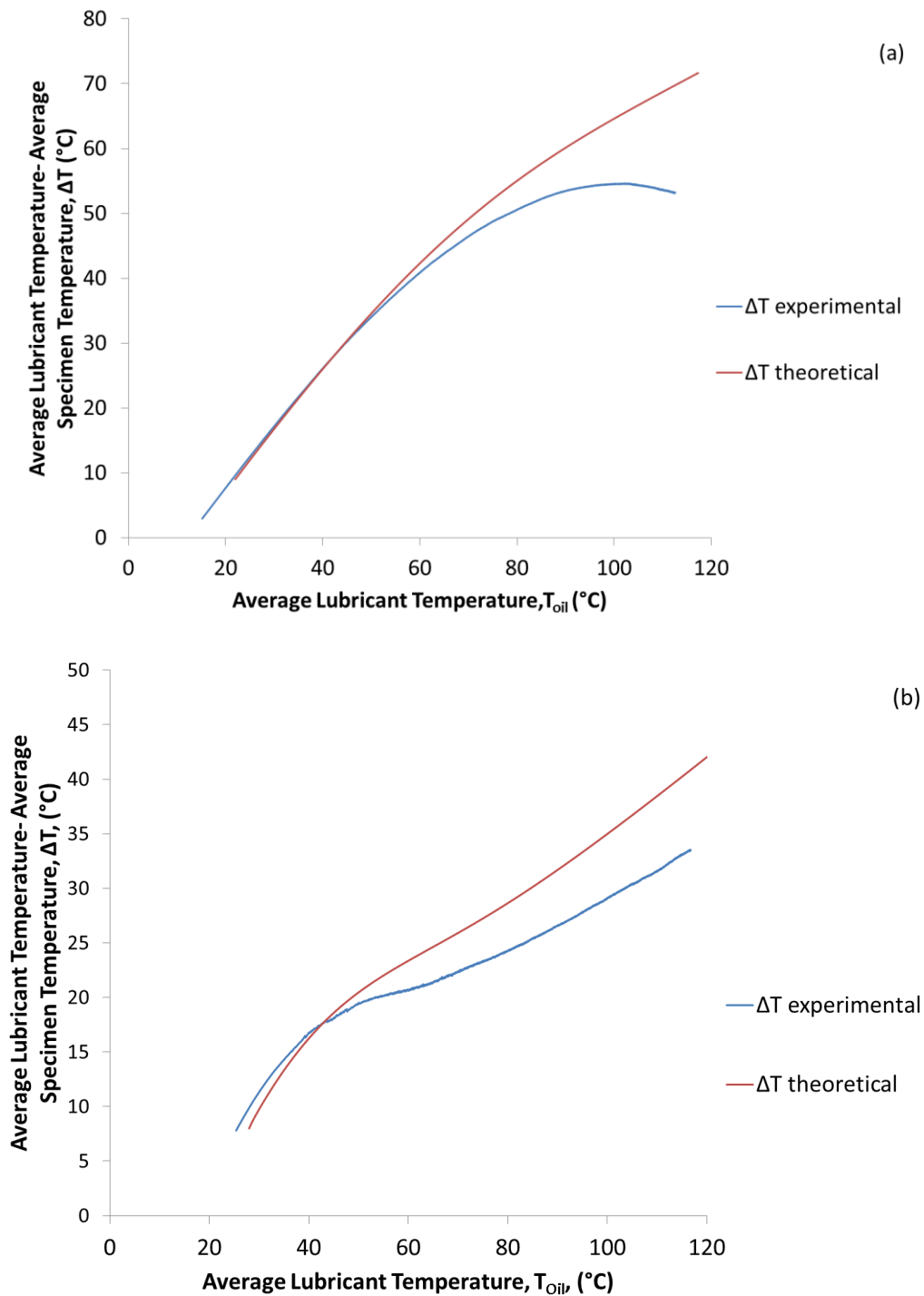


Figure 6.21: Comparison between theoretical and experimental data for the oil flow rig when 1200 W heater power is input using (a) 100 mm outer diameter and (b) 40 mm outer diameter specimens insulated with a 2 mm thick Nylon 12 insert and a lubricant flow rate of  $10 \text{ l min}^{-1}$

Given the issue with the model lay in predicting the temperature differential between the specimen and lubricant, the most logical parameter to investigate was that of the lubricant to specimen heat transfer coefficient,  $h_{oil}$ . When selecting an appropriate heat transfer coefficient, a range of correlations were compared against experimental data and discussed in Section 6.2.4.

Owing to the lower thermal mass of the specimen, the 40 mm outer diameter specimen is far more dynamic in its thermal behaviour as the heat transfer mechanism to ambient becomes significant sooner. The data for the 100 mm outer diameter specimen are easier to examine when considering heat flows at the internal bore as the external heat transfer mechanism takes much longer to become a significant factor.

The Dittus and Boelter correlation was selected owing to, with both specimen sizes, the correlation showing both the correct trend and being closest in magnitude. When studying Figure 6.5 it is clear that the experimentally derived heat transfer coefficient has an almost constant offset of  $40 \text{ W m}^{-2} \text{ K}^{-1}$  relative to the Dittus and Boelter correlation, particularly in the case of the 100 mm outer diameter specimen. Such a trend was not clearly evident in the case of the 40 mm outer diameter specimen however, as detailed above, it is likely that the onset of the external heat transfer mechanisms will have impacted on the ability to accurately calculate the value of  $h_{oil}$  from the experimental data for the 40 mm outer diameter specimen. With both test block specimens having been tested on the same rig and in the same laboratory conditions, there is no physical reason why such an offset would occur for one specimen and not the other. Consequently, having observed the offset in the value of  $h_{oil}$  between the experimental and correlation value in the case of the 100 mm outer diameter specimen the model was trialled with a modified value of  $h_{oil}$ , adding  $40 \text{ W m}^{-2} \text{ K}^{-1}$  to the correlation value for both specimen sizes. The resultant temperature differentials between the lubricant and specimen are shown in Figure 6.22 and Figure 6.23.

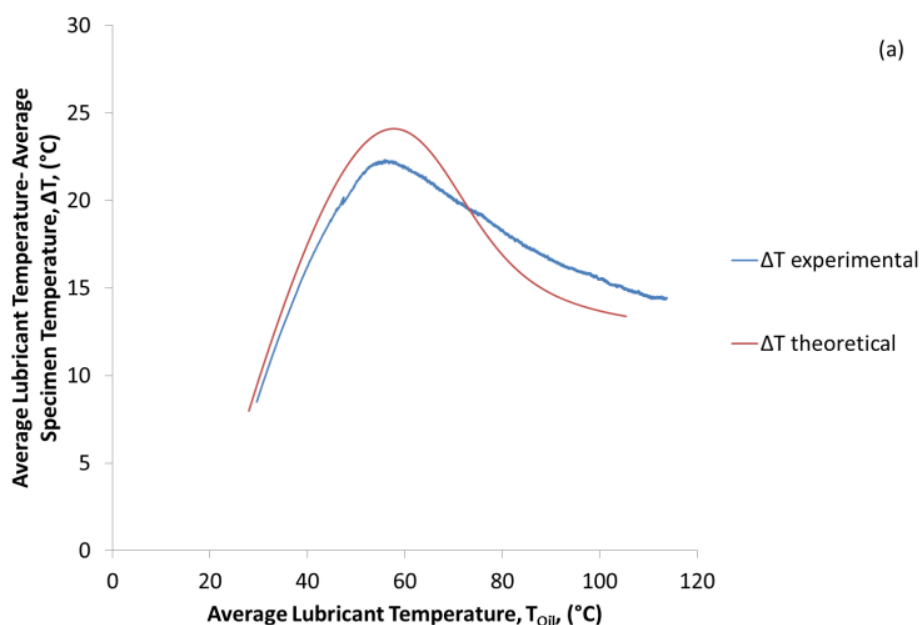


Figure 6.22a: Comparison between theoretical and experimental data for the oil flow rig when 1200 W heater power is input using 100 mm outer diameter uninsulated specimen and a lubricant flow rate of  $10 \text{ l min}^{-1}$  using a revised internal heat transfer coefficient

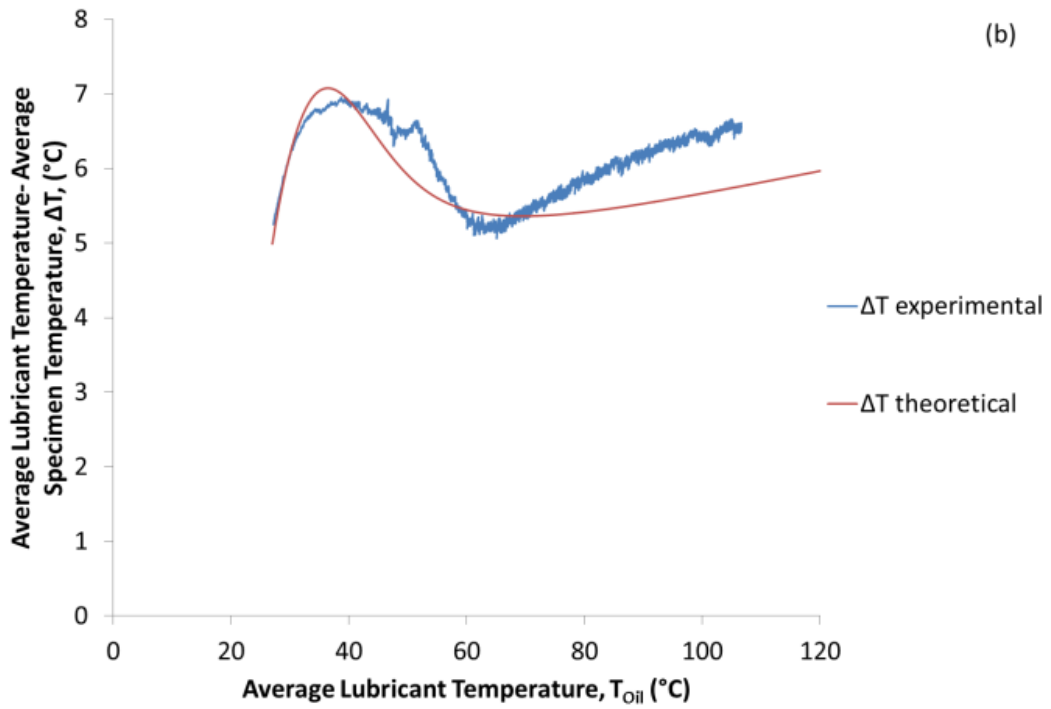


Figure 6.22b: Comparison between theoretical and experimental data for the oil flow rig when 1200 W heater power is input using a 40 mm outer diameter uninsulated specimen and a lubricant flow rate of 10 l min<sup>-1</sup> using a revised internal heat transfer coefficient

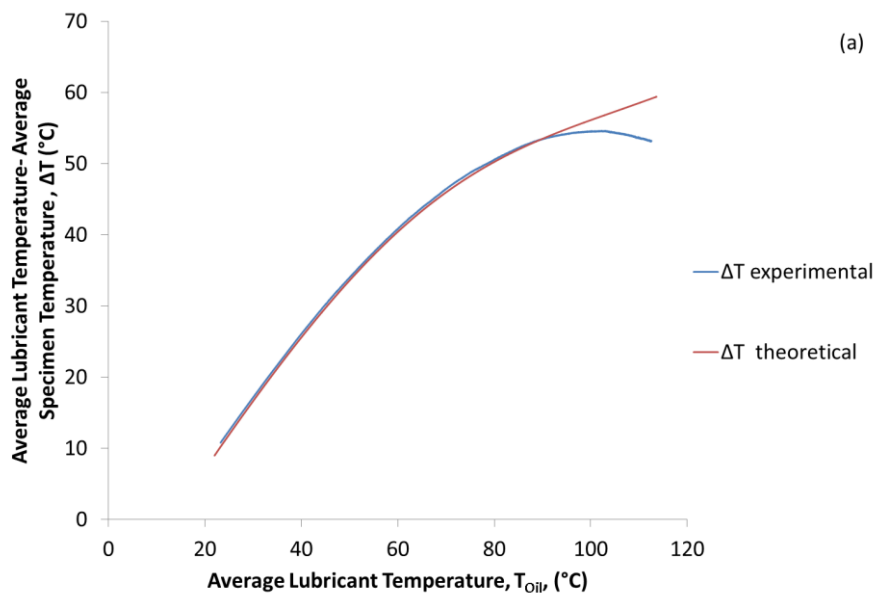
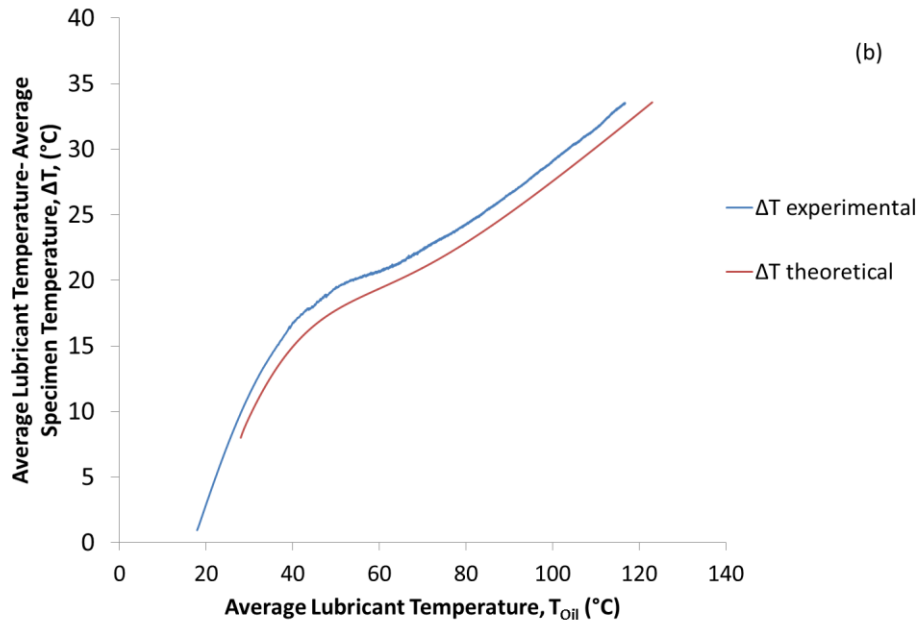


Figure 6.23a: Comparison between theoretical and experimental data for the oil flow rig when 1200 W heater power is input using a 100 mm outer diameter specimen insulated with a 2 mm thick Nylon insert and a lubricant flow rate of 10 l min<sup>-1</sup> using a revised internal heat transfer coefficient and a value for  $h_{\text{contact}}$  of 150 W m<sup>-2</sup> K<sup>-1</sup>



**Figure 6.23b : Comparison between theoretical and experimental data for the oil flow rig when 1200 W heater power is input using (a) 100 mm outer diameter and (b) 40 mm outer diameter specimen insulated with a 2 mm thick Nylon insert and a lubricant flow rate of  $10 \text{ l min}^{-1}$  using a revised internal heat transfer coefficient and a value for  $h_{contact}$  of  $150 \text{ W m}^{-2} \text{ K}^{-1}$**

Comparing Figure 6.20- Figure 6.21 with Figure 6.22-Figure 6.23 one can see the positive effect on the correlation increasing  $h_{oil}$  has had, particularly in the case of the insulated specimens. In the case of the 100 mm outer diameter insulated specimen, the peak discrepancy falls from 17 °C to 2.5 °C. Similarly for the 40 mm outer diameter insulated specimen, the discrepancy reduces from 7 °C to 1 °C. Typically, heat transfer coefficient correlations are quoted as being accurate to within 25% [50] or 40% [49]. Given that the heat transfer coefficients across the temperature range of the experiments vary from  $200 \text{ W m}^{-2} \text{ K}^{-1}$  to  $545 \text{ W m}^{-2} \text{ K}^{-1}$ , such a step is valid in terms of representing the underlying physical processes occurring. While difficult to quantify, the heat transfer coefficient even between the two uninsulated specimens may well vary owing to subtle differences in surface roughness between two drilled bores. It is also worth noting that it is possible that the heat transfer coefficient between the drilled, uninsulated bores will be different to that of the smooth, extruded Nylon tube owing to surface roughness effects.

Thus, in the final version of the model, all values of  $h_{oil}$  had a constant  $+40 \text{ W m}^{-2} \text{ K}^{-1}$  applied to the value relative to the Nusselt correlation.

### 6.5.3 The sensitivity of the specimen to ambient heat transfer coefficients

Adjustment of the internal heat transfer coefficient manifested significant improvements in the correlation of the theoretical model with experimental results. The specimen to ambient heat transfer coefficient,  $h_{outer}$ , is also subject to similar

variation. The value of  $h_{outer}$  only becomes significant in the late stages of any test, when the test block specimen is heated and an appreciable temperature differential between the specimen and ambient has developed. As such, it would be anticipated that any improvement in correlation from the model as a result of adjusting  $h_{outer}$  would be at higher lubricant temperatures. To investigate the sensitivity of  $h_{outer}$ , the four specimen simulations were investigated with the following variants of  $h_{outer}$ :

- $h_{outer} + 1$
- $h_{outer} + 3$
- $h_{outer} + 6$

Figure 6.24 shows plots of the temperature differential between the lubricant and specimen with different adjustments of the outer heat transfer correlation for the 100 mm and 40 mm outer diameter uninsulated specimens. It can be seen that the effect of such variations is limited to the high temperature region of the simulation. The addition of  $1 \text{ W m}^{-2} \text{ K}^{-1}$  to the value of  $h_{outer}$  appears to offer the optimum fit to the experimental data for the two specimen sizes. In the case of both specimens the addition of  $3 \text{ W m}^{-2} \text{ K}^{-1}$  to the value of  $h_{outer}$  provides a marginally improved fit at higher temperatures but in the instance of the 40 mm outer diameter specimen, the fit was detrimentally affected between lubricant temperatures of  $60 \text{ }^\circ\text{C}$  and  $80 \text{ }^\circ\text{C}$ .

Thus, in the final version of the model, all values of  $h_{outer}$  had a constant  $+1 \text{ W m}^{-2} \text{ K}^{-1}$  applied to the value relative to the Nusselt correlation.

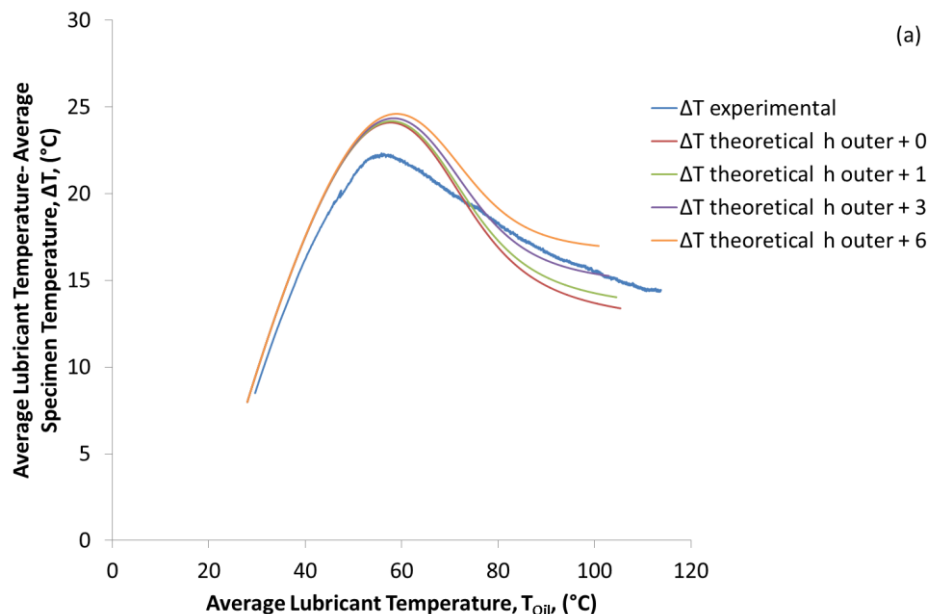


**Figure 6.24a:** Effect of modified external heat transfer coefficient on the temperature differential between the lubricant and specimen for the oil flow rig when 1200 W heater power is input using a 100 mm outer diameter uninsulated specimen and a lubricant flow rate of  $10 \text{ l min}^{-1}$  using a revised internal heat transfer coefficient

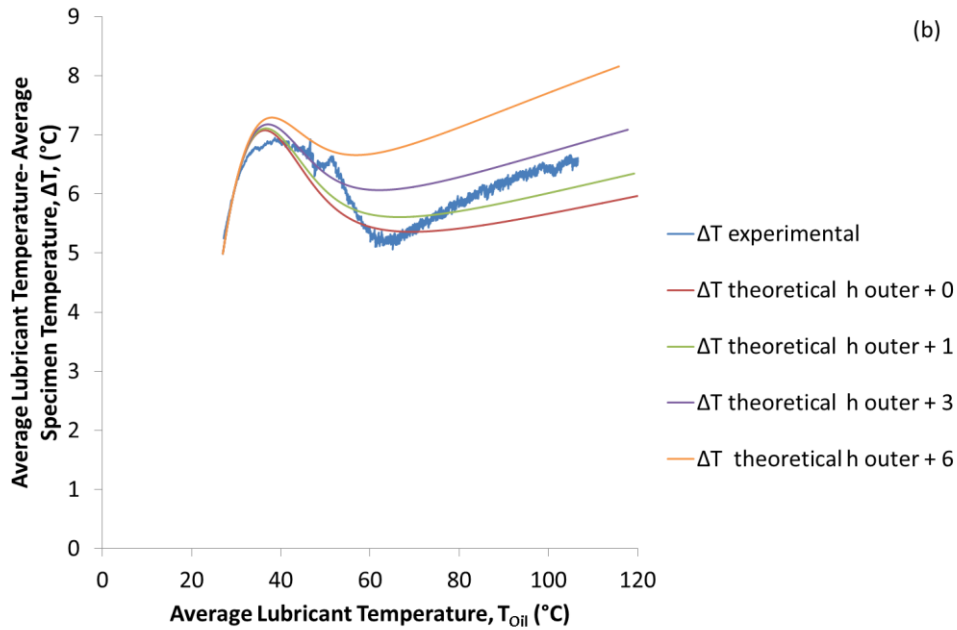
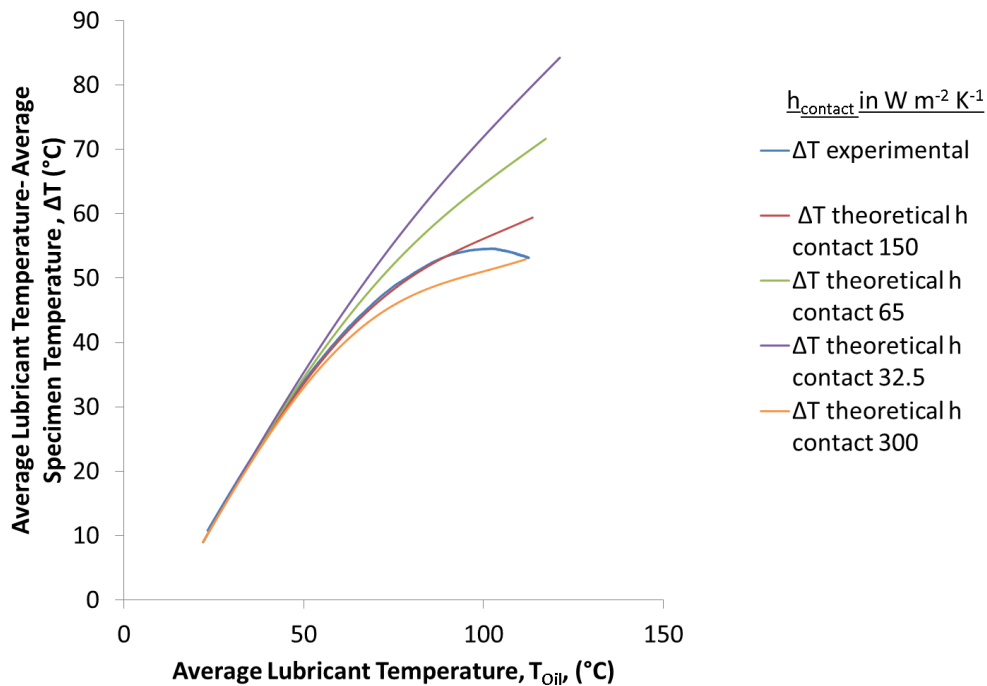


Figure 6.24b: Effect of modified external heat transfer coefficient on the temperature differential between the lubricant and specimen for the oil flow rig when 1200 W heater power is input a 40 mm outer diameter uninsulated specimen and a lubricant flow rate of 10 l min<sup>-1</sup> using a revised internal heat transfer coefficient

#### 6.5.4 Final model optimisation

The adjustment of both  $h_{oil}$  and  $h_{outer}$  to best replicate the interaction of the lubricant and specimen temperatures relative to each other required the value of  $h_{contact}$  to be re-assessed. When using the baseline correlations, the optimum value of  $h_{contact}$  was found to be 65 W m<sup>-2</sup> K<sup>-1</sup> however with the newly re-optimised model, this was found to be 150 W m<sup>-2</sup> K<sup>-1</sup> based upon the plot of the temperature differential between the lubricant and specimen against the lubricant temperature. Shown in Figure 6.25 is the change in behaviour of the model as a result of the change in  $h_{contact}$ . It can be seen that using the original value of 65 W m<sup>-2</sup> K<sup>-1</sup> for  $h_{contact}$  results in a nearly 20 °C peak overshoot and would therefore be wholly invalid. A further complexity is the likelihood that the contact resistance will change over the temperature range of the test procedure as a result of the differing coefficients of thermal expansion (CoE) between the Nylon 12 tube (CoE 4.5 x 10<sup>-5</sup> 2.3 K<sup>-1</sup>) [57] and aluminium 6082 ( CoE 2.3 x 10<sup>-5</sup> K<sup>-1</sup>) [93]. As a result, the contact resistance between the Nylon 12 insert and aluminium test block specimen is likely to decrease ( $h_{contact}$  therefore increasing) as the temperature increases and the polymer tube expands more than the aluminium. In studying Figure 6.25 it can be seen how, even with the lesser values of  $h_{contact}$  the temperature differential profile does present an overshooting and diverging trend at high lubricant temperatures. This would be consistent with the value of  $h_{contact}$  at high temperatures being too low and thus limiting heat transfer from the lubricant to the test block specimen and causing a higher temperature differential. Hence, in future work, it would be

desirable to develop further, an understanding into the sensitivity of the value of  $h_{contact}$  to changes in both material properties and changes in clearance between components as a result of changes in temperature.



**Figure 6.25: Sensitivity of predicted temperature differential between test block specimen as a result of varying the value of  $h_{contact}$  for a 100 mm outer diameter specimen with a 2 mm thick Nylon insert installed when 1200 W heater power is input and the flow rate is 10 l min<sup>-1</sup>**

A critical test of the robustness of the model is the ability to replicate accurately the trend of the experimental test where a 2 mm thick aluminium insert was inserted into the test block specimen. Such a test validates the effectiveness of the contact resistance when utilised with a large change in material thermal conductivity ( $193 \text{ W m}^{-1} \text{ K}^{-1}$  for aluminium compared to  $0.262 \text{ W m}^{-1} \text{ K}^{-1}$  for Nylon 12). Figure 6.26 shows a comparison between the experimental and theoretical data when using a 100 mm outer diameter specimen with a 2 mm thick aluminium insert. The agreement in trend that is obtained is good with a maximum discrepancy between theoretical and experimental data of 2 °C and is improved relative to the agreement in trend obtained with the Nylon 12 insert. One can see that the diverging trend that was present and highlighted in Figure 6.25 is absent in Figure 6.26. It should be remembered that no differential in coefficients of thermal expansion, or softening of the insert would be expected when using the aluminium insert and this this does further support the hypothesis that variation in the properties of the Nylon 12 insert, and the associated variation in  $h_{contact}$  were a limiting factor in achieving an acceptable correlation. In order to obtain the fit shown in Figure 6.26 the value of  $h_{contact}$  was increased to  $250 \text{ W m}^{-2} \text{ K}^{-1}$  from the previous value of  $150 \text{ W m}^{-2} \text{ K}^{-1}$  used with the polymer insert. It is briefly worth considering the validity of making

such a change. As highlighted earlier any contact resistance is incredibly difficult to quantify with no satisfactory empirical correlations existing. The contact resistance between the Nylon 12 insert and the aluminium insert will almost certainly not be the same (even though the same nominal fit was designed), owing to the clearance with the Nylon insert being 0.42 mm and the clearance of the aluminium insert being 0.23 mm (Section 5.7). Hence, given that Madhusudana [111] highlighted that the initial fit is critical in determining the contact resistance at the interface of two cylinders it is reasonable to expect that the initial value of  $h_{contact}$  to be higher in the case of the aluminium insert than in the case of the Nylon 12. However, the softening and expansion effects of the Nylon 12 insert relative to the aluminium that have been discussed will likely have led to the value of  $h_{contact}$  in the Nylon 12 increasing at higher temperatures and the insulating effect reducing.

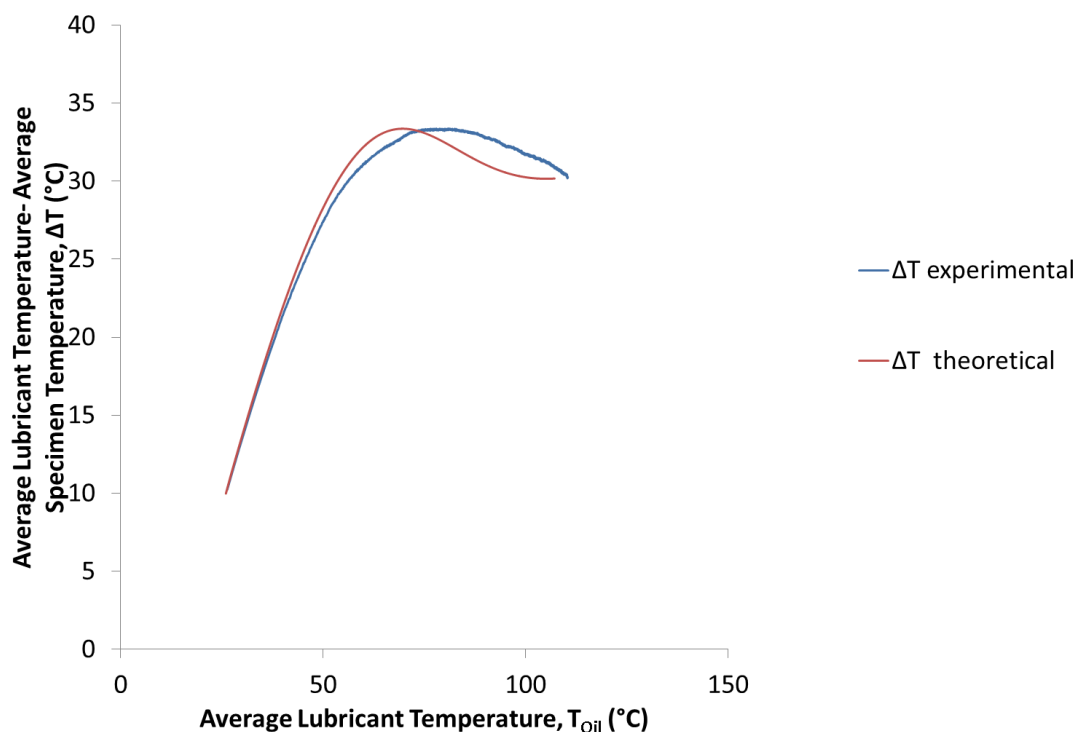


**Figure 6.26: Predicted and experimental temperature differential between the lubricant and test block specimen when using a 100 mm outer diameter specimen with a 2 mm thick aluminium insert with 1200 W heater input power and 10 l min<sup>-1</sup> flow rate and a value for  $h_{contact}$  of 150 W m<sup>-2</sup> K<sup>-1</sup>**

While only the trends of temperature differential have been presented for the model, the actual temperature profiles for the lubricant and specimen metal are included in Appendix C. In developing the model, the most appropriate values of  $h_{contact}$  for different insulating systems are listed in Table 6.5. Together with minor modifications to standard Nusselt number heat transfer coefficient correlations, that are within the stated percentage error of the correlation, the model has been able to replicate changes in the heat transfer dynamics of the oil flow rig for changing geometry or material properties.

Table 6.5: Optimised values of  $h_{contact}$  for the oil flow rig model simulation

Specimen Type	$h_{contact}$ ( $W\ m^{-2}\ K^{-1}$ )
Insulated with 2 mm thick Nylon 12 tube	150
Insulated with 2 mm thick aluminium tube	250

While the values of  $h_{contact}$ ,  $h_{outer}$ , and  $h_{oil}$  have proven critical to achieving a satisfactory correlation between experimental and theoretical data and have hence been subject to an in-depth investigation, there is also the ambient temperature to consider. In the case of each test, this was taken to be the soak temperature of the rig. However, the physical location of the rig was in a room where variations of up to 3 °C in ambient temperature were observed throughout the duration of a test. Thus, heat transfer from the test block specimen to ambient will have had an additional variable introduced as a result of the change in ambient temperature adjusting the temperature differential between the test block specimen and ambient. Changes in ambient temperature will also have affected the heat flow from the lubricant in the following ways:

- The sensible heat stored in the test block specimen will have been affected as the ambient temperature will dictate the steady state temperature of the test block specimen
- The heat flow from the lubricant to the test block specimen will have been affected as a result of the ambient temperature dictating the test block specimen temperature and subsequently the temperature differential between the lubricant and test block specimen.

For the model to replicate such effects exactly would require an ambient temperature profile to be input to the model which is beyond the scope and intention of the work. Instead, the aim of the work was to understand the sensitivity of thermal losses from the lubricant to different material and geometric parameters. Thus when using the model in Chapter 7 a constant ambient temperature is used and these effects are mitigated. However, Section 4.9 highlighted the ambient temperature as being a likely source of experimental noise and this is validated in an investigation of the effect of variations in ambient temperature in Section 7.4.

Therefore, accepting that a perfect correlation between experimental and theoretical data cannot be achieved owing to variations in ambient temperature and variations in  $h_{contact}$ , the correlation achieved is reasonable and the best possible without further increased instrumentation of the rig.

#### 6.5.4.1 The effect of adjusting $h_{contact}$ and $h_{outer}$ on energy flow predictions

While a good agreement between experimental and theoretical temperature profiles is necessary to prove the validity of the theoretical model, the most robust performance barometer of the success of different insulating strategies is the energy flow from the lubricant to the test block specimen. Having made adjustments to heat transfer coefficients, it is therefore necessary to understand the relative effect this has on the energy losses. Figure 6.27 shows a plot of the cumulative energy lost from the lubricant to a 100 mm outer diameter uninsulated test block specimen with three variants of heat transfer coefficient:

- The baseline correlations unadjusted.
- A constant offset of  $40 \text{ W m}^{-2} \text{ K}^{-1}$  applied to  $h_{oil}$  and the value of  $h_{outer}$  left unchanged.
- A constant offset of  $40 \text{ W m}^{-2} \text{ K}^{-1}$  applied to  $h_{oil}$  and a constant offset of  $1 \text{ W m}^{-2} \text{ K}^{-1}$  applied to  $h_{outer}$ .

If one first examines the percentage change plots one can see that the effect of increasing the outer heat transfer coefficient is only apparent at the end of the test, with the cumulative energy lost from the lubricant at 8000 seconds increasing from less than 1% when just the value of  $h_{oil}$  is adjusted to 4 % when both  $h_{oil}$  and  $h_{outer}$  are changed. The maximum percentage change in energy lost (indicated by the maximum point of the dashed lines) is observed to occur at 200 seconds with a 20% increase in energy lost to the specimen. While this is a large change, the baseline quantity of energy lost at this stage is only 8000 J and so represents a relatively small quantity of energy.

If one compares the absolute figures of energy transferred from the lubricant to the specimen, it can be seen that the baseline and increased  $h_{oil}$  scenario predict 970 kJ of energy to be transferred to the specimen over 8000 seconds, an average heat flux of 121 W whereas the increased  $h_{oil}$  and  $h_{outer}$  scenario, predicts 996 kJ of energy to be lost to the specimen, an average heat flux of 124 W. The comparative orders of magnitude of these predictions indicate that the minor modifications made to the heat transfer correlations to improve the fit between experimental and theoretical temperature profiles are not significant enough to affect the conclusions about the merits of different insulating mechanisms.

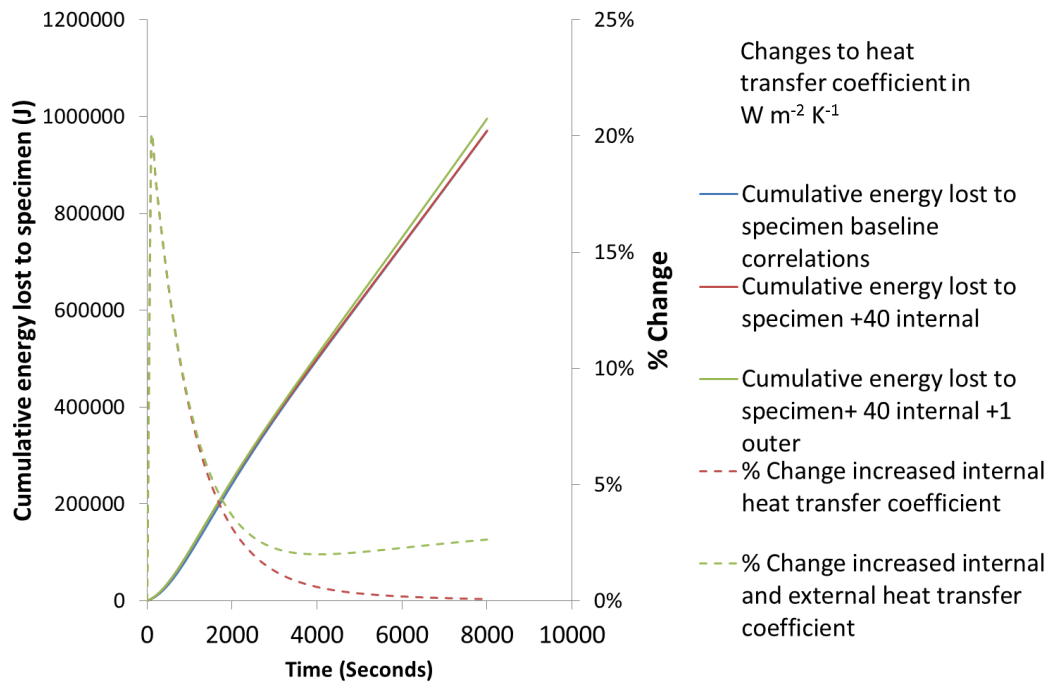


Figure 6.27: Cumulative energy lost from the lubricant to the test block specimen on the oil flow rig when a 100 mm outer diameter uninsulated specimen is installed with 1200 W heater input power and 10 l min<sup>-1</sup> flow rate

## 6.6 Mesh Sensitivity Study

The development of this model has focused on matching experimental data with simulated predictions. As such, the model has been configured to have either a homogenous solid aluminium test block specimen or to comprise of an aluminium test block specimen with the addition of an insert of aluminium or Nylon. In the instance of the 2 mm thick Nylon 12 insert, the nodal thickness of the model was set to 0.5 mm across a 2 mm thick wall, while the nodal spacing through the aluminium was set to 1.5 mm for both the 40 mm and 100 mm outer diameter specimen. Using these parameters, the time step was set to 0.002 seconds in order to maintain stability.

A significant factor in determining this nodal spacing was a physical limitation on computing power. The model was run on a desktop computer and while the number of radial nodes (28 metal nodes and 5 polymer nodes in the baseline configuration) was not a major consumer of computing power, the number of longitudinal steps (230 in the baseline configuration) was a limiting factor. The high thermal conductivity of the aluminium means the stability of the model is governed by the nodal spacing within the aluminium. At a nodal spacing of 1.5 mm, the model's time step was required to be 0.002 seconds. Therefore, in this mesh sensitivity study, where the nodal spacing of the aluminium has been decreased to 1 mm, the time step has had to be subsequently reduced to 0.001 seconds to maintain stability.

To ensure the nodal spacing was sufficiently discretised to not affect results, a full mesh sensitivity study of the mesh parameters was completed. This involved reducing the nodal spacing of the polymer from 0.5 mm to 0.25 mm and reducing the aluminium spacing from 1.5 mm to 1 mm and subsequently 0.75 mm. In all cases the baseline mesh was taken to be one with the following parameters:

- $\Delta r_{metal} = 1.5 \text{ mm}$
- $\Delta r_{polymer} = 0.5 \text{ mm}$
- $\Delta t = 0.002 \text{ s}$

The results presented in this section are from a mesh sensitivity study that was performed on the final optimised model and hence offer relevant values of the cumulative energy transferred from the lubricant to the test block specimen. However, similar mesh sensitivity checks were made to the model during its development to ensure that the results were not being unduly affected by the size of the mesh. In judging the validity of the mesh, the cumulative energy transferred to the test block specimen from the lubricant was used as a performance measure. In doing so, it was felt this allowed all the dynamics that may be sensitive to the mesh to demonstrate an effect. With both the value of  $h_{oil}$  and  $h_{outer}$  dependent on the inner and outer surface temperatures respectively, the cumulative energy transferred from the lubricant would show any change as a result of changing heat transfer coefficient values caused by sensitivity in the mesh. Similarly, as the heat flux from the lubricant is dependent on the temperature differential between the lubricant and the specimen, the cumulative energy lost would demonstrate any effect the mesh fidelity had on this relationship.

Table 6.6 summarises the percentage change as a result of changing different mesh parameters in the four baseline correlation cases. In the case of both the uninsulated scenarios, there is negligible change in predictions as a result of changing any of the parameters and the mesh has clearly proven that increasing the fidelity will not aid the model's predictions any further. In the case of the insulated 100 mm outer diameter specimen, the model proves to be more sensitive to the nodal spacing within the aluminium; showing a maximum change of 0.5% when reducing the nodal spacing to 1 mm and 0.68% when reduced further to 0.75 mm. It is felt that these changes are small enough to be able to confidently utilise the baseline nodal spacing, particularly given the vastly increased computing time to facilitate the finer mesh model. It is also worth noting that a small fraction (0.006%) of the change in prediction is related to the change in time step required to facilitate a denser mesh. Across all the specimens, just changing the time step from 0.002 s to 0.001 s, and leaving all other parameters the same, resulted in the energy transferred to the test block specimen varying by between 0.005 % and 0.007 %. This proves that the time step is sufficiently small to not warrant further reductions.

The 40 mm outer diameter insulated specimen clearly demonstrates the greatest sensitivity to changes in the mesh spacing. While a peak change in energy flow of 0.036 % as a result of halving the polymer nodal spacing demonstrates similar insensitivity to the 100 mm outer diameter specimen, the sensitivity to the nodal spacing in the aluminium is much more pronounced. Relative to the baseline mesh, reducing the metal spacing to 1 mm results in 2.3% change in predicted energy through the specimen and a reduction to 0.75 mm metal node spacing sees this increase to 3.6%. However, whereas in the other scenarios, the peak change in prediction occurs at the end of the simulation, in this scenario, the peak change occurs at 3000 seconds. At this point, the baseline mesh predicts 75 kJ of energy has been transferred to the specimen. Consequently, even with a 3.6% change, the change in predicted energy is 2.6 kJ. The reason behind this particular combination having higher mesh sensitivity can be attributed to this specimen having the least number of nodes through the metal thickness owing to the wall thickness being the thinnest.

**Table 6.6: Percentage change in cumulative energy transferred to the specimen from lubricant in the oil flow rig simulation as a result of adjusting the mesh parameters**

<u>Specimen outer diameter (mm)</u>	<u>Insulated/uninsulated</u>	<u>Maximum % change delta</u> <u><math>r_{\text{metal}} = 1 \text{ mm}</math></u>	<u>Maximum % change delta</u> <u><math>r_{\text{metal}} = 0.75 \text{ mm}</math></u>	<u>Maximum % change delta</u> <u><math>r_{\text{polymer}} = 0.25 \text{ mm}</math></u>	<u>Maximum % change <math>\delta t = 0.001 \text{ s}</math></u>
100	uninsulated	0.003	N/A	N/A	0.005
40	uninsulated	0.005	N/A	N/A	0.005
100	insulated	-0.50	-0.68	-0.084	-0.006
40	insulated	-2.3	-3.5	-0.036	-0.007

### 6.6.1 Reduced polymer thickness mesh sensitivity study

In carrying out the mesh sensitivity study using both a 40 mm and 100 mm outer diameter specimen, both the spacing of the nodes and the number of nodes through a given thickness of aluminium have been proven to be acceptable. However, in the case of the insulated specimens, the thickness of the polymer insert has remained constant. Consequently, a simulation was conducted where the polymer insert wall thickness was reduced to 1 mm and the value of  $\delta r_{\text{polymer}}$  was varied from 0.5 mm in the baseline mesh to 0.25 mm using a 100 mm outer diameter specimen. Figure 6.28 shows the predicted energy loss from the lubricant to the test block specimen using a polymer node spacing of 0.5 mm and 0.25 mm. In both cases, the aluminium node spacing was maintained at 1.5 mm and the time step used was 0.002 seconds. It can be seen that the maximum variation in predicted energy loss is 0.06% at 100 seconds when the baseline model predicts 1650 J of energy has been transferred to the specimen. The percentage difference between the two node spacing converges at 0.005%, indicating even with only 1 mm thick polymer, the

spacing of 0.5 mm is sufficient for the predictions to be valid and the mesh not to limit the model's performance.

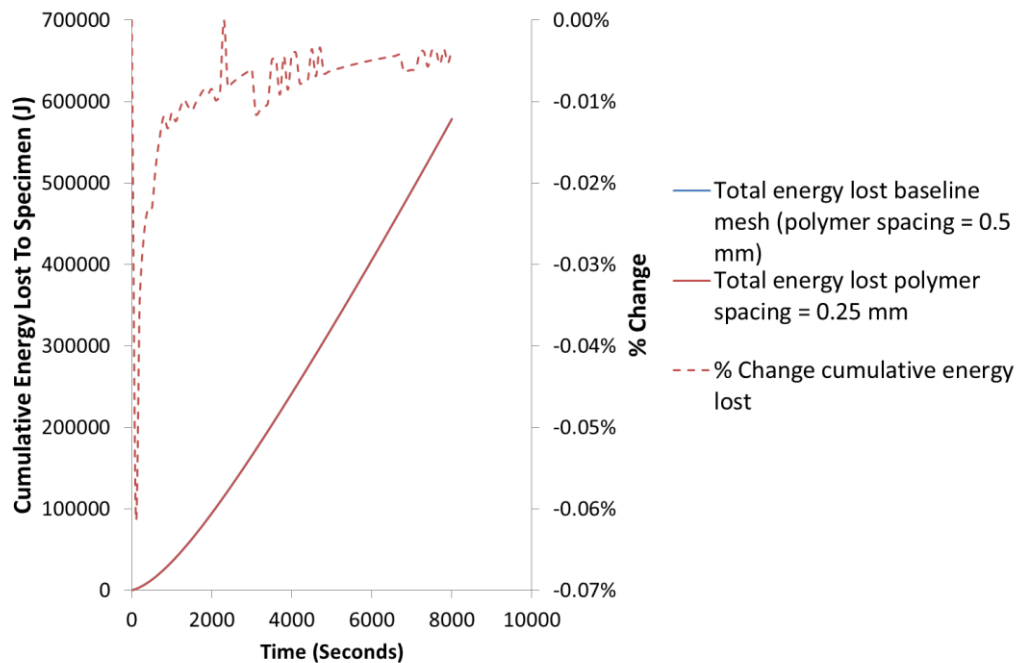


**Figure 6.28:** Predicted cumulative energy transferred from the lubricant to the test block specimen when simulating a 100 mm outer diameter specimen with a 1 mm thick Nylon insert and a heater power of 1200 W and a flow rate of 10 l min<sup>-1</sup> when varying mesh parameters

## 6.7 Conclusion

Through the work presented in this chapter it has been shown how a theoretical computational model of the oil rig has been developed. The model has been proven to provide an acceptable correlation between theoretical predictions and experimental data across a range of specimen sizes and configurations within the limitations of the instrumentation data from physical experiments. It has been highlighted how an important scope for future work is the need to incorporate a variable value of  $h_{contact}$  that reflects changes in the interface between metallic and polymeric materials with temperature and the associated impact on heat transfer.

Key to the structure of the model has been the development and explanation of an effective power method that accounts for energy transferred to parts of the rig other than the lubricant and the test block specimen.

In correlating the model with experimental data it has also been possible to calculate contact heat transfer coefficients between the insulator and the test block specimen. These vary from 150 W m<sup>-2</sup> K<sup>-1</sup> to 1000 W m<sup>-2</sup> K<sup>-1</sup> depending on the insert being used.

The mesh of the model has been proven to offer reliable predictions with a metal spacing of 1.5 mm, a polymer nodal spacing of 0.5 mm and a time step of 0.002 seconds.

## **7 Investigations into the effect of geometry and different material properties on transient warm-up of flowing automotive lubricants**

### **7.1 Introduction**

The experimental results presented in earlier chapters have been able to quantify the relative combined effects of a change in test parameters (e.g. testing an uninsulated gallery against an insulated gallery) but are unable to attribute the observed effect to any individual parameter. Thus, for example, it is not possible to quantify from the experimental results if the specific heat capacity of the Nylon 12 polymer insert provides the major benefit or if the low thermal conductivity is of greater significance.

Having correlated the theoretical model against experimental results; the model offers the flexibility to investigate the effect of individual parameters in isolation from one another and therefore gain further understanding into the significance of different parameters when trying to reduce thermal losses from the lubricant and achieve optimum lubricant warm-up times. This chapter seeks to investigate the following:

- The relative importance of different thermal properties of the materials surrounding the oil galleries.
- The importance of changing the geometry of the gallery and the flow velocity.
- Limitations of the experimental rig and the subsequent validity of the conclusions reached through Chapter 4 and Chapter 5.

When investigating the effect of different material thermal properties the thermal mass (through varying the specific heat capacity) and the thermal conductivity of both the substrate material and the insulator material are investigated in isolation of each other. A limitation of the experimental rig was that the test block specimen was manufactured from aluminium 6082 (a wrought alloy) while I.C. engine blocks are typically manufactured from a cast alloy. The variation in properties between the two grades of alloy, and the reasons behind using such a grade of alloy for the test block specimen has already been discussed in Chapter 3 (Section 3.3). However this chapter will investigate the combined effect of their different thermal properties and the effect that such a change in material specification has on energy flow away from the lubricant and into the surrounding structure. Similarly, the effect of changing the test block specimen from aluminium 6082 to both cast iron (a material still used in diesel C.I. engines) and a specimen made completely of Nylon 12 is also investigated. When considering the thermal properties of the insulator material, the effect of thermal mass and thermal conductivity of the insulator are investigated in the same

way as the substrate material, however the sensitivity of the energy flow to the insulator thickness and the value of  $h_{contact}$  are also investigated and quantified.

The experimental results were focused upon simulations of the 16 mm diameter bore of the test block specimen in the rig. However, Figure 1.17 [19] has highlighted how the gallery diameter can vary from diameters as small as 8 mm up to the diameter of the main gallery being 16 mm. Thus, investigations are carried out to appraise and understand the effect of increasing the bore diameter on heat transfer from the lubricant from the gallery to the surrounding wall. This includes understanding the interrelations of the bore diameter affecting both the heat transfer area but also the heat transfer coefficient as a result of the dependence of the fluid Reynolds Number on flow velocity.

## 7.2 Investigations in to the effect of material properties on energy flow from engine lubricant to the surrounding structure

### 7.2.1 Methodology

The experimental results have already proven how the characteristics of the oil flow rig are insensitive to flow rate with comparative results for 10 l min<sup>-1</sup> and 15 l min<sup>-1</sup> flow rates having been compared. Similarly, the effect of varying the heat input has been investigated by completing comparative tests at heat input rates of 600 W, 1200 W and 1800 W. Thus, in this chapter the simulated flow rate is maintained at 10 l min<sup>-1</sup> while the heater input power is simulated to be 1200 W. In doing so, the effective power function for use in the simulations is defined as:

$$Q_{effective} = 8709.6T_{specimen\ bore}^{-0.871}$$

Equation 7.1: Effective power function used in the simulation investigations

The investigations in this chapter aim not to repeat experimental work, but to advance knowledge and gain understanding beyond the physical limitations of the experimental rig.

#### 7.2.1.1 Uninsulated material investigation

When investigating the effect of physical properties associated with the uninsulated specimen, the specific heat capacity and the thermal conductivity of the substrate material are the only variables that warrant investigation. While the material density is variable, the effect of changing the density would be to alter the thermal mass of the specimen. Thus, such an effect is replicated by varying the specific heat capacity of the material. Hence, to investigate the effect of different material parameters, the specific heat capacity and thermal conductivity were varied in separate simulations

with the two suites of experiments shown in Table 7.1 for both the 40 mm and 100 mm outer diameter specimens.

**Table 7.1: Simulated variation in substrate specific heat capacity and thermal conductivity**

Baseline substrate thermal conductivity: $193 \text{ W m}^{-1} \text{ K}^{-1}$	Baseline substrate specific heat capacity: $900 \text{ J kg}^{-1} \text{ K}^{-1}$
<u>Cp of substrate (<math>\text{J kg}^{-1} \text{ K}^{-1}</math>)</u>	<u>Thermal conductivity of substrate (<math>\text{W m}^{-1} \text{ K}^{-1}</math>)</u>
480	35
585	56
900	73
1800	193

In addition, two further simulations were conducted whereby the properties of aluminium 6082 were replaced with the thermal properties of cast iron and aluminium casting alloy A319 (the comparative material properties are shown in Table 7.2). Such a comparison, in the case of the cast iron simulation would help determine if there is a significant difference in heat transfer between S.I. gasoline engines (typically manufactured from cast aluminium) and C.I. diesel engines (where cast iron blocks still have a presence in the market). The comparison between the wrought 6082 T6 alloy and the A319 casting alloy also allows for the limitations in the findings from the experimental rig, and subsequent simulations, as a result of manufacturing the test block specimen from 6082 T6 alloy rather than a cast alloy (which is a typical grade of aluminium used to manufacture I.C. engine blocks from) to be discussed.

**Table 7.2: Comparative material properties of aluminium alloy and cast iron**

<u>Material</u>	<u>Density (<math>\text{kg m}^{-3}</math>)</u>	<u>Thermal conductivity (<math>\text{W m}^{-1} \text{ K}^{-1}</math>)</u>	<u>Specific heat capacity (<math>\text{J kg}^{-1} \text{ K}^{-1}</math>)</u>
Aluminium alloy 6082 T6 (wrought)	2690 [93]	193 [93]	900 [57]
Aluminium alloy A319 (cast) [71]	2720	130	1000
Cast iron [57]	7150	56	460

### 7.2.1.2 Insulated material investigation

The insulated system presents significantly more variables to investigate. Aside from the specific heat capacity and density of the substrate, one must also consider the specific heat capacity and density of the insulator. Furthermore, the value of the contact heat transfer coefficient,  $h_{contact}$ , and the thickness of the insulator are also important parameters to investigate. Relative to metallic materials, polymeric materials tend to exhibit greater temperature sensitivity within the operating

temperature range of automotive lubricants. Hence there is also a need to assess the effect of the change in the material properties of the insulator (thermal conductivity, density and specific heat capacity) as the properties change with temperature. The material properties of the insulating insert are also seen to exhibit slight variations between different suppliers and there is therefore a need to understand if the magnitudes of such variations are significant in controlling thermal losses from automotive lubricants.

The investigation into the effect of insulator material properties on thermal losses from the lubricant therefore forms two parts. The first (Section 7.2.1.2.1) performs a general parametric study to assess, when considering the insulating insert material, which of the thermal properties are most significant in affecting thermal losses. Hence material properties are varied in isolation to remove the effect of any interactions between variables. The second part of the investigation (Section 7.2.1.2.2) investigates the effect of the reported variation in insulating insert material properties between suppliers of the same grade of material. In addition, the effects of the change in material property as a result of temperature variation are also investigated.

#### **7.2.1.2.1 Insulating material parameter parametric study**

To investigate the effect of individual insulating insert material properties on thermal losses, the design of experiments shown in Table 7.3 was conducted that varied each parameter independently of one another. Listed above the values of the variable being investigated are the other parameters in the simulation that were held constant. The simulations were only carried out using a 100 mm outer diameter specimen owing to both the experimental results (discussed in Chapter 4 and Chapter 5) and the simulations outlined in Section 7.2.1.1 sufficiently characterising the effect of a change in specimen size. Similar to that of the uninsulated simulations, the material properties of aluminium were replaced with those of cast iron in order to investigate any significant change that may be relevant when using C.I. engines. An additional simulation carried out was that of 5 mm thick insulation applied to the aluminium but the value of  $h_{contact}$  was increased to  $100000 \text{ W m}^{-2} \text{ K}^{-1}$ . Such a test indicates whether a greater thickness of insulation is able to replicate the insulating performance of the Nylon 12 tubing even if the contact resistance is reduced.

Finally, a simulation was conducted whereby the material properties of an uninsulated specimen were replaced with those of baseline Nylon 12 ( $C_p = 1760 \text{ J kg}^{-1} \text{ K}^{-1}$ ,  $\rho = 1015 \text{ kg m}^{-3}$ ,  $k = 0.262 \text{ W m}^{-1} \text{ K}^{-1}$ ) to observe if there is any benefit in trying to overcome the design challenges of manufacturing parts of the engine entirely out of polymeric materials rather than the strategy of insulating metallic components.

Table 7.3: Simulated test variations for the oil flow rig using a 100 mm outer diameter insulated specimen

Insulator thermal conductivity: 0.262 W m <sup>-1</sup> K <sup>-1</sup> Insulator specific heat capacity: 1760 J kg <sup>-1</sup> K <sup>-1</sup> Substrate thermal conductivity: 193 W m <sup>-1</sup> K <sup>-1</sup> h <sub>contact</sub> : 150 W m <sup>-2</sup> K <sup>-1</sup> Insulator thickness: 2 mm	Insulator thermal conductivity: 0.262 W m <sup>-1</sup> K <sup>-1</sup> Insulator specific heat capacity: 1760 J kg <sup>-1</sup> K <sup>-1</sup> Substrate specific heat capacity: 900 J kg <sup>-1</sup> K <sup>-1</sup> h <sub>contact</sub> : 150 W m <sup>-2</sup> K <sup>-1</sup> Insulator thickness: 2 mm	Insulator thermal conductivity: 0.262 W m <sup>-1</sup> K <sup>-1</sup> Substrate thermal conductivity: 193 W m <sup>-1</sup> K <sup>-1</sup> Substrate specific heat capacity: 900 J kg <sup>-1</sup> K <sup>-1</sup> h <sub>contact</sub> : 150 W m <sup>-2</sup> K <sup>-1</sup> Insulator thickness: 2 mm
<u>Cp of substrate (J kg<sup>-1</sup> K<sup>-1</sup>)</u>	<u>Thermal conductivity of substrate (W m<sup>-1</sup> K<sup>-1</sup>)</u>	<u>Cp of insulator (J kg<sup>-1</sup> K<sup>-1</sup>)</u>
480	35	880
585	56	1320
900	73	1760
1800	193	2640
		3520

Insulator specific heat capacity: 1760 J kg <sup>-1</sup> K <sup>-1</sup> Substrate thermal conductivity: 193 W m <sup>-1</sup> K <sup>-1</sup> Substrate specific heat capacity: 900 J kg <sup>-1</sup> K <sup>-1</sup> h <sub>contact</sub> : 150 W m <sup>-2</sup> K <sup>-1</sup> Insulator thickness: 2 mm	Insulator thermal conductivity: 0.262 W m <sup>-1</sup> K <sup>-1</sup> Insulator specific heat capacity: 1760 J kg <sup>-1</sup> K <sup>-1</sup> Substrate thermal conductivity: 193 W m <sup>-1</sup> K <sup>-1</sup> Substrate specific heat capacity: 900 J kg <sup>-1</sup> K <sup>-1</sup> Insulator thickness: 2 mm	Insulator thermal conductivity: 0.262 W m <sup>-1</sup> K <sup>-1</sup> Insulator specific heat capacity: 1760 J kg <sup>-1</sup> K <sup>-1</sup> Substrate thermal conductivity: 193 W m <sup>-1</sup> K <sup>-1</sup> Substrate specific heat capacity: 900 J kg <sup>-1</sup> K <sup>-1</sup> h <sub>contact</sub> : 150 W m <sup>-2</sup> K <sup>-1</sup>
<u>Thermal conductivity of insulator (W m<sup>-1</sup> K<sup>-1</sup>)</u>	<u>h<sub>contact</sub> (W m<sup>-2</sup> K<sup>-1</sup>)</u>	<u>Insulator thickness (mm)</u>
0.131	75	1
0.197	110	1.5
0.262	150	3
0.393	225	4
0.524	300	

### 7.2.1.2.2 The effect of insulating material thermal property variation caused by supplier variation and changes in operating temperature

It was discussed in Section 3.3.1.1.1 how, relative to the baseline properties of Nylon 12 that were presented in Table 3.2, the properties of Nylon 12 can vary between different suppliers and this is evident in the product data sheets shown in Appendix A. Thus, in order to understand if the variation in Nylon 12 properties that are observed between different suppliers have a significant effect on the thermal energy transferred from the lubricant to the test block specimen, an additional simulation was carried out whereby the baseline properties of Nylon 12 were replaced with supplier data (from two different suppliers) for Nylon 12; summarised in Table 7.4. In addition, a further simulation was carried out whereby the theoretical model was used to appraise whether or not the variation in the thermal properties of Nylon 12 and Nylon 6 (first discussed in Section 3.3.1.1.2) have a significant effect on the thermal losses from the lubricant to the test block specimen. Thus, comparative simulations were carried out whereby the baseline test block specimen properties were input into the model, together with the material properties data for different grades and suppliers of Nylon 12 and Nylon 6 (presented in Table 7.5) to investigate whether such variation in the insulating insert material properties were significant.

Finally, in order to appraise if the variation in the insulating material's thermal properties, caused by the polymer temperature rising, had a significant impact on the thermal losses from the lubricant to the test block specimen, a simulation was conducted whereby the thermal properties of the insulating insert were changed to match supplier data provided for the thermal properties of the insulator at 30 °C and 130 °C (see Table 7.6). In the case of the data for density and specific heat capacity, data were provided by Arkema for Nylon 12 [117] however such data were not available for the thermal conductivity. Instead data have been used for a Nylon 11 grade of the polymer [118] and reports the thermal conductivity increasing from 0.21 W m<sup>-1</sup> K<sup>-1</sup> to 0.24 W m<sup>-1</sup> K<sup>-1</sup> between 80 °C and 140 °C. The order of magnitude of this change is consistent with other sources with the work of do Santos et al. [119] reporting a change of 0.02 W m<sup>-1</sup> K<sup>-1</sup> for Nylon 6 between 20 °C and 120 °C.

Table 7.4: Thermal properties of Nylon 12 sourced from different suppliers

Property	Ensinger	PAR
Density (kg m <sup>-3</sup> )	1020	1020
Thermal conductivity (W m <sup>-1</sup> K <sup>-1</sup> )	0.30	0.23
Specific heat capacity (J kg <sup>-1</sup> K <sup>-1</sup> )	1800	2100

Table 7.5: Thermal properties of different grades of Nylon

Property	Nylon 12	Nylon 6
Density ( $\text{kg m}^{-3}$ )	1020	1130
Thermal conductivity ( $\text{W m}^{-1} \text{K}^{-1}$ )	0.30	0.23
Specific heat capacity ( $\text{J kg}^{-1} \text{K}^{-1}$ )	1800	1700

Table 7.6: Properties used to investigate the effect of Nylon 12 material property variation with temperature on thermal losses from the lubricant to the test block specimen

Property	30 °C	120 °C
Density ( $\text{kg m}^{-3}$ )	1025	987
Thermal conductivity ( $\text{W m}^{-1} \text{K}^{-1}$ )	0.21	0.24
Specific heat capacity ( $\text{J kg}^{-1} \text{K}^{-1}$ )	1791	2798

## 7.2.2 Results

### 7.2.2.1 Uninsulated results

The results from such comparative work are complex owing to the transient nature of the heat transfer being studied. The magnitude of any effect resulting from a change in material parameters varies over the duration of the test cycle and is demonstrated in Figure 7.1. The cumulative energy transferred from the lubricant to the test block specimen is plotted against time for a 100 mm outer diameter uninsulated specimen using different values for the specific heat capacity of the test block specimen. It can be seen how the maximum deviation between simulations of different specific heat capacity values occurs at approximately 2800 seconds before the results begin to converge. The reasoning behind such a trend is linked to when the temperature differential between the lubricant and specimen begins to reduce and the effect of the specific heat capacity on such dynamics has already been discussed both in Chapter 4 and Chapter 6. As a result of increasing the specimen specific heat capacity to  $1800 \text{ J kg}^{-1} \text{K}^{-1}$ , one observed a 39% peak increase in energy transferred to the specimen, relative to the baseline. Beyond the peak deviation, the specimen does begin to rise in temperature and the heat flux between the lubricant and specimen reduces and the cumulative energy lost from the lubricant also becomes dependent on the heat flux to ambient; owing to the specimen temperature being elevated relative to ambient. Thus the ambient heat flux limits the deviation of the different simulations and the results begin to converge. However, it can be seen that, owing to the specimen temperature still rising, the effect of the specific heat capacity is still present throughout the test and hence the results remain offset relative to each other throughout the test duration.

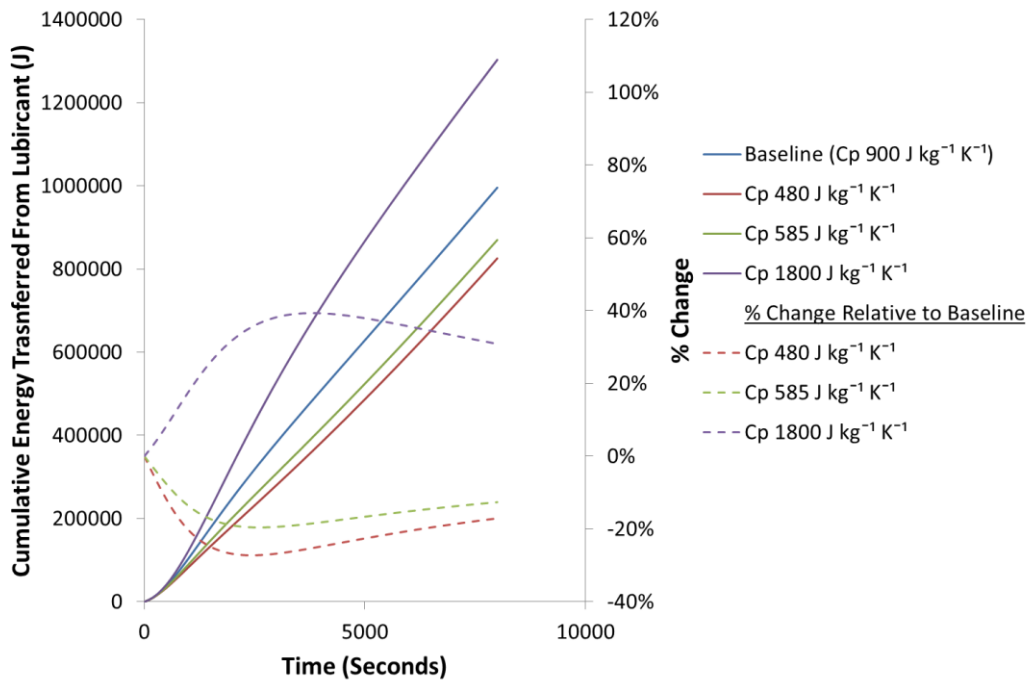


**Figure 7.1: Variation in cumulative energy lost from the lubricant to the specimen as a result of changing the specific heat capacity ( $C_p$ ) of a 100 mm outer diameter test block specimen. The lubricant flow rate was  $10 \text{ l min}^{-1}$  with 1200 W heater power input**

The example explained above (and shown in Figure 7.1) is demonstrative of the evolving thermal system that exists during warm-up. It must be remembered that the aim is to reduce thermal losses from the engine lubricant and that consequently, the most relevant performance measure in this work is to compare the cumulative energy transferred from the lubricant to the specimen. In doing so, it is desirable to observe a reduction in the cumulative energy transferred from the lubricant to the specimen which may therefore accelerate the rate of lubricant heating in an I.C. engine application. Thus, the results in this chapter compare the cumulative energy transferred from the lubricant to the specimen with the aim of determining the optimum material selection strategy to reduce thermal losses from the engine lubricant.

Table 7.7 compares the energy lost from the lubricant to the test block specimen for both the 100 mm and 40 mm outer diameter specimen. It can be seen that, in the case of both specimens, that the specific heat capacity is the dominant factor in reducing thermal losses from the lubricant to the specimen. By reducing the specific heat capacity of the test block specimen from  $900 \text{ J kg}^{-1} \text{ K}^{-1}$  to  $480 \text{ J kg}^{-1} \text{ K}^{-1}$  the thermal losses can be reduced by between 17% and 9% depending on size. Comparatively, doubling the specific heat capacity to  $1800 \text{ J kg}^{-1} \text{ K}^{-1}$  results in the thermal losses increasing by between 19% and 31%.

The thermal losses from the lubricant are much less sensitive to the thermal conductivity of the test block specimen with an 80% reduction in thermal

conductivity ( $193 \text{ W m}^{-1} \text{ K}^{-1}$  to  $35 \text{ W m}^{-1} \text{ K}^{-1}$ ) only reducing the thermal losses by between 1% and 3%. Doubling the thermal conductivity to  $386 \text{ W m}^{-1} \text{ K}^{-1}$  results in a less than 1% increase in thermal losses from the lubricant. Such a lack in sensitivity is a result of the lumped capacitance behaviour of the baseline specimen and, hence, increasing the thermal conductivity does not serve to increase the temperature gradient through the test block specimen any further. Consequently, the thermal losses from the lubricant to the specimen also do not increase any further.

The combined effects of different material parameter changes are shown when the baseline (aluminium alloy) test is compared with the cast iron simulation and increases in thermal losses of between 10% and 7% are observed. Of note also is how the specific heat capacity of the aluminium is higher than the cast iron (Table 7.1) but draws less energy from the lubricant. However in this instance, the volume of the two specimens have been kept equal and consequently, if one compares the volumetric heat capacity, the aluminium alloy has a volumetric heat capacity of  $2.4 \text{ MJ m}^{-3}$  which compares with  $3.3 \text{ MJ m}^{-3}$  for cast iron. Therefore, it can be seen that the heat capacity of the material remains dominant in dictating the warm-up performance of the material. However, the findings do highlight the need to consider the effect of material density carefully in any material selection process.

When comparing the results of the wrought aluminium 6082 alloy with those of the cast A319 alloy it can be seen that increased specific heat capacity and increased density (resulting in a 12% increase in volumetric heat capacity) result in the model predicting that the cast alloy would result in the energy flow from the lubricant increasing by between 2% and 4%, depending on specimen size, despite the cast alloy having a thermal conductivity that is 32% lower than the wrought alloy. This further confirms the domination of the heat capacity over the thermal conductivity of the substrate material. Thus, while the wrought alloy results in less heat flow away from the lubricant than the cast alloy (which would typically be used in the manufacture of an I.C. engine block), the change is small, relative to the 60% reduction in energy observed as a result of applying insulation in the experimental results. It can therefore be concluded that the choice of a wrought alloy over a cast alloy for use in the rig does not serve to limit the validity of the experimental findings. However, the fact that the cast alloy increases the energy flow from away from the lubricant, suggests that the application of insulation to galleries in an engine would result in energy savings of a higher magnitude than those observed on the rig.

**Table 7.7: Predicted cumulative energy transferred from the lubricant to a 100 mm and 40 mm outer diameter test block specimen over 8000 seconds with a lubricant heating rate of 1200 W and a flow rate of 10 l min<sup>-1</sup> when varying both the specific heat capacity and thermal conductivity of the specimen material**

<u>Specimen substrate property variation</u>	<u>Cumulative energy transferred to 100 mm outer diameter (MJ)</u>	<u>100 mm outer diameter % change (relative to baseline)</u>	<u>Cumulative energy transferred to 40 mm outer diameter (MJ)</u>	<u>40 mm outer diameter % change (relative to baseline)</u>
Baseline aluminium 6082 T6 specimen (wrought alloy) Cp = 900 J kg <sup>-1</sup> K <sup>-1</sup> K = 193 W m <sup>-1</sup> K <sup>-1</sup>	1.00		0.39	
Cp = 480 J kg <sup>-1</sup> K <sup>-1</sup>	0.83	-17%	0.36	-9%
Cp = 1800 J kg <sup>-1</sup> K <sup>-1</sup>	1.30	+31%	0.47	+19%
K = 35 W m <sup>-1</sup> K <sup>-1</sup>	0.97	-3%	0.39	-1%
K = 386 W m <sup>-1</sup> K <sup>-1</sup>	1.00	0%	0.39	0%
Aluminium A319 (cast alloy)	1.03	+4%	0.40	+2%
Cast Iron	1.1	+10%	0.42	+7%

Thus, the findings from this section indicate that where it is not possible to insulate the surrounding structure of the lubricant gallery, the optimum strategy to reducing thermal losses from the lubricant is to reduce the specific heat capacity of the surrounding substrate material.

## **7.2.2.2 100 mm insulated specimen results**

### **7.2.2.2.1 Material parameter parametric study**

As was highlighted in Table 7.3, the insulated specimen presents significantly more variables to be considered when trying to manage energy flows from the lubricant to the surrounding structure. This section therefore investigates the significance of different variables in isolation when implemented onto the insulated 100 mm outer diameter specimen. The baseline values for each of the variables are listed below:

- Insulator thermal conductivity: 0.262 W m<sup>-1</sup> K<sup>-1</sup>
- Insulator specific heat capacity: 1760 J kg<sup>-1</sup> K<sup>-1</sup>
- Substrate thermal conductivity: 193 W m<sup>-1</sup> K<sup>-1</sup>
- Substrate specific heat capacity: 900 J kg<sup>-1</sup> K<sup>-1</sup>
- h<sub>contact</sub>: 150 W m<sup>-2</sup> K<sup>-1</sup>
- Insulator thickness: 2 mm

Table 7.8 shows the change in energy transferred from the lubricant to the test block specimen as a result of changing the substrate material's specific heat capacity and

thermal conductivity. Compared to the data presented in Table 7.7, one can see the same trends are observed. The specific heat capacity of the material remains the dominant variable relative to the substrate thermal conductivity although the effect on thermal losses from the lubricant is reduced relative to the uninsulated case. For the same changes in specific heat capacity, the change in thermal losses from the lubricant are reduced to between -10% and 12% (Table 7.8) as opposed to -17% and +31% (Table 7.7). Similarly the sensitivity to the substrate thermal conductivity is reduced; a reduction in thermal conductivity from  $193 \text{ W m}^{-1} \text{ K}^{-1}$  to  $35 \text{ W m}^{-1} \text{ K}^{-1}$  (a reduction of over 80%) yielded only a 4.5 kJ reduction in thermal losses (less than 1%). The combined effect of varying such materials properties is again simulated by changing the material properties of the substrate from those of aluminium to those of cast iron (Table 7.2). The trend observed with the uninsulated results is repeated but with reduced sensitivity. Changing the substrate material from aluminium to cast iron increases the energy removed from the lubricant but by a reduced amount (a 5% increase from 0.48 MJ to 0.50 MJ rather than the 10% increase observed in the uninsulated scenario).

**Table 7.8: Predicted cumulative energy transferred from the lubricant to a 100 mm outer diameter test block specimen with a 2 mm thick Nylon 12 insert installed over 8000 seconds with a lubricant heating rate of 1200 W and a flow rate of  $10 \text{ l min}^{-1}$  while varying the substrate specific heat capacity and thermal conductivity**

<u>Specimen substrate property variation</u>	<u>Cumulative energy transferred to specimen (MJ)</u>	<u>% change (relative to baseline)</u>
Baseline aluminium substrate material properties $C_p = 900 \text{ J kg}^{-1} \text{ K}^{-1}$ $K = 193 \text{ W m}^{-1} \text{ K}^{-1}$	0.48	
$C_p = 480 \text{ J kg}^{-1} \text{ K}^{-1}$	0.43	-10%
$C_p = 1800 \text{ J kg}^{-1} \text{ K}^{-1}$	0.54	12%
$K = 35 \text{ W m}^{-1} \text{ K}^{-1}$	0.48	1%
$K = 386 \text{ W m}^{-1} \text{ K}^{-1}$	0.48	0%
Cast iron	0.50	+5%

Table 7.9 shows how the energy transferred to the test block specimen responds to changes in the insulator material properties. It can be seen how, relative to the trends observed when varying the substrate material properties (i.e. the aluminium), the sensitivity of the material properties is reversed when considering the insulator. Halving the specific heat capacity from  $1760 \text{ J kg}^{-1} \text{ K}^{-1}$  to  $880 \text{ J kg}^{-1} \text{ K}^{-1}$  only reduces the energy transferred from the lubricant to the specimen by just under 2 kJ (less than 1%) whereas a similar reduction in the specific heat capacity of the substrate (Table 7.8) achieved a 10% reduction in thermal losses. This is despite the sensitivity to substrate material properties being reduced in the insulated scenario. A similar

trend is observed when increasing the specific heat capacity of the insulator to 3520 J kg<sup>-1</sup> K<sup>-1</sup> (a doubling of the baseline value) which results in only a 1% increase in energy transferred.

The thermal conductivity of the insulator is a much more significant parameter than the insulator specific heat capacity; a direct contrast to the behaviour of the substrate in both the insulated and uninsulated studies. In halving the value of the thermal conductivity of the insulator from 0.262 W m<sup>-1</sup> K<sup>-1</sup> to 0.131 W m<sup>-1</sup> K<sup>-1</sup> the energy transferred to the specimen was reduced from 0.48 MJ to 0.37 MJ; a 23% reduction in energy transferred. Similarly, if the thermal conductivity of the insulator was doubled, then the energy transferred increased to 0.56 MJ (an increase of 17%).

**Table 7.9: Predicted cumulative energy transferred from the lubricant to a 100 mm outer diameter test block specimen with a 2 mm thick Nylon 12 insert installed over 8000 seconds with a lubricant heating rate of 1200 W and a flow rate of 10 l min<sup>-1</sup> while varying the insulator specific heat capacity and thermal conductivity**

<u>Insulating insert property variation</u>	<u>Cumulative energy transferred to specimen (MJ)</u>	<u>% change (relative to baseline)</u>
Baseline insulator material properties Cp = 1760 J kg <sup>-1</sup> K <sup>-1</sup> K = 0.262 W m <sup>-1</sup> K <sup>-1</sup>	0.48	
Cp = 880 J kg <sup>-1</sup> K <sup>-1</sup>	0.48	0%
Cp = 3520 J kg <sup>-1</sup> K <sup>-1</sup>	0.48	+1%
K = 0.131 W m <sup>-1</sup> K <sup>-1</sup>	0.37	-23%
K = 0.524 W m <sup>-1</sup> K <sup>-1</sup>	0.56	+17%

The response of the model to the variation in material parameters presents an overall trend that indicates, during warm-up, that the specific heat capacity of the specimen and that the thermal conductivity of the insulator (if present) should be minimised in order to minimise thermal losses from the lubricant to the surrounding metal. The specific heat capacity being as low as possible accelerates the rate of specimen heating and therefore reduces the temperature differential between the lubricant and specimen faster (thus reducing the heat flux). Such an effect is limited to the transient phase and during steady state situations, the heat transfer from the lubricant to the specimen would be a function of the thermal conductivity only. A lower thermal conductivity material results in a higher temperature gradient through the thickness of the test block specimen. The outer surface temperature of the test block specimen is limited by the ambient temperature and therefore a higher temperature gradient through the test block specimen must increase the inner bore temperature (rather than decrease the outer surface temperature). Hence, the

temperature differential between the lubricant and the bore is reduced and the heat flow to the specimen from the lubricant reduces also.

Of interest though is why a low thermal conductivity is of greater significance in the insulating insert and a low specific heat capacity is of greater significance when considering the specimen substrate. The volume of an insulating insert with a 16 mm bore and a 2 mm wall thickness is only  $4.3 \times 10^{-5} \text{ m}^3$ , as opposed to  $3.58 \times 10^{-4} \text{ m}^3$  and  $2.86 \times 10^{-3} \text{ m}^3$  in the case of the two test block specimens (100 mm and 40 mm outer diameter). The thermal mass of the insert is governed, not by the specific heat capacity of the material, but by the small volume of material present. Comparatively, any variation in specific heat capacity of the substrate is multiplied by the large volume of material present and hence has a greater impact on the warm-up performance.

Comparatively, when looking at the thermal conductivity, the test block specimens made of aluminium are already a highly effective thermal conductor (as are most metals). There is therefore negligible temperature gradient across the radial thickness of the specimen. Consequently, variations in the thermal conductivity of the substrate material will have little effect on thermal losses through the lubricant until such point that the thermal conductivity is low enough to produce a noticeable thermal gradient through the specimen's thickness. Comparatively, the already low thermal conductivity of the baseline insulator creates a 27 °C temperature drop across the radial thickness of the specimen, equivalent to a temperature gradient of  $13.5 \text{ °C mm}^{-1}$ . Hence, either an increase or decrease in insulator thermal conductivity has a direct result on such a temperature gradient and has a subsequent impact on thermal losses from the lubricant.

One can either increase the thermal resistance of a particular body by reducing the material thermal conductivity or by increasing the thickness. It has been seen how the low thickness of the insulator, relative to that of the specimen, results in the thermal resistance of the material being of greater significance than any thermal mass considerations. Table 7.10 reinforces such a finding by showing the response of the model to variations in the thickness of the insulating insert. It can be seen that changing the insert thickness results in the heat flow to the test block specimen varying by orders of magnitude similar to those observed when the insert thermal conductivity was adjusted (Table 7.9). Relative to the baseline 2 mm thick insulation, halving the insulator thickness to 1 mm increases the energy flow to the specimen by 11%. Comparatively, if one increases the thickness of the insulation to either 3 mm or 4 mm then the energy transferred from the lubricant can be reduced by 10% or 17% respectively. This confirms that it is the thermal resistance of the insert that is critical in reducing energy flow from the lubricant rather than the insulating insert's thermal mass. Of note is how the simulations presented in Table

7.10 all utilise a value for  $h_{contact}$  of  $150 \text{ W m}^{-2} \text{ K}^{-1}$  and both the experimental results (Chapter 5) and theoretical correlation (Chapter 6) highlighted how the contact resistance is a significant factor in achieving the insulation benefit. Thus, Table 7.10 also presents a simulation for a high thickness insulating insert of 5 mm but with a much higher value of  $h_{contact}$  ( $10000 \text{ W m}^{-2} \text{ K}^{-1}$ ) to simulate almost perfect contact between the specimen and insert. It must be highlighted that it is likely to be impractical to install an insert of such a thickness owing to the need to over bore the gallery of an engine to accommodate the thickness of the insulating insert. Indeed, similar concerns exist in relation to the installation of an insert with 3 mm or 4 mm wall thickness. However, in carrying out such a simulation, an understanding is developed as to whether the effect of the contact resistance is able to be replicated using additional insulating material. It can be seen that a 5 mm thick insert in perfect contact with the surrounding metal achieves a comparable performance to that of a 3 mm thick insert with the experimentally correlated contact resistance and that the contact resistance provides the equivalent insulating effect of increasing the thickness of the Nylon insert by 2 mm. Thus, while, the insulating effect of the contact resistance can be replicated with an increased thickness of insulating material, other design constraints related to the engine would currently prevent such an approach being achievable.

**Table 7.10: Predicted cumulative energy transferred from the lubricant to a 100 mm outer diameter test block specimen with a Nylon 12 insert installed over 8000 seconds with a lubricant heating rate of 1200 W and a flow rate of  $10 \text{ l min}^{-1}$  while varying the insert thickness**

<u>Insulating insert thickness variant</u>	<u>Cumulative energy transferred to specimen (MJ)</u>	<u>% change (relative to baseline)</u>
Baseline = 2 mm	0.48	
1 mm	0.53	+11%
1.5 mm	0.5	+5%
3 mm	0.43	-10%
4 mm	0.47	-17%
5 mm and $h_{contact} = 10000 \text{ W m}^{-2}$	0.43	-10%

Table 7.11 presents results showing the effect of varying  $h_{contact}$  on the energy transferred to the specimen from the lubricant. It can be seen how halving the heat transfer coefficient from  $150 \text{ W m}^{-2} \text{ K}^{-1}$  to  $75 \text{ W m}^{-2} \text{ K}^{-1}$  reduces the energy transferred to the lubricant by 18%, to 0.39 MJ. This is similar in performance to halving the thermal conductivity of the insulator (Table 7.9) but is more technically viable and is not limited by attempting to source a material that provides such a high thermal resistance while still having an acceptable peak operating temperature. Similarly, by doubling the contact heat transfer coefficient, one observes a 13% increase in the energy transferred to the specimen.

The significant effect of the contact heat transfer coefficient has implications on the validity of both the computational simulation findings and also the likelihood of success if such an insulation strategy were to be adopted in I.C. engines. It was discussed in Section 5.7 and Section 6.5.4 how Nylon 12 has a dissimilar coefficient of thermal expansion to aluminium 6082. Indeed, Nylon 12 (CoE between  $10 \times 10^{-5}$  and  $16 \times 10^{-5} \text{ }^\circ\text{C}^{-1}$ ) [97, 98] is seen to exhibit a coefficient of thermal expansion over four times that of aluminium 6082 (CoE  $2.3 \times 10^{-5} \text{ }^\circ\text{C}^{-1}$ ) [93]. As a result of different coefficients of thermal expansion for the two materials it is highly likely that the value of  $h_{contact}$  will vary across the temperature range of the test. Consequently, the model in its current form, with only a single value of  $h_{contact}$  for each test does need to address, in future work, the variation of  $h_{contact}$  with temperature. Having seen how the thermal losses from the lubricant to the test block specimen are so sensitive to the value of  $h_{contact}$  there is also a need to consider the effect of other parameters on the value of  $h_{contact}$ . This would include the initial fit between the insert and the surrounding metal and also the impact of the mating surfaces' surface roughness. The current methodology of manufacturing the engine block is to high speed drill the main gallery in to the block after it has been cast and one would therefore not expect dimensional tolerance to be greater than +/- 0.5 mm. The sensitivity that the thermal losses from the lubricant to the test block specimen exhibit to the clearance between the bore and the insulating insert has already been highlighted in Section 5.6 and Section 5.7 and places a limitation on the accuracy of being able to predict the thermal losses from the lubricant for a given material combination. However, based on the results presented in Table 7.10, it would be possible to observe variations in thermal losses from the lubricant to the gallery wall of up approximately 5% (the change in thermal losses observed as a result of a 0.5 mm change in dimension), between two engine blocks of the same nominal dimensions. Greater dimensional control would be achievable were the inserts secured in to the engine block however this would reduce the insulating effect and therefore increase the thermal losses from the lubricant.

**Table 7.11: Predicted cumulative energy transferred from the lubricant to a 100 mm outer diameter test block specimen with a 2 mm thick Nylon 12 insert installed over 8000 seconds with a lubricant heating rate of 1200 W and a flow rate of  $10 \text{ l min}^{-1}$  while varying the value of  $h_{contact}$**

<u><math>h_{contact}</math> variation</u>	<u>Cumulative energy transferred to specimen (MJ)</u>	<u>% change (relative to baseline)</u>
Baseline $h_{contact} = 150 \text{ W m}^{-2}$	0.48	
$75 \text{ W m}^{-2} \text{ K}^{-1}$	0.39	-18%
$110 \text{ W m}^{-2} \text{ K}^{-1}$	0.44	-8%
$225 \text{ W m}^{-2} \text{ K}^{-1}$	0.52	8%
$300 \text{ W m}^{-2} \text{ K}^{-1}$	0.54	13%

Thus from this work, it can be seen that in order to minimise the heat transfer from the lubricant to the specimen, one must aim to reduce the specific heat capacity of the substrate, increase the contact resistance between the substrate material and the insert or decrease the thermal conductivity of the insulating insert. Reducing the substrate specific heat capacity by 46% resulted in a 10% reduction in energy transferred to the test block specimen while a reduction of 50% in the insulator thermal conductivity and the contact resistance reduced the heat flow to the test block specimen by 23% and 18% respectively. However, achieving reductions in the thermal conductivity of the insulating insert beyond  $0.26 \text{ W m}^{-1} \text{ K}^{-1}$  is a significant material challenge if one looks at the limited scope for alternative materials in the material selection chart shown in Figure 2.5 of Chapter 2. The most effective and practical method of reducing heat flow from the lubricant to test block specimen when insulation is applied is to focus on increasing the contact resistance.

#### **7.2.2.2.2 100 mm outer diameter fully Nylon test block specimen**

The results presented in this chapter have indicated how it is desirable to reduce the specific heat capacity of the surrounding material of engine oil galleries in order to reduce thermal losses and aid warm-up. It has been seen how that, where an insulating insert is not present, reducing the specific heat capacity of the surrounding material is the most effective strategy while, where an insulating insert is present, one would aim to also reduce the thermal conductivity of the insulating insert or reduce the value of  $h_{contact}$ . While there has only been limited investigations into the extensive use of polymeric materials in engine applications [72, 74], a hypothetical scenario worthy of investigation is the relative performance of manufacturing the entire surrounding structure out of polymeric materials. Thus, a simulation was conducted whereby the material properties of the test block specimen were changed to match those of Nylon 12. A consequence of such a strategy is the removal of any potential benefit of a contact resistance but instead, the surrounding structure benefits from both a low thermal conductivity and low specific heat capacity. The result, shown in Figure 7.2, suggests that, were such a material choice possible, the energy transferred from the lubricant to the specimen could be reduced from 1 MJ (a baseline uninsulated aluminium test block specimen) to 0.22 MJ with a full Nylon insert; a reduction of 78%. Simulations of the baseline insulated scenario (a 2 mm thick Nylon 12 insert with a contact heat transfer coefficient of  $150 \text{ W m}^{-2} \text{ K}^{-1}$ ) predicted that 0.48 MJ of energy would be transferred from the lubricant to the specimen. Thus, manufacturing the entire thickness out of Nylon still represents a potential reduction in energy losses, relative to when an insulating insert is installed of 0.26 MJ (54 %). Such a simulation assumes that an equal volume of material is present. It is likely that a higher volume of material would be required to satisfy stiffness constraints were a fully polymeric solution

employed (the literature review highlighted that the stiffness of glass fibre reinforced resin systems could be up to 80% lower than that of aluminium). However, given the predicted benefits, one would still expect a reduced heat flow from the lubricant even if an increased volume, and hence mass of polymer, was needed to satisfy other design constraints.

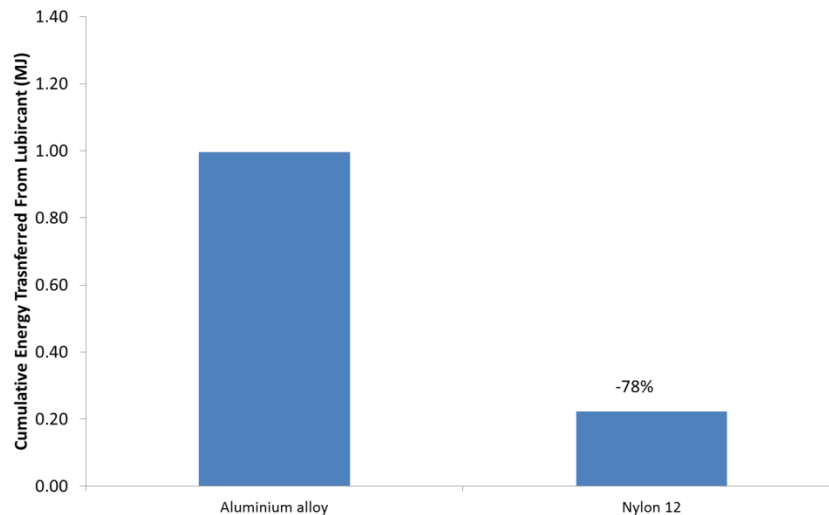


**Figure 7.2: Cumulative energy transferred from the lubricant to a 100 mm outer diameter test block specimen over 8000 seconds with a lubricant heating rate of 1200 W and a flow rate of 10 l min<sup>-1</sup> with aluminium alloy and Nylon 12 test block specimens**

### **7.2.2.2.3 The effect of insulating material thermal property variation caused by supplier variation and changes in operating temperature**

Table 7.12 presents data that shows how the variation in the thermal properties of Nylon 12, from different suppliers, affects the thermal losses from the lubricant. It can be seen that for the same nominal grade of Nylon 12, predicted variations of up to 4% are observed relative to the baseline material properties. Similarly, if one examines Table 7.13, it can be seen how a 4% increase in thermal losses is predicted if one uses the Ensinger material values as opposed to the baseline values presented in Table 3.2 while a 4% reduction in thermal losses is observed if one uses the Ensinger material properties for Nylon 6. Thus, if such technology were to be implemented into an I.C. engine, it must be accepted that the actual reduction in thermal realised would be subject to at least a 4% uncertainty. However, the magnitude of such uncertainty should be compared against the thermal benefits already realised throughout the work in this thesis. It has already been observed in Chapter 5 that reductions in thermal losses of up to 58% have been achieved as a result of optimising the insulating mechanism. In the instance where the contact resistance alone was installed by using a plain aluminium insert, a reduction of 27%

was achieved. Thus, the uncertainty introduced as a result of variation in either Nylon grade or supplier is not felt to be detrimental to the findings already reported.

**Table 7.12: Predicted cumulative energy transferred from the lubricant to a 100 mm outer diameter test block specimen with a Nylon 12 insert installed over 8000 seconds with a lubricant heating rate of 1200 W and a flow rate of 10 l min<sup>-1</sup> using different supplier material data**

<u>Supplier data</u>	<u>Cumulative energy transferred to specimen (MJ)</u>	<u>% change (relative to baseline)</u>
Baseline (Table 3.2)	0.48	
Ensinger	0.50	+4%
PAR	0.46	-4%

**Table 7.13: Predicted cumulative energy transferred from the lubricant to a 100 mm outer diameter test block specimen with a Nylon insulating insert installed over 8000 seconds using the thermal properties for different grades of Nylon with a lubricant heating rate of 1200 W and a flow rate of 10 l min<sup>-1</sup>**

<u>Supplier data</u>	<u>Cumulative energy transferred to specimen (MJ)</u>	<u>% change (relative to baseline)</u>
Baseline (Table 3.2)	0.48	
Ensinger Nylon 12	0.50	+4%
Ensinger Nylon 6	0.46	-4%

Table 7.14 presents data summarising the effect that the variation in Nylon 12 properties with temperature have on predicted thermal losses from the lubricant. It can be seen how, relative to the Arkema data for Nylon 12 at 30 °C, that using the Nylon 12 properties quoted for 130 °C results in the thermal losses increasing by 5% and would hence be comparable in effect to replacing the aluminium test block specimen with one manufactured from cast iron (Table 7.7) or reducing the insert by 0.5 mm in thickness in terms of the percentage change in thermal losses. Also presented in Table 7.14 is a third simulation, denoted 'Arkema Nylon 12 hybrid'. In this simulation the specific heat capacity and density were input as the values at 130 °C but the thermal conductivity was held at the value for 30 °C (0.21 W m<sup>-1</sup> K<sup>-1</sup>). It can be seen that as a result of such a simulation, the thermal losses from the lubricant to the test block specimen only increase by 0.45%; further confirming the findings in Section 7.2.2.2.1 that the insulating material thermal conductivity is the dominant parameter over the insulating material specific heat capacity. This is despite the specific heat capacity increasing by 56% relative to only a 14% change in thermal conductivity (0.21 W m<sup>-1</sup> K<sup>-1</sup> increasing to 0.24 W m<sup>-1</sup> K<sup>-1</sup>) and the density decreasing by 3%. It must be borne in mind when considering these results, that the simulations conducted for the purposes of the data in Table 7.14 assume that the high

temperature material properties have been active throughout the duration of the test simulation whereas the properties would progressively change from the low temperature values to the high temperature values were the physical test carried out. The actual effect on thermal losses from the lubricant as a result of accounting for thermal property variation of the polymer would therefore be reduced.

Thus, while the magnitude of the uncertainty produced through the change in polymer thermal properties with temperature needs consideration, it is again felt that such uncertainty is not overly detrimental to the findings presented in this thesis. When compared to the reductions in thermal losses achieved of up to 58% through the implementation of gallery insulation, the sensitivity to the changing thermal properties of polymers with temperature are relatively small and the 5% variation observed is a worst case scenario and would likely be smaller.

However, it should be highlighted as scope for further work, to account for such variations in material thermal properties with temperature in the simulation model in order to remove such uncertainty from the results.

**Table 7.14: Predicted cumulative energy transferred from the lubricant to a 100 mm outer diameter test block specimen with different grades of Nylon insulating insert installed over 8000 seconds with a lubricant heating rate of 1200 W and a flow rate of 10 l min<sup>-1</sup>**

<u>Supplier data</u>	<u>Cumulative energy transferred to specimen (MJ)</u>	<u>% change (relative to baseline)</u>
Arkema Nylon 12 (30 °C)	0.45	
Arkema Nylon 12 (130 °C)	0.47	+5%
Arkema Nylon 12 Hybrid	0.45	+0.45%

### 7.3 The significance of flow geometry on heat transfer

The experimental results presented in Chapter 5 explored, in depth, the potential methods of insulating engine lubricant from the surrounding metal structure. Through the oil flow rig, comparable conditions to that found in the main engine oil gallery of a typical I.C. engine were replicated with a 16 mm diameter bore gallery that is 380 mm in length. Both experimental and theoretical results have been presented and discussed for this particular scenario in in Chapter 5 and Chapter 7 (Section 7.2). However, it has already been discussed how the lubricant circuit within an I.C. engine is variable and there is therefore a need to consider the effects that such variations in geometry have on heat transfer from the lubricant to the surrounding metal structure.

The variations in gallery geometry, first shown in Figure 1.17, can affect the heat transfer mechanisms from the lubricant to the surrounding structure in two ways. It is worth remembering that the thermal energy transferred from the lubricant to the surrounding metal is defined by:

$$Q_{convection} = h_{oil}2\pi r_{inner}dx(T_{average} - T_{inner})\delta t$$

**Equation 7.2: Convective heat transfer from the lubricant to the gallery wall**

Consequently, a variation in the gallery diameter will affect the value of  $Q_{convection}$  by means of the impact of  $r_{inner}$ . Thus, an increase in the diameter of a given gallery would be expected to increase the heat transferred to the metal by virtue of the greater heat transfer area. However, one must remember that the value of  $h_{oil}$  is also dependent on the flow geometry. It was established in Chapter 6 that the heat transfer coefficient is best represented by the Dittus and Boelter Nusselt Number correlation, defined in Equation 7.3, and that the heat transfer coefficient is related to the Nusselt Number by Equation 7.4. The complexity of the relationship is increased by the presence of the Reynolds Number term in the Nusselt Number. The oil flow rig was operated in a fixed volumetric flow rate situation and hence for a given volumetric flow rate the velocity of the fluid is inversely proportional to the square of the diameter. Equation 7.5 presents a derivation of how, accounting for the Reynolds Effect, the internal heat transfer coefficient would be proportional to  $D_{inner}^{-1.8}$ . It can therefore be seen that for a given temperature differential between the lubricant and test block specimen, an increase in the bore diameter of the oil gallery would result in the cumulative energy transferred from the lubricant to be proportional to  $D_{inner}^{-0.8}$ . Thus, this section of the thesis seeks to investigate the effect that variations in bore diameter (and hence surface area) and flow velocity have on the heat transferred from the lubricant to the surrounding structure.

The dependence of convective heat transfer mechanisms on the flow geometry has been the subject of engines research in the past, albeit in the case of the coolant circuit rather than the lubricant circuit. The exhaust port bridge of an engine is an area that is subject to very high temperatures and subsequently dictates the cooling requirements of the engine, particularly during high load and low speed scenarios. Both Finlay et al. [108] and Clough [107] trialled using a reduced cross sectional area to increase convective heat transfer to the coolant in the exhaust port bridge area. Finlay et al. [108] experimented with a precision cooled head and was, depending on location, able to reduce metal surface temperatures by up to 50 °C on a 1.1 litre S.I. engine while the work of Clough [107] reported reducing the peak temperature of the cylinder head from 172 °C to 143 °C on a 6 cylinder 24 valve engine. Exact values of the heat transfer coefficient were not available in either reference but Finlay et al. did indicate that by changing the coolant velocity from 1 m s<sup>-1</sup> to 5 m s<sup>-1</sup> it was predicted that the heat flux in the cylinder head would increase from 530 kW m<sup>-2</sup> to

1270 kW m<sup>-2</sup>, an increase of 140%. Such an increase was predicted for metal temperatures of 150 °C and the benefit was reduced in magnitude at lower metal temperatures. However, it has been shown that reducing the hydraulic diameter can increase heat transfer owing to the Reynolds Effect and hence the reverse effect in the lubricant circuit (i.e. reduce the convective heat transfer coefficient with a larger diameter) may be advantageous in reducing thermal losses from the lubricant

$$Nu = 0.023Re^{0.8}Pr^{0.4}$$

**Equation 7.3: Dittus and Boelter Nusselt Number**

$$h = \frac{Nu k}{D}$$

**Equation 7.4: Relationship of heat transfer coefficient to Nusselt Number**

$$v = \frac{V}{A} = \frac{4V}{\pi D_{inner}^2}$$

$$Re = \frac{v D_{inner}}{\nu_{lubricant}} = Re = \frac{4V D_{inner}}{\pi D_{inner}^2 \nu_{lubricant}} = \frac{4V}{\pi D_{inner} \nu_{lubricant}}$$

$$Nu \propto Re^{0.8}$$

$$Nu \propto (D_{inner}^{-1})^{0.8}$$

$$Nu \propto D_{inner}^{-0.8}$$

$$h \propto \frac{Nu}{D_{inner}}$$

$$h \propto \frac{D_{inner}^{-0.8}}{D_{inner}}$$

$$h \propto D_{inner}^{-1.8}$$

**Equation 7.5: Derivation of dependence of internal heat transfer coefficient on hydraulic diameter**

Thus, in the sections that follow, this chapter aims to isolate the effect of varying the convective heat transfer area from the effect of the flow geometry changing the heat transfer coefficient. A limitation of the work is that the oil flow rig (and hence the computational model) concentrate on pressurised flow through a gallery of given dimensions. There are regions of the engine where such a flow regime is not representative of the conditions within the I.C. engine. An example is the return galleries which enables lubricant to return from the head of the engine, back to the sump. The entry to the gallery at the top of the cylinder block is shown in Figure 7.3 and the lubricant in these galleries flows back to the sump by gravity. Hence, the lubricant drains down the side of the return galleries as a film that is only a few

microns in thickness. Thus an area for both future computational and experimental work would be to further the work presented in this thesis by specifically investigating the merits of applying insulation to the return galleries and lubricant film flow. This is especially relevant, given that a significant lubricant temperature decrease has been observed along the length of the return galleries in Figure 1.18.

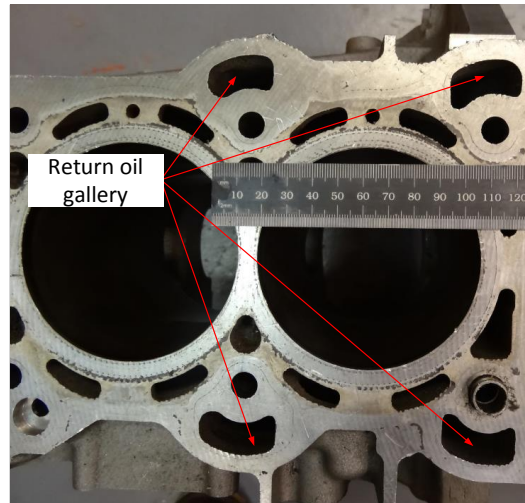
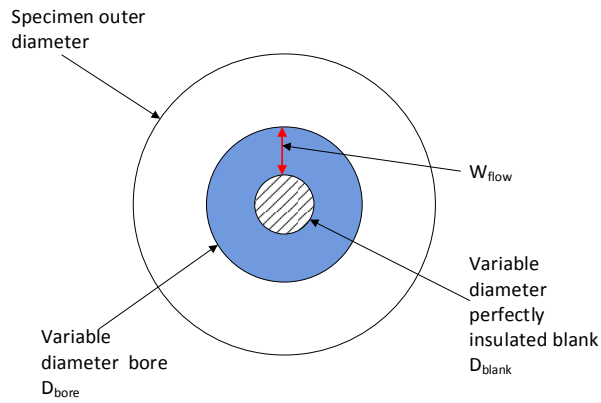


Figure 7.3: Typical return oil galleries on a 2.0 litre S.I. engine

### 7.3.1 The interaction between flow velocity and varying convective heat transfer area

One has established that the increase in surface area caused by increasing the bore diameter is counteracted by the Reynolds Effect of reducing the convective heat transfer coefficient. However, such an analysis ignores the effect that fluid properties can have on the heat transfer coefficient through the variation of viscosity and velocity (as a result of changing density) in a constant volumetric flow scenario.

Thus, to investigate the relative effects, the oil flow rig simulation was modified to enable the velocity of the fluid to be varied independently of the convective heat transfer area. To facilitate this, a thermally inert blank was placed in the mid flow of the test block specimen's bore, as shown in Figure 7.4. Thus, no heat transfer between the blank and the lubricant is modelled and hence adds no thermal inertia to the system. Instead, varying the size of the blank enables the velocity of the fluid to be varied independently of bore size. The lubricant flow rate was simulated at a constant  $10 \text{ l min}^{-1}$  and therefore, in order to maintain a constant volumetric flow rate through a restricted flow path, the velocity has to increase. In this investigative work, the outer diameter of the specimen was maintained at 100 mm while Table 7.15 details the combinations of bore diameter and blank diameter simulated with a heater power of 1200 W. The lubricant temperature commenced from a soak temperature of 28 °C while the specimen temperature commenced from a temperature of 20 °C.



**Figure 7.4: Schematic showing the use of a perfectly insulated blank to control fluid velocity independently of convective heat transfer area**

**Table 7.15: Flow cross sections examined using the oil flow rig simulation model at 1200 W heat input and 10 l min<sup>-1</sup> flow rate**

<u>Combination</u>	<u>D<sub>bore</sub> (mm)</u>	<u>D<sub>blank</sub> (mm)</u>	<u>W<sub>flow</sub> (mm)</u>	<u>Flow Velocity (m s<sup>-1</sup>)</u>
A	8.0	7.0	0.5	14.15
B	8.0	6.0	1.0	7.58
C	8.0	4.0	2.0	4.42
D	8.0	2.0	3.0	3.54
E	8.0	N/A	8.0	3.14
F	16.0	15.0	0.5	6.85
G	16.0	14.0	1.0	3.54
H	16.0	12.0	2.0	1.89
I	16.0	10.0	3.0	1.36
J	16.0	6.0	5.0	0.97
K	16.0	4.0	6.0	0.85
L	16.0	N/A	16.0	0.83
M	32.0	31.0	0.5	3.37
N	32.0	30.0	1.0	1.72
O	32.0	28.0	2.0	0.85
P	32.0	26.0	3.0	0.61
Q	32.0	22.0	5.0	0.40
R	32.0	20.0	6.0	0.34
S	32.0	N/A	16.0	0.21

### 7.3.1.1 Results

Figure 7.5 and Figure 7.6 show the cumulative energy transferred to the test block specimen for each of the cross section profiles detailed in Table 7.15. Figure 7.5 presents the results for an uninsulated bore while Figure 7.6 presents the results for a bore with a 2 mm thick Nylon 12 insert installed. In the case of the latter, the

contact heat transfer coefficient,  $h_{contact}$ , was set to the value of  $150 \text{ W m}^2 \text{ K}^{-1}$ , as derived in Chapter 6.

Across both the insulated and uninsulated results, one can see a constant trend of energy transferred to the specimen decreasing as the flow width,  $W_{flow}$ , increases. If one first examines the 8 mm uninsulated bore, it can be seen that as the flow width is increased from a 0.5 mm gap to an unrestricted 8 mm bore, the cumulative energy transferred to the specimen is reduced from 1035 kJ to 1025 kJ, a reduction of 1%. Comparatively, the 16 mm uninsulated bore sees a reduction from 1019 kJ to 996 kJ, a reduction of 2% as the bore is changed from a 0.5 mm gap to an unrestricted bore while the 32 mm diameter bore sees the energy transferred be reduce by 4%, from 1004 kJ to 961 kJ. Similar percentage changes are also observed when examining the changes presented in the insulated simulations in Figure 7.6.

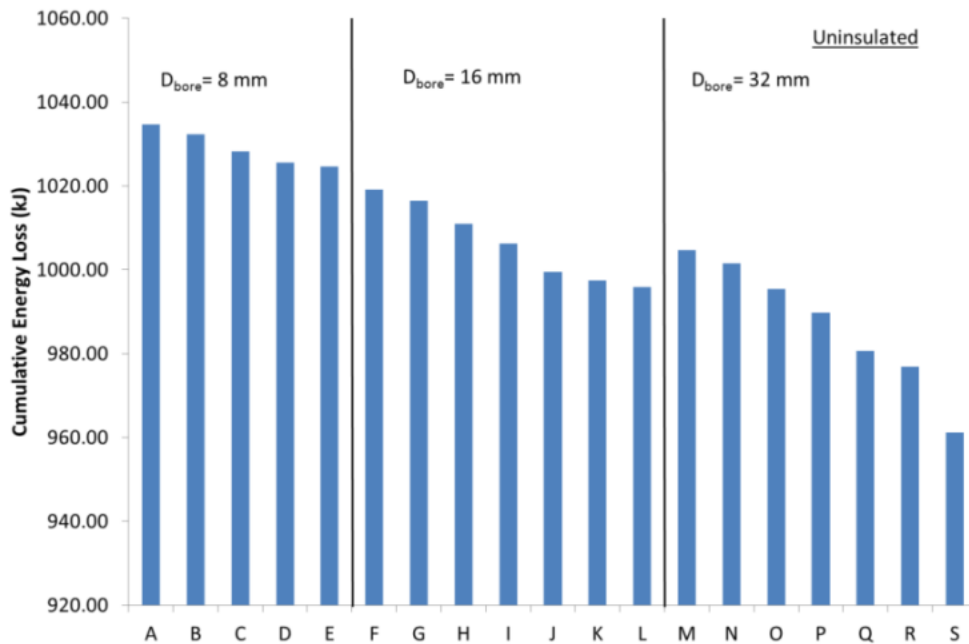


Figure 7.5: Cumulative energy transferred from the lubricant to the test block specimen in the oil flow rig simulation when testing bores of different diameters and flow velocities with  $10 \text{ l min}^{-1}$  flow rate and 1200 W heater input through an uninsulated test block specimen of 100 mm outer diameter

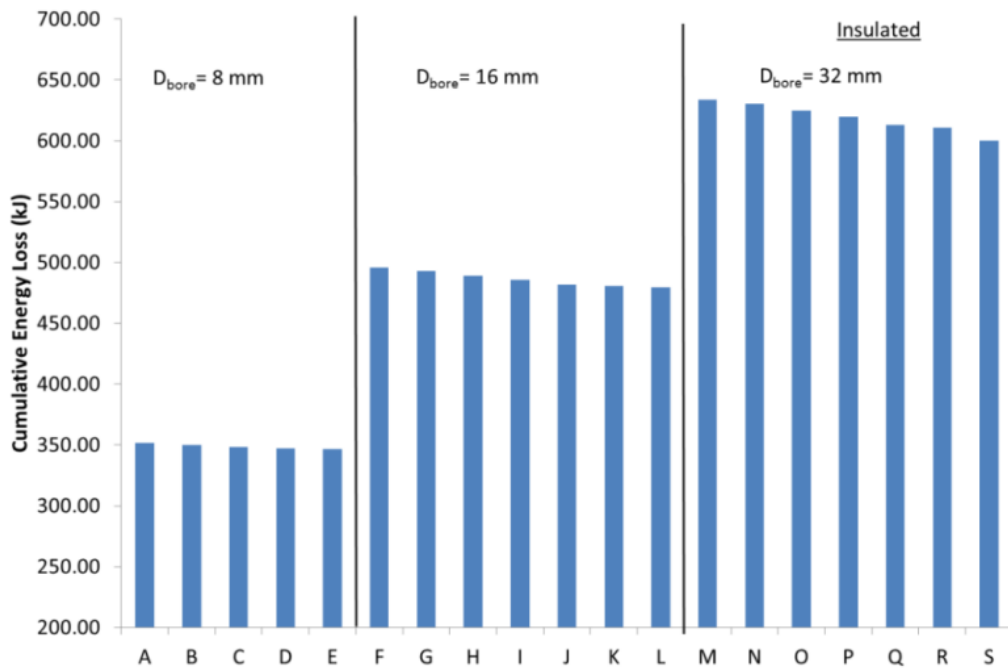


Figure 7.6: Cumulative energy transferred from the lubricant to the test block specimen in the oil flow rig simulation when testing bores of different diameters and flow velocities with  $10 \text{ l min}^{-1}$  flow rate and  $1200 \text{ W}$  heater input through a test block specimen of  $100 \text{ mm}$  outer diameter insulated with a  $2 \text{ mm}$  thick Nylon 12 insert

The changes discussed above occur as a result of a change in fluid velocity for a given convective heat transfer area. The flow restriction imposed increases the fluid velocity, as detailed in Table 7.15, and consequently increase the Reynolds Number of the fluid. Thus, the heat transfer coefficient increases. However, in both the insulated and uninsulated cases the magnitude of these changes are low in comparison with the effect of changing the bore diameter.

An interesting trend to note is the relative effect of the bore surface area when comparing the uninsulated results in Figure 7.5. It can be seen that during the transition from an unrestricted  $16 \text{ mm}$  bore (case L) to a  $32 \text{ mm}$  bore with a  $0.5 \text{ mm}$  flow gap (case M), the cumulative energy transferred to the specimen increases. Such a trend is to be expected between case L and case M, as the internal heat transfer area doubles and the convective heat transfer coefficient typically increases by 2.3 times.

The convective heat transfer area in case F was twice that seen in case E and the convective heat transfer coefficient also 1.5 times higher. Such trends would be expected to result in an increase in the energy transferred to the specimen from the lubricant and instead one observes a reduction in cumulative energy transferred when moving from case E to case F.

There are physical reasons as to why such an occurrence may happen. With a consistent outer diameter, a change in bore diameter would result in a slight change

in the thermal mass of the specimen. However the mass of a 16 mm bore diameter specimen would be expected to be 7.8 kg while an 8 mm diameter bore would be expected to have a mass of 8 kg. Thus, while the change in thermal mass may be contributory, this is unlikely to explain the trend between case E and case F.

The anomalous result between case E and F in Figure 7.5 can most likely be attributed to an over sensitivity in the theoretical model. Discussed in Chapter 6 was the development of an effective power methodology. Such an approach was required owing to the difficulty in modelling bespoke elements of the rig supporting hardware. Hence in order to focus on the heating of the lubricant and test block specimen it was found that an 'effective power' as a function of the specimen bore wall (Equation 6.13 in Chapter 6) was the best approach.

The function results in the power supplied to the rig in the simulation reducing as the specimen bore wall temperature rises and reflects the increasing heat flux to ambient from the rest of the rig. The function was optimised around extensive experimental data, all of which had a 16 mm bore diameter. In this work however, with the bore diameter varying there is evidence that the effective power function was too sensitive to changes in the specimen architecture.

The potential over sensitivity to the effective power function between case L and case M is likely to have been less significant owing to the higher order of magnitude change in the value of  $h_{oil}$ . To aid understanding as to why the cumulative energy transferred to the specimen decreases between cases E and F (an unexpected result) but increases between cases L and M, Figure 7.7 plots the instantaneous heat flux against time for the four following simulations:

- 8 mm unrestricted bore (case E).
- 16 mm bore with a 0.5 mm flow gap (case F).
- 16 mm unrestricted bore (case L).
- 32 mm bore with a 0.5 mm bore (case M).

If one first examines the change in performance between the 8 mm clear bore (shown in blue) and the heat flux with a 16 mm bore and a 0.5 mm flow gap (shown in red) it can be seen that, as expected, moving from the clear bore to the restricted flow with a higher surface area does result in a higher heat flux to the specimen. However this initial higher heat flux and accelerated heating of the bore wall causes the effective power supplied to the rig to be reduced much sooner. This results in a dramatic reduction in heat flux between the specimen and lubricant as the temperature differential between the lubricant and specimen subsequently reduces. A similar situation occurs during the transition from a 16 mm unrestricted bore (case L) to a 32 mm diameter bore with a 0.5 mm flow gap (case M). However, the differences in geometry between these two cases have been shown to result in a

greater change in the value of  $h_{oil}$  and hence the sensitivity of the model fails to mask the expected physical effect.

The structure of the model has been proven to produce reduced sensitivity to changes in flow geometry and the findings presented here are of a conservative nature. Consequently one would expect either higher velocity flow or a higher surface area to be of greater significance. However, while the concerns relating to the model's sensitivity remain valid, one can still draw meaningful insight from the comparison of the uninsulated results presented in Figure 7.5 with the insulated results presented in Figure 7.6.

The trends within the results presented in Figure 7.6 are more aligned to predictions. When comparing simulations of insulated specimens of the same diameter, the cumulative energy transferred from the lubricant to the specimen reduces as the flow gap widens and approaches that of an un-restricted bore. In moving from a 0.5 mm flow gap to an unrestricted 8 mm diameter bore one sees a 1% reduction from 351 kJ of energy transferred to the test block specimen to 347 kJ. Similarly the 16 mm diameter bore and 32 mm diameter bore see the energy transferred to the specimen reduce by 3% and 5% respectively as the flow restriction is reduced. Comparing the clear bore results in Figure 7.6 (cases E, L and S) showed that increasing the bore diameter from 8 mm to 16 mm results in a 38 % increase in the energy transferred to the specimen and a further 32 % increase results from increasing the bore diameter to 32 mm. From these results, it would appear that the convective heat transfer area is the dominant factor in dictating the flow of energy away from the lubricant rather than the flow velocity (which was the more dominant variable in the uninsulated results of Figure 7.5).

Worthy of discussion is why the insulated model appears less susceptible to the effective power being over sensitive to the effect of varying bore diameters. By installing the insulating insert, the effect is to de-couple the lubricant from the specimen and heat transfer is effectively between the lubricant and a 2 mm thick Nylon 12 insert. Thus, relative to an uninsulated specimen, the heating rate, and hence the effective power of specimens with a polymer insert bore wall is more consistent between different sized test block specimens.

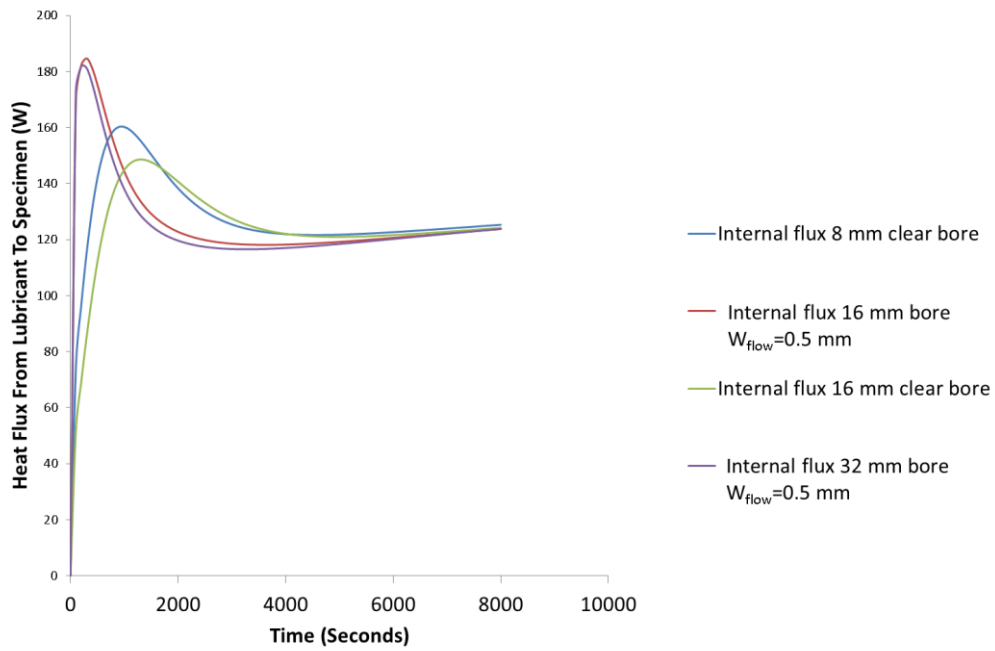


**Figure 7.7: Instantaneous heat flux from the lubricant to the 10 mm outer diameter test block specimen with varying bore diameters and flow gaps with a simulated lubricant flow rate of  $10 \text{ l min}^{-1}$  and a heater power of 1200 W**

Figure 7.5 and Figure 7.6 have both shown that, regardless of bore diameter, the heat transferred from the lubricant to the specimen reduces with falling fluid velocity. Thus, to appraise the merits of insulating different sized bores, the average cumulative heat transferred to the specimen for a given bore diameter across the spectrum of different flow velocities was calculated and compared between both the insulated and uninsulated scenario. These results are summarised in Table 7.16.

In the case of the 8 mm bore, the installation of an insulating insert has the potential to reduce the heat flow by a maximum of 66% while in the case of the baseline 16 mm diameter bore, the benefit reduces to 52% and this reduces further to a 38% improvement in the case of a 32 mm diameter bore. Thus, while the results indicate that the higher heat transfer coefficient dominates over the effect of a higher heat transfer area in the uninsulated scenarios, the results also indicate that insulation serves the greatest benefit in smaller diameter and high heat transfer coefficient regions.

**Table 7.16: Cumulative energy transferred from the lubricant to an insulated and uninsulated 100 mm outer diameter specimen when simulating different bore diameters with varying velocities when the lubricant flow rate is simulated to be 10 l min<sup>-1</sup> and the heater power simulated to be 1200 W**

<u>Bore diameter (mm)</u>	<u>Cumulative energy transferred to specimen uninsulated (kJ)</u>	<u>Cumulative energy transferred to specimen insulated (2 mm thick Nylon 12 insert) (kJ)</u>	<u>% Reduction</u>
8	1029	349	66%
16	1006	486	52%
32	987	616	38%

When studying the results presented in Table 7.16 one can see the apparent reversed trend of the energy transferred to the specimen increasing with bore diameter in the case of an insulated specimen and decreasing with bore diameter in the case of an uninsulated specimen. The discussion into these results has established that the overall effect of varying the flow geometry is governed by a complex combination of interrelations. These include varying the convective heat transfer area but also varying the convective heat transfer coefficient in an opposing manner by virtue of the variation in flow velocity. The situation is made more complex by any variation in the heat transfer coefficient as a result of flow geometry, altering the temperature profile of the fluid and thus having an even greater effect on the heat transfer coefficient. Such variations also affect the heat flow by virtue of changing the temperature differential between the lubricant and bore wall.

Such dynamic behaviour makes it very difficult to understand the exact cause of the switch in trends observed and to aid such understanding, the theoretical model was utilised using a static lubricant temperature scenario and this is discussed in Section 7.3.2.

### **7.3.2 Steady state lubricant temperature simulations**

To gain greater insight into the sensitivity of the cumulative energy transferred to the specimen, the simulation model of the oil rig was modified to operate in a semi-transient situation. In this work the lubricant temperature was held at a constant 90 °C and the specimen was heated from an initial soak temperature of 20 °C. The bore diameter was varied from the baseline 16 mm diameter to both 8 mm and 32 mm while the flow rate was maintained at 10 l min<sup>-1</sup>. Maintaining the lubricant at a constant temperature ensured both the Reynolds Number and heat transfer coefficient also remained constant throughout the duration of the test. Thus, any variation in heat flow from the lubricant to the specimen was purely as a result of changes in the flow geometry. Critically, such a strategy also removed any potential distortion on the predictions as a result of the effective power.

The simulations were conducted in both an insulated and uninsulated configuration for the three bore diameters specified above, using the convective heat transfer coefficients specified in Table 7.17. These values were determined by the model using the lubricant properties for dynamic viscosity and density at the constant temperature of 90 °C and therefore the variations in the values are a result solely of the varying cross sectional areas changing the velocity of the lubricant. The simulation conducted assumed that the insulation applied was a 2 mm thick Nylon 12 insert and thus, the contact coefficient between the Nylon and specimen was maintained at a constant 150 W m<sup>-2</sup> K<sup>-1</sup>. Figure 7.8 shows the cumulative energy transferred from the lubricant to the specimen for the three different bore diameters, both with and without insulation applied. It is important to note that the trend of the energy transferred to the specimen increasing with bore diameter in the insulated simulations but decreasing with the uninsulated specimens is still present. Indeed if one compares the insulated scenarios, the cumulative energy transferred from the lubricant to the specimen varies from 0.35 MJ with an 8 mm bore diameter to 0.59 MJ with a 32 mm bore diameter. Comparatively the uninsulated specimens predict 1.1 MJ of energy would be transferred from the lubricant to the specimen with an 8 mm bore and 0.93 MJ in the case of a 32 mm diameter bore.

The above results indicate that while the concerns about the effective power discussed in Section 7.3.1.1 are worthy of note, the issue has not affected the overall predicted trend (i.e. the energy transferred to the specimen decreases with increasing bore diameter in the case of uninsulated specimens and increases with increasing diameter in the case of insulated specimens).

**Table 7.17: Lubricant to specimen heat transfer coefficients for different bore diameters in the oil flow rig simulation when the lubricant temperature is maintained at a constant 90 °C and the flow rate maintained at 10 l min<sup>-1</sup>**

<u>Bore diameter (mm)</u>	<u>Lubricant to specimen heat transfer coefficient (W m<sup>-2</sup> K<sup>-1</sup>)</u>
8	1398.0
16	430.0
32	152.0

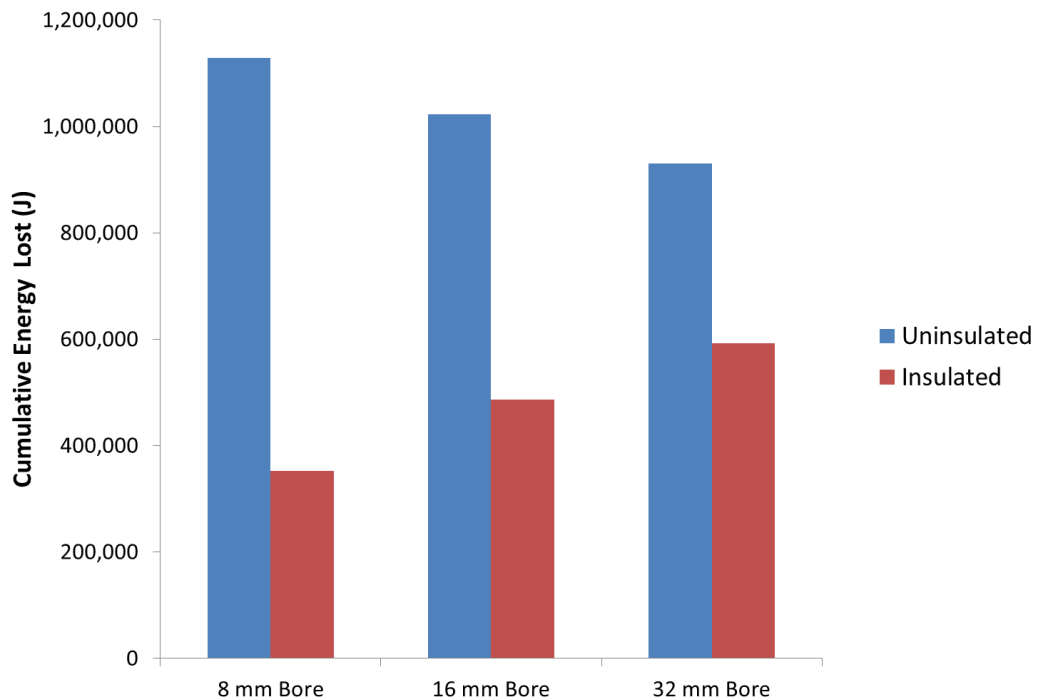


**Figure 7.8: Cumulative energy transferred from the lubricant to a 100 mm outer diameter specimen over 8000 seconds with differing test specimen bores when the lubricant is held at a constant temperature of 90 °C and a flow rate of 10 l min<sup>-1</sup>. The specimen is heated from a soak temperature of 20 °C while the insulation applied is a 2 mm thick insert of Nylon 12**

There is a need to understand why the energy transferred from the lubricant to the surrounding metal either increases or decreases with bore diameter depending on the presence or absence of insulation. Such a dynamic effect has major implications in understanding how to implement such technology effectively into an I.C. engine. One must remember that the quantity of energy transferred from the lubricant is governed by Equation 7.2. Within the equation are three variables:

- The convective heat transfer coefficient,  $h_{oil}$ .
- The convective area,  $2\pi r_{inner} dx$ , hence referred to in this section as,  $A$ ,
- The temperature differential between the lubricant and specimen bore wall,  $(T_{average} - T_{inner})$ , referred to as  $\Delta T$ .

For a test block specimen of a given bore, both the value of  $h_{oil}$  and the convective area is the same in these simulations. Hence, the change in trend must therefore result from the temperature differential. Table 7.18 lists the product of the heat transfer coefficient and convection areas for an 8 mm bore, 16 mm bore and 32 mm diameter bore. It can be seen that the product of the heat transfer coefficient and convection area in the case of the 8 mm bore is 1.63 times greater than in the instance of a 16 mm bore. Thus, if the energy transferred from the lubricant to the specimen is to be greater in the case of a 16 mm bore than in an 8 mm bore, the following condition must be satisfied:

$$\Delta T_{16} \geq 1.63\Delta T_8$$

**Table 7.18: Product of convective heat transfer coefficient and convective area for different bore diameters for lubricant held at 90 °C and flowing at 10 l min<sup>-1</sup>**

Bore Diameter (mm)	$h_{oil}A$ (W K <sup>-1</sup> )
8	13.37
16	8.21
32	5.80

Figure 7.9 shows the ratio of  $\Delta T_{16} : \Delta T_8$  for a 100 mm outer diameter specimen for both insulated and uninsulated scenarios. The green line represents the critical ratio of 1.63 where, above this point, a 16 mm bore has a higher heat flux than an 8 mm bore. Using this approach, it can be seen how the insulated case is always above the critical ratio and hence, the trend of a higher cumulative energy loss with a higher bore diameter is seen for insulated specimens in Figure 7.8. Comparatively, when one compares the uninsulated scenario, it can be seen how the critical ratio is only exceeded between 900 seconds and 3300 seconds. For the remainder of the test duration, the 8 mm bore has a higher heat flux than the 16 mm bore and hence, the cumulative energy transferred to the specimen, shown in Figure 7.8, is higher for an 8 mm uninsulated bore than it is for a 16 mm uninsulated bore.

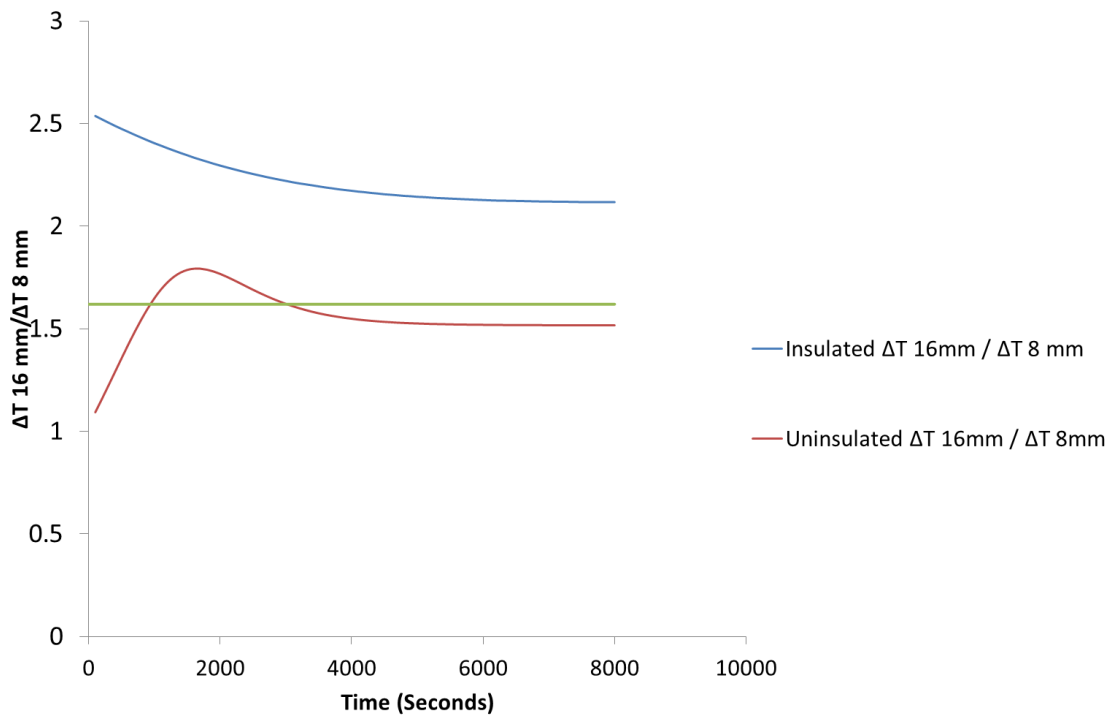


**Figure 7.9: Ratio of the temperature differential between the lubricant and specimen bore wall for bores of 8 mm and 16 mm diameter when heating a 100 mm outer diameter specimen from a soak temperature of 20 °C with lubricant at a constant temperature of 90 °C flowing at 10 l min<sup>-1</sup>**

Utilising the same logic, one can derive the critical temperature ratio for between a 16 mm bore and a 32 mm diameter bore. For a 32 mm bore to generate a higher heat flux than a 16 mm bore, the following condition must be met:

$$\Delta T_{32} \geq 1.42\Delta T_{16}$$

Figure 7.10 again shows how the ratio for the insulated case is always above that of the critical ratio meaning that the larger 32 mm diameter bore always has a higher heat flux than the 16 mm bore. Comparatively, in the case of the uninsulated specimens, it can be seen that the 32 mm diameter bore only has a higher heat flux between 2100 seconds and 2800 seconds.

It should be noted that the critical ratio is dependent on the flow rate and the temperature of the lubricant. The cases presented in this section are hypothetical examples, used to distinguish between the effects of fluid properties and the effects of geometry. In a situation where both the lubricant and specimen are being heated, the critical ratio at any given point will change owing to the changing fluid properties affecting the heat transfer coefficient.

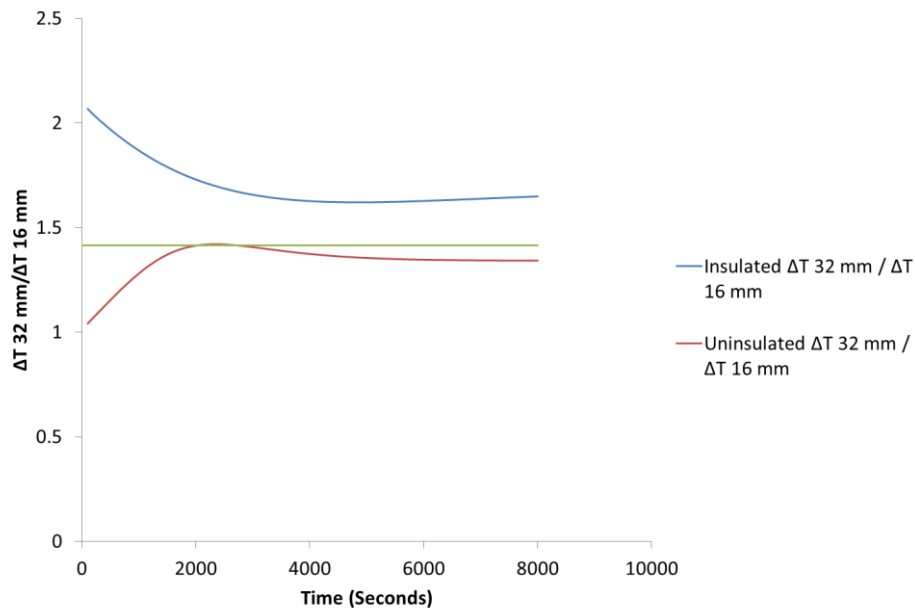


Figure 7.10: Ratio of the temperature differential between the lubricant and specimen bore wall for bores of 16 mm and 32 mm diameter when heating a 100 mm outer diameter specimen from a soak temperature of 20 °C with lubricant at a constant temperature of 90 °C flowing at 10 l min<sup>-1</sup>

### 7.3.2.1 Low flow rate steady state lubricant temperature simulations

The work presented in Section 7.3.2 explained how a variation in oil gallery bore diameter affects the heat transfer coefficient and convective heat transfer area in opposing manners. Whether the energy transferred from the lubricant increases or decreases is dependent upon the temperature differential between the lubricant

and specimen. This investigative work was all conducted at the baseline flow rate of  $10 \text{ l min}^{-1}$ . During such work it was seen that, without exception, an insulated oil gallery saw an increase in heat transferred from the lubricant to the specimen as the bore diameter increased. Conversely, uninsulated specimens showed a trend whereby the cumulative energy transferred from the lubricant to the specimen reduced with increasing diameter.

To establish that such a trend, and the explanations offered, is valid with different flow rates, the flow rate was reduced to  $2 \text{ l min}^{-1}$ . Figure 7.11 presents the cumulative energy transferred from the lubricant to the specimen for both insulated and uninsulated bores at a reduced flow rate of  $2 \text{ l min}^{-1}$ . It can be seen that once again, the cumulative energy transferred from the lubricant to the test block specimen rises with increasing bore diameter in the case of insulated specimens and reduces in the case of uninsulated specimens. In the uninsulated simulation it can be seen that the cumulative energy transferred to the specimen reduces by 0.09 MJ as the bore size increases from 8 mm to 12 mm and by 0.12 MJ as the bore size increases from 8 mm to 16 mm. This represents a percentage decrease from the 8 mm bore scenario of 10% and 14% respectively. Comparatively the insulated scenarios see the cumulative energy transferred from the lubricant increase by 0.05 MJ when increasing the bore from 8 mm to 12 mm and 0.09 MJ when increasing the bore diameter from 8 mm to 16 mm, a percentage change of 16% and 28% respectively.

From this additional study, the apparent trends and their associated physical explanations do appear to be repeatable and valid for different flow rates.

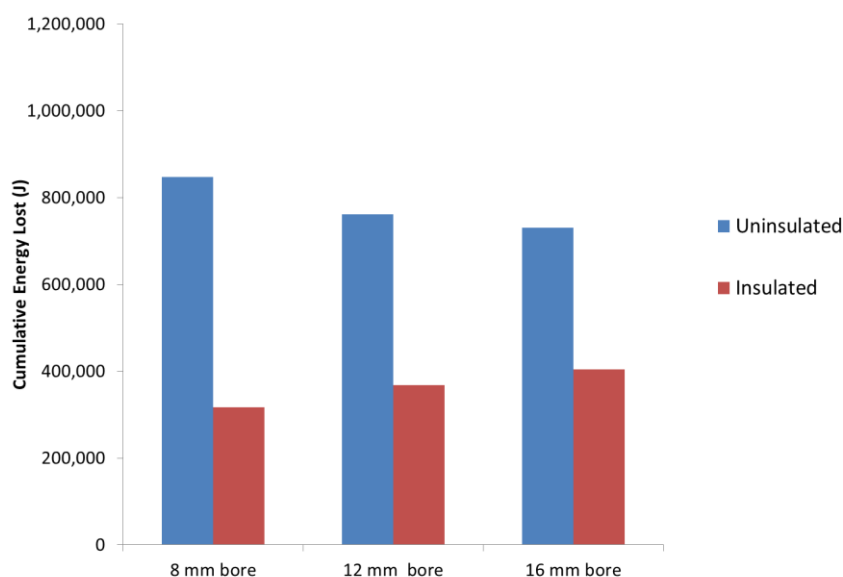


**Figure 7.11: Cumulative energy transferred from the lubricant to a 100 mm outer diameter specimen over 8000 seconds with differing test specimen bores when the lubricant is held at a constant temperature of  $90 \text{ }^\circ\text{C}$  and a flow rate of  $2 \text{ l min}^{-1}$  while the specimen is heated from a soak temperature of  $20 \text{ }^\circ\text{C}$ . The insulation applied is a 2 mm thick insert of Nylon 12**

## 7.4 Investigations into the effect of ambient temperature

Section 4.9 discussed investigations into the repeatability of the experimental rig. In the work, a 100 mm outer diameter uninsulated specimen was tested with a lubricant flow rate of  $10 \text{ l min}^{-1}$  and a heater input power of 1200 W. It was discussed how the temperature differential profile between the lubricant and test block specimen were in excellent agreement in the early phase of the test (prior to the peak temperature differential being achieved) but that the profiles deviated in the later regime of the test and resulted in a diverging trend that, at the termination of the test, was 2.5 °C higher. Such a trend was attributed to a variation in ambient temperature between the two tests and to validate such a hypothesis, the theoretical model was used to investigate the variation in temperature differential profile as a consequence of changing the ambient temperature. Figure 7.12 shows the temperature differential between the lubricant and test block specimen for the two tests presented in Figure 4.20 but in addition to the experimental data (shown in red and blue), the green and purple profiles show how the model would be expected to react to a change in ambient temperature. In the simulation of the June 2012 test, the ambient temperature and metal soak temperature were set to 20 °C while for the simulation of the June 2013 test the ambient temperature and metal soak temperature were set to 22.5°, in order to match the start conditions of the two experimental tests at the point the heater was activated. It can be seen how the model does capture the trend of the June 2012 experimental test reaching a higher peak temperature differential than the June 2013 simulation, thus validating the theory that the higher ambient temperature in the June 2013 test contributed to the specimen not being as heavily cooled by ambient and therefore reducing the temperature differential between the lubricant and the test block specimen.

Of concern is the continued divergence in trend of the two experimental results at the end of the test that is not reflected in the theoretical simulation. A limitation in the model is the use of a single ambient temperature and it is likely that the offset in ambient temperature between the two tests varied over the duration of the experimental procedure. Combined with an experimental set-up that was only able to log the initial soak temperature, it is not possible to comprehensively conclude that the divergence in the late regime of the temperature differential profile is a result of any change in ambient conditions. However, the model's verification of the change in peak temperature differential does suggest that this is a likely cause.

It is accepted that the absence of climatically controlled conditions around the experimental rig setup does limit both repeatability and hence confidence in the findings. However, using the simulation results discussed above, it has been possible to appraise the impact such changes have on the predicted cumulative energy flow

from the lubricant to the test block specimen over the time frame of the test. The simulation of the June 2012 test predicted that 1.0 MJ of energy would be transferred from the lubricant to the test block specimen over the duration of the 8000 second simulation (an average heat flux of 124 W). Comparatively, the June 2013 test with the warmer ambient conditions predicted that 0.95 MJ of energy would be transferred from the lubricant to the test block specimen over the same 8000 seconds (an average heat flux of 119 W). Such a change represents a 4% change in energy flow and while this is undesirable, and must be taken into consideration when appraising the results, it is must be compared relative to the magnitude of the changes in energy flows as a result of different insulation strategies

When comparing the findings to those reported in Table 7.7 it can be seen that the variations in energy flow predicted as a result of ambient temperature variation are equal in magnitude to those seen when varying the alloy grade between a wrought 6082 grade and a cast A319 grade. Thus, in using the model, it has been possible to investigate and quantify the effect of substrate material properties that would otherwise have been difficult to distinguish from experimental noise otherwise. However, if one compares the variation in heat flow observed in these simulations with the experimental results summarised in Table 5.2 it can be seen that the variations in energy flow observed as a result of different insulation strategies are far greater than any uncertainty introduced through a change in ambient temperature. The minimum change in energy flow to the specimen as a result of insulation strategies was 27% (127 W to 92 W). It is therefore felt that the variation observed through this simulation of ambient temperature, while acknowledging it introduces an undesirable cause of uncertainty into the results, is insufficient to discredit the overall conclusions from the experimental findings.

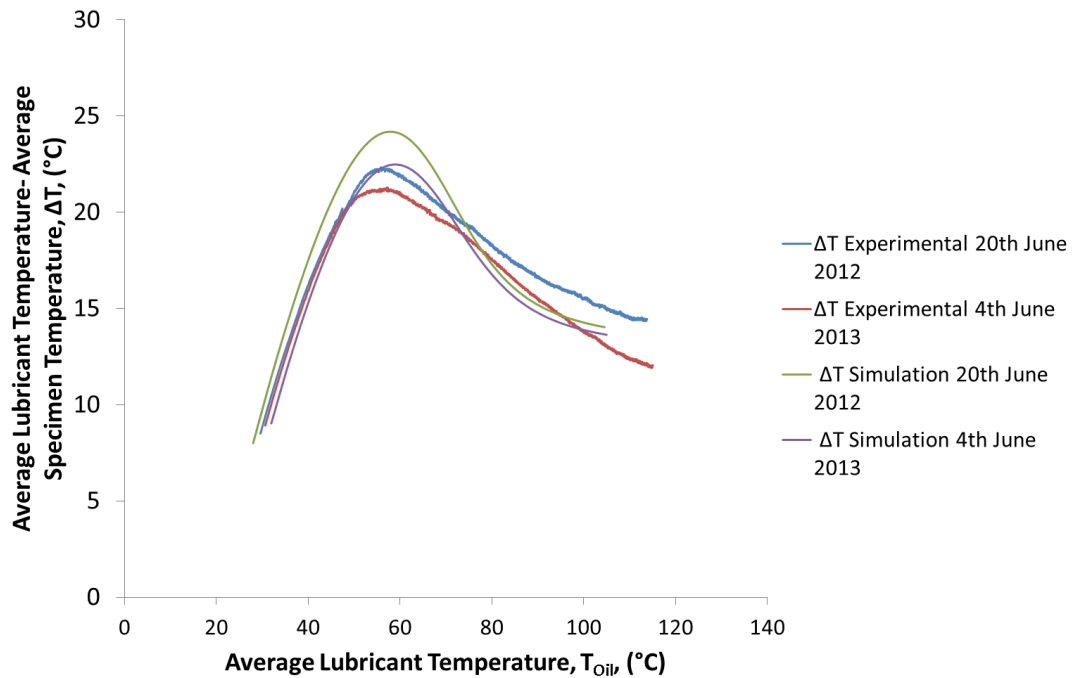


Figure 7.12: Temperature differential between the lubricant and test block specimen when using a 100 mm outer diameter uninsulated specimen with 1200 W heater input power and  $10 \text{ l min}^{-1}$  flow rate on two respective dates for both experimental data and theoretical data

## 7.5 Conclusions

### 7.5.1 Investigations in to the effect of material properties on energy flow

Through this chapter, it has been possible to gain a deeper understanding of the sensitivity of material properties into limiting the energy transferred from the lubricant to the surrounding structure. In addition to the experimental findings already reported, it has been seen how the specific heat capacity of the surrounding metal does have a significant effect on the total energy transferred from the lubricant to the surrounding metal structure. It was seen how, when simulating an uninsulated 100 mm outer diameter aluminium specimen, a total of 1 MJ of energy was transferred to the specimen from the lubricant. Reducing the specific heat capacity of the surrounding material by 46% can reduce total energy losses from the lubricant by 17%. Conversely, doubling the specific heat capacity of the surrounding material increases the energy losses from the lubricant by 31%. Comparatively, reducing the thermal conductivity of the specimen by 80% only reduced the thermal losses from the lubricant by 3%, with negligible change observed when increasing the thermal conductivity beyond the baseline value of  $193 \text{ W m}^{-1} \text{ K}^{-1}$ . The model predicts that the combined effect of these material property variations would result in a cast iron specimen (a material still used in diesel engines) removing 10% more energy from the lubricant than an aluminium specimen. The specific heat capacity remains the dominant variable when investigating the smaller 40 mm outer

diameter specimen with the same 46% reduction in specific heat capacity resulting in a 9% reduction in the energy transferred to the specimen. Meanwhile, reducing the thermal conductivity by 80% only results in a 1% reduction in thermal losses from the lubricant while a cast iron specimen removes 7% more energy from the lubricant than an aluminium specimen of equivalent size. A key validation of the experimental findings in this chapter was a comparative simulation of an uninsulated specimen manufactured from wrought aluminium 6082 T6 alloy (the same grade that the physical test block specimens were manufactured from) against a test block specimen manufactured from a cast A319 aluminium alloy that is typically used to manufacture I.C. engine blocks. The simulations showed that manufacturing the test block specimen from the A319 alloy, increased the thermal losses from the lubricant by between 2% and 4% depending on specimen size. Thus, while the grade of aluminium alloy does affect the energy losses from the lubricant, the order of magnitude of the change is insignificant relative to the changes observed as a result of insulation (between 27% and 60%). In addition, the changes observed are in line with those observed in the sensitivity study of different material parameters.

Investigations into the sensitivity of an insulated 100 mm outer diameter specimen indicated that again, the specific heat capacity of the substrate material is a significant parameter although its impact is reduced relative to an uninsulated specimen. Reducing the specific heat capacity of the substrate material by 46% reduced the energy removed from the lubricant by 10% while doubling the specific heat capacity increased the energy losses from the lubricant by 12%. The thermal conductivity of the specimen substrate material also remained an insensitive parameter with an 80% reduction in thermal conductivity achieving less than a 1% reduction in energy losses from the lubricant.

Comparatively the specific heat capacity of the insulator was found to be an insensitive parameter with less than 1% variation in the energy removed from the lubricant for a twofold increase or decrease in the specific heat capacity. Meanwhile, halving the thermal conductivity of the insulator resulted in a 23% reduction in thermal losses from the lubricant while doubling the thermal conductivity increased lubricant thermal losses by 17%

The thickness of the insulator has also been proven to be a significant factor with a doubling of the insulator thickness reducing lubricant thermal losses by 17% and halving the thickness, increasing losses by 11% relative to the 2 mm thick baseline.

As observed in the experimental results, the value of the contact heat transfer coefficient has the potential to reduce energy losses from the lubricant significantly. By halving the value of  $h_{contact}$ , thermal losses from the lubricant were reduced by 18% while doubling the heat transfer coefficient increased thermal losses from the lubricant by 13%.

In the hypothetical case of it being possible to manufacture regions of the engine block entirely out of polymeric materials, the simulations predicted that such a strategy could reduce thermal losses from the lubricant by 78% relative to an uninsulated aluminium baseline scenario.

Investigations into the variation in properties between different grades of Nylon and also Nylon of the same grade but from different suppliers have shown that the variation in properties are likely to affect thermal losses from the lubricant to the specimen by up to 4% relative to the baseline Nylon 12 result when 0.48 MJ of energy was seen to be transferred from the lubricant to the test block specimen. Using specific supplier data provided by Arkema it has also been observed how, when the variation in the thermal properties of the insulating insert as a result of the temperature increasing from 30 °C to 130 °C are investigated, that the cumulative energy flow from the lubricant to the specimen is seen to increase from 0.45 MJ to 0.47 MJ (an increase of 5%). Thus, in a warm-up simulation the effect would be reduced in magnitude owing to the gradual change in material properties, rather than assuming the more conductive scenario for the entire simulation. It has also been proven in this work, how the change in thermal conductivity of the insulating material is the dominant factor, rather than any change in the specific heat capacity.

Thus, from these findings it can be concluded that the following material selection and design criteria will achieve the greatest reductions in thermal losses from automotive lubricants:

- Use a block material with as low a thermal mass as possible (including aiming to replace metallic components with polymeric equivalents where possible).
- Where possible install an insulating insert with as low a thermal conductivity as possible and as high a thickness as possible.
- Design any insulating insert to have a low contact heat transfer coefficient (high contact resistance).

### **7.5.2 The significance of flow geometry on heat transfer**

Through the work presented in this chapter, a detailed examination has taken place into the effects of varying the flow geometry on transient heat transfer. Such changes have been proven to be complex owing to the dependency of the lubricant to specimen heat transfer coefficient on lubricant properties. It has been shown that, when the convective heat transfer area is held constant, the energy transferred to the test block specimen can be reduced as a result of reduced lubricant velocity. In both the insulated and uninsulated scenarios, it was found that the largest 32 mm diameter bore was most sensitive to velocity changes with the cumulative energy transferred to the specimen increasing by 5% (961 kJ to 1005 kJ) in the uninsulated

scenario as the velocity increased from  $3.37 \text{ m s}^{-1}$  to  $0.21 \text{ m s}^{-1}$  and by 6% in the insulated scenario (600 kJ to 634 kJ).

The effect of the bore surface area was shown to be more complex and the effect was dictated by the temperature regime the rig was being operated in. By increasing the gallery bore diameter, the surface area for heat transfer is increased but the convective heat transfer coefficient reduced owing to the reduced velocity of the lubricant. It was observed in the fully transient scenario, where both the lubricant and specimen were heated, that the uninsulated specimen showed reduced sensitivity to the surface area effects (shown in Figure 7.5) relative to the insulated specimen results (shown in Figure 7.6). While, the comparison between insulated and uninsulated scenarios does represent a variation in the thermal mass of the metal owing to over boring to accommodate the installation of an insulating insert, such a variation is unlikely to account for the change seen. The results presented therefore potentially indicate an over sensitivity in the model to the bore wall temperature owing to the effective power function. That said, the comparative nature of the results is still valid and does show that there is a greater reduction in energy loss to be achieved with small diameter galleries than with larger diameter galleries when the combined effect of differing heat transfer coefficients and heat transfer areas are considered. It was seen that when applied to an 8 mm diameter bore, a 2 mm thick Nylon 12 insert was able to reduce the energy transferred from the oil by 66% from 1025 kJ to 347 kJ. Comparatively, a 32 mm diameter bore saw only a 38 % reduction from 961 kJ to 600 kJ.

In carrying out simulations of holding the lubricant temperature constant and heating the specimen, it was seen how the temperature differential between the lubricant and surrounding specimen is pivotal in the observed change. Increasing the bore diameter from 8 mm to 32 mm for an insulated scenario saw the cumulative energy transferred to the specimen increase by 68% owing to the higher heat transfer area. Comparatively the uninsulated case saw the cumulative energy transferred to the specimen decrease by 15% for the same change in bore diameter. Such findings place confidence in the more dynamic model as the prediction of the trends reversing between the insulated and uninsulated simulations remain consistent, and hence mitigate concern that the effective power dominates predictions. For any insulation strategy to be effective, the thermal mass of concern (in this case the lubricant oil), must be hotter than the surroundings it is being insulated against. The absence of a heavily instrumented engine block makes it difficult to judge where in the engine this would happen but the experimental data from the test bed engine do indicate that the lubricant temperature reduces by up to  $5 \text{ }^{\circ}\text{C}$  along the length of the return. Such data suggest this is likely to be the most beneficial location to implement internal insulation.

It is felt that through this work, an important advancement in knowledge has been achieved in understanding the complexities of transient heat transfer including the conflicting effect of varying the bore diameter on heat transfer area and the heat transfer coefficient. Through the simulations carried out in Section 7.3 it has been shown that, depending on the magnitude of the temperature differential between the lubricant and bore wall, that an increase in the bore diameter can either increase the thermal losses from the lubricant (owing to an increased heat transfer area) or reduce the thermal losses owing to the lubricant's reduced velocity decreasing the convective heat transfer coefficient.

The simulations discussed in this work have centred on lubricant flow through galleries that are pressurised. However, there are regions of the engine where the lubricant is gravity fed and flows down the side of component surfaces. These include the return flows from the cylinder head and the main bearings (Figure 1.17). The flow in these regions is considerably different in nature with a thin film of lubricant draining down the walls in the case of the head return galleries and the return from the main bearings falling directly into the sump after being ejected from the bearing. In the case of the latter, the rotating crankshaft throws the lubricant around the block and hence, the unpredictable nature of this flow is outside the scope of the current model and would be an area for future work. The return galleries, with the data in Figure 1.18 having indicated that this is region where the greatest reduction in lubricant temperature occurs, is also an area for further modelling refinement to focus on; in particular the need to account for film flow rather than pressurised flow.

### **7.5.3 Investigations into the effect of ambient temperature**

Through simulations carried out on a 100 mm uninsulated outer diameter specimen it has been seen how variations in ambient temperature of 2.5 °C (equivalent in magnitude to those seen in experimental results) result in changes in energy flow of up to 4%. This compares with changes in energy flow of between 27% and 60% as a result of applying different insulation strategies to the bore wall. Thus, while the variations in ambient temperature are undesirable, it has been seen that the impact of such variations is insufficient to discredit the validity of the experimental findings.

## **8 Conclusions and scope for further work**

### **8.1 Conclusions**

#### **8.1.1 Experimental investigations into the effect of applying insulation on oil gallery thermal losses**

The use of the oil flow rig has been utilised to both appraise and understand the potential benefits of applying internal insulation to engine oil galleries. Through the use of variable sized specimens (a 100 mm outer diameter test block specimen and a 40 mm outer diameter test block specimen) it has been proven that the greatest thermal losses from the lubricant will occur in regions where the casting thickness is high and that the associated benefit of applying insulation is also reduced when insulating against a smaller mass. Such findings are based on the following key results:

- An uninsulated 100 mm outer diameter specimen (giving an effective wall thickness of 40 mm) transferred, on average, 124 W of energy from the lubricant to the specimen and this could be reduced by 56% to 54 W using a 2 mm thick Nylon 12 insert.
- An uninsulated 40 mm outer diameter specimen (giving an effective wall thickness of 10 mm) transferred, on average, 39 W of energy from the lubricant to the specimen and this could be reduced by 25% to 29 W using a 2 mm thick Nylon 12 insert.

#### **8.1.2 Experimental investigations into the effect of contact resistance on oil gallery thermal losses**

The installation of an insulating insert provides an insulating effect using more than just the low thermal conductivity of the chosen material. A contact resistance is also introduced at the interface of the insert and the surrounding metal structure. Through the work presented in this thesis, it has been seen how the contact resistance is an equally important insulating mechanism relative to the low thermal conductivity material. It was seen, using the 100 mm outer diameter specimen over a time frame of 10400 seconds, that a 2 mm thick aluminium insert was able to reduce the heat flux from the lubricant to the specimen by 27% relative to the uninsulated baseline of 127 W. Such a result is critical as there is no insulation benefit of a low thermal conductivity material, nor is there any change in thermal mass. Combining a high contact resistance with a low thermal conductivity material enabled the thermal losses from the lubricant to the specimen to be reduced by 58%. However, it is accepted that the differing coefficients of thermal expansion between the aluminium and Nylon 12, together with the Nylon 12 softening will reduce the contact resistance as temperatures rise. While investigations were carried out to assess the impact that the surface roughness of the internal bore would have on heat transfer, such work demonstrated only that its effect was

minimal relative to any variation in fit and subsequent contact resistance. Consequently such effects could not be determined from the experimental data.

### **8.1.3 Computational investigations into the effect of substrate material properties on oil gallery thermal losses**

The development of a correlated theoretical model has enabled the sensitivity of different material parameters to be investigated and understood. Where insulation has not been applied it has been observed how the specific heat capacity of the surrounding material (and thus the thermal mass of the substrate material) is of critical importance. Increasing the specific heat capacity of the substrate material results in thermal losses from the lubricant increasing while reducing the specific heat capacity of the substrate causes the thermal losses from the lubricant to decrease. From the baseline specific heat capacity value of  $900 \text{ J kg}^{-1} \text{ K}^{-1}$  the thermal losses were seen to increase by up to 31% as a result of doubling the specific heat capacity and reduce by 17% in response to a 47% reduction in specific heat capacity. The thermal losses from the lubricant to the test block specimen were far less sensitive to changes in the substrate thermal conductivity with an 80% reduction, from the baseline value  $193 \text{ W m}^{-1} \text{ K}^{-1}$ , only reducing the thermal losses by 3% while doubling the thermal conductivity only increased the thermal losses by 1%. Similar trends were observed in the case of the 40 mm outer diameter specimen simulations although the magnitude of the response for the same change in parameter was reduced relative to the 100 mm outer diameter specimen.

The above simulations were all carried out for uninsulated specimens. Using a 100 mm outer diameter with a 2 mm thick Nylon insert, it was found that the sensitivity to the substrate material properties were reduced (a consequence of the insulating insert decoupling the heat flow between the specimen and lubricant from the specimen metal temperature) but the trend remained unchanged. In reducing the specific heat capacity from  $900 \text{ J kg}^{-1} \text{ K}^{-1}$  to  $480 \text{ J kg}^{-1} \text{ K}^{-1}$  a reduction of 10% was observed in the energy transferred from the lubricant to the specimen (where the baseline was 0.48 MJ). Similarly, increasing the substrate specific heat capacity to  $1800 \text{ J kg}^{-1} \text{ K}^{-1}$  increased the energy transferred to the specimen by 12%.

### **8.1.4 Computational investigations into the effect of insulating material properties, insulating thickness and contact conditions on oil gallery thermal losses**

The sensitivity to the insulating material's properties was in direct contrast to those observed when investigating the substrate material. In halving the specific heat capacity of the insulating insert from  $1760 \text{ J kg}^{-1} \text{ K}^{-1}$  to  $880 \text{ J kg}^{-1} \text{ K}^{-1}$  a reduction of less than 1% was observed in the energy transferred from the lubricant to the specimen (where the baseline was 0.48 MJ). Similarly, doubling the insulator specific

heat capacity to  $3520 \text{ J kg}^{-1} \text{ K}^{-1}$  only increased the energy transferred to the specimen by 1%.

Comparatively, the thermal conductivity of the insulating insert is the more dominant factor. Reducing the thermal conductivity of the insulating material from  $0.262 \text{ W m}^{-1} \text{ K}^{-1}$  to  $0.131 \text{ W m}^{-1} \text{ K}^{-1}$  reduced the energy transferred to the specimen by 23%, while increasing the thermal conductivity to  $0.52 \text{ W m}^{-1} \text{ K}^{-1}$  increased the energy transferred to the specimen by 17%. Increasing the thickness of the insulating insert to 4 mm (compared to the baseline value of 2 mm) reduced the energy transferred to the specimen by 17% while halving the insulating material thickness to 1 mm increased the energy transferred to the specimen by 11%.

Halving the value of the contact heat transfer coefficient,  $h_{contact}$ , from  $150 \text{ W m}^{-2} \text{ K}^{-1}$  to  $75 \text{ W m}^{-2} \text{ K}^{-1}$  reduced the energy transferred to the specimen by 18% to 0.39 MJ while doubling the value to  $300 \text{ W m}^{-2} \text{ K}^{-1}$  increased the energy transferred to the specimen by 13% to 0.54 MJ.

### **8.1.5 Computational investigations into oil gallery thermal losses using different engine block materials**

The combined effect of varying different material parameters was investigated by means of changing the material properties of the specimen from those representative of aluminium to those of cast iron. The two materials are the two primary materials used to manufacture I.C. engine blocks with aluminium alloys being used for the manufacture of S.I. engines and light duty C.I. engines and cast iron still being used for heavy duty C.I. engines. Such a change increased the energy transferred to the specimen by 10% in the case of a 100 mm outer diameter uninsulated specimen, 7% in the case of the 40 mm outer diameter uninsulated specimen and 5% in the case of the 100 mm outer diameter insulated specimen (consistent with the presence of insulation reducing the sensitivity of thermal losses to the substrate material thermal properties). It was also predicted that if the entire test block specimen were made of Nylon 12 (with no insert installed), then the energy transferred from the lubricant could be reduced by 78%, relative to the baseline in the case of the 100 mm outer diameter specimen.

The sensitivity of thermal losses from the lubricant to the specimen as a result of variations in material properties caused by differences in polymer grade was assessed to be of the order of 4% in the case of the insulating insert (including using the thermal properties of Nylon 6 instead of Nylon 12). The simulations were carried out using thermal properties for the Nylon insert that were constant across the temperature range. Investigations into the effect that changes in the Nylon thermal properties with temperature would have on thermal losses indicated that the thermal losses could increase by up to 5%. There is therefore scope to incorporate

such variations into future modelling work. In the case of the substrate, using the thermal properties of a cast alloy as opposed to a wrought alloy (that being the grade the physical test block specimen was manufactured from) was assessed to be of the order of between 2% and 4% depending on the test block specimen size.

Thus, the work has indicated that the optimum strategy to reducing thermal losses from the lubricant to the engine block is to ensure that the thermal conductivity of the insulator is as low as possible and, to combine this with a low specific heat capacity substrate material and a low contact heat transfer coefficient.

#### **8.1.6 Computational investigations into the effect of flow geometry and conditions on oil gallery thermal losses**

A key factor to understand is the effect that flow geometry can have on heat transfer. The convective heat transfer coefficient is dependent on flow rate and velocity through the correlation with the Nusselt Number. Consequently, if the bore of an oil gallery is reduced, for a fixed volumetric flow rate, the velocity of the fluid will rise resulting in a higher convective heat transfer coefficient. However the heat transfer area is reduced as a result of the smaller bore. The overall combined effect of these two mechanisms is that the instantaneous heat flux is proportional to  $D^{-0.8}$  (where  $D$  is the bore diameter) for a given temperature differential between the lubricant and bore wall. Investigations into the sensitivity of energy transferred from the lubricant to the gallery wall were carried out using the oil flow rig simulation model by varying the velocity of the lubricant independently of both the bore diameter and the volumetric flow rate with the following findings reported:

- Reducing the lubricant velocity by 78% in the case of an 8 mm diameter bore reduced the energy transferred from the specimen by 1% for both the insulated and uninsulated variants.
- Reducing the lubricant velocity by 87% in the case of the 16 mm diameter bore reduced the energy transferred to the specimen by 2% and 5% for the uninsulated and insulated variants respectively.
- Reducing the lubricant velocity by 94% in the case of the 32 mm diameter bore reduced the energy transferred to the specimen by 4% and 5% (uninsulated and insulated).

In the case of the uninsulated bore, the cumulative energy transferred to the specimen decreased with increasing bore diameter while the increased bore diameter in the insulated specimen caused the cumulative energy transferred to the specimen to increase. By conducting simulations whereby the lubricant was held at a static temperature of 90 °C and the specimen heated from an initial temperature of 20 °C such a trend was able to be understood. Assuming a constant lubricant temperature, the product of the convective heat transfer area and convective heat transfer coefficient reduces with increasing bore diameter owing to the lower

lubricant velocity decreasing the Reynolds number. There therefore exists a critical temperature differential, above which the reduced convective heat transfer coefficient is counteracted and the heat flow to the test block specimen increases. The critical temperature differential varies between two comparative bore sizes but the trend and explanation has also been proven to be valid at lower flow rates of  $2 \text{ l min}^{-1}$ ; although the critical temperature differential is different owing to a change in the value of the lubricant to specimen heat transfer coefficient.

### **8.1.7 Final conclusions and advances in knowledge**

In conclusion, it has been proven through the work presented in this thesis that there is significant scope to reduce the thermal losses from automotive lubricants by insulating the engine oil galleries. Using an insulating insert presents the opportunity to utilise the contact resistance between the insert and the surrounding metal insert and this alone was proven to reduce thermal losses from the lubricant by 40%. Where one combined the high contact resistance with a low thermal conductivity material (Nylon 12) these benefits could be increased to a 58% reduction in thermal losses. It has been shown that the optimum strategy to achieve minimum thermal losses from the lubricant to the surrounding metal structure is to ensure that the thermal conductivity of any insulating layer applied to the gallery walls is as low as possible and that the thermal mass (either through reduced mass or specific heat capacity) is minimised. One should, where possible, attempt to incorporate a high contact resistance between the substrate material and the insulator.

The advancements in knowledge arising from this thesis are:

- The contact resistance between the interface of two separate bodies is a highly effective insulator and can provide an insulating benefit without the need to consider low thermal conductivity materials.
- The installation of inserts to engine oil galleries has the potential to reduce heat transfer from the lubricant to the bore wall by up to 58% owing to the combination of low thermal conductivity materials and contact resistance.
- The areas targeted for internal insulation in the I.C. engine need careful consideration to ensure that the insulation provides a benefit to lubricant heating and doesn't isolate a heat source. This also requires careful consideration of the implications of the gallery geometry and flow regime and heat transfer area. The work of this thesis suggests that the returns represent the area most likely to benefit from such insulation strategies.

## **8.2 Scope for further work**

Through the work presented in this thesis, it has been shown how it is possible to reduce the thermal losses from automotive engine lubricant to the surrounding

gallery structure by means of introducing a combination of both low thermal conductivity materials and an interface thermal resistance. However, in carrying out such work areas for further work and advancement in knowledge have also been identified and these are identified in the following sections:

### 8.2.1 Refinements to computational modelling

The model presented and used in this thesis was shown in Chapter 6 to require further development in order to improve the correlation with experimental results. A significant area for advancement in knowledge is understanding the complexities of the contact resistance between an insulating insert and the surrounding structure. Through the work in this thesis it has been discussed how the magnitude of the contact resistance, and the associated value of  $h_{contact}$ , is difficult to determine for a given set of physical parameters. Moreover, such a value will likely vary between two repeat situations of the same nominal material and geometric parameters. Thus, there is a need for further research into the variation of the contact resistance between different combinations of materials and also between different geometric layouts (i.e. the clearance between components). It would be desirable, as an output from such work, to be able to predict the contact resistance for a given physical set-up and be able to use such a value to predict thermal losses from automotive lubricants. Such work should also take account of the variation that is introduced as a result of parameter inconsistencies such as the clearance and the surface roughness.

It has been discussed how the value of  $h_{contact}$  is likely to vary across the operating temperature window of the experimental work presented in this thesis and hence also vary across the operating temperature window of an I.C. engine. This is a result of the clearance between the insulating insert and the surrounding metal changing with temperature owing to dissimilar coefficients of thermal expansion causing the contact pressure to change but also as a result of the polymer insert (in the case of the experimental work, Nylon 12) softening. Thus, as was highlighted in Section 6.5.4, the use of a constant value of  $h_{contact}$  is likely to be an over simplification and will have contributed to the difficulties in obtaining an acceptable level of correlation between computational and experimental results. Future work should therefore, seek to address such an issue and introduce a method of accounting for the variation in  $h_{contact}$  with temperature, should the material combination merit such a feature.

It would also be desirable to develop an alternative form of the model that would accurately model the flow of lubricant through the return galleries from the cylinder head of an I.C. engine. It was discussed in Section 7.3 how the lubricant in the returns, rather than being pressurised flow, as is the case in the galleries that feed lubricant from the oil pump to components, is instead film flow down the gallery wall that is gravity fed. Hence, the velocity of the lubricant is much slower and the

model is not currently able to accurately reflect such a flow regime. Given that experimental evidence has indicated that, depending on the specific engine, the lubricant return galleries are likely to be the regions of greatest loss, it would be desirable to develop a methodology of accurately predicting the benefits of insulating the lubricant return galleries. Such a methodology would need to incorporate a detailed knowledge of the temperatures of the metal locally surrounding the return gallery to avoid the introduction of errors caused by over simplifying the temperature distribution of the engine block. Such issues were first highlighted in Section 2.4.2 where it was highlighted how the engine block is currently sparsely instrumented. Hence, a rig based set-up, similar to the one utilised for the purposes of this work, would be desirable to remove the complex system interactions of a full I.C. engine and to facilitate effective understanding of the heat transfer mechanism between the return lubricant film and the surrounding metal structure.

### **8.2.2 Development of implementation methodologies**

This thesis has investigated the potential to reduce thermal losses from automotive lubricants by means of insulating the engine oil galleries with different designs of insulating insert. However, as was highlighted in Section 5.10, the geometry of an I.C. engine is such that it is not feasible to use such a methodology for the entire lubricant circuit. There is therefore a need to develop an alternative method of implementing I.C. engine insulation before the concept can be applied to a full working engine.

One possible method of achieving effective insulation around the entire lubricant circuit is to rely upon the contact resistance alone. It was established that the contact resistance between the insulating insert and the surrounding metal was a powerful variable in reducing the thermal losses from the lubricant circuit to the surrounding structure. Hence one could attempt to replicate the stepped aluminium insert philosophy throughout the entire engine by using cast in features to achieve a reduced effective heat transfer area throughout the lubricant circuit.

Alternatively, it was proven that the low thermal conductivity of the Nylon 12 insert did demonstrate an increased thermal insulating effect relative to relying on the contact resistance alone. There is therefore merit in investigating further, ways of applying polymer insulation to the lubricant circuit and, in particular, ensuring that areas of limited access can be coated. One method worthy of consideration is to use thermal spraying of polymers. This is where the substrate (in this case the I.C. engine) is heated and electrostatically charged polymer powder is sprayed on to the engine block. The charged powder is naturally attracted to uncoated regions of the engine and this would therefore facilitate the coating of areas of the engine where there is poor access. Moreover, depending on the polymer chosen, multiple coats

can be applied to achieve the required thickness and insulating effect. Were such an approach to be investigated, long term durability of the coating would need to be considered and investigated thoroughly to ensure such a process were suitable for use in I.C. engines. Amongst the factors that would require consideration are:

#### Lubricant and coating compatibility

The chemistry of a modern synthetic I.C. engine is complex and when submerged in hot, aerated lubricant (as would be the case in an I.C. engine) there is a risk of unwanted and detrimental chemical reaction between the lubricant and the coating. A possible method of investigating this would be to use the hardness and mass of a coating prior to and after exposure to hot, aerated lubricant. The hardness and mass of a coating are convenient measures of changes in the mechanical properties of the coating following lubricant exposure as recommended by Galipeau [120] and Hulme and Cooper [121]. If the lubricant effectively acts as a plasticiser to the polymer coating, then the coating stiffness would be seen to reduce in addition to the hardness decreasing [120]. The mass of the test specimen would also be expected to increase as the lubricant, acting as a plasticiser, became entrapped between polymer chains. An alternative effect would be if the lubricant were to act as a solvent to the polymer coating. In this instance, the mass of the test specimen would be expected to reduce as the polymer coating is dissolved into the lubricant. However, solvation of the coating causes the polymer chains to become unravelled and therefore a reduction in stiffness and hardness would still be expected [120]. Alternatively, the lubricant could act as, or contain, cross-linking agents to the polymer. In such an instance, the de-mobilising of polymer chains would be expected to result in an increase in hardness and stiffness [121].

It would also be desirable to monitor the condition of the lubricant as well as the condition of the coating in such work. Typically, the total acid number (TAN) and total base number (TBN) would be used to monitor the condition of the lubricant in service. The TAN is a measure of the acidity of a lubricant. As a lubricant ages in service, the acidity of the lubricant would be expected to increase owing to the production of acidic products from combustion (sulphuric acid is a particular problem in the case of diesel engines) [32]. The TAN is the amount of potassium hydroxide required to neutralise 1 g of lubricant and hence has units of  $\text{mg KOH g}^{-1}$ . The TAN therefore increases as the lubricant becomes more acidic. Lubricants are designed to have a composition that incorporates a 'reserve alkalinity' to prevent the lubricant becoming acidic during the service interval of the lubricant. The lubricant manufacturers use a process known as over basing to increase the level of alkali reserves in the lubricant [32] and the TBN is a measure of how much base product remains in the lubricant. The base in the lubricant is intended to be consumed during the service interval of the lubricant in order to prevent the acidity of the lubricant

rising and causing corrosion issues and hence the TBN would be expected to decrease over time. The TBN is measured by identifying how much hydrochloric acid is required to neutralise 1 g of the lubricant and subsequently calculating the amount of potassium hydroxide required to neutralise the hydrochloric acid used. This additional step enables the TAN and TBN to be compared using consistent units. Thus in appraising the condition of the lubricant, and hence suitability of a coating material, one would aim for the TAN to remain as low as possible and for the TBN to remain as high as possible. In addition to monitoring the TAN and TBN one would also monitor the condition of other specific chemical elements in the lubricant in order to observe if any detergent additives were being consumed.

### Thermal Cycling

The coefficient of thermal expansion of polymers is different to that of an aluminium substrate as highlighted earlier in the thesis for the specific example of aluminium 6082 and Nylon 12. The magnitude of this difference will vary depending on the specific polymer and substrate metal used however there is a risk that repeated thermal cycling of the coating and substrate, as would be the case during the service life of an I.C. engine, could cause the coating to debond and hence cause reliability issues. It would therefore be recommended that repeated thermal cycling tests be carried out to ensure that the adherence between the coating and substrate is sufficiently robust to cope with the thermal cycling that occurs in a working I.C. engine. This would include the need to reflect the fact that the typical operating temperatures of components in an I.C. engine can vary between 85 °C and 120 °C but that the cold-start temperatures, even in the European market, can be as low as -20 °C.

### Process Consistency

In order to ensure that the desired insulating effect is achieved, and that required clearances and tolerances can be adhered to, there would need to be tight control on any coating thickness. Thus, investigations into the consistency and repeatability of the coating would be required. One would also need to investigate any impact on the thermal conductivity and density that may result from process variation. In applying a coating via a spray methodology, there is a possibility of introducing a void content to the coating. While this is likely to be of benefit in creating a thermal insulating effect (the void content would reduce the thermal conductivity of the coating) such variation needs to be accounted for when specifying the required thicknesses. As scope for further work, there would be merit in investigating methods of purposefully reducing the thermal conductivity of coating materials to provide a greater insulating effect. Possible methods of achieving this would be the inclusion of filler materials such as glass spheres within the coating or to aerate the

coating to increase the void content further. However, the process would need to be proven to provide repeatable coating thermal properties.

### **8.2.3 Alternative methods to address I.C. engine cold-start efficiency**

Section 2.3.7 discussed previous work into the use of PCMs to improve I.C. engine cold start efficiency. Such an approach was shown to have benefits on I.C. engine systems either through reduced exhaust emission levels or through higher temperatures being retained for a longer period of time after the engine had been switched off (therefore facilitating a higher re-start temperature). There are similar challenges related to implementing PCMs as is the case with implementing insulation strategies including long term durability, chemical compatibility and economic cost. Depending on the method of application (i.e. on the outside of an I.C. engine), the PCM also effectively acts as an insulator from the ambient air; although it has been discussed how the thermal conductivity of the PCM needs to be enhanced to facilitate an effective charging process and this insulating effect is therefore dramatically reduced [41, 64].

The aim of using phase change materials is to capture waste energy during periods of engine running and subsequently use this energy during periods of none operation to reduce the rate of temperature reduction in the engine. The phase change process facilitates a high energy density storage system that, if implemented correctly, can be used as an energy source to supply thermal energy to the lubricant and therefore reduce the rate of temperature decrease. Consequently, when the engine is re-started, the lubricant temperature is elevated relative to a normal situation. Thus, while the aim of using PCM systems is the same as engine oil gallery insulation (i.e. reduce the lubricant warm-up time) the method of achieving this is subtly different with PCMs as the reduced lubricant warm-up time is achieved by virtue of the lubricant warm-up process commencing at a higher temperature rather than by reducing thermal losses via the gallery walls.

It was felt that investigations into the use of PCMs was too complex to feature in this thesis owing to the vast array of PCM variants available on the commercial market and the need to ensure that the optimum PCM and installation configuration had been selected. However, the potential benefits of using PCM materials, particularly if installed around the oil sump of an engine, would be of interest and enable a comparison to be made of the relative benefits of engine oil gallery insulation and PCM encapsulation. As part of the work, the following would need consideration:

- Ensuring the thermal conductivity of the PCM was as high as possible to facilitate effective charging.
- Ensuring that the thermal energy stored can be effectively transferred back to the target destination and not dissipated to ambient.

- Variability of the PCM properties (specific heat capacity, and latent heat capacity) as a result of manufacturer inconsistencies.
- Life-span relative to the life of the vehicle.
- Investigation as to whether the additional thermal mass of the PCM results in any increase in the lubricant warm-up time if the PCM is completely discharged.

## 9 References

1. Grove, J., *Vehicle Licensing Statistics: 2012*, 2012, Department for Transport.
2. Fly, A. and Thring, R.H. *System thermal and water balance in an evaporatively cooled PEM fuel cell vehicle*. presented at VTMS 11, 2013. Coventry, UK: IMechE.
3. Barlow, T.J., Latham, S., McCrae, I.S., and Boulter, P.G., *A Reference Book of Driving Cycles For Use In the Measurement of Road Vehicle Emissions*, IHS, ISBN: 0968-4093, 2009
4. *Council Directive of 6th February 1970 on the approximation of the laws of the Member States relating to the type-approval of motor vehicles and their trailers*. 1970.
5. *Regulation (EC) No 715/2007 On Type Approval Of Motor Vehicles With Respect To Emissions From Light Passenger and Commercial Vehicles (Euro 5 and Euro 6) and on Access to Vehicle Repair and Maintenance Information*, 2007.
6. *Regulation (EC) No 443/2009 Setting Emission Performance Standards For New Passenger Cars As Part of the Community's Integrated Approach to Reduce CO<sub>2</sub> Emissions From Light Duty Vehicles*, 2009.
7. Heywood, J., *Internal Combustion Engine Fundamentals*, McGraw-Hill, ISBN: 0-07-100499-8, 1988
8. Will, F. and Boretti, A. *A New Method to Warm Up Lubricating Oil To Improve the Fuel Efficiency During Cold Start*. 2011. SAE Technical Paper 2011-01-0318.
9. Andrews, G., Ounzain, A., Li, H., Bell, M., Tate, J., and Ropkins, K. *The Use of a Water/Lube Oil Heat Exchanger and Enhanced Cooling Water Heating to Increase Water and Lube Oil Heating Rates in Passenger Cars for Reduced Fuel Consumption and CO<sub>2</sub> Emissions During Cold Start*. 2007. SAE Technical Paper 2007-01-2067.
10. Goettler, H.J., Vidger, L.J., and Majkrzak, D.S. *The effect of Exhaust-to-Coolant Heat Transfer on Warm-up Time and Fuel Consumption of Two Automobile Engines*. 1986. SAE Technical Paper 860363.
11. Bent, E., Shayler, P., and La Rocca, A. *The effectiveness of stop-start and thermal management measures to improve fuel economy*. presented at VTMS 11, Coventry, 2013.
12. Kunze, K., Wolff, S., Lade, I., and Tonhauser, J. *A Systematic Analysis of CO<sub>2</sub>-Reduction by an Optimized Heat Supply during Vehicle Warm-up*. 2006. SAE Technical Paper 2006-01-1450.
13. Will, F., *Fuel conservation and emission reduction through novel waste heat recovery for internal combustion engines*. *org. Fuel*, 2012. **102**(0): p. 247-255.
14. Samhaber, C., Wimmer, A., and Loibner, E. *Modeling of Engine Warm-Up with Integration of Vehicle and Engine Cycle Simulation*. 2001. SAE Technical Paper 2001-01-1697.
15. Kauranen, P., Elonen, T., Wikström, L., Heikkinen, J., and Laurikko, J., *Temperature Optimisation of a Diesel Engine Using Exhaust Gas Heat Recovery and Thermal Energy Storage (Diesel Engine With Thermal Energy Storage)*. *Applied Thermal Engineering*, 2010. **30**: p. 631-638.
16. Jarrier, L., Champoussin, J.C., and Yu, R. *Warm-Up of a D. I. Diesel Engine: Experiment and Modeling*. 2000. SAE Technical Paper 2000-01-0299.
17. Andrews, G.E., Harris, J.R., and Ounzain, A. *SI Engine Warm-up: Water and Lubricating Oil Temperature Influences*. 1989. SAE Technical Paper 892103.
18. André, M. *In Actual Use Car Testing: 70,000 kilometers and 10,000 trips by 55 French Cars Under Real Conditions*. 1991. SAE Technical Paper 910039.

19. Gardiner, R., Zhao, C., Addison, J., and Shayler, P.J. *The effects of thermal state changes on friction during the warm up of a spark ignition engine*. presented at VTMS 11, Coventry, UK, 2013.
20. Trapy, J.D. and Damiral, P. *An Investigation of Lubricating System Warm-Up for the Improvement of Cold Start Efficiency and Emissions of S.I. Automotive Engines*. 1990. SAE Technical Paper 902089.
21. Li, H., Andrews, G.E., Savvidis, D., Daham, B., Ropkins, K., Bell, M., and Tate, J., *Study of Thermal Characteristics and Emissions during Cold Start using an on-board Measuring Method for Modern SI Car Real World Urban Driving*. SAE International Journal of Engines: Paper No: 2008-01-1307, 2009. **1**(1): p. 804-819.
22. Kamo, R., Bryzik, W., Reid, M., and Woods, M. *Coatings For Improved Engine Performance*. 1997. SAE Technical Paper 970204.
23. Finlay, I.C., Tugwell, W., Biddulph, T., and Marshall, R.A. *The Influence of Coolant Temperature on the Performance of a Four Cylinder 1100cc Engine Employing a Dual Circuit Cooling System*. presented at *Heat and Mass Transfer in Gasoline and Diesel Engines*, 1989. Taylor and Francis.
24. Shayler, P., Leong, D., and Murphy, M. *Contributions to Engine Friction During Cold, Low Speed Running and the Dependence on Oil Viscosity*. 2005. SAE Technical Paper 2005-01-1654.
25. Shayler, P.J., Baylis, W.S., and Murphy, M. *Main Bearing Friction and Thermal Interaction During the Early Seconds of Cold Engine Operation*. presented at *ASME 2002 Internal Combustion Engine Division Fall Technical Conference*, New Orleans, USA, 2002.
26. Burke, R.D., Brace, C.J., Hawley, J.G., and Pegg, I., *Review of the systems analysis of interactions between the thermal, lubricant, and combustion processes of diesel engines*. Proceedings of the Institution of Mechanical Engineers, Part D: Journal of Automobile Engineering, 2010. **224**(5): p. 681-704.
27. Zammit, J.-P., Shayler, P.J., Gardiner, R., and Pegg, I., *Investigating the Potential to Reduce Crankshaft Main Bearing Friction During Engine Warm-up by Raising Oil Feed Temperature*. SAE International Journal of Engines: Paper 2012-01-1216, 2012. **5**(3).
28. Comfort, A. *An Introduction to Heavy-Duty Diesel Engine Frictional Losses and Lubricant Properties Affecting Fuel Economy-Part 1*. 2004. SAE Technical Paper 2003-01-3225.
29. Glaeser, W.A., *Characterization of Tribological Materials*, Butterworth- Heinemann, ISBN: ISBN: 0-7506-9297-9, 1993
30. Vick, G.K. *The Role of the Engine Oil in Cold Weather Starting*. 1965. SAE Technical Paper 650446.
31. Selby, T.W. *A Comparison of the Effects of Cranking Speed and Oil Viscosity on Low-Temperature Engine Starting*. 1964. SAE Technical Paper 640427.
32. Haycock, R.F. and Hillier, J.E., *Automotive Lubricants Reference Book (2nd Edition)*, Society of Automotive Engineers, Inc., ISBN: 978-0-7680-1251-4, 2004
33. Pulkrabek, W.W., *Engineering Fundamentals of the Internal Combustion Engine*. Vol. 2. Pearson Prentice Hall New Jersey, ISBN: 0-13-140570-5, 2004
34. Cameron, A., *Basic Lubrication Theory*. Ellis Horwood Series in Engineering Science, Chichester, John Wiley & Sons, ISBN: 85132 057 9, 1976
35. Leong, D., *Investigations of Friction Losses In Automotive Internal Combustion Engines*, PhD thesis, Department of Mechanical, Materials and Manufacturing Engineering, The University of Nottingham, Nottingham, 2004.
36. Shayler, P.J., Allen, A.J., Leong, D.K.W., Pegg, I., Brown, A.J., and Dumenil, J.-C. *Characterising lubricating oil viscosity to describe effects on engine friction*. 2007. SAE Technical Paper 2007-01-1984.

37. Leong, D.K.W., Shayler, P.J., Pegg, I.G., and Murphy, M., *Characterizing the effect of viscosity on friction in the piston assembly of internal combustion engines*. Proceedings of the Institution of Mechanical Engineers, Part J: Journal of Engineering Tribology, 2007. **221**(4): p. 469-478.
38. Andrews, G.E., Harris, J.R., and Ounzain, A. *Transient Heating and Emissions of an SI Engine during the Warm-up period*. 1988. SAE Technical Paper 880264.
39. Shayler, P. and Christian, S. *A model for the investigation of temperature, heat flow and friction characteristics during engine warm-up*. 1993. SAE Technical Paper 931153.
40. Gardiner, R., Zhao, C., Addison, J., and Shayler, P., *Private Communication Containing Experimental Test Bed Engine Experimental Data*, September 2013.
41. Korin, E., Reshef, R., Tshernichovesky, D., and Sher, E., *Reducing cold-start emission from internal combustion engines by means of a catalytic converter embedded in a phase-change material*. Proceedings of the Institution of Mechanical Engineers, Part D: Journal of Automobile Engineering, 1999. **213**(6): p. 575-583.
42. Shayler, P., Chick, J., Hayden, D., Yuen, H., and Ma, T. *Progress on Modelling Engine Thermal Behaviour for VTMS Applications*. 1997. SAE Technical Paper 971852.
43. Zhao, Y. and Winterbone, D.E. *A Study of Warm-Up Processes in SI Engine Exhaust Systems*. 1993. SAE Technical Paper 931094.
44. Gumus, M., *Reducing cold-start emission from internal combustion engines by means of thermal energy storage system*. Applied Thermal Engineering, 2009. **29**(4): p. 652-660.
45. Shayler, P.J., Davies, M.T., and Scarisbrick, A. *Audit of Fuel Utilisation During the Warm-Up of SI Engines*. 1997. SAE Technical Paper 971656.
46. Yu, C. and Chau, K.T., *Thermoelectric automotive waste heat energy recovery using maximum power point tracking*. Energy Conversion and Management, 2009. **50**(6): p. 1506-1512.
47. Uzun, A., Çevik, İ., and Akçil, M., *Effects of thermal barrier coating on a turbocharged diesel engine performance*. Surface and Coatings Technology, 1999. **116–119**(0): p. 505-507.
48. Brito, F.P., Martins, J., Goncalves, L., and Sousa, R. *Temperature Controlled Exhaust Heat Thermoelectric Generation*. 2012. SAE Technical Paper 2012-01-1214.
49. Bejan, A., *Heat Transfer*, John Wiley & Sons, ISBN: 0-471-50290-1, 1993
50. Çengel, Y.A., *Heat and mass transfer: a practical approach*, McGraw-Hill, 2007
51. Welty, J.R., *Fundamentals of momentum, heat, and mass transfer*, Wiley, ISBN: 9780471381495, 2001
52. Holman, J.P., *Heat transfer*, McGraw-Hill Higher Education, ISBN: 9780072406559, 2002
53. Kumar, S., Heister, S.D., Xu, X., Salvador, J.R., and Meisner, G.P., *Thermoelectric Generators for Automotive Waste Heat Recovery Systems Part I: Numerical Modeling and Baseline Model Analysis*. Journal of Electronic Materials, 2013. **42**(4): p. 665-674.
54. Crane, D., Jackson, G., and Holloway, D. *Towards Optimization of Automotive Waste Heat Recovery Using Thermoelectrics*. 2001. SAE Technical Paper 2001-01-1021.
55. Matsubara, K. *Development of a high efficient thermoelectric stack for a waste exhaust heat recovery of vehicles*. presented at *Twenty-First International Conference on Thermoelectrics*, Long Beach, USA, 2002.
56. Bose, S., *High Temperature Coatings*, Butterworth- Heinemann, ISBN: 978-0-75068252-7, 2007
57. *CES Version 5.0 (Software)*, 2009, Granta Design Limited.

58. Yilmaz, İ.T., Gumus, M., and Akçay, M. *Thermal Barrier Coatings for Diesel Engines*. presented at *International Scientific Conference*, 2010.
59. Ciniviz, M., Hasimoglu, C., Şahin, F., and Salman, M.S., *Impact of thermal barrier coating application on the performance and emissions of a turbocharged diesel engine*. Proceedings of the Institution of Mechanical Engineers, Part D: Journal of Automobile Engineering, 2008. **222**(12): p. 2447-2455.
60. Taymaz, I., Çakır, K., and Mimaroglu, A., *Experimental study of effective efficiency in a ceramic coated diesel engine*. Surface and Coatings Technology, 2005. **200**(1): p. 1182-1185.
61. Dahotre, N.B. and Nayak, S., *Nanocoatings for engine application*. Surface and Coatings Technology, 2005. **194**(1): p. 58-67.
62. Ciulli, E., *A Review of Internal Combustion Engine Losses Part 1: Specific Studies on the Motion of Pistons, Valves and Bearings*. Proceedings of the Institution of Mechanical Engineers, Part D: Journal of Automobile Engineering, 1992. **206**(4): p. 223-236.
63. Bürgin, T. *CO<sub>2</sub> and emission reduction by means of heat storage in the powertrain*. presented at *VTMS 10*, Gaydon, UK, 2011.
64. Stouffer, S.B., Lewis, A.B., Whitney, T.J., and Drake, M.L., *Diesel Cold Start Improvement Using Thermal Management Techniques*, 2000, University of Drayton Research Institute.
65. Zammit, J.P., Shayler, P.J., and Pegg, I. *Thermal coupling and energy flows between coolant, engine structure and lubricating oil during engine warm-up*. presented at *VTMS 10*, Coventry, United Kingdom, 2010.
66. Brace, C.J., Hawley, G., Akehurst, S., Piddock, M., and Pegg, I., *Cooling system improvements — assessing the effects on emissions and fuel economy*. Proceedings of the Institution of Mechanical Engineers, Part D: Journal of Automobile Engineering, 2008. **222**(4): p. 579-591.
67. Law, T., Shayler, P., and Pegg, I. *Investigations of sump design to improve the thermal management of oil temperature during engine warm up*. presented at *VTMS 8*, Nottingham, UK, 2007.
68. Dubouil, R., Hetet, J., and Maiboom, A. *Modelling of the Warm-up of a Spark Ignition Engine: Application to Hybrid Vehicles*. 2011. SAE Technical Paper 2011-01-1747.
69. Burke, R., Brace, C., Cox, A., Lewis, A., Hawley, J.G., Pegg, I., and Stark, R., *Systems approach to the improvement of engine warm-up behaviour*. Proceedings of the Institution of Mechanical Engineers, Part D: Journal of Automobile Engineering, 2011. **225**(2): p. 190-205.
70. Bettles, C.J., Forwood, C.T., Jones, D.S., Griffiths, J.R., Frost, M.T., St. John, D.H., Qian, M., Song, G.L., and Nie, J.F. *AMC-SC1: A New Magnesium Alloy Suitable For Powertrain Applications*. 2003. SAE Technical Paper 2003-01-1365.
71. Overfelt, R. and Bakhtiyarov, S., *Thermophysical Properties of A201, A319 and A356 Aluminium Casting Alloys*. High Temperatures, High Pressure, 2002. **34**: p. 401-409.
72. Bowman, T.J., Cumming, B.S., and Gilmore, P.J., *Final Summary Report: Fibre Reinforced Composite Engine, BRITE Contract Number RI1B-0115-D(B)*, ISBN: 9822631419, 1990
73. Hughes, D., *Summarised Presentation of the Findings and Recommendations of a Study Undertaken at the National Engineering Laboratory for Ford of Europe into the Feasibility of a Fibre Reinforced Plastics Engine Block*, 1986.
74. Guimond, D. and Muench, R. *Composite V-6 Diesel Engine Concept*. 1992. SAE Technical Paper 920084.
75. *Materials Handbook: Volume 2, Properties and Selection: Nonferrous Alloys and Special-Purpose Materials*, ASM International, ISBN: 0-87-170378-5, 1990

76. *AMC-SC1: Sand Casting Alloy For High Temperature Powertrain*, 2006.
77. Krigbaum, R.S., *Advantages of Thermoset Composites in Automotive Engine Applications*. 1993.
78. Pegguleruz, M. and Celikin, M., *Creep Resistance In Magnesium Alloys*. International Materials Review, 210. **55**(4): p. 197-217.
79. Sharma, A., Tyagi, V.V., Chen, C.R., and Buddhi, D., *Review On Thermal Energy Storage With Phase Change Materials And Applications*. Renewable and Sustainable Energy Reviews, 2009. **13**: p. 318-345.
80. Farid, M.M., Khudhair, A.M., Razack, S.A.K., and Al-Hallaj, S., *A review on phase change energy storage: materials and applications*. Energy Conversion and Management, 2004. **45**(9–10): p. 1597-1615.
81. Agyenim, F., Hewitt, N., Eames, P., and Smyth, M., *A review of materials, heat transfer and phase change problem formulation for latent heat thermal energy storage systems (LHTESS)*. Renewable and Sustainable Energy Reviews, 2004. **14**(2): p. 615-628.
82. Sharma, S.D. and Sagara, K., *Latent Heat Storage Materials and Systems: A Review*. International Journal of Green Energy, 2005. **2**(1): p. 1-56.
83. Shukla, A., Buddhi, D., and Sawhney, R.L., *Thermal cycling test of few selected inorganic and organic phase change materials*. Renewable Energy, 2008. **33**(12): p. 2606-2614.
84. Sharma, S.D., Buddhi, D., and Sawhney, R.L., *Accelerated thermal cycle test of latent heat-storage materials*. Solar Energy, 1999. **66**(6): p. 483-490.
85. Sharma, A., Sharma, S.D., and Buddhi, D., *Accelerated thermal cycle test of acetamide, stearic acid and paraffin wax for solar thermal latent heat storage applications*. Energy Conversion and Management, 2002. **43**(14): p. 1923-1930.
86. Salunkhe, P.B. and Shembekar, P.S., *A review on effect of phase change material encapsulation on the thermal performance of a system*. Renewable and Sustainable Energy Reviews, 2012. **16**(8): p. 5603-5616.
87. Kaplan, J.A. and Heywood, J.B. *Modeling the Spark Ignition Engine Warm-up Process to Predict Component Temperatures and Hydrocarbon Emissions*. 1991. SAE Technical Paper 910302.
88. Seider, G., Mehring, J., and Weber, C. *A high-resolution warm-up simulation model for a gasoline engine with advanced thermal control*. presented at *Vehicle Thermal Management Systems Conference*, 2011.
89. Jasak, H., Luo, J., Kaluderčić, B., Gosman, A., Echtele, H., Liang, Z., Wirbeleit, F., Wierse, M., Rips, S., and Werner, A. *Rapid CFD simulation of internal combustion engines*. 1999. SAE Technical Paper 1999-01-1185.
90. Tiney, N., Spiller, M., Pržulj, V., and Penning, R., *Conjugate Heat Transfer Modelling of Internal Combustion Engine*. MTZ worldwide, 2012. **73**(12): p. 44-49.
91. Rakopoulos, C.D., Kosmadakis, G.M., and Pariotis, E.G., *Critical evaluation of current heat transfer models used in CFD in-cylinder engine simulations and establishment of a comprehensive wall-function formulation*. Applied Energy, 2010. **87**(5): p. 1612-1630.
92. Uppuluri, S., Proulx, J., Marovic, B., and Naiknaware, A. *Characterizing Thermal Interactions Between Engine Coolant, Oil and Ambient for an Internal Combustion Engine*. 2013. SAE Technical Paper 2013-01-0960.
93. Gale, W.F. and Totemeier, T.C., *Smithells Metals Reference Book*, Elsevier Science, ISBN: 9780080480961, 2003
94. *The Properties of Aluminium and Its Alloys*. 8th ed, The Aluminium Federation, 1983
95. Rana, R.S., Purohit, R., and Das, S., *Reviews on the Influences of Alloying elements on the Microstructure and Mechanical Properties of Aluminum Alloys and Aluminum*

- Alloy Composites*. International Journal of Scientific and Research Publications, 2012. **2**(6).
96. Stadler, F., Antrekowitsch, H., Fragner, W., Kaufmann, H., Pinatel, E.R., and Uggowitz, P.J., *The effect of main alloying elements on the physical properties of Al-Si foundry alloys*. Materials Science and Engineering: A, 2013. **560**(0): p. 481-491.
  97. *Product Data Sheet: Nylon 12*, 2014, PAR Group.
  98. *Product Data Sheet: Tecamid 12*, 2014, Ensinger.
  99. Harper, C.A., *Handbook of Plastics, Elastomers, and Composites*. 4th ed. Vol. 2. McGraw-Hill Inc, 2002
  100. *Product Data Sheet: Nylon 6*, 2014, PAR Group.
  101. *Product Data Sheet: Ertalon 6*, 2014, Quadrant Engineering Plastic Products.
  102. *Product Data Sheet: Tecamid 6*, 2014, Ensinger.
  103. Lacey, P.I., Gonsel, S., Ferner, M.D., Pozebanchuk, M., and Alim, A. *Effect of Oil Drain Interval on Crankcase Lubricant Quality*. 2003. SAE Technical Paper 2003-01-1957.
  104. Tseregounis, S.I. and McMillan, M.L. *Engine Oil Aging Effects on Fuel Economy as Measured by the EPA FTP Vehicle Dynamometer Test in a GM Engine*. 2002. SAE Technical Paper 2002-01-1635.
  105. Moseley, A., *Product Data Sheet*, 2012, Chevron.
  106. *TC Guide to Thermocouple and Resistance Thermometry Issue 6.1*, 2013
  107. Clough, M. *Precision cooling of a four valve per cylinder engine*. 1993. SAE Technical Paper 931123.
  108. Finlay, I., Gallacher, G., Biddulph, T., and Marshall, R. *The Application of Precision Cooling to the Cylinder-Head of a Small, Automotive, Petrol Engine*. 1988. SAE Technical Paper 880263.
  109. Tye, R.P., *Thermal conductivity*. Vol. 2, London, Academic press, 1969
  110. Fletcher, L.S., *Recent Developments in Contact Conductance Heat Transfer*. Journal of Heat Transfer, 1988. **110**(4b): p. 1059-1070.
  111. Madhusudana, C. *Contact Heat Transfer Between Coaxial Cylinders of Similar or Dissimilar Materials*. presented at *Proceedings of the ASME-JSME Thermal Engineering Joint Conference, Honolulu, Hawaii*, 1983.
  112. Madhusudana, C.V. and Litvak, A.L., *Thermal contact conductance of composite cylinders - An experimental study*. Journal of Thermophysics and Heat Transfer, 1990. **4**(1): p. 79-85.
  113. Fuller, J.J. and Marotta, E.E., *Thermal Contact Conductance of Metal/Polymer Joints: An Analytical and Experimental Investigation*. Journal of Thermophysics and Heat Transfer, 2001. **15**(2): p. 228-238.
  114. Yuan, M., *Thermal Conductivity Measurements of Polyamide Powder*, PhD thesis, The Graduate School, Texas, Austin, 2011.
  115. DeGarmo, E.P., Black, J.T., and Kohser, R.A., *DeGarmo's Materials and Processes in Manufacturing*. 11th ed, Wiley, ISBN: 9780470924679, 2011
  116. Zammit, J.P.S., P. J.; Gardiner, R., *Investigating the Potential to Reduce Crankshaft Main Bearing Friction During Engine Warm-up by Raising Oil Feed Temperature*. SAE Paper 2012-01-1216, 2012.
  117. Dang, P., *Product Data Sheet: Nylon 12*, 2014, Arkema.
  118. Dang, P., *Product Data Sheet: Nylon 11*, 2014, Arkema.
  119. dos Santos, W.N., de Sousa, J.A., and Gregorio Jr, R., *Thermal conductivity behaviour of polymers around glass transition and crystalline melting temperatures*. Polymer Testing, 2013. **32**(5): p. 987-994.
  120. Galipeau, R.J. *Predicting The Effects Of Contact Materials and Their Environments On Thermoplastics Through Chemical Compatibility Testing*. presented at ANTEC 95, 1995. Boston: Society of Plastics Engineers.

121. Hulme, A. and Cooper, J., *Life prediction of polymers for industry*. Sealing Technology, 2012(9): p. 8-12.

# Appendix A Manufacturer data of Nylon properties

## A.1 Nylon 12 data

### A.1.1 Ensinger data



### TECAMID 12 natural - Stock Shapes

**Chemical Designation**  
PA 12 (Polyamide 12)

**Colour**  
Ivory opaque

**Density**  
1.02 g/cm<sup>3</sup>

Data generated directly after machining  
(standard climate Germany).

**Main features**

- + high toughness
- + resistant to many oils, greases and fuels
- + good wear properties
- + high dimensional stability
- + good slide and wear properties
- + low density
- + low moisture absorption
- + good weldable and bondable

**Target industries**

- + conveyor technology
- + textile industry
- + printing machines
- + food engineering
- + precision engineering
- + packaging and paper machinery
- + electrical engineering
- + automotive industry

Mechanical properties	parameter	value	unit	norm	comment
Modulus of elasticity (tensile test)	1mm/min	1800	MPa	DIN EN ISO 527-2	1)
Tensile strength	50mm/min	53	MPa	DIN EN ISO 527-2	
Tensile strength at yield	50mm/min	53	MPa	DIN EN ISO 527-2	
Elongation at yield	50mm/min	9	%	DIN EN ISO 527-2	
Elongation at break	50mm/min	200	%	DIN EN ISO 527-2	
Flexural strength	2mm/min, 10 N	88	MPa	DIN EN ISO 178	2)
Modulus of elasticity (flexural test)	2mm/min, 10 N	1700	MPa	DIN EN ISO 178	
Compression strength	1% / 2% 5mm/min, 10 N	13 / 24	MPa	EN ISO 604	3)
Compression modulus	5mm/min, 10 N	1800	MPa	EN ISO 604	4)
Impact strength (Charpy)	max. 7,5J	n.s.	kJ/m <sup>2</sup>	DIN EN ISO 179-1eU	5)
Notched impact strength (Charpy)	max. 7,5J	7	kJ/m <sup>2</sup>	DIN EN ISO 179-1eA	
Ball indentation hardness		105	MPa	ISO 2008-1	6)
Thermal properties	parameter	value	unit	norm	comment
Glass transition temperature		37	°C	DIN 53765	1)
Melting temperature		180	°C	DIN 53765	
Service temperature	short term	150	°C		2)
Service temperature	long term	110	°C		
Thermal expansion (CLTE)	23-80°C, long.	15	10 <sup>-6</sup> K <sup>-1</sup>	DIN EN ISO 11359-1:2	
Thermal expansion (CLTE)	23-100°C, long.	16	10 <sup>-6</sup> K <sup>-1</sup>	DIN EN ISO 11359-1:2	
Specific heat		1.8	J/(g·K)	ISO 22007-4:2008	
Thermal conductivity		0.30	W/(K·m)	ISO 22007-4:2008	
Electrical properties	parameter	value	unit	norm	comment
Specific surface resistance		10 <sup>14</sup>	Ω	DIN IEC 60093	
Specific volume resistance		10 <sup>14</sup>	Ω·cm	DIN IEC 60093	
Other properties	parameter	value	unit	norm	comment
Water absorption	24h / 96h (23°C)	0.04 / 0.07	%	DIN EN ISO 62	1)
Resistance to hot water/ bases		-	-	-	2)
Resistance to weathering		-	-	-	3)
Flammability (UL94)	corresponding to	HB		DIN IEC 60695-11-10;	4)

Our information and statements reflect the current state of our knowledge and shall inform about our products and their applications. They do not assure or guarantee chemical resistance, quality of products and their processability in a legally-binding way. Our products are not defined for use in medical or dental implants. Existing commercial patents have to be observed. The corresponding values and information are no minimum or maximum values, but guideline values that can be used primarily for comparison purposes for material selection. These values are within the normal tolerance range of product properties and do not represent guaranteed property values. Therefore they shall not be used for specification purposes. Unless otherwise noted, these values were determined by tests at reference dimensions (typically rods with diameter 40-60 mm) according to DIN EN 15868 on extruded and machined specimens. As the properties depend on the dimensions of the semi-finished products and the orientation in the component (esp. in reinforced grades), the material may not be used without a separate testing under individual circumstances. The customer is solely responsible for the quality and suitability of products for the application and has to test usage and processing prior to use. Data sheet values are subject to periodic review, the most recent updates can be found at [www.ensinger-online.com](http://www.ensinger-online.com). Technical changes reserved.

Ensinger Ltd  
Wilfried Way  
Tongrefail, Mid Glamorgan CF39 8JQ  
Great Britain

Phone: (01443) 670400  
Fax: (01443) 675777  
[www.ensinger.co.uk](http://www.ensinger.co.uk)

Date: 2014/07/21

Version: AA

## A.1.2 PAR data



# PAR GROUP

[www.par-group.co.uk](http://www.par-group.co.uk)

<b>PAR (MANCHESTER) LTD</b> Warrin Street Ashton-Under-Lyne Lancashire OL6 8NW t : +44(0) 161 339 6608 f : +44(0) 161 343 2088 e : sales@par-group.co.uk	<b>PAR (PRESTON) LTD</b> Club Street Bamber Bridge Lancashire PR5 6FN t : +44(0) 1772 322 114 f : +44(0) 1772 627 524 e : preston@par-group.co.uk	<b>PAR (YORKSHIRE) LTD</b> Warrin Street Ashton-Under-Lyne Lancashire OL6 8NW t : +44(0) 1924 444 529 f : +44(0) 161 343 2088 e : sales@par-group.co.uk
---	--	--

### Nylon 12

A semi-crystalline engineering plastic with very high toughness and good chemical resistance for varied applications.

The main characteristics of Nylon 12 are as follows:

- Extremely tough
- Good sliding properties
- Abrasion resistant
- Good chemical resistance to many oils, greases, diesel, petrol and cleaning fluids
- Light
- Low water absorption
- Good electrical insulation
- Easily machined
- Dimensionally accurate
- Easily welded and bonded

Nylon 12 is commonly used in transport and conveyor technology, food technology, textile, packing and paper processing machinery, printing and drinks dispensing machinery, electrical engineering and the automotive industry.

Typical applications of Nylon 12 include:

- Conveyor screw sleeves
- Friction strips
- Gear wheels
- Fan impellers
- Castors
- Impact plates
- Cutting pads
- Friction bearings
- Housing parts
- Switch parts
- plug parts
- Damping plates



## PAR (MANCHESTER) LTD

Wern Street  
Ashton-Under-Lyne  
Lancashire  
OL6 8NW  
t : +44(0) 161 338 8600  
f : +44(0) 161 343 2088  
e : sales@par-group.co.uk

## PAR (PRESTON) LTD

Club Street  
Bamber Bridge  
Lancashire  
PR5 6FN  
t : +44(0) 1772 322 114  
f : +44(0) 1772 627 524  
e : preston@par-group.co.uk

## PAR (YORKSHIRE) LTD

Wern Street  
Ashton-Under-Lyne  
Lancashire  
OL6 8NW  
t : +44(0) 1924 444 529  
f : +44(0) 161 343 2088  
e : sales@par-group.co.uk

## Technical Information

Information to be used as a guide only. It corresponds with our current knowledge and indicates possible applications. We cannot guarantee suitability for a specific application. Unless otherwise stated these values represent averages taken from injection moulded samples.

Properties	Unit	Test Method DIN	Result Dry	Result Wet
<b>MECHANICAL</b>				
Density	g/cm <sup>3</sup>	53479	1.02	-
Tensile strength at yield	MPa	53455	85	-
Tensile strength at break	MPa	53455	82	88
Elongation at Break	%	53455	240	-
Modulus of elasticity in tension	MPa	53457	1800	-
Modulus of elasticity in flexure	MPa	53457	-	-
Ball indentation hardness	MPa	53456	95	-
Impact strength (Charpy)	KJ/m <sup>2</sup>	53453	no break	-
Creep rupture strength after 1000 hours with static load	MPa	-	23	-
Time yield limit for 1% elongation after 1000 hours	MPa	-	3.5	-
Coefficient of friction against hardened and ground steel p=0,05 N/mm <sup>2</sup> , v=0.6 m/s	-	-	0.32 - 0.38	-
Wear conditions as above	µm/km	-	0.8	-
<b>THERMAL</b>				
Crystalline melting point	°C	53736	179	-
Glass transition temperature	°C	53736	41	5
Heat distortion temperature method A	°C	ISO 75	50	-
Heat distortion temperature method B	°C	ISO 75	140	-
Max. service temperature short term	°C	-	140	-
Max. service temperature long term	°C	-	80	-
Coefficient of thermal conductivity	W/(m K)	-	0.23	-
Specific heat	J/(g K)	-	2.1	-
Coefficient of thermal expansion	10 <sup>-5</sup> /K	-	10	-
<b>ELECTRICAL</b>				
Dielectric constant at 10 (5) Hz	-	53483	3.1	3.6
Dielectric loss factor at 10(5) Hz	-	53483	0.03	0.04
Specific Volume Resistance	Ωcm	53482	2 x 10 <sup>15</sup>	10 <sup>14</sup>
Surface Resistance	Ω	53482	10 <sup>14</sup>	10 <sup>12</sup>
Dielectric strength 1mm	kV/mm	53481	33	30
Tracking resistance	-	53480	KB 3b	CT600
<b>MISCELLANEOUS</b>				
Moisture Absorption: Equilibrium in standard atmosphere (23°C / 50% relative humidity)	%	53714	0.7	-
Water absorption at saturation at 23°C	%	53495	1.6	-
Resistance to hot water, washing soda	-	-	resistant	-
Flammability	-	UL 94	V2	-
Resistance to weathering	-	-	not resistant	-

## A.2 Nylon 6 data

### A.2.1 Ensinger data



## TECAMID 6

---

Chemical Designation:	Polyamide 6 ( Nylon 6 )
DIN Abbreviation:	PA 6
Colour, Filler:	Opaque

---

TECAMID 6 is a semi-crystalline engineering thermoplastic with high toughness for varied applications.

Main characteristics:	- Good sliding properties	- Very tough
	- Very abrasion resistant	- Rigid
	- Good chemical resistance to many oils, greases, diesel, petrol, cleaning fluids	- Electrically Insulating
		- Easily machined
		- Easily welded and bonded

Preferred fields: Mechanical engineering, automotive engineering, transport and conveyor technology, textile, packaging and paper processing machinery, printing and drinks dispensing machinery, household articles, electrical engineering, building machinery, agricultural machinery

Applications:	- Gear wheels	- Friction bearings
	- Friction strips	- Conveyor screws
	- Bushes, spindle nuts	- Cam discs
	- Piston guides	- Rope pulleys
	- Castors	- Plug parts
	- Impact plates	- Damping plates

---

Ensinger Ltd  
Wilfried Way  
Tonyrefail  
Mid Glam CF39 8JQ

Tel: 01443 678400  
Fax: 01443 675777  
Web: [www.ensinger.ltd.uk](http://www.ensinger.ltd.uk)  
Email: [sales@ensinger.ltd.uk](mailto:sales@ensinger.ltd.uk)

## TECAMID 6

The following information corresponds with our current knowledge and indicates our products and possible applications. We cannot give a legally binding guarantee of certain properties or the suitability for a specific application. Existing commercial patents must be observed. A definitive quality guarantee is given in our general conditions of sales. Unless otherwise stated, these values represent averages taken from injection moulding samples. We reserve the right of technical alterations.

Properties	Unit	Test method DIN EN ISO / ASTM	Dry / Wet*
<b>Mechanical</b>			
Density	g/cm <sup>3</sup>	527 / D 790	1.13
Tensile strength at yield	MPa	527 / D 638	95 / 90*
Tensile strength at break	MPa	527 / D 638	
Elongation at break	%	527 / D 638	70 / 200*
Modulus of elasticity in tension	MPa	527 / D 638	3000 / 1800*
Modulus of elasticity in flexure	MPa	179 / D 790	
Ball indentation hardness	MPa	2036 / I	180 / 70*
Impact strength	kJ/m <sup>2</sup>	179 / D 256	no. br.
Creep rupture strength after 1000 hrs with static load	MPa		45
Time yield limit for 1% elongation after 1000 hrs	MPa		4.5
Coefficient of friction against hardened and ground steel $\mu = 0.25$ (static), $\nu = 0.6$ (slip)	-		0.38 - 0.45
Wear conditions as above	µm <sup>3</sup> /km		0.23
<b>Thermal</b>			
Crystalline melting point	°C	DIN 53 736	220
Glass transition temperature	°C	DIN 53 736	90 / 15*
Heat distortion temperature Method A, Method B	°C °C	R 75 R 75	75 190

Properties	Unit	Test method DIN EN ISO / ASTM	Dry / Wet*
<b>Thermal</b>			
Max. service temperature short term	°C		150
long term	°C		100
Coefficient of thermal conductivity	W/(m · K)		0.23
Specific heat	J/(kg · K)		1.7
Coefficient of thermal expansion	10 <sup>-6</sup> /K	DIN 53 463 / D 990	8
<b>Electrical</b>			
Dielectric constant at 10 <sup>3</sup> Hz		DIN 53 483	3.7 / 3*
Dielectric loss factor at 10 <sup>3</sup> Hz		DIN 53 483	0.021 / 0.3*
Specific volume resistance	Ω · cm	DIN 50090	10 <sup>16</sup>
Surface resistance	Ω	DIN 50090	10 <sup>16</sup>
Dielectric strength 1 mm	kV/mm	ASTM 149	50 / 25*
Tracking resistance		52 480	CTI 900
<b>Fluorescence</b>			
Moisture absorption: Equilibrium in standard atmosphere (23 °C / 50 % relative humidity)	%	52	3
Water absorption at saturation at 23 °C	%	52	9.5
Resistance to hot water, wetting acids			limited resistant
Flammability according to UL standard 94			H0
Resistance to weathering			not resistant

\* after storage in a standard 23/50 atmosphere (DIN 50 014) to equilibrium

ENSINGER: Production and stock programme

- Semi-finished product, finished parts, injection moulded parts and profiles in more than 500 materials and modifications.
- Engineering plastics: PA extruded or cast, POM, PC, PET, PBT, PPE, PP, PE
- High temperature plastics: PI, TPI, PEEK, PPS, PES, PPSU, PEL, PSU, PVDF, PCTFE, PTFE
- Stock length: Standard 3 metres. Cast rod and sheet 2 mts. Tube up to 3.5 mts. PE, PP, PVC, and PTFE 2 mts
- Pressed/airtreated semi-finished product: PI, PEEK, PPS, PTFE/PI and modifications, as well as PCTFE in special sizes ie, large discs, tubes and rings with diameters up to about 1400 mm
- Material modifications: eg. glass, carbon and aramid fibre, talc, MoS<sub>2</sub>, graphite, PTFE, PE, silicone oil, internal lubrication

## A.2.2 Quadrant data

POLYMER (PA 6)		QUADRANT	
ERTALON® 6 PLA		ENGINEERING PLASTIC PRODUCTS	
<p>Unmodified cast nylon 6 grade exhibiting characteristics which come very close to those of ERTALON 66 SA. It combines high strength, stiffness and hardness with good creep and wear resistance, heat aging properties and machinability.</p>			
<p><b>Physical properties (indicative values *)</b></p>			
PROPERTIES	Test methods	Units	VALUES
<p><b>MOQs</b></p>			
Density	ISO 1183-1	g/cm <sup>3</sup>	1.15
Water absorption:		mg	440
	- after 24h in immersion in water at 23 °C (1)	ISO 62	0.05/ 20
	- at saturation in air at 23°C / 50 % RH	-	3.2
	- at saturation in water at 23 °C	-	6.5
<p><b>Thermal Properties (2)</b></p>			
Melting temperature (DSC, 10 °C/min)	ISO 11357-1/3	°C	255
Glass transition temperature (DSC, 10 °C/min, 20)	ISO 11357-1/2	°C	-
Thermal conductivity at 23 °C	-	W/m.K	0.39
<p><b>Coefficient of linear thermal expansion:</b></p>			
- average value between 23 and 60 °C	-	µm/m.K	80 x 10 <sup>-6</sup>
- average value between 23 and 100 °C	-	µm/m.K	90 x 10 <sup>-6</sup>
<p><b>Temperature of deflection under load:</b></p>			
- method A: 1.8 MPa	ISO 75-2/3	°C	80
<p><b>Max. allowable service temperature in air:</b></p>			
- for short periods (3)	-	°C	170
- continuous - for 5,000 / 20,000 h (5)	-	°C	125/90
<p><b>Min. service temperature (6)</b></p>			
-	-	°C	-30
<p><b>Flammability (7)</b></p>			
- "Oxygen Index"	ISO 4589-1/2	%	25
- according to UL 94 (3 / 6 mm thickness)	-		HB / H-0
<p><b>Mechanical Properties at 23 °C (8)</b></p>			
<p><b>Tension test (9)</b></p>			
- tensile stress at yield / tensile stress at break (10)	ISO 527-2/3	MPa	80 / 85.1
- tensile strength (10)	ISO 527-2/3	MPa	85.1
- tensile stress at yield (10)	ISO 527-2/3	MPa	80
- tensile strain at yield (10)	ISO 527-2/3	%	5
- tensile strain at break (10)	ISO 527-2/3	%	25
- tensile modulus of elasticity (11)	ISO 527-2/3	MPa	3000
-	ISO 527-2/3	MPa	1750
<p><b>Compression test (12)</b></p>			
- compressive stress at 1 / 2 / 5 % nominal strain (13)	ISO 604	MPa	26 / 31 / 32
<p><b>Creep test in tension (9)</b></p>			
- stress to produce 1 % strain in 1000 h (at 23°C)	ISO 899-1	MPa	22
-	ISO 899-1	MPa	10
<p><b>Impact strength - Charpy (14)</b></p>			
- Charpy impact strength - Notched	ISO 179-1/A	kJ/m <sup>2</sup>	no break
- Charpy impact strength - Notched	ISO 179-1/A	kJ/m <sup>2</sup>	3.5
<p><b>Ball impact strength - Notched</b></p>			
-	ISO 1824	kJ/m <sup>2</sup>	3.5
-	ISO 1824	kJ/m <sup>2</sup>	7
<p><b>Ball indentation hardness (14)</b></p>			
-	ISO 2039-1	N/mm <sup>2</sup>	195
<p><b>Rockwell hardness (14)</b></p>			
-	ISO 2039-2	-	M 88
<p><b>Electrical Properties at 23 °C</b></p>			
<p><b>Electric strength (15)</b></p>			
-	IEC 60243-1	kV/mm	25
-	IEC 60243-1	kV/mm	17
<p><b>Volume resistivity</b></p>			
-	IEC 60093	Ohm.cm	> 10 <sup>14</sup>
-	IEC 60093	Ohm.cm	> 10 <sup>12</sup>
<p><b>Surface resistivity</b></p>			
-	IEC 60093	Ohm	> 10 <sup>14</sup>
-	IEC 60093	Ohm	> 10 <sup>12</sup>
<p><b>Relative permittivity ε<sub>r</sub> - at 100 Hz</b></p>			
-	IEC 60250	-	3.0
-	IEC 60250	-	6.6
- at 1 MHz	IEC 60250	-	3.2
-	IEC 60250	-	9.7
<p><b>Dielectric dissipation factor tan δ - at 100 Hz</b></p>			
-	IEC 60250	-	0.012
-	IEC 60250	-	0.14
- at 1 MHz	IEC 60250	-	0.010
-	IEC 60250	-	0.05
<p><b>Compressive tracking index (CTI)</b></p>			
-	IEC 60112	-	600
-	IEC 60112	-	600

Note: 1 g/cm<sup>3</sup> = 1000 kg/m<sup>3</sup>; 1 MPa = 1 N/mm<sup>2</sup>; 1 kV/mm = 1000 V/mm.

### AVAILABILITY

Round Rods: Ø 50-500 mm - Plates: Thicknesses 10-100 mm - Tubes: O.D. 50-600 mm

ERTALON® is a registered trademark of the Quadrant Group.

All information supplied by or on behalf of Quadrant Engineering Plastic Products in relation to its products, in any form, is supported by research and believed to be reliable, but Quadrant Engineering Plastic Products assumes no liability whatsoever in respect of application, processing or use made of the aforementioned information or products, or any consequence thereof. The buyer undertakes all liability in respect of the application, processing or use of the aforementioned information or product, whose quality and other properties he shall verify, or any consequence thereof. No liability whatsoever shall attach to Quadrant Engineering Plastic Products for any infringement of the rights owned or controlled by a third party in intellectual, industrial or other property by reason of the application, processing or use of the aforementioned information or products by the buyer.

Quadrant Engineering Plastic Products

global leader in engineering plastics for machining

www.quadrantplastics.com

### Legend:

- + : values referring to dry material
  - ++ : values referring to material in equilibrium with the standard atmosphere 23 °C / 50 % RH (mostly derived from literature)
  - (1) According to method 1 of ISO 62 and equal on discs Ø 50 x 3 mm.
  - (2) The figures given for these properties are for the most part derived from the material supplier data and other publications.
  - (3) Values for this property are only given here for amorphous materials and not for semi-crystalline ones.
  - (4) Only for short time exposure (a few hours) in applications where not or only a very low load is applied to the material.
  - (5) Temperature not stable over a period of 5,000/20,000 hours. After these periods of time, there is a decrease in tensile strength - measured at 23 °C - of about 50 % as compared with the original value. The temperature values given here are thus based on the thermal-oxidative degradation which takes place and causes a reduction in properties. Note, however, that the maximum allowable service temperature depends in many cases essentially on the duration and the magnitude of the mechanical stresses to which the material is subjected.
  - (6) Impact strength decreasing with decreasing temperature, the minimum allowable service temperature is practically mainly determined by the extent to which the material is subjected to impact. The value given here is based on unfavourable impact conditions and may consequently not be considered as being the absolute practical limit.
  - (7) These estimated ratings, derived from raw material supplier data and other publications, are not intended to reflect factors presented by the material under actual fire conditions. There is no UL File Number available for ERTALON 6 PLA stock shapes.
  - (8) The figures given for the properties of dry material (+) are for the most part average values of tests run on test specimens machined out of rods Ø 50 mm. Except for the hardness tests, the test specimens were then taken from an area mid between centre and outside diameter, with their length in longitudinal direction of the rod.
  - (9) Test specimens: Type 1 B
  - (10) Test speed: 50 mm/min (phase acc. to: ISO 13303-1 as a function of the ductile behaviour of the material (tough or brittle))
  - (11) Test speed: 1 mm/min
  - (12) Test specimens: cylinders Ø 12 x 30 mm
  - (13) Pendulum used: 10 J
  - (14) Measured on 10 mm thick test specimens (discs), mid between centre and outside diameter.
  - (15) Electrode configuration: Ø 25 / Ø 75 mm coaxial cylinders; in transformer oil according to IEC 60250; 1 mm thick test specimens.
- \* This table is a valuable help in the choice of a material. The data listed here fall within the normal range of product properties. However, they are not guaranteed and they should not be used to establish material specification limits nor used alone as the basis of design.

## A.2.3 PAR data



Physical Properties	Value	Unit	Method of verification
Density:	1.15	g/cm <sup>3</sup>	ISO 1183
Moisture pick-up till saturation (in normal climate 23 °C) :	2.3	%	ISO 62
Moisture pick-up till saturation (in normal climate 23 °C) :	6.5	%	ISO 62

Mechanical properties	Value	Unit	Method of verification
Tensile stress at yield (v = 50 mm/min):	85	N/mm <sup>2</sup>	ISO 527-2
Tensile stress at break (v = 5 mm/min):	-	N/mm <sup>2</sup>	ISO 527-2
Nominal percentage elongation at break:	25	%	ISO 527-2
Tensile modulus of elasticity:	3500	N/mm <sup>2</sup>	ISO 527-2
Flexural modulus of elasticity:	-	N/mm <sup>2</sup>	ISO 178
Ball indentation hardness (value at 30 s):	165	N/mm <sup>2</sup>	ISO 2039-1
Rockwell hardness:	M 88	-	ISO 2039-2
Charpy impact strength (23 °C) :	n. br. **	kJ/m <sup>2</sup>	ISO 179/1eU
Charpy impact strength - notched (23 °C) :	3.5	kJ/m <sup>2</sup>	ISO 179/1eA

Thermal properties	Value	Unit	Method of verification
Temperature for using in air (maximum):	170	°C	Max. short term
Temperature for using in air (maximum):	105	°C	Max. lasting
Temperature for using in air (minimum):	-30	°C	-
Heat distortion temperature (HDT A process):	80	°C	ISO 75-2
Coefficient of linear expansion, at length (23-60)°C :	0.8·10 <sup>-4</sup>	1/K	DIN 53752
Thermal conductivity (23 °C):	0.29	W/(K·m)	DIN 52612
Flammability according UL standard:	HB	Grade	UL 94
Vicat softening temperature (VST/B/50):	-	°C	ISO 306
Melting point DSC (10 K/min):	220	°C	ISO 3146

Electrical properties	Value	Unit	Method of verification
Specific volume resistivity:	10 <sup>12</sup>	Ω·m	IEC 60093
Specific surface resistivity:	10 <sup>13</sup>	Ω	IEC 60093
Dielectric factor (at 1 MHz)*:	3.2	-	IEC 60250
Dielectric factor (at 100 Hz)*:	3.6	-	IEC 60250
Dissipation factor (at 1 MHz)*:	0.016	-	IEC 60250
Dissipation factor (at 100 Hz)*:	0.012	-	IEC 60250
Dielectric strength K20/K20:	25	kV/mm	IEC 60243-1
Comparative tracking Index (CTI):	600	-	IEC 60112

Values may vary depending on the manufacturer. If you require a specific value for anything above please state at time of enquiry.

All recommendations and information contained on this website are, to the best of our knowledge, correct. Product specifications are intended as guidelines. Since conditions of service are beyond our control, users must satisfy themselves that products are suitable for the intended use. No guarantee or warranty is given or implied in respect of information or recommendations, or that any use of products will not infringe rights belonging to other parties. We reserve the right to change product design and properties without notification.

### A.3 Variation of Nylon properties with temperature

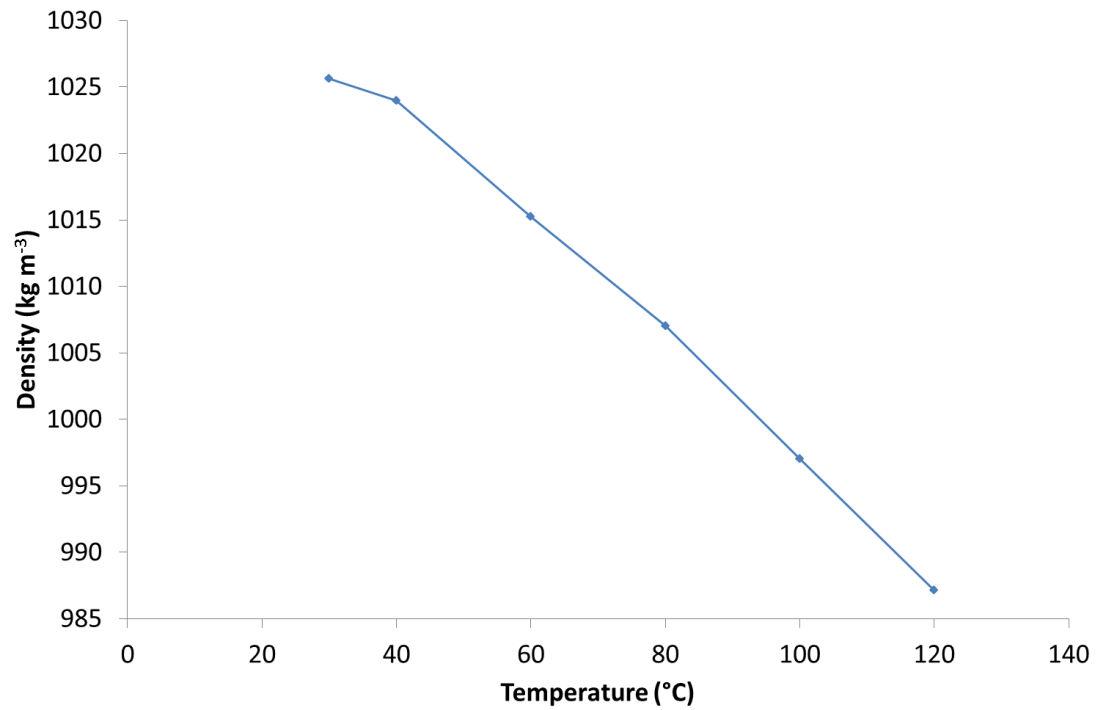


Figure A.1 Variation in Nylon 12 density with temperature [118]

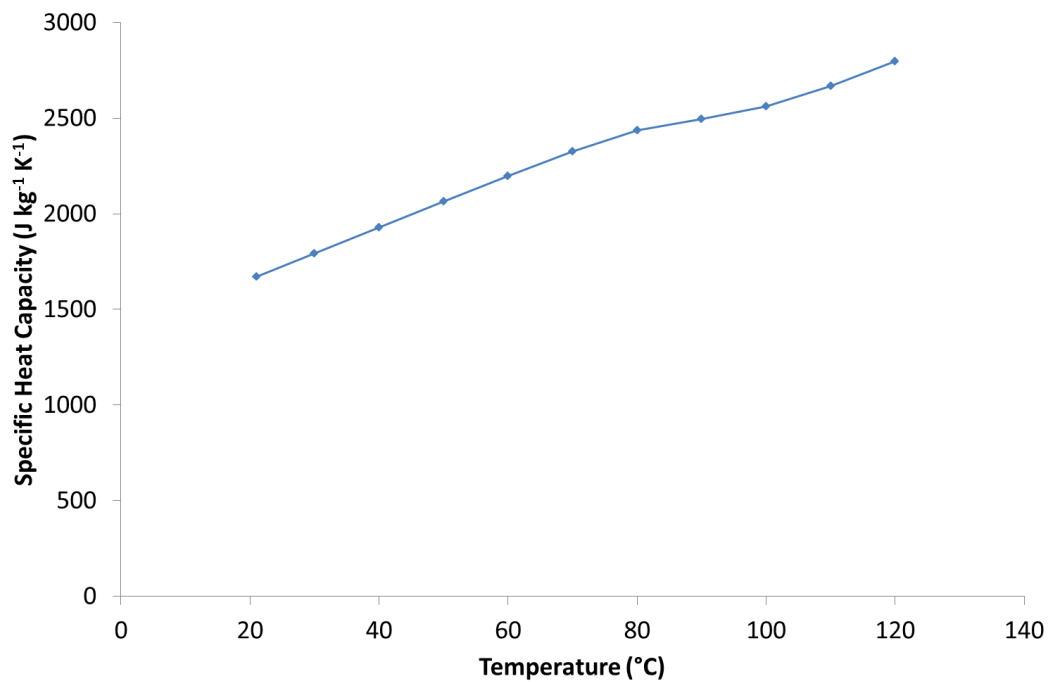


Figure A.2 Variation in Nylon 12 specific heat capacity with temperature [118]

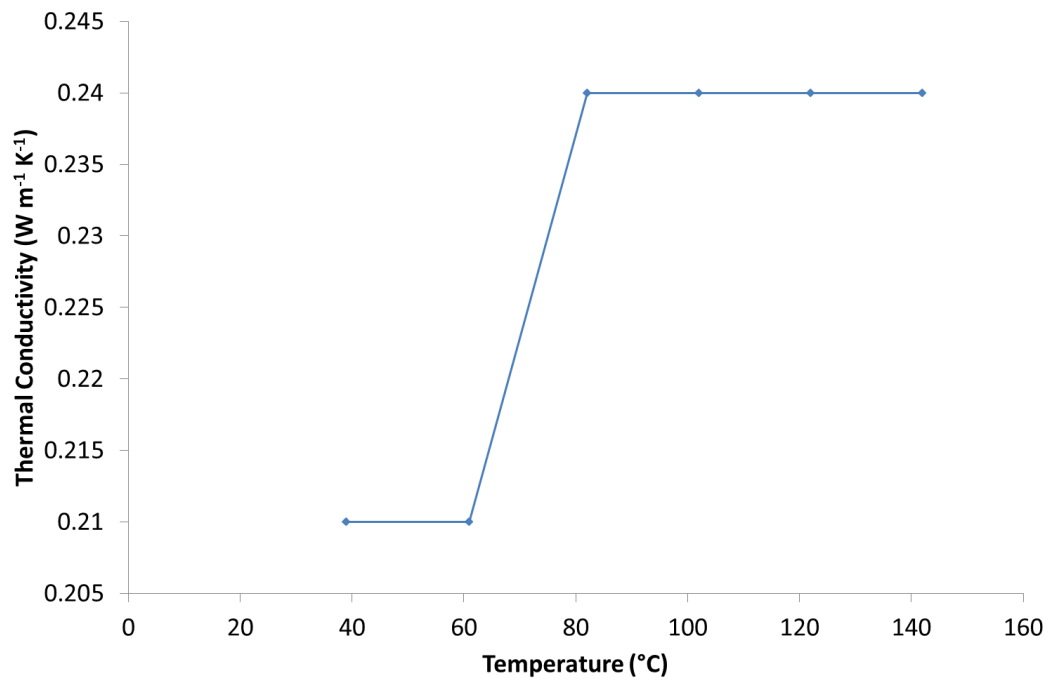


Figure A.2 Variation in Nylon 11 thermal conductivity with temperature [118]

## Appendix B Oil rig theoretical model nodal equation derivations

### B.1 Internal surface node exchanging heat with the lubricant

Taking the average lubricant temperature across the specimen from the current time step,  $T_{Average}^n$ , the heat flux from the lubricant to the surface node in time step  $\delta t$  is defined as:

$$Q_{convection} = h_{oil} \delta t 2\pi r_{inner} (T_{average}^{n-1} - T_{inner}^{n-1})$$

The surface node also exchanges heat with the rest of the specimen by conduction hence,

$$Q_{conduction} = \frac{k_{metal} \delta t 2\pi (r_{inner} + \frac{\Delta r}{2})}{\Delta r} (T_{inner+1}^{n-1} - T_{inner}^{n-1}):$$

The summation of the convection and conduction heat fluxes results in a subsequent change in temperature of the inner bore surface of the test bock specimen. The change in thermal energy of the surface node over a given time step is given by

$$Q_{accumulation} = m_{metal} C p_{metal} (T_{inner}^n - T_{inner}^{n-1})$$

$$Q_{accumulation} = \rho_{metal} C p_{metal} \pi \left( \left( r_{inner} + \frac{\Delta r}{2} \right)^2 - r_{inner}^2 \right) (T_{surface}^n - T_{surface}^{n-1})$$

$$Q_{accumulation} = \rho_{metal} C p_{metal} \pi r_{inner} \Delta r (T_{surface}^n - T_{surface}^{n-1})$$

$$Q_{accumulation} = Q_{convection} + Q_{conduction}$$

$$\rho_{metal} C p_{metal} r_{inner} \Delta r (T_{inner}^n - T_{inner}^{n-1}) = h_{oil} \delta t 2\pi r_{inner} (T_{Average}^{n-1} - T_{inner}^{n-1}) + \frac{k_{metal} \delta t 2\pi (r_{inner} + \frac{\Delta r}{2})}{\Delta r} (T_{inner+1}^{n-1} - T_{inner}^{n-1})$$

The Fourier number,  $FO$ , is defined as

$$\left( \frac{k_{metal} \delta t}{\rho_{metal} C p_{metal} \Delta r^2} \right)$$

Equation B.1: Definition of Fourier Number

The temperature of the inner surface node,  $T_{Surface}^n$ , following re-arrangement and substitution is given by Equation B.2:

$$T_{surface}^n = T_{surface}^{n-1} \left( 1 - F_{O_{metal}} \left( \left( 2 + \frac{\Delta r}{r_{inner}} \right) + \frac{\Delta r h_{oil}}{k_{metal}} \right) \right) + F_{O_{metal}} \left( 2 + \frac{\Delta r}{r_{inner}} \right) T_{inner+1}^N + \frac{2F_{O_{metal}} \Delta r h_{oil}}{k_{Metal}} T_{oil}^{n-1}$$

**Equation B.2: Definition of the surface temperature of the inner bore of the test block specimen**

It should be noted that in the instance where a polymer insert is installed,  $F_{O_{metal}}$  would be replaced with  $F_{O_{polymer}}$ .

## B.2 Internal node exchanging heat by conduction with two neighbouring nodes

The interaction of a metallic node, sandwiched between two other metallic nodes is a scenario repeated cyclically throughout the radial distribution of the test block specimen. The derivation presented here is focused on the node  $T_{inner+1}$

The node receives heat flow from the node  $T_{inner}$  by conduction:

$$Q_{conduction T_{inner}} = \frac{2\pi\delta tk_{metal} \left( r_{inner+1} - \frac{\Delta r}{2} \right)}{\Delta r} (T_{inner}^{n-1} - T_{inner+1}^{n-1})$$

The node receives heat flow from the node  $T_{inner+2}$  by conduction:

$$Q_{conduction T_{inner+2}} = \frac{2\pi\delta tk_{Metal} \left( r_{inner+1} + \frac{\Delta r}{2} \right)}{\Delta r} (T_{inner+2}^{n-1} - T_{inner+1}^{n-1})$$

The summation of the conduction heat fluxes result in a subsequent change in temperature of the metal at the node of interest. The change in thermal energy of the sandwich node over a given time step is given by

$$Q_{accumulation} = m_{metal} C_{p_{metal}} (T_{inner+1}^N - T_{inner+1}^{N-1})$$

$$Q_{accumulation} = \pi\rho_{metal} C_{p_{metal}} \left( \left( r_{inner+1} + \frac{\Delta r}{2} \right)^2 - \left( r_{inner+1} - \frac{\Delta r}{2} \right)^2 \right) (T_{inner+1}^n - T_{inner+1}^{n-1})$$

$$Q_{accumulation} = \pi\rho_{metal} C_{p_{metal}} 2\Delta r r_{inner+1} (T_{inner+1}^n - T_{inner+1}^{n-1})$$

$$Q_{accumulation} = Q_{conduction T_{inner}} + Q_{conduction T_{inner+2}}$$

$$\begin{aligned} & \rho_{metal} C_{p_{metal}} 2\Delta r r_{inner+1} (T_{inner+1}^n - T_{inner+1}^{n-1}) \\ &= \frac{2\pi\delta tk_{Metal} \left( r_{inner+1} - \frac{\Delta r}{2} \right)}{\Delta r} (T_{inner}^{n-1} - T_{inner+1}^{n-1}) + \frac{2\pi\delta tk_{Metal} \left( r_{inner+1} + \frac{\Delta r}{2} \right)}{\Delta r} (T_{inner+2}^{n-1} - T_{inner+1}^{n-1}) \end{aligned}$$

Following re-arrangement and substitution, the final equation for the temperature at  $T_{inner+1}$  is derived and is shown in Equation B.3:

$$T_{inner+1}^n = T_{inner+1}^{n-1} (1 - 2Fo_{metal}) + T_{inner}^{n-1} \left( Fo_{metal} \left( 1 - \frac{\Delta r}{2r_{inner+1}} \right) \right) + T_{inner+2}^{n-1} \left( Fo_{metal} \left( 1 + \frac{\Delta r}{2r_{inner+1}} \right) \right)$$

Equation B.3: Derivation of the temperature at a sandwich node within the aluminium test block specimen

### B.3 External surface node exchanging heat with the ambient air

When exchanging heat with the ambient air, the node's thermal balance has a form very similar to that described in Appendix B.1 in that there is one convective heat transfer to the node and one conduction heat transfer mechanism to the node. Heat transfer from the outer surface by radiation has not been considered in this case due to the low emissivity of the surface (highlighted as significant parameter in radiation heat transfer in Section 2.2.1). The emissivity of aluminium is reported to be of the order of 0.07 at 23 °C [50] while Welty et al. [51] reported the emissivity of oxidised aluminium at 199 °C to be 0.11. Thus, the combination of the surface temperature causing the emissivity to rise and any change in the optical properties of the aluminium as a result of oxidation do not appear to increase the emissivity to such an extent that it would become significant. In addition, the outer surface temperature of the specimen only reaches a maximum temperature of 100 °C. In the case of the outer surface node the convective heat flux is between the outer surface and ambient air.

$$Q_{convection} = h_{ambient} \delta t 2\pi r_{outer} (T_{ambient}^{n-1} - T_{outer}^{n-1})$$

$$Q_{conduction} = \frac{k_{metal} \delta t 2\pi (r_{outer} - \frac{\Delta r}{2})}{\Delta r} (T_{outer-1}^{n-1} - T_{outer}^{n-1}):$$

The summation of the convection and conduction heat fluxes result in a subsequent change in temperature of the outer surface node. The change in thermal energy of the surface node over a given time step is given by

$$Q_{accumulation} = m_{metal} C p_{metal} (T_{outer}^n - T_{outer}^{n-1})$$

$$Q_{accumulation} = \rho_{metal} C p_{metal} \pi (r_{outer}^2 - \left( r_{outer} - \frac{\Delta r}{2} \right)^2) (T_{outer}^n - T_{outer}^{n-1})$$

$$Q_{accumulation} = \rho_{metal} C p_{metal} \pi r_{outer} \Delta r (T_{outer}^n - T_{outer}^{n-1})$$

$$Q_{accumulation} = Q_{convection} + Q_{conduction}$$

Following substitution for the Fourier Number,  $Fo_{metal}$ , the resulting equation for the temperature at the node  $T_{outer}$  follows a near identical form to that presented for  $T_{inner}$ :

$$T_{outer}^n = T_{outer}^{n-1} \left( 1 - Fo_{metal} \left( \left( 2 - \frac{\Delta r}{r_{outer}} \right) + \frac{\Delta r h_{outer}}{k_{metal}} \right) \right) + Fo_{metal} \left( 2 - \frac{\Delta r}{r_{outer}} \right) T_{outer-1}^n + \frac{2Fo_{metal} \Delta r h_{outer}}{k_{metal}} T_{ambient}^{n-1}$$

**Equation B.4: Derivation of the temperature at the outer surface node of the aluminium test block specimen exchanging heat to the ambient air**

## B.4 Internal node at the interface of a material change where an insulator has been applied

The transfer of heat at the interface of two surfaces is modelled in a near identical way to that of convective heat transfer from a surface to a fluid. Hence, where an insert has been installed in the test block specimen the outer surface of the insert and the inner surface of the specimen bore have energy balances almost identical in form to that of the nodes described in Appendix B.1 and Appendix B.3 respectively. However, the value of  $h_{oil}$  or  $h_{outer}$  is replaced by a different value,  $h_{contact}$ .

The temperature of the inner bore is now calculated using Equation B.5 to allow interaction with a polymer liner:

$$T_{inner\ metal}^n = T_{inner\ metal}^{n-1} \left( 1 - Fo_{metal} \left( \left( 2 + \frac{\Delta r}{r_{inner\ metal}} \right) + \frac{\Delta r h_{contact}}{k_{metal}} \right) \right) + Fo_{metal} \left( 2 + \frac{\Delta r}{r_{inner\ metal}} \right) T_{inner\ metal+1}^n + \frac{2Fo_{metal} \Delta r h_{contact}}{k_{metal}} T_{outer\ polymer}^{n-1}$$

**Equation B.5: Derivation of the inner metal bore temperature when in contact with the outer surface of a polymer liner**

Similarly, the outer temperature of the polymer is modified to transfer heat to the bore of the surrounding metal, as shown in Equation B.6.

$$T_{outer\ polymer}^n = T_{outer\ polymer}^{n-1} \left( 1 - Fo_{polymer} \left( \left( 2 - \frac{\Delta r}{r_{outer\ polymer}} \right) + \frac{\Delta r h_{contact}}{k_{polymer}} \right) \right) + Fo_{polymer} \left( 2 - \frac{\Delta r}{r_{outer}} \right) T_{outer\ polymer-1}^n + \frac{2Fo_{polymer} \Delta r h_{contact}}{k_{polymer}} T_{inner\ metal}^{n-1}$$

**Equation B.6: Derivation of the outer surface temperature of a polymer tube when inserted into a metal bore**

## Appendix C Temperature profiles for model predictions

### C.1 100 mm outer diameter uninsulated specimen

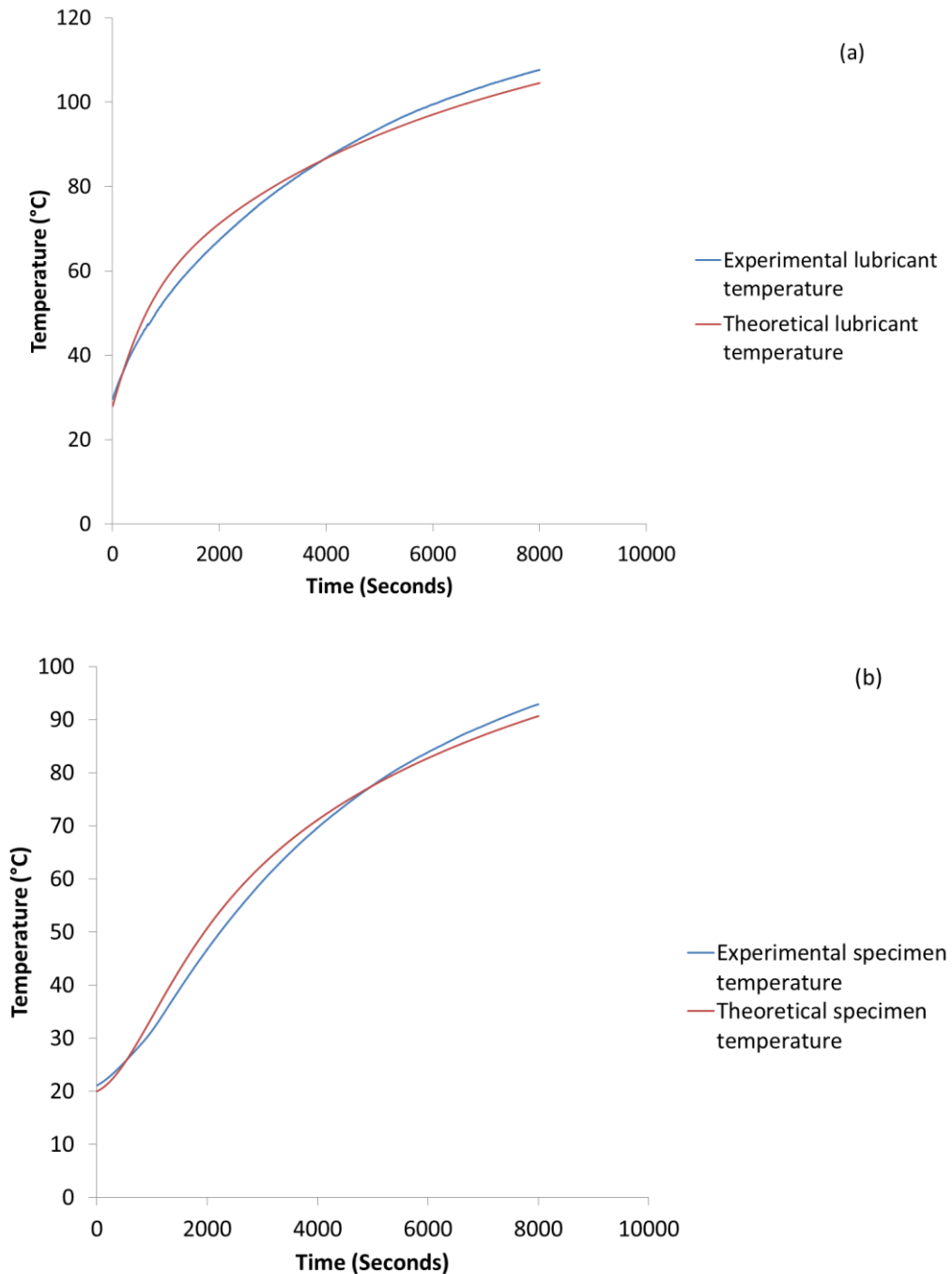


Figure C.1: Comparison between theoretical and experimental data for the oil flow rig when 1200 W heater power is input using a 100 mm outer diameter uninsulated specimen and a lubricant flow rate of  $10 \text{ l min}^{-1}$

## C.2 40 mm outer diameter uninsulated specimen

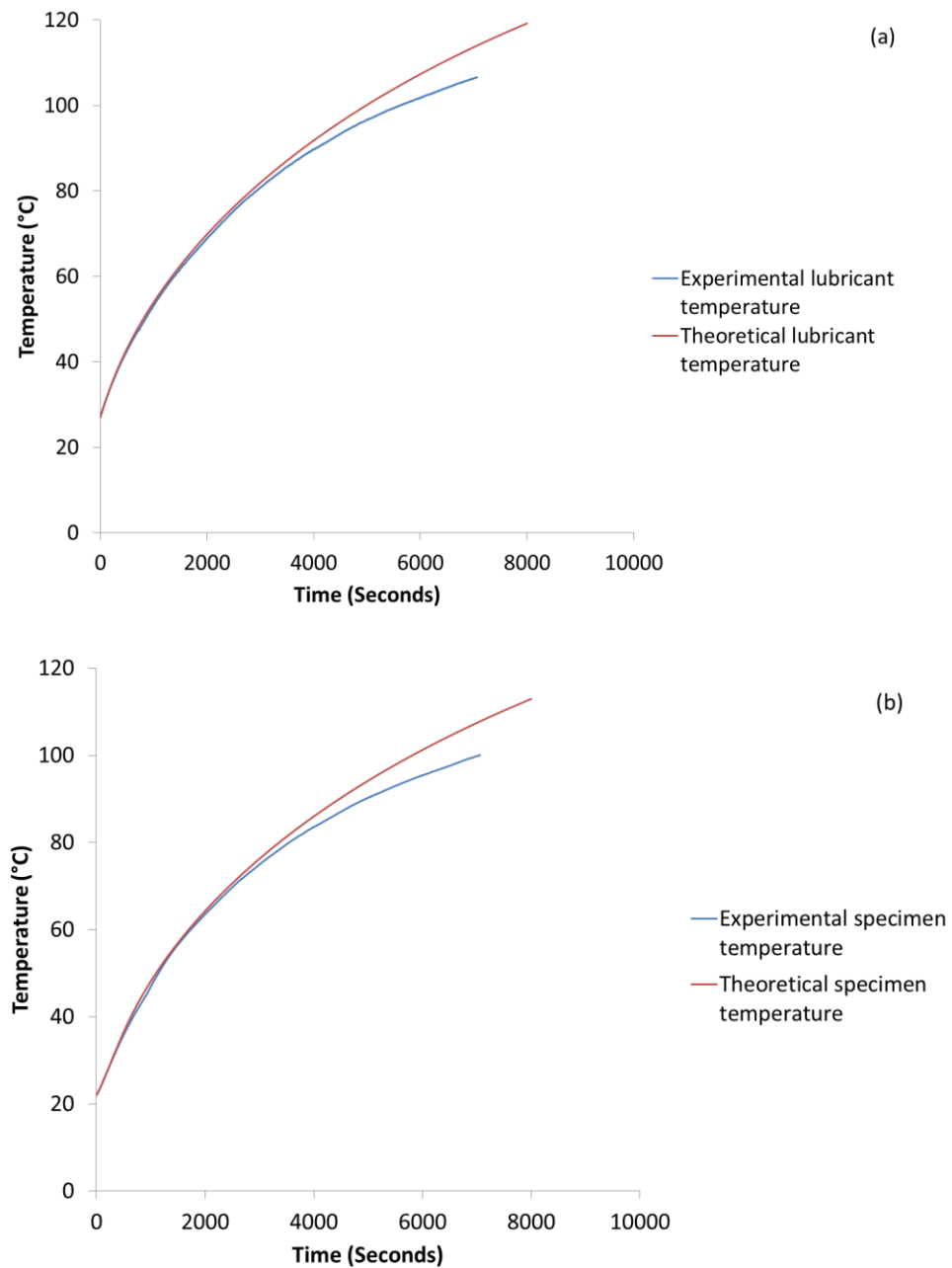


Figure C.2: Comparison between theoretical and experimental data for the oil flow rig when 1200 W heater power is input using a 40 mm outer diameter uninsulated specimen and a lubricant flow rate of  $10 \text{ l min}^{-1}$

### C.3 100 mm outer diameter insulated specimen

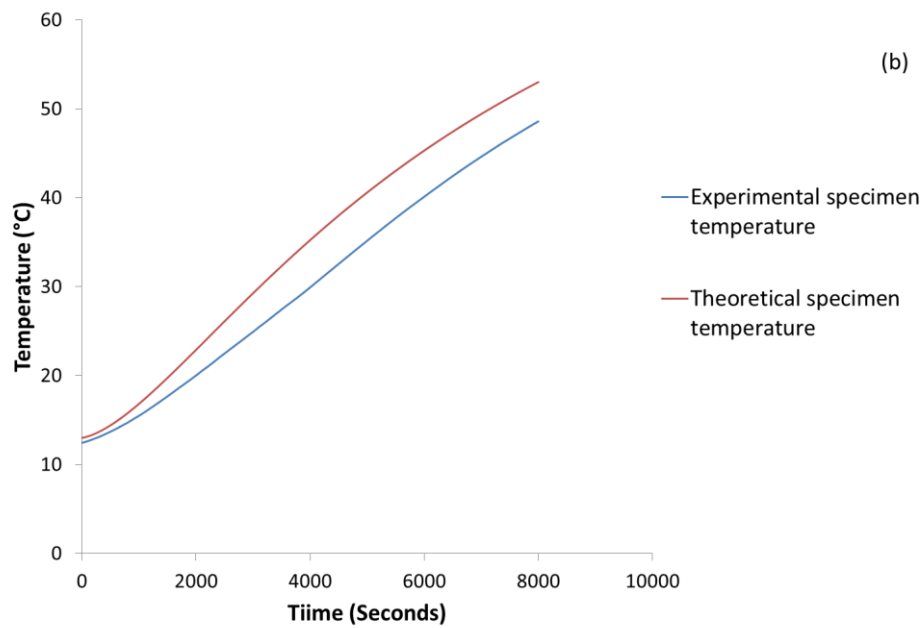
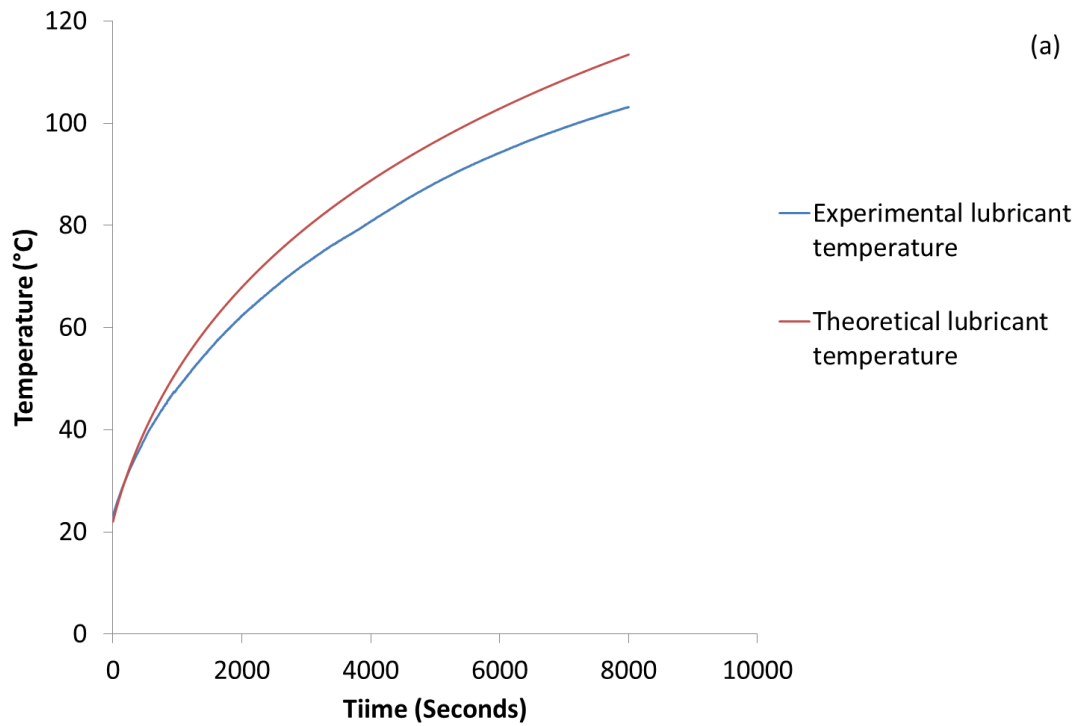


Figure C.3: Comparison between theoretical and experimental data for the oil flow rig when 1200 W heater power is input using a 100 mm outer diameter specimen with a 2 mm thick Nylon insert and a lubricant flow rate of  $10 \text{ l min}^{-1}$

## C.4 40 mm outer diameter insulated specimen

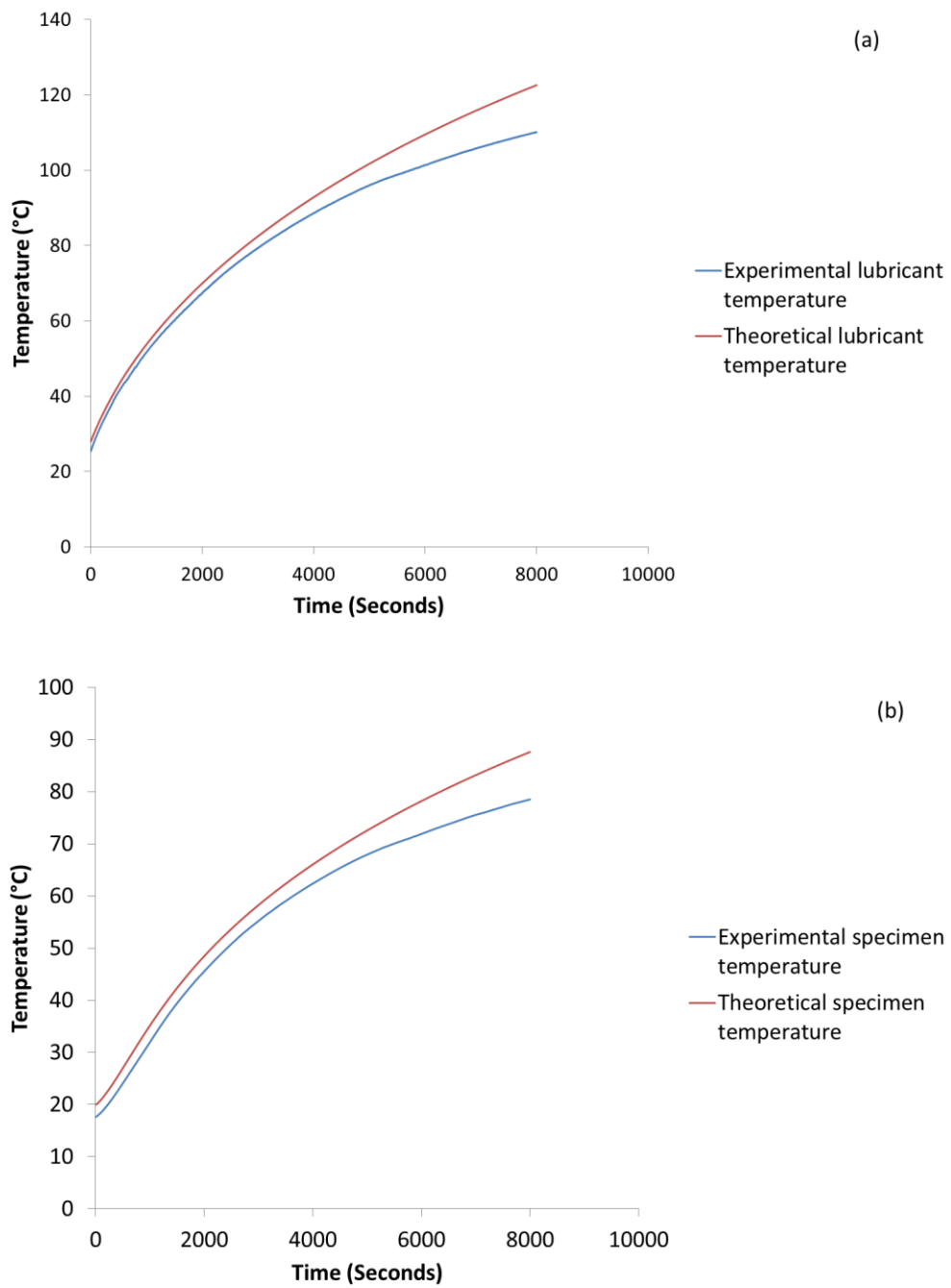


Figure C.4: Comparison between theoretical and experimental data for the oil flow rig when 1200 W heater power is input using a 40 mm outer diameter specimen with a 2 mm thick Nylon insert and a lubricant flow rate of  $10 \text{ l min}^{-1}$

## C.5 100 mm outer diameter plain aluminium insert

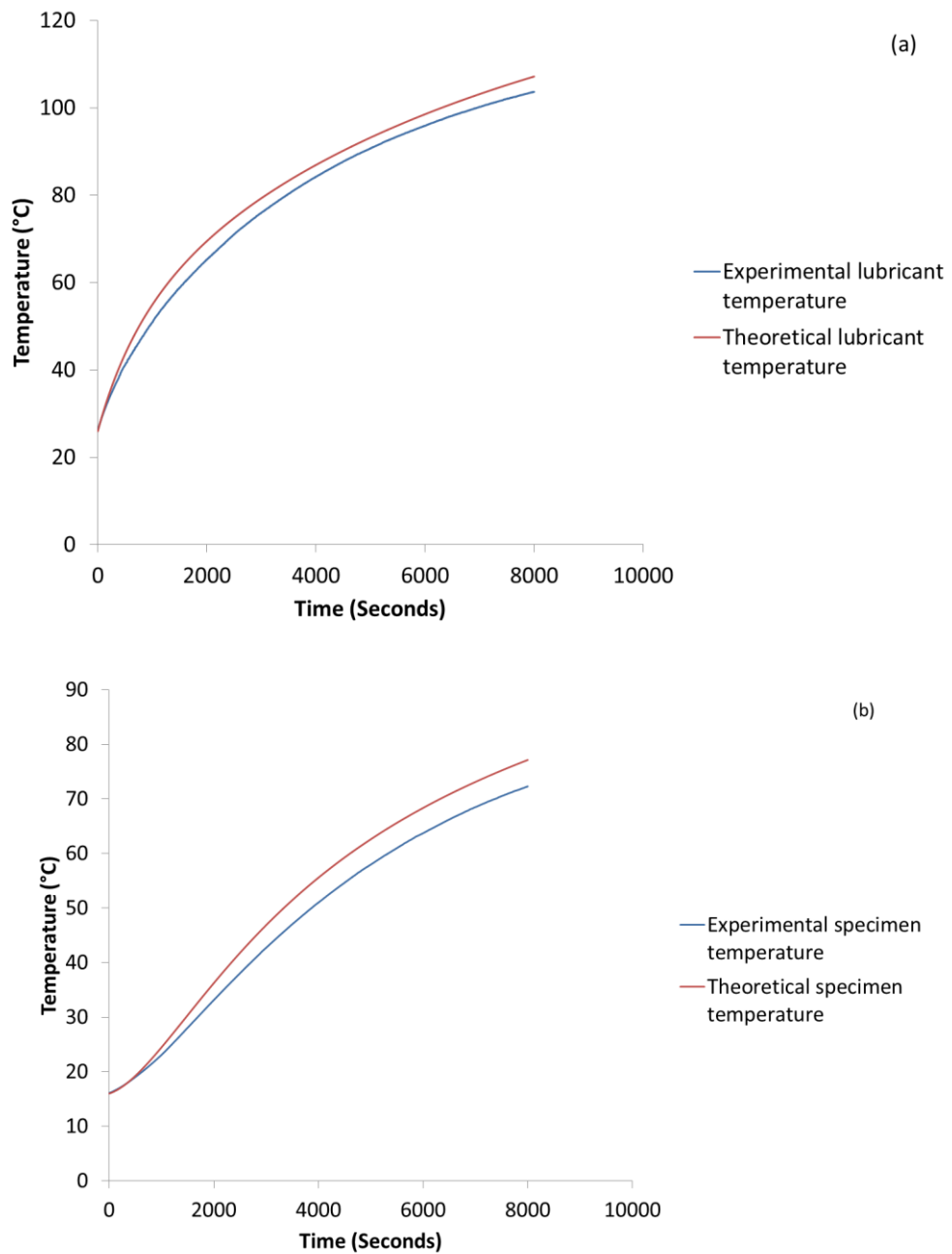


Figure C.5: Comparison between theoretical and experimental data for the oil flow rig when 1200 W heater power is input using a 100 mm outer diameter specimen with a 2 mm thick aluminium insert and a lubricant flow rate of 10 l min<sup>-1</sup>

## **Appendix D   Flow Chart of Model Structure**

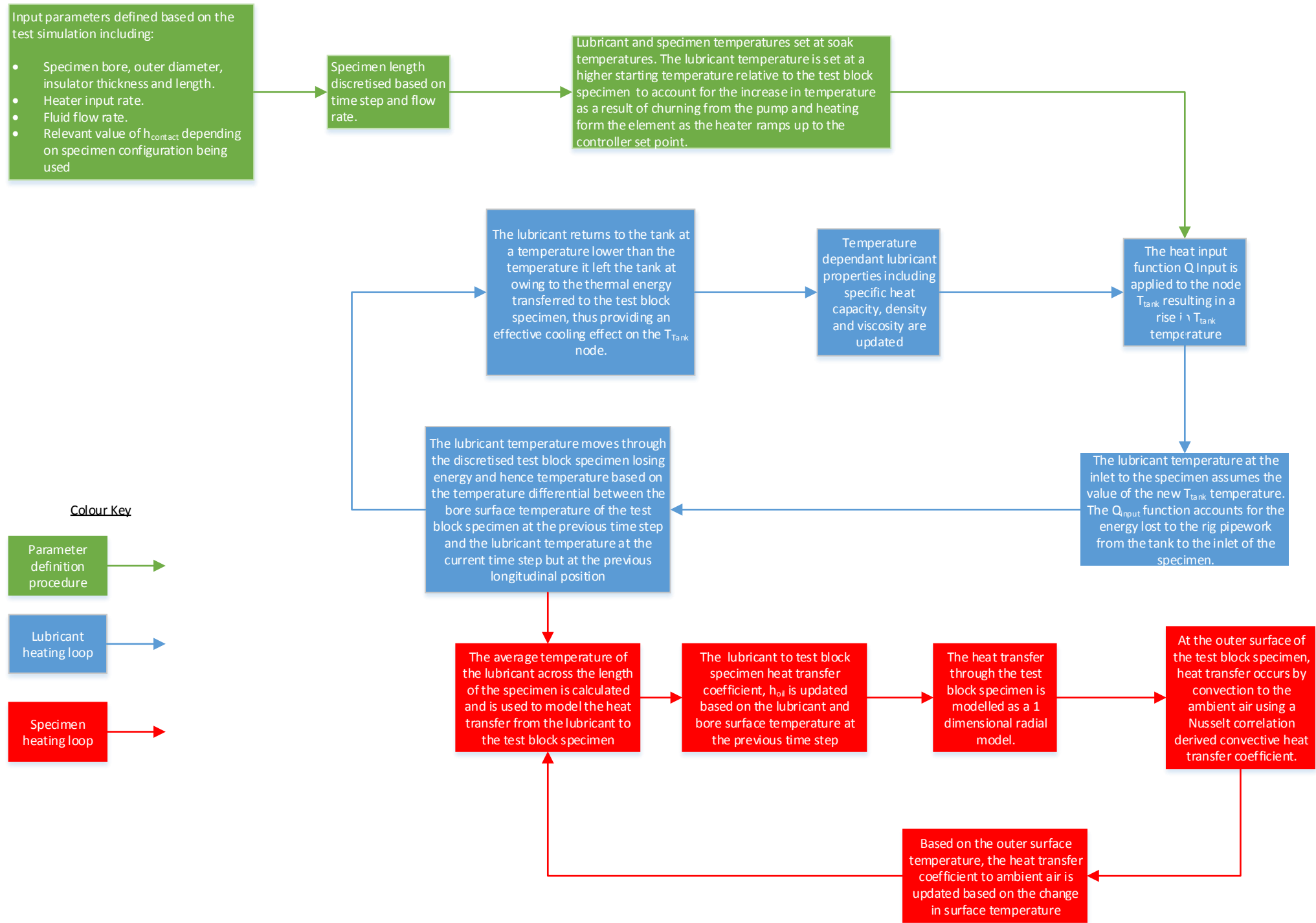


Figure D.1: Flow chart of oil circuit model

## Appendix E Publications arising from this thesis

- Roberts, A, Brooks, R.; Shipway, P.; Dominy, J.; Gilchrist, R.; Helle-Lorentzen, R.; Reducing thermal losses from automatic lubricant circuits during cold start by the application of polymer insulation presented at VTMS 11, Coventry, UK, 2013.
- Roberts, A; Brooks, R.; Shipway, P.; Gilchrist, R.; Pegg I., "Reducing Energy Losses from Automotive Engine Lubricants by Thermal Isolation of the Engine Mass," SAE Technical Paper 2014-01-0672, 2014
- Roberts, A.; Brooks, R.; Shipway P., Internal combustion engine cold-start efficiency: A review of the problem, causes and potential solutions. Energy Conversion and Management, 2014. **82**(0): p. 327-350